...CAN
J... 1951
...CS
...ARY

THE JOURNAL OF CHEMICAL PHYSICS

Volume 19 Number 7

JULY, 1951

AMERICAN INSTITUTE OF PHYSICS

Physics
Room

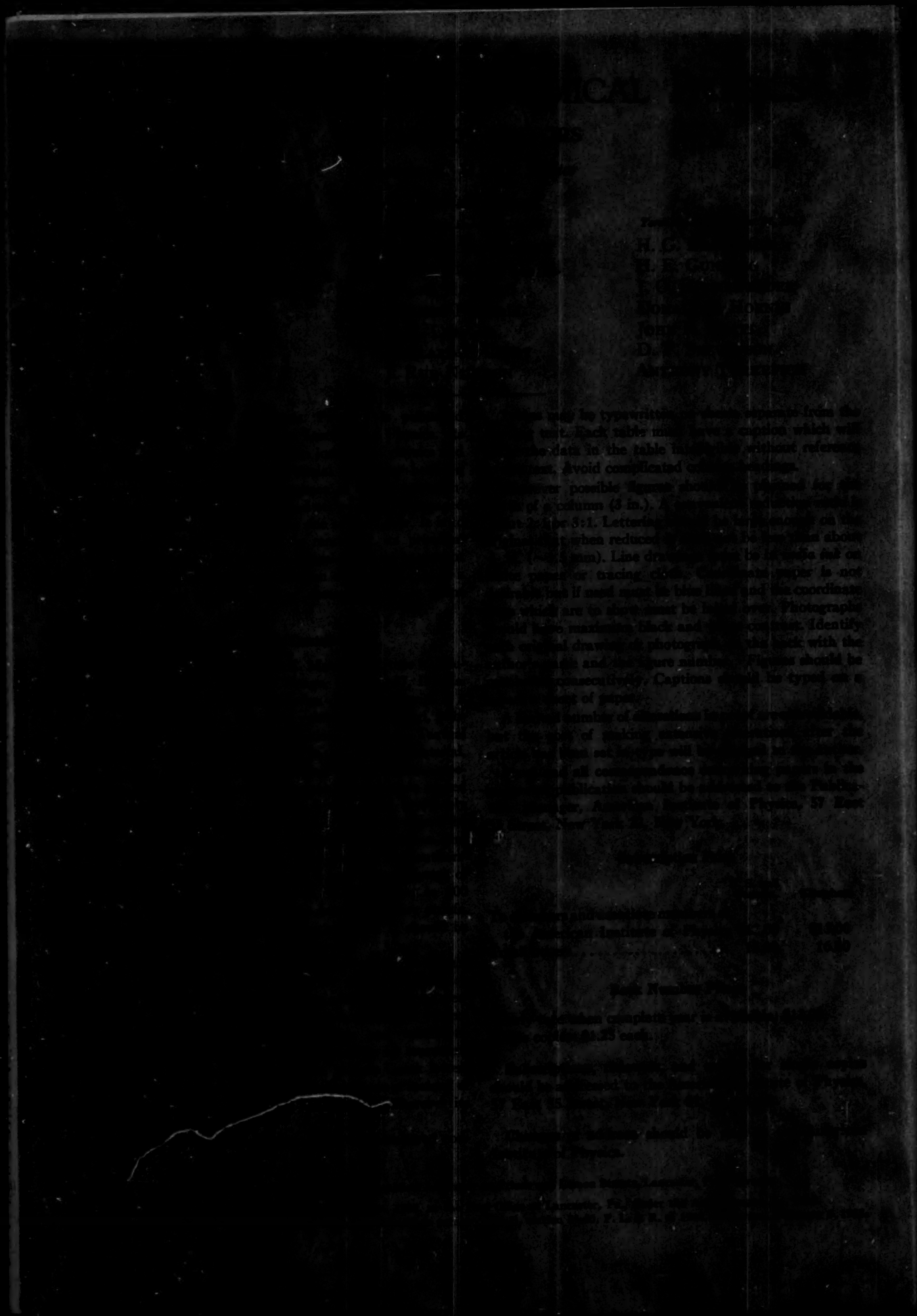

Physics
Faxon

THE JOURNAL
OF
CHEMICAL PHYSICS

VOLUME 19, NUMBER 7 JULY, 1951

Quantitative Infrared Intensity Measurements. I. Carbon Monoxide Pressurized with Infrared-Inactive Gases*

S. S. PENNER AND D. WEBER
Jet Propulsion Laboratory, California Institute of Technology, Pasadena, California
(Received February 26, 1951)

Quantitative infrared intensity measurements on CO pressurized with H_2, He, A, O_2, and N_2 for total pressures up to 700 psia have been carried out. The values of integrated absorption for the fundamental and first overtone of CO have been found to be 237 cm^{-2} $atmos^{-1}$ and 1.64 cm^{-2} $atmos^{-1}$, respectively. The numerical values of integrated absorption were obtained by using an indirect method for the interpretation of experimental data, similar to the extrapolation technique of Wilson and Wells.

The experimental data obtained at very large values of the total pressure should yield correctly the numerical values of the spectral absorption coefficients. This statement is supported by the fact that the integral over the spectral absorption coefficients at a total pressure of 700 psia yields values for the integrated absorption of fundamental and first overtone of CO which are in excellent agreement with results obtained by indirect methods.

I. INTRODUCTION

MOST of the recently published measurements on integrated absorption of diatomic and polyatomic gases involve the use of an extrapolation technique which was introduced by Wilson and Wells in 1946.[1] In particular, measurements have been reported on ethylene,[2] nitrous oxide,[2] carbon dioxide,[3] methane,[3] ethane,[3] aliphatic hydrocarbons,[4] cyanogen,[5] cyanogen hydrochloride,[5] nitric oxide,[6] and carbon monoxide.[6] Earlier infrared intensity measurements for carbon monoxide, using a novel indirect method, have been reported by Matheson,[7] whereas infrared dispersion measurements, which also give information concerning the effective charge and integrated absorption, have been described by Havens.[8]

Compared with the work of Dinsmore and Crawford[6] and of Matheson,[7] the studies described in the present report differ in several important details. In particular, the present studies have been extended to large values of the total pressure (up to 700 psia) in order to minimize the curvature in the Wilson-Wells extrapolation plot and thus yield a more reliable estimate of the limiting slope corresponding to the integrated absorption. The use of pressures of this order of magnitude is not new, having been reported by Bartholomé,[9] who attempted to measure the integrated absorption for three of the hydrogen halides. Bartholomé's experimental technique was inadequate because very low spectral resolution was used,[10] as explained in a previous discussion.[11]

It is well known that pure gases, especially at elevated pressures, may diffuse so slowly as to require very long periods of time in order to produce a uniform mixture. The present investigation has yielded ample evidence of the prevalence of errors resulting from imperfect mixing. These errors were ultimately eliminated by providing the infrared absorption cell with a grid to produce mixing by forced convection. Finally it appeared in the course of the present studies that the concentration of gas mixtures may be falsified by the oc-

* This paper presents the results of one phase of research carried out at the Jet Propulsion Laboratory, California Institute of Technology, under Contract No. W-04-200-ORD-455, sponsored by the U. S. Army Ordnance Department.

[1] E. B. Wilson, Jr., and A. J. Wells, J. Chem. Phys. 14, 578 (1946).
[2] Thorndike, Wells, and Wilson, Jr., J. Chem. Phys. 15, 157 (1947).
[3] A. M. Thorndike, J. Chem. Phys. 15, 868 (1947).
[4] S. A. Francis, J. Chem. Phys. 18, 861 (1950).
[5] E. R. Nixon and P. C. Cross, Technical Report No. 15, Brown University, May 15, 1950.
[6] H. L. Dinsmore and B. L. Crawford, Jr., Report NR-019-104, University of Minnesota, October, 1949.
[7] L. A. Matheson, Phys. Rev. 40, 813 (1932).
[8] R. J. Havens, Dissertation, University of Wisconsin, 1938.
[9] E. Bartholomé, Z. physik. Chem. B23, 131 (1933).
[10] E. C. Kemble, J. Chem. Phys. 3, 316 (1935).
[11] S. S. Penner, J. Appl. Phys. 21, 685 (1950).

TABLE I. Composition of gases.

Gas	Manufacturer	Nominal purity (%)	Nominal concentrations of impurities
CO	Matheson Company	96.8	CO, 0.36%; N_2, 1.0%; H_2, 0.97%; saturated hydrocarbons, 0.8%
H_2	Linde Air Products Company	99.5±1	—
A	Linde Air Products Company	99.8	O_2, 20 ppm (max) H_2, 40 ppm (max)
O_2	Linde Air Products Company	99.5	N_2, 0.25%; A, 0.25%
N_2 (dry)	Linde Air Products Company	99.7	O_2, 0.3%; A, trace
He	Air Reduction Company	98.4±0.15	O_2, 0.01%; H_2, 0.08 to 0.12%; N_2, 1.4 to 1.6%; hydrocarbons 0 to 0.01%

currence of selective adsorption on the walls of the infrared absorption cells. At small optical densities it is necessary to introduce suitable corrections for adsorption phenomena. These corrections can be estimated empirically by checking gas concentrations through independent analysis of the mixtures present in the cell. Gas analyses were performed by the use of a mass spectrometer at the Consolidated Engineering Corporation in Pasadena. The design of several high pressure, infrared absorption cells, together with the experimental technique used, is described in Sec. II.

Infrared intensity measurements on mixtures of CO form the subject of Sec. III. As the result of careful studies on gas mixtures containing carbon monoxide with hydrogen, helium, argon, oxygen, or nitrogen as broadening agents, it is concluded that the integrated absorption for the fundamental of CO has the value 237 cm^{-2} $atmos^{-1}$ at 297±2°K (see Sec. III-B), a result which is in good agreement with the value 255 cm^{-2} $atmos^{-1}$ obtained from infrared dispersion measurements[8] but which is considerably smaller than indicated by the best previously published infrared intensity measurements.[6,7] The integrated absorption for the first overtone of CO is 1.64 cm^{-2} $atmos^{-1}$ at 297±2°K (see Sec. III-C), which agrees reasonably well with the value of 2.30 cm^{-2} $atmos^{-1}$ reported by Dinsmore and Crawford,[6] but which again is much smaller than Matheson's value[7] of 5.13 cm^{-2} $atmos^{-1}$. The effective charge (see Sec. III-D), corresponding to an integrated absorption of 237 cm^{-2} $atmos^{-1}$, is 3.14×10^{-10} esu.

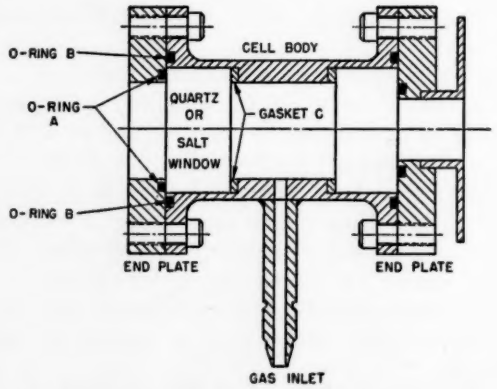

FIG. 1. Cross-sectional representation of high pressure gas cell for infrared-absorption studies (type A).

Examination of experimental results obtained at a total pressure of 700 psia shows that significant values for the spectral absorption coefficients, as well as for integrated absorption, have been obtained. Thus it is found that the integral of the spectral absorption coefficients leads to values for the integrated absorption which are in excellent agreement with the results obtained by other methods (see Sec. IV).

II. EXPERIMENTAL TECHNIQUE AND APPARATUS

All of the experimental studies on infrared absorption by carbon monoxide were carried out with a model 12C Perkin-Elmer infrared spectrometer using a lithium fluoride prism. The spectral resolution obtained with the spectrometer slit widths employed for the present study corresponds to about 4 cm^{-1} for the fundamental and 30 cm^{-1} for the first overtone. Commercially available gas supplies were used without further purification. The various gases, their source, and nominal compositions are listed in Table I.

Pressure readings were performed by use of a Wallace and Tiernan precision mercury manometer for the pressure range 0 to 800 mm with a maximum error of ±0.2 mm. Pressures from 0 to 200 psig were read on an Ashcroft test gage 1850 with a precision of ±0.3 psig. Pressures up to 1000 psig were read on a Marsh gage, model 100 FCPSR, with a precision greater than ±2 psig. Several high pressure, infrared absorption cells have been constructed.

A. Details of Cell Design

The cells and window assemblies were machined from 18–8 stainless steel stock. Neoprene O-rings and Neoprene or Teflon gaskets were used to support the windows. The principal features of two similar cell arrangements are shown in Figs. 1 and 2.

In the design shown in Fig. 1 the end plate contains two concentric O-rings which are aligned with the smaller ring *A* seating against the window and the larger ring *B* placed between the end plate and the body of the cell. A gasket *C* made of Neoprene or plastic such as Teflon was used between the window and its support in the body of the cell. A gasket rather than an O-ring was employed at this point in order to facilitate the use of windows of slightly different thicknesses by merely varying the thickness of the gasket.

In the design shown in Fig. 2 the window is housed in the end plate and supported by an O-ring *A* and a gasket *C*. A second O-ring *B* is placed between the end

plate and the cell body. The design shown in Fig. 2 has the advantage of facilitating the removal of the windows for cleaning and polishing, particularly if the circumferential surfaces of the crystals have been coated with Glyptal varnish or a similar cement.

The end plates can be provided with special holes in order to permit flushing of the outside surface with N_2 (see *D* in Fig. 2), thereby minimizing selective absorption of light caused by atmospheric CO_2 or H_2O.

The cells shown in Figs. 1 and 2 were fitted with flanges to slide into the receptable for the gas absorption cells provided on Perkin-Elmer infrared spectrometers. These cells have only one inlet. Since the mixing of gases at elevated pressures may take place very slowly, cells of the type shown in Figs. 1 and 2 may not be useful for studies on gas mixtures unless the chemical composition of the cell contents is determined by analysis after each measurement of infrared absorption. In practice it was found that significant concentration gradients existed over long periods of time in the gas handling system leading to the infrared absorption cell. As the result of such gradients, the gas composition in the cell is not related, in any simple way, to the partial pressures of the gases admitted to the system. For this reason cells of the type shown in Fig. 1 and 2 were used only for infrared transmission studies on pure gases.

Incomplete mixing in the lines leading to the absorption cell can be avoided by using a design of the type shown in Fig. 3, which contains separate inlets for each of the gases. This cell is provided with the window assembly shown in Fig. 1 and is large enough to permit incorporation of stirring equipment to assure uniform mixing. The stirrer shown in Fig. 3 consists of a flat plate containing a large number of small holes. Complete mixing by forced convection occurs very rapidly when the perforated grid is plunged along the axis of the cylindrical absorption chamber to the bottom of the cell. At elevated pressures the uncompensated pressure on the supporting rod of the perforated grid is sufficient to push the plunger to its topmost position. All of the experimental data on gas mixtures described in the present report were obtained in the absorption cell shown in Fig. 3. In each experiment care was taken to assure uniform mixing of the gases in the absorption cell by adequate use of the stirrer. It was assumed that a uniform gas mixture had been obtained when additional stirring produced no measurable change in infrared transmission.

B. Operational Problems

The principal problem in obtaining satisfactory performance of the high pressure gas cells is, of course, that of retaining leakproof window closures. No particular difficulties were encountered in the use of the quartz crystals, for they did not develop fractures or cracks, even at the highest pressures used thus far. On the other hand, at pressures exceeding about 300 psia the NaCl crystals (20×40 mm) tended to fracture on the supporting edges. The extent and further development of these cracks could be minimized greatly by painting the supporting surfaces with one or more thin coats of Glyptal varnish. Presumably difficulties of this sort can be eliminated by using larger and more expensive crystals with large supporting surfaces. Of four sodium chloride windows (20×40 mm) which were in almost continuous use for more than 12 months, none developed cracks which were so large that the window could no longer be used for high pressure infrared studies.

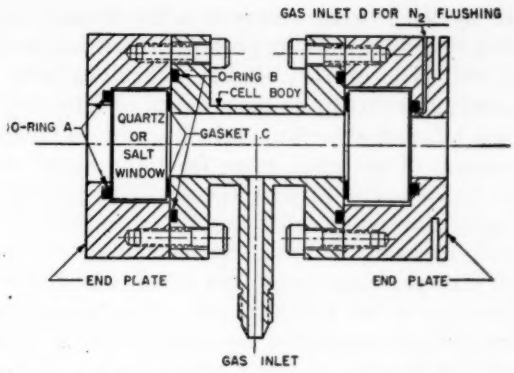

FIG. 2. Cross-sectional representation of high pressure gas cell for infrared-absorption studies (type B).

Selective adsorption of polar gases on the stainless steel walls may be an important factor in falisfying experimental results by altering the gas composition in the absorption cell. For example, absorption bands

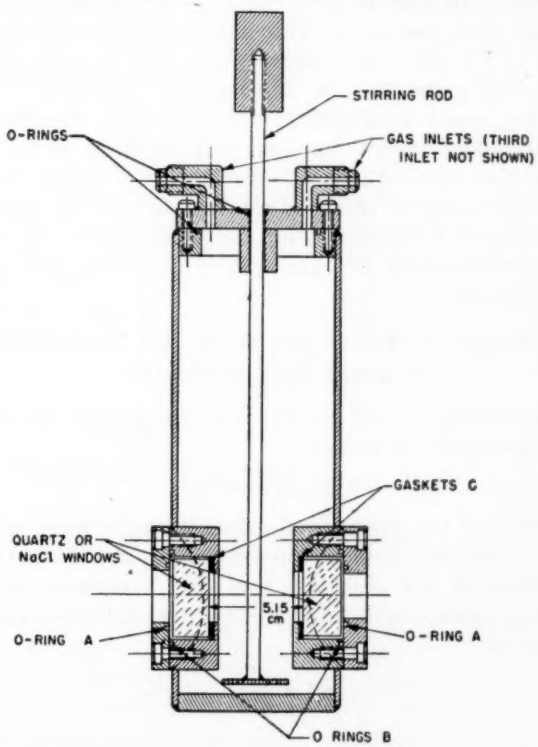

FIG. 3. Assembly drawing of large, high pressure gas cell for infrared-absorption studies.

caused by HCl were observed after several dozen repeated evacuations of the absorption cell followed by filling with HBr or HF. Similar difficulties were encountered subsequently in the removal of HBr and HF from the infrared absorption cell. In order to facilitate the removal of adsorbed gases from the metal walls, it may be desirable to heat the entire cell assembly. Heating of the cell assembly can be accomplished conveniently by using Nichrome heater wire covered with flexible glass sleeving around the metal cells. However, temperatures of 100 to 200°C are not sufficiently high to permit rapid removal of adsorbed hydrogen halides from the metal walls. For this reason the use of coated cells may be indicated in some cases.

In the case of experimental studies on carbon monoxide the existence of adsorption of the gas by stainless steel occurred to an extent sufficient to cause significant errors, particularly at very low partial pressures of infrared active gas. This problem and suitable corrections are discussed more fully in Sec. III, which is concerned with a description of experimental results and calculation of integrated absorption.

III. MEASUREMENT OF INTEGRATED ABSORPTION OF CO

The integrated absorption α for a given vibration-rotation band is defined by the relation,

$$\alpha=\int P_\nu d\nu, \tag{1}$$

where P_ν represents the spectral absorption coefficient at the wave number ν. Although the limits of integration in Eq. (1) should extend from $-\infty$ to $+\infty$, it is sufficient in practice to restrict the integration to a narrow wave number interval bracketing the band center. The reason for this simplification is to be sought in the fact that P_ν decreases very rapidly with ν in the wings of vibration-rotation bands. The values of integrated absorption for the fundamental and the first overtone of CO are designated as α_F and α_O, respectively.

A. Method of Wilson and Wells and Its Extension to Large Total Pressures

According to the well-known absorption law for monoenergetic radiation,

$$I_\nu=I_{0\nu}\exp(-P_\nu pl), \tag{2}$$

where I_ν is the transmitted intensity at the wave number ν when the incident intensity is $I_{0\nu}$, p is the partial pressure of the absorbing gas, and l represents the optical path length. Hence the integrated absorption becomes

$$\alpha=(1/pl)\int \ln(I_{0\nu}/I_\nu)d\nu, \tag{3}$$

where the integration in Eq. (3) is to be performed over the entire vibration-rotation band under study.

The apparent intensities observed without absorber and with absorber, when the instrument is set at ν, are not $I_{0\nu}$ and I_ν, respectively, but rather

$$T_{0\nu}=\int I_{0\nu'}g(\nu,\nu')d\nu', \tag{4}$$

and

$$T_\nu=\int I_{\nu'}g(\nu,\nu')d\nu', \tag{4a}$$

where $g(\nu,\nu')$ represents the fraction of light of actual wave number ν' to which the instrument responds when it is set at ν. The dependence of $g(\nu,\nu')$ on ν' can be approximated by a triangular distribution in a prism spectrometer, provided the prism has infinite resolution.[12] Some of the difficulties inherent in the accurate calculation of P_ν, utilizing corrections discussed by Dennison[12] and Slater,[13] do not arise in the determination of the integrated absorption. From the experimentally determined values of $T_{0\nu}$ and of T_ν it is possible to determine an apparent absorption coefficient α', which is defined by the relation,

$$\alpha'=(1/pl)\int \ln(T_{0\nu}/T_\nu)d\nu=\mathfrak{B}/pl. \tag{5}$$

It has been shown by Wilson and Wells[1] that

$$\lim_{pl\to 0}\alpha'=\alpha, \tag{6}$$

provided a number of specified conditions are met. These conditions include the requirement that $I_{0\nu}$ is independent of ν in the resolved spectral range, a condition which can be approached closely by eliminating atmospheric absorption and using sufficiently narrow spectrometer slits to give high spectral resolution. In addition to requiring constant $I_{0\nu}$, Wilson and Wells have shown that Eq. (6) will hold only if either the variation of P_ν with ν can be neglected in the resolved spectral range or the resolution of the instrument does not vary appreciably over the entire vibration-rotation band under study. Of these two requirements the latter constitutes an intrinsic property of the instrument and is not entirely met in practice. On the other hand, the variation of P_ν in the resolved spectral interval can be minimized by pressure broadening; i.e., as pl is decreased, α' will approach α more rapidly, the larger the constant total pressure at which the observations are made.

In the experimental work described by Wilson and his collaborators,[2,3] as well as in the studies of integrated absorption of NO and CO recently reported by Dinsmore and Crawford,[6] the total pressure has not exceeded a few atmospheres. As the result of the small total pressure the plots of $\mathfrak{B}$ *vs* pl may show considerable curvature as the optical density is decreased. The

[12] D. M. Dennison, Phys. Rev. **31**, 503 (1928).
[13] J. C. Slater, Phys. Rev. **25**, 783 (1925).

presence of this curvature introduces an appreciable error into the extrapolation required to determine α. Presumably the curvature and hence the experimental error can be minimized by increasing the total pressure. At sufficiently high total pressures p_T, the variation of $\mathfrak{B}$ with pl should follow a linear relation in accord with the fact that the true integrated absorption is measured at every value of the optical density, whence Eq. (3) should apply directly.

It is a simple matter to demonstrate the result,

$$\alpha' \rightarrow \alpha \text{ as } p_T \text{ is increased,} \tag{7}$$

by proceeding according to the method of Wilson and Wells.[1] From Eqs. (3), (4), (4a), and (5) it is apparent that

$$\alpha - \alpha' = \frac{1}{pl} \int \ln \left[\frac{I_{0\nu} \int I_{\nu'} g(\nu, \nu') d\nu'}{I_\nu \int I_{0\nu'} g(\nu, \nu') d\nu'} \right] d\nu. \tag{8}$$

For the experimental conditions usually encountered it is not difficult to obtain a sufficiently small resolved spectral interval $\Delta\nu'$ to make $I_{0\nu'}$ constant in the interval $\Delta\nu'$. Hence Eq. (8) becomes, using Eq. (2),

$$\alpha - \alpha' = \frac{1}{pl} \int \ln \left[\frac{\int \exp(-P_{\nu'} pl) g(\nu, \nu') d\nu'}{\exp(-P_\nu pl) \int g(\nu, \nu') d\nu'} \right] d\nu. \tag{9}$$

The principal effect of increased total pressure is broadening of the rotational lines. That is, $P_{\nu'}$ becomes a slowly varying function of ν'; for sufficiently large total pressures and sufficiently small values of $\Delta\nu'$, the variation of $\exp(-P_{\nu'} pl)$ with ν' can be neglected, and

$$\exp(-P_{\nu'} pl) \rightarrow \exp(-P_\nu pl),$$

whence by Eq. (9)

$$\alpha' \rightarrow \alpha \text{ as } p_T \text{ is increased.}$$

As the result of these considerations it is apparent that the true value of the integrated absorption α can be obtained either by extrapolating α' to zero values of pl at constant total pressure or by finding the limiting value of α' at constant optical density as the total pressure is increased. Of these two alternate procedures the latter has proved to be the more reliable for carbon monoxide. Plots exemplifying both methods of approach are described in Secs. III-B and III-C for the fundamental and the first overtone of carbon monoxide, respectively.

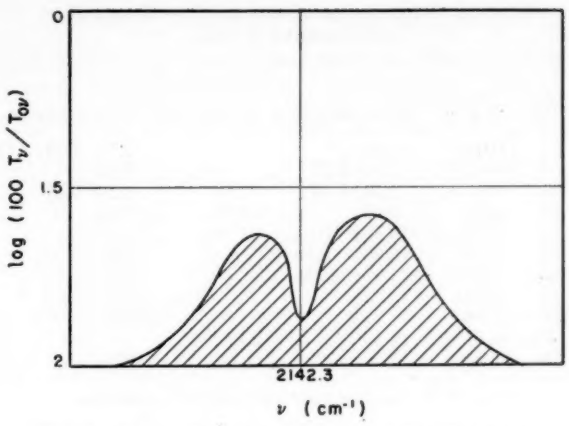

FIG. 4. Plot for the determination of $\int \log(T_{0\nu}/T_\nu) d\nu$.

B. Experimental Measurements on the Fundamental Vibration-Rotation Band of CO

Following the notation which is usually employed, a quantity $\mathfrak{B}$ is defined by the relation,

$$\mathfrak{B} = pl\alpha' = 2.303 \int \log(T_{0\nu}/T_\nu) d\nu. \tag{10}$$

The quantity $\int \log(T_{0\nu}/T_\nu) d\nu$ can be obtained conveniently from experimental transmission measurements on an evacuated cell and the same cell filled with absorbing gas, by plotting $\log(100\ T_\nu/T_{0\nu})$ *vs* ν, using an inverted ordinate, as shown in Fig. 4 for a representative transmission spectrum for CO. The area of the entire rectangle is

$$2 \int_{\Delta\nu} d\nu,$$

where $\Delta\nu$ represents an effective width of the vibration-rotation band, which is chosen so large that $\log(100\ T_\nu/T_{0\nu})$ has increased to 2 in the wings of the absorption band, corresponding to 100 percent transmission of light. The unshaded area in Fig. 4 evidently represents

$$\int_{\Delta\nu} \log(100 T_\nu/T_{0\nu}) d\nu,$$

whence the shaded area equals

$$\int_{\Delta\nu} [2 - \log(100 T_\nu/T_{0\nu})] d\nu = \int_{\Delta\nu} \log(T_{0\nu}/T_\nu) d\nu,$$

which is the desired quantity.

The experimental results for carbon monoxide pressurized with hydrogen are summarized in Table II. Data for CO–He mixtures are given in Table III, and the results for CO containing added A, O_2, or N_2 are represented in Table IV. The data shown in Tables II, III, and IV include results obtained at total pressures

TABLE II. Experimental results for CO−H_2 mixtures (fundamental of CO).

p (mm of Hg)	pl (cm atmos)	$\mathfrak{B}/2.303$ (cm^{-1}) at p_T=50 psia	at p_T=100 psia	at p_T=700 psia
3	0.0203	1.80	—	2.14; 2.03; 2.51
5	0.0339	2.74; 3.22	—	3.32
10	0.0678	5.40; 5.46	7.07	6.59; 6.65
15	0.102	8.97	9.29	9.51
20	0.136	10.70;[a] 10.92	11.96	13.6
40	0.271	18.96;[a] 18.16	—	26.4
60	0.407	23.90;[a] 25.56	—	39.7
80	0.542	32.28	—	53.6
200	1.356	—	—	105.8
40	0.271	18.48[a, b]	22.52[a, b]	—
150	1.016	47.2	—	88.1[a, b]

Results of analyses for CO in CO−H_2 mixtures.

Nominal P_1 (% CO)	Analyzed P_2 (% CO)	P_2-P_1 (% CO)	$100\frac{P_2-P_1}{P_1}$
0.74	0.89	0.15	20.3
1.45	1.68	0.23	15.7
2.21	2.46	0.25	11.3
1.45[b]	1.44[b]	−0.01[b]	−0.7[b]
0.72[b]	0.72[b]	0[b]	0[b]
5.62[b]	5.50[b]	−0.12[b]	−2.1[b]
0.40[b]	0.43[b]	−0.03[b]	−7.5[b]

[a] Gas mixtures analyzed by the Consolidated Engineering Corporation of Pasadena. The probable accuracy of these analyses is ±0.03 percent.
[b] Absorption cell coated with Glyptal varnish.

p_T between 3.87 and 700 psia. Also indicated are the results of representative mass spectrometric analyses of the mixed gases. Duplicate listings in any of the tables indicate independent duplicate measurements. Reference to the experimental results shows that the absolute reproducibility (observed scatter about 5 to 10 percent) is less than would be expected for the spectrometer used. Hence it must be concluded that errors introduced by faulty concentration readings and uncontrolled temperature fluctuations are, in general, much larger than errors resulting from inadequacies in pressure readings or infrared-transmission measurements.

TABLE III. Experimental results for CO−He mixtures (fundamental of CO).

p (mm of Hg)	pl (cm atmos)	p_T (psia)	$\mathfrak{B}/2.303$ (cm^{-1})
3	0.0203	700	1.88
60	0.407	16	14.5
60	0.407	20	15.6
60	0.407	25	17.0
60	0.407	40	21.5
60	0.407	50	25.6; 22.2*
60	0.407	75	29.4
60	0.407	100	32.1
60	0.407	300	41.0
60	0.407	500	40.7
60	0.407	700	39.7
200	1.356	3.87	16.9
200	1.356	15	23.9
200	1.356	20	32.8
200	1.356	25	36.8
200	1.356	30	40.2
200	1.356	50.5	51.4: 49.1*
200	1.356	75	68.3
200	1.356	100	76.8
200	1.356	300	107.4
200	1.356	500	111.4
200	1.356	700	113.6; 109.1

Results of analyses for CO in CO−He mixtures.

Nominal P_1 (% CO)	Analyzed P_2 (% CO)	P_2-P_1 (% CO)	$100\frac{P_2-P_1}{P_1}$
2.24	2.42	0.18	8.0
7.41	7.72	0.31	4.2

* Gas mixtures analyzed by the Consolidated Engineering Corp. of Pasadena. The probable accuracy of these analyses is ±0.03 percent.

The analyses of the gas mixtures shown in Tables II, III, and IV show that the actual concentrations of CO in uncoated absorption cells invariably exceed the values calculated from the measured partial pressures. Furthermore, the discrepancies are so large, especially for small concentrations of CO, that they cannot be attributed to inaccurate readings of the pressure gauges. The probable cause of the excessively large CO concentrations is adsorption of the gas on the metal walls when it is first introduced into the absorption cell, followed by partial or complete desorption when H_2, He, or some other gas is added in order to increase the total pressure in the absorption cell. This mechanism explains not only the fact that the actual CO concentration exceeds the calculated value, but also the relative increase in the discrepancy which is observed as the partial pressure of CO is decreased or the total pressure is increased. It is at once apparent that any extrapolation technique to zero optical density, ignoring the occurrence of adsorption and desorption processes of the type described, will inevitably yield excessively large values for the integrated absorption. This fact may explain some of

TABLE IV. Experimental results for CO−A, CO−O_2, CO−N_2 mixtures (fundamental of CO).

p (mm of Hg)	pl (cm atmos)	p_T (psia)	$\mathfrak{B}/2.303$ (cm^{-1})	Added gas
200	1.356	700	110.0	O_2
200	1.356	700	107.7	N_2
200	1.356	700	106.9	A
80	0.542	50	26.1	A
80	0.542	100	37.6	A
80	0.542	300	47.9	A
80	0.542	700	48.8	A
100	0.678	50	30.6	A
100	0.678	100	43.0	A
100	0.678	300	59.0	A
100	0.678	700	63.1	A
40	0.271	50.0±0.2	15.7	A[a, b]
300	2.033	50.0±0.2	60.8	A[a, b]

Results of analyses for CO in CO−A mixtures

Nominal P_1 (% CO)	Analyzed P_2 (% CO)	P_2-P_1 (% CO)	$100\frac{P_2-P_1}{P_1}$
1.50[b]	1.54[b]	0.04[b]	2.7[b]
11.24[b]	11.56[b]	0.32[b]	2.8[b]

[a] Gas mixtures analyzed by the Consolidated Engineering Corporation of Pasadena. The probable accuracy of these analyses is ±0.03 percent.
[b] These data were obtained in a cell coated with Glyptal varnish.

the discrepancies between the present measurements and those reported by other investigators. In support of this adsorption-desorption hypothesis may be quoted the results of gas analysis obtained after the absorption cell had been coated with Glyptal varnish. In particular, reference to Table II shows that the actual CO concentrations agree well with the calculated values for coated cells and, furthermore, never exceed the calculated values.† For CO—A mixtures the discrepancies between calculated and observed analyses are also small for the coated absorption cell (see Table IV).

Since the purpose of the present studies is the measurement of integrated absorption, not of selective adsorption of gases on metals, the validity of the suggested mechanism for the change in concentration is of no particular importance. It is important, however, to correct for or eliminate concentration errors in order

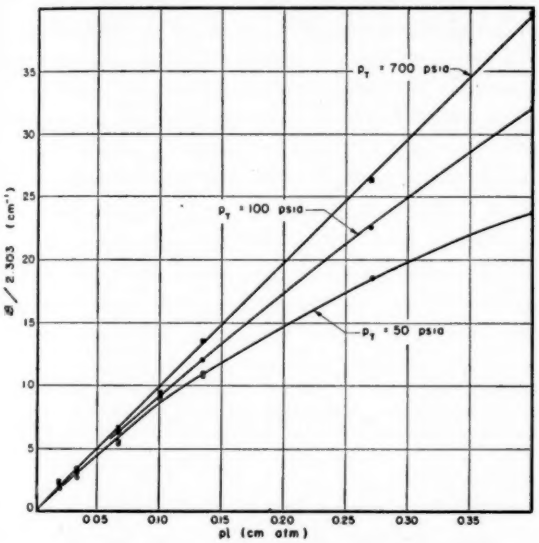

FIG. 5. $\mathfrak{B}/2.303$ as a function of pl for CO pressurized with H_2 (fundamental of CO).

to permit correlation between partial pressures and concentrations. Since the development of suitable coating material to prevent adsorption completely appeared to be a major task, it seemed preferable to abandon attempts at measurement of integrated absorption by extrapolating to zero optical density. Instead the alternate technique described in Sec. III-A, which involves application of large total pressures, seems to be more reliable. Thus it should be possible to obtain an absolute intensity measurement at optical densities large enough to permit neglect of concentration changes induced by adsorption-desorption phenomena.

The data summarized in Tables II, III, and IV are

† It should be noted that for a nominal CO concentration of 0.40 percent, for example, an error of 7.5 percent is within the limits of accuracy of the analyses, whereas for a nominal concentration of 2.21 percent an error of 11.3 percent is approximately ten times as large as the analytical error.

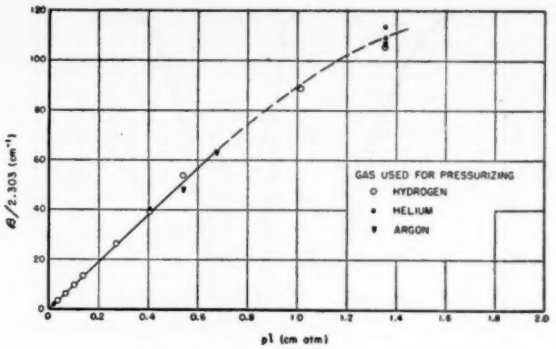

FIG. 6. $\mathfrak{B}/2.303$ as a function of pl at $p_T=700$ psia (fundamental of CO).

plotted in Figs. 5, 6, and 7 without correcting the nominal values of the optical density. Results for CO—H_2 mixtures are shown in Fig. 5 at total pressures of 50, 100, and 700 psia. In Fig. 6 the CO—H_2, CO—He, and CO—A data obtained at $p_T=700$ psia are plotted, whereas in Fig. 7 the corresponding results obtained at $p_T=50$ psia are shown. No data are shown for total pressures intermediate between 100 and 700 psia since experimental results at total pressures between 300 and 700 psia are practically independent of the total pressure. This last statement is substantiated, for example, by the results shown for CO—A mixtures at 300, 500, and 700 psia in Table III as well as by the representative transmission plot given in Fig. 8.

Reference to Fig. 5 clearly indicates that the experimental results at $p_T=50$ psia do not permit a reliable estimate of the limiting slope $d\mathfrak{B}/d(pl)$ at zero optical density even if the nominal partial pressure of CO was a quantitative indication of the concentration in the absorption cell. On the other hand, at $p_T=700$ psia the plot of $\mathfrak{B}/2.303$ *vs* pl is seen to be very nearly linear for optical densities up to about 0.7 cm-atmos (see Figs. 5 and 6), corresponding to a partial pressure of CO of approximately 100 mm of Hg. However, for partial pressures of CO as large as this, concentration changes produced by adsorption-desorption processes should be of minor importance and hence can be ignored in the

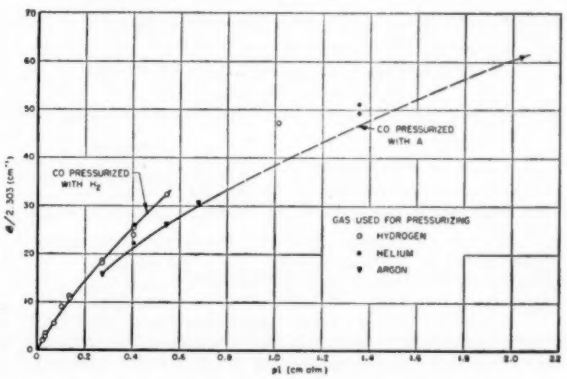

FIG. 7. $\mathfrak{B}/2.303$ as a function of pl at $p_T=50$ psia (fundamental of CO).

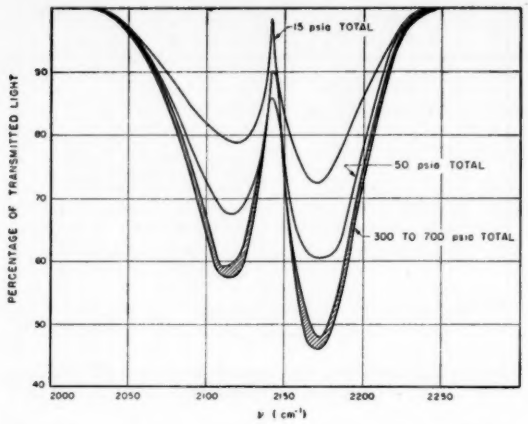

FIG. 8. Transmission spectrum of a 6.22-cm cell of CO (partial pressure of CO=60 mm) pressurized with N_2 at room temperature (fundamental of CO).

calculation of the integrated absorption. It is perhaps noteworthy that at $p_T=700$ psia the experimental value of $\mathfrak{B}$ is almost independent of the nature of the added gas (see Tables II, III, and IV and Fig. 6). On the other hand, at $p_T=50$ psia, H_2 is a more efficient broadening agent than either He or A (see Fig. 7). These results indicate that the optical collision diameter of H_2 is greater than that of either He or A, which, in turn, should have approximately equal optical collision diameters with respect to CO.‡ The fact that practically identical infrared transmission is obtained at 700 psia for gases of different optical collision diameter merely indicates that a total pressure of 700 psia is large enough, even for CO—He and CO—A mixtures, to broaden the rotational lines sufficiently in order to assure that the infrared transmission is practically independent of total pressure.

The integrated absorption for the fundamental of CO, calculated from the experimental results obtained at $p_T=700$ psia for CO—H_2, CO—He, and CO—A mixtures, has the value 237 cm^{-2} $atmos^{-1}$, a value which is probably accurate to within ± 5 percent. This experimental result is contrasted with the findings of other investigators in Table V. Reference to the data listed in this table shows that the results of the present investigation§ agree with the infrared-dispersion measurements of Havens,[8] being appreciably smaller than the experimental values reported by either Matheson[7] or by Dinsmore and Crawford.[6]

TABLE V. Experimental results for α_F reported by different investigators.

	Matheson[a]	Havens[b]	Dinsmore and Crawford[c]	Present study
α_F (cm^{-2} $atmos^{-1}$)	394; 413[d]	255	419	237

[a] Reference 7. [b] Reference 8. [c] Reference 6.
[d] Recalculated by Dinsmore and Crawford (reference 6).

‡ It is possible that selective adsorption-desorption of CO on the metal walls varies from one gas to another. In this case the apparent optical collision diameters would require correction for concentration changes.

§ In this connection it may also be of interest to note that numerical emissivity calculations for CO based on the value $\alpha=237$ cm^{-2} $atmos^{-1}$ are in satisfactory agreement with the experimental findings. A value of $\alpha=419$ cm^{-2} $atmos^{-1}$ leads to emissivities much larger than the observed values.

The results of integrated-absorption measurements will be used in Sec. III-D to calculate the dependence of the electric moment of CO on internuclear distance.[14–16]

C. Experimental Measurements on the First Overtone of CO

The experimental results for the first overtone of CO obtained with CO—He mixtures are summarized in Table VI. Large discrepancies were observed for the overtone data unless uniform mixing was assured by stirring of the gases, stirring being more important than for the fundamental because of the higher pressures of gas used, which, in turn, cause an appreciable decrease in the binary diffusion coefficients.[17] A very simple experiment can be performed to demonstrate the need for mixing by forced convection. Thus, the observed infrared transmission when a pressure of 20 psia of CO is admitted first to the absorption cell and then pressurized with H_2 to 100 psia is seen to be quite different from the results obtained when the same nominal amounts of each gas are introduced into the absorption cell in reverse order (see Fig. 9). In this particular case the mixture obtained when H_2 is admitted first to the absorption cell is almost uniform, as can be verified by comparison of infrared-transmission records for stirred and unstirred cells. The transmission is, of course, independent of the order of admission of the gases if the gases are stirred. The larger transmission observed when the CO is admitted first to the absorption cell is the result of imperfect mixing resulting in abnormally large CO concentrations at the bottom of

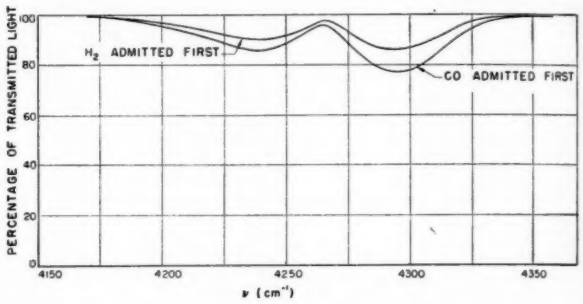

FIG. 9. Dependence of infrared transmission on the order of introduction of gases, illustrating the need for mixing by forced convection (20 psia of CO, 80 psia of H_2, $l=5.15$ cm; first overtone of CO).

[14] B. L. Crawford, Jr., and H. L. Dinsmore, J. Chem. Phys. **18**, 983, 1682 (1950).
[15] R. S. Mulliken, J. Chem. Phys. **2**, 400 (1934).
[16] J. L. Dunham, Phys. Rev. **35**, 1347 (1930).
[17] S. Chapman and T. G. Cowling, *The Mathematical Theory of Nonuniform Gases* (Cambridge University Press, Cambridge, England, 1939).

TABLE VI. Experimental results for the first overtone of CO at $p_T=300$ psia.

p (psia)	pl (cm atmos)	$\mathcal{B}/2.303$ (cm^{-1})	Added gas
7.73	2.71	1.88	He
15.5	5.43	4.20	He
20	7.01	4.84	He
40	14.0	9.60	He
60	21.0	14.6	He
80	28.0	19.3; 19.0	He
100	35.1	23.9	He
20	7.01	4.54	H_2

TABLE VII. Experimental results for the first overtone of CO at $p_T=700$ psia.

p (psia)	pl (cm atmos)	$\mathcal{B}/2.303$ (cm^{-1})	Added gas
7.73	2.71	2.20	He
15.5	5.43	4.49	He
20	7.01	4.60	He
40	14.0	10.1	He
60	21.0	14.9	He
80	28.0	19.4; 19.7	He
100	35.1	24.2	He
20	7.01	5.50	H_2

the absorption cell (see Fig. 3) and hence in the path of the light beam.

Since the partial pressures of CO used for integrated-absorption measurements on the first overtone of CO are generally large, no measurable errors are introduced as the result of the occurrence of adsorption-desorption phenomena.

The results of experimental measurements for the first overtone of CO are summarized in Table VII for $p_T=700$ psia. The quantity $\mathcal{B}/2.303$ is plotted as a function of pl in Fig. 10 for $p_T=300$ or 700 psia. Reference to Fig. 10 shows that the observed infrared transmission is independent of p_T for $p_T=300$ or 700 psia and furthermore is substantially the same for $CO-H_2$ and $CO-He$ mixtures. These results are in agreement with those described in Section III-B for the fundamental of CO, where it was noted that at $p_T=300$ psia the rotational lines of the fundamental of CO are sufficiently broadened to make the apparent integrated absorption practically independent of total pressure.

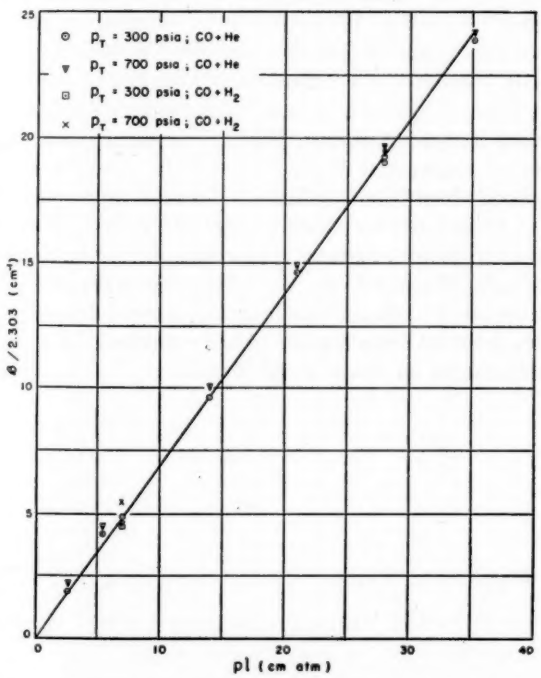

FIG. 10. $\mathcal{B}/2.303$ as a function of pl for CO pressurized with He or H_2 at $p_T=300$ and 700 psia (first overtone of CO).

The slope of the plot of $\mathcal{B}/2.303$ as a function of pl given in Fig. 10 leads to the conclusion that

$$\alpha_0=1.64 \text{ cm}^{-2} \text{ atmos}^{-1},$$

if allowance is made for the fact that the CO contains 3.2 percent impurities. This experimental value, which should be reliable to ± 5 percent, is contrasted in Table VIII with the results of other investigators.

Reference to Table VIII shows that the present study leads to a much smaller value of α_0 than was reported by Matheson, whereas the agreement with the results of Dinsmore and Crawford is almost within the claimed limits of accuracy (± 20 percent for the work of Dinsmore and Crawford). The value of α_0 has also been determined, entirely independently of the present studies, from an analysis of high pressure, infrared-absorption measurements on unpressurized CO.||

D. Determination of Electric Moment as a Function of Internuclear Distance for CO

The electric moment can be calculated as a function of internuclear distance from the measured infrared intensities of the fundamental and overtones. Early calculations of this type have been carried out by Dunham[16] and Mulliken.[15] Recently, Crawford and Dinsmore[14] have reconsidered this problem in detail and have succeeded in obtaining a more rigorous solution to the problem of the relation between infrared intensities and the coefficients occurring in the expressions for the electric moment and the potential energy as a function of internuclear distance. The experimental data described in Secs. III-B and III-C lead to the

TABLE VIII. Experimental results for α_0 reported by different investigators.

	Matheson[a]	Dinsmore and Crawford[b]	Present study
α_0 (cm^{-2} $atmos^{-1}$)	5.13	2.30	1.64

[a] Reference 7. [b] Reference 6.

|| Details concerning this work are described in Part II of the present investigations.

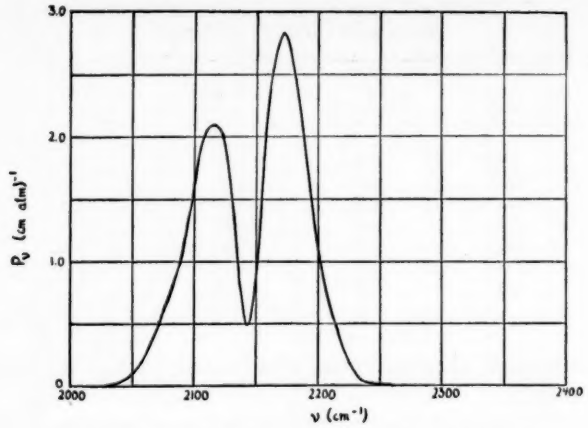

FIG. 11. P_ν as a function of ν for the fundamental of CO at $p_T=700$ psia (CO−H_2 mixtures).

result

$$p(\xi)\simeq -0.118\times10^{-18}\pm[3.55\times10^{-18}\xi + (9.785\times10^{-18}\xi^2 \text{ or } 0.165\times10^{-18}\xi^2)], \quad (11)$$

where $p(\xi)$ is the electric moment as a function of internuclear distance, and

$$\xi=(r-r_e)/r_e.$$

Here r equals the internuclear distance, and r_e is the equilibrium value of the internuclear distance. In Eq. (11) a negative sign has been chosen for the permanent electric moment according to a suggestion by Mulliken.[15] The effective charge ϵ, corresponding to the value $\pm3.55\times10^{-18}$ esu-cm for $(dp/d\xi)_{\xi=0}$, is 3.14×10^{-10} esu.

IV. DIRECT DETERMINATION OF INTEGRATED ABSORPTION AS INTEGRAL OF SPECTRAL ABSORPTION COEFFICIENTS

At elevated total pressures each experimentally determined transmission value should give a valid result, since P_ν is no longer a rapidly varying function of ν. Hence the transmission data can be used directly to calculate P_ν. Thus

$$d\log(T_\nu/T_{0\nu})/d(pl)\simeq d\log(I_\nu/I_{0\nu})/d(pl) = -P_\nu/2.303. \quad (12)$$

The results of calculations of P_ν according to Eq. (12) are plotted in Figs. 11 and 12 for the fundamental and first overtone, respectively, at $p_T=700$ psia. It should be noted that each of the plots leading to the appropriate value of P_ν has been found to be accurately linear at least for small values of pl.

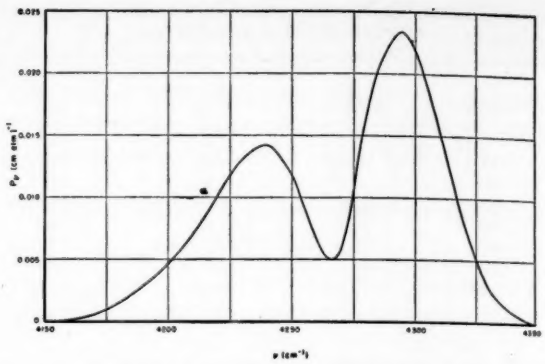

FIG. 12. P_ν as a function of ν for the first overtone of CO at $p_T=700$ psia (CO−He mixtures).

The statement that the values of P_ν determined from Eq. (12) and plotted in Figs. 11 and 12 are correct absolute values can be verified by referring to the original definition of α as the integrated absorption. Thus

$$\alpha_F=\int_{\Delta\nu F} P_\nu d\nu,$$

$$\alpha_O=\int_{\Delta\nu O} P_\nu d\nu.$$

The value of α_F determined as the integrated absorption for the fundamental is found to be 230 cm^{-2} $atmos^{-1}$ (see Fig. 11), which is in excellent agreement with the value of 237 cm^{-2} $atmos^{-1}$ obtained in Sec. III-B. Similarly it is found from Fig. 12 that $\alpha_O=1.68$ cm^{-2} $atmos^{-1}$, which is in excellent agreement with the results deduced in Sect. III-C. The direct determination of integrated absorption as the integral of the spectral absorption coefficients does not appear to have been attempted by other investigators. It is evidently a much more laborious procedure than the indirect methods discussed in Sec. III. Nevertheless, it is gratifying to obtain excellent agreement between results deduced from a given set of experimental data by independent methods of calculation.

Quantitative Infrared Intensity Measurements. II. Studies on the First Overtone of Unpressurized CO

S. S. PENNER AND D. WEBER
*Jet Propulsion Laboratory, California Institute of Technology, Pasadena, California**

(Received February 26, 1951)

Quantitative infrared absorption measurements on unpressurized CO have been carried out for the first overtone in cells of different lengths and at different pressures of gas. The experimental data lead to a value for the integrated absorption of the first overtone of CO of 1.69 cm^{-2} $atmos^{-1}$, which is in excellent agreement with results obtained previously from the study of mixtures of CO pressurized with infrared inert gases.

I. INTRODUCTION

INFRARED absorption studies on pure gases have the obvious advantage of eliminating the possibility of experimental error resulting from imperfect mixing or from the occurrence of adsorption-desorption phenomena. On the other hand, they possess the severe disadvantage of always involving the effect of significant self-broadening associated with increased pressure of the absorber. Since self-broadening of rotational lines is understood only imperfectly, the interpretation of low resolution data on pure gases involves serious difficulties, at least at low pressures.

For low pressure and low resolution studies on pure gases, it seems possible, in principle, to determine the integrated absorption α by extrapolating to zero optical density at constant pressure for experimental results obtained in absorption cells of different lengths.[1,2] Under these conditions Eq. (6) of Part I[3] should hold. The difficulty with this procedure is the result of large curvature of the extrapolation curve in the vicinity of zero optical density. It is therefore scarcely possible to obtain reliable values for integrated absorption unless the resolving power of the instrument is high, and very long absorption cells are used for measurement. On the other hand, if reliable measurements on pure gases can be carried out at sufficiently high pressures, then α' will approach α according to Eq. (9) of I. Therefore, in this instance it should be possible to determine α from measurements on pure gases. Successful experimental studies of this type have been carried out for the first overtone of CO.

The present investigations show that under suitable conditions self-broadening of the infrared-active gas can be utilized to carry out quantitative infrared absorption measurements. Unfortunately, the path length of the absorption cell must be so chosen that appreciable changes in infrared transmission are observed at pressures of absorbing gas which are sufficiently high to produce extensive overlapping of rotational lines. For weak absorbers such as the first overtone of CO this restriction is not serious. In particular, for the studies described in this paper, cells several cm in length were used (see Figs. 1 and 2 of I). In order to perform similar measurements on the fundamental vibration-rotation band of CO, it is necessary to construct infrared absorption cells with path lengths of the order of 0.05 cm. Cells of this type have been built and are currently being used to measure integrated absorption of strong absorbers according to the technique described in this paper for measurements on the first overtone of CO.

TABLE I. Experimental results for self-broadening on the first overtone of CO ($l=6.22$ cm).

p (psia)	pl (cm atmos)	$\mathcal{B}/2.303$ (cm^{-1})
20	8.47	4.64
30	12.7	6.39
40	16.9	9.35
60	25.4	14.1
70	29.6	16.5
100	42.3	26.7
200	84.6	58.6
300	127	87.2
400	169	116
500	212	147
600	254	159
700	296	174

II. EXPERIMENTAL RESULTS AND INTERPRETATION OF DATA

Experimental results obtained on the first overtone of unpressurized CO are summarized in Tables I and II for

TABLE II. Experimental results for self-broadening on the first overtone of CO ($l=3.57$ cm).

p (psia)	pl (cm atmos)	$\mathcal{B}/2.303$ (cm^{-1})
15	3.64	2.32
20	4.86	3.74
30	7.29	4.26
40	9.72	6.06
60	14.6	8.00
70	17.0	9.55
100	24.3	15.5
200	48.6	32.8
300	72.9	52.5
400	97.2	67.1
500	121	84.6
600	146	104
700	170	119.5

* This paper presents the results of one phase of research carried out at the Jet Propulsion Laboratory, California Institute of Technology, under Contract No. W-04-200-ORD-455, sponsored by the U. S. Army Ordnance Department.

[1] E. C. Kemble and D. G. Bourgin, Nature **117**, 789 (1926).
[2] D. G. Bourgin, Phys. Rev. **29**, 794 (1927).
[3] S. S. Penner and D. Weber, J. Chem. Phys. **19**, 807 (1951), the preceding paper, hereafter referred to as I.

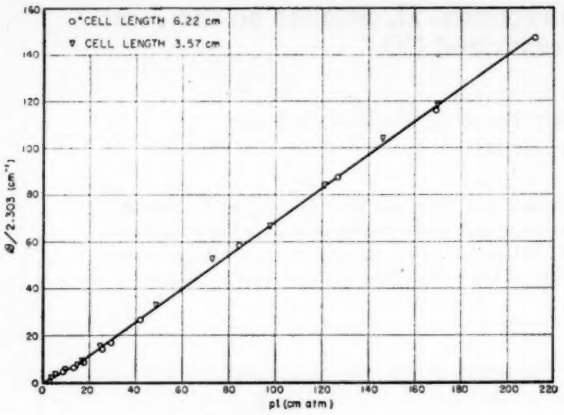

FIG. 1. Dependence of $\mathfrak{B}/2.303$ on pl for the first overtone of unpressurized CO.

data obtained in cells 6.22 and 3.57 cm in length, respectively. Since the infrared absorption by the overtone is relatively weak, it is possible to study the dependence of absorption on pressure up to relatively high pressures. Accordingly the present investigations were extended up to 700 psia.

In Fig. 1 the quantity $\mathfrak{B}/2.303$ is plotted as a function of optical density pl. As was pointed out in I (see Fig. 8), when the pressure is sufficiently high, the dependence of P_r and hence of α_0 on pressure becomes slight. It is, therefore, to be expected that, for sufficiently large values of the pressure, $\mathfrak{B}$ will depend on optical density uniquely and independently of the cell length. Furthermore, $\mathfrak{B}$ will become a linear function of pl, and α_0 should be calculable from Eq. (10) of I; i.e.,

$$\alpha_0 = d\mathfrak{B}/d(pl).$$

These predictions are completely verified by the data given in Fig. 1. At elevated pressures it is seen that

$$d(\mathfrak{B}/2.303)/d(pl) = 0.710 \text{ cm}^{-2} \text{ atmos}^{-1},$$

whence

$$\alpha_0 = 1.69 \text{ cm}^{-2} \text{ atmos}^{-1}.$$

Reference to I shows that this value for α_0, obtained from the self-broadening of unpressurized CO, is in excellent agreement with the independently determined value of

$$\alpha_0 = 1.64 \text{ cm}^{-2} \text{ atmos}^{-1},$$

based on absorption studies of CO—He and CO—H_2 mixtures. The method for the determination of α_0 described in this paper does not appear to have been used by other investigators. It seems to be a simple and reliable method for all absorbers provided a suitable cell length has been chosen.

THE JOURNAL OF CHEMICAL PHYSICS VOLUME 19, NUMBER 7 JULY, 1951

Transport Phenomena in Dense Media. II. Thermal Diffusion in Compressed Gases*†

W. L. ROBB AND H. G. DRICKAMER
University of Illinois, Urbana, Illinois

(Received March 12, 1951)

From the thermodynamics of irreversible processes, values of the thermal diffusion ratio α have been calculated using (1) the virial equation of state, (2) generalized reduced enthalpies, (3) the Lennard-Jones and Devonshire "cage" model for liquids. These results are compared with experiment and with previously published calculations for a van der waals gas. Only the LJD model gave results markedly superior to van der Waals' equation. The LJD model predicts very large positive values of α for compressed liquids.

THE thermal diffusion ratio α is defined by the transport equation

$$\mathbf{J}_1 = -D_{12}[\mathbf{grad}\, x_1 + \alpha x_1 x_2\, \mathbf{grad}(\ln T)]. \quad (1)$$

For simple gases at low pressures, the kinetic theory of Enskog and Chapman[1] is adequate to predict the first-order transport properties (diffusion, viscosity, and thermal conductivity). Whether it adequately describes thermal diffusion at atmospheric pressure is still open to question.[2] The dense gas theory of Enskog reproduces the viscosity well and the thermal conductivity fairly well up to densities considerably greater than the critical. (It is now being tested for self-diffusion.) It has been shown[3,4] that this dense gas theory fails to predict the thermal diffusion ratio even qualitatively. The experimental results from the previous work on the system ethane-xenon are shown in Fig. 1. A double sign change, from positive to negative below the critical density and then to positive again at high density, is noted. The dense gas theory as developed by Enskog predicts no sign change unless a clustering effect, really foreign to the theory, is assumed.

In a previous paper[5] an equation for α in terms of

* For Part I of the present paper see W. L. Robb and H. G. Drickamer, J. Chem. Phys. **18**, 1380 (1950).

† This work was supported in part by the AEC.

[1] S. Chapman and T. G. Cowling, *Mathematical Theory of Non-Uniform Gases* (Cambridge University Press, Cambridge, England, 1939).

[2] E. W. Becker, J. Chem. Phys. **19**, 131 (1951).

[3] Pierce, Duffield, and Drickamer, J. Chem. Phys. **18**, 950 (1950).

[4] Giller, Duffield, and Drickamer, J. Chem. Phys. **18**, 1027 (1950).

[5] W. L. Robb and H. G. Drickamer, J. Chem. Phys. **18**, 1380 (1950).

thermodynamic quantities was obtained from the thermodynamics of irreversible processes:

$$\alpha=\frac{A(\bar{H}_1M_2-\bar{H}_2M_1)-BM_1M_2}{A\bar{M}x_1(\partial M_1/\partial x_1)}, \tag{2}$$

where $\bar{H}$ and μ can be evaluated in terms of the equation of state from

$$\bar{H}_1=\bar{H}_1^*-RT^2\left[\frac{\partial \ln f}{\partial T}+x_2\frac{\partial}{\partial T}\frac{\partial \ln f}{\partial x_1}\right], \tag{3a}$$

$$x_1\frac{\partial M_1}{\partial x_1}=RT\left[1+x_1x_2\frac{\partial^2 \ln f}{\partial x^2}\right]. \tag{3b}$$

For a mixture of isotopes, Eq. (2) reduces to

$$\alpha=[\bar{H}(M_2-M_1)A-BM_1M_2]/A\bar{M}RT. \tag{2a}$$

Since the molecular constants of xenon and ethane are not greatly different, Eq. (2a) is used in this work. Here A and B are phenomenological constants whose values cannot, at present, be calculated in general. To the first approximation, it will be assumed here that the ratio B/A is constant for any given system. It can be shown from experimental data that it does not vary radically from gas to liquid.

In the previous paper van der Waals' equation was used, and the results were shown to be in qualitative agreement with the experimental data. The double change of sign obtained experimentally was reproduced by the theory, but the sign changes occurred at reduced densities considerably different than those found experimentally, and the absolute values of α were of the wrong order of magnitude.

In this paper results are presented as calculated from Eq. (2a) for the following relationships:

(1) The virial equation was used in the form,

$$pv/RT=1+[B(T)/V]+[C(V)/V^2], \tag{4}$$

with the second and third virial coefficients evaluated by Bird and Spotz[6] using the Lennard-Jones model for molecular interaction. For this case Eq. (2a) reduces to the form,

$$\alpha=\alpha_0-\frac{M_2-M_1}{\bar{M}V}\left[T\frac{\partial(B(T))}{\partial T}-B+\frac{1}{V}\left(\frac{T}{2}\frac{\partial C(T)}{\partial T}-C\right)\right]. \tag{5}$$

(2) A generalized correlation[7] for enthalpy as a function of reduced temperature and pressure was used.

(3) The value of α was calculated using the enthalpy obtained from the values for thermodynamic variables given by Hirschfelder[8] *et al.* as evaluated using the Lennard-Jones and Devonshire "cage" model for liquids. Since this model is satisfactory for dense systems, the results are presented only for densities greater than the critical.

The results are shown in Figs. 2–4. The dotted curve on each figure is the line for $\alpha=0$ obtained from van der Waals' equation. Although the virial Eq. (4) reproduces qualitatively the features found experimentally, the agreement with experiment is poorer than that obtained from van der Waals' equation. Calculations were made using the second virial coefficient only, but these did not even reproduce the data qualitatively.

The results obtained from the use of generalized

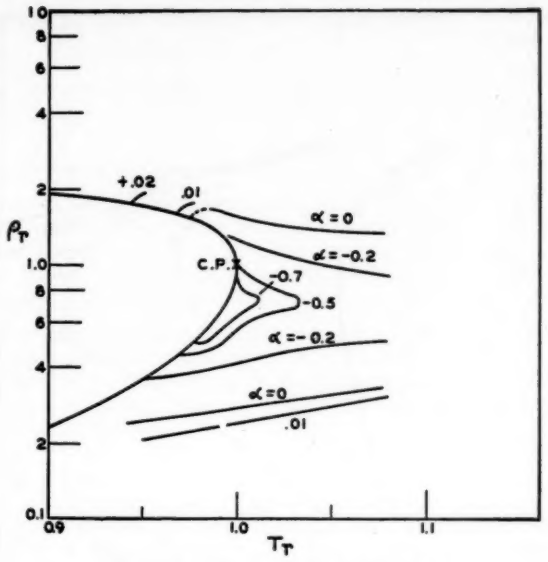

FIG. 1. $\rho_r-T_r-\alpha$ plot experimental.

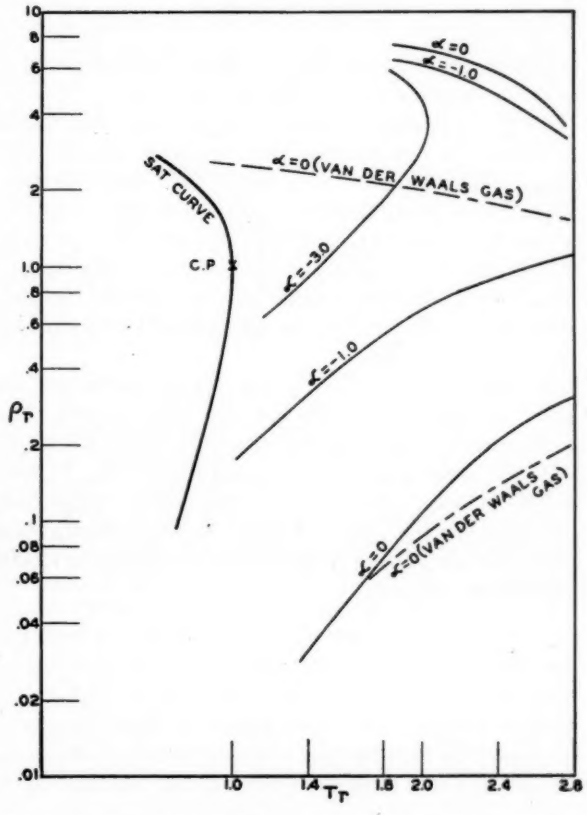

FIG. 2. $\rho_r-T_r-\alpha$ plot (using second and third virial coefficients).

[6] R. B. Bird and E. Spotz, NOrd 9938 TASK WISC-1-C, University of Wisconsin, CM-508.

[7] O. A. Hougen and K. M. Watson, *Chemical Process Principles* (John Wiley and Sons, Inc., New York, 1946), Vol. II, pp. 494–495.

[8] Hirschfelder, Wentdorf, Buehler, and Curtiss, J. Chem. Phys. 18, 1484 (1950).

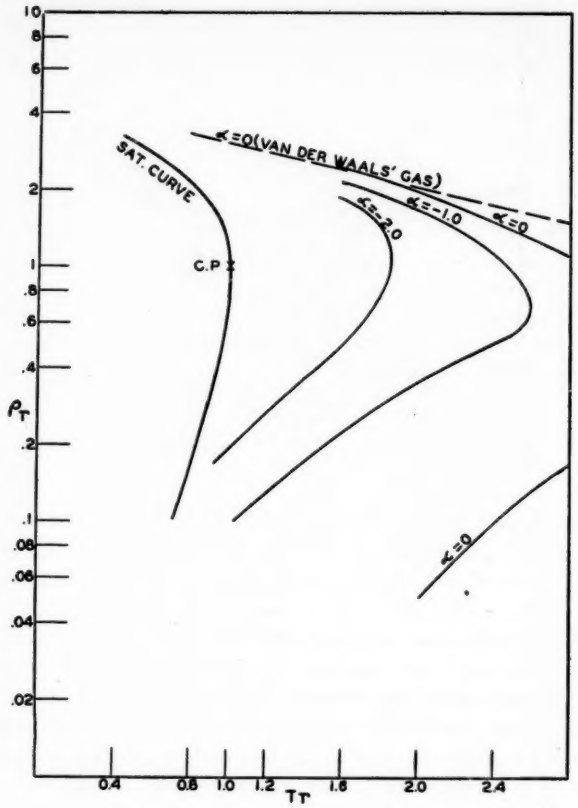

FIG. 3. $\rho_r - T_r - \alpha$ plot (using generalized enthalpies of Hougen and Watson).

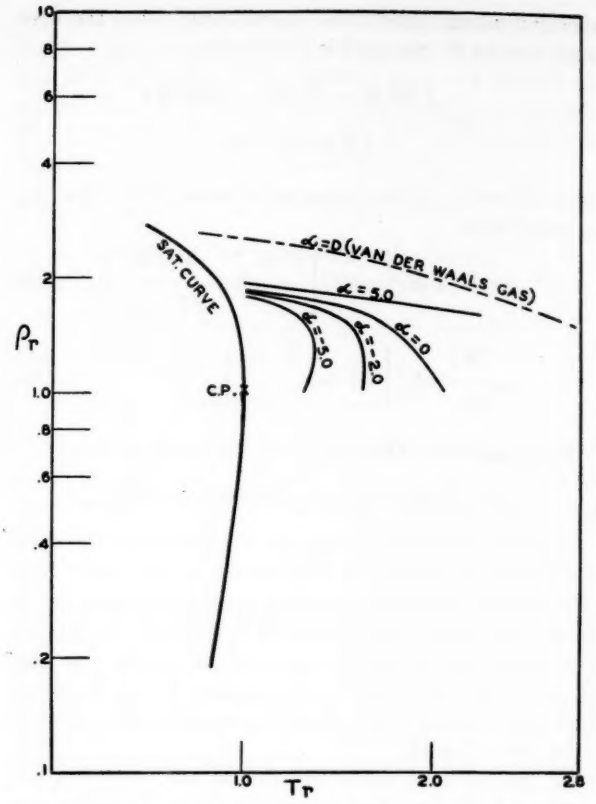

FIG. 4. $\rho_r - T_r - \alpha$ plot from Lennard-Jones–Devonshire model for liquids.

enthalpies are shown in Fig. 3. Again, the agreement is no better than for van der Waals' equation.

In Fig. 4 the results using the LJD model for liquids are shown. It can be seen that the high density sign change is reproduced at very nearly the correct density. This would indicate that the use of this model is superior for predicting properties of dense systems, such as compressed liquids or highly compressed gases. The magnitude is not of the same order as that obtained experimentally, but in view of the approximations involved, this is not surprising.

An interesting feature is the results predicted for highly compressed liquids by the LJD model. The calculations indicate that the value of α remains positive and gets very large. The magnitude at the highest density is over twenty times the largest magnitude calculated for the critical region. An experimental test of this feature is being prepared for liquids up to 12,000 atmospheres pressure.

NOMENCLATURE

A, B = phenomenological constants.
$B(T), C(T)$ = virial coefficients (functions of temperature).
D = diffusion coefficient.
f = fugacity.
$\bar{H}_i$ = partial molar enthalpy of component i.
H_i^* = partial molar enthalpy of component i in the standard state.
J_i = flux of component i.
M_i = molecular weight of component i.
$\bar{M}$ = mean molecular weight.
p = pressure.
R = gas constant.
T = temperature.
T_c = critical temperature.
T_r = reduced temperature T/T_c.
V = molar volume.
X_i = mole fraction of component i.
α = thermal diffusion ratio.
α_0 = thermal diffusion ratio for ideal gas.
μ_i = chemical potential of component i.
ρ = mean density of system.
ρ_c = critical density.
ρ_r = reduced density ρ/ρ_c.

The Solution of Some Potential Problems in the Theory of Electrolytes

F. Booth
Department of Theoretical Physics, Wheatstone Laboratory, King's College, London, England
(Received April 4, 1951)

The Poisson-Boltzmann equation for the potential in an electrolyte is solved for the following cases:

(a) Electrolyte bordered by a uniformly charged plane; (b) two semi-infinite electrolytes of different composition separated by a plane boundary; (c) electrolyte confined between parallel charged planes; (d) uniformly charged cylinder immersed in an electrolyte; (e) electrolyte in a cylinder with charged walls; (f) electrolyte between two concentric charged cylinders; (g) solid charged sphere in an electrolyte; and (h) sphere of electrolyte immersed in another electrolyte extending to infinity, and of different composition.

All the problems discussed are of interest in the theory of colloids or emulsions. In each case a series solution in powers of a parameter involving the charge or charges on relevant surfaces is given. The first term of each series is the solution of the Poisson-Boltzmann equation when the so-called Debye-Hückel approximation is applied to the equation. The additional terms are built up from the first by an iterative method. No restrictions on the compositions of the electrolytes are required.

INTRODUCTION

Section 1.

IN this note we shall obtain the solutions of some potential problems which are of interest in the theory of colloidal electrolytes. According to Debye's theory,[1] the fundamental differential equation which must be satisfied by the electrostatic potential ψ in an electrolye is

$$\nabla^2\psi=-\frac{4\pi e}{\epsilon}\sum_{i=1}^{s}n_i\exp(-ez_i\psi)/\mathbf{k}T, \tag{1.1}$$

where e is the electronic charge, ϵ the dielectric constant of the solvent, $\mathbf{k}$ Boltzmann's constant, and T the absolute temperature. The summation extends over the s ionic species present in solution, n_i being the concentration of ions of type i when $\psi=0$, and z_i their valency. Equation (1.1) combines the poisson and Boltzmann equations; the complete nonlinear equation has been criticized,[2,3] but a more correct equation has not so far been obtained.

If we assume electroneutrality of the solution as a whole, then we have

$$\sum_{i=1}^{s}n_iz_i=0. \tag{1.2}$$

Also, if the condition

$$e\psi/\mathbf{k}T\ll 1 \tag{1.3}$$

holds everywhere, then Eq. (1.1) can be written

$$\nabla^2\psi=\kappa^2\psi, \tag{1.4}$$

where

$$\kappa^2=4\pi e^2\sum_{i=1}^{s}n_iz_i^2/\epsilon\mathbf{k}T. \tag{1.5}$$

A considerable amount of work has been done based on the approximate equation (1.4), which is associated with the names of Debye and Hückel. The more exact Eq. (1.1) has received much less attention, doubtless owing to its nonlinearity. The most important development using (1.1) is due to Gronwall, LaMer, and Sandved,[4] who gave a theory for electrolytes in statistical equilibrium which is formally similar to the Debye-Hückel theory. Their work was entirely confined to a study of ordinary solutions of strong electrolytes; but it is of interest to notice that the idea underlying their method can be adapted so as to furnish solutions of a wide variety of problems which arise in another field, that of colloidal solutions. Here, instead of all the charges in the assembly being associated with free ions, some may be attached to solid boundaries or solid or liquid particles, of dimensions which may be large on the atomic scale. In most cases it is not difficult to solve Eq. (1.4) for the potential, but quite impossible to integrate (1.1) directly. Experimental work on colloidal systems indicates that the potentials may reach values as high as 200 millivolts, giving for $e\psi/\mathbf{k}T$ a value of about 8 at room temperatures. For these cases it is obviously a very bad approximation to use Eq. (1.4) in view of condition (1.3). However, in the following paragraphs it will be shown how solutions of Eq. (1.1) can be built up from those of (1.4). The general method is to assume a series development for ψ in powers of a suitable parameter. Substitution of the series in Eq. (1.1) gives a sequence of differential equations which can be handled without difficulty. Any term in the series for ψ can be expressed in terms of preceding terms. Since the *first* term of the series turns out to be simply the solution of Eq. (1.4), the members of the series may be calculated successively, and so a complete solution of Eq. (1.1) obtained.

Although the solutions developed should be more satisfactory than those derived from Eq. (1.4) unless ψ is very small, in which case both methods give the same result, it must be pointed out that the usefulness of the method is limited by three factors. In the first

[1] P. Debye and E. Hückel, Physik. Z. **24**, 185 (1923).
[2] L. Onsager, Chem. Revs. **13**, 73 (1933).
[3] J. G. Kirkwood, J. Chem. Phys. **2**, 767 (1934).
[4] Gronwall, LaMer, and Sandved, Physik. Z. **28**, 358 (1928).

place, it has been shown that Eq. (1.1) is not strictly thermodynamically consistent.[2] It is of interest to notice however that in cases where it *has* been applied, better results have emerged than when the simpler Debye-Hückel theory was used. For example, the Gronwall-LaMer-Sandved theory gives a better account of the properties of electrolytes in equilibrium; in particular, it gives more reasonable estimates of ionic radii. In another connection, Verwey and Overbeek[5] have shown that the Schulze-Hardy rule on the dependence of the coagulating properties of electrolytes on their valency can be explained if the analysis is based on Eq. (1.1), but not if Eq. (1.4) is used. Another difficulty arises in connection with the convergence of the solutions. Since in all cases a power series solution is derived, strictly it is necessary in each case to find the radius of convergence. This is difficult to calculate, since the method does not give the general term of the power series in a simple expression. It is easy in some cases to devise dominant series, but then it is found that these have finite radii of convergence which are less than the values sometimes indicated by experiment. A further difficulty lies in the mathematical complexity of the higher terms of the series for ψ. Although in theory it is possible to calculate any desired number of terms, in practice this becomes impracticable beyond a certain stage.

In spite of the three limitations we have mentioned, however, it seems likely that the solutions should be suitable for a useful range of potential above the upper limit for which the simple theory based on Eq. (1.4) can be legitimately employed. The next section deals with problems involving plane boundaries. First, the potential near an infinite uniformly charged plane in contact with a semi-infinite electrolyte is found. The next solution given is the potential near the plane boundary between two semi-infinite electrolytes. Then follows the general solution for an electrolyte between two infinite parallel charged planes. The next section deals with similar problems involving cylindrical boundaries; finally, questions with spherical boundaries are examined. The cases we have dealt with do not exhaust all the problems which could be solved by the method. We have confined attention to those cases which are or are likely to be of interest in the interpretation of experimental data. For example, all the solutions involving solids may be useful in refinements of the theory of the stability of colloids.

PROBLEMS INVOLVING PLANE BOUNDARIES

Section 2. The Potential near an Infinite Uniformly Charged Plane

Let σ be the surface density of the charge on the plane and ζ the potential at the surface, the potential zero being taken at infinity. If x denotes distance measured normal to the plane, the equation to be solved is

$$\frac{d^2\psi}{dx^2}=-\frac{4\pi e}{\epsilon}\sum_{i=1}^{s} n_i \exp\left(\frac{-ez_i\psi}{\mathbf{k}T}\right), \tag{2.1}$$

with the boundary conditions

$$\psi=0,\quad x=\infty\,;\quad \psi=\zeta,\quad d\psi/dx=-4\pi\sigma/\epsilon,\quad x=0. \tag{2.2}$$

The solution is well known in the case $i=2$, $z_1=-z_2$ and $n_1=n_2$;[6] Eq. (2.1) is then immediately integrable, giving

$$\log_e \tanh(z_1e\psi/4\mathbf{k}T)=\log_e \tanh(z_1e\zeta/4\mathbf{k}T)-\kappa x, \tag{2.3}$$

and

$$\sinh(z_1e\zeta/2\mathbf{k}T)=2\pi ez_1\sigma/\kappa\epsilon\mathbf{k}T, \tag{2.4}$$

where

$$\kappa^2=8\pi e^2n_1z_1^2/\epsilon\mathbf{k}T. \tag{2.5}$$

When n_i and z_i are not restricted in the above manner, Eq. (2.1) can be integrated once to give $d\psi/dx$. From the resulting equation, σ and ζ can be related:

$$\sigma=\left(\frac{\epsilon\mathbf{k}T}{2\pi}\right)^{\frac{1}{2}}\left[\sum_{i=1}^{s} n_i\left\{\exp\left(\frac{-ez_i\zeta}{\mathbf{k}T}\right)-1\right\}\right]^{\frac{1}{2}}. \tag{2.6}$$

Unfortunately the integration cannot be carried a stage further to give ψ. For some purposes, for example, the determination of σ from measurements of the electrokinetic potential ζ, Eq. (2.6) gives all that is required. It is of interest, however, to be able to find the complete solution for ψ in the general case.

Equation (2.1) may be written in the form,

$$(d^2\psi/dx^2)-\kappa^2\psi=\kappa^2\Psi, \tag{2.7}$$

where

$$\Psi=\sum_{\nu=2}^{\infty}\frac{(-1)^{\nu-1}}{\nu!}\left(\frac{e}{\mathbf{k}T}\right)^{\nu-1}q_\nu\psi^\nu, \tag{2.8}$$

and

$$q_\nu=\sum_{i=1}^{s} n_iz_i^{\nu+1}/\sum_{i=1}^{s} n_iz_i^2. \tag{2.9}$$

κ has been defined in Eq. (1.5); also it has been assumed that condition (1.2) is satisfied. The general solution of Eq. (2.7) is

$$\psi=C_1e^z+C_2e^{-z}+\frac{1}{2}\int^{z}\Psi(u)(e^{z-u}-e^{u-z})du, \tag{2.10}$$

where we have put $z=\kappa x$.[7] The first two terms represent the general solution of Eq. (2.7), and it is easily verified that the third term is a particular integral. Using the boundary conditions (2.2), we may write Eq. (2.10) as

$$\psi=(4\pi\sigma/\kappa\epsilon)e^{-z}+\int_0^{\infty} f(u,z)\Psi(u)du, \tag{2.11}$$

[5] E. J. W. Verwey and J. Th. G. Overbeek, Philips. Tech. Research Repts, No. I.

[6] A. J. Rutgers and E. Verlende, Proc. Acad. Sci. Amsterdam 42, 71 (1939).

[7] A. R. Forsyth, *A Treatise on Differential Equations* (Macmillan and Company, Ltd., London, 1888), second edition, p. 78.

where

$$f(u, z) = -\tfrac{1}{2}(e^{u-z}+e^{-u-z}), \quad 0<u<z,$$
$$= -\tfrac{1}{2}(e^{z-u}+e^{-u-z}), \quad u>z. \tag{2.12}$$

The expression on the right-hand side of Eq. (2.11) vanishes for x large, since it can easily be shown that

$$|f(u, z)| \leqslant e^{u-z}. \tag{2.13}$$

To solve Eq. (2.11) we write ψ as an expansion in powers of σ:

$$\psi = \sum_{m=1}^{\infty} e^{m-1}(\kappa\epsilon)^{-m}(-\mathbf{k}T)^{1-m}(4\pi\sigma)^m\theta_m(z). \tag{2.14}$$

The $\theta_m(z)$ are functions of z only, which must now be determined. From Eq. (2.8) we find that Ψ can be written in the form,

$$\Psi = \sum_{m=2}^{\infty} e^{m-1}(\kappa\epsilon)^{-m}(-\mathbf{k}T)^{1-m}(4\pi\sigma)^m\Psi_m(z), \tag{2.15}$$

where

$$\Psi_m(z) = \sum_{\substack{m_1+\cdots m_\nu=m \\ \nu\geqslant 2,\ m_\nu\geqslant 1}} \frac{q_\nu}{\nu!}\prod_{s=1}^{\nu}\theta_{m_s}(z). \tag{2.16}$$

Substituting from Eq. (2.14) for ψ in Eq. (2.11) and using Eq. (2.15), we can then determine the functions $\theta_m(z)$ by comparing coefficients of like powers of σ:

$$\theta_1(z) = e^{-z}, \tag{2.17}$$

$$\theta_m(z) = \int_0^\infty f(u, z)\Psi_m(u)du, \quad m>1. \tag{2.18}$$

From Eqs. (2.18) and (2.16), it is clear that $\theta_m(z)$ for m greater than 1, can be expressed in terms of the same functions with smaller suffixes. Hence, since $\theta_1(z)$ is known, all the $\theta_m(z)$ can be evaluated. By direct calculation we find

$$\theta_2(z) = q_2(\tfrac{1}{6}e^{-2z}-\tfrac{1}{3}e^{-z}),$$

$$\theta_3(z) = q_2^2[(1/48)e^{-3z}-(1/9)e^{-2z}+(23/144)e^{-z}] + q_3[(1/48)e^{-3z}-(1/16)e^{-z}],$$

$$\theta_4(z) = q_2^3[(1/432)e^{-4z}-(1/48)e^{-3z}+(31/432)e^{-2z} -(13/144)e^{-z}]+q_2q_3[(1/144)e^{-4z}-(1/48)e^{-3z} -(1/48)e^{-2z}+(11/144)e^{-z}] +q_4[(1/360)e^{-4z}-(1/90)e^{-z}],$$

$$\theta_5(z) = q_2^4[(5/20{,}736)e^{-5z}-(1/324)e^{-4z} +(13/768)e^{-3z}-(31/648)e^{-2z}+(581/10{,}368)e^{-z}] +q_2^2q_3[(5/3{,}456)e^{-5z}-(1/108)e^{-4z} +(5/384)e^{-3z}+(7/216)e^{-2z}-(2/27)e^{-z}] +q_2q_4[(11/8640)e^{-5z}-(1/270)e^{-4z} -(1/270)e^{-2z}+(137/8640)e^{-z}] +q_3^2[(1/2304)e^{-5z}-(1/256)e^{-3z}+(11/1152)e^{-z}] +q_5[(1/2880)e^{-5z}-(1/576)e^{-z}]. \tag{2.19}$$

Although we have tabulated only the first five terms of Eq. (2.14), the series can, in theory at any rate, be carried through to any desired value of m, and so the potential completely determined. The terms soon become very complicated.

To complete the solution, strictly we should examine the convergence of series (2.14), and either establish its validity for all values of σ or find its radius of convergence. Unfortunately, the radius of convergence cannot be found directly, since the method does not give a general formula for any term. For the case of ions, Gronwall, LaMer, and Sandved use a dominant series to examine the convergence. The same method can be used in the present problem, but it is not very helpful. For example it can be shown that Eq. (2.14) is certainly convergent provided that

$$|4\pi ez_0\sigma/\kappa\epsilon\mathbf{k}T| < 2\log_e 2-1 = 0.386, \tag{2.20}$$

where $z_0 \geqslant |z_i|$. This gives a low value for σ. If we substitute $x=0$ in the right-hand side of Eq. (2.14), and then revert the resulting series, so as to give σ as a power series in ζ, then it can be shown that this series is certainly convergent provided that

$$|e\zeta/\mathbf{k}T| < 4\log_e 2-1-2[\log_e 2(3\log_e 2-1)]^{\frac{1}{2}} = 0.0426. \tag{2.21}$$

This is a very small value; with this order of magnitude the first term only of series (2.14) should be sufficient. It seems very likely, however, that the series is convergent for much larger values of $\zeta e/\mathbf{k}T$. For it is easily shown that the corresponding series derived from Eq. (2.4) is certainly convergent provided

$$e\zeta/\mathbf{k}T < 2/3. \tag{2.22}$$

The results embodied in Eqs. (2.20), (2.21), and (2.22) are significant, since they indicate that the series (2.14) cannot be used indiscriminately. The only safe procedure in any particular case would seem to be a comparison of the orders of magnitude of successive terms.

Section 3. Potential at the Plane Interface between Two Different Electrolytes

This is a simple variant of the above problem; instead of a plane solid boundary, the electrolyte is bordered by another semi-infinite electrolyte of different composition. For the case of simple electrolytes dissociating into two ions only, this problem has been solved by Verwey and Niessen.[8] At a large distance from the interface in either direction, the potential is uniform; but, in general, the potential for x large and positive will differ from its value for x large but negative. We shall indicate all quantities to the right of the boundary by the superscript (1) to the left by the superscript (2). For complete generality it will be assumed that there is an adsorbed charge of surface density σ_s, and also a potential jump of ψ_s due to oriented dipoles,

[8] E. J. Verwey and K. F. Niessen, Phil. Mag (7), **28**, 435 (1939).

at the interface. The boundary conditions are

$$\psi^{(2)}=0, \quad x=-\infty; \quad \psi^{(1)}=\zeta, \quad x=\infty; \tag{3.1}$$

$$\psi^{(2)}=\psi_s+\psi^{(1)}, \quad x=0. \tag{3.2}$$

$$\epsilon^{(2)}d\psi^{(2)}/dx|_0-\epsilon^{(1)}d\psi^{(1)}/dx|_0=4\pi\sigma_s. \tag{3.3}$$

When the method of Sec. 2 is used, the series expressions for the potentials are

$$\psi^{(2)}=\sum_{m=1}^{\infty} e^{m-1}(\kappa^{(2)}\epsilon^{(2)})^{-m}(-\mathbf{k}T)^{1-m} \times(4\pi[\sigma_s-\sigma])^m\theta_m(-\kappa^{(2)}x), \quad x<0, \tag{3.4}$$

$$\psi^{(1)}=\zeta+\sum_{m=1}^{\infty} e^{m-1}(\kappa^{(1)}\epsilon^{(1)})^{-m}(-\mathbf{k}T)^{1-m} \times(4\pi\sigma)^m\theta_m(\kappa^{(1)}x), \quad x>0, \tag{3.5}$$

where σ is now effectively a parameter given by

$$\epsilon^{(1)}d\psi^{(1)}/dx|_0=-4\pi\sigma. \tag{3.6}$$

In general σ will not be specified; to find it in terms of the known quantities ζ, ψ_s, and σ_s, the solutions with x set equal to 0 must be substituted in Eq. (3.2) and the resulting series solved by reversion.

Section 4. Electrolyte between Two Parallel Charged Planes

The potential in an electrolyte confined between two parallel planes whose inner surfaces have uniform charge densities σ and σ' is required. This problem is of interest in the theory of the stability of colloids.[9] Solutions for the particular case $s=2$, $\sigma=\sigma'$, $n_1=n_2$, and $z_1=-z_2$, have previously been given by Corkill and Rosenhead[10] and Verwey.[11] Equation (2.7) again holds, provided the potential zero is chosen in such a manner that the n_i satisfy the electroneutrality equation (1.2). But instead of Eq. (2.2) the boundary conditions are now

$$d\psi/dx|_0=-4\pi\sigma/\epsilon, \quad d\psi/dx|_d=4\pi\sigma'/\epsilon, \tag{4.1}$$

where d is the distance between the planes. Integrating Eq. (2.7), we again get Eq. (2.10); but conditions (4.1) now give

$$\psi=\frac{4\pi e^z}{\kappa\epsilon}\left[\frac{\sigma e^{-2b}+\sigma' e^{-b}}{1-e^{-2b}}\right]+\frac{4\pi e^{-z}}{\kappa\epsilon}\left[\frac{\sigma+\sigma' e^{-b}}{1-e^{-2b}}\right] +\int_0^b g(u,z)\Psi(u)du, \tag{4.2}$$

where

$$\left.\begin{aligned} g(u,z)&=-[1/2(1-e^{-2b})] \\ &\times[e^{u-z}+e^{-u-z}+e^{-2b}(e^{u+z}+e^{z-u})], \quad 0<u<z \\ &=-[1/2(1-e^{-2b})] \\ &\times[e^{z-u}+e^{-u-z}+e^{-2b}(e^{u+z}+e^{u-z})], \quad z<u<b \end{aligned}\right\} \tag{4.3}$$

and

$$b=\kappa d, \quad z=\kappa x. \tag{4.4}$$

To solve Eq. (4.2), the potential ψ is expanded as a double series in powers of both σ and σ',

$$\psi=\sum_{m+m'>1}^{\infty} e^{m+m'-1}(\kappa\epsilon)^{-m-m'}(-\mathbf{k}T)^{1-m-m'} \times(4\pi\sigma)^m(4\pi\sigma')^{m'}\theta_{m,m'}(z). \tag{4.5}$$

It can now be shown as before that Ψ may be written

$$\Psi(z)=\sum_{m+m'>0}^{\infty} e^{m+m'-1}(\kappa\epsilon)^{-m-m'}(-\mathbf{k}T)^{1-m-m'} \times(4\pi\sigma)^m(4\pi\sigma')^{m'}\Psi_{m,m'}(z), \tag{4.6}$$

where

$$\Psi_{m,m'}(z)=\sum_{\substack{m_1+\cdots m_\nu=m \\ m_1'\cdots m_\nu'=m' \\ \nu\geq 2,\ m_\nu+m_\nu'\geq 1.}} \frac{q_\nu}{\nu!}\prod_{s=1}^{\nu}\theta_{m_s,m_s'}(z). \tag{4.7}$$

Proceeding as before, we find

$$\begin{aligned} \theta_{1,0}(z)&=(e^{z-2b}+e^{-z})/(1-e^{-2b}), \\ \theta_{0,1}(z)&=(e^{z-b}+e^{-z-b})/1-e^{-2b}), \end{aligned} \tag{4.8}$$

and the functions of higher order are derived from $\theta_{1,0}(z)$ and $\theta_{0,1}(z)$ by the formula,

$$\theta_{m,m'}(z)=\int_0^b g(u,z)\Psi_{m,m'}(u)du, \quad m+m'>1. \tag{4.9}$$

From Eqs. (4.8) and (4.9) the whole series of functions can be built up to any desired order of m and m'.

PROBLEMS INVOLVING CYLINDRICAL BOUNDARIES

Section 5. Infinite Charged Cylinder Immersed in an Electrolyte

Let the charge on the surface of the cylinder be uniformly distributed and of density σ. If r is the distance from the axis of the cylinder, the equation for the potential is

$$(d^2\psi/dr^2)+(1/r)(d\psi/dr)-\kappa^2\psi=\kappa^2\Psi, \tag{5.1}$$

and the boundary conditions,

$$d\psi/dr|_a=-4\pi\sigma/\epsilon, \quad \psi=0, \quad r=\infty, \tag{5.2}$$

where a is the radius. The general integrals of Eq. (5.1) are $I_0(\kappa r)$ and $K_0(\kappa r)$, the bessel functions with imaginary argument of the first and second kind. The

[9] E. J. W. Verwey and J. Th. G. Overbeek, *Theory of the Stability of Lyophobic Colloids* (Elsevier Publishing Company, Inc., New York, 1948), Part II.

[10] A. J. Corkill and L. Rosenhead, Proc. Roy. Soc. (London) **A172**, 410 (1939).

[11] E. J. W. Verwey, Trans. Faraday Soc. **36**, 192 (1940).

determination of the potential follows closely the method of Sec. 2, and so we shall only set down the principal results. Integration gives

$$\psi=-(4\pi\sigma/\kappa\epsilon)\cdot[K_0(z)/K_0'(b)]+\int_b^\infty f(u,z)\Psi(u)udu, \quad (5.3)$$

where

$$\left.\begin{aligned} f(u,z)&=-K_0(z)[I_0(u)-I_0'(b)K_0(u)/K_0'(b)], \quad b<u<z,\\ &=-K_0(u)[I_0(z)-I_0'(b)K_0(z)/K_0'(b)], \quad z<u<\infty. \end{aligned}\right\} \quad (5.4)$$

and

$$z=\kappa r, \quad b=\kappa a, \quad I_0'(z)=dI_0/dz, \quad K_0'(z)=dK_0/dz. \quad (5.5)$$

If ψ is again expanded as in Eq. (2.14), the solutions for the θ functions are

$$\theta_1(z)=-K_0(z)/K_0'(b),$$

$$\theta_m(z)=\int_b^\infty f(u,z)\Psi_m(u)udu, \quad m>1, \quad (5.6)$$

where Ψ_m is given by Eq. (2.16). Hence, the problem is completely solved. The integrals of the second of Eq. (5.6) cannot be evaluated in finite terms and resort must be made to numerical integration.

Section 6. Cylinder Containing Electrolyte

This problem might be of interest in the analysis of streaming potentials and electro-osmosis through tubes sufficiently narrow for the double-layer thickness to be comparable with the radius. The equation for the potential is again Eq. (5.1), but the boundary conditions are now

$$d\psi/dr|_0=0, \quad d\psi/dr|_a=4\pi\sigma/\epsilon, \quad (6.1)$$

where a is again the radius and σ the charge density on the *inner* surface. The final solutions for the θ-functions are

$$\theta_1(z)=I_0(z)/I_0'(b);$$

$$\theta_m(z)=\int_0^b f(u,z)\Psi_m(u)udu, \quad m>1, \quad (6.2)$$

where now

$$\left.\begin{aligned} f(u,z)&=-I_0(u)[K_0(z)-K_0'(b)I_0(z)/I_0'(b)], \quad o<u<z,\\ &=-I_0(z)[K_0(u)-K_0'(b)I_0(u)/I_0'(b)], \quad z<u<b, \end{aligned}\right\} \quad (6.3)$$

and z, b, $I_0'(z)$, and $K_0'(z)$ have the same meaning as in Eq. (5.5).

Section 7. Electrolyte Confined between Charged Coaxial Cylinders

This problem is formally very similar to the one solved in section 4. The boundary conditions are

$$d\psi/dr|_a=-4\pi\sigma/\epsilon, \quad d\psi/dr|_{a'}=4\pi\sigma'/\epsilon, \quad (7.1)$$

where a is the radius, σ the charge density on the inner cylinder, and a' and σ' the corresponding quantities for the outer cylinder. Assuming an expansion for ψ of the same form as Eq. (4.5), where z is now equal to κr, the $\theta_{m,m'}(z)$ functions are given by the equations

$$\left.\begin{aligned} \theta_{1,0}(z)&=\frac{I_0(z)K_0'(b')-K_0(z)I_0'(b')}{I_0'(b')K_0'(b)-I_0'(b)K_0'(b')},\\ \theta_{0,1}(z)&=\frac{I_0(z)K_0'(b)-K_0(z)I_0'(b)}{I_0'(b')K_0'(b)-I_0'(b)K_0'(b')},\\ \theta_{m,m'}(z)&=\int_b^{b'} g(u,z)\Psi_{m,m'}(u)udu, \quad m+m'>1, \end{aligned}\right\} \quad (7.2)$$

where

$$\left.\begin{aligned} g(u,z)&=[I_0(z)I_0(u)K_0'(b)K_0'(b')+K_0(z)K_0(u)I_0'(b)I_0'(b')-K_0(z)I_0(u)I_0'(b')K_0'(b)\\ &\quad -I_0(z)K_0(u)I_0'(b)K_0'(b')]/[I_0'(b')K_0'(b)-I_0'(b)K_0'(b')], \quad b<u<z,\\ &=[I_0(z)I_0(u)K_0'(b)K_0'(b')+K_0(z)K_0(u)I_0'(b)I_0'(b')-K_0(z)I_0(u)I_0'(b)K_0'(b')\\ &\quad -I_0(z)K_0(u)K_0'(b)I_0'(b')]/[I_0'(b')K_0'(b)-I_0'(b)K_0'(b')], \quad z<u<b', \end{aligned}\right\} \quad (7.3)$$

$b=\kappa a$, $b'=\kappa a'$,

and $\Psi_{m,m'}$ is given by Eq. (4.7).

PROBLEMS INVOLVING SPHERICAL BOUNDARIES

Section 8. Solid Sphere with Uniform Surface Charge in an Infinite Electrolyte

The solution in this case is of importance in the theory of cataphoresis.[12] If a is the radius of the sphere and Qe the total charge upon it, the potential in the electrolyte is given by

$$(d^2\psi/dr^2)+(2/r)(d\psi/dr)-\kappa^2\psi=\kappa^2\Psi, \tag{8.1}$$

$$\psi=0, \quad r\to\infty\,; \quad d\psi/dr|_a=-Q/\epsilon a^2, \tag{8.2}$$

where r is the distance from the center of the sphere, and Ψ is again determined by Eq. (2.8). The solution follows the lines of the previous cases, and so we shall merely give the final results. If the ψ is expanded as a power series in Q

$$\psi=\sum_{m=1}^{\infty} e^{2m-1}(\epsilon a)^{-m}(-\mathbf{k}T)^{1-m}Q^m\theta_m(\kappa r), \tag{8.3}$$

then the θ_m functions are given by the relations

$$\theta_1(x)=be^{b-x}/(1+b)x, \tag{8.4}$$

$$\theta_m(x)=\int_b^{\infty} f(u,x)\Psi u\,du, \quad m>1, \tag{8.5}$$

where

$$\left.\begin{aligned} f(u,x)&=-\frac{1}{2x}\left[e^{u-x}+\frac{(b-1)}{(b+1)}e^{2b-u-x}\right], \quad u<x;\\ &=-\frac{1}{2x}\left[e^{x-u}+\frac{(b-1)}{(b+1)}e^{2b-u-x}\right], \quad u>x,\end{aligned}\right\} \tag{8.6}$$

and $b=\kappa a$; Ψ_m is again defined by Eq. (2.16).

Section 9. Sphere of Electrolyte Immersed in Another Electrolyte of Different Composition

This may be regarded as an extension of the previous problem. It may be of interest in the study of the properties of emulsions, which consist of liquids dispersed in small droplets in a medium formed by another liquid. The solution outside the sphere will again be given by a series of the type (8.3), if Qe is the total charge contained in the sphere; for the solution inside we have to obtain the appropriate series in powers of Q. Suppose all quantities for $r<a$, where a is the radius, are distinguished by the superscript (1) and for $r>a$ by the superscript (2). The potential $\psi^{(1)}$ obeys an equation of the form of Eq. (8.1), but the boundary conditions are different,

$$(d^2\psi^{(1)}/dr^2)+(2/r)(d\psi^{(1)}/dr)+\kappa^{(1)2}\psi^{(1)}=\kappa^{(1)2}\Psi^{(1)}, \tag{9.1}$$

$$d\psi^{(1)}/dr|_0=0, \quad d\psi^{(1)}/dr|_a=-eQ/a^2\epsilon^{(1)}. \tag{9.2}$$

The first of Eq. (9.2) follows, since the charge density must remain finite at the origin. In the above equations, the zero of the potential $\psi^{(1)}$ is the potential which gives electroneutrality; this means that if $n_i^{(1)}(i=1,\cdots s^{(1)})$ denote the concentrations when $\psi^{(1)}$ is zero, then we have

$$\sum_{i=1}^{s^{(1)}} n_i^{(1)}z_i^{(1)}=0. \tag{9.3}$$

In general, the zero of the two potentials $\psi^{(1)}$ and $\psi^{(2)}$ will differ; but this raises no difficulties, as we shall see. The general solution of Eq. (9.1) is

$$\psi^{(1)}=\frac{C_1e^{y}}{y}+\frac{C_2e^{-y}}{y}-\frac{1}{2y}\int_0^{y}\Psi^{(1)}u(e^{u-y}-e^{y-u})du, \tag{9.4}$$

where

$$y=\kappa^{(1)}r, \tag{9.5}$$

and C_1 and C_2 are constants. From the first of Eq. (9.2), it follows that

$$C_1=-C_2, \tag{9.6}$$

and from the second we find

$$C_1=-F(c)\left[eQc/\epsilon^{(1)}a + \frac{1}{2}\int_0^{c}\Psi^{(1)}u[e^{u-c}(c+1)+e^{c-u}(c-1)]du\right], \tag{9.7}$$

where

$$F(c)=[e^c(c-1)+e^{-c}(c+1)]^{-1}; \quad c=\kappa^{(1)}a. \tag{9.8}$$

If we now let

$$\psi^{(1)}=\sum_{m=1}^{\infty} e^{2m-1}(\epsilon^{(1)}a)^{-m}(-\mathbf{k}T)^{1-m}Q^m\theta_m{}^{(1)}(\kappa^{(1)}r), \tag{9.9}$$

then we find

$$\left.\begin{aligned} \theta_1{}^{(1)}(y)&=cF(c)[e^{-y}-e^{y}]/y,\\ \theta_m{}^{(1)}(y)&=\int_0^{b}\Psi_m{}^{(1)}f^{(1)}(u,y)u\,du, \quad m>1,\end{aligned}\right\} \tag{9.10}$$

where

$$\left.\begin{aligned} f^{(1)}(u,y)&=\tfrac{1}{2}F(c)[(c+1)e^{y-c}+(c+1)e^{c-y}]\\ &\qquad\times(e^{-u}-e^{u}), \quad 0<u<y,\\ &=\tfrac{1}{2}F(c)[(c+1)e^{u-c}+(c-1)e^{c-u}]\\ &\qquad\times(e^{-y}-e^{y}), \quad y<u<c.\end{aligned}\right\} \tag{9.11}$$

The potential is now completely determined. For any point with r greater than a, a series of the type (8.3) suffices. The potential at any point for r less than a, referred to the potential at infinity as zero, is simply

$$\psi(r)=\psi^{(2)}(a)+\psi^{(1)}(r)-\psi^{(1)}(a). \tag{9.12}$$

[12] F. Booth, Proc. Roy. Soc. (London) **A203**, 514 (1950).

The Third Virial Coefficients of Polar Gases*

J. S. ROWLINSON
The Naval Research Laboratory, Department of Chemistry, University of Wisconsin, Madison, Wisconsin
(Received April 9, 1951)

The third virial coefficient is calculated for a gas composed of spherical molecules whose intermolecular potential has a repulsive term proportional to r^{-12}, an attractive term proportional to r^{-6}, and which have point-dipoles at their centers. The calculated values are compared with the experimental results for steam and ammonia, using parameters previously calculated from the second virial coefficient. The agreement is good for ammonia but poor for steam. It is suggested that this is because of the neglect of the higher multipoles in the interaction potential.

INTRODUCTION

THE equation of state of a gas may be written as a power series in the density,

$$pV/RT=1+(B/V)+(C/V^2)+\cdots, \quad (1)$$

where V is the volume per mole. The second and third virial coefficients, B and C, are functions only of the temperature and of the intermolecular potential. They have been calculated for several molecular models, and the results have been compared with experiment to give information about the forces acting between molecules. It is simpler to use the second virial coefficient, as this is the more easily measured and calculated. However, the third has the advantage that it is much more sensitive to the shape of the potential, and so provides a more severe test of the molecular models. For example, the potential proposed by Lennard-Jones

$$E(r)=ar^{-12}-br^{-6} \quad (2)$$

is sufficiently accurate to represent the second virial coefficient of most nonpolar gases, whether their molecules are symmetrical or not. However, recent calculations[1,2] have shown that, for the third virial coefficient, this potential is only moderately satisfactory even for the simplest molecules such as argon, nitrogen, and methane.

In this paper the third virial coefficient is calculated for polar molecules whose energy of interaction may be expressed by terms proportional to r^{-12} and r^{-6} (as in Eq. (2)) with an additional term to represent the interaction of two point-dipoles. This is the potential first used by Stockmayer.[3] It has been used in calculations of the second virial coefficient,[3,4] where it was very successful even for molecules in which the charge distribution differs considerably from that of a point-dipole. The change in the second virial coefficient due to the complexity and finite size of the charge distribution has been calculated for water[5] and shown to be small. This, though, does not imply that it will be small for the third virial coefficient too. Another approximation must be made whose effect it is hard to foresee. The third virial coefficient depends upon the simultaneous interaction of three molecules; and, so that the mathematics shall not become too complicated, it must be assumed that the energy of interaction between any two of these is not affected by the presence of the third. This is strictly true both for the first-order London forces (r^{-6} term) and for the interaction of permanent charge distributions. It is not true, though, for the forces between permanent charges and the charges they induce in polarizable molecules, the principal part of which is also included in the r^{-6} term. However, these forces are known to be small.

CALCULATION OF THE THIRD VIRIAL COEFFICIENT

The third virial coefficient is given by

$$C=-\tfrac{1}{3}N^2\int\int f_{12}f_{13}f_{23}d\mathbf{r}_1d\mathbf{r}_2, \quad (3)$$

where

$$f_{ij}=\exp(-E_{ij}/kT)-1 \quad (4)$$

and E_{ij} is the energy of interaction between molecules i and j, which depends on their distance apart r_{ij} and on their relative orientation. E_{ij} may be written

$$E_{ij}/kT=(4/\tau)(R_{ij}^{-12}-R_{ij}^{-6}-(t_1/\sqrt{2})\cdot R_{ij}^{-3}\cdot F_{ij}), \quad (5)$$

where

$$R_{ij}=r_{ij}/r_0, \quad (6)$$

$$t_1=(1/2\sqrt{2})(p^2/\epsilon r_0^2), \quad (7)$$

$$\tau=kT/\epsilon. \quad (8)$$

It is convenient to introduce another parameter with the units of volume per mole:

$$b_0=\tfrac{2}{3}\pi N r_0^3. \quad (9)$$

The expressions ϵ and r_0 are the energy and distance characteristic of the nonpolar part of the potential.†

* This work was carried out under Contract NOrd-9938 with the Navy Bureau of Ordnance.
[1] T. Kihara, J. Phys. Soc. Japan **3**, 265 (1948).
[2] Bird, Spotz, and Hirschfelder, J. Chem. Phys. **18**, 1395 (1950).
[3] W. H. Stockmayer, J. Chem. Phys. **9**, 398, 863 (1941).
[4] J. S. Rowlinson, Trans. Faraday Soc. **45**, 974 (1949).
[5] J. S. Rowlinson, Trans. Faraday Soc., **47**, 120 (1951).

† Unfortunately there are several contradictory notations for these parameters. The symbol r_0 is often used (references 1, 4, and 5) for the distance at which E is a minimum. When $t_1=0$, this is larger than the present r_0 by a factor of $2^{1/6}$.

If the dipole moment p is zero, then r_0 is the distance at which $E=0$ and $-\epsilon$ is the minimum value of E. The symbol t_1 is a pure number which may be called the reduced dipole-dipole energy,[4,5] and τ is the reduced temperature.

F_{ij} is a function both of the angles specifying the orientation of the two molecules and of the positions of their centers. Let the three molecules be arranged as shown in Fig. 1. The parameters x and y fix the position of molecule 3. They are given by

$$R_{13}^2=R_{12}^2(x^2+y^2), \tag{10a}$$

$$R_{23}^2=R_{12}^2[(1-x)^2+y^2]. \tag{10b}$$

Let the dipole of each molecule make an angle θ_i with the line joining 1 and 2 and let the azimuthal angle which it makes with the plane of the three molecules be ϕ_i. Then one obtains

$$\begin{aligned}
F_{12}&=2\cos\theta_1\cos\theta_2-\sin\theta_1\sin\theta_2\cos(\phi_1-\phi_2),\\
F_{13}&=\alpha\cos\theta_1\cos\theta_3+\sin\theta_1\sin\theta_3[(1-\alpha)\cos\phi_1\cos\phi_3\\
&\quad-\sin\phi_1\sin\phi_3]+\beta(\cos\theta_1\sin\theta_3\cos\phi_3\\
&\quad+\sin\theta_1\cos\theta_3\cos\phi_1),\\
F_{23}&=\gamma\cos\theta_2\cos\theta_3+\sin\theta_2\sin\theta_3[(1-\gamma)\cos\phi_2\cos\phi_3\\
&\quad-\sin\phi_2\sin\phi_3]+\delta(\cos\theta_2\sin\theta_3\cos\phi_3\\
&\quad+\sin\theta_2\cos\theta_3\cos\phi_2),
\end{aligned} \tag{11}$$

where

$$\begin{aligned}
\alpha&=(2x^2-y^2)/(x^2+y^2),\\
\beta&=3xy/(x^2+y^2),\\
\gamma&=[2(1-x)^2-y^2]/[(1-x)^2+y^2],\\
\delta&=-3(1-x)y/[(1-x)^2+y^2].
\end{aligned} \tag{12}$$

The energy of interaction, given by Eqs. (5) and (11), is now put into Eq. (3) and the integral evaluated. There are several ways of doing this. The most convenient is that of Kihara,[1] who expands in powers of R_{12} and integrates to a sum of Γ-functions. This is the method by which Lennard-Jones first integrated the expression for the second virial coefficient. Kihara shows that

$$\begin{aligned}
&\frac{1}{3}\int\int d\mathbf{r}_1 d\mathbf{r}_2\\
&\quad=4\pi^2 r_0^6\int_0^{\frac{3}{4}} d(y^2)\int_{1-(1-y^2)^{\frac{1}{2}}}^{(1-y^2)^{\frac{1}{2}}} dx\int_0^{\infty} R_{12}^5 dR_{12}.
\end{aligned} \tag{13}$$

The integration over x and y allows molecule 3 to move over the area shown in Fig. 1, in which $R_{12}\geq R_{13}$, R_{23}. If the molecules are not spherical, then the integration must be taken over the six angles θ_1, θ_2, θ_3, ϕ_1, ϕ_2, ϕ_3. This gives

$$\begin{aligned}
C=-9b_0^2\int_0^{\frac{3}{4}}\int_{1-(1-y^2)^{\frac{1}{2}}}^{(1-y^2)^{\frac{1}{2}}}\int_0^{\infty}\int_0^{\pi}\int_0^{\pi}\int_0^{\pi}\int_0^{2\pi}\int_0^{2\pi}\int_0^{2\pi} f_{12}f_{13}f_{23}\\
\cdot R_{12}^5\sin\theta_1\sin\theta_2\sin\theta_3 d(y^2)dx dR_{12}d\theta_1 d\theta_2 d\theta_3 d\phi_1 d\phi_2 d\phi_3.
\end{aligned} \tag{14}$$

Multiplying out the product of $f_{12}f_{13}f_{23}$ gives

$$f^{(0)}-f^{(1)}-f^{(2)}-f^{(3)}+f_{12}+f_{13}+f_{23},$$

where

$$\begin{aligned}
f^{(0)}&=\exp[-(E_{12}+E_{13}+E_{23})/kT]-1,\\
f^{(1)}&=\exp[-(E_{12}+E_{13})/kT]-1,\\
f^{(2)}&=\exp[-(E_{12}+E_{23})/kT]-1,\\
f^{(3)}&=\exp[-(E_{13}+E_{23})/kT]-1.
\end{aligned} \tag{15}$$

When these expressions are expanded and integrated over R_{12}, all terms which are independent of t_1 may be dropped, as these can contribute only to the nonpolar part of C. Very accurate calculations were made of this by Bird, Spotz, and Hirschfelder.[2] This leaves for ΔC, the difference between the polar and nonpolar virial coefficient,

$$\Delta C=\tfrac{2}{3}b_0^2\sum_{n=2}^{\infty}\sum_{\kappa=2}^{n}\frac{2^n}{n!}\binom{n}{\kappa}\frac{t_1^{\kappa}}{\tau^{\frac{1}{4}(2n+\kappa+2)}}\cdot Q_{n,\kappa}. \tag{16}$$

If κ is even, it follows that

$$\begin{aligned}
Q_{n,\kappa}&=-(1/8\pi)^3\cdot\Gamma(\tfrac{1}{4}(2n-\kappa-2))\\
&\times\int\int\int\int\int\int\int\int\int[A_{n,\kappa}(F_{12}+\xi^3F_{13}+\eta^3F_{23})^{\kappa}\\
&-B_{n,\kappa}(F_{12}+\xi^3F_{13})^{\kappa}-C_{n,\kappa}(F_{12}+\eta^3F_{23})^{\kappa}\\
&-D_{n,\kappa}(\xi^3F_{13}+\eta^3F_{23})^{\kappa}+F_{12}^{\kappa}+\xi^6F_{13}^{\kappa}+\eta^6F_{23}^{\kappa}]\\
&\times\sin\theta_1\sin\theta_2\sin\theta_3 d(y^2)dx d\theta_1 d\theta_2 d\theta_3 d\phi_1 d\phi_2 d\phi_3.
\end{aligned} \tag{17}$$

If κ is odd, all the terms except the first, in the integrand of $Q_{n,\kappa}$, vanish on integrating over angles. Here ξ and η are given by

$$\begin{aligned}
\xi&=R_{12}/R_{13}=(x^2+y^2)^{-\frac{1}{2}},\\
\eta&=R_{12}/R_{23}=[(1-x)^2+y^2]^{-\frac{1}{2}},
\end{aligned} \tag{18}$$

$$\begin{aligned}
A_{n,\kappa}&=(1+\xi^6+\eta^6)^{n-\kappa}(1+\xi^{12}+\eta^{12})^{\frac{1}{4}(2-2n+\kappa)},\\
B_{n,\kappa}&=(1+\xi^6)^{n-\kappa}(1+\xi^{12})^{\frac{1}{4}(2-2n+\kappa)}\\
C_{n,\kappa}&=(1+\eta^6)^{n-\kappa}(1+\eta^{12})^{\frac{1}{4}(2-2n+\kappa)},\\
D_{n,\kappa}&=(\xi^6+\eta^6)^{n-\kappa}(\xi^{12}+\eta^{12})^{\frac{1}{4}(2-2n+\kappa)}.
\end{aligned} \tag{19}$$

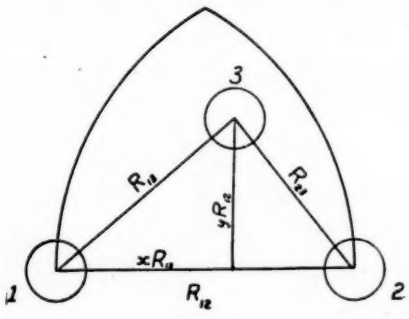

FIG. 1.

TABLE I. $Q_{n,\kappa}$.

κ / n	2	3	4	5	6	7	8
2	+0.4995						
3	+0.3364	+0.9414					
4	+0.3189	+0.4305	+1.0421				
5	+0.3008	+0.4423	+0.7495	+1.367			
6	+0.0981	+0.6383	+0.6667	+1.458	+1.811		
7	−0.7378	+1.145	+0.3033	+2.170	+0.916	+5.670	
8	−4.259	+2.407	−1.140	+3.996	−1.050	+8.024	−2.982
9	−15.10	+5.744	−6.491	+8.652	−7.147	+15.33	−14.42
10	−53.68	+15.10	−25.62	+20.92	−26.97	+33.74	−46.17
11	−197.5	+43.41	−93.87	+55.02	−92.77	+82.85	−140.8
12	−754.3	+135.1	−340.7	+161.1	−316.7	+221.1	−462.5
13	−2995	+450.4	−1262	+508.1	−1103	+646.1	−1401
14	−12340	+1593	−4785	+1710	−3964	+2032	−4689
15	−52650	+5950	−18715	+6099	−14790	+6817	−16380
16	−232400	+23340	−75590	+22920	−57390	+24100	−59710

If $n=\kappa=2$, then Q becomes indefinite as the Γ-function is infinite and the integrand zero. However, by putting $\kappa=2$ and taking the limit as $n\to 2$, one finds that, after integrating over angles

$$Q_{2,2}=\frac{4}{3}\int\int\left[\ln\frac{A_{3,2}}{B_{3,2}\cdot C_{3,2}\cdot D_{3,2}}+\xi^6\ln\frac{A_{3,2}}{B_{3,2}\cdot D_{3,2}}+\eta^6\ln\frac{A_{3,2}}{C_{3,2}\cdot D_{3,2}}\right]d(y^2)dx. \tag{20}$$

Each value of $Q_{n,\kappa}$ can be reduced to such an integral over x and y^2 by integration over the six angles. Integrals of the F_{ij} functions (Eq. (11)) and their products will be written $\{F_{ij}\}$. It may be shown that $\{F_{ij}{}^q\}$ and $\{F_{ij}{}^qF_{jk}{}^r\}$ vanish unless both q and r are even. Also, $\{F_{12}{}^qF_{13}{}^rF_{23}{}^s\}$ vanishes unless q, r, and s are either all even or all odd. If rotations of the whole system of three molecules are considered, it follows that $\{F_{ij}{}^qF_{jk}{}^r\}=\{F_{ij}{}^rF_{jk}{}^q\}$, etc., and that

$$\{F_{12}{}^q\}=\{F_{13}{}^q\}=\{F_{23}{}^q\}=\frac{(8\pi)^3}{1+q}\sum_{m=0}^{q/2}\binom{q/2}{m}\frac{3^m}{1+2m}\quad\text{(Stockmayer}^3\text{)}$$

and so are independent of x and y. More complicated products of the F terms lead to cumbersome functions of α, β, γ, and δ (and so of x and y) which only varied slowly over the area accessible to the third molecule. And so for $\kappa\geq 5$ some of the more complicated products were replaced by simpler ones, e.g., $\{F_{13}{}^4F_{23}{}^2\}$ and $\{F_{13}{}^2F_{23}{}^4\}$ by $\frac{1}{2}[\{F_{12}{}^4F_{13}{}^2\}+\{F_{12}{}^4F_{23}{}^2\}]$. This simplified the computing. Where the terms for $\kappa=4$ were worked out both with and without these approximations, it was found that they were unlikely to make the integrand more than one percent in error. Sufficient terms were worked out to give $Q_{n,\kappa}$ for $\kappa=2, 3, \cdots 8$ and $n=2, 3, \cdots 16$.

The last step is to integrate over x and y^2. This cannot be done analytically. Only half the area shown in Fig. 1 need be considered as the integrand is symmetrical about $x=\frac{1}{2}$. Gauss' method of numerical integration was used. Six values of y^2 were taken and, for each, 4, 4, 4, 4, 3, and 1 values of x. The integrands are well behaved and never have more than one point of zero slope with respect to changes of x or y^2. As a check on the accuracy this method was used to find one value for a nonpolar molecule by Kihara's method. The result agreed with the punched-card calculations of Bird, Spotz, and Hirschfelder within one part in 4000. The values of $Q_{n,\kappa}$ are given in Table I.

The value of $\Delta C/b_0{}^2$ was computed from these by means of Eq. (16) and added to the values of $C/b_0{}^2$ for nonpolar gases[2] to give the results shown in Table II and plotted in Fig. 2. It is hard to assess the accuracy

TABLE II. $C/b_0{}^2$.

t_1 / τ	0.0	0.1	0.2	0.3	0.4	0.5	0.6	0.7	0.8	1.0	1.2
1.0	0.4297	0.4440	0.5304	0.740							
1.2	0.5924	0.6177	0.7162	0.9216	1.268	1.78	2.5	3.4	4.6	7	
1.4	0.5683	0.5900	0.6679	0.8221	1.075	1.451	2.0	2.7	3.7	6.3	9
1.6	0.5180	0.5351	0.5940	0.7075	0.8899	1.158	1.53	2.03	2.69	4.72	7.0
1.8	0.4728	0.4861	0.5311	0.6161	0.7507	0.9455	1.214	1.572	2.03	3.36	5.2
2.0	0.4371	0.4476	0.4826	0.5478	0.6496	0.7957	0.995	1.257	1.595	2.46	4.0
2.5	0.3811	0.3873	0.4076	0.4445	0.5195	0.5807	0.6871	0.825	0.999	1.482	2.19
3.0	0.3523	0.3563	0.3692	0.3924	0.4275	0.4761	0.5403	0.6223	0.7248	1.002	1.401
4.0	0.3266	0.3286	0.3350	0.3463	0.3630	0.3859	0.4156	0.4529	0.4986	0.6194	0.7857
6.0	0.3077	0.3085	0.3109	0.3151	0.3213	0.3296	0.3401	0.3532	0.3690	0.4095	0.4640
8.0	0.2962	0.2966	0.2978	0.3000	0.3031	0.3072	0.3124	0.3188	0.3265	0.3459	0.3715
10.0	0.2861	0.2863	0.2871	0.2884	0.2902	0.2926	0.2957	0.2995	0.3039	0.3151	0.3297

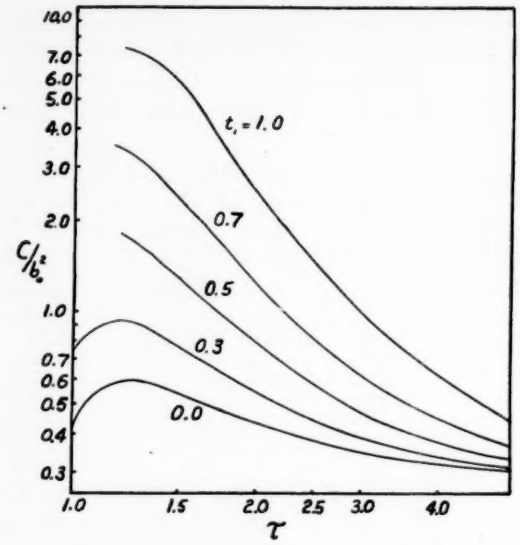

FIG. 2. The third virial coefficient as a function of the temperature (τ) and the dipole energy (t_1).

of these numbers. The integrand of $Q_{n,\kappa}$ changes with x more rapidly for the polar than for the nonpolar case. The values of $\Delta C/bo^2$ are computed from sums of many terms of the $Q_{n,k}$, some positive and some negative. The sums over n and κ converge very slowly for low values of τ and high values of t_1. Hence, the figures may not always be accurate to as many places as they are given. This, though, is unimportant, as the experimental results themselves are not very accurate.

DISCUSSION

The difference ΔB, between the value of the second virial coefficient for a polar and a nonpolar gas, is always negative and increases in size with increasing t_1. The difference ΔC is positive for the temperatures shown in Fig. 2. However, at lower temperatures the terms of $Q_{n,k}$ which contribute most to the virial coefficient are those where n is large; and Table I shows that here the negative terms (k even) are larger than the positive

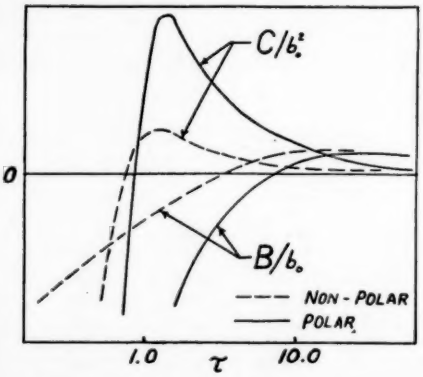

FIG. 3. The approximate form of the second and third virial coefficients of nonpolar and polar gases as a function of the reduced temperature (τ). The curves for the polar gas correspond to $t_1 \sim 1$.

terms (k odd). That is, ΔC will become negative at low enough temperatures. This would be expected, as a negative C corresponds to increased compressibility. For $t_1=1.0$ it is estimated that C will become negative at about $\tau=1.0$. The trend of the curves is shown in Fig. 3.

There are experimental measurements of the third virial coefficients of ammonia and steam. Those for ammonia may be calculated from the measurements of Beattie and Lawrence[6] by finding the slope at zero pressure of $(V-RT/p)$ as a function of the density. The measurements of Meyers and Jessup[7] are all at low pressures. Keyes, Smith, and Gerry[8] have determined the equation of state of steam. The third virial coefficient may be found approximately from the equation which they fit to their results. The parameter t_1, ϵ/k, and b_0 must be known in order to compare the observed and calculated values of C/b_0^2. These have been determined from the second virial coefficient:[4]

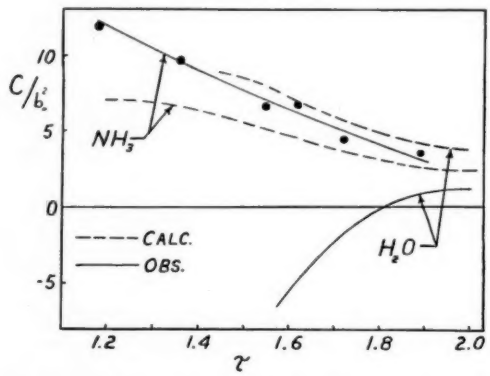

FIG. 4. The observed and the calculated values of the third virial coefficient of ammonia and water.

Ammonia, $t_1=1.0$, $\epsilon/k=320°K$, $b_0=22.12$ cm³/mole;
Water, $t_1=1.2$, $\epsilon/k=380°K$, $b_0=23.42$ cm³/mole.

The comparison of theory with experiment is shown in Fig. 4. The agreement is good for ammonia but very bad for steam. This is undoubtedly due to the neglect of the higher multipoles in the interaction potential. Even for the second virial coefficient, the effect of these is several times larger for water than for a symmetrical molecule such as ammonia.[5] Apparently, this difference is even larger in the third coefficient. This effect is to make the water molecules cluster together more than would be expected, so that C becomes negative at temperatures below $\tau=1.8$, instead of at about $\tau=1.0$. The geometry of the water molecules is probably a

[6] J. A. Beattie and C. K. Lawrence, J. Am. Chem. Soc. **52**, 6 (1930).
[7] C. H. Meyers and R. S. Jessup, Refrig. Eng. **11**, 345 (1925).
[8] Keyes, Smith, and Gerry, Proc. Am. Acad. Arts. Sci. **70**, 319 (1936).

factor which favors this clustering, as it allows them to pack together to form a lattice of the wurtzite type where each molecule attracts all its neighbors equally. This is not possible with either point-dipoles or ammonia molecules.

I would like to thank Marjorie Leikvold (director), Catherine Denton, Alice Epstein, and Ruth Straus, of the computing section of the University of Wisconsin Naval Research Laboratory, who calculated the integrals $Q_{n,k}$.

THE JOURNAL OF CHEMICAL PHYSICS VOLUME 19, NUMBER 7 JULY, 1951

The Critical Constants of Polar Gases

J. S. ROWLINSON
The Naval Research Laboratory, Department of Chemistry, University of Wisconsin, Madison. Wisconsin
(Received April 9, 1951)

The range of usefulness of the virial expansion is discussed. It is shown that this expansion closely resembles the Beattie-Bridgman equation if terms up to the third virial coefficient are included. This suggests that the ranges of validity of the two equations may be similar—namely, almost up to the critical density. The virial expansion is therefore used to calculate the critical constants of both nonpolar and polar gases. These constants are much less sensitive to the dipole-energy than are the virial coefficients. The agreement with experiment is satisfactory.

NO exact equation of state of dense gases has yet given numerical results. Two approximate methods have been used. In the first, the gas is regarded as a rarified liquid in which molecules spend most of their time imprisoned by a cage of their nearest neighbors. The second method, which will be discussed here, starts from the equation of state of a perfect gas and considers the effect of interactions, first of pairs of molecules, then of triplets, etc. (the virial expansion). The first method has the advantage that the equation of state is formally valid over the whole range of density from solid and liquid to a perfect gas. However, the physical approximations, which have had to be introduced to give numerical results, are such that the equation is good only at densities considerably above the critical.[1–3] These approximations have been improved recently and better results have been obtained.[4,5] These calculations are restricted, though, to nonpolar molecules.

In the second method, the equation of state is expanded in a power series of the density,

$$pV/RT=1+B/V+C/V^2+D/V^3+\cdots. \qquad (1)$$

The lower virial coefficients, B, C, etc., are functions of the temperature only. The very high ones will depend also on the volume, though the nature of this dependence is not known. The expansion is valid only in the gas region. Elsewhere, the series diverges. However, convergence is very rapid over most of the gas region; and it is only close to the critical point that the sum of the terms beyond C/V^2 is important. Thus, although Eq. (1) cannot be used beyond the critical point, it might still be capable of giving reasonable values of the critical constants. This view is supported by its resemblance to the well-known empirical equation of Beattie and Bridgman, which is also reliable up to, but not beyond, the critical density.[6] This resemblance will be examined a little more closely, before discussing the critical constants of Eq. (1).

The Beattie-Bridgman equation may be written as a virial expansion where

$$\begin{aligned} B&=b_1-(b_2/T)-b_3/T^3,\\ C&=c_1+(c_2/T)-c_3/T^3,\\ D&=d_1/T^3. \end{aligned} \qquad (2)$$

Here $b_1\cdots$, $c_1\cdots$, and d_1 are compounded of five adjustable parameters which are determined from the experimental measurements of the compressibility. These empirical expressions for the virial coefficients B and C show a similar dependence on temperature to

TABLE I.

	τ_c	$\left(\frac{p_c b_0}{\epsilon}\right)$	$\left(\frac{V_c}{b_0}\right)$	$\left(\frac{p_c V_c}{RT_c}\right)$
Mean value for Ne, A, N_2[a]	1.28	0.256	1.47	0.293
From Eqs. (5)–(8)	1.45	0.376	1.29	0.333
Lennard-Jones-Devonshire treatment[a]	1.30	0.909	0.84	0.591
Peek and Hill's[b] modification of L.J.D.	1.18	0.547	1.55	0.72

[a] Reference 3.
[b] Reference 5.

[1] J. E. Lennard-Jones and A. F. Devonshire, Proc. Roy. Soc. (London) **A163**, 53 (1937).
[2] I. Prigogine and G. Garikian, J. chim. Phys. **45**, 273 (1948).
[3] Wentorf, Buehler, Hirschfelder, and Curtiss, J. Chem. Phys. **18**, 1484 (1950).
[4] S. Ono, Mem. Faculty Eng., Kyushu Imp. Univ. **10**, No. 4, 196 (1947); T. Sato and S. Ono, J. Phys. Soc. Japan **4**, 103 (1949).
[5] H. M. Peek and T. L. Hill, J. Chem. Phys. **18**, 1252 (1950).
[6] J. A. Beattie and W. H. Stockmayer, Rept. Progress Phys. **7**, 195 (1940), give a good account of the validity and characteristics of the Beattie-Bridgman and similar empirical equations.

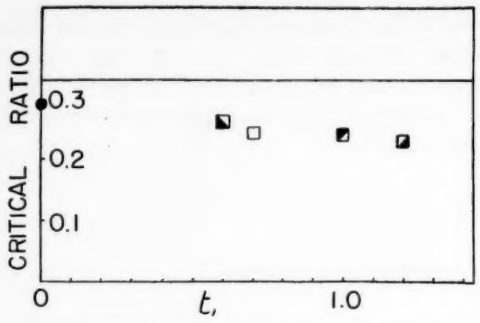

FIG. 1. The critical ratio, $p_c V_c/RT_c$, as a function of the dipole energy, t_1.

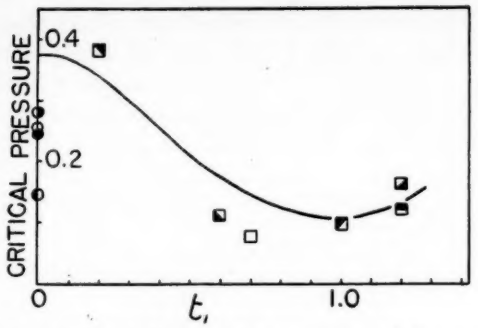

FIG. 3. The reduced critical pressure, $p_c b_0/\epsilon$, as a function of the dipole energy, t_1.

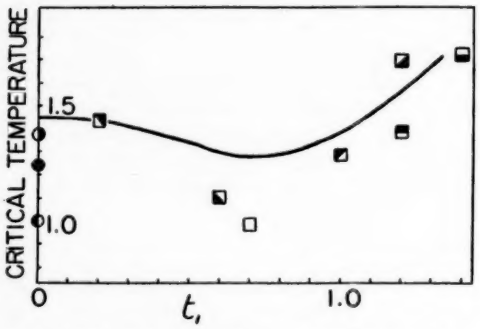

FIG. 2. The reduced critical temperature, τ_c, as a function of the dipole energy, t_1.

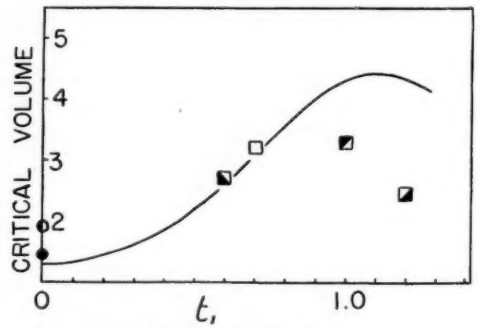

FIG. 4. The reduced critical volume, V_c/b_0, as a function of the dipole energy, t_1.

Key for Figs. 1 - 4

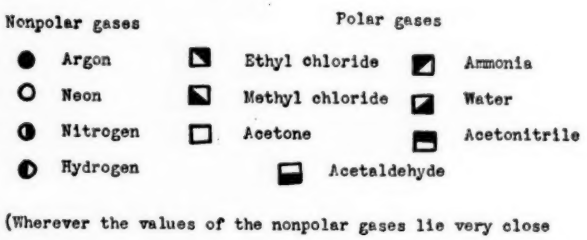

(Wherever the values of the nonpolar gases lie very close together, only the symbol for argon is shown.)

the theoretical values (see Fig. 3 of preceding paper, reference 7). This resemblance between the Beattie-Bridgman equation and the virial expansion has been commented on before. Hirschfelder and Roseveare[8] compared the temperature-dependence of the second virial coefficient, and Corner[9] the dependence of the third. It is emphasized here because it suggests that the virial expansion up to the third virial coefficient should have as wide a range of usefulness as the Beattie-Bridgman equation. The fourth virial coefficient, D, which appears in Eqs. (2), may be ignored. In fitting the parameters, d_1 is put equal to zero for He, Ne, and A, and small but negative for H_2, N_2, and CH_4. Theoretical indications are that it should be small but positive for these gases.[10] It is probable, therefore, that it has little effect except very close to the critical point.*

A very sensitive test of any equation of state is the curvature of the isochores. Experiment shows that for nonpolar gases, $(\partial^2 p/\partial T^2)_V$ is always very small. It is negative in the gas region but becomes positive near the critical density.[6] (At the critical *point* it is identically zero.) The sign of this curvature is given by various equations of state, thus—zero (van der waals), positive (Dieterici), and negative (Berthelot and Beattie-Bridgman). From Eq. (1), it may be shown

[7] J. S. Rowlinson, J. Chem. Phys. **19**, 827 (1951).
[8] J. O. Hirschfelder and W. E. Roseveare, J. Phys. Chem. **43**, 15 (1939).
[9] J. Corner, Trans. Faraday Soc. **37**, 358 (1941).

[10] R. B. Bird and E. L. Spotz, University of Wisconsin CM-599, Project NOrd 9938 (May 10, 1950).

* Recent calculations have shown that even the exact theoretical equation of state of Born and Green is accurate only to the third virial coefficient, when the "superposition" approximation is introduced. The apparent fourth virial coefficient is 78 percent of its true value for hard spheres. G. S. Rushbrooke and H. I. Scoines, Nature **167**, 366 (1951); Hart, Wallis, and Pode, J. Chem. Phys. **19**, 139 (1951).

that at low densities this curvature has the same sign as $[2T(dB/dT)+T^2(d^2B/dT^2)]$. Bird and Spotz[10] have computed derivatives of B for nonpolar gases. This function is negative over the whole temperature range. A similar term with derivatives of C becomes more important at high densities. This is positive except at very low or very high temperatures. It is too small, though, to do more than reduce the amount of the negative curvature at any density below the critical. Equation (1), therefore, predicts isochores of nonpolar gases with negative curvature at all densities up to the critical. In this, it again resembles the Beattie-Bridgman equation.

THE CRITICAL CONSTANTS

Equation (1) may be written

$$p=RT(\rho+B\rho^2+C\rho^3+\cdots), \tag{3}$$

where ρ, the density, is the reciprocal of the molar volume. The critical point is given by

$$(\partial p/\partial\rho)_T=(\partial^2 p/\partial\rho^2)_T=0. \tag{4}$$

Using subscript c to denote values at the critical point gives

$$p_cV_c/RT_c=1/3 \tag{5}$$

and

$$3C_c=B_c^2. \tag{6}$$

Equation (6) determines the critical temperature.[11] Tables of B[10,12] and C[7,10,13] have recently been computed for both polar and nonpolar gases. The intermolecular potential and the notation used to express it are the same as in the preceding paper. The critical temperature τ_c was found from the tables of B and C by graphical interpolation. When τ_c is known, the other reduced critical constants may be found from the two relations which may be derived from Eqs. (3), (5), and (6),

$$(p_cb_0/\epsilon)=-(\tau_cb_0/3B_c), \tag{7}$$

$$(V_c/b_0)=-(B_c/b_0). \tag{8}$$

[11] T. Kihara used this relation between the virial coefficients to determine the critical temperature in his discussion of the square-well potential. Proc. Phys.-Math. Soc. Japan **17**, 11 (1943) (in Japanese).

[12] J. S. Rowlinson, Trans. Faraday Soc. **45**, 974 (1949).

[13] Bird, Spotz, and Hirschfelder, J. Chem. Phys. **18**, 1395 (1950).

TABLE II.

	t_1	b_0(cm³/mole)	ϵ/k(°K)
Ethyl chloride	0.2	199.7	320
Methyl chloride	0.6	50.7	380
Acetone	0.7	66.9	520
Ammonia	1.0	22.1	320
Water	1.2	23.4	380
Acetonitrile	1.2	82.0	400
Acetaldehyde	1.4	62.8	270

For nonpolar gases, Eqs. (5)–(8) lead to the values shown in Table I.

It is seen that the approach to the critical point from the virial expansion gives better values for the constants than the crude treatment of Lennard-Jones and Devonshire, and values which are as good as those of Peek and Hill, who modified their treatment to allow for the presence of "holes" in the liquid.

Figures 1–4 show the predicted variation of these quantities[14] with the reduced dipole-energy t_1, which is a measure of the relative importance of the polar to the nonpolar forces.[7,12] Although both B and C change very rapidly with t_1, it is found that the critical constants only change slowly. The critical ratio (Fig. 1) is determined by the form of Eq. (1) and so is independent of t_1. The reduced critical temperature (Fig. 2) is almost independent of t_1, and the critical pressure (Fig. 3) and volume (Fig. 4) tend to fall and rise, respectively. These predictions are compared with the experimental results for the gases for which the parameters t_1, ϵ, and b_0 have been derived. These parameters (Table II) were found by fitting the second virial coefficient.[12] Methyl alcohol has been omitted, as the value previously given to b_0 is anomalous. It was smaller than that of water, owing to the unsymmetrical arrangement of the electric charges.

The agreement with experiment is very satisfactory, in view of the approximations involved. The critical ratio apparently decreases slowly with t_1, rather than remaining constant. The trends of T_c, p_c, and V_c are reproduced quite satisfactorily. Only the calculated critical volumes of water and ammonia are badly in error.

[14] Experimental values for the critical constants were obtained from the *Tables* of Landolt-Bornstein and from the *Handbook of Chemistry and Physics* (Chemical Rubber Publishing Company, Cleveland, Ohio). Values for steam are from the tables of J. H. Keenan and F. G. Keys (John Wiley and Sons, Inc., New York, 1936).

The Stability of Gaseous Diatomic Oxides*

LEO BREWER AND DONALD F. MASTICK†
Chemistry and Chemical Engineering Department and Radiation Laboratory, University of California, Berkeley, California‡

(Received October 30, 1950)

The instabilities of FeO, NiO, MnO, and SiO_2 upon vaporization, and upper limits to the heats of dissociation of these oxides and SiO have been determined by effusion experiments. The data available in the literature have been treated to obtain the heats of dissociation, or the upper limits thereof, of the gaseous oxides SnO, ZnO, CdO, CuO, PbO, GeO, and TiO.

The linear Birge-Sponer extrapolation of vibrational levels appears to give correct dissociation energies for the fourth-group oxides.

INTRODUCTION

THE vapor pressure of several diatomic oxides have been studied by the measurement of rates of vaporization from a free surface into a vacuum or by the rates of effusion from a Knudsen cell. In essentially all such studies the stability of the gaseous oxide has been assumed, and the vapor pressures and heats of sublimation have been calculated on this basis.

If one considers the types of reactions that may occur upon vaporization of metal oxides, one can divide them into three classes. The first class, which is probably the most common, includes those oxides which have a high oxygen decomposition pressure and which decompose to a lower oxide with no appreciable loss of metal as the elemental vapor or as a gaseous oxide. These oxides may be readily distinguished experimentally by the observation that heating causes a change in the x-ray pattern of the sample without any appreciable loss of the metal.

The second class, which appears to be relatively uncommon, includes those oxides which vaporize to a stable gaseous molecule of approximately the same composition as the condensed phase. The third class includes those oxides which vaporize by a process of decomposition almost completely to the gaseous elements or to a stable gaseous oxide of considerably different composition than the condensed phase.

The three classes can be illustrated using oxides considered in this paper. The decomposition of Fe_2O_3 to Fe_3O_4 or of Mn_3O_4 to MnO upon heating illustrates the first class. During the heating of these oxides, oxygen is evolved with no detectable amounts of iron or manganese vaporizing. The second class may be illustrated by the vaporization of PbO. The solid of composition approximately PbO vaporizes to a gas consisting almost entirely of PbO gaseous molecules. The third class may be illustrated by the vaporization of NiO and SiO_2. NiO appears to vaporize largely by decomposition to gaseous nickel and oxygen which are present in the gaseous phase in higher concentrations than any gaseous nickel oxide molecules. SiO_2 also appears to vaporize by decomposition, but elemental silicon is not the main species. SiO and O_2 gases appear to be the main gaseous species when SiO_2 vaporizes.

It is the purpose of this work to consider an experimental method for distinguishing between the second and third classes discussed above. In any case, the partial pressures of the elements in equilibrium with the condensed oxide phase can be calculated when the heat and entropy of formation of the oxide are known as a function of temperature. When stable gaseous oxide molecules are unimportant, the volatility of the oxide has thus been determined when the partial pressures of the elements are known. The effect of the existence of a stable gaseous molecule which would be present in higher concentration than the gaseous elements is to increase the total volatility. Thus, a clear distinction can be made between an oxide which vaporizes largely by decomposition to the elements and one which vaporizes largely to a stable oxide molecule. In the first situation the total volatility should agree with the decomposition pressures of the elements calculated from the thermodynamic data for the oxide. In the second situation the total volatility should be greater than that calculated on the basis of decomposition to only the elements. Using this in reverse as an experimental criterion, we can say that the existence of a stable gaseous oxide species has been demonstrated when the total observed volatility is greater than the calculated volatility due only to decomposition to the elements. When the total observed volatility is of the order of the calculated volatility due to decomposition to the elements, then any gaseous oxide molecules will be of smaller concentration than the elements or in a few intermediate cases will approach the concentration of the elements. When the gaseous oxide is more important than the elements, the vapor pressure data can be used directly to determine a heat of formation of the gaseous oxide. When it is less important than the elements, only an upper limit to its stability can be given. Since it is not common to have experimental or thermodynamic data which will fix the pressures to better than a factor of two, the simplest way to fix the upper limit to the partial pressure of the gaseous oxide species is to take it equal to the decomposition pressure

* Abstracted in part from the thesis by Donald F. Mastick in partial satisfaction of the requirements for the degree of Doctor of Philosophy in Chemistry at the University of California.

† Atomic Energy Commission Fellow, 1948–1949; present address: Technical Information Division, U. S. Atomic Energy Commission, Washington 25, D. C.

‡ This document is based in part on work performed under Contract No. W-7405-eng-48B for the AEC.

of the elements. From this pressure value together with entropy values one can then calculate the upper limit to the heat of formation. In most cases it will be a very high upper limit, since the oxide gaseous species will be very much less important than the gaseous elemental species.

When decomposition takes place to a stable gaseous species such as the vaporization of SiO_2 as SiO and O_2 gases, the same procedure as described above can be used to determine if other oxide species such as SiO_2 gas, for example, are important if the thermodynamic data for the decomposition products are available.

Of the oxide systems considered in this paper, stable gaseous oxide species have been demonstrated for the Pb, Cu, Sn, and Si oxide systems. For the oxides MnO, FeO, NiO, ZnO, CdO, and TiO, the observed total volatility has agreed with the calculated decomposition pressure of the elements within experimental error. Thus, they clearly belong to the third class discussed above. Any possible gaseous oxide species in these systems cannot be more important than the elemental species and undoubtedly are of negligible importance in reducing atmospheres. Also, the total volatility of SiO_2 has been shown to agree within experimental error with the decomposition pressure of SiO and O_2, which demonstrates that SiO_2 gas cannot be more important than SiO and indicates that SiO_2 is most likely a quite unimportant gaseous species.

If the spectroscopic value for the heat of dissociation is well established, one may combine this value with the heat of formation of the oxide and heat of sublimation of metal and of dissociation of O_2 to calculate the vapor pressure of the gaseous oxide at the appropriate temperatures. If these values are much lower than those observed, further verification of dissociation is obtained. Actually, the spectroscopic values are rarely of value, because of the uncertainties in fixing the ground states of the molecule and resulting atoms and the difficulties in extrapolating observed vibrational levels to the true dissociation limit. In many cases, it is the chemical determination which allows one to decide which of several possible spectroscopic values is correct.

The studies of FeO, NiO, MnO, and SiO_2 were conducted by measuring the rate of effusion from an inert Knudsen cell. The FeO, MnO, and SiO_2 were contained in platinum cells and the NiO in a BeO cell. These cells were crucibles with snug-fitting lids with concentric knife-edged effusion holes, about $\frac{1}{8}$ inch in diameter. A series of thin molybdenum spirals surrounded the crucibles, and a series of molybdenum disks supported on $\frac{1}{16}$-inch pins served to decrease heat loss outward and downward from the crucibles. Heat flow out the top was decreased by having above the crucibles a series of tantalum disks, each of which had a hole in the center. The size of each hole increased regularly with the distance from the effusion hole, so that an unobstructed cone was available for the escape of the molecular beam. Above these shields was a thin platinum collector plate suspended in a water-cooled copper holder. The geometry was such that about five percent of the vapor leaving the hole was collected.

The crucible and all the molybdenum and tantalum shielding were contained in a zircon crucible about 5.5 inches tall, 2.25 inches in diameter at the bottom, and 2.5 inches in diameter at the top. The zircon crucible rested on a zircon stand inside an externally water-cooled Pyrex tube. The vacuum within this tube was maintained between 1×10^{-5} mm and 4×10^{-5} mm during each run by a system of two oil diffusion pumps backed by a mechanical pump.

Energy was applied to the crucible from a water-cooled copper coil which surrounded the Pyrex water jacket. This coil was in series with a 20-kw spark gap converter. The temperature inside the crucible was read with a calibrated optical pyrometer focused through a hole in the collector plate at the plane of the effusion hole. Because of the small ratio of hole area to total inside area, no deviation from blackbody conditions was assumed. The temperature measurements were corrected for reflection and absorption by the windows of the vacuum system. Details of the equipment and procedure are given elsewhere.[1]

RESULTS AND CALCULATIONS

FeO

The instability of gaseous ferrous oxide has been indicated by the experimental work of Darken and Gurry.[2] They prepared the constant boiling oxide mixture at 1600°C, whose composition in atom ratio was O/Fe=1.116. From the known activity of iron in this mixture, the equilibrium oxygen pressure, and the vapor pressure of iron at 1600°C, they conclude the pressure of FeO(g) over this constant boiling mixture is negligibly small, since their calculation actually leads to a negative FeO(g) pressure.

In attempt to establish an upper limit to the FeO vapor pressure by an effusion method, the stationary constant boiling composition mentioned above is unsatisfactory because of the relatively high iron activity at this composition. It is desirable, then, to utilize another stationary composition or composition range in the iron-oxygen system in which the iron activity is greatly reduced relative to the FeO activity. The two-phase system liquid iron oxide—solid magnetite (Fig. 1) affords such a situation as the activity of iron and the oxygen pressure are constant for all compositions in this region along any given isotherm, and the iron activity is quite low.

The experimental data for the activity of iron and FeO and the equilibrium oxygen pressure in the iron-oxygen system are taken from Darken and Gurry's comprehensive paper[2] for the purposes of the thermodynamic calculations made herein.

[1] L. Brewer and D. F. Mastick (to be published). Brewer, Gilles, and Jenkins, J. Chem. Phys. **55**, 707 (1948).

[2] L. S. Darken and R. W. Gurry, J. Am. Chem. Soc. **68**, 798 (1946).

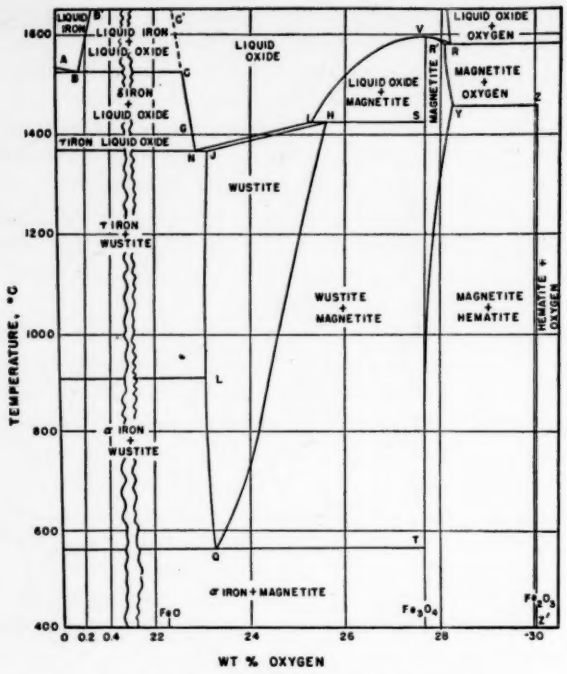

FIG. 1. Phase diagram for iron-iron oxides.

In the liquid oxide-solid magnetite region the partial pressure of oxygen is 3.02×10^{-5} atmos at 1773°K; and the activity of iron, relative to metallic iron as unity, is 3.47×10^{-3} at 1773°K. Combining this information with the hole area and given initial weight of Fe_3O_4, one can calculate the time required to lose an amount of $O_2(g)$ from the cell sufficient to cause the disappearance of the solid magnetite phase. The duration of each run was accordingly at least a factor of two lower than this calculated time interval. This precaution was necessary, since one cannot determine the phases present at the end of the run by x-ray diffraction analysis, because a final composition either in the two-phase region or in the liquid oxide region upon cooling will pass into the solid wustite and magnetite region (Fig. 1) and result in the identification of the magnetite phase.

The Fe_3O_4 was prepared by heating Baker's cp Fe_2O_3 in vacuum to 1300°C. At this temperature, the partial pressure of oxygen is initially 1 atmos over $Fe_2O_3(s)$ and drops to 1.48×10^{-2} atmos, at which point the $Fe_3O_4(s)$ phase appears. The oxygen pressure remains constant at this value until the $Fe_2O_3(s)$ phase disappears and then drops to 2.40×10^{-8} atmos as the composition changes by loss of oxygen through the magnetite solid solution region until the magnetite-wustite edge is reached. By observing the pressure changes when Fe_2O_3 is heated in an open platinum crucible one can easily tell when the conversion to Fe_3O_4 is complete. An added advantage of preparing Fe_3O_4 by this method is that volatile impurities are essentially excluded. This is quite important, since collections of the order of a few micrograms of iron are to be expected during the effusion runs and a small amount of chloride impurity, for instance, might introduce a great error by virtue of the high volatility of the iron chlorides. The weight change during the conversion was within 0.02 percent of the calculated stoichiometric value. Spectrochemical analysis showed less than 0.01 percent platinum was present in the iron oxide after heating at 1778°K for 30 minutes in the platinum effusion cell. Analysis of the resulting Fe_3O_4 indicated the following level of impurity: As, Co, Cr, Pb, Sn, not detected; Mo, Ni, 0.01–0.1 percent. X-ray diffraction pattern showed no iron oxide phases other than $Fe_3O_4(s)$ to be present. The lattice constant determined with $CuK\alpha_1$ radiation was $a=8.394\pm0.003$A.

TABLE I. Observed volatility of liquid FeO and calculated vapor pressure of FeO and Fe from effusion data.

Run	°K	Time sec$\times10^{-3}$	Wt. Fe on collector g$\times10^{6}$	P_{FeO} (atmos), assuming only FeO(g)	P_{Fe} (atmos), assuming only Fe(g)
1	1776	1.20	4.38	1.01×10^{-7}	0.89×10^{-7}
2	1776	1.80	9.33	1.44×10^{-7}	1.27×10^{-7}
3	1776	2.40	17.8	2.05×10^{-7}	1.81×10^{-7}

The deposits on the platinum collector plates were very difficult to dissolve. Consequently, the collector plates were sealed in thick-walled Pyrex tubes with 9N HCl and heated for six hours at 140°C. The resultant solutions were analyzed colorimetrically by a Carey recording spectrophotometer by 5100A, using orthophenanroline as the colorimetric reagent.

Table I gives the essential results of these measurements. The vapor pressures were calculated by use of the expression provided by kinetic theory of gases:

$$p=z(MT)^{\frac{1}{2}}/44.383a\cdot t, \qquad (1)$$

where p is the vapor pressure in atmospheres, z is the number of moles of the particular species effusing, M the molecular weight, a the area of the effusion hole in cm^2, and t the duration of the run in seconds. The vapor pressures given in columns 5 and 6 were calculated by Eq. (1), assuming first that FeO(g) was the only vaporizing species and secondly that Fe(g) was the only vaporizing species. The average value for $P_{Fe}=(1.32\pm0.47)\times10^{-7}$ atmos agrees exceptionally well with the value $P_{Fe}=1.59\times10^{-7}$ atmos from the activity of iron[2] and the vapor pressure of iron at this temperature.[3] Although it is apparent that the amount of iron collected may be accounted for by Fe(g) as the only important effusing species, the vapor pressures given in column five for FeO(g) serve as an upper limit for P_{FeO} in this system.

If one takes the values of the $(\Delta F-\Delta H_0)/T$ functions given by Johnston and Marshall[4] for the reaction NiO(s)=NiO(g) as being a reasonable approximation to the reaction under consideration, the average value for the upper limit of the vapor pressure of FeO, 1.50×10^{-7} atmos, may be used to calculate an upper limit to the

[3] K. K. Kelley, U. S. Bureau of Mines Bulletin 383 (1935).
[4] H. L. Johnston and A. L. Marshall, J. Am. Chem. Soc. **62**, 1382 (1940).

heat of dissociation of FeO(g) at 0°K. Using the available values for the heat of formation[5] of $Fe_{0.95}O(s)$, the heat of sublimation of iron,[6] and the heat of dissociation[6] of $O_2(g)$, one obtains

$$FeO(g)=Fe(g)+O(g), \quad \Delta H_0 \leq 98 \text{ kcal/mole}.$$

A definitive determination of this quantity from spectroscopic data is not possible since the ground state of FeO has not been fixed. Gaydon[7] has reviewed the spectroscopic data which give a linear Birge-Sponer[8] extrapolation to $\Delta H_0=115$ kcal/mole, which Gaydon reduces to $\Delta H_0=92\pm23$ kcal/mole to take into account the deviation from linearity. Comparison of this value with the upper limit $\Delta H_0 \leq 98$ kcal/mole indicates that the electronic state for which the Birge-Sponer extrapolation has been carried out must be the ground state or very close in energy to the ground state if the extrapolation is to the ground state atoms.

NiO

The apparent instability of FeO with respect to dissociation upon vaporization leads one to suspect that NiO would behave in a similar fashion by virtue of the close similarity in the chemical properties of iron and nickel. However, Johnston and Marshall[9] report that gaseous NiO shows only a negligible tendency to dissociate between the temperatures 1438 and 1566°K. There are other reports in the literature which conflict with this,[10] indicating in some cases a high dissociation pressure at lower temperatures.

The stability of gaseous NiO has been investigated by a thermodynamic treatment of Johnston and Marshall's excellent data and by experimental studies of the phase changes in solid NiO at high temperatures and the composition of the condensate resulting from effusion from a Knudsen cell containing NiO(s).

Johnston and Marshall determined the vapor pressure of NiO by measuring the rate of vaporization from a nickel ring which was slightly oxidized on its surface to NiO. The ring was supported in high vacuum and heated by induction. A determination of total weight loss per unit time was supplemented by a determination of the weight of oxygen lost during each run by subsequent reduction of the oxide film by hydrogen. Thus, assuming the only species which transported oxygen from the solid to the gas phase was NiO(g), the weight loss of Ni and NiO per unit time was determined.

In the calculation of vapor pressures from these data, Johnston and Marshall used the expression,

$$\log p+\log\alpha=\log m-\tfrac{1}{2}\log M+\tfrac{1}{2}\log T-1.647, \quad (2)$$

in which p is the pressure in atmospheres, α is the sticking coefficient, m is the weight loss in grams per cm² per second, and T is the temperature in °K. In their treatment α was assumed to be essentially unity, which is in accord with other results in the literature.[11]

They combine their calculated free energy functions for Ni(s) and NiO(s) with the free energy functions for $O_2(g)$ given by Johnston and Walker[12] and the standard heat of formation of NiO(s) at 298.1°K as given by Roth[13] in order to calculate the dissociation pressure of oxygen to be expected under their experimental conditions. The pertinent results of their treatment of the NiO vapor pressure data and their calculated O_2 dissociation pressure are given in Table II.

By using the $(F-H_0)/T$ functions of NiO(s) and NiO(g) in conjunction with the ΔF values as calculated from the NiO(g) vapor pressures given in Table II, Johnston and Marshall calculated the ΔH_0 for the sublimation of NiO(s). This value, $\Delta H_0=117{,}055\pm1000$ cal, was found to be essentially constant over the temperature range investigated. This fact and the calculated low values for the oxygen dissociation pressures were taken as definite indication that the dissociation of NiO(s) was quite negligible at these temperatures.

TABLE II. Observed vapor pressure of NiO reported by H. L. Johnston and A. L. Marshall (reference 9).

T°K	Initial O_2, g	Evap. loss total, g	Residual O_2, g	Time, sec	NiO evap. g	P_{NiO} atmos	P_{O_2} atmos
1438	0.01424	0.01732	0.01381	6930	0.00200	2.43×10^{-9}	
1441	0.00759	0.01160	0.00722	7001	0.00173	2.09×10^{-9}	7.76×10^{-10}
1495	0.01840	0.01803	0.01770	2286	0.00327	1.23×10^{-8}	3.29×10^{-9}
1511	0.00917	0.00465	0.00877	609	0.00187	2.66×10^{-8}	5.00×10^{-9}
1529	0.00921	0.01139	0.00837	1340	0.00392	2.72×10^{-8}	7.37×10^{-9}
1566	0.0044	0.01893	0.00289	759	0.0070	8.51×10^{-8}	1.84×10^{-8}

Now it was found that during their NiO vapor pressure runs the underlying Ni continued to vaporize essentially unimpeded through the NiO layer. Actually, their analyses show that the weight loss assumed to be due to NiO(g) varied from 12 to 46 percent of the total loss in their heatings. Thus, since the weight loss of oxygen is quite small relative to the total, it would be exceedingly difficult to fix the actual species responsible for the transference of the oxygen to the gas phase from their data alone.

In regard to their derivation of oxygen dissociation pressures it should be pointed out that the ratio of P_{NiO} to P_{O_2} is not actually as large as is indicated by their calculated pressures given in Table II. It will be

[5] L. Brewer, Atomic Energy Commission Declassified Paper UCRL-104 (1948).

[6] L. Brewer, *National Nuclear Energy Series* (McGraw-Hill Book Company, Inc., New York, 1950), Vol. 19B, Paper 3.

[7] A. G. Gaydon, *Dissociation Energies and Spectra of Diatomic Molecules* (John Wiley and Sons, Inc., New York, 1947).

[8] R. T. Birge and H. Sponer, Phys. Rev. **28**, 259 (1936).

[9] H. L. Johnston and A. L. Marshall, J. Am. Chem. Soc. **62**, 1383 (1940).

[10] H. W. Foote and E. K. Smith, J. Am. Chem. Soc. **30**, 1344 (1908); R. N. Pease and R. S. Cook, *ibid.*, **48**, 1199 (1926); L. Wohler and O. Balz, Z. Elektrochem. **27**, 406 (1931); A. Skapsky and J. Dabrowsky, *ibid.*, **38**, 365 (1932); A. F. Kapustinsky and L. Shamovsky, Z. anorg. u. allgem. Chem. **216**, 10 (1933).

[11] I. Langmuir, Phys. Rev. **2**, 329 (1913), and subsequent papers; F. H. Verhoek and A. L. Marshall, J. Am. Chem. Soc. **61**, 2737 (1939); Brewer, Gilles, and Jenkins, J. Chem. Phys. **16**, 797 (1948).

[12] H. L. Johnston and M. K. Walker, J. Am. Chem. Soc. **55**, 172 (1933); *ibid.*, **57**, 682 (1935).

[13] W. A. Roth, Z. angew. Chem. **42**, 981 (1929).

seen that the pressure which is obtained by Eq. (2) is a rather sensitive function of the molecular weight of species chosen for the calculation, this choice affecting the terms m and M. For instance, given the weight loss of oxygen per unit time, one can assume that either the species NiO(g) or $O_2(g)$ is responsible for the loss of oxygen from the solid NiO. The same oxygen weight loss then allows a calculated P_{NiO} *or* P_{O_2} which will have the ratio $P_{O_2}=0.327P_{NiO}$. The ratio of P_{O_2} to P_{NiO} as calculated by Johnston and Marshall (Table II) varies from 0.373 to 0.187. Thus, actually, the oxygen pressures which they have calculated from thermodynamic data appear to agree reasonably well with those which they would have obtained if they had treated their experimental data for the species $O_2(g)$ rather than NiO(g). In other words, the ΔH_0 of formation of NiO(s) which they used would agree very well with the average ΔH_0 which one would obtain by a treatment of their oxygen loss data assuming only dissociation to be occurring. From their calculated O_2 pressures (Table II) and the free energy functions which they used, one finds they had used $\Delta H_0=59.5$ kcal. Again using the same functions and the O_2 pressures derived from their experimental data, one obtains $\Delta H_0=59.3$ kcal.

The second point to be made concerning the ratio of P_{NiO} to P_{O_2} given by Johnston and Marshall concerns the ΔH_0 which they have used in calculating their dissociation pressures. The National Bureau of Standards[14] gives $(\Delta H_{298}-\Delta H_0)=0.6$ for the reaction NiO(s) $=$Ni(s)$+\frac{1}{2}O_2(g)$. The heat of the reaction is greater at 298.1°K than at 0°K. However, Roth's value, which they use as ΔH_{298}, is 58.9 kcal. The only explanation for the $\Delta H_0=59.5$, which they apparently use in calculating their O_2 pressures, is that they added the $(\Delta H_{298}-\Delta H_0)$ correction to Roth's heat rather than subtracting. This then introduces an error of about one kilocalorie in their ΔF of dissociation and results in O_2 pressures which are roughly a factor of two lower than would result from the proper use of the $(\Delta H_{298}-\Delta H_0)$ correction. In view of these two factors, one is no longer justified in concluding that dissociation is negligible relative to direct vaporization.

A recent evaluation by Brewer[5] of existing data on the heat of dissociation places the most probable value at $\Delta H_{298}=57.5$ kcal. If this were used instead of Roth's value, even higher dissociation pressures would result from such calculations. However, it will be recalled that the treatment of Johnston and Marshall's experimental data gave the still higher heat $\Delta H_{298}=59.9$, which, of course, means that the oxygen pressures calculated from their data will be lower than those calculated by the use of Brewer's heat and the free energy functions used by Johnston and Marshall. Thus, use of either value supports the dissociation mechanism. Therefore, it appears that the dissociation mechanism is the only hypothesis by which Johnston and Marshall's data assumes the best fit to existing thermodynamic data.

With respect to the discrepancy between the heat of formation of NiO(s) derived from Johnston and Marshall's data and that which Brewer gives, it should be mentioned that there is apparently some error in the high temperature heat capacity data[15] which Johnston and Marshall used in calculating the free energy functions for NiO(s).[16] However, the main difference is probably due to the greater heat of formation of nickel oxide of a composition saturated with Ni (as in the experiments discussed above) compared with the heat of formation of nickel oxide compositions of high oxygen content which would be expected to be present in systems at lower temperatures.

The NiO used in the experimental studies reported below was obtained from a bottle of Baker's cp NiO and gave the following spectrochemical analysis: Be, Co, Fe, Ti, and V, not detected. The carbon content, determined by microcombustion, was 0.006 percent. No further purification was attempted. All samples were air dried at 140°C for 48 hours prior to use.

While, in general, it is desirable thermodynamically to use refractory metal containers for oxides at high temperatures, it was found that W was very unsatisfactory as rapid reduction of the NiO occurred, forming the volatile tungsten oxides and the low melting W-Ni eutectic. By this one could rule out Ta and Mo, as the former was quite unstable towards FeO at 1600°C within one hour, and the latter has essentially the same electronegativity as W, oxides of high volatility at these temperatures, and a low melting eutectic. Considering the high difference in the ionic radii of Be^{++} and Ni^{++}, which would lead one to expect only slight solid formation between BeO(s) and NiO(s), and the fact that the minimum in the NiO-BeO liquidus curve occurs at 1890°C, which is well above the temperature range investigated, BeO was used as the container.

Three effusion runs were made, two at 1816°K for 60 minutes each, and one at 1782°K for 100 minutes. After the first run tiny globules of metallic Ni were found on the crucible walls as a result of condensation. Otherwise, the walls and lid were clean except for a continuous blue coloration. X-ray diffraction and spectrochemical analyses were made of the effusate which collected on a water-cooled Pt plate and of the solid remaining in the crucible.

The effusate, aside from large amounts of Ni, showed the following spectrochemical analysis: Co, V, Ti, not detected; Be and Fe, ~0.01 percent. X-ray diffraction showed the existence of two phases: Ni(s) and NiO(s). The same analyses carried out on the solid remaining in the crucible after heating for 220 minutes showed spectrochemically: Co, V, T, not detected; Be, Fe,

[14] *Selected Values of Chemical Thermodynamic Properties*, National Bureau of Standards (U. S. Government Printing Office, Washington, D. C.), 1947 et seq.

[15] A. F. Kapustinsky and Novoseltsev, J. Phys. Chem. (U.S.S.R.) **11**, 61 (1938).

[16] Personal communication from K. K. Kelley, U. S. Bureau of Mines, Berkeley, California.

<0.01 percent; by x-ray diffraction, two phases were present: Ni(*s*) and NiO(*s*). It is seen that BeO is a satisfactory container for NiO(*s*) at these temperatures.

At first inspection, these results appear to show dissociation occurring in such a manner to bring about a continuous production of a Ni phase by virtue of the loss of oxygen. However, from Johnston and Marshall's data one calculates that at 1438°K, for example, the ratio of oxygen atoms to nickel atoms vaporizing from a surface mixture of nickel and nickel oxide or from an effusion chamber containing both nickel and nickel oxide phases should be about 0.1. Thus, if one vaporizes such a mixture at constant temperature, the nickel phase will eventually disappear, leaving a nickel oxide phase which will continue to lose nickel. As the nickel content of the nickel oxide solid solution decreases, the nickel partial pressure will decrease and the oxygen partial pressure will rise until the composition of the solid is equal to the composition of the vapor. When this is reached, one will have a constant vaporizing mixture which will vaporize without change in composition. If one starts well inside the nickel oxide solid-solution range, the rate of escape of oxygen is higher than the rate of escape of nickel and the oxygen content of the solid solution decreases until the constant vaporizing mixture is reached.

Thus, upon heating NiO one should not form any Ni metal phase at the high temperature. However, if the solubility of Ni in the nickel oxide phase or the extreme limit of the nickel oxide solid-solution range decreases with decreasing temperature sufficiently, and if the constant vaporizing composition is close enough to the Ni-rich limit of the nickel oxide solid-solution range, then one can obtain a nickel phase upon cooling the single phase constant vaporizing nickel oxide solid solution due to disproportionation to metallic nickel and a nickel oxide solid solution higher in oxygen content. This appears to be the case for nickel oxide, since one obtains a mixture of nickel metal phase and nickel oxide phase upon cooling the constant vaporizing nickel oxide. Also, one obtains nickel and nickel oxide phases in the sublimate because of the disproportionation of the same constant vaporizing composition.

No data are available in the literature on the Ni-NiO phase diagram, but these results indicate that study of this system will show a wide solid-solution range for the nickel oxide range with an increasing solubility of nickel in the oxide phase with increasing temperature.

In order to establish definitely the absence of reducing agents in the Baker's NiO which could account for the presence of nickel after heating, the nickel oxide was heated for 90 minutes at 1302°K. In a second run, the NiO was heated to 1629°K for 4 minutes, cooled to 1296°K over 12 minutes, and held at 1296°K for 60 minutes. Under these conditions, essentially no change in composition will result from volatilization; and if a metallic nickel phase is found after the heating, it must be due to a reducing impurity in the NiO. In both cases the x-ray diffraction pattern was exactly similar to that of the original nickel oxide with no metallic nickel lines being visible. These results exclude the possibility of reducing agents being responsible for the appearance of the metallic nickel phase in the effusion runs. Furthermore, the second heating to 1629°K and subsequent slow cooling shows that the NiO was not originally a metastable phase as no metallic nickel phase resulted from this treatment. Since analysis indicates the composition of the starting nickel oxide is $NiO_{0.995}$, the constant vaporizing composition at 1800°K must be richer in nickel than $NiO_{0.995}$ and the nickel-rich solid-solution limit at 1800°K must be even richer in nickel content.

From these results one is led to conclude that vaporization by dissociation is the major way in which NiO vaporizes, since loss of only the species NiO(*g*) would not account for the observed phase changes.

Taking the vapor pressures for NiO(*g*) given by Johnston and Marshall as an upper limit, the upper limit to the heat of dissociation of NiO(*g*) at 0°K is ≤ 99 kcal/mole. Spectroscopic D_0 values for this reaction are not available for comparison.

MnO

Relatively little is known concerning the manganese-oxygen phase diagram. Le Blanc and Wehner[17] have found that MnO prepared in a vacuum takes up oxygen up to the composition $MnO_{1.13}$ with no change in phase. Assuming the activity of MnO to be essentially unity throughout the MnO solid-solution range, one may investigate the volatilization of MnO by measuring the rate of weight loss from an effusion cell containing manganese oxide whose composition falls within this range. Such measurements may be conducted by heating Mn_3O_4 to high temperatures in vacuum. At 1767°K the partial pressure of oxygen over Mn_3O_4 is about 1.9 atmos; and therefore, the composition changes rapidly by loss of oxygen until the MnO solid-solution edge is reached. During this time interval a negligible amount of Mn will volatilize, since the Mn activity is very low in the Mn_3O_4 region. Owing to the high decomposition pressure of Mn_3O_4, it is not possible to determine the vapor pressure of an invariant two-phase system containing both Mn_3O_4 and MnO in a manner similar to the above study of the $FeO-Fe_3O_4$ system.

The Mn_3O_4 used in these determinations was prepared by heating Merck's Reagent grade MnO_2 at 950°C in vacuum. Krüll[18] has observed that dissociation of MnO_2 and Mn_2O_3 occur readily in the range 900–1000°C, whereas Mn_3O_4 was not observed to dissociate to MnO at an appreciable rate below 1300°C. The MnO_2 was consequently heated at 950°C until the pressure in the vacuum line dropped to a value which indicated that rapid gas evolution was occurring no longer. The resultant Mn_3O_4 was a deep rust color and upon x-ray

[17] M. Le Blanc and G. Wehner, Z. Physik. Chem. **A168**, 59 (1933).

[18] F. Krüll, Z. anorg. Chem. **208**, 134 (1932).

TABLE III. Observed volatility of MnO and calculated pressures of MnO and Mn from effusion data.

Run	°K	Time sec×10⁻³	Wt. Mn collected (g×10⁶)	P_{Mn} (atmos) assuming Mn(g) species	P_{MnO} (atmos) assuming MnO(g) species
1	1767	1.80	49	6.7×10^{-7}	7.6×10^{-7}
2	1767	2.40	73	7.55×10^{-7}	8.55×10^{-7}

diffraction examination was shown to contain no other phases than Mn_3O_4. The tetragonally distorted spinel structure had the lattice constants $a=5.76\pm0.01$A, $c=9.44\pm0.01$A with Cu$K\alpha_1$ radiation. Spectrochemical analysis indicated the following level of impurities: As, Co, Ni, Sn, Pb, Cr, not detected; Mo, 0.1–1 percent; Na, 0.2 percent; Fe<0.01 percent.

Spectrochemical analysis of the resultant MnO after a 40-minute heating at 1767°K showed <0.01 percent platinum was picked up from the container. The deposit was dissolved from the 2-mil platinum collector plate with 36N H_2SO_4, oxidized with KIO_4 and determined colorimetrically as permanganate on a Carey Recording Spectrophotometer. X-ray diffraction patterns of the residue in the effusion cell after each run showed that only the MnO phase was present. The lattice constants for the face-centered cubic phase were $a_0=4.438\pm0.004$A and $a_0=4.441\pm0.002$A for the MnO resulting from runs 1 and 2, respectively (Table III), as determined with Cu$K\alpha_1$ radiation.

Table III gives the results of the effusion measurements. Columns 5 and 6 were calculated from the data, assuming the gaseous manganese species in equilibrium with MnO(s) to be Mn(g) and MnO(g), respectively.

In view of the agreement between the results of runs 1 and 2 the average values $P_{Mn}=7.1\times10^{-7}$ atmos and $P_{MnO}=8.1\times10^{-7}$ atmos are used in the calculation of the value of $\Delta F/T$ for the two possible reactions under consideration:

$$MnO(s)=Mn(g)+\tfrac{1}{2}O_2(g), \quad (3)$$

$$MnO(s)=MnO(g). \quad (4)$$

Within the desired accuracy of this research it is assumed that $P_{Mn}=2P_{O_2}$ in reaction (3) and that the pressures of Mn(g) and MnO(g) given above are upper limits. For reaction (3), $\Delta F/T=42.23$ kcal/mole. Combining this value with available $(F-H_0)/T$ values[5,19,20] for the species in reaction (3), one obtains the heat for the reaction: $\Delta H_{298}=161.5$ kcal/mole. Brewer[5,6] gives $\Delta H_{298}=-92.0$ kcal/mole for the reaction $Mn(s)+\frac{1}{2}O_2(g)=MnO(s)$ and $\Delta H_{298}=68.63$ kcal/mole for the heat of sublimation of manganese. Thus, for the reaction (3) the thermochemical value for the heat is $\Delta H_{298}=160.6$ kcal/mole. Since the difference of one kcal/mole is probably within the accuracy allowed by the assumptions made herein, this constitutes very good agreement between the value calculated on the assumption of a dissociation mechanism and the thermochemical value for the same reaction.

The $\Delta F/T$ value for reaction (4), as calculated from the experimental P_{MnO}, is $\Delta F/T=27.8$ kcal/mole. Assuming the $(F-H_0)/T$ functions for MnO(g) to be essentially equal to those for NiO(g),[9] allowing for the difference in molecular weights, the experimentally determined lower limit to the heat for reaction (4) is $\Delta H_0\geq113$ kcal/mole. Combining this value with those for the heat of formation of MnO(s),[5] the heat of sublimation of Mn(s),[6] and the heat of dissociation of $\frac{1}{2}O_2(g)$,[6] one calculates the value $\Delta H_0\leq107$ kcal/mole for the reaction

$$MnO(g)=Mn(g)+O(g).$$

The value given for this reaction by Gaydon[7] from an inspection of spectroscopic data is $D_0=92$ kcal/mole. The divergence between these two values is indication that the vapor pressure of MnO(g) is much lower than the upper limit given above if the value given by Gaydon is for the dissociation of the MnO molecule from its ground state. The upper limiting value obtained in this work establishes Gaydon's value as resulting from the ground state or one quite close to the ground state.

SiO

The results obtained by heating high purity SiO_2 in a platinum effusion cell are given in Table IV. After each run the deposit on the platinum collector plate was heated in air to 600°C. No weight increase was observed, showing the deposit to be SiO_2. The vapor pressures for SiO(g) were calculated assuming SiO_2 vaporizes chiefly in accord with the reaction:

$$SiO_2(s)=SiO(g)+\tfrac{1}{2}O_2.$$

The calculated ΔF for this reaction for each run is given in column six.

From these data the heat of reaction for the dissociation of SiO(g) is calculated:

$$SiO(g)=Si(g)+O(g),$$
$$\Delta H_0=165 \text{ kcal/mole or } 7.2 \text{ ev/molecule.}$$

Since this agrees within experimental error with the ΔH_0 of SiO(g) obtained from the data described below, it would appear that SiO_2 molecules are less important than SiO molecules in the vapor. The SiO and O_2 molecules apparently recombine on the collector plate to give SiO_2.

The vapor pressure of SiO(g) over the mixture

TABLE IV. Observed vapor pressure of SiO_2.

Run	°K	Time sec×10⁻³	Wt. on collector g×10⁹	P_{SiO} atmos	ΔF
1	1840	2.40	0.5	4.06×10^{-6}	69.3
2	1933	3.72	1.4	7.47×10^{-6}	69.5
3	1951	6.60	2.3	7.02×10^{-6}	70.2

[19] K. K. Kelley, U. S. Bureau of Mines Bulletin 434 (1948).
[20] K. K. Kelley, U. S. Bureau of Mines Bulletin 476 (1949).

$Si(s)+SiO_2(s)$ has been studied by Geld and Kochnev,[21] who measured the rate of weight loss from a quartz effusion cell in which the mixture was heated in vacuum. The existence of $SiO(g)$ as a stable gaseous species was established by the observed volatility under conditions where neither $Si(s)$ nor $SiO_2(s)$ has appreciable vapor pressure.[21] Their observed entropy of vaporization, 35 eu, indicates that at the temperatures 900–1155°C the Si and SiO_2 solid phases may react to form a $SiO(s)$ phase, since the expected entropy of sublimation $SiO(s)=SiO(g)$ should be about 34 eu, whereas for the reaction $\frac{1}{2}Si(s)+\frac{1}{2}SiO_2(s)=SiO(g)$ the entropy is about 42 eu.

Because of the uncertainty of the actual reaction occurring under their experimental conditions, it is not possible to make a conclusive calculation of the heat of dissociation of the SiO molecule from their data. Assuming only the $SiO(s)$ phase present during volatilization, one calculates $D_0(SiO)=170$ kcal/mole or 7.4 ev; and assuming the phases $Si(s)+SiO_2(s)$ present, one calculates $D_0(SiO)=160$ kcal/mole or 7.0 ev. From a linear Birge-Sponer extrapolation of the ground $^1\Sigma$-state of SiO Herzberg[22] obtains $D_0(SiO)=7.4$ ev, and Gaydon[7] gives $D_0(SiO)=7.8$ ev (correcting for slight positive curvature) assuming unexcited atomic products. Linear extrapolation of the $^1\Pi$-state of SiO yields $D_0(SiO)=8.9$ ev for the ground $^1\Sigma$-state if the $^1\Pi$-state goes to unexcited atoms as Gaydon suggests. However, $D_0(SiO)$ may assume lower values if the $^1\Pi$-state goes to excited atoms. Gaydon chose 8 ± 1 ev but indicated it as very uncertain.

The chemical values of 7.0, 7.2, and 7.4 ev indicate that the linear extrapolation of the $^1\Sigma$-state gives a reasonably correct value for the heat of dissociation of $SiO(g)$.

The Remaining Oxides

In the calculations of reported experimental results on the vapor pressure of SnO and the oxides which follow, the sources of thermochemical data are as follows: heats of formation of solid oxides, Brewer;[5] National Bureau of Standards, *Selected Values of Chemical Thermodynamic Properties*;[14] thermodynamic properties of the elements, Brewer;[6] entropies of inorganic compounds and elements at 298.1°K, Kelley;[19] S_T-S_{298} and H_T-H_{298} and heat capacity values for inorganic compounds and elements, Kelley;[20] dissociation energies of diatomic oxides, Gaydon[7] and Herzberg.[22]

SnO

The recent investigation of the stability and volatility of tin oxides carried out by Vesselovsky[23] essentially establishes the fact that SnO is a stable gaseous species. The volatility of a mixture of $SnO_2(s)+Sn(l)$ was studied in vacuum at temperatures where neither $SnO_2(s)$ nor $Sn(l)$ have an appreciable volatility (721–893°C).[23] The thirteen vapor pressure measurements were combined with high temperature heat content and entropy data to yield

$$Sn(s)+SnO_2(s)=2SnO(g),$$
$$\Delta H_{298}=136.9\pm0.7 \text{ kcal/mole}.$$

The heat of dissociation of the SnO molecule was calculated by use of the following thermochemical data:

$$\begin{aligned}
Sn(s)+O_2(g)=SnO_2(s), &\quad \Delta H_{298}=-138.8 \text{ kcal/mole};\\
2Sn(g)=2Sn(s), &\quad \Delta H_{298}=-140.0 \text{ kcal/mole};\\
2O(g)=O_2(g), &\quad \Delta H_{298}=-118.6 \text{ kcal/mole};\\
Sn(g)+O(g)=SnO(g), &\quad \Delta H_{298}=-130.2 \text{ kcal/mole};\\
&\quad \Delta C_p=-1.4 \text{ cal/mole/deg},\\
&\quad \Delta H_0=-131.6 \text{ kcal/mole},\\
D_0(SnO)=131.6 &\text{ kcal/mole},\\
=5.70 &\text{ ev/molecule}.
\end{aligned}$$

It is of interest that Herzberg obtains the value 5.6 ev by a long linear extrapolation of lower vibrational levels and that Gaydon reduces this value to 3.2 ev by empirical methods to correct for nonlinearity of the vibrational levels. It appears that an uncorrected linear extrapolation of the vibrational levels gives the correct dissociation limit.

ZnO

Although the experimental techniques employed by Feiser[24] in the determination of the volatility of ZnO are not commensurate with high accuracy, the values so obtained are the only ones available. The volatility was measured by the rate of weight loss from an open sample heated in a static atmosphere. The vapor pressure of metallic zinc was calculated from the heat of formation of ZnO and the heat of sublimation of Zn at the temperatures which Feiser reported. The calculated Zn partial pressures over ZnO are a factor of 2–3 greater than the ZnO pressures reported by Feiser. This is undoubtedly due to presence of oxygen in the atmosphere used. Therefore, one can conclude that the Zn partial pressure over ZnO is much higher than the ZnO partial pressure in an inert atmosphere.

Taking Feiser's values as upper limits to the vapor pressure of $ZnO(g)$, the calculated value for the heat of dissociation of $ZnO(g)$ to the gaseous atoms is $\Delta H_0\leq92$ kcal/mole.

CdO

Ueno[25] has reported the results of measurements of the vapor pressure of CdO which were made by the effusion method. Since his experimental techniques were of an accurate nature and he gives a comprehensive report of the data taken, a more extensive treatment of his results has been made.

[21] P. V. Geld and M. I. Kochnev, Repts. Acad. Sci. U.S.S.R. **61**, No. 4 (1948).
[22] G. Herzberg, *Molecular Spectra and Molecular Structure* (D. Van Nostrand Company, Inc., 1950), second edition, Vol. I.
[23] B. K. Vesselovsky, J. Appl. Chem. (U.S.S.R.) **16**, 397 (1943).
[24] J. Feiser, Metall u. Erz **26**, 269 (1929).
[25] K. Ueno, J. Chem. Soc. Japan **62**, 990 (1941).

TABLE V. Vapor pressures of CdO and Cd calculated from effusion data, and heat of formation of CdO.

T°K	P_{CdO} (atmos)	P_{Cd} (atmos)	$-\Delta H_{298}$
1003	1.27×10^{-6}	1.45×10^{-6}	66.03
1013	1.68×10^{-6}	2.00×10^{-6}	66.08
1023	1.27×10^{-6}	2.46×10^{-6}	65.90
1033	3.00×10^{-6}	3.17×10^{-6}	65.89
1043	4.16×10^{-6}	4.27×10^{-6}	65.80
1053	5.30×10^{-6}	5.76×10^{-6}	65.95

In Table V, column 2, the vapor pressures of $CdO(g)$ reported by Ueno are given. Column 3 gives the vapor pressures of $Cd(g)$ as calculated from thermochemical data. The calculated values for P_{Cd} are in very good agreement with those for P_{CdO}. Thus, the CdO vaporization falls in the third class of vaporization and must vaporize largely by the reaction $CdO(s)=Cd(g)+\frac{1}{2}O_2(g)$.

From the weight loss of the effusion cell per unit time which Ueno reports, the standard heat of formation of CdO may be calculated. In order to do this it is necessary to have some knowledge of the ratio of escaping $O_2(g)$ molecules to $Cd(g)$ atoms in order to apply the reported weight losses to such a calculation. During the vapor pressure measurement the composition of the solid necessarily falls within the CdO solid-solution range because at the Cd−CdO edge the vapor pressure of Cd is about 0.9 atmos and $P_{O_2}=3.0\times10^{-5}$ atmos and at the CdO−O_2 edge, $P_{Cd}=7.3\times10^{-9}$ atmos and $P_{O_2}=1$ atmos at 1000°K. It is assumed that the composition change in the solid is so small that its composition is essentially stoichiometric CdO. Since the Cd atoms and O_2 molecules are escaping in the ratio $Cd:\frac{1}{2}O_2$, the square-root dependence of the rate of escape will not give pressures of $Cd(g)$ and $O_2(g)$ of this same ratio. This effect has been taken into account in the calculations. The equilibrium constants obtained in this manner have been combined with available free energy functions to give the standard heat of formation for the reaction $Cd(s)+\frac{1}{2}O_2(g)=CdO(s)$. The value for each experimental temperature is given in column 4, Table V, the average value being $\Delta H_{298}=-65.9\pm0.1$ kcal/mole. Bichowsky and Rossini[26] give for the same reaction $\Delta H_{298}=-65.2$ kcal/mole, whereas the Bureau of Standards Tables give $\Delta H_{298}=-60.86$ kcal/mole.

If one takes the vapor pressures given by Ueno as an upper limit to P_{CdO} at the reported temperatures, the calculated upper limit to the heat of dissociation of the gaseous CdO molecule to gaseous atoms is $\Delta H_0\leq88$ kcal/mole.

CuO

The stability of gaseous CuO is indicated by the measurement of the vapor pressure of solid CuO by Mack, Osterhof, and Krauer.[27] Although their experimental methods are subject to large error, the vapor pressures of $Cu(s)$ which they determined in conjunction with those of $CuO(s)$ agree reasonably with those given by Kelley;[3] and, therefore, it is assumed that the values given for CuO are reasonably accurate. The values given by Mack *et al.* for the vapor pressures of $CuO(g)$ between 873° and 1223°K are a factor of 10^6–10^8 higher than the vapor pressure of $Cu(g)$ in equilibrium with $CuO(s)$ as calculated from the heat of formation of $CuO(s)$. Since these experiments were conducted in 1 atmos O_2, it must be concluded that the principal gaseous species is $CuO(g)$.

Since this stability is out of line with that of $FeO(g)$ and $NiO(g)$, it is possible that polymerization to $Cu_2O_2(g)$ is contributing to the observed stability.

From the vapor pressures given by Mack *et al.* one calculates the heat of dissociation of $CuO(g)$ to gaseous atoms to be $\Delta H_0=113$ kcal/mole.

PbO

Feiser[24] also reports measurements of the volatility of PbO by the same method used to determine the vapor pressure of ZnO described above. The values given for temperatures between 1023° and 1323°K are at least a factor of 10^2 higher than those which one calculates for the vapor pressure of $Pb(g)$ in equilibrium with $PbO(s)$ at those temperatures. Thus, one is led to conclude that $PbO(g)$ is a stable gaseous species under these conditions. From the vapor pressures given by Feiser one calculates the heat of dissociation of $PbO(g)$ to gaseous atoms to be $\Delta H_0=98$ kcal/mole. Herzberg gives for this value $D_0(PbO)=99$ kcal/mole from a linear Birge-Sponer extrapolation, and Gaydon gives $D_0(PbO)=76$ kcal/mole by correction of the extrapolated value for nonlinearity by empirical methods. As in the case of SnO, it appears that the linear extrapolation gives the better agreement with the chemical value.

GeO

No experimentally determined values for the vapor pressures of GeO are available. However, Herzberg gives $D_0(GeO)=159$ kcal/mole by a linear extrapolation, and Gaydon gives $D_0(GeO)=127$ kcal/mole. Although the results for PbO and SnO indicate that the linear extrapolation given by Herzberg is probably a better value than that given by Gaydon, the latter is taken as a lower limit to the stability of the $GeO(g)$ molecule. If the standard heat of formation of $GeO(s)$ is taken as $\Delta H_{298}=-64$ kcal/mole, one then may calculate that at 1000°K the vapor pressures of $GeO(g)$ and $Ge(g)$ in equilibrium with $GeO(s)$ are, respectively, 6.2×10^{-8} atmos and 3.6×10^{-14} atmos. If the values given by Herzberg and Gaydon are for the ground state of GeO molecule dissociating to unexcited atoms, then the stability of gaseous GeO at 1000°K is strongly indicated by these calculations.

[26] F. R. Bichowsky and F. D. Rossini, *The Thermochemistry of Chemical Substances* (Reinhold Publishing Company, New York, 1936).

[27] Mack, Osterhof, and Krauer, J. Am. Chem. Soc. **45**, 617 (1923).

TiO

From Ehrlich's[28] observation that about 1 percent of a sample of TiO volatilized in 15 min at 1600°C and from the dimensions of the containing vessel, one can calculate an approximate vapor pressure of TiO at 1873°K: $P_{TiO}=1.1\times10^{-5}$ atmos. Using $\Delta H_{298}=-124.2$ kcal/mole for the heat of formation of TiO(s)[29] for its entire homogeneity range, one calculates $P_{Ti}=2.5\times10^{-6}$ atmos and $P_O=10^{-14}$ atmos at 1873°K for the TiO phase saturated with titanium metal. That the oxygen partial pressure will not increase greatly across the homogeneity range can be seen by calculating the oxygen partial pressure for the composition saturated by Ti_2O_3 using $\Delta H_{298}=-367$ kcal for Ti_2O_3.[14] Thus, the solid TiO must lose more Ti atoms than O atoms, and the composition must change towards an oxide of lower Ti content. Therefore, there is no invariant vaporizing composition within the TiO homogeneity range. The factor of four between the P_{TiO} calculated from Ehrlich's observation and P_{Ti} over the TiO solid solution must be attributed to the very crudeness of the observational data.

An upper limit to the heat of dissociation of TiO(g) to gaseous atoms is $\Delta H_0\leq184$ kcal/mole, calculated by assuming $P_{TiO}=1.1\times10^{-5}$ atmos as a generous upper limit. That the actual partial pressure of TiO(g) must be much smaller is shown by comparison of the value $\Delta H_0\leq184$ kcal/mole with the spectroscopic values D_0(TiO)=159 and 127 kcal/mole given, respectively, by Herzberg by a linear Birge-Sponer extrapolation and by Gaydon, who corrects the extrapolation for nonlinearity.

SUMMARY

The results of the above investigation are summarized in Table VI. The first column gives the oxide, the second column the temperature or temperature range for which the vapor pressure has been measured or calculated, the third, the predominate gaseous species in equilibrium with the oxide at the indicated temperature; the fourth, the calculated upper limit to, or the value for, the heat of dissociation as determined by chemical means; the sixth, the values given by Herzberg (LB) and Gaydon (LBC), in which the former has used a linear Birge-Sponer extrapolation of vibrational levels and the latter corrected the linear extrapolation by empirical methods.

It is evident that a large uncertainty is inherent is the spectroscopic values for D_0 for two reasons: (1) when only a few lower vibrational levels are available for extrapolation to the dissociation limit, one cannot be certain of the linearity of the change in energy between successive levels, and (2) in many cases it is not known whether or not the particular set of vibrational levels is for the ground-state molecule dissociating to unexcited atoms. Chemical determination of the D_0 are necessary in many cases to establish the ground state dissociation energy.

TABLE VI. Gaseous species in equilibrium with solid diatomic oxides, temperature ranges, chemical and spectroscopic heats of dissociation of the gaseous oxides.

Oxide	Temp. range, °K	Gaseous species	D_0 (kcal/mole)	Spectroscopic D_0 (kcal/mole) LB	LBC
FeO	1776	Fe, O_2	$\leq$98	···	92±23
NiO	1400–1566	Ni, O_2	$\leq$99	···	···
MnO	1767	Mn, O_2	$\leq$107	101	92±13
SiO_2	1173–1428, 1900	SiO	160, 165, 170	170	184±23
SnO	994–1166	SnO	132	129	74±23
ZnO	1673–1748	Zn, O_2	$\leq$92	···	···
CdO	1003–1053	Cd, O_2	$\leq$88	···	···
CuO	873–1223	CuO	113	156	104±35
PbO	1023–1323	PbO	98	99	76± 9
GeO	1000	GeO	···	159	127±23
TiO	1873	Ti, O_2	$\leq$184	159	127±23

Such is the case for PbO; Table VI gives $D_0=99$ kcal/mole in which Herzberg chose the $^1\Sigma$-state as the ground state and applied a linear extrapolation to the seven available levels. On the other hand, Gaydon assumed the $^1\Sigma$-state probably goes to the Pb ($^3P_1$) atom, which would give $D_0=78$ kcal/mole, which he lowered to 76 kcal/mole by empirical methods. It is evident that if the chemical evidence is correct, the linear extrapolation of the $^1\Sigma$-state to unexcited Pb and O atoms is the proper interpretation. Vago and Barrow[30] give the heat of dissociation of PbO, which is in agreement with the value given by Herzberg, and give the reasoning by which they conclude PbO dissociates to the unexcited atoms.

Another conclusion which may be drawn from Table VI is that for the oxides of the fourth-group elements the linear extrapolation appears to be correct, rather than Gaydon's application of an empirical corrective factor to the extrapolation. This is shown particularly by the chemical D_0 values for SnO and PbO, and less conclusively by SiO. While not discussed in this paper, it is of interest to note that the D_0 for CO obtained by a linear extrapolation is in good agreement with thermochemical values obtained from a recent determination[31] of the heat of sublimation of graphite.

Of course, this behavior cannot be a general one, since Gaydon[7] has clearly demonstrated that many molecules display a linear decrease in vibrational spacing only for a relatively small number of levels, and the correction factors that he applies for nonlinearity should, in general, give better D_0 values. As more D_0 values become firmly established by direct chemical studies, it should become possible to give a firmer basis to these correction factors. It is encouraging that a group of related molecules like CO, SiO, SnO, and PbO show a similar behavior in regard to the correction to the Birge-Sponer extrapolation.

[28] P. Ehrlich, Z. Electrochem. **45**, 362 (1939).
[29] K. K. Kelley, U. S. Bureau of Mines, Berkeley, California, private communication.
[30] E. E. Vago and R. F. Barrow, Proc. Phys. Soc. (London) **59**, 449 (1947).
[31] Brewer, Gilles, and Jenkins, J. Chem. Phys. **16**, 797 (1948).

Photoneutron Fission Analysis for U-235 in High Purity U-238*†

R. L. Macklin and J. H. Lykins
K-25 Laboratories, Carbide and Carbon Chemicals Division, Union Carbide and Carbon Corporation, Oak Ridge, Tennessee

(Received March 22, 1951)

The photoneutron method for the analysis of U-235 in high purity U-238 is described. Special samples have been found to contain as little as 5 parts per million U-235. An upper limit for the thermal neutron fission cross section of U-238 can be set at 5×10^{-28} cm².

INTRODUCTION

A QUANTITY of high purity U-238 was prepared in 1946 for use in special research problems. The analysis of residual impurities, particularly U-235, was achieved by the photoneutron fission method to be described.

METHOD

The use of moderated radium gamma-beryllium photoneutrons for the analysis of U-235 had been suggested earlier by Beyer.[1] The advantage of this method lies in the virtual elimination of U-238 fission, so that the fission rate is strictly proportional to the U-235 content of the sample measured. The threshold for U-238 fission[2] is 1.0±0.1 Mev, while the maximum energy of the neutrons from the radium *C*-beryllium, gamma-neutron reaction[3] is 0.69 Mev.

Fission counters of the parallel plate ionization chamber type were used. A central well in a six-inch cube of beryllium contained the radium source (usually 2 grams). The ionization chamber containing the sample was placed at a face of the beryllium cube. The whole assembly was surrounded with about a six-inch layer of petrolatum and an outer lead shield. The ionization chamber was continually flushed with a slow stream of dry nitrogen to permit electron collection. This gave pulses with a quite fast rise time. The electronic amplifier incorporated a filter to cut off lower frequencies and thereby eliminated almost all spurious counts due to circuit "noise." The total background count, including also any spontaneous fission in the sample and fission by stray neutrons from nearby radium alpha-beryllium sources, was held below 0.3 counts per hour.

The samples for counting were electrolytically deposited by the method of Cohen and Hull[4] on 22-cm² circular nickel disks used as the collector plate in the ionization chamber. Because of the low counting rates anticipated, the maximum weight of U_3O_8 available as an adherent layer by the electrodeposition method was used for both the U-238 samples and the natural uranium standards counted for calibration.

Because of the very low counting rates found (about 4 counts per hour) it was convenient to record pulses on a strip chart recorder. The chart from an overnight run could then be examined to determine whether the distribution of pulses had been abnormal by applying statistical tests. The procedure was to find the mean time interval between counts and the sample variance. These were checked with an F test to demonstrate the improbability of malfunction of the recording equipment, and the mean counting rate and its precision at the 95 percent probability level (L.E.) were computed. The calibration standards were counted before and after the samples and the rates checked statistically for possible change in sensitivity of the counting equipment. Fortunately, these precautionary tests showed no abnormalities after the first few exploratory runs.

Table I.

Sample	Total counts	Rate (counts/min)	F test value	95% F limit	% L.E.
N	627	41.80			7.8
KX	56	0.055	1 09	1.70	26.2
N	2776	42.06			3.7
N	2429	43.38			4.0
Bkg*	17	0.0049			48
(Av N)	(5832)	(42.57)	1.35	3.69	2.56

* The background was taken with the KX material in the counter but with the radium source removed. It represents stray neutron fission from nearby fast neutron sources as well as electrical transients and spontaneous fission.

DATA

A sample set of counting data is given in Table I. The F test ratios obtained, the average counting rates for sample background and standard, and the 95 percent confidence intervals (L.E.) for each count are given. For the particular sample shown, the indicated

Table II.

Batch	U-235 (parts per million U-238)
K-1	4.5±1.5
K-2	13.5±1.4
K-3	16.2±2.2
K-4	10.0±5.0
K-5	18.5±2.1

* This is a revision of the report A-3654 issued October 23, 1946.

† This document is based on work performed for the AEC by Carbide and Carbon Chemicals Division, Union Carbide and Carbon Corporation, at Oak Ridge, Tennessee.

[1] H. G. Beyer, Report A-1235, Part III, April 4, 1946.

[2] W. E. Shoupp, and J. E. Hill, Phys. Rev. **75**, 785 (1949).

[3] B. W. Sargent, "Photoneutron sources," NRCC Declassified Report PD-206.

[4] D. E. Hull, "The counting method of isotopic analysis of uranium," parts i and ii, Declassified Report MDDC 387.

U-235 content is 1/851 that of natural uranium or about 8.4 ppm. The precision is about 2.5 ppm (L.E.) for this single measurement. Several other batches of U-238 were analyzed by the same method, some repeatedly. Values obtained are listed in Table II.

DISCUSSION

As can be seen from Table II, at least one batch of high purity U-238 practically reached the limit of 5 ppm impurity expected, but several were not as pure as expected. Slight errors in adjustment of the electromagnetic separators or contamination in subsequent chemical processing are likely causes. Contamination of the counting samples was feared but check determinations, in some cases several months apart and on samples prepared in different laboratory rooms, failed to show any significant differences. Analyses of U-238 containing thirty to forty times as much U-235 impurity by the photoneutron method have shown excellent agreement with mass spectrometric assays and the emulsion track counting of pile neutron fissions.

High purity U-238 offers several attractive research applications. It has been used in the preparation of synthetic standards for high precision isotope analysis.[5] The specific alpha-activity of U-238 has been remeasured by Kienberger.[6] U-238 fission has been employed as a fast neutron detector with a sharp cutoff at 1 Mev.

From a comparison of the minimum U-235 content found with the quoted limit of the method of preparation, it is apparent that the U-238 fission cross section for thermal neutrons is less than about one-seven-thousandth that of natural uranium. Taking the natural uranium thermal fission cross section[7] as 3.9×10^{-24} cm², the U-238 thermal fission cross section is less than 5×10^{-28} cm².

[5] W. W. Boardman and A. B. Meservey, "U-235 content of natural uranium," Carbide and Carbon Chemicals Divisions, K-25 Plant, Report K-248 (1948).
[6] C. A. Kienberger, Phys. Rev. **76**, 336 (1949).
[7] Chem. and Eng. News **28**, 4470 (1950).

THE JOURNAL OF CHEMICAL PHYSICS VOLUME 19, NUMBER 7 JULY, 1951

Compressibility of Gases at Pressures up to 50 Atmospheres. V. Carbon Tetrafluoride in the Temperature Range 0°–400°C. VI. Sulfur Hexafluoride in the Temperature Range 0°–250°C

K. E. MacCormack* and W. G. Schneider
National Research Council, Ottawa, Canada
(Received April 12, 1951)

The gaseous compressibilities of carbon tetrafluoride in the temperature range 0–400°C, and sulfur hexafluoride in the temperature range 0–250°C have been measured at pressures up to 50 atmospheres by a method employing gas expansion. The data have been fitted to a series equation of the type,

$$PV \text{ (Amagat units)} = A_T + B_T P + C_T P^2 + D_T P^4,$$

and the virial coefficients are tabulated.

INTRODUCTION

THE primary object in making compressibility measurements on carbon tetrafluoride and sulfur hexafluoride has been to provide accurate values of the second virial coefficients which could then be used in the computation of intermolecular force fields pertaining to each of these substances. In order to minimize the complexity of the series of equations involved, the maximum working pressures were confined to the neighborhood of 50 atmospheres, where terms involving powers of pressure greater than the second become very small.

METHOD

The experimental procedure followed closely that described in earlier publications.[1–3] The main features of the method involved the measurement of the pressure and temperature of a gas confined in a stainless steel pipet whose volume need not be known accurately. The gas was then expanded into a smaller pipet maintained at the same temperature and the new pressure determined. After evacuation of the second pipet, further expansions could be performed and a series of pressure ratios determined therefrom. Assuming that the equation of state of a gas may be adequately represented by the equation,

$$PV = A_T + B_T P + C_T P^2 + D_T P^4, \tag{1}$$

it is easily shown that the following relation exists for an expansion of the type described:

$$\frac{P_1}{P_2} = N + (N-1)\frac{B_T}{A_T}P_1 + \left(N - \frac{P_2}{P_1}\right)\frac{C_T}{A_T}\cdot P_1^2 + \left(N - \frac{P_2^3}{P_1^3}\right)\frac{D_T}{A_T}P_1^4. \tag{2}$$

* National Research Laboratories Postdoctorate Fellow.
[1] W. G. Schneider, Can. J. Research **27B**, 339 (1949).
[2] W. G. Schneider and J. A. H. Duffie, J. Chem. Phys. **17**, 751 (1949).
[3] K. E. MacCormack and W. G. Schneider, J. Chem. Phys. **18**, 1269 (1950).

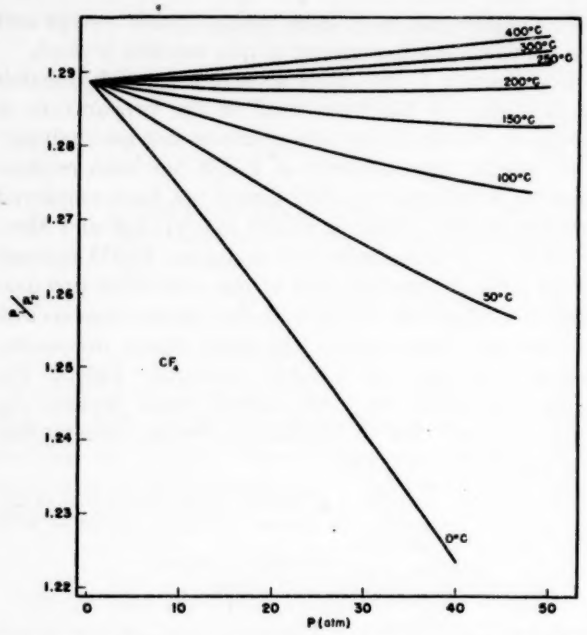

FIG. 1. Plots of pressure ratio P_1/P_2 *vs* initial pressure P_1 for CF_4.

In the foregoing equations, P_1 and P_2 represent the pressures before and after expansion from the first pipet of volume V_1, to the second pipet of volume V_2. N is the ratio of the volumes $(V_1+V_2)/V_1$; B_T, C_T, and D_T are the second, third, and fourth virial coefficients at temperature T. Amagat units are used throughout so that V in Eq. (1) is the ratio of the true volume, v_{TP}, to the normal volume, V_N, defined at 0°C and 1 atmosphere as the volume occupied by one mole of the gas. Thus,

$$V=v_{TP}/V_N.$$

It follows from Eq. (1) that at 0°C and 1 atmos,

$$PV=1=A_0+B_0+C_0+D_0. \tag{3}$$

In addition, for an ideal gas,

$$PV=RT_0/V_N,$$

where V is expressed in Amagat units, and R is the g-molecular gas constant in liter-atmospheres-deg^{-1}. Therefore,

$$A_0=RT_0/V_N \tag{4}$$

and $A_T=A_0T/T_0$. The series evaluations have been performed by a method employing least mean squares which has been fully described in a previous publication[3] relating to work on carbon dioxide. The probable error in B_T has been estimated to be approximately 1 percent at 0°C and 1.5 percent at 200°C and higher temperatures.

TABLE I. Virial coefficients for CF_4 (Amagat units).

T°K	A_T	10^3B_T	10^6C_T	10^9D_T	Max'm deviations $(P_1/P_2)_{calc}-(P_1/P_2)_{exp}$
273.16	1.004988	−4.977	−10.64	—	0.00015
323.16	1.188944	−3.155	+1.06	+0.81	0.00007
373.16	1.372900	−1.931	+3.52	+0.50	0.00006
423.16	1.556856	−1.164	+5.98	—	0.00005
523.16	1.924768	+0.056	+3.63	—	0.00005
573.16	2.108724	+0.416	+3.18	—	0.00005
673.16	2.476635	+1.056	+1.63	—	0.00005

CARBON TETRAFLUORIDE

(a) Purity of Gas

This gas was supplied by the Minnesota Mining and Manufacturing Company with a purity of at least 99 percent. A further sample was kindly prepared by Mr. H. W. Dale which had the following approximate composition: CF_4, 95 percent; C_2F_6, 2–3 percent; C_3F_8, 1 percent; C_4 upward, present as traces. These compounds have boiling points which differ by approximately 50°C, and it was thus possible to effect a reliable separation employing a low temperature Stedman column. A mass spectrogram of the fractionated sample compared with the unfractionated commercial sample indicated that the latter was free from air, water, and compounds of fluorine containing two or more carbon atoms. Frequent comparison of samples during the course of compressibility experiments provided reliable means of checking the purity of the gas.

(b) Corrosion

Carbon tetrafluoride is extremely stable to heat and to most reagents, but it was considered necessary to be sure that no chemical reaction would occur with stainless steel over the temperature range to be investigated. A steel vessel with removable screw head and pressure seating was constructed for testing various metal samples at high temperatures and pressures. Since the compressibility apparatus had already been made from stainless steel (Carpenter Type 304), only the results of tests on this sample will be quoted here. After a period of 20 hr at 425°C, and at a pressure of 400 lb/sq in., only very pale brown coloration of the sample was noticed. A fresh sample treated for the same period at 500°C was much more noticeably attacked, being covered by a dull gray film. It was therefore considered impossible to make reliable measurements at temperatures exceeding 400°C. In order to provide a protective film, the apparatus was filled with CF_4 at 500 lb/sq in. pressure and 420°C for a period of 24 hr prior to making compressibility measurements at 400°C.

(c) Results

Figure 1 shows pressure ratio *vs* pressure curves for CF_4 over the pressure and temperature range studied. Experimental points have been omitted for the sake of clarity, though scatter about these curves would not be evident on the scale used. Contrary to observations made on carbon dioxide[3] and also on sulfur hexafluoride of the following section, it will be noted that in no case could linearity of the isotherms be assumed over the

whole pressure range employed. It was necessary, therefore, to express the P–V–T relationships by a series equation which incorporates the third, and in some cases, the fourth virial coefficient, as shown in Eq. (1). The virial coefficients of this equation at seven temperatures between 0° and 400°C are presented in Table I. These coefficients are expressed in units of Amagat volume and may be converted to units of cm³/mole by multiplying by the normal volume V_N of CF_4. This may be calculated from the standard volume of a perfect gas, *viz.*, 22414.6±0.6 cm³/mole,[4] using the relation given in Eq. (4)

$$V_N=\frac{22414.6}{A_0}\ \text{cm}^3/\text{mole}.$$

A_0 was found to have the value 1.004988, giving the normal volume the value 22303.3$_5$ cm³/mole.

The final column of Table I indicates the maximum deviations encountered between an experimental value of P_1/P_2 and a value calculated from Eq. (2) by substitution of the calculated coefficients.

The second virial coefficient B_T (Amagat) has been plotted as a function of temperature in Fig. 2. Computed coefficients for 200°C have been omitted from the tabulated data because of their unreliable nature. As can be seen from Fig. 1 the isotherm at 200°C is very nearly horizontal over the central portion of the pressure range and forms a very shallow U-shape for which experimental points could not be accurately measured below 10 atmospheres. The mean deviation of the P_1/P_2 ratios relative to the total change in P_1/P_2 over the whole pressure range is thus too large to warrant a reliable fitting of the data by mean squares.

Also included in Fig. 2 is the plot of C_T (Amagat) *vs* temperature; this may be found useful for interpolation purposes though the accuracy of these data cannot be assumed to be better than that shown by the graphical deviations.

SULFUR HEXAFLUORIDE

(a) Purity of Gas

The samples of gas used in the earlier part of this work were kindly prepared by Mr. H. W. Dale. These had been purified chemically for removal of all fluorine compounds of sulfur of greater complexity than SF_6. Subsequent samples were purchased from the Matheson Company with a specified minimum purity of 99 percent. All samples were further purified by a multiple trap sublimation at dry-ice temperature. Final portions were rejected each time followed by evacuation of the condensate for approximately 20 minutes at liquid air temperature. Analysis of several of these purified samples by mass spectrometer showed no trace of air, water, or any other known compounds of sulfur and fluorine.

[4] J. W. Dumond and E. R. Cohen, Revs. Modern Phys. **20**, 82 (1948).

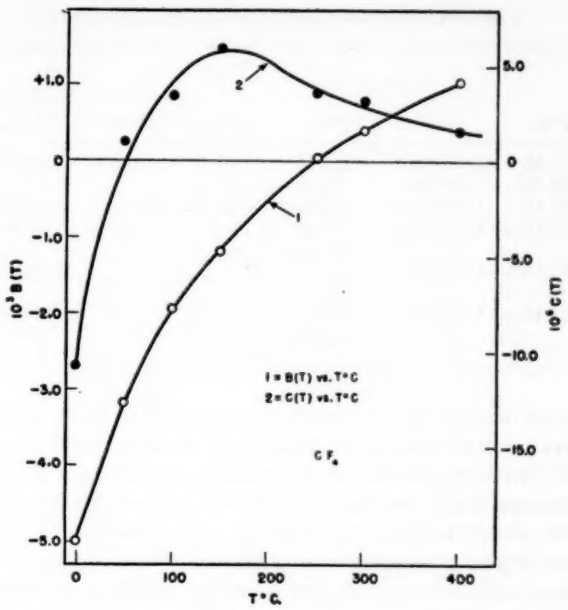

FIG. 2. Second and third virial coefficient *vs* temperature for CF_4.

(b) Corrosion

The chemical properties of sulfur hexafluoride show it to be an extremely stable gas, and it has been reported[5] that copper and silver are not attacked at the melting

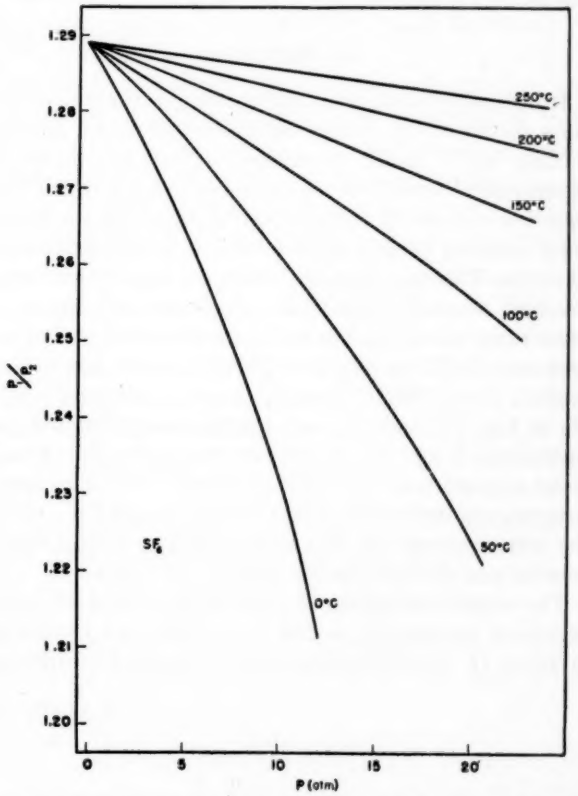

FIG. 3. Plots of pressure ratio P_1/P_2 *vs* initial pressure P_1 for SF_6.

[5] Bulletin issued by General Chemical Division, Allied Chemical and Dye Corporation.

TABLE II. Virial coefficients for SF_6 (Amagat units).

T°K	A_T	10^3B_T	10^5C_T	10^7D_T	Max'm deviations $(P_1/P_2)_{calc}-(P_1/P_2)_{exp}$
273.16	1.015317	−15.114	−20.25	−6.81	0.00020
323.16	1.201164	−9.823	−10.17	—	0.00015
373.16	1.387011	−7.212	−2.29	—	0.00006
423.16 (a)	1.572858	−5.367	—	—	0.00006
(b)		−5.360	—	—	
473.16 (a)	1.758704	−3.573	—	—	0.00005
(b)		−3.621	—	—	
523.16 (a)	1.944551	−2.436	—	—	0.00005
(b)		−2.332	—	—	

point of glass. It was, however, essential to be sure that no chemical reaction occurred with stainless steel (Type 304) from which the compressibility apparatus was constructed and corrosion tests similar to those described in the case of carbon tetrafluoride were therefore carried out. Up to a temperature of 250°C, there appeared to have been no reaction with a sample of this steel after a period of 20 hours at a pressure of approximately 300 lb/sq in. A further period of 20 hours at 320°C did produce evidence of some attack, the original polished surface having become a blue-black color. It was therefore considered essential to confine working temperatures to an upper limit of 250°C, and tests for small changes in pressure using the piston gauge indicated this to be a safe limit.

(c) Results

It became evident from the pressure ratio *vs* pressure plots shown in Fig. 3 that the isotherms above and including 150°C could be treated within the limits of experimental error by assuming a linear form of the equation of state. It will be noted further that the maximum working pressures were limited to approximately 24 atmos. This was necessary, since the apparatus design involved a small "dead space" volume maintained at room temperature and to avoid condensation the vapor pressure of SF_6 at room temperature could not be exceeded. From 150°C upwards terms involving C_T and D_T in Eqs. (1) and (2) were therefore omitted, and the coefficients N and B_T/A_T were evaluated by simple least mean squares treatment for a straight line. The lower temperature isotherms were, however, treated in exactly the same manner as that employed for carbon tetrafluoride and carbon dioxide referred to earlier.

The virial coefficients of these equations at six temperatures between 0° to 250°C inclusive, are presented in Table II. These coefficients are expressed in units of

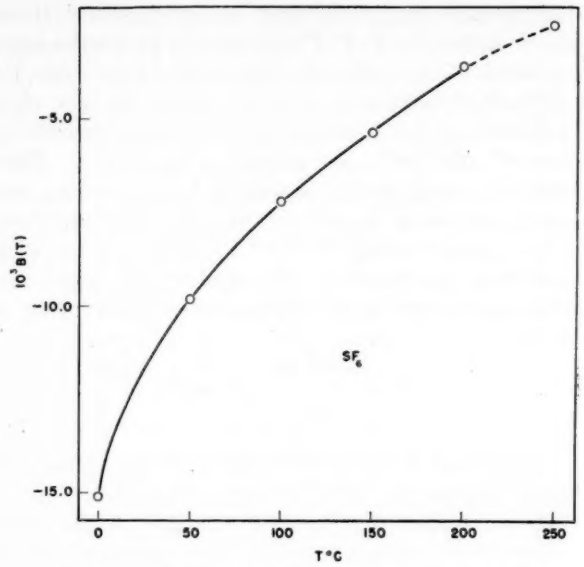

FIG. 4. Second virial coefficient *vs* temperature for SF_6.

Amagat volume and may be converted to units of cm^3/mole by multiplying by the normal volume, V_N, of SF_6. This was found to be 22,076.4 cm^3/mole from Eq. (5) employing the value of A_0 found to be equal to 1.015317. The final column of Table II gives the maximum deviations encountered between experimental values of P_1/P_2 and those calculated by resubstituting the calculated coefficients into the appropriate series equation. During subsequent measurements with this apparatus, a failure developed in one of the pipets necessitating an entirely new pipet system. This provided the opportunity of checking some of the foregoing work with both new volume ratios and gas samples. At 150°, 200°, and 250°C, the values of B_T are presented for both groups of experiments under (a) and (b). The discrepancy at 250°C is somewhat larger than is expected, but may be due in part to slight decomposition of the sulfurhexafluoride.

The final values of the second virial coefficient B_T (Amagat) are plotted in Fig. 4, the dotted portion of the curve indicating the possible uncertainty in the high temperature values by virtue of corrosion, but as pointed out earlier, the effect of corrosion even at 250°C was not considered serious.

ACKNOWLEDGMENTS

We wish to thank Mr. K. Milliken for computational assistance and Mr. Y. Lupien for help in the experimental measurements.

Intermolecular Potentials. I. Carbon Tetrafluoride and Sulfur Hexafluoride. II. Carbon Dioxide

K. E. MacCormack* and W. G. Schneider
Division of Chemistry, National Research Laboratories, Ottawa, Canada
(Received April 12, 1951)

Experimental second virial coefficient data for carbon tetrafluoride, sulfur hexafluoride, and carbon dioxide have been used to investigate the intermolecular potentials of these molecules on the basis of a Lennard-Jones model. Force constants for the fluoride molecules can be fitted rather satisfactorily, but the constants so derived do not agree with those derived from other gaseous properties, e.g., the critical data. This result may be due to the assumption of central forces for the symmetrical fluoride molecules.

For carbon dioxide it was found that the derived force constants varied with temperature, the high temperature data yielding lower values of the collision diameter r_0. The results can be interpreted on the basis of a partial association. A likely configuration for the resulting dimer is suggested.

INTRODUCTION

BECAUSE of the symmetrical structure of molecules such as carbon tetrafluoride and sulfur hexafluoride it is of interest to investigate the force field surrounding these molecules. In particular, the question arises whether the forces responsible for molecular interaction can be regarded as central forces or whether the force field is localized in the outer fluorine atoms. In the case of the larger tetrachloride molecules (CCl_4, $SiCl_4$, $GeCl_4$, $SnCl_4$, etc.) Hildebrand[1] has suggested that the behavior of these molecules can be explained by assuming the force field to reside in the outer halogen atoms. Using the data for the second virial coefficients of carbon tetrafluoride and sulfur hexafluoride of the preceding paper, we have attempted to obtain a fit to a Lennard-Jones potential. The second virial coefficient $B'(T)$ is related to the energy of interaction between a pair of molecules as follows:

$$B'(T)=2\pi N\int_0^\infty (1-e^{-\epsilon(r)/kT})r^2dr, \qquad (1)$$

where N is the avogadro number and $\epsilon(r)$ is the potential energy of interaction as a function of the separation r. Equation (1) is based on the assumption of central forces. Accordingly, substitution of a Lennard-Jones potential for $\epsilon(r)$ and use of Eq. (1) to compare the experimentally measured second virial coefficients of the fluoride molecules might be expected to yield good agreement only if the molecular force fields are to be treated as central. On the other hand, it is possible that a reasonably good fit can be obtained even though the molecules do not behave strictly as centers of force. Such a result could mean that the second virial coefficient is not a sufficiently sensitive property to make a clear-cut distinction.

The results presented below show that for carbon tetrafluoride in particular, an excellent fit to the experimental second virial data over the entire temperature range can be obtained with a Lennard-Jones potential. The fit for sulfur hexafluoride is not quite as satisfactory although this may be attributed in part to the experimental difficulty of measuring the 0°C isotherm for this gas with sufficient precision. For both gases, however, it is felt that the model is sufficiently good to employ the derived potentials for a number of physical applications, particularly those involving gaseous properties. The question regarding the exact nature of the force fields of these molecules cannot, however, be conclusively decided on the basis of the present results.

In the second part of this paper an attempt has been made to treat second virial coefficient data for carbon dioxide over a much wider temperature range than that hitherto employed. In spite of the nonspherical nature of this molecule, the application of Eq. (1) in conjunction with a Lennard-Jones-type potential has previously met with success in the temperature range 0–150°C. It is here shown, however, that the experimental data obtained by the present authors in the range 0–600°C cannot be adequately fitted by such a model. Although the lower temperature data gives rise to a set of force constants in good agreement with the previous investigation, it is found that an entirely new set of force constants must be used in the application of the same type of model to the high temperature data. This indicates, of course, that the usefulness of such a model lies only in its value for purposes of interpolation within the temperature range for which the fit has been made.

The second virial coefficient $B'(T)$ appearing in Eq. (1) is defined by the series expression,

$$Pv/RT=1+[B'(T)/v]+[C'(T)/v^2]+\cdots. \qquad (2)$$

Compressibility measurements higherto made in this laboratory[2] have been computed on the basis of the following series,

$$PV=A(T)+B(T)P+C(T)P^2+\cdots, \qquad (3)$$

in which units of Amagat volume are used. The coeffi-

* National Research Laboratories Postdoctorate Fellow.
[1] J. H. Hildebrand, J. Chem. Phys. **15**, 727 (1947).
[2] K. E. MacCormack and W. G. Schneider, J. Chem. Phys. **19**, 845 (1951) (previous paper). See also reference 13.

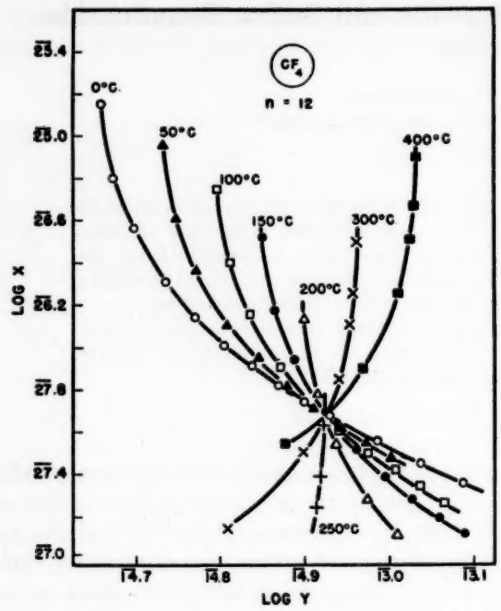

FIG. 1. Log$X$−log$Y$ curves of the Buckingham method (CF_4).

cients of Eqs. (2) and (3) are related as follows:

$$A(T)=RT/V_N,$$
$$B'(T)=V_N B(T),$$
$$C'(T)=V_N^2(AC+B^2),$$

where V_N is the volume occupied by one mole of gas at NTP.

The Lennard-Jones potential is given by,

$$\epsilon(r)=(\lambda/r^{12})-\mu/r^6, \tag{4}$$

in the special case of twelfth and sixth powers of repulsion and attraction, respectively. With this potential, Eq. (1) yields

$$B'(T)=\tfrac{2}{3}\pi N(\lambda/\mu)^{\frac{1}{4}}F(y), \tag{5}$$

where $F(y)$ is a function which has been tabulated by Lennard-Jones[3] and others.[4] The argument y is given by

$$y=\mu/kT(kT/\lambda)^{\frac{1}{4}}. \tag{6}$$

To evaluate the constants λ and μ we have used a method described by Buckingham.[5] This has the advantage of indicating any variation of the derived constants with temperature when sufficient experimental data are available. To apply the method a plot is made of the quantities log$X$ and log$Y$ given by,

$$\log X=\log[3B'(T)/2\pi N]-\log F(y),$$
$$\log Y=2\log y+\log kT. \tag{7}$$

The relation between log$X$ and log$Y$ can be shown in the (log$X$, log$Y$) plane, and the intersection of two such curves obtained by plotting Eqs. (7) and (8) for the observed values of $B'(T)$ at their respective temperatures determines the constants λ and μ by the relations,

$$\log\lambda=4\log X+\log Y, \tag{9}$$

$$\log\mu=2\log X+\log Y. \tag{10}$$

When all the intersections in the log$X$−log$Y$ plot obtained with data over a wide temperature range occur at a single point, the constants λ and μ are uniquely determined and can be considered to be nonvariant with temperature. On the other hand, if the points of intersection in the log$X$−log$Y$ plane are not well localized, a temperature dependence of λ and μ is indicated, or perhaps more correctly, the assumed potential is not capable of fitting the experimental data over the entire temperature range.

PART I

Carbon Tetrafluoride

Figure 1 shows a log$X$−log$Y$ plot for carbon tetrafluoride. The intersections of the curves for different temperatures are localized in a surprisingly small area, considering that the temperature range covered is 400°C. The values of λ and μ obtained from the plot are presented in Table I.

In order to verify the suitability of this model these values were used to calculate the second virial coefficient at each temperature and the latter were compared with the original experimental values. To do this the tables published by Hirschfelder *et al.*[4] were used. These authors employ the Lennard-Jones potential in the alternative form,

$$\epsilon(r)=4\epsilon_0[(r_0/r)^{12}-(r_0/r)^6], \tag{11}$$

TABLE I. Values for parameters of Lennard-Jones potential ($m=6$; $n=9$ or 12).

Units	λ erg−$(A)^9$ ×10^{6}	λ erg−$(A)^{12}$ ×10^{6}	μ erg−$(A)^6$×10^{10}		ϵ_0/k degrees K		r_0 (A)		$r(\min^m)$ (A)	
Gas \ n	9	12	9	12	9	12	9	12	9	12
SF_6	1.097	87.21	54.86	31.10	147.3	200.9	5.85	5.51	6.70	6.19
CF_4	0.1830	9.782	15.28	9.075	114.8	152.5	4.93	4.70	5.64	5.28

[3] J. E. Lennard-Jones, Proc. Roy. Soc. (London) **A106**, 463 (1924).
[4] Hirschfelder, Bird, and Spotz, Trans. Am. Soc. Mech. Engrs. **71**, 921 (November, 1949). Also publication CM-599 University of Wisconsin, Project NOrd 9938 (May 10, 1950).
[5] R. A. Buckingham, Proc. Roy. Soc. (London) **A168**, 264 (1938).

where r_0 is the so-called low velocity collision diameter and ϵ_0 is the minimum value of the potential energy curve (see Fig. 2). These parameters are related to λ and μ by,

$$\epsilon_0=\mu^2/4\lambda$$

$$r_0=(\lambda/\mu)^{1/6}.$$

Then Eq. (5) becomes

$$B'(T)=b_0B^0(\tau), \tag{12}$$

where

$$b_0=\tfrac{2}{3}\pi N r_0^3$$

and

$$\tau=kT/\epsilon_0=4/y^2.$$

The values of $B'(T)$ for CF_4 shown in Table II were calculated using tabulated values for $B^0(\tau)$ given in reference 4. The agreement with the experimental values is very satisfactory over the whole temperature range.

As a matter of interest a fit was also tried with a Lennard-Jones potential having a repulsive term proportional to the inverse ninth power of the separation. In this case the fit was not as good as with a twelfth-power repulsion though the sensitivity to such a variation was not very marked. The results for both $n=12$ and $n=9$ are summarized in Table I, and the potential energy curve for $n=12$ is shown in Fig. 2.

Approximate expressions for the relation between the force constants and the critical constants have been derived[6] from the Lennard-Jones and Devonshire theory of gases and liquids.[7] These are found to be in fair agreement with experimentally derived data for inert gas-type molecules. On the basis of the force constants for argon, nitrogen, and helium, derived from viscosity data, the relation becomes[4]

$$b_0=0.68V_c. \tag{13}$$

Using the value 146.7 cm³/mole for the critical volume V_c of CF_4[8] we obtain $b_0=99.8$ cm³/mole. This compares with $b_0=131.0$ cm³/mole when the value of r_0 (4.70A) derived from the second virial is used. The difference between the two values of b_0 is considerably larger than that which has been observed for a number of smaller molecules,[4] as will be indicated below.

Sulfur Hexafluoride

Approximate values for λ, μ, ϵ_0, and r_0 for this gas are also shown in Table I. In contrast to the excellent fit obtained for CF_4, the fit for SF_6 was not nearly as satisfactory as can be seen from the $\log X-\log Y$ plot shown in Fig. 3. An exact determination of the parameters is accordingly not possible although a twelfth-power repulsion term was considered an improvement over a ninth-power term. Table II contains a comparison of the calculated virial coefficients with the corresponding experimental values. The simplified potential here used is thus not capable of fitting the experimental data within the estimated error of the latter.

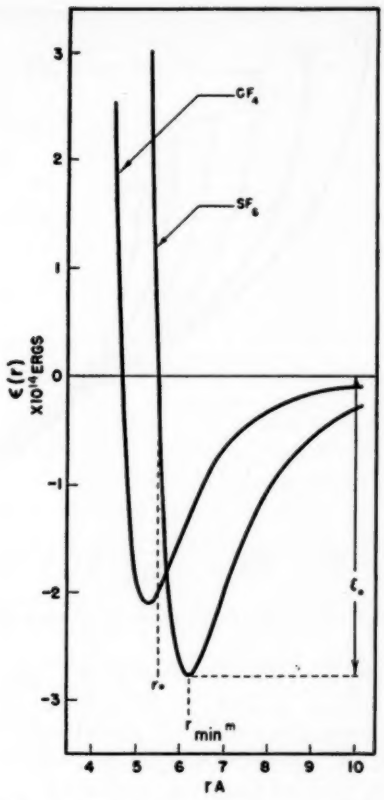

FIG. 2. Potential energy curves for SF_6 and CF_4. ($n=12$)

As in the case of CF_4 the value of $b_0=132.0$ cm³/mole for SF_6 obtained from the critical volume[9] is considerably smaller than the value 211.1 cm³/mole, calculated from the derived value of r_0. In fact for both gases b_0

TABLE II. Comparison of experimental and calculated second virial coefficients.

	SF_6 $\epsilon_0/k=200.9$°K, $r_0=5.51$A, $b_0=211.1$ cm³/mole		CF_4 $\epsilon_0/k=152.5$°K, $r_0=4.70$A, $b_0=131.0$ cm³/mole	
T°C	$B'(T)$ exptl. cm³/mole	$B'(T)$ calcd. $=b_0B^0(\tau)$ cm³/mole	$B'(T)$ exptl. cm³/mole	$B'(T)$ calcd. $=b_0B^0(\tau)$ cm³/mole
0	−333.7	−307.2	−111.0	−112.0
50	−216.9	−219.3	−70.4	−70.3
100	−159.2	−158.8	−43.1	−44.3
150	−118.6	−114.8	−26.0	−25.7
200	−78.9	−81.5	—	—
250	−54.8	−56.2	$+1.2_5$	$+3.5_2$
300			+9.3	+9.5
350			—	—
400			+23.6	+23.0

[6] Butler, Wentorf, Hirschfelder, and Curtiss, University of Wisconsin, CM-565, Project NOrd 9938 (February 3, 1950).

[7] J. E. Lennard-Jones and A. F. Devonshire, Proc. Roy. Soc. (London) **A163**, 53 (1937).

[8] Bulletin on fluorocarbons issued by Minnesota Mining and Mfg. Co.

[9] Bulletin issued by General Chemical Division, Allied Chemical and Dye Corporation, New York.

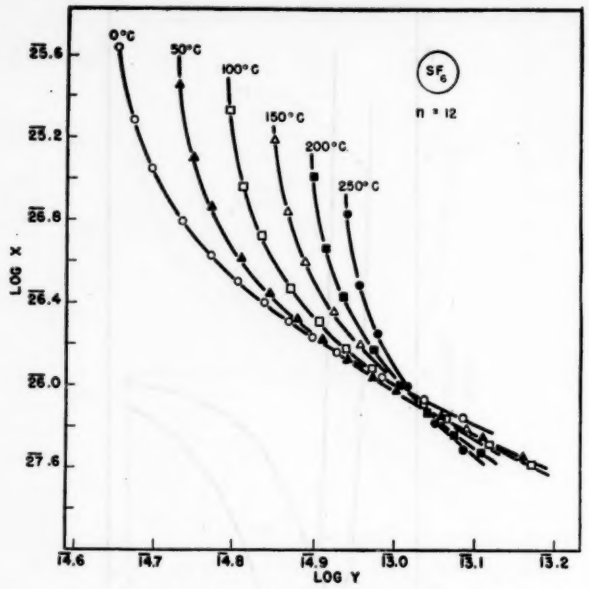

FIG. 3. Log$X$ − log$Y$ curves of the Buckingham method (SF_6).

derived from the virial data is almost as large or larger than the critical volume itself, a behavior which is somewhat anomalous when compared with that of the inert gases. A somewhat similar behavior is exhibited by CCl_4; b_0 derived from viscosity data[4] is 256.6 cm³/mole while the value of b_0 derived from V_c is 187 cm³/mole.

A similar anomaly is to be noted when the values of ϵ_0 obtained from the virial data are compared with the ϵ_0 values derived from the relation[4]

$$\epsilon_0/k = 0.79T_c. \tag{14}$$

If we let $b_0 = \alpha V_c$ and $\epsilon_0/k = \beta T_c$ then the values of α and β obtained for the respective gases are as follows:

	α	β
Average for A, N_2, and He	0.68	0.79
CF_4	0.90	0.67
SF_6	1.09	0.63
CCl_4	0.93	0.59.

In other words, the last three substances behave relative to argon, nitrogen, and helium as though their collision diameter were abnormally large and also, or perhaps in consequence, the interaction energy considerably smaller. It appears reasonable to interpret this as evidence that the molecular interaction is almost entirely the result of outer halogen atoms. The relationship between the force constants derived from critical data and those from virial or viscosity data for a variety of molecules is being investigated further.

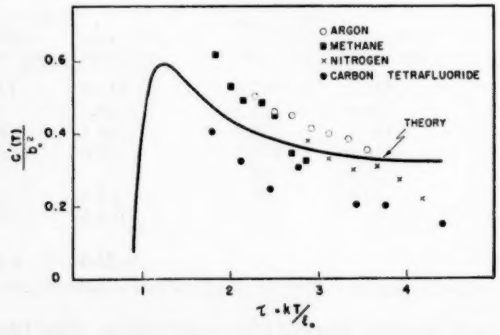

FIG. 4. Theoretical and experimental third virial coefficients.

The Third Virial Coefficient

An attempt was made to correlate the third virial data for carbon tetrafluoride with the theoretical values for nonpolar gases.[10] The data for $C(T)$ presented in the previous paper[2] were converted to units $C'(T)$ in Eq. (2) using the relation given earlier. The function $C^0(\tau)$ has been tabulated[4,10] for the Lennard-Jones model ($n=12$: $m=6$) where $\tau = kT/\epsilon_0$ as before. Then with $C'(T) = b_0^2 C^0(\tau)$ it is possible to compare experimental values with theory, using the force constants ϵ_0 and b_0 obtained from the second virial coefficient data. For argon, methane, and nitrogen Hirschfelder *et al.*[10] have obtained reasonably satisfactory agreement between experimental and calculated results, though both the values of the virial and their temperature variation differ by about 20 percent. In Fig. 4 the theoretical curve has been redrawn as in Hirschfelder's paper to show the comparison with the third virial coefficients of CF_4 and the aforementioned molecules. In all cases the slope of the experimental curves is steeper than that of the theoretical. As Kihara[11] has pointed out, this probably signifies a steeper repulsive region to the negative potential energy part of the function than that given by the Lennard-Jones model. The numerical comparison of the data is presented in Table III. If the curve for CF_4 were transposed upward and to the left in order to bring the experimental values into line, a new set of force constants relating to three-body collisions would be needed to describe this particular kind of interaction. Such an adjustment necessarily signifies a lower value for the maximum interaction energy.

TABLE III. Comparison of experimental and theoretical third virial coefficients for carbon tetrafluoride. (From second virial coefficient data $\epsilon_0/k = 152.5°K$; $b_0 = 131.0$ cm³/mole.)

T°C	τ	$C^0(\tau)$[10]	$C'(T)/(b^0)^2$ exptl.
0	1.79	0.47486	0.408
50	2.12	0.42008	0.325
100	2.45	0.38525	0.248
150	2.77	0.36342	0.309
250	3.43	0.33817	0.203
300	3.76	0.33080	0.199
400	4.41	0.32104	0.149

If, as is suggested from considerations of the second virial coefficients, the halogen atoms themselves offer

[10] Bird, Spotz, and Hirschfelder, J. Chem. Phys. **18**, 1395 (1950).
[11] T. Kihara, J. Phys. Soc. Japan **3**, 265 (1948).

an important contribution to the binary interaction, it might conceivably be expected that a ternary collision would involve interaction very different from that which would obtain for molecules having central force fields. For large polyatomic molecules, therefore, there is no reason to expect that the force constants for a binary collision will be the same as those for a ternary collision.

PART II

Carbon Dioxide

Second virial coefficient data obtained by Michels[12] over the temperature range 0–150°C have been used by Hirschfelder *et al.*[4] to determine the force constants of

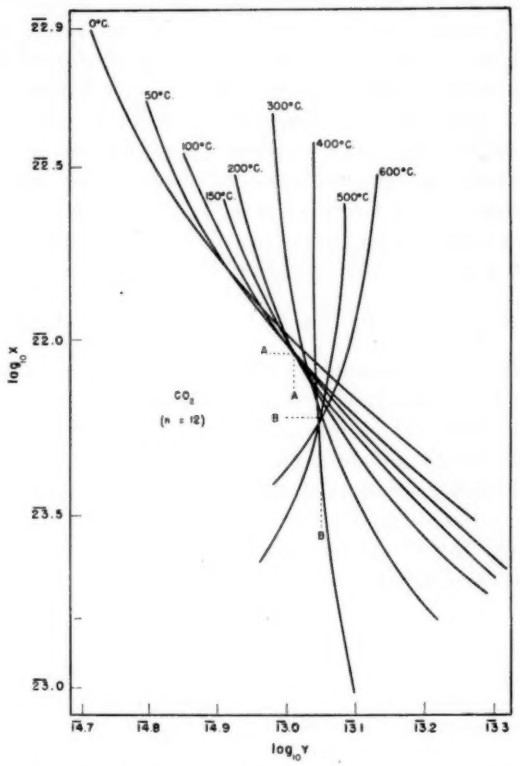

FIG. 5. Log$X$ − log$Y$ curves of the Buckingham method (CO_2).

the Lennard-Jones model applied to carbon dioxide. These were found to be $\epsilon_0/k = 189°K$, $r_0 = 4.486A$.

Similar data obtained by the present authors[13] over a much wider temperature range 0–600°C have now been used to test the applicability of the same model. The method employed was that developed by Buckingham as described in the previous section, and Fig. 5 indicates the moderate success of such a fit. It is clear that the Lennard-Jones (12.6) model is inadequate to represent experimental data over the whole range of temperature, but it is surprising to note that the log$X$, log$Y$ intersections seem to fall into two well-defined areas. Over the range 0–200°C the intersection marked A yields force constants in good agreement with those obtained from Michel's data. The data over the range 300–600°C (intersection B) are covered very well by another set of constants, as shown in Table IV. Also presented are comparisons of the experimental second virial coefficients and those calculated on the basis of these parameters, showing agreement within the limits of accuracy expected in the experimental measurements.

TABLE IV. Comparison of experimental and calculated values of the second virial coefficient for carbon dioxide.

Force constants	T°C	$B'(T)$ calc. cm³/mole	$B'(T)$ exptl. cm³/mole
	0	−156.4	−145.0
$\epsilon/k = 187.5°K$	50	−101.7	−102.6
$r_0 = 4.47A$	100	−71.87	−71.85
$b_0 = 113.0$ cm³/mole	150	−51.63	−50.59
	200	−34.27	−34.08
	300	−13.33	−13.58
$\epsilon/k = 203.3°K$	400	−2.00	−1.58
$r_0 = 3.91A$	500	+6.04	+6.05
$b_0 = 75.20$ cm³/mole	600	+12.01	+12.11

It becomes evident, therefore, that in the case of carbon dioxide the low temperature range parameters may not be reliably used for extrapolation of the data to higher temperatures. Some idea of the error involved can be judged from the plots of experimental values of

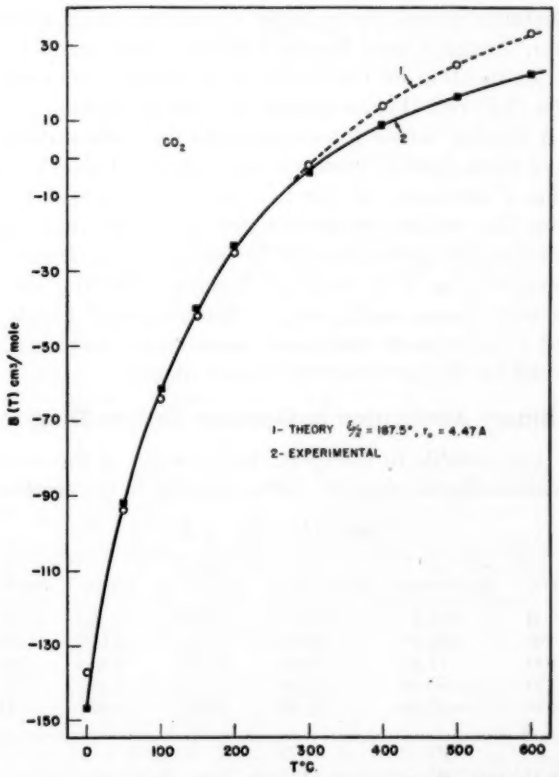

FIG. 6. Theoretical and experimental second virial coefficients for CO_2.

[12] A. Michels and C. Michels, Proc. Roy. Soc. (London) **A153**, 201 (1936).

[13] K. E. MacCormack and W. G. Schneider, J. Chem. Phys. **18**, 1269 (1950).

TABLE V. Values of the L-J force constants for carbon dioxide derived from various sources.

	ϵ_0/k/(°K)	r_0/(A)
Second virial coefficient		
(a) 0°–200°C	187.5	4.47
(b) 300°–600°C	203.3	3.91
Third virial coefficient	221	4.11
Critical temperature data	240.3	3.70
Viscosity	190	4.00

$B'(T)$ and those calculated on the basis of the low temperature parameters shown in Fig. 6.

The effect of the ellipsoidal shape of the CO_2 molecule has been mentioned by Hirschfelder *et al.*[10] in relation to the force constants obtained from second and third virial coefficient data. The latter were reasonably well accounted for theoretically on the basis of a new set of force constants, *viz.*, $\epsilon_0/k=221°K$, $r_0=4.11A$. In view of the fact that the force constants must be a function of the orientation of the molecules involved in collision, there results a set of average constants for two-body collisions from second virials and another set for three-body collisions from third virials. This concept appears to be justified when use is made of Eqs. (13) and (14). The critical temperature and volume for CO_2 are 31.04°C and 94.22 cm³/mole,[14] respectively. Thus $\epsilon_0/k=240.3°$ and $r_0=3.70A$. Since it may be expected that there is a tendency for molecular alignment to occur in the critical region, it is not particularly surprising that third virial data yield force constants approaching those calculated from critical data, though it must be admitted that there seems to be no justification for the choice of the parameters used in Eqs. (13) and (14) as applied to carbon dioxide.

A further set of force constants for carbon dioxide have been derived from viscosity data.[15] Table V contains a summary of the L-J force constants derived from the various properties indicated; the maximum variation is approximately 25 percent in ϵ_0/k and 20 percent in r_0. It is evident therefore that the simple Lennard-Jones model with a twelfth-power repulsion and a sixth-power attraction represents a rather crude model for the force field of carbon dioxide.

Binary Association in Gaseous Carbon Dioxide

It is possible to interpret the behavior of the second virial coefficient data of carbon dioxide in the temperature range 0° to 600°C on the basis of a binary association. As pointed out in the previous section the Lennard-Jones model derived from the experimental virials at the higher temperatures (300° to 600°) yields values of r_0 which are considerably smaller than the value obtained from the data in the lower temperature range (0° to 200°). This trend is contrary to what one would expect if the failure of the Lennard-Jones model were ascribed to the "cigar" shape of the carbon dioxide molecule, a suggestion recently discussed by Hirschfelder.[10] At high temperatures there must be a greater tendency for the molecules to find sufficient space to sweep out spheres by virtue of the lower gas density. Hence r_0 would be expected to be as large or larger than r_0 derived from the low temperature data. Moreover, it has been shown by Corner[16] that the second virial coefficient is not very sensitive to the shape of a molecule, the value calculated for a slightly elongated molecule differing but little from that for a spherical molecule. Evidence for dimerization (dipole association) in polar vapors such as alcohol and acetone has been reported by Eucken and Meyer,[17] Shafer and Foz Gazulla,[18] and Lambert *et al.*[19] While carbon dioxide has an over-all zero moment, the partial moment represented by each CO bond may be expected to be of the same order as the $\diagdown\!\!\diagup C=O$ moment in acetone (2.74×10^{-13} esu). According to Briegleb[20] the dipole association in carbon dioxide is represented by the configuration shown in Diagram (A). However, it is easy to show that taking all coulombic interactions into account, this configuration is unstable by +375 cal/mole. For this calculation the CO bond distance was taken as 1.16A, the C−O moment as 2.78×10^{-18} esu, and a value of d equal to 2.75A (see below).

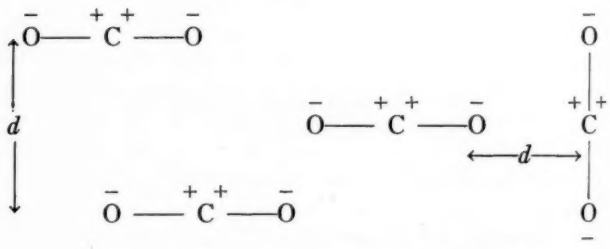

Diagram (A) Diagram (B)

However, using the same value of d, the configuration in Diagram (B) leads to a coulomb interaction energy of −2060 cal/mole.

The degree of association, α, should be negligible at temperatures above 300°C so that on the basis of the

TABLE VI. Values of K_P.

T°C	B_0(cm³/mole)	B(cm³/mole)	10^3K_P (atmos^{-1})	$\log_{10}K_P$	$10^3/T$°K
0	−156.5	−112.6	1.959	$\bar{3}.292$	3.66
50	−102.6	−80.18	0.845	$\bar{4}.927$	3.09
100	−71.85	−50.02	0.451	$\bar{4}.653$	2.68
150	−50.59	−42.60	0.230	$\bar{4}.362$	2.36
200	−34.08	−30.30	0.097	$\bar{5}.987$	2.11

[14] Michels, Blaisse, and Michels, Proc. Roy. Soc. (London) **A160**, 358 (1937).
[15] Hirschfelder, Bird, and Spotz, J. Chem. Phys. **16**, 968 (1948).
[16] J. Corner, Proc. Roy. Soc. (London) **A192**, 275 (1948).
[17] A. Eucken and L. Meyer, Z. physik. Chem. **B5**, 452 (1929).
[18] K. Schafer and O. R. Foz Gazulla, Z. physik. Chem. **B52**, 299 (1942).
[19] J. D. Lambert *et al.*, Proc. Roy. Soc. (London) **B196**, 113 (1949).
[20] G. Briegleb, *Zwischenmolekulare Krafte und Molekulstruktur* (Ferdinand Enke, Stuttgart, 1937), p. 61.

force constants derived from the high temperature second virial data it is possible to compute values for the lower temperature virials in the range 0–200°C, which would be measured experimentally only in the absence of dimerization. This assumes further that the Lennard-Jones model is correct and adequate to allow extrapolation of the high temperature data. The fact that the low velocity collision diameter, r_0, was earlier found to increase towards lower temperatures may well be due to the fact that the low temperature virials are measured for gas mixtures of dimer and monomer. From high temperature data, $r_0=3.91$A. In Diagram (B), therefore, it can easily be shown that the distance, d, will be in the order of 2.75A, and the energy estimates made above were based on this approximate value.

The association reaction is taken to be

$$2CO_2 \leftrightarrows (CO_2)_2.$$

For very small values of α relative to unity,

$$\alpha/2 = PK_P, \tag{15}$$

where P is the total pressure and K_P is the equilibrium constant defined by

$$K_P = p(CO_2)_2/p^2(CO_2),$$

the small p's denoting partial pressures of the particular molecular kind. By reasoning similar to that outlined by Eucken[17] it can be shown that

$$B_0 = B - RTK_P,$$

where B_0 is the observed second virial coefficient and B is that calculated for a monomeric gas on the basis of the Lennard-Jones parameters obtained from the high temperature data. In Table VI these values are presented along with the corresponding values of K_P. By plotting $\log_{10}K_P$ *vs* $1/T$°K a linear relation was found to exist over the lower half of the temperature range, from which the heat of dimerization was estimated to be −2980 cal/mole. It can be seen that this order of magnitude compares favorably with that estimated above for Diagram (B). The degree of association has been calculated according to Eq. (15) and presented in Table VII.

TABLE VII. Values of the degree of association, α, at various temperatures and pressures (units of mole percent).

T°C	1 atmos	10 atmos	50 atmos
0	0.40	4.00	—
50	0.17	1.69	8.45
100	0.09	0.90	4.51
150	0.05	0.46	2.30
200	0.02	0.19	0.97

THE JOURNAL OF CHEMICAL PHYSICS VOLUME 19, NUMBER 7 JULY, 1951

Substituted Ethanes. III. Raman and Infrared Spectra, Assignments, Force Constants, and Calculated Thermodynamic Properties for 1,1,1-Trichloroethane*

M. ZAKI EL-SABBAN,† ARNOLD G. MEISTER, AND FORREST F. CLEVELAND
Spectroscopy Laboratory, Department of Physics, Illinois Institute of Technology, Chicago, Illinois

(Received March 19, 1951)

Raman displacements, semiquantitative relative intensities, and quantitative depolarization factors for liquid 1,1,1-trichloroethane, and infrared wave numbers and percentage absorption for both the liquid and gaseous states in the region 400–5000 cm^{-1} were obtained and compared with previous data. A normal coordinate treatment, using the Wilson *FG* matrix method, was carried out, and a reasonable set of force constants was determined. Assignments were made for all observed bands of the infrared and Raman spectra. The heat content, free energy, entropy, and heat capacity at constant pressure were calculated for 9 temperatures in the range 298.16° to 1000°K. A comparison of calculated and observed entropy values indicated that the potential barrier hindering the internal rotation is about 2840 cal/mole, which leads to a value of 205±20 cm^{-1} for the torsional frequency and to 0.786×10^{-12} erg/radian for the torsional force constant.

THE Raman spectrum of 1,1,1-trichloroethane (methyl chloroform, Cl_3C-CH_3) has been obtained in the liquid state in 4 different investigations,[1–4] and very recently by Smith, Nielsen, and Liang,[5] but in only two cases[3, 5] were depolarization factors determined. The first infrared information was of the strong band at 343 cm^{-1} reported by Hyde[6] who investigated the gas in the limited region 270–500 cm^{-1}. More complete infrared data were reported[7] as a result of the

* Presented at the Chicago meetings of the American Physical Society, November, 1949, and November, 1950; abstracts in Phys. Rev. **77**, 740 (1950); and **81**, 302 (1951). For I and II, see J. Chem. Phys. **12**, 249 (1944); **18**, 1320 (1950).

† This paper is a report on an investigation carried out by Mr. M. Zaki El-Sabban in partial fulfillment of the requirements for the Ph.D. degree at the Illinois Institute of Technology, Chicago, Illinois.

[1] K. W. F. Kohlrausch and F. Köppl, Monatsh. Chem. **65**, 185 (1935).

[2] G. F. Hull, Jr., J. Chem. Phys. **3**, 534 (1935).

[3] J. Wagner, Z. physik. Chem. **B45**, 341 (1940).

[4] Rubin, Levedahl, and Yost, J. Am. Chem. Soc. **66**, 279 (1944).

[5] Smith, Nielsen and Liang, private communications (February 9 and 22, 1951).

[6] W. Lewis Hyde, J. Chem. Phys. **16**, 744 (1948).

[7] M. Z. El-Sabban and F. F. Cleveland, American Physical Society Meeting, November, 1949; abstract in Phys. Rev. **77**, 740 (1950).

TABLE I. Raman spectral data for liquid 1,1,1-trichloroethane (methyl chloroform, Cl_3C-CH_3).[a]

$\Delta\nu$ PR	N	PV	AD	I PR	W	SNL	ρ PR	PS	ν_c	Assignment	Type
									205[c]	ν_6	A_2
242	5	241	0.8	45	0.81	0.82	0.86	D	**241**[c]	ν_{12}	E
	3	306	3.0						295	$\nu_3-\nu_{10}'$	E
344	5	343	1.2	74	0.48	0.49	0.58	P	**343**[c]	ν_5	A_1
									363	ν_{11}	E
	1	480							482[c]	$2\nu_{12}$	A_1+E
523	5	522	0.8	100	0.03	<0.1	0.12	P	**521**[c]	ν_4	A_1
544	2	542	2.0	w					548	$\nu_9'-\nu_4$	E
698	2	694	4.0	vw					686	$2\nu_5$	A_1
710		710		19	0.78	0.87	0.84	D	**716**[c]	ν_{10}', ν_{10}'' $2\nu_{11}$	E, E A_1+E
721		721									
	2	759	1.5						763[c]	$\nu_4+\nu_{12}$	E
									1002	ν_3	A_1
1073	5	1070	1.8	3	0.64	0.6	0.82	D	**1074**	ν_9', ν_9'' $\nu_{10}'+\nu_{11}$	E, E A_1+A_2+E
1083	4	1084	1.5	3		0.86					
1383	4	1379[b]	3.3	1		0.4		P	**1377**[c]	ν_2	A_1
1422	5	1421	2.0	2	0.81	0.8	0.81	D	**1434**[c]	ν_8', ν_8'' $\nu_9'+\nu_{11}$	E, E A_1+A_2+E
1449	5	1447	2.6	4		0.9					
	1	1592							1592	$\nu_4+\nu_9'$	E
	1	1730							1726	$\nu_3+\nu_{10}''$	E
1789	2	1790	0.5	vvw					1790[c]	$\nu_5+\nu_8''$	E
	1	2133							2142[c]	$\nu_8'+\nu_{10}''$	A_1+A_2+E
2740	5	2741	1.2	1		0.2		P	2758[c]	$2\nu_2$	A_1
	2	2853	5.0						2868	$\nu_8'+\nu_8''$	A_1+A_2+E
2880	3	2882	2.7	2					2894	$2\nu_8''$	A_1+E
2938	5	2939	1.9	80	(0.32)	0.1	0.15	P	**2943**[c]	ν_1	A_1
3005	5	3005	2.8	21	(0.97)	0.9	0.81	D	**3010**[c]	ν_7	E

[a] $\Delta\nu$ = Raman displacement in cm^{-1}; PR = present results; N = number of times the line has been obtained in apparently reliable, independent investigations, including the present one; PV = probable value (mean of the N values); AD = average deviation from the mean; I = relative intensity (w = weak, m = medium, s = strong, v = very); ρ = depolarization factor; W = Wagner, reference 3 (values enclosed with parentheses are uncertain); SNL = Smith, Nielsen, and Liang, reference 5; PS = polarization state (P = polarized, D = depolarized); ν_c = calculated wave number (the calculated fundamentals, being more reliable than the overtones and combinations, are set in bold face type); braces are used to indicate resonance doublets; and primes (′) and double primes (″) refer to the energy levels of these resonance doublets.

[b] This band was reported by Hull (reference 2) as the doublet 1361, 1384 cm^{-1}.

[c] Same as assignment of Smith, Nielsen, and Liang (reference 5).

present investigation. Later, Karplus and Halford[8] reported infrared data in the three phases, gas, liquid, and solid. Very recently, Smith, Nielsen, and Liang[5] have obtained gas and liquid infrared data, together with assignments. The later investigators[5, 8] made an assignment of the fundamentals on the basis of their data and the previous Raman data. However, there has always been a lack of agreement as to the location of the carbon-carbon stretching fundamental. Also, there was still doubt about a doubly degenerate deformation frequency. Moreover, no previous normal coordinate treatment had been carried out, and only a few thermodynamic functions had been calculated or obtained calorimetrically.[4] So, in order to close some of these gaps, the present investigation was undertaken.

EXPERIMENTAL DETAILS

Purification of the Sample

The liquid used in this work was furnished by the Dow Chemical Company, Midland, Michigan. It was purified by distillation, the distilling apparatus having only glass seals to avoid contact of the sample with rubber stoppers. The first $\frac{1}{3}$ of the distillate was discarded, and the sample used was collected from the middle portion in order to eliminate low or high boiling point impurities. Redistillation of the substance directly into the Raman tube was then carried out.

Spectroscopic Technique

Raman displacement spectrograms were obtained with different exposures, using a 2-prism spectrograph, constructed in this laboratory, having a dispersion of 162 cm^{-1}/mm (33A/mm) at 4500A. The spectrograms were taken on Eastman 103-J plates, with Hg 4358A as the exciting line. Depolarization spectrograms with different exposures were obtained with a Hilger E-518 spectrograph having a dispersion of 307 cm^{-1}/mm (63A/mm) at 4500A. The relative intensities[9] and depolarization factors[10] were determined by previously described methods, using a Gaertner microdensitometer. The depolarization factors were checked later with a Leeds and Northrup recording microphotometer. Infrared data were secured from records obtained with a Beckman IR-2 recording spectrophotometer equipped with KBr optics. Records of the atmospheric absorption were taken immediately preceding the sample record in order to make possible the elimination of spurious bands. The thickness of the liquid in the absorption cell was 0.11 mm. The gaseous sample was contained in an absorption cell 10 cm in length and at a vapor pressure of 114 mm of Hg.

[8] R. Karplus and R. S. Halford, J. Chem. Phys. **18**, 910 (1950).

[9] F. F. Cleveland, J. Chem. Phys. **11**, 1 (1943).

[10] F. F. Cleveland, J. Chem. Phys. **13**, 101 (1945).

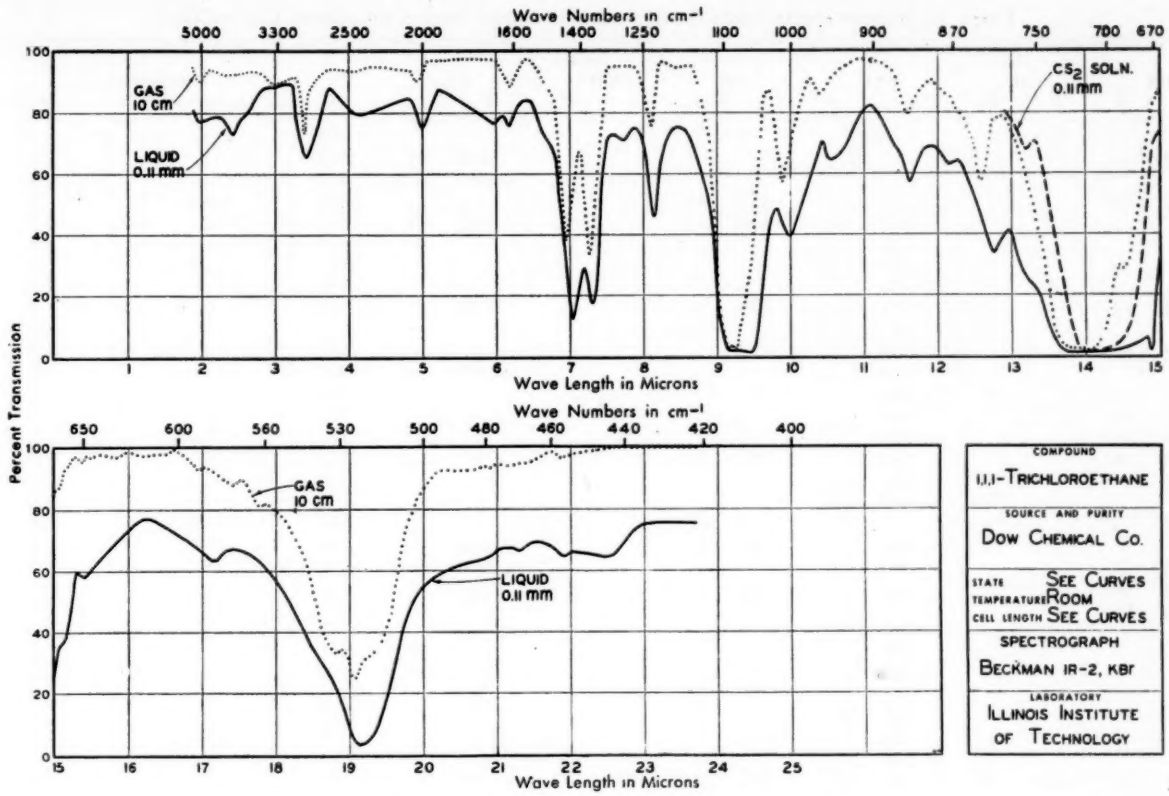

FIG. 1. Infrared absorption bands for 1,1,1-trichloroethane.

RESULTS

The present results and the probable values for the Raman spectral data are listed in Table I. The previously reported relative intensities were only visual estimates, except those of Wagner,[3] which are in qualitative agreement with the present values.

The fundamental frequencies were chosen by considering the depolarization state and the relative intensities, and by comparison with the values of the fundamentals in similar molecules. A splitting of the line in the 710- to 721-cm^{-1} region was detected in the present work. No such splitting was reported by previous investigators, which may indicate the reason for the quite low value given by Kohlrausch and Köppl[1] for this line as compared with later values. Kohlrausch and Köppl may have obtained only the 710-cm^{-1} line, while the other investigators may have determined the mean value of the broad band. Due to the discrepancy between the values obtained by different investigators, it was decided to leave the space, under N in Table I, blank for these frequencies and to include under the probable values only the present, resolved values. Two frequencies at 1172 cm^{-1} and 1242 cm^{-1} were observed; the former was reported by both Hull[2] and Wagner,[3] the latter frequency was reported only by Hull.[2] It is believed that these two lines correspond to the Raman displacements 2939 and 3005 cm^{-1}, respectively, excited by the Hg 4047A, and so they were not included in Table I.

It should be noticed that the values of the fundamentals reported by Rubin, Levedahl, and Yost[4] were not considered in the probable values; these values are 2939 (1), 1471 (1), 977 (1), 523 (1), 345 (1) and 3000 (2), 1450 (2), 1086 (2), 713 (2), 340 (2), 241 (2); the numbers between parentheses give the degeneracy of the corresponding frequency assigned from rough polarization measurements. One observes that some of these frequencies differ considerably from the corresponding values reported by the other investigators; for this reason, it was preferred to await the more complete discussion promised by the authors before including any of these values in the mean.

The infrared spectral data for the present as well as for the previous investigations are given in Table II, and the percent trasmission curve is shown in Fig. 1.

SYMMETRY AND SELECTION RULES

The 1,1,1-trichloroethane molecule belongs to the C_{3v} point group whether it is in the staggered or the eclipsed position. It should execute 18 normal vibrations: 5 type A_1, totally symmetric, 1 type A_2, and 6 type E, doubly degenerate; all of which are allowed by the selection rules in both the Raman and infrared spectra, except the type A_2 torsional vibration which is forbidden in both spectra. All overtones and binary combinations also are allowed in both spectra, except A_2^n (n odd) and $A_1 \times A_2$ which are forbidden in both spectra.

TABLE II. Infrared spectral data for 1,1,1-trichloroethane (methyl chloroform, Cl_3C-CH_3).[a]

Gas PR ν	Gas PR I	Gas KH ν	Gas KH I	Gas SNL ν	Gas SNL I	Liquid PR ν	Liquid PR I	Liquid KH ν	Liquid KH I	Liquid SNL ν	Liquid SNL I	ν_e	Theoretical Assignment	Type
												205[e]	ν_6	A_2
343[b]	vs									344	vs	343[e]	ν_5	A_1
										~ 411	w	410[e]	$2\nu_6$	A_1
457	3					457	35					446	$\nu_6+\nu_{12}$	E
				482	vw	470	34			~ 483	vw	482[e]	$2\nu_{12}$	A_1+E
				516								509[f]	$\nu_{10}'-\nu_6$	E
				519								521	$\nu_{10}''-\nu_6$	E
				~ 524								521	$2\nu_{11}-\nu_6$	A_2+E
524	75			526	s	523	97			524	s	521[e]	ν_4	A_1
				~ 527										
532	67			~ 533								532	$\nu_9'-(\nu_5+\nu_6)$	E
				548						~ 541	vw	548	$\nu_9'-\nu_4$	E
				~ 556								564	$\nu_3'-(\nu_6+\nu_{12})$	E
562	19			565								568	$\nu_6+\nu_{11}$	E
575	11			~ 576								570	$\nu_9''-\nu_4$	E
590	6			~ 588		582	37			587	vw	584[e]	$\nu_5+\nu_{12}$	E
				~ 621	vw							604	$\nu_{11}+\nu_{12}$	A_1+A_2+E
				~ 632	vw							647	$\nu_3'-\nu_{11}$	E
652	2					649	42					658	$\nu_2-\nu_{10}''$	E
				~ 686		672	(73)[d]			~ 662	vw	669	$\nu_2-\nu_{10}'$	E
690	71			690						~ 690		686[e]	$2\nu_5$	A_1
714	99												ν_{10}'	E
726	98	720	100	~ 725	vs	714	98	713	100	~ 713	vs	716[e]	ν_{10}'' $2\nu_{11}$	E A_1+E
				~ 749								742	$\nu_8''-\nu_{10}'$	A_1+A_2+E
				755								751	$\nu_9''-\nu_5$	E
				~ 760								762	$(\nu_{10}''+\nu_{12})-\nu_6$	A_1+A_2+E
		766	?	763	m	759	73	766	?	~ 763	m	763[e]	$\nu_4+\nu_{12}$	E
				767	m							769	$\nu_3'-\nu_{12}$	E
				773								775	$\nu_3''-\nu_{12}$	E
				~ 779								777	$\nu_2-(\nu_{11}+\nu_{12})$	A_1+A_2+E
795	42	802[g]	13	~ 796	m	784	66	792	?	~ 790	m	789	$(\nu_9'+\nu_{12})-\nu_4$ or CCl_4 impurity	A_1+A_2+E
				~ 806	w							808	$(\nu_3'+\nu_4)-\nu_{10}''$	E
				~ 819	w							820	$(\nu_3'+\nu_4)-\nu_{10}'$	E
		820[g]		~ 835	vw	824	37	830	5	~ 829	w	829	$\nu_9'-\nu_{12}$	A_1+A_2+E
				~ 843	vw							853	$\nu_9''-\nu_{12}$	A_1+A_2+E
				864								857	$\nu_2-\nu_4$	A_1
864	21	866	10	868	w	861	43	868	19	~ 867	w	865[e]	$\nu_4+\nu_5$	A_1
				872	w							875	$\nu_9'-\nu_6$	E
				~ 876						883	vw	879	$\nu_9''-\nu_6$	E
				~ 926	vvw							931[e]	$\nu_6+\nu_{10}''$	E
				~ 952								955	$\nu_{10}'+\nu_{12}$	A_1+A_2+E
963	14	960	8	962	w	947	35	955	12	~ 951	w	962[e]	$\nu_{10}''+\nu_{12}$	A_1+A_2+E
				~ 971								971	$\nu_2-2\nu_6$	A_1
				~ 997								998	$(\nu_2+\nu_5)-\nu_{10}''$	E
				~1003								1009	$(\nu_4+\nu_{10}'')-\nu_{12}$	A_1+A_2+E
1012	42	1010	28	1010	m	1002	61	1007	35	~1005	m	1002	ν_3' ν_3'' $\nu_4+2\nu_{12}$	A_1 A_1 A_1+E
				1016	m									
				~1040								1038[e]	$\nu_2-\nu_5$	A_1
				~1046								1048	$2\nu_4$	A_1
1080	98	1068	?	1075	vs	1059	98	1068	?	~1071	vs	1074	ν_9' ν_9'' $\nu_{10}'+\nu_{11}$	E E A_1+A_2+E
1094	98	1088	100	1089	vs	1082	98	1084	100	1086				
				1096	vs					~1100		1084	$\nu_{10}''+\nu_{11}$	A_1+A_2+E
				~1149	vvw							1140[e]	$\nu_2-\nu_{12}$	E
				~1190	vvw							1186[e]	$\nu_8'-\nu_{12}$	A_1+A_2+E
				~1227								1222	$\nu_8'-\nu_6$	E
1235	25	1246	19	1236	m	1229	54	1238	24	1232	m	1232[e]	$\nu_4+\nu_{10}'$	E
				1242	m							1250	$\nu_4+\nu_{10}''$	E
				~1282								1285	$\nu_6+\nu_9'$	E
				1290		1290	28	1289	3	1290	w	1289[e]	$\nu_6+\nu_9''$	E
				1299								1300	$(\nu_3'+\nu_3'')-\nu_{10}''$	E
				~1309								1321	$\nu_9'+\nu_{12}$	A_1+A_2+E
				1319				1313	2	1309	w	1325	$\nu_9''+\nu_{12}$	A_1+A_2+E
				~1337								1353	$\nu_3'+\nu_5$	A_1
				1376								1373	$\nu_3'+\nu_{11}$	E
1381	66	1386	68	1383	m	1376	83	1382	86	1379	s	1377[e]	ν_2	A_1
				1391								1379	$\nu_3''+\nu_{11}$	E
				~1418								1423	$\nu_5+\nu_9'$	E
		1426	37	1427	m			1423	60	1420	m		ν_8'	E
				~1439[e]		1424	88					1434[e]	$\nu_9'+\nu_{11}$	A_1+A_2+E
1445	61			~1445[e]									ν_8''	E
		1454[f]	58	1456	m			1448	83	1447	m	1457	$\nu_9''+\nu_{11}$	A_1+A_2+E
				~1462								1504	$2\nu_6+\nu_9''$	E
				1504	vvw									
				1575	vvw					~1600	vvw	1592	$\nu_4+\nu_9'$	E

TABLE II.—(*Continued*).

Gas PR ν	Gas PR I	Gas KH ν	Gas KH I	Gas SNL ν	Gas SNL I	Liquid PR ν	Liquid PR I	Liquid KH ν	Liquid KH I	Liquid SNL ν	Liquid SNL I	ν_c	Theoretical Assignment	Type
												1626	$\nu_6+\nu_8'$	E
				~1667		1621	24							
						1678	23			~1653	vvw	1662[c]	$\nu_8'+\nu_{12}$	A_1+A_2+E
				1695	vvw							1697[c]	$\nu_8''+\nu_{12}$	A_1+A_2+E
				~1709								1724	$\nu_3'+\nu_{10}'$	E
				~1718								1724	$\nu_2+\nu_5$	A_1
		1730	vw	1733	vvw			1740	?	1721	w	1726	$\nu_3+\nu_{10}''$	E
				1745	vvw							1742	$\nu_3''+\nu_{10}''$	E
				~1751								1744	$\nu_2+\nu_{11}$	E
										1779	w	1784	$\nu_8'+\nu_{11}$	A_1+A_2+E
		1790	?	~1795	vw			1800	?			1790[c]	$\nu_5+\nu_8''$	E
				1832	vvw							1820	$\nu_9''+\nu_{10}''$	A_1+A_2+E
				1910	vw					1898	vw	1901	$\nu_2+\nu_4$	A_1
				1919								1919	$(\nu_3''+\nu_8')-\nu_4$	E
2041	6					2000	23					2010	$2\nu_3$	A_1
				~2110								2104	$\nu_3'+\nu_9''$	E
				2114						~2092		2100	$\nu_2+\nu_{10}''$	E
				~2128								2110	$\nu_3''+\nu_9''$	E
				~2132								2141	$\nu_8'+\nu_{10}'$	A_1+A_2+E
		2130	9	2137	w[d]			2130	15	2128	w	2142[c]	$\nu_8'+\nu_{10}''$	A_1+A_2+E
				~2141								2160	$2\nu_9'$	A_1+E
				~2155								2170	$\nu_8''+\nu_{10}'$	A_1+A_2+E
				2179								2188	$2\nu_9''$	A_1+E
				~2445								2443	$\nu_3''+\nu_8'$	E
				2451	w					2445	m	2449	$\nu_2+\nu_9'$	E
2475	6	2460	10	2460		2439	12	2460	15	2460	m	2463[c]	$\nu_2+\nu_9''$	E
				2509						2500	vw	2505[c]	$\nu_8'+\nu_9''$	A_1+A_2+E
				~2538						2525	vw	2531[c]	$\nu_8''+\nu_9''$	A_1+A_2+E
										2597	vw	2596[c]	$\nu_1-\nu_5$	A_1
				~2660								2654	$\nu_7-\nu_{11}$	A_1+A_2+E
				2670	vvw					2660	vw	2662[c]	$\nu_7-\nu_5$	E
										~2695		2698[c]	$\nu_1-\nu_{12}$	E
				2755	vvw					2740	vw	2758[c]	$2\nu_2$	A_1
										2762	vw	2764[c]	$\nu_7-\nu_{12}$	A_1+A_2+E
				~2809						~2801		2800[c]	$\nu_2+\nu_8'$	E
				~2825								2812	$\nu_7-\nu_8$	E
				2829								2837	$\nu_2+\nu_8''$	E
		2845	30	2837						2825	w	2842	$2\nu_8'$	A_1+E
				~2857						2857		2868	$\nu_8'+\nu_8''$	A_1+A_2+E
				2874						2882		2894[c]	$2\nu_8''$	A_1+E
				~2899								2895	$(\nu_7+\nu_{12})-\nu_{11}$	A_1+A_2+3E
				2946								2942	$(\nu_1+\nu_{10}')-\nu_{10}''$	A_1+A_2+E
		2935	50	2954	w					2941	w	**2943**[c]	ν_1	A_1
				2963								2967	$\nu_3''+\nu_4+\nu_8'$	E
2950	26					2941	27							
				~3008								3013	$\nu_2+\nu_6+\nu_8'$	E
		3010	35	3017	m					3003	m	**3010**[c]	ν_7	E
				~3021								3030	$3\nu_3'$	A_1
										~3077		3083	$2\nu_5'+\nu_{12}$	A_1+A_2+2E
				3175	vw					3175	w	3180[c]	$\nu_1+\nu_{12}$	E
				3247	w					3247	w	3246	$\nu_7+\nu_{12}$	A_1+A_2+E
				3289	w					3289	w	3282[c]	$\nu_1+\nu_5$	A_1
3378	11			3356	w	3356	2			3344	w	3348[c]	$\nu_5+\nu_7$	E
										3460	vw	3461[c]	$\nu_1+\nu_4$	A_1
										3584	vw	3589	$\nu_6+\nu_7+\nu_{12}$	A_1+A_2+E
										3636	vvw	3649	$\nu_1+\nu_{10}'$	E
										3704	vw	3715	$\nu_7+\nu_{10}'$	A_1+A_2+E
										3774	vw	3769	$(\nu_3+\nu_7)-\nu_{12}$	A_1+A_2+E
										~3922		3944	$\nu_1+\nu_3$	A_1
				4000	w					4016	w	4009	$\nu_1+\nu_9'$	E
				4065	w					4065	w	4075	$\nu_7+\nu_9'$	A_1+A_2+E
						4132	19					4089	$\nu_7+\nu_9''$	A_1+A_2+E
				4348	w					4367		4360[c]	$\nu_1+\nu_8'$	E
				4405	w					4425	w	4426[c]	$\nu_7+\nu_8'$	A_1+A_2+E
										4651	vvw	4654	$\nu_1+\nu_3+\nu_{10}'$	E
5155	10					5102	14					5105	$\nu_2+\nu_7+\nu_{10}''$	A_1+A_2+E

[a] KH = infrared data of Karplus and Halford, see reference 8; ν = infrared wave number in cm^{-1}; braces enclose unresolved bands or resonance doublets; other symbols have the same meaning as in Table I.
[b] Reported by W. L. Hyde (reference 6).
[c] Same as assignment of Smith, Nielsen, and Liang (reference 5).
[d] This intensity is uncertain because of its proximity to the strong 714 band.
[e] These two bands can be assigned as $\nu_{10}'+\nu_{10}''=1440(A_1+A_2+E)$ and $2\nu_{10}''=1452$ cm^{-1} (A_1+E), respectively.
[f] Gas fundamentals were used in the calculation for bands reported in the gas only; otherwise, liquid fundamentals were used.
[g] In the paper of Karplus and Halford (reference 8), apparently the bands 802 and 820 are interchanged, and the 1454 band is incorrectly given as 1554 cm^{-1}. In a prepublication copy of their data, handed to the authors at the Chicago meeting of the American Physical Society, November, 1949, the 802 (intensity 13) line was listed opposite their liquid 792 line, and the 1554 line was given correctly as 1454 cm^{-1}.

NORMAL COORDINATE TREATMENT

A normal coordinate treatment was carried out using the Wilson *FG* matrix method.[11] The various bond distances and interbond angles used to determine the internal coordinates are shown in Fig. 2.

From the internal coordinates the following orthonormal symmetry coordinates were formed:

for the A_1 vibrations,

$$R_1=(\Delta d_1+\Delta d_2+\Delta d_3)/3^{\frac{1}{2}},$$
$$R_2=(\Delta D_1+\Delta D_2+\Delta D_3)/3^{\frac{1}{2}},$$
$$R_3=\Delta r,$$
$$R_4=(\Delta a_{12}+\Delta a_{23}+\Delta a_{31}-\Delta b_1-\Delta b_2-\Delta b_3)/6^{\frac{1}{2}},$$

and

$$R_5=(\Delta A_{12}+\Delta A_{23}+\Delta A_{31}-\Delta B_1-\Delta B_2-\Delta B_3)/6^{\frac{1}{2}};$$

for the two redundant coordinates,

$$R_6=(\Delta a_{12}+\Delta a_{23}+\Delta a_{31}+\Delta b_1+\Delta b_2+\Delta b_3)/6^{\frac{1}{2}},$$

and

$$R_7=(\Delta A_{12}+\Delta A_{23}+\Delta A_{31}+\Delta B_1+\Delta B_2+\Delta B_3)/6^{\frac{1}{2}};$$

and for the E vibrations,

$$R_{1a}=(2\Delta d_2-\Delta d_1-\Delta d_3)/6^{\frac{1}{2}},$$
$$R_{1b}=(\Delta d_1-\Delta d_3)/2^{\frac{1}{2}},$$
$$R_{2a}=(2\Delta D_2-\Delta D_1-\Delta D_3)/6^{\frac{1}{2}},$$
$$R_{2b}=(\Delta D_1-\Delta D_3)/2^{\frac{1}{2}},$$
$$R_{3a}=(2\Delta a_{13}-\Delta a_{12}-\Delta a_{23})/6^{\frac{1}{2}},$$
$$R_{3b}=(\Delta a_{23}-\Delta a_{12})/2^{\frac{1}{2}},$$
$$R_{4a}=(2\Delta A_{13}-\Delta A_{12}-\Delta A_{23})/6^{\frac{1}{2}},$$
$$R_{4b}=(\Delta A_{23}-\Delta A_{12})/2^{\frac{1}{2}},$$
$$R_{5a}=(2\Delta b_2-\Delta b_1-\Delta b_3)/6^{\frac{1}{2}},$$
$$R_{5b}=(\Delta b_1-\Delta b_3)/2^{\frac{1}{2}},$$
$$R_{6a}=(2\Delta B_2-\Delta B_1-\Delta B_3)/6^{\frac{1}{2}},$$

and

$$R_{6b}=(\Delta B_1-\Delta B_3)/2^{\frac{1}{2}}.$$

The f matrix was

f	Δd_1	Δd_2	Δd_3	ΔD_1	ΔD_2	ΔD_3	Δr	Δa_{12}	Δa_{23}	Δa_{31}	ΔA_{12}	ΔA_{23}	ΔA_{31}	Δb_1	Δb_2	Δb_3	ΔB_1	ΔB_2	ΔB_3
Δd_1	f_d	f_{dd}	f_{dd}	f_{dD}	f_{dD}	f_{dD}	f_{dr}	df_{da}	df'_{da}	df_{da}	Df_{dA}	Df_{dA}	Df_{dA}	df_{db}	df'_{db}	df'_{db}	Df_{dB}	Df_{dB}	Df_{dB}
Δd_2		f_d	f_{dd}	f_{dD}	f_{dD}	f_{dD}	f_{dr}	df_{da}	df_{da}	df'_{da}	Df_{dA}	Df_{dA}	Df_{dA}	df'_{db}	df_{db}	df'_{db}	Df_{dB}	Df_{dB}	Df_{dB}
Δd_3			f_d	f_{dD}	f_{dD}	f_{dD}	f_{dr}	df'_{da}	df_{da}	df_{da}	Df_{dA}	Df_{dA}	Df_{dA}	df'_{db}	df'_{db}	df_{db}	Df_{dB}	Df_{dB}	Df_{dB}
ΔD_1				f_D	f_{DD}	f_{DD}	f_{Dr}	df_{Da}	df_{Da}	df_{Da}	Df_{DA}	Df'_{DA}	Df_{DA}	df_{Db}	df_{Db}	df_{Db}	Df_{DB}	Df'_{DB}	Df'_{DB}
ΔD_2					f_D	f_{DD}	f_{Dr}	df_{Da}	df_{Da}	df_{Da}	Df_{DA}	Df_{DA}	Df'_{DA}	df_{Db}	df_{Db}	df_{Db}	Df'_{DB}	Df_{DB}	Df'_{DB}
ΔD_3						f_D	f_{Dr}	df_{Da}	df_{Da}	df_{Da}	Df'_{DA}	Df_{DA}	Df_{DA}	df_{Db}	df_{Db}	df_{Db}	Df'_{DB}	Df'_{DB}	Df_{DB}
Δr							f_r	df_{ra}	df_{ra}	df_{ra}	Df_{rA}	Df_{rA}	Df_{rA}	df_{rb}	df_{rb}	df_{rb}	Df_{rB}	Df_{rB}	Df_{rB}
Δa_{12}								d^2f_a	d^2f_{aa}	d^2f_{aa}	dDf_{aA}	dDf_{aA}	dDf_{aA}	d^2f_{ab}	d^2f_{ab}	$d^2f'_{ab}$	dDf_{aB}	dDf_{aB}	dDf_{aB}
Δa_{23}									d^2f_a	d^2f_{aa}	dDf_{aA}	dDf_{aA}	dDf_{aA}	$d^2f'_{ab}$	d^2f_{ab}	d^2f_{ab}	dDf_{aB}	dDf_{aB}	dDf_{aB}
Δa_{31}										d^2f_a	dDf_{aA}	dDf_{aA}	dDf_{aA}	d^2f_{ab}	$d^2f'_{ab}$	d^2f_{ab}	dDf_{aB}	dDf_{aB}	dDf_{aB}
ΔA_{12}											D^2f_A	D^2f_{AA}	D^2f_{AA}	dDf_{Ab}	dDf_{Ab}	dDf_{Ab}	D^2f_{AB}	D^2f_{AB}	$D^2f'_{AB}$
ΔA_{23}												D^2f_A	D^2f_{AA}	dDf_{Ab}	dDf_{Ab}	dDf_{Ab}	$D^2f'_{AB}$	D^2f_{AB}	D^2f_{AB}
ΔA_{31}							$(f_{ij}=f_{ji})$						D^2f_A	dDf_{Ab}	dDf_{Ab}	dDf_{Ab}	D^2f_{AB}	$D^2f'_{AB}$	D^2f_{AB}
Δb_1														d^2f_b	d^2f_{bb}	d^2f_{bb}	dDf_{bB}	dDf_{bB}	dDf_{bB}
Δb_2															d^2f_b	d^2f_{bb}	dDf_{bB}	dDf_{bB}	dDf_{bB}
Δb_3																d^2f_b	dDf_{bB}	dDf_{bB}	dDf_{bB}
ΔB_1																	D^2f_B	D^2f_{BB}	D^2f_{BB}
ΔB_2																		D^2f_B	D^2f_{BB}
ΔB_3																			D^2f_B

In this matrix, two interaction constants differing only by a prime mean an interaction between the same two elements, except that in the primed constant the interacting elements have no bond in common, whereas in the unprimed one there is a common bond. The equilibrium values of the bond lengths were[12] $d=1.093$, $D=1.76$, and $r=1.54$A. All angles were assumed to be tetrahedral.

From the f matrix and the U matrix, formed from the coefficients in the symmetry coordinates, one gets the following F matrix elements: for the A_1 vibrations,

$$F_{11}=f_d+2f_{dd},\ F_{12}=3f_{dD},\ F_{13}=3^{\frac{1}{2}}f_{dr},$$
$$F_{14}=2^{-\frac{1}{2}}d(2f_{da}+f'_{da}-f_{db}-2f'_{db}),\ F_{15}=3D2^{-\frac{1}{2}}(f_{dA}-f_{dB}),$$
$$F_{22}=f_D+2f_{DD},\ F_{23}=3^{\frac{1}{2}}f_{Dr},\ F_{24}=3d2^{-\frac{1}{2}}(f_{Da}-f_{Db}),$$
$$F_{25}=2^{-\frac{1}{2}}D(2f_{DA}+f'_{DA}-f_{DB}-2f'_{DB}),\ F_{33}=f_r,$$
$$F_{34}=3d6^{-\frac{1}{2}}(f_{ra}-f_{rb}),\ F_{35}=3D6^{-\frac{1}{2}}(f_{rA}-f_{rB}),$$
$$F_{44}=d^2(f_a+2f_{aa}-4f_{ab}-2f'_{ab}+f_b+2f_{bb})/2,$$
$$F_{45}=3dD(f_{aA}-f_{aB}-f_{bA}+f_{bB})/2,$$
$$F_{55}=D^2(f_A+2f_{AA}-4f_{AB}-2f'_{AB}+f_B+2f_{BB})/2,$$

and $F_{ij}=F_{ji}$;

and for the E vibrations,

$$F_{11}=f_d-f_{dd},\ F_{12}=0,\ F_{13}=-d(f_{da}-f'_{da}),\ F_{14}=0,$$
$$F_{15}=d(f_{db}-f'_{db}),\ F_{16}=0,\ F_{22}=f_D-f_{DD},\ F_{23}=0,$$
$$F_{24}=-D(f_{DA}-f'_{DA}),\ F_{25}=0,\ F_{26}=D(f_{DB}-f'_{DB}),$$
$$F_{33}=d^2(f_a-f_{aa}),\ F_{34}=0,\ F_{35}=-d^2(f_{ab}-f'_{ab}),\ F_{36}=0,$$
$$F_{44}=D^2(f_A-f_{AA}),\ F_{45}=0,\ F_{46}=-D^2(f_{AB}-f'_{AB}),$$
$$F_{55}=d^2(f_b-f_{bb}),\ F_{56}=0,\ F_{66}=D^2(f_B-f_{BB}),\ \text{and}\ F_{ij}=F_{ji}.$$

[11] E. B. Wilson, Jr., J. Chem. Phys. **7**, 1047 (1939); **9**, 76 (1941).
[12] J. Y. Beach and D. P. Stevenson, J. Am. Chem. Soc. **61**, 2643 (1939).

The following G matrix elements were obtained from the relations given by Wilson:[11] for the A_1 vibrations,

$G_{11}=\mu_H+\mu_C/3$, $G_{12}=0$, $G_{13}=-3^{-\frac{1}{2}}\mu_C$,
$G_{14}=-4\mu_C/3d$, $G_{15}=0$, $G_{22}=\mu_{Cl}+\mu_C/3$, $G_{23}=-3^{-\frac{1}{2}}\mu_C$,
$G_{24}=0$, $G_{25}=-4\mu_C/3D$, $G_{33}=2\mu_C$, $G_{34}=4\mu_C/3^{\frac{1}{2}}d$,
$G_{35}=4\mu_C/3^{\frac{1}{2}}D$, $G_{44}=2d^{-2}(\mu_H+8\mu_C/3)$, $G_{45}=0$,
$G_{55}=2(\mu_{Cl}+8\mu_C/3)D^{-2}$, and $G_{ij}=G_{ji}$;

and for the E vibrations, $G_{11}=\mu_H+4\mu_C/3$, $G_{12}=0$,
$G_{13}=4\mu_C 2^{\frac{1}{2}}/3d$, $G_{14}=0$, $G_{15}=-2^{\frac{1}{2}}\mu_C(r^{-1}+3^{-1}d^{-1})$,
$G_{16}=0$, $G_{22}=\mu_{Cl}+4\mu_C/3$, $G_{23}=0$, $G_{24}=4\mu_C 2^{\frac{1}{2}}/3D$,
$G_{25}=0$, $G_{26}=-2^{\frac{1}{2}}\mu_C(r^{-1}+3^{-1}D^{-1})$,
$G_{33}=(5\mu_H/2+8\mu_C/3)d^{-2}$, $G_{34}=0$,
$G_{35}=\frac{1}{2}d^{-2}\mu_H-2d^{-1}(r^{-1}+3^{-1}d^{-1})\mu_C$, $G_{36}=0$,
$G_{44}=(5\mu_{Cl}/2+8\mu_C/3)D^{-2}$, $G_{45}=0$,
$G_{46}=\frac{1}{2}D^{-2}\mu_{Cl}-2D^{-1}(r^{-1}+3^{-1}D^{-1})\mu_C$,
$G_{55}=d^{-2}\mu_H+3\mu_C[r^{-2}+(r^{-1}+3^{-1}d^{-1})^2]/2$, $G_{56}=0$,
$G_{66}=D^{-2}\mu_{Cl}+3\mu_C[r^{-2}+(r^{-1}+3^{-1}D^{-1})^2]/2$, and $G_{ij}=G_{ji}$;

where $\mu_H=0.99216$, $\mu_C=0.083264$, and $\mu_{Cl}=0.028203$ (awu)$^{-1}$ are the reciprocals of the masses of the H, C, and Cl atoms, respectively.

As an aid in determining some of the force constants, the results from previous investigations of ethane and hexadeuteroethane,[13] and of methylacetylene, some trichloromethanes, and hexachloroethane[14] were used. The method of splitting out frequencies given by Wilson[11] was first used to get an approximate value for the C−H stretching force constant. The other constants were transferred from the above molecules,[13,14] and after several modifications it was possible to get agreement to within 1 percent of the observed values. The set of force constants that gave the best agreement with the observed fundamentals is given in Table III. In this table $f_{r\gamma}=f_{ra}-f_{rb}$, and $f_{rC}=f_{rA}-f_{rB}$, since these constants could be obtained only in such combinations. One notices that all interactions between the CH_3 and CCl_3 groups were ignored; this was done because these interactions are believed to be very small and also because there were not sufficient data to permit their determination. The combination $(f_{aA}+f_{bB})-(f_{aB}+f_{bA})$ was assumed to be zero, since it also involves interaction constants between the CCl_3 and CH_3 groups.

For comparison, the CCl_3 group force constants and other corresponding constants found for hexachloroethane[14] are given in Table IV.

One notices that f_D is slightly lower than for hexachloroethane. The value of f_{AA} is very small, about $\frac{1}{10}$ that for C_2Cl_6, while f_B is considerably higher. The constants f_{AB} and f_{BB} changed sign, but the order of magnitude is about the same as that found for C_2Cl_6. The constant f'_{AB} was set equal to zero, and the value of f_r was assumed to be 4.5×10^5 dynes/cm as for

[13] F. Stitt, J. Chem. Phys. **7**, 297 (1939).
[14] A. G. Meister, J. Chem. Phys. **16**, 950 (1948); Zietlow, Cleveland, and Meister, J. Chem. Phys. **18**, 1076 (1950); also work on hexachloroethane by Miss Rose A. Carney, to be published.

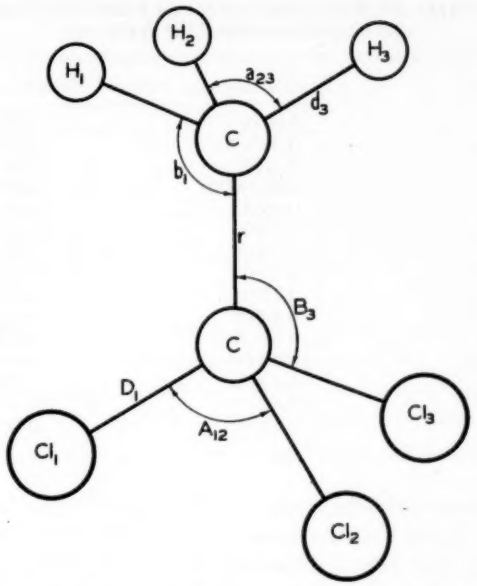

FIG. 2. Bond distances and interbond angles for 1,1,1-trichloroethane.

C_2Cl_6[14], C_2H_6[13], and C_2D_6[13]. The value of f_{Dr} is higher than for C_2Cl_6.

ASSIGNMENT OF THE FUNDAMENTALS

The frequencies chosen as fundamentals are those given in Table V.

There has been a lack of agreement among previous workers as to the location of the C−C stretching fundamental ν_3; in four investigations it was given as 714[2], 977[4], 1070[5], and 1007[8]. The present calculations showed clearly that ν_3 should lie in the range 1000–1100 cm^{-1}.

TABLE III. Force constants for 1,1,1-trichloroethane (10^5 dynes/cm).

Type	Value	Type	Value
f_d	4.9402[a]	f_D	3.0076
f_{dd}	0.023633	f_{DD}	0.30760[d]
f_a	0.43948[b]	f_A	0.37094[d]
f_{aa}	−0.0048900	f_{AA}	0.0010600
f_b	0.61739	f_B	0.38733
f_{bb}	−0.015030	f_{BB}	0.10977
f_{ab}	0.012850[c]	f_{AB}	0.041274
f_{ab}'	0.00000	f_{AB}'	0.00000
f_{da}	0.20586	f_{DA}	0.20000
f_{da}'	−0.087840	f_{DA}'	−0.14501
f_{db}	0.24129	f_{DB}	0.21056
f_{db}'	0.041293	f_{DB}'	−0.10528
f_r	4.5000[d]		
$f_{r\gamma}$	−0.25000	f_{rC}	−0.32893[d]
f_{dr}	0.00000	f_{Dr}	0.37576
f_{dD}	0.00000		
f_{dA}	0.00000	f_{Da}	0.00000
f_{dB}	0.00000	f_{Db}	0.00000
$(f_{aA}+f_{bB})-(f_{aB}+f_{bA})=0$			

[a] This number of significant figures is not really justified but is necessary to give the best reproduction of the observed frequencies and to secure internal consistency in the calculations.
[b] Transferred without modification from B. Stepanov, Acta Physicochim. U.R.S.S. **20**, 174 (1945).
[c] Transferred without modification from methylacetylene (reference 14).
[d] Transferred without modification from hexachloroethane (reference 14).

TABLE IV. Force constants for 1,1,1-trichloroethane and hexachloroethane (10^5 dynes/cm).

Type	1,1,1-trichloroethane	Hexachloroethane
f_D	3.0076	3.4580
f_{DD}	0.30760	0.30760
f_A	0.37094	0.37094
f_{AA}	0.0010600	0.019760
f_B	0.38733	0.29559
f_{BB}	0.10977	−0.16402
f_{DA}	0.20000	0.20584
f_{DA}'	−0.14501	−0.15413
f_{DB}	0.21056	0.22684
f_{DB}'	−0.10528	−0.11342
f_{AB}	0.041274	−0.072394
f_{AB}'	0.00000	0.036197
f_r	4.5000	4.5000
f_{rC}	−0.32893	−0.32893
f_{Dr}	0.37576	0.26531

The most probable value in this region is the band at 1005 (liquid) or the band at 1070. The F-matrix elements that primarily affect this fundamental are $F_{22}=f_D+2f_{DD}$, $F_{23}=3^{\frac{1}{2}}f_{Dr}$, and $F_{33}=f_r$. The value f_r was fixed at 4.5×10^5 dynes/cm, the value it has in C_2Cl_6[14], C_2H_6[13], and C_2D_6[13]. The value of F_{22} and F_{23}, then, could be varied so as to keep the frequency pattern undistorted while giving values for ν_3 ranging from 1005 to 1070 cm^{-1}. It was found that going from 1070 down to 1005 cm^{-1} (by adjusting F_{22} and F_{23} slightly) moved some frequencies in the right direction (towards the observed values), whereas going up from 1005–1070 cm^{-1} moved the same frequencies in the wrong direction (away from the observed values). This may indicate that 1005 is more likely to be ν_3 than 1070 which would be extraordinarily high for a C−C frequency. Furthermore, the values of F_{22} and F_{23} so obtained are a little better, comparing with hexachloroethane constants, than those obtained if one assumes $\nu_3=1070$ cm^{-1}. Moreover, the 1010 and 1016 cm^{-1} (gas values) in the data of Smith, Nielsen, and Liang[5] seem quite likely to be a resonance doublet, which thus points to the presence of a fundamental there. Unless these form a resonance doublet, it is hard to assign them both as binary combinations. Only one of them was assigned by Smith, Nielsen, and Liang[5] using their 301 cm^{-1} fundamental, which is assigned in the present paper as a difference band. On the other hand, the frequency at 1070 cm^{-1} can easily be assigned. All these indications tend to put more weight on the side of the 1005 as ν_3. The C−C band for many molecules is very weak in the Raman spectrum, and it apparently has not been observed for Cl_3C-CH_3.

TABLE V. The fundamentals of 1,1,1-trichloroethane.

Designation	Wave number Calculated	Observed Liquid	Observed Gas	Degeneracy	Type
ν_1	2943	2939	2954	1	A_1
ν_2	1377	1379	1381	1	A_1
ν_3	1002	1005	1012	1	A_1
ν_4	521	522	524	1	A_1
ν_5	343	343	343	1	A_1
ν_6	205	—	—	1	A_2
ν_7	3010	3005	3017	2	E
ν_8	1434	1434[a]	1445	2	E
ν_9	1074	1077[a]	1087[a]	2	E
ν_{10}	716	716[a]	720[a]	2	E
ν_{11}	363	—	—	2	E
ν_{12}	241	241	—	2	E

[a] Mean of resonance doublets, see Tables I and II.

The frequency ν_{11} was obtained in the present investigation by calculation only. It was not observed in either the Raman or infrared. It was suspected by Karplus and Halford[8] to be the twice reported[1,3] very weak band at 308 cm^{-1} and was believed by Smith, Nielsen, and Liang[5] to be the very, very weak band at 301 cm^{-1}. It is interesting to examine closely the E frequencies and the corresponding A_1 frequencies. The C−H stretching are ($3005E$, $2939A_1$), the C−Cl stretching are ($716E$, $522A_1$), the CH_3 deformation are ($1434E$, $1379A_1$) and the CCl_3 deformation are ($\nu_{11}E$, $343A_1$). So it is very reasonable from such a comparison to believe that ν_{11} should be higher than $\nu_5=343A_1$ frequency. The calculated value for ν_{11} was found to be 363 cm^{-1}. In order to see how reliable this calculated value is, the value of the combination (f_B-f_{BB})—which determines primarily the frequency in question—was changed to that of C_2Cl_6. It was found that this change distorted the frequency pattern appreciably, which means that this F-matrix element should have a value around that found in the present investigation. Consequently, the present calculated value (363) should be reliable to within the usual uncertainty limits of calculation (∼2 percent). It is then conceivable that this band is unresolved from the very strong band at 343 cm^{-1}. The fact that the observed depolarization factor was 0.58, which is about the value one would expect if an A_1 and an E fundamental were overlapping, may be used as an argument in favor of this supposition. The present calculated value is further substantiated by the fact that the Fermi resonance doublet 710–721 cm^{-1} can be accounted for satisfactorily only with the help of the overtone of this frequency. It is seen from Tables I and II that the two fundamentals ν_3 and ν_{11} have been used in many assignments, some of which could not be assigned otherwise.

Other observed wave numbers and their assignments as combinations or overtones are given in Tables I and II. It is seen that Smith, Nielsen, and Liang[5] have listed a large number of bands, some of which may be due to rotational structure, but a more detailed rotational analysis has to be carried out in order to settle this point. However, an assignment of all the present and previously reported bands has been attempted in this present investigation. The majority of these bands have been assigned as binary combinations or first overtones, but it was necessary to use ternary combinations in the remaining cases.

THE TORSIONAL FREQUENCY

The A_2, torsional frequency ν_6 can be evaluated if the height of the potential barrier hindering the internal rotation is known. The form of the potential barrier adopted in the present investigation is the usual $V=\frac{1}{2}V_0(1-\cos 3\phi)$, V_0 being the height of the potential barrier, and ϕ the torsional angle. To get V_0, the entropies for the ideal gaseous state at the temperatures 286.53°K and 298.16°K were calculated to a rigid rotator, harmonic oscillator approximation, assuming the internal rotation to be unrestricted. A comparison with the experimental values of Yost and co-workers[4] made it possible, using Pitzer and Gwinn's tables,[15] to get the corresponding two values[16] of V_0. The entropies, entropy differences, and the corresponding values of V_0 are given in Table VI.

The uncertainty ±0.16 cal deg^{-1} mole^{-1} was not taken into account in obtaining the values of V_0 given in the table. From this uncertainty in the experimental entropy values, the upper and lower limits for V_0 were then evaluated in a similar manner. These were found to be 3397 and 2363 cal mole^{-1}, respectively. The values of the principal moments of inertia were I_A (about the symmetry axis)$=492\times10^{-40}$ and $I_B=354\times10^{-40}$ g cm^2. In evaluating the entropy contribution of a free rotator, a quantity called the reduced moment of inertia is needed; this is defined as $I_r=I_1I_2/(I_1+I_2)$, where I_1 and I_2 are the moments of inertia of the CH_3 and CCl_3 groups about the symmetry axis. The value of I_r was found to be 5.27×10^{-40} g cm^2, corresponding to I_1 and $I_2=5.33\times10^{-40}$ g cm^2 and 486×10^{-40} g cm^2, respectively. The atomic masses and fundamental constants were taken from Birge's tables.[17]

The torsional frequency ν_6 can now be obtained from V_0. The Schrödinger wave equation for this torsional motion, using the above cosine potential function, is the Mathieu equation, which has been solved exactly for certain values of V_0. Wilson[18] has tabulated the first 7 eigenvalues corresponding to several values of V_0. The first 2 eigenvalues corresponding to each of the present values of V_0 were obtained from Wilson's tables by graphical interpolation, and these, together with the Bohr formula $(W_2-W_1)/hc=\nu_6$, were used to get ν_6. Here W_1 and W_2 are the first 2 energy levels, which can be obtained from the tabulated eigenvalues using known constants,[19] h is Planck's constant, and c is the velocity of light. Table VII shows the ν-values corresponding to the aforementioned values of V_0. It is seen that the mean of the first two values (at temperatures 286.53°K and 298.16°K, respectively) is 205 cm^{-1} and the mean corresponding to the upper and lower limits of V_0 is 205.5 cm^{-1}; hence, a mean value of 205±20 cm^{-1} was considered reasonable for ν_6. The value V_0 corresponding to this adopted mean value of ν_6 was found to be 2840±500 cal/mole. It should be noticed that the uncertainty in V_0 (±500 cal/mole) and the corresponding uncertainty in ν_6 (±20 cm^{-1}) is due only to the uncertainty given by the investigators[4] for their experimental entropies and does not include any uncertainties in the spectroscopic observations or in the method of calculation given in the present investigation. The calculated value for ν_6 (205 cm^{-1}) is believed to be not far from the real value, since a band at 457 cm^{-1} was found in the present infrared investigation which could be assigned satisfactorily only as a combination with ν_6. Moreover, this frequency ν_6 was used in quite a few cases in making assignments for the observed bands.

Having established a value for the torsional fundamental, a normal coordinate treatment was carried out for this vibration. Of course, the value of the force constant thus obtained will be approximate, since in this treatment a harmonic oscillator approximation was assumed and in addition the frequency itself is not known accurately. The potential energy function for such a vibration will simply be $2V=f_\phi(\Delta\phi)^2$, where ϕ is the torsional angle, and f_ϕ is the force constant associated with this motion. The kinetic energy is $2T=I_r\dot{\phi}^2$, where I_r is again the reduced moment of inertia for the molecule; and hence, the secular equation will simply be $f_\phi=I_r\lambda$, where $\lambda=4\pi^2\nu_6^2c^2$, ν_6 being the wave number corresponding to the torsional frequency, and c the velocity of light. The value of f_ϕ was found to be 0.786×10^{-12} erg/radian. It is interesting to compare this value with the value 0.71×10^{-12} erg/radian for the similar force constant in ethane given by Pitzer.[20] A more accurate determination of the torsional frequency for Cl_3C-CH_3 is necessary before a critical comparison can be made of the torsional force constants of the two molecules.

TABLE VI. Potential barrier hindering the internal rotation in 1,1,1-trichloroethane.[a]

Temp. (°K)	Calculated entropy, $S°_{calc}$ (cal deg^{-1} mole^{-1}) T+R	Vib	IRF	Total	$S°_{exp}$	$S°_{calc}-S°_{exp}$	V_0 (cal mole^{-1})
286.53	65.96	7.97	3.55	77.48	76.22±0.16	1.26±0.16	2680
298.16	66.28	8.45	3.59	78.32	76.97±0.16	1.35±0.16	2993

[a] T+R = translational+rotational contribution; Vib = vibrational contribution; IRF = internal free rotational contribution; $S°_{exp}$ = experimental value of the entropy.

TABLE VII. The calculated values of the torsional fundamental ν_6 for 1,1,1-trichloroethane.

V_0	2680	2993	2363	3397
ν (cm^{-1})	199	211	186	225

[15] K. S. Pitzer and W. D. Gwinn, J. Chem. Phys. **10**, 428 (1942).
[16] H. Taylor and S. Glasstone, *A Treatise on Physical Chemistry*, Vol. I, *Atomistics and Thermodynamics* (D. Van Nostrand Company, Inc., New York, 1942), third edition, p. 599.
[17] R. T. Birge, Revs. Modern Phys. **13**, 233 (1941).
[18] E. B. Wilson, Jr., Chem. Revs. **27**, 17 (1940).
[19] Eyring, Walter, and Kimball, *Quantum Chemistry* (John Wiley and Sons, Inc., New York, 1944), p. 358.
[20] K. S. Pitzer, J. Chem. Phys. **12**, 310 (1944).

TABLE VIII. Heat content, free energy, entropy, and heat capacity of 1,1,1-trichloroethane for the ideal gaseous state at one atmosphere pressure.[a]

T	$(H^0-H_0^0)/T$	$-(F^0-H_0^0)/T$	S^0	C_p^0
286.53			76.15	
298.16	14.71	62.33	77.03	22.37
300	14.75	62.42	77.17	22.44
400	17.11	66.99	84.10	25.80
500	19.12	71.03	90.15	28.37
600	20.83	74.67	95.51	30.36
700	22.31	78.00	100.31	31.96
800	23.60	81.06	104.67	33.29
900	24.75	83.91	108.66	34.41
1000	25.76	86.61	112.37	35.36

[a] T is in °K, other quantities are in cal mole^{-1} deg^{-1}.

THERMODYNAMIC PROPERTIES

The heat content, free energy, entropy, and heat capacity for 1,1,1-trichloroethane were calculated at 9 different temperatures from 298.16 to 1000°K, to a rigid rotator, harmonic oscillator approximation for the ideal gaseous state at one atmosphere pressure. The entropy at 286.53°K was calculated also so that it could be compared with the experimental value given by Yost and co-workers.[4] The wave numbers given in Table V for the gaseous state were used, when available; otherwise the liquid values or (for ν_6 and ν_{11}) calculated values were used. In the present calculations, nuclear spins and the effect of the isotopic mixing have been neglected. The values of the principal moments of inertia are those given in the section on the torsional frequency. The symmetry number has been taken equal to 3, and Birge's 1941 values[17] of the physical constants have been used throughout. The results obtained for the thermodynamic properties, including the contribution of the torsional fundamental 205 cm^{-1}, are given in Table VIII. The contribution of the torsional frequency was obtained with the aid of Pitzer and Gwinn's Tables.[15]

ACKNOWLEDGMENTS

The Hilger E518 spectrograph used for the depolarization spectrograms was obtained in part with a grant from the American Academy of Arts and Sciences, and the optical parts of the 2-prism spectrograph used for the Raman displacement spectrograms were secured with a grant from the Society of the Sigma Xi. The sample of 1,1,1-trichloroethane was kindly furnished by the Dow Chemical Company, Midland, Michigan. The diagrams used as Figs. 1 and 2 were prepared by Mr. Alfons Weber. The authors are grateful for this assistance. They also wish to express their thanks to Dr. Don C. Smith, of the Naval Research Laboratory and to Professor J. Rud Nielsen, Physics Department, University of Oklahoma, for making their infrared and Raman data available before publication. One of us (M.Z.S.) wishes to express his gratitude to the Egyptian Government for the fellowship which made it possible for him to carry out this work.

Unimerism

JAMES K. SENIOR
George Herbert Jones Laboratory, University of Chicago, Chicago, Illinois
(Received October 31, 1949)

It is pointed out that, in the development of structural organic chemistry, those compounds which have no structural isomers play a crucial role. Since no general name has ever been given to compounds which meet this condition, they are here called "unimers." It is further shown that the molecular formula of a unimer must necessarily fulfill certain mathematical conditions. These conditions are set forth in nine theorems. Some of these theorems are almost self-evident; for others, the proofs, although simple in plan, are exceedingly intricate in application. Consequently, the reader is referred for all proofs to a purely mathematical paper which will be published in the *American Journal of Mathematics*. Finally, a complete list of unimeric types is given.

THE methods used by organic chemists to determine molecular structures differ widely in detail, but most of the procedures employed for that purpose fit into the general scheme illustrated by the following outline. Let A be a pure compound of unknown molecular structure, but of known molecular formula fixed by qualitative and quantitative analysis together with a molecular weight determination. A is converted by (supposedly) well-understood type reactions into the compounds $B_1 \cdots B_m$, the structures of which are known. The structure of A is then determined by reversing (at least in thought) the conversion reactions. In most instances, some of the substances $B_1 \cdots B_m$ are compounds the structures of which were at one time unknown. The structure of any one of them (say B_i) was previously determined by converting B_i into the compounds $C_1 \cdots C_n$, the structures of which were known at the time when the structure of B_i was under investigation. And so the process of successive conversion may be traced back through an indefinite number of stages.

Since the number of compounds of known structure is finite, reasoning of the sort just indicated cannot lead to an infinite regression. It may, however, easily lead to a vicious circle; for, unless due caution is exercised, the structure of X may first be derived from the assumed structure of Y, and the structure of Y may then be derived from the structure of X thus obtained. To avoid this fallacy, it is essential, in using the recursive reasoning described, to arrive finally at compounds the structures of which are known independently—that is, without any further conversion. These compounds are obviously the ones where, under the assumed rules of valence, the molecular formula uniquely determines the structural formula—in other words, the compounds with molecular formulas which permit no structural isomerism. Such compounds will hereafter be called *unimers*.

Certain unimers such as methane, ethane, propane, ethylene, methyl alcohol, methyl chloride, chloroform, etc., will at once occur to almost any chemist. But, for a thorough understanding of unimerism, no such list drawn up at random is adequate. What is here required is a statement of necessary and sufficient conditions, which, when applied to a molecular formula, assure that the corresponding compound (if one exists) shall be a unimer. In the present paper, such conditions are established. Once they have been determined, the construction of a complete list of unimers turns out to be surprisingly easy.

A convenient way to investigate unimerism is first to lay aside (temporarily) its chemical aspects, and to treat it as a problem in mathematics. In this approach, the initial step is to establish the parallelism between certain chemical and certain mathematical terms. This may be done by considering butane as an example.

Chemical term	Butane	Mathematical term
Molecular formula	C_4H_{10} or CCCCHHHHHHHHHH	——
Type molecular formula	$4_4 1_{10}$ or 4,4,4,4,1,1,1,1,1,1,1,1,1,1	(Additive) partition
Structural formulas	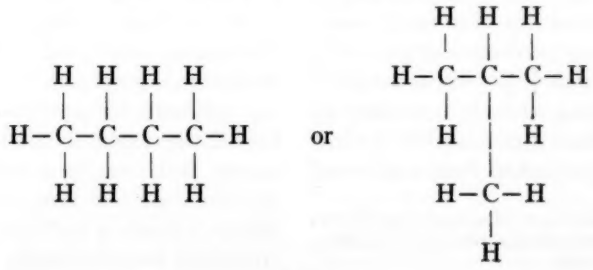 or	——

Type structural formulas

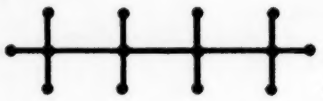

Covalence (of an atom).

or

Graphs (of a particular kind).

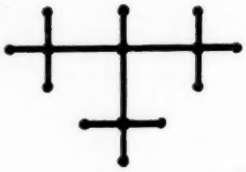

Multiplicity (of a point).

That is to say, what chemists might call "type molecular formulas" correspond to what mathematicians call "additive partitions"; what chemists might call "type structural formulas" correspond to what mathematicians call "graphs"[1] (of a particular kind); what chemists call the "covalence" of an atom in a structural formula corresponds to what mathematicians call the "multiplicity" of a point in a graph. In the remainder of this paper, a mixed dialect will be used. The mathematical terms "graph" and "additive partition" (hereafter abbreviated to "partition") will be used instead of the cumbersome chemical phrases "type structural formula" and "type molecular formula." On the other hand, the chemical term "valence" will be used instead of the mathematical term "multiplicity," for, since no other sort of valence besides covalence will be considered, the prefix "co" may be dropped. According to this usage, the word "valence" refers both to the number of covalent bonds ending in any one atom in a structural formula and to the number of line segments ending in any one point in a graph.

In mathematical terminology, a graph is a set of "points" joined to one another by "edges." The number of edges joining the members of any particular pair of points may be zero or any positive integer, but each point must lie at the end of at least one edge. The relative positions of the points (in euclidean space), the lengths or shapes of the edges, and the magnitudes of the angles between these edges are here of no significance. Various kinds of graph are recognized. If the number of points in the graph and the numbers of edges between the members of each pair of points are all finite, then the graph is also called "finite." If the edges are regarded as directed lines (usually represented by arrows), the graph is "directed"; if each edge is regarded merely as the symbol of a symmetric relation between its two end points, the graph is "undirected." An edge terminating at both ends in the same point forms with that point a "loop." If, in the graph G, it is possible to start at each point c_i and to reach every other point c_j by passing along successive edges of G, then G is "connected"; otherwise it is "disconnected."

Chemical structural formulas written according to the dot-atom line-valence system introduced by Crum-Browne are chemical representatives of *finite undirected graphs*. Hence, hereafter, for the sake of brevity, the unmodified word "graph" will be used only in this restricted sense. If any graph is represented by chemical structural formulas, it must be loopless; and if it is represented by single structural formulas, it must also be connected.

At this stage, it is well to introduce an appropriate notation. Let P be any finite set of finite positive integers. Every such set may be regarded as a partition of the finite integer ΣP where $\Sigma P = p_1 + p_2 \cdots + p_n$. Assume (solely for the sake of convenience) that the integers $p_1 \cdots p_n$ are so arranged that $p_1 \overline{\overline{>}} p_2 \cdots \overline{\overline{>}} p_{n-1} \overline{\overline{>}} p_n$. Let C be a set of points $c_1, c_2, \cdots c_n$. If a graph G is constructed by drawing undirected edges (loops being excluded) between the points of C in such a way that each point c_i is an end point of p_i edges, then G will be called a loopless *graph for* P. In such a graph, each integer p_i is the *valence* of the point c_i.

For any partition P, let the number of distinct connected loopless graphs be $ZCL(P)$. Where $ZCL(P)=0$, the partition will be called "nullgraphic"; where $ZCL(P)=1$, the partition will be called "unigraphic," and the one connected loopless graph for P will be called "unique"; where $ZCL(P)>1$, the partition will be called "multigraphic."

In order to give meaning to the word "distinct" used in the definition of $ZCL(P)$, it is necessary to explain what is meant by the identity or distinctness of two loopless graphs. Let G be one such graph for the partition $P(=p_1, p_2 \cdots p_n)$. If G' is any other loopless graph, and if the points of G' can be labeled $c_1', c_2' \cdots c_n'$ in such a way that, for every pair of points c_i', c_j', the number of edges joining c_i' directly to c_j' is equal to the number of edges joining c_i directly to c_j, then G and G' are identical; otherwise they are distinct. It follows at once from this definition that no two graphs can be identical unless they are graphs for the same P; but that two graphs may well be graphs for the same P without being identical.

It is a chemical truism that every structural formula determines one and only one molecular formula. Similarly, every connected loopless graph determines one and only one partition—which is merely an ordered list of the valences of the constituent points of that graph. But usually a molecular formula does not determine just one structural formula, and, as already stated, usually a partition does not determine just one connected loopless graph. In the special cases where the

[1] For a general mathematical treatment of graphs, see Denes König, *Theorie der endlichen und unendlichen Graphen* (Akademische Verlagsgesellschaft, Leipzig, 1936).

molecular formula does determine just one structural formula, the compound is a unimer. For the corresponding partition P, $ZCL(P)=1$; that is, the partition P is unigraphic and the corresponding graph is unique. The mathematical part of determining a complete list of unimers is to determine a complete list of unigraphic partitions, and thus a complete list of unique connected loopless graphs.

Before undertaking the determination just mentioned, it is, however, desirable to state a larger problem of which that determination is a part. Every P uniquely determines its $ZCL(P)$; but each $ZCL(P)$ determines only a class (in the cases here considered an infinite class) of distinct P's. Thus there arise two converse problems:

(A) For any given P, determine the single value of $ZCL(P)$.

(B) For any given non-negative integer taken as $ZCL(P)$, determine the class of Ps.

Problem (*A*). It is easy, where $ZCL(P)>0$ and ΣP is small, to construct one or more distinct connected loopless graphs for P and to prove that no other such graph for P exists. Thus a value of $ZCL(P)$ is obtained for the particular P in question. But where P is expressed in terms of one or more variables each of which may take the value of any finite integer, to determine $ZCL(P)$ as a function of these variables may be very difficult. As long ago as 1874, the mathematician Cayley[2] attempted to obtain the value of $ZCL(P)$ for all P's of the form 4_x1_{2x+2}. He was of course led to consider this particular class of P's because one of the corresponding generalized molecular formulas, C_xH_{2x+2}, is the general formula for the saturated hydrocarbons. Since the appearance of this first work, there has grown up a considerable literature dealing with Cayley's problem and other problems of a similar nature.

Problem (*B*). It is again easy to find by trial and error particular P's which can be proven to correspond to given (small) values of $ZCL(P)$. But the author is not aware of any previous work dealing with problem (B) in any more general fashion. The main object of the present paper is to solve this problem for the case $ZCL(P)=1$—that is to determine necessary and sufficient conditions to be imposed on a P in order to make that P unigraphic. Unavoidably, however, necessary and sufficient conditions for nullgraphism ($ZCL(P)=0$) must be determined before unigraphism can be successfully treated. If $ZCL(P)=0$, then P, since it has no corresponding connected loopless graph, can find no application in structural chemistry; but (as will be shown) the condition $ZCL(P)>0$ is not the only condition which must be placed on a P in order to assure the applicability of that P in the structural field.

Bearing in mind the application of the mathematical results to chemical problems, it is evident that, in one respect at least, the theory thus far outlined requires elaboration. From the definition already given for the identity of the two graphs G and G', it follows that the point c_i in G and the point c_i' in G' can correspond to one another only if they have the same valence and are similarly joined by edges to the other points of G and G' respectively. If graphs in which these conditions are sufficient for the correspondence of c_i and c_i' are represented by structural formulas, they must be represented by the structural formulas of compounds in which all the atoms of like valence are atoms of the same element.[3] The reason for this limitation is that it is impossible, on grounds so far discussed, to distinguish (for example) between the graphs represented by methane and by methyl chloride, or between those represented by 1,4-dioxane and by 1,4-thioxane. Such distinctions may, however easily be made if the individual points in the graphs are endowed with some intrinsic property such as color. Then necessary and sufficient conditions for the identity of the two graphs G and G' are fixed as follows: The corresponding points c_i and c_i' must not only be (as heretofore) of equal valence and similarly connected to the other points of G and G' respectively, but, in addition, the like-valent points c_i' and c_j' in G' must be alike in color if and only if the corresponding like-valent points c_i and c_j in G are alike in color. A graph in which all the points of like valence are of the same color will be called "monochromatic"; a graph in which this condition is not met will be called "polychromatic"; and the same terminology will be applied to the chemical formulas and compounds which represent these graphs. There is no object in distinguishing by color between points of different valence. In any two graphs, no two such points can correspond with one another, whether they are of the same color or not.

Only one very simple theorem concerning polychromatic graphs need here be introduced. Evidently, if a graph is to involve m colors (i.e., to be m-chromatic), it must contain at least m points of like valence. If $ZCL(P)>0$ and P contains $m(>1)$ like integers, then, for P, at least one connected loopless graph involving y colors ($2\leqq y\leqq m$) can be constructed. Furthermore, if, for P, the number of distinct connected loopless monochromatic graphs is x, then, for P, the number of distinct connected loopless graphs involving y colors is $\geqq x$. In more definite chemical terms, if there are (for example) x monochromatic structural isomers with the formula C_aH_b, there must be at least x polychromatic structural isomers with the formula $C_aH_eCl_f$, where $e+f=b$ and $e>0<f$. Consequently, if it be asked whether the polychromatic formula $C_aH_eCl_f$ corresponds to one or more than one structural isomer, the first question to be answered is whether the associated monochromatic formula C_aH_b corresponds to one or

[2] Arthur Cayley, Brit. Assoc. Advancement Sci. Repts., p. 275 (1875); Phil. Mag. (4) **47**, 444 (1874); (5), **3**, 34 (1877). These papers are reprinted in Vol. IX of Cayley's collected works.

[3] Isotopism is here neglected, but solely for the sake of simplicity. The entire ensuing argument would hold equally well if the word "isotope" were substituted for the word "element."

more than one structural isomer. If it corresponds to only one hydrocarbon, there may be one or more than one chlorine derivative of the stated composition. But if C_aH_b corresponds to several structurally isomeric hydrocarbons, there cannot be only one chlorine derivative $C_aH_eCl_f$.

As a result of these considerations, the determination of all unique connected loopless graphs falls definitely into two stages. The first stage is to determine all monochromatic graphs which meet this condition; the second stage is to determine under what conditions each of these monochromatic graphs, if it is made polychromatic, remains unique. If a monochromatic graph is not unique, then no polychromatic graph derived from it can possibly be so.

It is well to consider in advance the results which may be expected from a mathematical inquiry of the kind just outlined. All that mathematics can here given is a complete list of unigraphic partitions and their corresponding unique graphs. Any compound which has a molecular formula representing one of the unigraphic partitions on the mathematically determined list may be expected to have a structural formula representing the corresponding unique connected loopless graph. But whether chemists have been or ever will be able to prepare a stable representative for a particular unigraphic partition, and, if they have succeeded in so doing, whether the chemical and physical behavior of any such representative is in agreement with the corresponding unique connected loopless graph, are questions upon which the mathematical theory of graphs throws no light whatever.

The number of unique connected loopless monochromatic graphs is infinite, and the class of the corresponding unigraphic partitions falls into a complex set of infinite and partially overlapping subclasses. To translate the mathematical findings into chemical terms would therefore be a most laborious task, were it not for the fortunate fact that one mathematically arbitrary but chemically important limitation readily lends itself to mathematical expression. When attention is restricted (as in this paper) to covalence, it may be assumed that no atom, and thus no point in any chemically represented graph, has a valence greater than four. Hence no integer in any chemically represented unigraphic partition is greater than four. The whole class of unigraphic partitions which meet this restriction consists of two non-overlapping infinite series (which fortunately may be summarily treated) and about thirty individual cases. Moreover, the corresponding unique connected loopless monochromatic graphs give rise to unique polychromatic graphs which are also few in number.

The molecular and structural formulas representing these unique connected loopless graphs (both monochromatic and polychromatic) must be subjected to chemical scrutiny. But since the valence rules by themselves tell nothing about the stability of any compound which might represent a particular graph, no automatic exclusion principles can be set up in advance. It is necessary to rely on chemical good sense, guided in part by such considerations as the strain theory. Forms like I and II, when considered merely as Crum-Browne structures, are quite as admissible as III, for they fully conform to the valence rules that oxygen is bivalent, nitrogen trivalent and carbon quadrivalent. Nevertheless, the first two of these putative compounds have never been made, and their future preparation would be regarded by most chemists as improbable to the verge of absurdity.

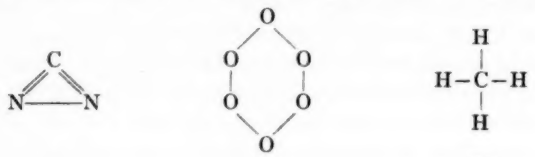

I II III

The object of an exhaustive chemical scrutiny would be to determine, for every unigraphic partition containing no integer greater than four,

(1) How many distinct chemical representatives have been isolated, and

(2) Whether, for each particular representative, the uniquely determined structural formula is in satisfactory agreement with the physical properties and chemical behavior of the compound in question.

Since a decision of either one of these two questions partakes of the nature of a value judgment, complete unanimity of opinion is here not to be expected. In the present paper, no such exhaustive chemical scrutiny is attempted. A serious effort is made to indicate all those unigraphic partitions for which no chemical representative exists, and all those where the chemical behavior of no representative is in accord with the required structural formula. But, where one or more satisfactory representatives are known, one good example is given, without any attempt to make the list of examples complete.

The purely mathematical aspects of the relations between partitions and their associated graphs will be discussed in another publication.[4] To that paper the reader is referred for proofs of the following theorems.

Theorem (*1.1*) $\Sigma P=2x$ (where x is any positive integer) is a necessary and sufficient condition for the existence of at least one graph (connected or disconnected, with or without loops) for P.

Theorem (*1.2*) $(\Sigma P/2)-(n-1)\overline{\geq}0$ is a necessary and sufficient condition for the existence of at least one connected graph for P.

Theorem (*1.3*) $(\Sigma P/2)-p_1\overline{\geq}0$ is a necessary and sufficient condition for the existence of at least one loopless graph for P.

[4] Paper entitled "Partitions and their representative graphs," Am. J. Math. **73** (1951), to be published.

Theorem (1.4) $(\Sigma P/2)-(n-1)\gtreqless 0\lesseqgtr(\Sigma P/2)-p_1$ is a necessary and sufficient condition for the existence of at least one connected loopless graph for P.

Any P which meets conditions (1.1) and (1.4), and thus corresponds to at least one loopless connected graph, will hereafter be called a Π. Evidently, every unigraphic partition must be a Π.

Theorem (2). Where polychromism is excluded, any one of the following conditions, if imposed on a Π, is sufficient, and at least one of them is necessary to make that Π unigraphic.

(a)	$(\Sigma\Pi/2)-p_1=0$.	One-half of the sum of all the integers in Π is equal to the largest integer in Π.
(b)	$n=3$.	The number of integers in Π is three.
(c)	$p_3=1$.	Π consists of at least three integers, but not more than two of them are >1.
(d)	$p_1=2$.	The largest integer in Π is 2.
(e)	$(\Sigma\Pi/2)-p_1-1$; $p_2=p_n$.	The largest integer in Π is one less than half the sum of all the integers in Π; excepting this largest integer, all the integers in Π are equal.
(f)	$p_1=p_3$; $p_4=1$.	The three largest integers in Π are all equal to one another; the fourth integer is 1.
(f′)	$n=4$.	The number of integers in Π is four.
(f″)	$(\Sigma\Pi/2)-(n-1)=0$.	The number of integers in Π is $(\Sigma\Pi/2)+1$.

Conditions 2a$\cdots$2f″ are independent of one another, but they partially overlap.[5] For this reason, in dealing with unigraphic Π's, it is better to be guided by the following rubric, where the same conditions are restated in a form which prevents overlapping.

Rubric

$(\Sigma\Pi/2)-p_1=0$	Class I
$(\Sigma\Pi/2)-p_1>0$ $n=3$ $n>3$	Class II
$p_3=1$ $p_3>1$	Class III
$p_1=2$ $p_1>2$	Class IV
$(\Sigma\Pi/2)-p_1=1$, $p_2=p_n$ $(\Sigma\Pi/2)-p_1>1$, $p_1=p_3$, $p_4=1$	Class V
$n=4$	Class VI
$n=(\Sigma\Pi/2)+1$	Class VII

The existence conditions (1.1) and (1.4) which apply to connected loopless monochromatic graphs need only a little strengthening to make them apply in the polychromatic case.

Theorem (3.1) For any Π which meets conditions (1.1) and (1.4) an additional condition necessary and sufficient for the existence of an m-chromatic graph is $p_i=p_{i+m-1}$ for at least one p_i. (Where $m=1$, this condition reduces to the identity $p_i=p_i$.)

The uniqueness conditions 2a$\cdots$2f″ which hold for monochromatic graphs must be successively strengthened as the number of colors is increased from one to four. For more than four colors, the uniqueness conditions are the same as for four colors.

Theorem (3.2) (a) Every connected loopless polychromatic graph for a Π of class I or class II is unique.

(b) No connected loopless polychromatic graph for a Π of class V or class VI or class VII is unique.

(c) A connected loopless polychromatic graph for a Π of class III or class IV is unique only under the following special conditions.

Class III.

Here an additional condition is $p_1=p_2$.

(1) The two polyvalent points are of different colors; all the univalent points are of one color,

(2) The two polyvalent points are of one color; all but one of the univalent points are of one color.

Class IV.

(1) $p_n=2$. All the points but one are of one color.

(2) $p_n=1$. All the bivalent points are of one color; the two univalent points are of different colors.

From theorems (3.1) and (3.2) it follows that a loopless connected graph with three colors is unique if and only if its Π contains at least three like integers and is of class I or class II; a loopless connected graph with x (>3) colors is unique if and only if its Π contains at least x like integers and is of class I.

The last condition to be imposed on a Π in order to

[5] For example, the partition 2, 1, 1 meets the first four conditions. Hence there are four independent reasons why any one of the representative compounds (e.g., H_2O) should be a unimer.

CLASS	π	UNIQUE GRAPHS WITH y COLORS			
		y=1	y=2	y=3	y=4
I	4,4	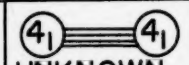 UNKNOWN	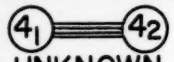 UNKNOWN		
	4,3,1	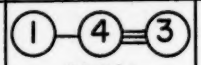 ClCN			
	4,2,2	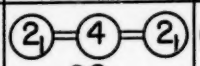 CO_2	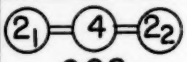 COS		
	4,2,1,1	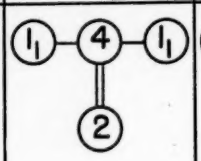 $COCl_2$	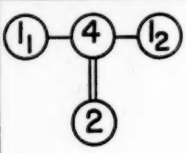 COFCl		
	4,1,1,1,1	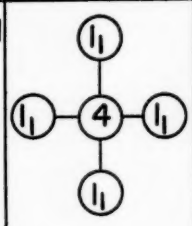 CH_4	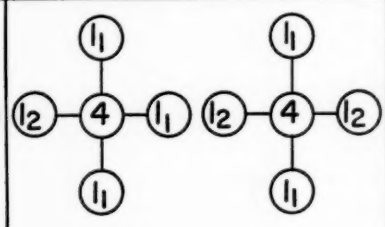 CH_3Cl CH_2Cl_2	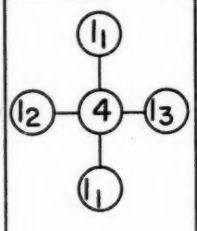 CH_2ClF	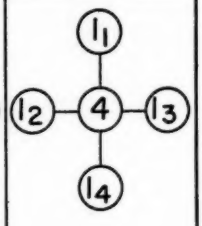 CHFClBr
	3,3	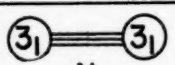 N_2	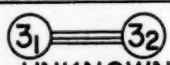 UNKNOWN		
	3,2,1	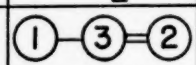 NOCl			
	3,1,1,1	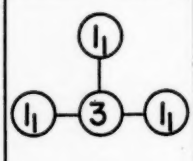 NH_3	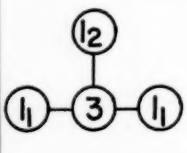 NH_2Cl	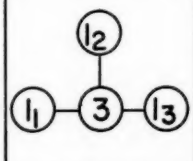 UNKNOWN	
	2,2	O_2 (UNSAT.)	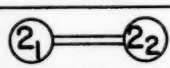 SO(UNSAT.)		
	2,1,1	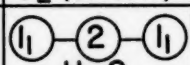 H_2O	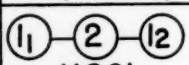 HOCl		
	1,1	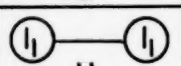 H_2	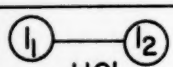 HCl		

FIG. 1a.

CLASS	π	UNIQUE GRAPHS WITH y COLORS		
		y = 1	y = 2	y = 3
II	4,4,4	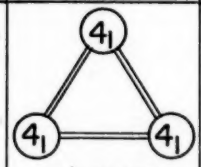 UNKNOWN	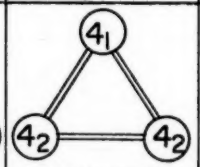 UNKNOWN	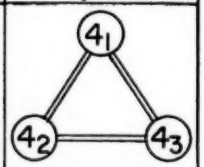 UNKNOWN
	4,4,2	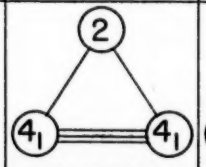 UNKNOWN	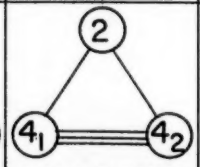 UNKNOWN	— — — —
	4,3,3	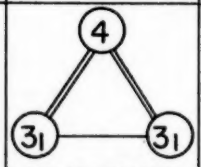 UNKNOWN	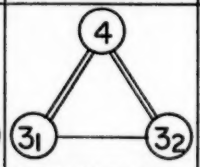 UNKNOWN	— — — —
	3,3,2	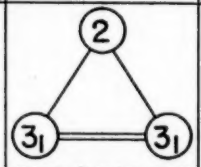 N_2O (UNSAT.)	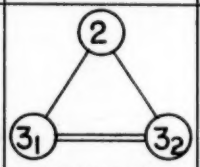 UNKNOWN	— — — —
	2,2,2	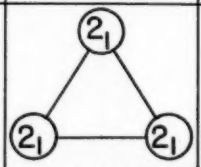 O_3 (UNSAT.)	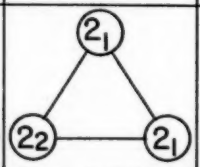 SO_2 (UNSAT.)	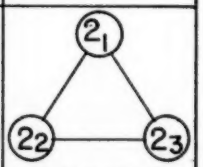 UNKNOWN

CLASS	π	UNIQUE GRAPHS WITH y COLORS	
		y = 1	y = 2
IV	2,2,2,2 ETC.	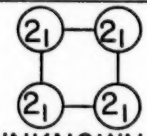 UNKNOWN	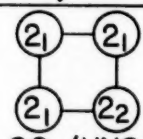 SO_3 (UNSAT.)
	2,2,2,1,1 ETC.	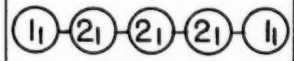 UNKNOWN	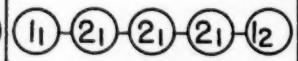 UNKNOWN
V	4,2,2,2	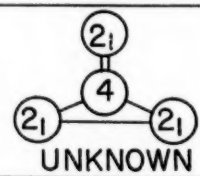 UNKNOWN	— — — — — —
VI	3,3,3,1	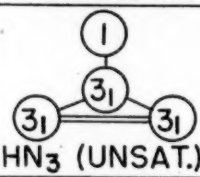 HN_3 (UNSAT.)	— — — — — —
VII	3,3,3,1,1,1,1,1	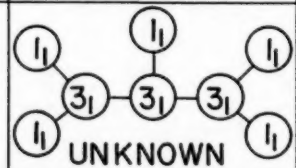 UNKNOWN	— — — — — —
	4,4,4,1,1,1,1,1,1,1	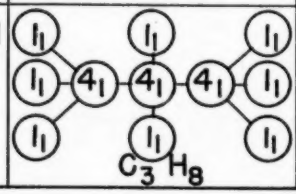 C_3H_8	— — — — — —

FIG. 1b.

CLASS	π	UNIQUE GRAPHS WITH y COLORS	
		y = 1	y = 2
III	4,4,1,1	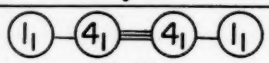 C_2H_2	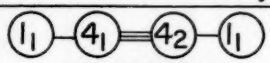 UNKNOWN 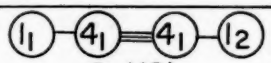 C_2HCl
	4,4,1,1,1,1	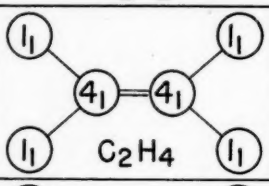 C_2H_4	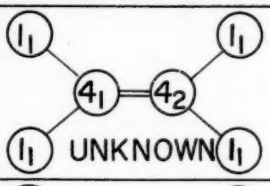 UNKNOWN 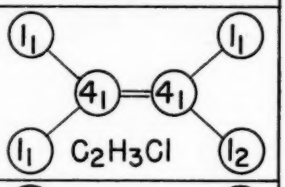 C_2H_3Cl
	4,4,1,1,1,1,1,1	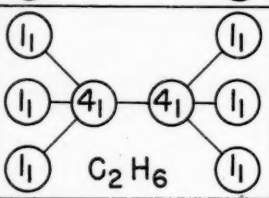 C_2H_6	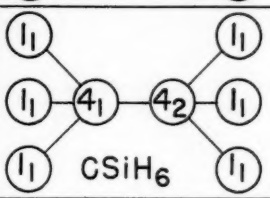 $CSiH_6$ 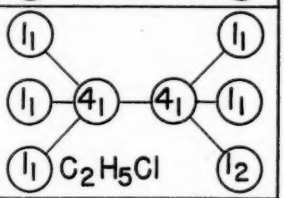 C_2H_5Cl
	4,3,1,1,1	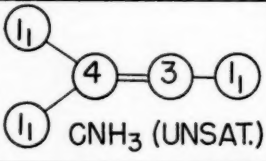 CNH_3 (UNSAT.)	— — — — — —
	4,3,1,1,1,1,1	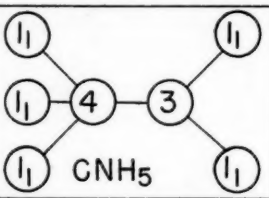 CNH_5	— — — — — —
	4,2,1,1,1,1	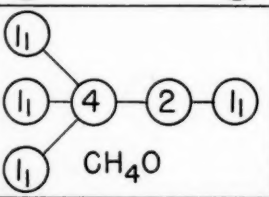 CH_4O	— — — — — —
	3,3,1,1	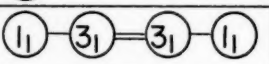 N_2F_2	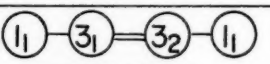 UNKNOWN 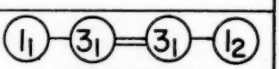 UNKNOWN
	3,3,1,1,1,1	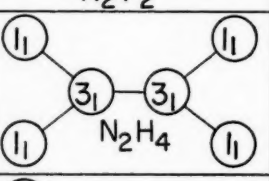 N_2H_4	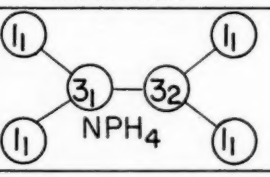 NPH_4 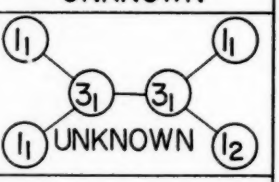 UNKNOWN
	3,2,1,1,1	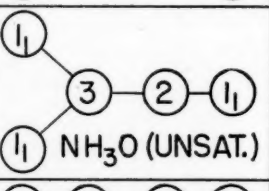 NH_3O (UNSAT.)	— — — — — —
	2,2,1,1	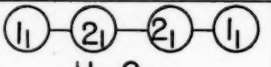 H_2O_2	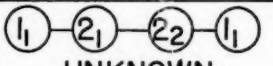 UNKNOWN 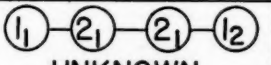 UNKNOWN

FIG. 1c.

make that Π chemically applicable is the mathematically arbitrary but chemically important limitation (2g): $p_1 < 5$. The only Π's which fulfill condition (2g) as well as at least one of the conditions (2a)$\cdots$(2f″) are those given in Figs. 1a, 1b, and 1c. Certain of the compounds with molecular formulas corresponding to these partitions *form the foundation upon which is erected almost the whole edifice of structural organic chemistry.*

In the figures, the partitions are classified according to the rubric, and with each partition are given the unique monochromatic and polychromatic graphs to which that partition corresponds. The symbol a stands for an atom of valence a. The symbols a_1, a_2, etc., stand for atoms of different elements with the same valence.

Where there exists at least one stable compound representing a particular unigraphic partition, and where the behavior and properties of at least one of these representatives is satisfactorily depicted by the corresponding structural formula, the molecular formula of one satisfactory representative is given below the graph. Where there exist stable compounds representing a particular unigraphic partition, but where the properties and behavior of no such representative are satisfactorily depicted by the corresponding structural formula, the molecular formula of one representative, followed by the word "unsatisfactory" (abbreviated to "unsat") is given below the graph. Where no compound representing a particular unigraphic partition is known, the word "unknown" is given below the graph.

The figures are drawn up on the assumption that polychromism within any subset of live-valent atoms refers to differences between the atomic numbers of these atoms. With this assumption, of the 66 graphs listed, 25 have no chemical representatives, 9 are unsatisfactorily represented, and 32 have satisfactory representatives. Of the satisfactorily represented graphs, 20 correspond to saturated compounds which require no molecular weight determination to fix their molecular formulas. If isotopism is recognized as a source of polychromism, the number of satisfactorily represented polychromatic graphs is somewhat increased. For example, such compounds as H−C≡Si−H and $H_2C=SiH_2$ probably do not exist, whereas $HC^{12}\equiv C^{13}H$ and $H_2C^{12}=C^{13}H_2$ are, respectively, normal constituents of ordinary acetylene and ethylene.

Only two of the unigraphic partitions listed permit of stereoisomerism among their representative compounds. These are the partitions 3,3,1,1 and 4,1,1,1,1. For the partition 3,3,1,1 there should be a pair of optically inactive syn-anti isomers in the monochromatic and in each of the two possible dichromatic cases. For the partition 4,1,1,1,1 there should be no stereoisomerism except in the tetrachromatic case, where there should be a pair of enantiomorphs.

20th Anniversary

of the

AMERICAN INSTITUTE OF PHYSICS

OCTOBER 23–27 HOTEL SHERMAN CHICAGO, ILLINOIS

A Joint Meeting of the American Institute of Physics and its Founder Societies

- **AMERICAN PHYSICAL SOCIETY (OCT. 25–27)**
- **OPTICAL SOCIETY OF AMERICA (OCT. 23–25)**
- **ACOUSTICAL SOCIETY OF AMERICA (OCT. 23–25)**
- **SOCIETY OF RHEOLOGY (OCT. 24–26)**
- **AMERICAN ASSOCIATION OF PHYSICS TEACHERS (OCT. 25–27)**

The American Crystallographic Association, an Affiliated Society of the American Institute of Physics, will participate in the Anniversary Meeting.

On Thursday, October 25, there will be an all-day symposium organized upon the theme "physics today", which will feature invited papers by:

ENRICO FERMI—The Nucleus
E. U. CONDON—The Atom
J. C. SLATER—The Solid State
HARVEY FLETCHER—Acoustics
EDWIN H. LAND—Optics
K. K. DARROW—Physics as Science and as Art

A JOINT BANQUET on Thursday evening, October 25, will have Senator Brien McMahon and K. T. Compton as guest speakers.

AN INDUSTRIAL EXHIBIT of scientific instruments and apparatus will provide manufacturers with an excellent opportunity to show their products to men who are responsible for many of the major scientific and technological advances of the past twenty years.

A PLACEMENT SERVICE for the benefit of employers and potential employees will be available during the meeting, and space in the Hotel Sherman will be reserved for this purpose.

Address inquiries to: The Secretary, American Institute of Physics, 57 East 55th Street, New York 22, New York

Magnetic Susceptibilities of Praseodymium Oxides*

SHERMAN W. RABIDEAU
University of California, Los Alamos Scientific Laboratory, Los Alamos, New Mexico
(Received January 19, 1951)

The magnetic susceptibilities of the three oxides of praseodymium, Pr_2O_3, PrO_2, and Pr_6O_{11}, have been measured with the faraday magnetic balance over a range of temperatures from 80° to 300°K. The sesquioxide and the dioxide have been found to have moments of 3.55 and 2.48 Bohr magnetons, respectively, and to obey the Weiss modification of the Curie law, $\chi(T+\Delta)=C$, over the range of temperatures studied with corresponding values of Δ equal to 55.0° and 104°. A curvature was noted in the plot of $1/\chi$ *vs* T for the oxide Pr_6O_{11}. Thus the Weiss-Curie law does not adequately express the relationship between the susceptibility and the temperature for this oxide. A moment of 2.8 Bohr magnetons was calculated for Pr_6O_{11} from the slope of the above plot between 200° and 300°K.

INTRODUCTION

IN spite of the large number of investigations of the magnetic properties of the rare earths, relatively few measurements have been made on the oxides of praseodymium as a function of temperature. Selwood[1] apparently overlooked the work of Cabrera and Duperier[2] and that of Klemm and Koczy,[3] for he estimated a value for the gram susceptibility of the sesquioxide of praseodymium. To the author's knowledge no susceptibility data have been reported for the oxide Pr_6O_{11} as a function of temperature, and only Cabrera and Duperier[2] appear to have measured PrO_2 in this manner.

Susceptibility measurements have been made on analyzed samples of the three oxides of praseodymium, Pr_2O_3, Pr_6O_{11}, and PrO_2 over a range of temperatures from 80° to 300°K.

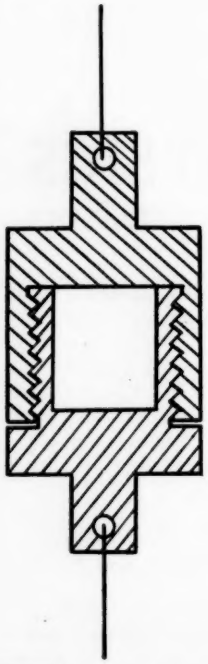

FIG. 1. Phosphor-bronze capsule.

EXPERIMENTAL

The susceptibilities were measured by the vertical force method with a faraday magnetic balance. The apparatus was assembled by Lewis and Elliott.[4] The magnet and the power supply were manufactured by the Consolidated Engineering Corporation of Pasadena, California. An Ainsworth type TCX semimicro balance was used to measure the force exerted on the sample. A phosphor-bronze capsule of the type shown in Fig. 1 was used to contain the specimen under investigation. The mapping of the field to locate the region of maximum HdH/dx was accomplished by reading the position of the capsule relative to a fixed reference point by means of a Gaertner cathetometer. The temperature of the sample was measured with copper-constantan thermocouples which had been checked against a platinum resistance thermometer certified by the Bureau of Standards.

The phosphor-bronze capsule was surrounded by a copper tube which was placed inside a silvered Pyrex glass Dewar flask. Around the copper tube was placed a copper spiral coil through which liquid nitrogen was pumped. The desired temperature was achieved by a proper selection of the length of the pump stroke and the number of strokes per minute. The emf of the controlling copper-constantan thermocouple was opposed with a Rubicon precision potentiometer. The condition of unbalance was indicated by a Leeds and Northrup moving coil, reflecting galvanometer, and the reflected light beam was projected on a photoelectric cell which activated the relay controlling the operation of the liquid nitrogen pump. With this assembly the temperature of the copper tube surrounding the phosphor-bronze capsule could be controlled to within a few tenths of a degree. Additional details of the apparatus will be found in the paper of Lewis and Elliott.[4]

The rare earth sample was obtained in the form of the oxide, Pr_6O_{11}, from Professor F. H. Spedding at the Institute for Atomic Research, Ames, Iowa. A spectrographic analysis of this oxide indicated 0.005 percent magnesium, and the quantities of other rare earths

* This work was done under the auspices of the AEC.
[1] P. W. Selwood, *Magnetochemistry* (Interscience Publishers, Inc., New York, 1943), p. 232.
[2] B. Cabrera and A. Duperier, Compt. rend. **188**, 1640 (1929).
[3] W. Klemm and A. Koczy, Z. anorg. Chem. **233**, 84 (1937).
[4] W. B. Lewis and N. Elliott (to be published).

present were beyond the limit of detection. The absence of ferromagnetic impurities in the oxide was demonstrated by measuring the susceptibility as a function of the magnetic field strength.

The oxide Pr_2O_3 was prepared by inductively heating Pr_6O_{11} at a temperature of about 1400° for sixteen hours at a pressure of about 5 microns. An x-ray analysis of this sample showed it to be the A (hexagonal) form of Pr_2O_3. No other component was indicated by the x-ray diffraction pattern.

Pr_6O_{11} was prepared for the magnetic measurement by heating the sample as received for one hour in air at approximately 1000° in a platinum crucible to remove any moisture and to decompose any carbonates which might have formed. The resulting oxide was shown by its x-ray pattern to consist of a single component.

The method of McCullough[5] was used in the preparation of PrO_2. This procedure consisted of heating the oxide Pr_6O_{11} to 300° for 48 hours under a pressure of 60 atmospheres of oxygen in a quartz capillary. Again an x-ray diffraction pattern of this material failed to reveal the presence of a second component. The lattice constants of Pr_6O_{11} and of PrO_2 are in agreement with those obtained by McCullough,[5] while those for Pr_2O_3 are in accord with the results of Eyring, Cunningham, and Lohr[6] for the A form of this oxide. The "active oxygen" method of analysis developed by Barthauer and Pearce[7] was used to serve as an additional check on the composition of the praseodymium oxides. Whereas the theoretical percentages of "active oxygen" are 0.0, 3.13, and 4.63 for the oxides Pr_2O_3, Pr_6O_{11}, and PrO_2, respectively, the experimentally observed percentages were 0.0, 3.14, and 4.7. The latter value is within the experimental error because of the limited sample.

The magnetic balance was calibrated with potassium chrome alum as the standard of susceptibility, and the values obtained by de Haas and Gorter[8] were used for this salt. A crystal of manganous sulfate tetrahydrate was measured over the range of temperature from 80° to 300°K as a check on the reliability of the calibration. A linear relation between $1/\chi$ and T was obtained. A moment of 5.86 Bohr magnetons was obtained for this salt, and the absolute values of the susceptibility were within approximately 1 percent of the values obtained by Jackson.[9]

The contribution of the empty phosphor-bronze capsule was measured as a function of temperature. This blank was also measured both before and after each measurement. The phosphor-bronze capsule was loaded with the oxide samples in an inert "drybox" to prevent the reaction of either carbon dioxide or moisture with the sample.

[5] J. D. McCullough, J. Am. Chem. Soc. **72**, 1386 (1950).
[6] Eyring, Cunningham, and Lohr, UCRL-791, July (1950).
[7] G. L. Barthauer and D. W. Pearce, Ind. Eng. Chem., Anal. Ed. **18**, 479 (1946).
[8] W. J. de Haas and C. J. Gorter, Proc. Acad. Sci. Amsterdam **33**, 676 (1930).
[9] L. C. Jackson, Proc. Roy. Soc. (London) **A140**, 704 (1933).

TABLE I. The susceptibility of praseodymium sesquioxide as a function of temperature.

T, °K	$\chi_g \times 10^6$	$\chi'_M \times 10^6$	$\chi_M \times 10^6$	$1/\chi_M \times 10^{-4}$
297.9	26.80	4420	4478	2.233
263.4	29.63	4887	4945	2.022
243.4	31.67	5223	5281	1.894
215.6	34.84	5746	5804	1.723
182.3	39.60	6530	6588	1.518
149.2	46.58	7681	7739	1.292
83.3	68.87	11358	11416	0.876

EXPERIMENTAL RESULTS

In Table I are given the values for the susceptibility per gram of Pr_2O_3, χ_g, and the susceptibility of Pr_2O_3 per gram atom of praseodymium as a function of temperature. A correction of -58×10^{-6} was applied for the diamagnetism of the oxide. In calculating the diamagnetic correction to be applied, a value of -13×10^{-6} was used as the contribution of the oxygen and -38×10^{-6} was used for the rare earth ions in all three oxides. The latter value is that given by Pauling[10] for La^{+++}. While both Pr^{+++} and Pr^{++++} have $4f$ electrons, whereas La^{+++} does not, it is believed that the diamagnetic corrections for these rare earth ions are approximately correct, since, as Van Vleck[11] has stated, the electrons in the $4f$ shell contribute less to the diamagnetism than the surrounding $5s$ and $5p$ shells. The values of the susceptibility of Pr_2O_3 in Table I are approximately 2 to 3 percent less than the values of Cabrera and Duperier[2] and Velayos,[12] and 3 percent greater than the values of Klemm and Koczy.[3] The susceptibility of Pr_2O_3 can be satisfactorily represented by the Weiss-Curie law from 80° to 300°K. A moment of 3.55 Bohr magnetons was calculated for this oxide and a value of 55.0° was found for Δ, the molecular field constant. The moment was calculated from the relation $\mu=2.83[\chi(T+\Delta)]^{\frac{1}{2}}$. The χ' values have not had the diamagnetic correction for the ions applied.

The Weiss-Curie law has also been found to express adequately the relation between the susceptibility and temperature for the oxide PrO_2. See Table II. A correction of -64×10^{-6} was applied to the measured results

TABLE II. Susceptibility-temperature relation for PrO_2.

T, °K	$\chi_g \times 10^6$	$\chi'_M \times 10^6$	$\chi_M \times 10^6$	$1/\chi_M \times 10^{-4}$
298.6	10.75	1858	1922	5.203
267.9	11.53	1994	2058	4.859
242.2	12.50	2162	2226	4.492
201.6	14.17	2450	2513	3.979
174.4	15.62	2700	2764	3.618
82.9	23.44	4052	4116	2.430

[10] L. Pauling, Proc. Roy. Soc. (London) **114A**, 181 (1927).
[11] J. H. Van Vleck, *The Theory of Electric and Magnetic Susceptibilities* (Oxford University Press, London, 1932), p. 252.
[12] S. Velayos, Anales españ. fís. quím. **33**, 5 (1935).

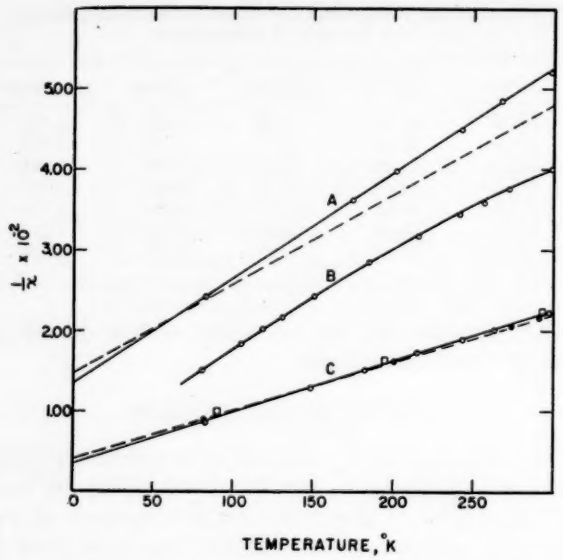

FIG. 2. Reciprocal of the magnetic susceptibility of the praseodymium oxides as a function of temperature. (A) PrO_2, (B) Pr_6O_{11}, (C) Pr_2O_3. -●-●-●- Velayos; ——— Cabrera and Duperier; -□-□-□- Klemm and Koczy; -○-○-○- This investigation.

for the diamagnetism of the ions. A moment of 2.48 Bohr magnetons and a Δ value of 104° were found for PrO_2. A comparison of the results of the present work with that of other investigators is given in Fig. 2.

The susceptibility-temperature relationship for the oxide Pr_6O_{11} is not adequately expressed by the Weiss-Curie law over the temperature range studied. Measurements on four independent samples of Pr_6O_{11} with an average weight of 30 mg gave concordant results for the susceptibilities of this oxide. Since a plot of $1/\chi$ *vs* T shows a definite curvature, no attempt was made to calculate a value for the molecular field constant. A moment of 2.8 Bohr magnetons was calculated for the oxide Pr_6O_{11} from the slope of the above plot in the temperature range between 200° and 300°K. A diamagnetic correction of -62×10^{-6} has been applied to the susceptibility values per gram atom of rare earth as given in Table III.

TABLE III. Susceptibility of Pr_6O_{11} as a function of temperature.

T, °K	$\chi_g\times10^6$	$\chi'_M\times10^6$	$\chi_M\times10^6$	$1/\chi_M\times10^{-2}$
299.3	14.30	2435	2494	4.010
272.2	15.27	2600	2659	3.761
256.9	15.91	2709	2768	3.589
241.4	16.65	2835	2894	3.455
215.9	18.11	3083	3142	3.183
184.7	20.23	3444	3503	2.855
150.4	23.83	4057	4116	2.430
130.9	26.67	4540*	4599	2.174
118.9	28.56	4862*	4921	2.032
105.5	31.51	5365*	5424	1.844
80.8	38.50	6555*	6614	1.512

* Independent sample.

DISCUSSION

The experimentally observed moment of 3.55 Bohr magnetons obtained for Pr^{+++} is in good agreement with the results of other investigators (Fig. 2) and with the theoretical value of 3.62 calculated by Van Vleck and Frank.[13] Cabrera and Duperier[2] stated that the oxides Pr_2O_3 and PrO_2 do not conform to the Weiss-Curie law and proposed the formula $(\chi+k)(T+\Delta)=C$ as best representing the susceptibility-temperature relationship for these oxides. Their values for the Curie constant, C, for these two oxides were 1.617 ± 0.005 and 0.861 ± 0.010, respectively. However, in this study it has been found that between 80° and 300°K the Curie-Weiss relation, $\chi(T+\Delta)=C$ satisfactorily represents the susceptibilities of Pr_2O_3 and of PrO_2 as a function of temperature. Values of 1.575 ± 0.004 and 0.769 ± 0.002 were found for the Curie constants of the sesquioxide and the dioxide, respectively.

Van Vleck and Frank[13] have calculated that Ce^{+++} should possess a moment of 2.56 Bohr magnetons. According to the Sommerfeld-Kossel rule, since Pr^{++++} is isoelectronic with Ce^{+++}, the moments of the two ions should be very nearly equal. The experimental value of 2.48 Bohr magnetons obtained for Pr^{++++} is in satisfactory agreement with this prediction. Since Cabrera and Duperier[2] did not report on the purity of their preparation of PrO_2, it is believed that their susceptibility measurements of this oxide are approximately 9 percent too large at room temperature.

A departure from the Weiss-Curie law was observed for the oxide Pr_6O_{11} as evidenced by the curvature of the $1/\chi$ *vs* T plot shown in Fig. 2. A moment of 2.8 Bohr magnetons was calculated for this oxide from the slope of the above plot in the temperature range of 200° to 300°K, since in the high temperature region the uncertainty in the molecular field constant is less important in calculations of the moment. It is not possible to distinguish between the formulas $Pr_2O_5\cdot2Pr_2O_3$ and $Pr_2O_3\cdot4PrO_2$ which have been proposed for the composition of the oxide Pr_6O_{11} from the magnetic moments of the trivalent and the tetravalent praseodymium ions, since nearly identical calculated moments of about 2.86 Bohr magnetons are found for each of the proposed formulas.

ACKNOWLEDGMENT

The author wishes to express his appreciation to Professor George Glocker and to J. F. Lemons for their interest and helpful discussions relative to this investigation. The use of the magnetic balance of W. B. Lewis and the induction furnace apparatus of C. E. Holley, Jr. is gratefully acknowledged.

[13] J. H. Van Vleck and A. Frank, Phys. Rev. **34**, 1494, 1625 (1929).

Thermodynamics and Chemical Kinetics of One-Dimensional Nonviscous Flow through a Laval Nozzle

S. S. PENNER
Guggenheim Jet Propulsion Center, California Institute of Technology, Pasadena, California
(Received February 13, 1951)

Explicit relations have been obtained for the enthalpy changes in one-dimensional nonviscous flow through a Laval nozzle, where arbitrary deviations from thermodynamic equilibrium of chemical composition and of internal electronic, vibrational, or rotational energy states may occur. These relations are of interest in connection with calculations on the effect of deviations from equilibrium on performance of jet engines.

Starting with the equation of continuity for a multicomponent mixture of reacting gases, criteria for near-equilibrium and for near-frozen flow with respect to chemical reactions are derived. The near-equilibrium criteria agree with results obtained previously. The near-frozen flow criteria are new and have not yet been applied to the study of chemical reactions during nozzle flow.

I. INTRODUCTION

THE determination of translational energy for fluid mixtures after expansion through a Laval nozzle involves use of a well-known procedure, at least for the special case of one-dimensional adiabatic expansion with complete chemical equilibrium or without composition change.[1–4] It has usually been assumed that complete thermodynamic equilibrium is maintained during flow with respect to vibrational and rotational energy states, although numerical calculations for a few representative cases of vibrationally frozen flow have been discussed.[5] The calculation of exhaust velocity after one-dimensional adiabatic expansion through a Laval nozzle can be carried out for arbitrary distributions of internal energy and for arbitrary composition changes. It is the purpose of Section II to present a systematization of calculations of this type in a convenient form for practical applications.

Closely connected with the essentially thermodynamic calculations of exhaust velocity are the kinetic problems of rates of chemical reactions and rates of adjustment of internal equilibrium states during nozzle flow. Of these kinetic problems only the former has been treated in connection with the evaluation of rocket performance. The methods which have been used fall into two categories: those concerned with exact stepwise numerical calculations[2,3,6] and those involving the application of near-equilibrium criteria.[7–9] Exact calculations are extremely laborious and, in view of the lack of adequate information concerning reaction-rate constants, seem hardly worth while. On the other hand, the use of near-equilibrium criteria is at least of qualitative value and in selected cases may even be used for the analysis of a complete propellant system.[9] Up to the present time only near-equilibrium criteria, that is, methods for allowing rapid screening of reactions which occur so rapidly that they almost maintain concentration changes consistent with local thermodynamic equilibrium, have been used. It is evident that near-frozen flow criteria should be just as useful as near-equilibrium criteria. Accordingly Section III will be devoted to the development of near-frozen flow criteria, as well as of near-equilibrium criteria, from rather general considerations. With the aid of this new tool for studying kinetic processes during nozzle flow, additional numerical calculations on selected propellant systems should become possible. For complex reactions of the type which occur in the hydrogen-oxygen motor the interdependence of chemical reactions will have to be considered according to a scheme described in an earlier publication.[8]

II. CALCULATION OF TRANSLATIONAL ENERGY FOR FLUID MIXTURES DURING ADIABATIC FLOW

The principle of conservation of energy for fluid mixtures, during steady one-dimensional adiabatic flow, may be expressed by the relation[10]

$$H+\tfrac{1}{2}u^2=\text{constant}, \tag{1}$$

where H represents the enthalpy per gram of fluid mixture and u is the linear flow velocity. Equation (1) forms the basis for the calculation of exhaust velocities after flow through a Laval nozzle. In particular, if it is assumed that the translational velocity at the nozzle entrance (conditions at the nozzle entrance are identified by the subscript c corresponding to the chamber temperature T_c) is zero, then the translational velocity at the nozzle exit (identified by the subscript e corresponding to the exhaust temperature T_e) is given by the relation

$$\tfrac{1}{2}u_e^2=H_c-H_e=\Delta H_e^c. \tag{2}$$

It is well known that the numerical value of u_e depends on the nature of the flow process and will assume

[1] F. J. Malina, J. Franklin Inst. **230**, 433 (1940).
[2] S. S. Penner and D. Altman, J. Franklin Inst. **245**, 421 (1948).
[3] D. Altman and S. S. Penner, J. Chem. Phys. **17**, 56 (1949).
[4] S. R. Brinkley, Jr., J. Chem. Phys. **15**, 107 (1947).
[5] S. S. Penner, J. Appl. Phys. **20**, 445 (1949).
[6] H. Behrens, Z. physik. Chem. **195**, 1 (1950).
[7] S. S. Penner, J. Am. Chem. Soc. **71**, 788 (1949).
[8] S. S. Penner, J. Chem. Phys. **17**, 841 (1949).
[9] S. S. Penner, J. Franklin Inst. **249**, 441 (1950).

[10] H. W. Liepmann and A. E. Puckett, *Aerodynamics of Compressible Flow* (John Wiley and Sons, Inc., New York, 1947).

different values depending on the extent of chemical reaction and redistribution of internal energy during flow. In order to exhibit this dependence of u_e on the flow process in some detail, it is desirable to express $\Delta H_e{}^c$ in such a form as to demonstrate explicitely its dependence on the occurrence or nonoccurrence of chemical reactions and internal energy adjustments. The term equilibrium flow will be understood to mean flow in which equilibrium is maintained at each point with respect to chemical reaction, whereas frozen or constant-composition flow means flow without chemical reaction. The state of the electronic, vibrational, and rotational distribution will be identified by a statement concerning the internal energy distribution. Let $H_0{}^0$ = enthalpy per gram of fluid mixture if complete chemical and internal equilibrium is maintained for all constituents; H^0 = enthalpy per gram of fluid mixture if complete chemical equilibrium is maintained for all components but internal-energy lags may exist; H_0 = enthalpy per gram of fluid mixture if complete internal equilibrium exists for all constituents but the chemical composition may depart from equilibrium. It is convenient to form the following identity

$$H=H_0{}^0-\tfrac{1}{2}[(H_0{}^0-H_0)+(H_0-H)+(H_0-H^0)+(H^0-H)], \quad (3)$$

whence

$$\Delta H_e{}^c=(H_{0c}{}^0-H_{0e}{}^0)-\tfrac{1}{2}\{[(H_{0c}{}^0-H_{0c})+(H_{0c}-H_c)+(H_{0c}{}^0-H_c{}^0)+(H_c{}^0-H_c)]-[(H_{0e}{}^0-H_{0e})+(H_{0e}-H_e)+(H_{0e}{}^0-H_e{}^0)+(H_e{}^0-H_e)]\}. \quad (4)$$

Let $(H_{0c}{}^0-H_{0e}{}^0)=\Delta H_{0e}{}^{0c}$ = enthalpy change for complete chemical and internal equilibrium. In general, the fluid mixture of density ρ contains N different chemical species. The equilibrium concentration of the k'th species is $C_k{}^0$ in moles per cubic centimeter of mixture or $C_k{}^0/\rho$ in moles per gram of mixture. The corresponding actual concentrations are C_k in moles per cubic centimeter of mixture or C_k/ρ in moles per gram of mixture. Setting the molecular weight of the k'th component equal to M_k, it is apparent that

$$H_0{}^0=\sum_{k=1}^{N}(M_kC_k{}^0/\rho)H_{0k} \quad (5)$$

$$H^0=\sum_{k=1}^{N}(M_kC_k{}^0/\rho)H_k \quad (5a)$$

$$H_0=\sum_{k=1}^{N}(M_kC_k/\rho)H_0{}^k, \quad (5b)$$

where H_{0k} is the enthalpy per gram of the kth component with equilibrium internal energy distribution and H_k is the corresponding enthalpy per gram without equilibrium internal-energy distribution. Introducing Eqs. (5), (5a), and (5b) into Eq. (4), the following relation is obtained:

$$\tfrac{1}{2}u_e{}^2=\Delta H_e{}^c=\Delta H_{0e}{}^{0c}-\tfrac{1}{2}\sum_{k=1}^{N}M_k\{(1/\rho_c)[(C_{kc}{}^0-C_{kc})(H_{0kc}+H_{kc})+(C_{kc}{}^0+C_{kc})(H_{0kc}-H_{kc})]-(1/\rho_e)[(C_{ke}{}^0-C_{ke})(H_{0ke}+H_{ke})+(C_{ke}{}^0+C_{ke})(H_{0ke}-H_{ke})]\}. \quad (6)$$

Equation (6) is the desired result and can be used directly to calculate u_e for the most general type of information which may be available. The utility of Eq. (6) will now be demonstrated by considering a number of special cases, some of which have been employed previously for the calculation of exhaust velocities from conventional rocket motors.

A. Equilibrium Concentration and Equilibrium Internal Energy at T_e and T_c

In this case $C_{kc}=C_{kc}{}^0$, $C_{ke}=C_{ke}{}^0$, $H_{kc}=H_{0kc}$, $H_{ke}=H_{0ke}$. Hence Eq. (6) becomes

$$\tfrac{1}{2}u_e{}^2=\Delta H_{0e}{}^{0c}=\sum_{k=1}^{N}M_k[(C_{kc}{}^0H_{0kc}/\rho_c)-(C_{ke}{}^0H_{0ke}/\rho_e)]. \quad (7)$$

Equation (7) shows how the exhaust velocity is calculated for equilibrium flow. For practical purposes it may be convenient to replace the enthalpies in Eq. (7) by heat capacity integrals. Thus

$$\tfrac{1}{2}u_e{}^2=\sum_{k=1}^{N}\left\{M_k\left[(C_{kc}{}^0/\rho_c)\int_{298}^{T_c}C_{pk}dT-(C_{ke}{}^0/\rho_e)\int_{298}^{T_e}C_{pk}dT\right]+H_{0k}{}^{298}[(C_{kc}{}^0/\rho_c)-(C_{ke}{}^0/\rho_e)]\right\}, \quad (7a)$$

where C_{pk} is the specific heat at constant pressure per gram of k for equilibrium electronic, vibrational, and rotational excitation, and $H_{0k}{}^{298}$ denotes the standard heat of formation of species k at 298°K.

B. Equilibrium Concentration at T_c followed by Frozen Flow to T_e and Equilibrium Internal Energy at T_e and T_c

In this case $C_{kc}=C_{kc}{}^0$, $H_{kc}=H_{0kc}$, $H_{ke}=H_{0ke}$, $C_{ke}/\rho_e=C_{kc}{}^0/\rho_c$. Hence Eq. (6) becomes

$$\tfrac{1}{2}u_e{}^2=\sum_{k=1}^{N}(M_kC_{kc}{}^0/\rho_c)(H_{0kc}-H_{0ke}). \quad (8)$$

Equation (8) is the usual relation for frozen-flow calculations. In terms of heat capacities it becomes

$$\tfrac{1}{2}u_e{}^2=\sum_{k=1}^{N}(M_kC_{kc}{}^0/\rho_c)\int_{T_e}^{T_c}C_{pk}dT, \quad (8a)$$

since no composition changes occur during flow.

C. Equilibrium Concentration at T_c with Arbitrary Concentration at T_e and Equilibrium Internal Energy at T_e and T_c

In this case $C_{kc}=C_{kc}{}^0$, $H_{kc}=H_{0kc}$, $H_{ke}=H_{0ke}$, $C_{ke}\neq C_{ke}{}^0$. Hence Eq. (6) becomes

$$\tfrac{1}{2}u_e{}^2=\sum_{k=1}^{N}\left\{M_k\left[(C_{kc}{}^0/\rho_c)\int_{298}^{T_c}C_{pk}dT-(C_{ke}/\rho_e)\int_{298}^{T_e}C_{pk}dT\right]+H_{0k}{}^{298}[(C_{kc}{}^0/\rho_c)-(C_{ke}/\rho_e)]\right\}. \quad (9)$$

D. Equilibrium Internal Energy and Arbitrary Concentration at T_e and T_c

In this case $H_{kc}=H_{0kc}$, $H_{ke}=H_{0ke}$, $C_{kc}\neq C_{kc}^0$, $C_{ke}\neq C_{ke}^0$. Hence Eq. (6) becomes

$$\tfrac{1}{2}u_e^2=\sum_{k=1}^{N} M_k[(C_{kc}H_{0kc}/\rho_c)-(C_{ke}H_{0ke}/\rho_e)]. \quad (10)$$

E. Equilibrium Concentration at T_c and T_e and Internal-Energy Lag at T_e

In this case $C_{kc}=C_{kc}^0$, $C_{ke}=C_{ke}^0$, $H_{kc}=H_{0kc}$, $H_{ke}\neq H_{0ke}$. Hence Eq. (6) becomes

$$\tfrac{1}{2}u_e^2=\Delta H_{0e}^{0c}+\sum_{k=1}^{N}(M_kC_{ke}^0/\rho_e)(H_{0ke}-H_{ke}). \quad (11)$$

The term $H_{0ke}-H_{kc}$ can be conveniently expressed as the sum of electronic, vibrational, and rotational enthalpy lags; i.e.,

$$H_{0ke}-H_{ke}=(H_{0ke}^{el}-H_{ke}^{el})+(H_{0ke}^{vib}-H_{ke}^{vib})+(H_{0ke}^{rot}-H_{ke}^{rot})$$

or

$$H_{0ke}-H_{ke}=\int_{T_{ke}^{el}}^{T_e}C_k^{el}dT+\int_{T_{ke}^{vib}}^{T_e}C_k^{vib}dT+\int_{T_{ke}^{rot}}^{T_e}C_k^{rot}dT,$$

where the superscripts el, vib, and rot denote, respectively, the electronic, vibrational, and rotational contributions to the heat capacity.* The notation T_{ke}^{el}, T_{ke}^{vib}, T_{ke}^{rot} has been adopted in order to emphasize the fact that, for lagging internal-energy distribution, the electronic, vibrational, and rotational temperatures at the nozzle exit may be different. Since electronic and rotational energy lags are less likely to occur during flow through a Laval nozzle than are vibrational lags, it is of interest to consider Eq. (11) when only vibrational lags occur. In this case

$$\tfrac{1}{2}u_e^2=\Delta H_{0e}^{0c}+\sum_{k=1}^{N}(M_kC_{ke}^0/\rho_e)\int_{T_{ke}^{vib}}^{T_e}C_k^{vib}dT. \quad (11a)$$

Equation (11a) has been used previously to estimate an upper limit for the effect of vibrational lags on exhaust velocity for equilibrium flow by setting $T_{ke}^{vib}=T_c$.[5]

F. Equilibrium Concentration and Internal Energy at T_c Followed by Frozen Flow to T_e with Arbitrary Internal-Energy Lags at T_e

In this case $C_{kc}=C_{kc}^0$, $C_{ke}/\rho_e=C_{kc}^0/\rho_c$, $H_{kc}=H_{0kc}$, $H_{ke}\neq H_{0ke}$. Hence Eq. (6) becomes

$$\tfrac{1}{2}u_e^2=\Delta H_{0e}^{0c}+\tfrac{1}{2}\sum_{k=1}^{N}M_k\{(H_{0ke}-H_{ke})[(C_{ke}^0/\rho_e)+(C_{kc}^0/\rho_c)]+(H_{0ke}+H_{ke})[(C_{ke}^0/\rho_e)-(C_{kc}^0/\rho_c)]\}. \quad (12)$$

A comparison of Eqs. (11) and (12) shows very clearly that the effect of vibrational lag on exhaust velocity will depend on the occurrence or nonoccurrence of chemical reaction during flow, a conclusion which was reached previously as the result of numerical calculations.[5] It is possible to derive a quantitative expression for the interdependence of internal and chemical equilibrium. Denoting by $\frac{1}{2}\Delta(u_e^2)$ the difference in exhaust velocity between equilibrium and frozen flow for nonequilibrium internal energy at T_e and subtracting Eq. (12) from Eq. (11) it is found that

$$\tfrac{1}{2}\Delta(u_e^2)=\sum_{k=1}^{N}M_k[(C_{kc}^0/\rho_c)-(C_{ke}^0/\rho_e)][H_{0ke}-(H_{0ke}-H_{ke})]. \quad (13)$$

In terms of heat capacity integrals Eq. (13) becomes for equilibrium electronic and rotational distribution, with the vibrational temperature at the nozzle exit of each of the k components lagging at T_e

$$\tfrac{1}{2}\Delta(u_e^2)=\sum_{k=1}^{N}M_k[(C_{kc}^0/\rho_c)-(C_{ke}^0/\rho_e)]\times\left[\int_{298}^{T_e}C_{pk}dT-\int_{T_e}^{T_e}C_k^{vib}dT+H_{0k}^{298}\right]. \quad (14)$$

Hence the occurrence of vibrational lag for frozen and equilibrium flow with $T_k^{vib}=T_c$ has increased the difference between equilibrium and frozen flow by the term

$$\sum_{k=1}^{N}M_k[(C_{kc}^0/\rho_c)-(C_{ke}^0/\rho_e)]\int_{T_e}^{T_e}C_k^{vib}dT.$$

This last result serves as a good illustration of the utility of Eq. (6) for the analysis of complicated flow problems.

Further results for various specific chemical and internal-energy distributions can be obtained by using the general relation given in Eq. (6) for the solution of particular problems. The more complex the problem at hand, i.e., the more detailed the knowledge concerning concentrations and internal-energy distributions, the more desirable will it be to proceed from Eq. (6) in order to calculate exhaust velocities.

III. NEAR-EQUILIBRIUM AND NEAR-FROZEN FLOW THROUGH A LAVAL NOZZLE

As was pointed out in Sec. I, the analysis of kinetic changes during flow has been facilitated in the past by the use of near-equilibrium criteria. Reference to Sec. II shows that full use of available thermodynamic techniques for the calculation of exhaust velocity must await far more complete information concerning the kinetic changes during nozzle flow than are available at the present time. It is therefore of obvious interst to extend the useful kinetic methods by the development of criteria for near-frozen flow. It will be shown in this section how near-frozen as well as near-equilibrium criteria follow from the equation of continuity for a multicomponent mixture of reacting ideal gases.

The equation of continuity for species k of a multicomponent mixture of reacting gases can be written in the form[11]

$$DC_k/Dt=\Gamma_k+(C_k/\rho)(D\rho/Dt)-\nabla\cdot[(C_k\mathbf{V}_k)], \quad (15)$$

where $D/Dt=(\partial/\partial t)+\mathbf{v}\cdot\nabla$ is the euler total time derivative moving with the fluid; Γ_k = net rate of production of species k in moles per cubic centimeter, as the result of chemical reaction; t = time; $\mathbf{v}$ = mass weighted average velocity $=(1/\rho)\sum_k C_kM_k\mathbf{v}_k$; $\mathbf{v}_k$ = actual velocity of species k; ρ = density of fluid mixture (gm/cc); C_k = concentration of species k (mol/cc); M_k = molecular weight of species k; $\mathbf{V}_k$ = diffusion velocity of species k.

For flow through a Laval nozzle the diffusion term is small and may be neglected. Assuming the presence of ideal gases, the equation of state is

$$\rho=p/\dot{R}T, \quad (16)$$

* It should be noted that individual electronic, vibrational, and rotational contributions to specific heats are readily calculated by standard statistical methods. See J. E. Mayer and M. E. Mayer, *Statistical Mechanics* (John Wiley and Sons, Inc., New York, 1946).

[11] C. F. Curtiss, and J. O. Hirschfelder, "Kinetic theory of multi-component systems of gases," C. F. 727 (University of Wisconsin, Naval Research Laboratory, Madison, 1947).

and for adiabatic flow

$$Dp/DT=\gamma p/T(\gamma-1), \tag{17}$$

whence Eq. (15) becomes

$$D\ln C_k/Dt=\Gamma_k/C_k+[1/T(\gamma-1)](DT/Dt). \tag{18}$$

Here p=mean hydrostatic pressure; T=temperature; R'=gas constant per g; γ=ratio of specific heat at constant pressure to the specific heat at constant volume, including[2] any contributions resulting from the occurrence of chemical reactions.

The most general type of chemical reaction may be represented by the relation

$$\sum_k \nu_k' M_k=\sum_k \nu_k'' M_k, \tag{19}$$

where ν_k' and ν_k'' are the coefficients which multiply the chemical symbol M_k of species k in the relation representing the stoichiometry of the reaction. For a reaction of the type shown in Eq. (19) it is apparent that

$$\Gamma_k=(\nu_k''-\nu_k')[k_f\prod_j C_j^{\nu_j'}-k_b\prod_j C_j^{\nu_j''}] \tag{20}$$

where k_f and k_b are specific reaction-rate constants for the forward and reverse reactions represented in Eq. (19) by an arrow pointing to the right or to the left, respectively.

From Eqs. (18) and (20) it is apparent that

$$D\ln C_k/Dt=(\nu_k''-\nu_k')k_f(\prod_j C_j^{\nu_j'}/C_k)\times\{1-[K_e(T)\prod_j C_j^{\nu_j''}/\prod_j C_j^{\nu_j'}]\}+[1/T(\gamma-1)](DT/Dt), \tag{21}$$

where use has been made of the relation

$$K_e(T)=\prod_j C_j^{0\nu_j'}/\prod_j C_j^{0\nu_j''}=k_b/k_f \tag{22}$$

and the superscript zero indicates that the equilibrium concentrations prevail at the local temperature T.

A temperature T' is next defined by the relation

$$K_e(T')=\prod_j C_j^{\nu_j'}/\prod_j C_j^{\nu_j''}, \tag{23}$$

whence

$$D\ln C_k/Dt=(\nu_k''-\nu_k')k_f(\prod_j C_j^{\nu_j'}/C_k)\times\{1-[K_e(T)/K_e(T')]\}+[1/T(\gamma-1)](DT/Dt). \tag{24}$$

Equation (24) represents the desired general result and may now be examined for various special cases.

A. Near-Equilibrium Flow

Near-equilibrium flow is defined as nozzle flow for which the difference $T'-T$ is small during the entire flow process. More specifically it has been defined as flow for which only the first two terms of the Taylor expansion for $K_e(T')$ about $K_e(T)$ need be included in calculations.[7-9] Since $T'\gtrless T$, it follows that $K_e(T')\gtrless K_e(T)$ for dissociation reactions and

$$K_e(T')\simeq K_e(T)+K_e(T)[d\ln K_e(T)/dT]_T(T'-T). \tag{25}$$

Hence Eq. (24) becomes for near-equilibrium flow, since

$$[d\ln K_e(T)/dT]_T(T'-T)\ll 1,$$

$$D\ln C_k/Dt=(\nu_k''-\nu_k')k_f(\prod_j C_j^{\nu_j'}/C_k)\times[d\ln K_e(T)/dT]_T(T'-T)+[1/T(\gamma-1)](DT/Dt). \tag{26}$$

It has been shown previously that the second term on the right-hand side of Eq. (26) is, in general, negligibly small compared to the first term.[6] Proceeding in the usual way,[6] it is readily shown that Eq. (26) leads to the following general criterion for near-equilibrium flow:

$$T'-T=\left[1+\frac{\sum_j(\nu_j''-\nu_j')}{(\gamma-1)T(d\ln K_e/dT)_{T'\simeq T}}\right]\left(-\frac{DT}{Dt}\right)\times[k_f\prod_j C_j^{\nu_j'}\sum_j(\nu_j''-\nu_j')^2/C_j]^{-1}. \tag{26a}$$

B. Near-Frozen Flow

Near-frozen nozzle flow is defined as flow for which $T'\sim T_c$ where T_c represents the temperature at the nozzle entrance. Since $T'\lesseqgtr T_c$, it follows that $K_e(T')\lesseqgtr K_e(T_c)$ for dissociation reactions. More specifically near-frozen flow may be defined as flow for which all terms higher than the second in the Taylor expansion of $K_e(T')$ about $K_e(T_c)$ may be neglected. Thus

$$K_e(T')\simeq K_e(T_c)-K_e(T_c)[d\ln K_e(T)/dT]_{T_c}(T_c-T') \tag{27}$$

and Eq. (24) becomes, since

$$[d\ln K_e(T)/dT]_{T_c}(T_c-T')\ll 1,$$

$$D\ln C_k/Dt=(\nu_k''-\nu_k')k_f(\prod_j C_j^{\nu_j'}/C_k)\times\{1-[K_e(T)/K_e(T_c)]\times[1+(d\ln K_e(T)/dT)_{T_c}(T_c-T')]\}+[1/T(\gamma-1)](DT/Dt). \tag{28}$$

Proceeding in the usual way,[6] the following general

criterion for near-frozen flow is obtained:

$$\left[\left(\frac{d\ln K_e}{dT}\right)_{T'\simeq T_c}+\sum_j (\nu_j''-\nu_j')/(\gamma-1)T\right]\times\left(-\frac{DT}{Dt}\right)=k_f\prod_j C_j^{\nu_j'}\sum_j\frac{(\nu_j''-\nu_j')^2}{C_j}\times\left\{1-\frac{K_e(T)}{K_e(T')}\left[1+\left(\frac{d\ln K_e}{dT}\right)_{T'\simeq T_c}(T_c-T')\right]\right\}. \quad (28a)$$

C. Flow with Arbitrary Composition Changes

Flow with arbitrary composition changes can evidently be described by using a Taylor series expansion of $K_e(T')$ about either $K_e(T)$ or $K_e(T_c)$ and retaining an adequate number of terms in the power series to assure convergence. Depending upon the particular chemical reaction under study, it may be more convenient to use either a generalized near-equilibrium criterion or a generalized near-frozen-flow criterion.

THE JOURNAL OF CHEMICAL PHYSICS VOLUME 19, NUMBER 7 JULY, 1951

The Experimental Determination of the Intensities of Infrared Absorption Bands. IV. Measurements of the Stretching Vibrations of OCS and CS_2*†

DAVID Z. ROBINSON‡
Mallinckrodt Chemical Laboratory, Harvard University, Cambridge, Massachusetts

(Received March 5, 1951)

The absolute intensity of the infrared stretching vibrations of the molecules CS_2 and OCS have been measured. For CS_2, the intensity of ν_3 was found to be 7560×10^{10} cycles sec^{-1} (cm of vapor at NTP)$^{-1}$. For OCS, the results were 110 and 7900×10^{10} for ν_1 and ν_3. A normal coordinate analysis of the stretching vibrations of OCS was carried out to obtain $\partial\mu/\partial r$ for the bonds and to compare them with those for CS_2 and the previously obtained results for CO_2. The results for a reasonable value of the interaction constant were 6.7 and 4.3×10^{-10} esu for the CO and CS bonds, while in CO_2 and CS_2 they were 6.0 and 5.6×10^{-10} esu. The bearing of these results on the amount of resonance in OCS is discussed. Arguments are presented which suggest that, in spite of the electronegativity difference between oxygen and sulfur, resonance in OCS is not markedly different from that in CO_2 and CS_2.

THE work done here was carried out as part of a study of the measurement and interpretation of the absolute intensity of infrared absorption bands.[1–3] The first reference discussed the method of measuring directly reliable absolute intensities even with a spectrograph of low resolving power, and the second and third papers described the interpretation of measurements made on some simple gases and the comparison with results of dispersion measurements.[4] The present paper deals with the molecules carbon disulfide and carbon oxysulfide. The intensities of the stretching modes of both CS_2 and OCS have been measured and the results discussed in connection with previous work on carbon dioxide.[3]

ABSOLUTE INTENSITY

The absolute intensity of the ith absorption band is defined by

$$A_i=\int\alpha d\nu=-(1/PL)\int\ln\frac{I}{I_0}d\nu, \quad (1)$$

where A_i is the intensity of the band, α is the absorption coefficient, ν is the frequency, P is the pressure of the gas, L is the length of the gas cell, and I/I_0 is the fraction of light transmitted by the gas The integral is taken over the whole band.

In order to obtain correct absolute intensities from the observed transmission curves, it is necessary to eliminate the errors caused by rapid variations in transmission over a single slit width. To eliminate the effect of these variations two steps must be taken:

(1) The rapid fluctuations due to the rotational fine structure can be removed by adding a foreign gas to broaden the individual rotational lines.

(2) The variations in absorption coefficient over the band envelope can be eliminated by taking spectra of the gas at smaller and smaller partial pressures. The limit of the observed absolute intensity at zero partial pressure is the true absolute intensity.

* Presented before the Symposium on Molecular Spectra and Molecular Structure, Columbus, June, 1949.

† The research reported here was partially supported by funds extended to Harvard University by the ONR under contract N-5-ori-76, T.O.5.

‡ Present address: Baird Associates, Inc., 33 University Road, Cambridge, Massachusetts.

[1] E. B. Wilson, Jr., and A. J. Wells, J. Chem. Phys. **14**, 578 (1946).

[2] Thorndike, Wells, and Wilson, J. Chem. Phys. **15**, 157 (1947).

[3] A. M. Thorndike, J. Chem. Phys. **15**, 868 (1947).

[4] R. Rollefson and A. H. Rollefson, Phys. Rev. **48**, 779 (1935).

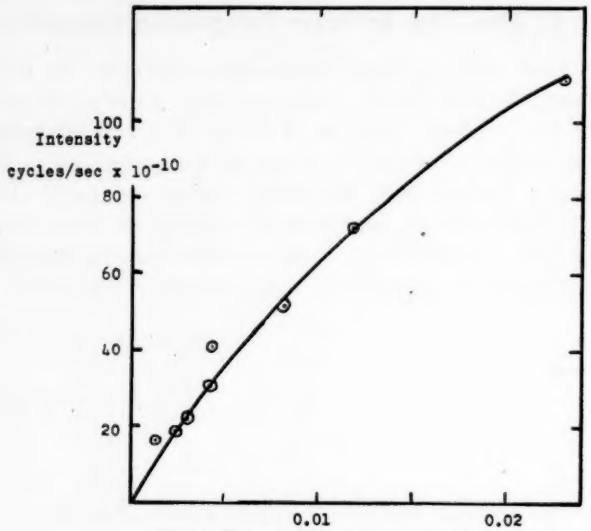

FIG. 1. The apparent intensity of the CS_2 1523-cm^{-1} band as a function of path length.

The Absolute Intensity of the CS_2 Stretching Vibration

Carbon disulfide is a linear symmetric molecule with an active infrared stretching fundamental vibration occurring at 1523 cm^{-1}. Since the structure of carbon disulfide is similar to that of carbon dioxide, the bond properties, including the effect of resonance, would be expected to be quite similar.[3]

The intensity of the 1523-cm^{-1} band was obtained with a Baird Associates double-beam spectrophotometer. The partial pressures which gave absorptions in the correct range were of the order of a few hundredths of a millimeter. These partial pressures were obtained by diluting mixtures of CS_2 and air, one atmosphere of air being sufficient to broaden the band. The path length was varied by further dilution. The spectra were obtained directly as percent transmittance *vs* wavelength. Since the integral of the absorbance on a linear frequency scale was needed, the spectra were replotted on semilogarithmic paper and the areas obtained with a planimeter. The apparent intensity of the band as a function of path length is shown in Fig. 1. The apparent integrated absorption coefficient is obtained by dividing the values of the intensities on the smooth curve by the corresponding values of the path length. The extrapolation of these ratios to zero path length gave the absolute intensity of 7560×10^{10} cycles sec^{-1} (cm of vapor at NTP)$^{-1}$ (Fig. 2).

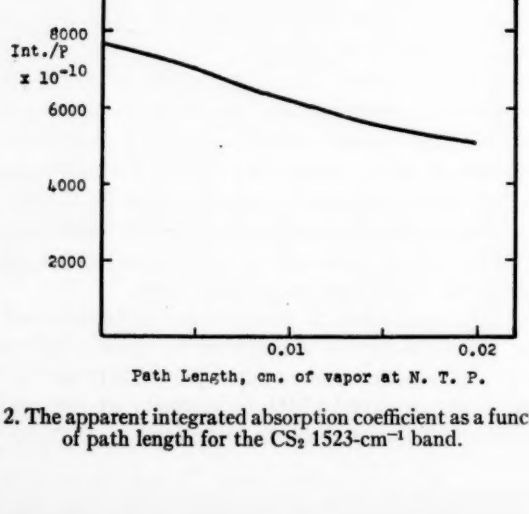

FIG. 2. The apparent integrated absorption coefficient as a function of path length for the CS_2 1523-cm^{-1} band.

The Intensity of the OCS Stretching Vibration

Carbonyl sulfide was prepared by the method described by Partington[5] and was purified by distillation at low temperatures under vacuum. OCS has two active stretching vibrations: ν_3 an unsymmetrical stretching vibration at 2079 cm^{-1} and ν_1 at 859 cm^{-1}. The spectra were recorded and the intensities measured and plotted on Figs. 3 and 4. Since all the points fell on straight lines, there was no need to extrapolate the slope. The results for OCS, CS_2, and CO_2[3] are shown in Table I.

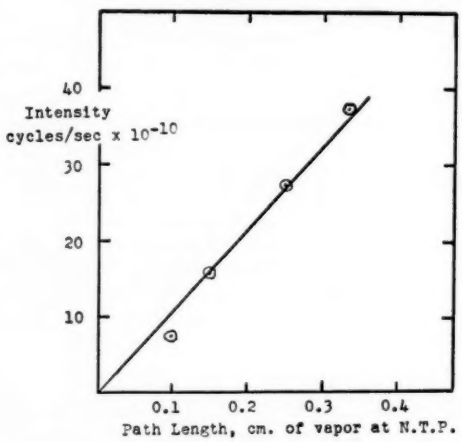

FIG. 3. The intensity of the 859-cm^{-1} band of OCS as a function of path length. The slope of this line is 110×10^{10} cycles sec^{-1} (cm of vapor at NTP)$^{-1}$.

Method of Interpretation of Infrared Intensities

It is well known that the absolute intensity of a band depends on the change of dipole moment as the molecule goes through its normal mode of motion. The actual formula can be represented by

$$A_i=(N\pi/3c)\,|\partial\boldsymbol{\mu}/\partial Q_i|^2, \qquad (2)$$

where A_i is the intensity of the band, N the number of molecules per cm^3, c the velocity of light, and $\partial\boldsymbol{\mu}/\partial Q_i$ the rate of change of dipole moment with the particular normal mode Q_i. The assumptions made in deriving this formula are that the molecule undergoes harmonic

[5] J. R. Partington, *Textbook of Inorganic Chemistry* (Macmillan and Company, Ltd., London, 1939), p. 695.

vibrations and that the dipole moment is a linear function of the displacement.[6]

The absolute intensity can therefore give quantitatively the change in the dipole moment of the molecule for each normal mode. We would, however, like to relate this change with the properties of the individual bonds. To do this, two things are needed: first, the actual changes in bond length and bond angle during the normal vibrations; second, enough intensity data to assign unambiguously changes in moments to the bonds. For example, in OCS, since the vibration at 2079 cm^{-1} involves only the stretching of the C=O and the C=S bonds, the intensity of only one other stretching vibration involving these bonds is needed. Once the changes in moments for two stretching vibrations have been determined, the change for the individual bonds can be found.

Algebraically, we have

$$Q_i=\sum_k L_{ik}^{-1}R_k, \tag{3}$$

where the L^{-1} are the normalized transformation coefficients relating the internal coordinates and the normal modes Q.

Using Eq. (3) we obtain,[2]

$$\partial\mu/\partial R_k=\sum_i L_{ik}^{-1}\partial\mu/\partial Q_i. \tag{4}$$

Here $\partial\mu/\partial R$ is the change of dipole moment of the molecule that occurs when the internal coordinate R is changed. Thorndike tried the approximation, following Wolkenstein,[7] and Rollefson and Havens,[8] that if R was a bond distance, $\partial\mu/\partial R$ was the change in the bond dipole moment as the bond was stretched, while if R was a bond angle, $\partial\mu/\partial R$ was the bond moment.

Unfortunately, this approximation does not seem to agree well with experiment, as Thorndike found. To the change in dipole moment of a given bond must be added the change of dipole moment thereby produced in the rest of the molecule. The existence of an interaction term in the potential energy function shows that this latter contribution is important because it implies that changes in one coordinate will alter the character of the other bond. It is only by considering such secondary effects that the discrepancy between the values of the dipole moment of the CH_2 band in ethylene can be accounted for.[2]

In any event, to obtain $\partial\mu/\partial R$, it is necessary to know not only the normal frequencies but also the normal coordinates. Accurate normal modes are hard to obtain. The complete force field is necessary for their calculation, and the complete force field is known for very few polyatomic molecules. Most often the assumption of a valence force field is made. It is then possible to calculate force constants that will fit the known frequencies. However, there are $n!$ sets of constants (where n is the order of the secular equation being solved), and some of the constants have to be brought over from other molecules.

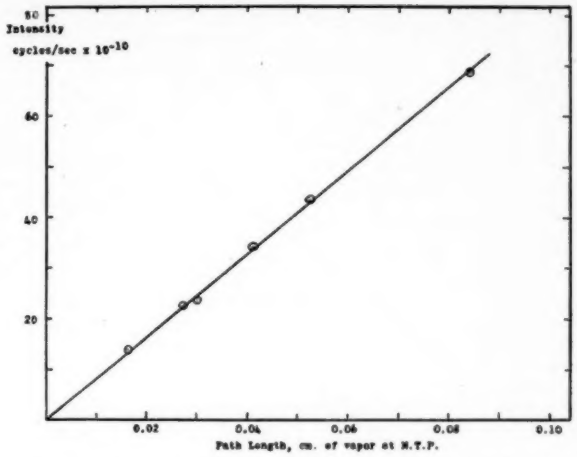

FIG. 4. The intensity of the 2079-cm^{-1} band of OCS as a function of path length. The slope of this line is 7900×10^{10} cycles sec^{-1} (cm of vapor at NTP)$^{-1}$.

Even when we know the normalized modes, we have to know the direction of $\partial\mu/\partial Q$. Different signs for these quantities will lead to different values of $\partial\mu/\partial R$. It is necessary to use data from other similar molecules and physical arguments in order to eliminate as many of these combinations as possible.

Interpretation of the CS_2 Result

Since the 1523-cm^{-1} vibration of CS_2 is the only one in its symmetry class, the symmetry coordinate and the unnormalized normal coordinate are the same In OCS, however, the symmetry is lost; and it is necessary to calculate the actual normal modes. The calculations of the $\partial\mu/\partial r$ of CS_2 will be done first.

Let the molecule be written as S=C=S, and let Δr_1 be a change in bond distance of the C=S bond and Δr_2 be a change in the S=C bond. The symmetry coordinate is then

$$\Re_3=2^{-\frac{1}{2}}(\Delta r_1-\Delta r_2). \tag{5}$$

To normalize this coordinate[9] it is necessary to multiply it by $(G_{33})^{-\frac{1}{2}}$, where G_{33} is given by

$$G_{33}=(m_s)^{-1}+2(m_c)^{-1}. \tag{6}$$

The normal mode is then

$$Q_3=2.8\times10^{-12}\Re_3.$$

TABLE I. Intensities of stretching vibrations of XCY molecules $\times10^{-10}$ cycle sec^{-1} (cm of vapor at NTP)$^{-1}$.

Molecule	CO_2	OCS	CS_2
ν_1 unsym. stretch	8600	7900	7560
ν_3 sym. stretch	0	110	0

[6] B. L. Crawford, Jr., and H. L. Dinsmore, J. Chem. Phys. **18**, 983 (1950).
[7] M. W. Wolkenstein, J. Phys. (U.S.S.R.) **5**, 185 (1941).
[8] R. Rollefson and R. Havens, Phys. Rev. **57**, 710 (1940).
[9] E. B. Wilson, Jr., J. Chem. Phys. **9**, 76 (1941).

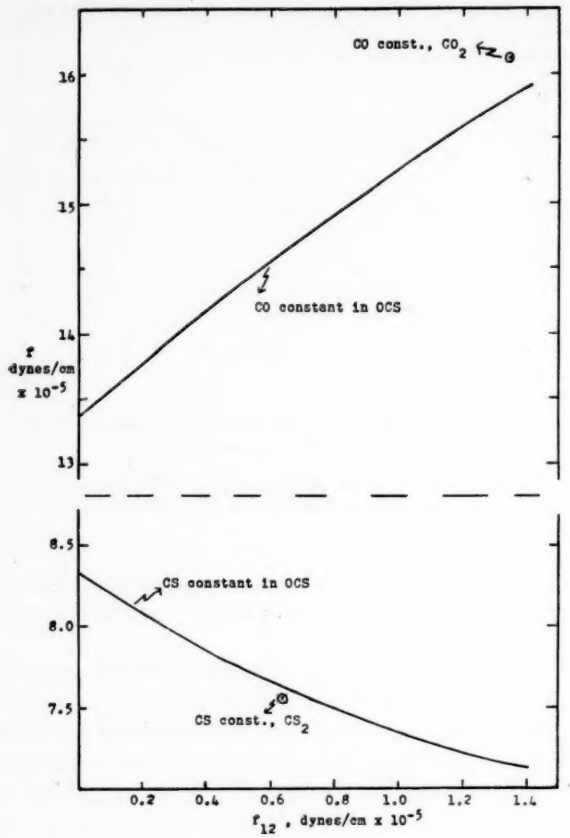

FIG. 5 The CO and CS force constants in OCS as a function of f_{12}.

From Eq. (2) and Table I we can obtain $\partial\mu/\partial Q_3$, the rate of change of moment during the normal vibration:

$$\partial\mu/\partial Q_3=\pm 283. \tag{7}$$

The change of moment for a unit change in symmetry coordinate is, from Eq. (4),

$$\partial\mu/\partial\Re_3=2.8\times10^{-12}\partial\mu/\partial Q_3$$
$$=\pm 7.93\times10^{-10}\text{ esu}. \tag{8}$$

To convert this value to the property of the individual bonds we need the relationship between the symmetry and the internal coordinate:

$$(\partial\mu/\partial r_1)=(\partial\mu/\partial\Re_3)(\partial\Re_3/\partial r_1)+(\partial\mu/\partial\Re_1)\partial\Re_1/\partial r_1. \tag{9}$$

Since $\Re_1$, the symmetric stretching vibration, is inactive, $\partial\mu/\partial\Re_1$ is zero. From Eqs. (8) and (5) we obtain

$$\partial\mu/\partial r=-5.6\times10^{-10}\text{ esu}. \tag{10}$$

The sign of the change of moment of the AB bond will be considered negative if atom B becomes more negative when the bond is stretched. Since stretching the CS bond will favor a single-bonded structure with a negative sulfur atom, the sign in Eq. (10) is negative.

Calculation of the COS Bond Properties

Since there are two vibration frequencies and three force constants (the CO stretching constant, the CS stretching constant, and the interaction constant), no unique set of force constants can be calculated from these data alone. In order to see what effect reasonable values of the interaction, f_{12}, would have on the calculated bond properties, it was felt that a complete normal coordinate treatment would be useful. A comparison with the constants for CO_2 and CS_2 would be also of value.

FORCE CONSTANTS FOR CO_2, CS_2, AND OCS

It can be shown that for CO_2 or CS_2 the force constants, the frequencies, and the reciprocal masses have the following relationship:

$$\lambda_1=(f_1+f_{12})\mu_1,$$
$$\lambda_3=(f_1-f_{12})(\mu_1+2\mu_3),$$

where $\lambda_n=4\pi\nu_n^2$, and μ_1, μ_3 are the reciprocal masses (μ_3 is the carbon reciprocal mass, and μ_1 the O or S mass). Using 2396 and 1361 for ν_3 and ν_1 for CO_2, and 1523 and 660 for ν_3, ν_1 for CS_2, we obtain the following force constants (in units of 10^5 dynes/cm). (All frequencies are in cm^{-1}.)

for CO_2: $f_{co}=16.11$,
$f_{12}=1.34$;
for CS_2: $f_{cs}=7.56$,
$f_{12}=0.63$.

In OCS the potential energy can be written in the form (r_1 is the C=O bond, r_2 the CS bond):

$$2V=f_1\Delta r_1^2+f_2\Delta r_2^2+2f_{12}\Delta r_1\Delta r_2.$$

The kinetic energy can be written in the form

$$2T=(\mu_1+\mu_3)\Delta r_1^2+(\mu_2+\mu_3)\Delta r_2^2-2\mu_3\Delta r_1\Delta r_2.$$

If we solve for the frequencies in terms of the constants, we get the equations

$$\lambda_1\lambda_3=[f_1f_2-f_{12}^2][(\mu_1+\mu_3)(\mu_2+\mu_3)-\mu_3^2],$$
$$\lambda_1+\lambda_3=(\mu_1+\mu_3)f_1-2\mu_3f_{12}+(\mu_2+\mu_3)f_2.$$

We can solve for f_1 and f_2 as a function of f_{12} if we use the known (uncorrected) frequencies. They are plotted in Fig. 5.

From resonance theory, f_{12} should be positive. Wu has suggested that the average value 0.9 of the CO_2 and CS_2 cases be used. However, the resonance might mainly be between the structures

$$^-O-C\equiv S^+, \quad O=C=S.$$

TABLE II. Bond lengths in XCY molecules.

Bond	CO_2[a]	CS_2[b]	OCS[b]	OCS[c]
C=O	1.15A		1.16A	1.165A
C=S		1.54±0.03A	1.56A	1.558A

[a] P. E. Martin and E. F. Barker, Phys. Rev. **41**, 291 (1932).
[b] P. C. Cross and L. O. Brockway, J. Chem. Phys. **3**, 821 (1935).
[c] C. H. Townes, Phys. Rev. **74**, 1113 (1948).

If the magnitude of the interaction constant is due to resonance and only two structures of about equal energy are resonating, we might expect the interaction constant to be smaller than either the CO_2 or CS_2 interaction constants. This assumption is normally made; but the evidence for less resonance is not certain, as will be discussed later.

In any event, the stretching constant of the C=S bond in OCS should be greater than that of CS_2, and the C=O constant in OCS should be less than that in CO_2 because of the resonance. If the bond force constant for the CS bond is to be greater in OCS than in CS_2, the interaction constant must be less than 0.7. We can take $0.5\times10^5\pm0.2$ as a value that is probably correct. We might perhaps get some information from the bond distances. They are given in Table II. The CO bond is probably longer in OCS than in CS_2, but nothing can be said about the CS, bond because of the experimental uncertainty in the electron diffraction determination for CS_2. However, the CS bond in OCS is unlikely to be more than 0.01A shorter than the bond in CS_2. These distances therefore suggest that the bonds in OCS are similar to those in CS_2 and CO_2. Consequently, f_{12} was taken as near the average of CO_2 and CS_2 as is compatible with having the C−S constant in OCS larger than in CS_2. This value is approximately 0.7×10^5.

OCS NORMAL COORDINATES

Once we have the force constants and the frequencies, there is no difficulty in solving for the normal coordinates. They can be written in the following form:

$$Q_1=L_{11}^{-1}R_1+L_{12}^{-1}R_2,$$

$$Q_3=L_{31}^{-1}R_1+L_{32}^{-1}R_2,$$

where the Q_n are the normal coordinates associated with ν_n, R_k are the internal coordinates, and L_{nk}^{-1} is the transformation coefficient.

Then it can easily be shown[9] that

$$L_{n2}^{-1}/L_{n1}^{-1}=-[(GF)_{11}-\lambda_n]/(GF)_{21}.$$

The ratios obtained are plotted in Figs. 6 and 7.

It is worth noting that the exact form of the normal coordinates is a sensitive function of the interaction constant. For example, a change in the interaction force constant by 0.5×10^5 dynes per centimeter makes a 25 percent change in L_{31}^{-1}/L_{32}^{-1} for the 2079-cm^{-1} band.

The 2079 band can be described as an unsymmetrical stretching vibration mainly involving the C=O bond and the 859 band as an asymmetrical stretching vibration with the CS bond mainly involved.

From the calculation of the ratios it is easy to normalize the coefficients using the method of Wilson.[9] If we take $L_{n1}^{-1}=1$, then the normalization constant K_n which multiplies each coefficient is given by

$$K_n=(G_{11}+2L_{n2}^{-1}G_{12}+(L_{n2}^{-1})^2G_{22})^{-\frac{1}{2}}.$$

$\partial\mu/\partial r$ FOR OCS

Once we have the normalization constants, we can obtain $\partial\mu/\partial Q$ from the intensities:

$$\partial\mu/\partial Q_1=\pm33.2,$$

$$\partial\mu/\partial Q_3=\pm288.$$

The ± signs are due to the fact that we can measure only $(\partial\mu/\partial Q)^2$. We can obtain the relationship between

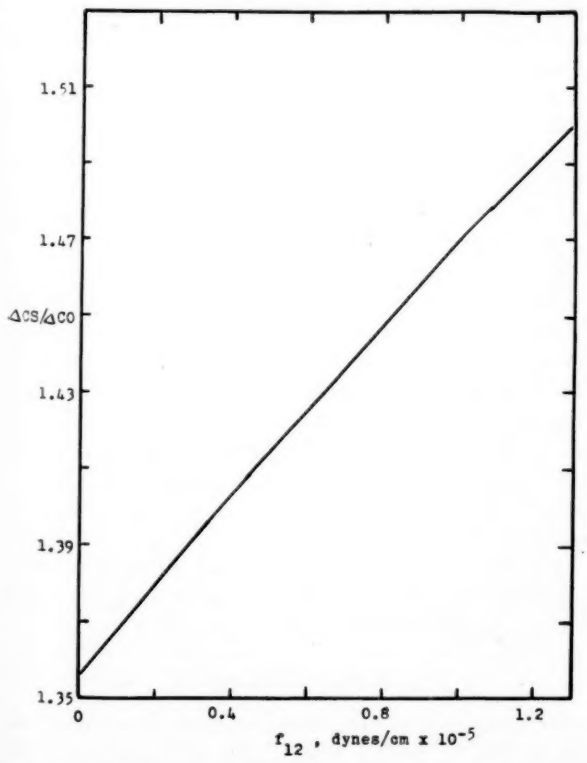

FIG. 6. ΔCS/ΔCO for the OCS 859-cm^{-1} band as a function of f_{12}.

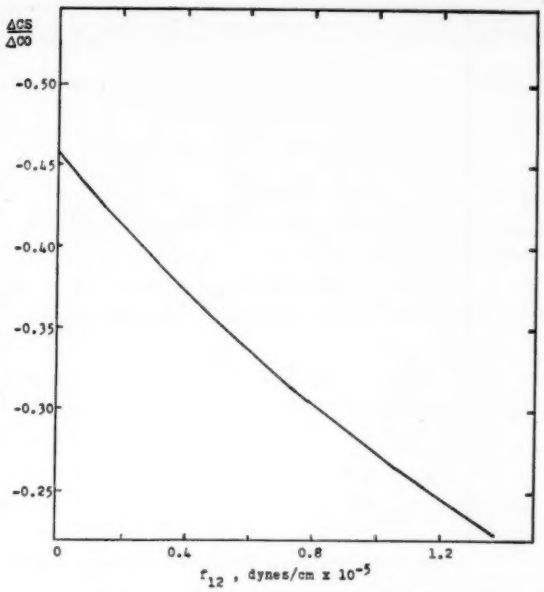

FIG. 7. ΔCS/ΔCO for the OCS 2079-cm^{-1} band as a function of f_{12}.

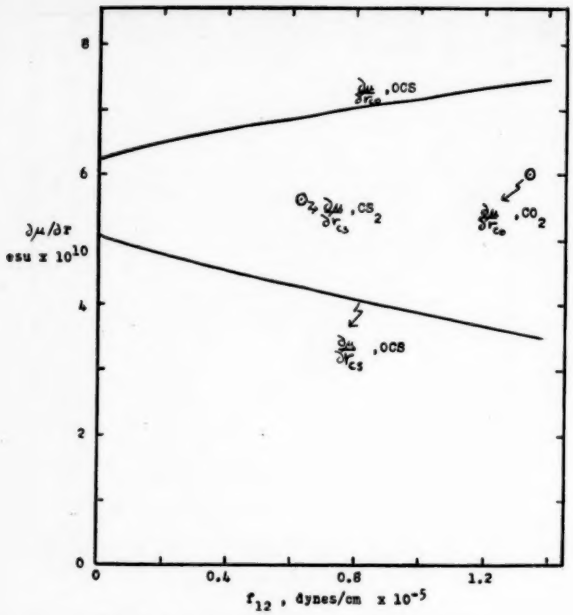

FIG. 8. $\partial\mu/\partial r$ for OCS as a function of f_{12}.

the $\partial\mu/\partial Q$'s and $\partial\mu/\partial r$'s:

$$\partial\mu/\partial r_1 = L_{11}^{-1}(\partial\mu/\partial Q_1) + L_{31}^{-1}\partial\mu/\partial Q_3,$$

$$\partial\mu/\partial r_2 = L_{12}^{-1}(\partial\mu/\partial Q_1) + L_{32}^{-1}\partial\mu/\partial Q_3.$$

In order to determine the signs, the following considerations were used. If we try giving the $\partial\mu/\partial Q$ both the same sign, we obtain

$$\partial\mu/\partial r_1 = \pm 8.7\times 10^{-10} \text{ esu},$$

$$\partial\mu/\partial r_2 = \pm 1.72\times 10^{-10} \text{ esu},$$

if we use the L^{-1} for the case $f_{12}=0$. Both these values are quite different from the CO_2 and CS_2 results and are not near each other. If, on the other hand, we try

$$\partial\mu/\partial Q_1 = \mp 33.2,$$

$$\partial\mu/\partial Q_3 = \pm 288,$$

we obtain

$$\partial\mu/\partial r_1 = \pm 6.3\times 10^{-10},$$

$$\partial\mu/\partial r_2 = \mp 5.0\times 10^{-10}.$$

The numbers are close to the results for CO_2 and CS_2. They have different signs, which is to be expected, since the bonds point in different directions. We therefore accept this choice of signs. These values are plotted as a function of f_{12} in Fig. 8.

It is interesting to note that these values are not nearly so sensitive a function of f_{12} as are the normal modes. A change of 0.5 in the force constants makes only a 10 percent change in the values of the $\partial\mu/\partial r$'s.

We can summarize the results in Table III if we use the value 0.7 for f_{12}. Owing in part to the larger error in measuring the intensity of the CO_2 2350 band, it is difficult to determine if there is any real difference in the values obtained. However, it is reasonably certain that the $\partial\mu/\partial r$ for the CS bond is smaller in OCS than in CS_2.

TABLE III. $\partial\mu/\partial r\times 10^{10}$ for CX bonds.

	CO_2	OCS	CS_2
$(\partial\mu/\partial r)_{CO}$	-6.0 ± 0.6 esu	-6.7 ± 0.5 esu	
$(\partial\mu/\partial r)_{CS}$		-4.3 ± 0.5	-5.6 ± 0.5 esu

CONCLUSIONS

As discussed by Thorndike,[3] these very high values of $\partial\mu/\partial r$ can be ascribed to the effect of resonance between the structures:

$$X^+\equiv C-Y^-, \quad X=C=Y, \quad X^--C\equiv Y^+.$$

Stretching a bond tends to favor the resonance structure in which that bond is single and thus induces a dipole moment in the molecule. This induced moment is much greater that would be expected if a final effective charge of a size high enough to give the observed bond moment were used to calculate the intensity.

The most striking feature of these results is the great similarity between these OCS bond moments and the CO and CS moments in CO_2 and CS_2. This indicates that the resonance in OCS is about the same order of magnitude in OCS as in the other molecules, while considerations of electronegativity might give the impression that there would be resonance between only two forms instead of three.

It is of interest to examine the evidence for the amount of resonance in OCS. If only two forms were resonating, the CO bond length in OCS should be longer than in CO_2, while the CS bond distance should be shorter than in CS_2. Table II shows that the CO bond distance in OCS is about 0.015A longer than in CO_2, while the CS distance can be no more than 0.01A shorter. These results certainly do not indicate that there is such difference in resonance.

Many authors have shown that the bond force constants in OCS are quite different from those in the parent molecules. However, these authors have usually not taken into account the interaction constant. From Fig. 5 it can be seen that for $f_{12}=0$ the CO and CS constants are 13.3 and 8.3 for OCS compared with 16.1 and 7.6 for CO_1 and CS_2. However, if $f_{12}=0.7$, a reasonable value, the OCS constants become 14.5 and 7.6, respectively. This procedure lowers the difference markedly.

In general, it can be concluded that the evidence from molecular data does not seem to point to great differences in resonance between OCS, CS_2, and CO_2.

ACKNOWLEDGMENT

For his helpful advice, I wish to express my appreciation to Dr. E. Bright Wilson, Jr., who suggested this problem.

Determination of Isotope Ratios, e.g., in Tracer Work, by an Infrared Absorption Method

J. M. W. MILATZ, J. C. KLUYVER, AND J. HARDEBOL
Physical Laboratory, University of Utrecht, Utrecht, The Netherlands
(Received January 26, 1951)

WE have studied the possibility of using infrared absorption spectra for the determination of isotope abundances. For this purpose the isotope is measured in the form of a chemical compound, showing absorption in the infrared.

The frequencies of the centers of the vibration-rotation bands of a molecule depend on the interatomic forces and on the masses of the constitutive atoms. Substitution of some atom in the molecule by one of its isotopes will therefore cause a change in the infrared absorption spectrum of the molecule.[1]

For the development of a method based on this effect carbon dioxide with variable C^{13} contents appeared to be a most suitable test object for several reasons. Carbon dioxide has strong absorption bands and this holds in particular for the ν_3 vibration band near 4.3μ. Moreover, the position of this band has been accurately determined, both[2] for $C^{12}O_2$ and[3] for $C^{13}O_2$; and the isotope shift is rather considerable. An additional advantage from the point of view of practical application is the easy convertibility of all molecules containing labeled carbon into carbon dioxide.

To select the spectral region, where only the molecule with the isotope wanted shows absorption, we did not use a spectrograph but a detector selective for each isotope. This detector consists of a cell (D_1) filled with the gas component to be measured (compare Fig. 1). For measuring the C^{13}/C^{12} ratio the detector cell should be filled with pure $C^{13}O_2$.

A beam of unresolved infrared light from a Nichrome filament S_1 is projected in the detector and interrupted 50 times per second by the chopper disk C. The part of the radiation with wavelengths in the spectral region of the absorption band of the component to be detected ($C^{13}O_2$) causes temperature oscillations in D_1 and consequently pressure oscillations. This sound of the frequency 50 is detected by a condenser microphone M, which is backed by a set constructed by one of us for the detection of small photoelectric currents.[4]

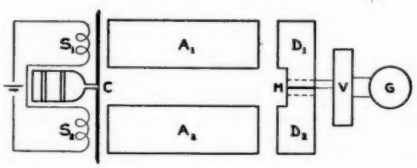

FIG. 1. Experimental arrangement. S_1=Source, C=Chopper disk. A_1=Analysis cell. D_1=Detection cell. V=Amplifier. G=Ac galvanometer. M=Microphone membrane. S_2, A_2, D_2 source, and analysis and detection cells for compensation method.

This set consists of a two-valve ac amplifier and an alternating current galvanometer (sensitive to 50 ± 1 period only: favorable signal-to-noise ratio; mean square error 10^{-14} amp).

When the absorption cell A_1 is filled with a gas containing $C^{13}O_2$, the galvanometer shows a decrease of the deflection.

The instrument described is a gas analyzer of the positive filtering type similar to those constructed by Luft *et al.*[5] for ordinary gas analysis.

Provided the gas mixture to be analyzed in A_1 does not contain any other gas that absorbs in the same region, or consists of only two gases with overlapping (but not coinciding) spectra, the change in the reading is a measure for the concentration in A_1 of the gas to be determined.

Since the spectra of $C^{12}O_2$ and $C^{13}O_2$—although overlapping—do not coincide, the method is adequate for the determination of the abundance of $C^{13}O_2$ in $C^{12}O_2-C^{13}O_2$ mixtures. As no pure $C^{13}O_2$ was at our disposal, we had to fill the detection cells with a mixture 52.5 percent $C^{13}O_2-47.5$ percent $C^{12}O_2$ made from a corresponding $BaCO_3$ preparation kindly provided by the Eastman Kodak Company. This limitation implies a certain decrease in sensitivity and an obvious ambiguity of the result, which however, is scarcely a drawback in view of the rarity of carbon with more than 50 percent C^{13}.

The instrument is calibrated with the help of standard isotope mixtures. A typical calibration curve of percentage transmission *versus* abundance C^{13} is shown

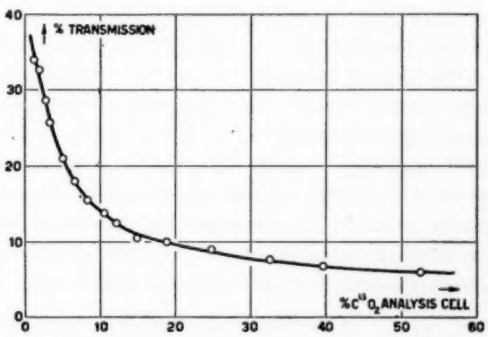

FIG. 2. Percentage transmission *versus* C^{13} abundance in sample.

[1] G. Herzberg, *Infrared and Raman Spectra of Polyatomic Molecules* (D. Van Nostrand Company, Inc., New York, 1947), p. 227.
[2] D. M. Cameron and H. H. Nielsen, Phys. Rev. **53**, 246 (1938).
[3] A. H. Nielsen, Phys. Rev. **53**, 983 (1938).
[4] J. M. W. Milatz, thesis Utrecht, 1937. J. M. W. Milatz and N. Bloembergen, Physica **11**, 449 (1946).
[5] K. F. Luft, Z. tech. Physik **24**, 97 (1943). A. H. Pfund, Science **90**, 236 (1939).

in Fig. 2. The accuracy with which C^{13}/C^{12} ratios between 0.011 and 0.10 have been determined using one beam of light is 0.002.

To increase the sensitivity the instrument is constructed as a double-beam analyzer. Both detector cells are filled with the same gas and are separated by the membrane of the microphone. Compensation will be achieved either by adjusting a diaphragm in one beam or by filling the dummy analysis cell (A_2) with a reference isotope mixture.

In this way we hope to attain an accuracy of about 1 percent of the C^{13}/C^{12} ratio near 0.011 and about 2 percent in the interval 0.03–0.07. This is sufficient for a large number of biological tracer experiments.

In principle the same method can be applied to the determination of other isotope abundance ratios in appropriate molecules.

This work is part of the research programme of the "Stichting voor Fundamenteel Onderzoek der Materie" and was made possible by financial support from the "Nederlandse Organisatie voor Zuiver-Wetenschappelijk Onderzoek."

THE JOURNAL OF CHEMICAL PHYSICS VOLUME 19, NUMBER 7 JULY, 1951

Kinetics of OH Radicals from Flame Emission Spectra. III. Total Transition Probabilities and the Energetic Distribution of $OH(^2\Sigma^+)$ and $O_2(^3\Sigma_u^-)$ in the Oxy-Hydrogen Flame

KURT E. SHULER*
Applied Physics Laboratory,† The Johns Hopkins University, Silver Spring, Maryland
(Received March 13, 1951)

The energetic distribution of $OH(^2\Sigma^+)$ and $O_2(^3\Sigma_u^-)$ in hydrogen-oxygen flames has been investigated. The measurements were made in the inner cones of these flames burning with various fuel ratios (lean, stoichiometric, and rich) at atmospheric pressure. The relative concentrations of the excited species were determined by comparing the calculated equilibrium intensity ratios of $OH(^2\Sigma^+)$ and $O_2(^3\Sigma_u^-)$ with the experimental intensity ratios. The electronic, vibrational, and rotational transition moments relevant to this calculation have been computed. The good agreement between the experimental intensity ratios and the calculated equilibrium intensity ratios indicates that the electronically excited $O_2(^3\Sigma_u^-)$ is in thermal equilibrium with $OH(^2\Sigma^+)$. It is possible, therefore, that O_2 is excited thermally in the hydrogen-oxygen flame.

I. INTRODUCTION

IN Parts I and II of this series[1] there has been discussed the determination of the rotational and vibrational distribution of electronically excited OH radicals from flame emission spectra. With the methods and data of these papers it is possible to ascertain whether electronically excited OH radicals are in rotational and vibrational equilibrium distributions; this, however, still leaves open the question as to whether the OH is in an *electronic* equilibrium distribution as given by the usual Boltzmann expression. The determination of the distribution of a molecular or atomic species among its various electronic states is of great help in elucidating the possible origin and role of this species in the flame reaction mechanism. Thus, for instance, an electronic non-equilibrium distribution such as the finding that a certain electronically excited species is present in a flame in great excess over its thermal equilibrium concentration may give valuable clues as to the elementary reactions occurring in the flame.[2,3] If, on the other hand, a state of complete thermal equilibrium is found for the flame, no direct information can be extracted in regard to the possible kinetic mechanisms and recourse must be had to further experimental work under different conditions of fuel ratios and total pressure.[4]

For certain molecular species such as CH or C_2, which have several rather closely spaced electronic energy levels, the general methods discussed in I and II may be applied to determine the distribution of the molecules among the various energy levels. In the case of CH, for instance, one may compare the experimental and theoretical (thermal) intensity distribution among the $^2\Pi$, $^2\Delta$, $^2\Sigma^-$, and $^2\Sigma^+$ levels which have a spread of only about 4 ev. This method cannot, however, be used for the OH radical, which has only one excited electronic state ($^2\Sigma^+$) which has been identified with certainty; and it is therefore necessary to proceed in a different manner.[5]

The method adopted here is to compare the experimental intensity ratio of an $OH(^2\Sigma^+ \rightarrow {}^2\Pi)$ and an $O_2(^3\Sigma_u^- \rightarrow {}^3\Sigma_g^-)$ transition in an hydrogen-oxygen flame

* Research Fellow of the Applied Physics Laboratory, The Johns Hopkins University.

† The work described in this paper was supported by the Bureau of Ordnance, U. S. Navy, under Contract NOrd-7386.

[1] K. E. Shuler, J. Chem. Phys. **18**, 1221, 1466 (1950).

[2] V. F. Griffing and K. J. Laidler, in *Third Symposium on Combustion, Flame and Explosion Phenomena* (Williams and Wilkins Company, Baltimore, 1949), p. 432.

[3] K. J. Laidler and K. E. Shuler, Chem. Revs. **48**, 153 (1951).

[4] For a more detailed discussion on this point see K. J. Laidler and K. E. Shuler, Ind. Eng. Chem., to be published.

[5] It would of course be possible to make "absolute" intensity measurements similar to those of V. Kondratjew, Acta Physicochim. U.R.S.S. **2**, 126 (1935); **4**, 547 (1936); **6**, 625, 748 (1936); and subsequent publications, to obtain the desired results. There is, however, some question as to the accuracy of these types of experiments.

with that calculated on the basis of complete thermal equilibrium.[6] While this will not give direct information as to the separate electronic distribution of OH or O_2 it will permit a determination of the *relative* concentration of OH and O_2 in their electronically excited states and thus enable one to draw conclusions as to the equilibrium or non-equilibrium conditions in the flame. It may be pointed out that the method to be described here for the case of $OH(^2\Sigma^+)$ and $O_2(^3\Sigma_u^-)$ should be of general utility in these types of studies; it could be used, for instance, in conjunction with the recent accurate calculation[7] of the oscillator strength f for C_2 to determine the relative concentration of electronically excited C_2 and OH in hydrocarbon flames.

It is desired to determine the intensity ratio of the $R_1(10)$ line in the (0,1) band of the $^2\Sigma^+\rightarrow{}^2\Pi$-transition of OH and the $P(31)+R(35)$ lines of the (0,14) band of the $^3\Sigma_u^-\rightarrow{}^3\Sigma_g^-$ transition of O_2. The $P(31)$ and $R(35)$ lines of (0,14) O_2 are separated by only 1.1 cm^{-1} and could not be resolved by our spectrograph so that they can be considered as forming one "line" which will hereafter be referred to as $PR(31,35)$. The choice of these particular lines of OH and O_2 was dictated by the fact that they are only about 8A apart, so that it will not be necessary to be concerned with the wavelength response of the plate. The intensity ratio is given by

$$\frac{I(\mathrm{OH})}{I(\mathrm{O_2})}=\frac{N[\mathrm{OH}(^2\Sigma^+)]A_{nm}(\mathrm{OH})}{N[\mathrm{O_2}(^3\Sigma_u^-)]A_{nm}(\mathrm{O_2})}, \tag{1}$$

where the frequency dependence has been canceled out, since $\nu_{nm}(O_2)\sim\nu_{nm}(OH)$ for the lines chosen. To calculate the desired equilibrium intensity ratio it is necessary to calculate the equilibrium population of the electronically excited levels, $N[OH(^2\Sigma^+)]$ and $N[O_2(^3\Sigma_u^-)]$, and the Einstein transition probability coefficients, $A_{nm}(OH)$ and $A_{nm}(O_2)$, for the particular total transitions, i.e., electronic, vibrational, and rotational.

II. CALCULATION OF MATRIX ELEMENTS AND TRANSITION PROBABILITIES

a. The Electronic Matrix Elements

The electronic matrix elements of the dipole moment, $\mathbf{R}_{el}=\int\psi_{el}'M\psi_{el}''d\tau_{el}$, may be determined by evaluating the above integral after the electronic wave functions have been expressed in the appropriate AO or LCAO MO approximation. This method has been developed extensively in a series of papers by Mulliken;[8,9] however, owing to the difficulty encountered in the exact representation of the electronic wave functions, these calculations are of necessity rather approximate. It is therefore preferable, in the present state of the subject, to determine the electronic matrix elements from experimental data on intensities. Fortunately, the electronic absorption spectra of OH and $O_2(^3\Sigma_g^-\rightarrow{}^3\Sigma_u^-)$ have been studied rather thoroughly, and the necessary data can thus be readily obtained.[10]

The experimental data of absorption are frequently expressed in terms of the "oscillator strength" f^{nm}. This quantity is related to the electronic dipole moment matrix element by

$$f^{nm}=\frac{8\pi^2\mu c\nu_{nm}}{3he^2}\frac{1}{g_m}\sum|\mathbf{R}_{el}^{ni,mk}|^2, \tag{2}$$

where g_m is the electronic statistical weight of the lower state m and where the summation extends over all the allowed combinations of the component sublevels i and k of the states n and m. The quantities μ and e are, respectively, the mass and charge of the electron. The oscillator strength f^{nm} of Eq. (2) refers to the absorption intensity summed over all the rotational and vibrational levels of the final state n with which the initial rotational-vibrational level of the state m can combine; it is thus, for discrete bands, the sum of the oscillator strengths of the separate transitions starting from a common level. This relationship between f^{nm} and $|\mathbf{R}_{el}^{nm}|^2$ arises from the application of the rotational and vibrational sum rules to the total transition moment $|\mathbf{R}^{nm}|^2$, which may be written as

$$|\mathbf{R}^{nm}|^2=|\mathbf{R}_{el}^{nm}|^2|\mathbf{R}_{vibr}^{v'v''}|^2|\mathbf{R}_{rot}^{j'j''}|^2, \tag{3}$$

where the terms on the right-hand side are the squares of the electronic, vibrational, and rotational matrix elements. The neglect of the interaction of the internal degrees of freedom implicit in writing $\mathbf{R}^{nm}$ as a product function of the various transition moments will introduce a certain amount of inaccuracy in these calculations; the approximation in writing $\mathbf{R}^{nm}$ as in Eq. (3) seems, however, to be unavoidable if the problem is to be tractable at all.[11]

The oscillator strengths $f^{j'v'nj''v''m}$ for the various rotational lines of the (0,0) band OH have been measured by Oldenberg and Rieke[12] and subsequently been corrected by Dwyer and Oldenberg.[13] According to this correction, the f-values of reference 12 should be multiplied by 4.2. Forming the sum[14] $\sum_{v'}\sum_{j'}f^{nmv'v''j'j''}$ from the corrected data of Oldenberg and Rieke, one finds $f^{nm}=1.26\times10^{-3}$. Substitution of this value into Eq. (2) with $g_m=2$ (ground state is a doubly-degenerate Π) and $\sum_{i,k}|\mathbf{R}_{el}^{ni,mk}|^2=2|\mathbf{R}_{el}^{nm}|^2$ (since $i=1$, $k=1$, 2,

[6] $O_2(^3\Sigma_u^-)$, which gives rise to the Schumann-Runge bands $(^3\Sigma_u^-\rightarrow{}^3\Sigma_g^-)$, has recently been identified in various flames of oxygen. For the CO—O_2 flame, see G. A. Hornbeck and H. S. Hopfield, J. Chem. Phys. **17**, 982 (1949), for the H_2—O_2 flame see H. G. Wolfhard and A. G. Gaydon, Nature **164**, 22 (1949).

[7] H. Shull, Astrophys. J. **112**, 352 (1950).

[8] R. S. Mulliken, J. Chem. Phys. **7**, 14 (1939), and subsequent publications in this Journal.

[9] R. S. Mulliken and C. A. Rieke, Phys. Soc. Rept. Progress Phys. **8**, 237–273 (1941).

[10] The matrix elements calculated by Mulliken for OH and O_2 are in good agreement with these experimentally determined values.

[11] The principal interaction is that of the electronic and vibrational motions; this has been discussed in I and in more detail by Mulliken (reference 9).

[12] O. Oldenberg and F. F. Rieke, J. Chem. Phys. **6**, 439 (1938).

[13] R. J. Dwyer and O. Oldenberg, J. Chem. Phys. **12**, 351 (1944).

[14] R. S. Mulliken, J. Chem. Phys. **8**, 382 (1940).

and $|\mathbf{R}_{el}^{n_1m_1}|^2=|\mathbf{R}_{el}^{n_1m_2}|^2$) gives

$$|\mathbf{R}_{el}^{nm}|^2_{OH(^2\Sigma^+\to{}^2\Pi)}=8.3\times10^{-38}\text{ g cm}^5\text{ sec}^{-2}. \quad (4)$$

The f-value for the $O_2(^3\Sigma_g^--{}^3\Sigma_u^-)$ transition has been determined by Ladenburg and Van Voorhis.[15] Their value of $f=0.193$ was obtained for the continuous absorption of O_2 between 1300 and 1750A with an absorption maximum at 1450A (69,000 cm^{-1}). An analysis of their data indicates that the continuum investigated by them is indeed due principally to the Schumann-Runge transition.[16] Since their absorption measurements correspond to molecules going principally from the level $v''=0$ to all of the Franck-Condon allowed unquantized vibrational and rotational "levels" of the upper electronic state, their oscillator strength is the f^{nm} of Eq. (2), i.e., an f-value integrated over all the upper state levels which combine with the initial level of the ground state. For ν_{nm} of Eq. (2) one can take ν_{max} for the absorption intensity maximum. The value which should be used is an average $\bar{\nu}_{nm}$; however, since the absorption curve is very symmetrical and since the shift between the overlap and the intensity maximum is very small, the choice of ν_{max} for $\bar{\nu}_{nm}$ should be sufficiently accurate. Substitution of $f^{nm}=0.193$ into Eq. (2) gives

$$|\mathbf{R}_{el}^{nm}|^2_{O_2(^3\Sigma_u^-\to{}^3\Sigma_g^-)}=5.8\times10^{-36}\text{ g cm}^5\text{ sec}^{-2}. \quad (5)$$

b. The Vibrational Transition Moments (Overlap-Integrals)

Since the lines whose intensity ratio is to be determined are in the (0,1) band of OH and in the (0,14) band of O_2, respectively, it is necessary to calculate $|\mathbf{R}_{vibr}^{v'v''}|=\int\psi_v'\psi_v''dr$ for these transitions. For the (0,1) transition of OH the values calculated in I can be used. The values quoted there (Table III) are, however, the squares of the matrix elements relative to the (0,0) transition and thus cannot be used directly. Absolute values of $\int\psi_v'\psi_v''dr$ were, however, calculated for the construction of Table III, Part I; and for the (0,1) transition the square of the matrix element was found to be

$$|\mathbf{R}_{vibr}^{0-1}|^2_{OH}=9.3\times10^{-2}. \quad (6)$$

This value corresponds to $\rho=0$ [see Eq. (7), I], i.e., it is calculated for an electronic dipole moment matrix component which does not vary with internuclear distance. As mentioned before, this is an approximation which must be made for Eqs. (2) and (3) to be applicable.

It is most probable that $|\mathbf{R}_{vibr}^{v'v''}|^2$ for O_2 would show a similar dependence upon r as was found for OH in Part I. Since this cannot be taken into account within the framework of Eqs. (2) and (3), the effort involved in making a very accurate calculation of $|\mathbf{R}_{vibr}^{v'v''}|^2$ similar to that of Part I would not be warranted by the results; this may readily be seen from the data of Part I, where it was shown that the variation of $|\mathbf{R}_{vibr}^{v'v''}|^2$ with r is a much more important factor in the calculation than the use of more exact wave functions taking explicit account of the anharmonicity. The vibrational transition moments for $O_2(^3\Sigma_u^-\to{}^3\Sigma_g^-)$ have been calculated by Pillow[17] using wave functions distorted graphically to fit the proper Morse curves.[18] While Miss Pillow's paper[17] lists only the ratios of the transition moments relative to that of the (0,12) transition, she has very kindly communicated to me the absolute value for the (0,14) transition, which is

$$|\mathbf{R}_{vibr}^{0-14}|^2_{O_2}=0.54. \quad (7)$$

This result should be of an accuracy comparable to that for OH (Eq. 6).

c. Rotational Transition Moments (Intensity Factors)

The rotational transition moment for the $R_1(10)$ line of OH was calculated from the intensity factors given by Earls[19] for the $^2\Sigma-{}^2\Pi$-transitions. The "coupling constant" λ, which takes account of the intermediate character of the $^2\Pi$-state between Hund's case a and b was taken[20] as $\lambda=-7.55$. For the $R_1(10)$ line, Earls' formulas gave

$$|\mathbf{R}_{rot}^{R_1(10)}|^2_{OH}=2.5. \quad (8)$$

The rotational transition moment for the O_2 "line" $PR(31,35)$ can be obtained from the Hönl-London line strength formulas.[21] Since the Schumann-Runge bands are a $\Sigma-\Sigma$-transition, the formulas for $\Delta\Lambda=0$ must be used. The Hönl-London equations are, however, derived on the assumption of negligible interaction of electronic and rotational motion (Hund's case a) so that they would be applicable principally to singlet systems, while the Schumann-Runge bands, being a $^3\Sigma-{}^3\Sigma$-transition obey Hund's case b. Mulliken[22] has given formulas for line strengths in a $^2\Sigma-{}^2\Sigma$-transition to which Hund's case b is applicable. A comparison of these formulas with those of Hönl and London for Hund's case a show that there is only a negligible difference between the two sets, especially for large values of K. If the reasonable assumption is made that this is also the case for the $^3\Sigma-{}^3\Sigma$-transition, it follows that the Hönl-London equations should give results of sufficient accuracy. Application of these equations to the $R(35)$ and $P(31)$ lines, bearing in mind that each of these lines really consists of an unresolved triplet, gave

$$|\mathbf{R}_{rot}^{PR(31,35)}|^2_{O_2}=33.5 \quad (9)$$

[15] R. Ladenburg and C. C. Van Voorhis, Phys. Rev. **43**, 315 (1933).
[16] R. S. Mulliken, J. Chem. Phys. **7**, 20 (1939).
[17] M. E. Pillow, Proc. Phys. Soc. (London) **63A**, 940 (1950).
[18] M. E. Pillow, Proc. Phys. Soc. (London) **62A**, 237 (1949).
[19] L. T. Earls, Phys. Rev. **48**, 423 (1935).
[20] G. H. Dieke and H. M. Crosswhite, *The Ultraviolet Bands of OH, Fundamental Data*, Bumblebee Report No. 87, The Johns Hopkins University, 1948. The spectroscopic notation of the present paper corresponds to that of this report.
[21] See e.g., G. Herzberg, *Spectra of Diatomic Molecules* (D. Van Nostrand Company, Inc., New York, 1950), second edition, p. 208.
[22] R. S. Mulliken, Revs. Modern Phys. **3**, 89 (1931).

as the *average* value of the line strength. The composite nature of this "line" in regard to the P and R components with their triplet structure must be taken into account in calculating the population of the emitting level. The line strengths [Eqs. (8) and (9)] include the rotational degeneracy $g_{\text{rot}}=2J+1$, which therefore does not have to be taken into account again in computing the population of these levels.

d. The Einstein Transition Probabilities

The Einstein coefficient for spontaneous emission A_{nm} is related to the total transition moment by

$$A_{nm}=(64\pi^4\nu_{nm}^3/3h)(1/g_n)\sum|\mathbf{R}^{n_im_k}|^2, \quad (10)$$

where g_n is the electronic statistical weight of the upper state n and where the summation extends again over all the possible combinations of the degenerate sublevels i and k of the states n and m. For OH, using the values of Eqs. (4), (6), and (8) in Eq. (3), one obtains $|\mathbf{R}^{nm}|^2_{\text{OH}}=1.9\times10^{-38}$. With $\nu_{nm}=29{,}138$ cm^{-1}, corresponding to the $R_1(10)$ line of the (0,1) band, $g_n=1$ for the nondegenerate upper $^2\Sigma^+$ state and $\sum_{ik}|\mathbf{R}^{n_im_k}|^2=2|\mathbf{R}^{nm}|^2$ (see Sec. IIa), the Einstein coefficient A_{nm} is given by

$$A_{nm}(\text{OH})[R_1(10),\ (0,1)]=2.9\times10^5\ \text{sec}^{-1}. \quad (11)$$

There is no orbital degeneracy in the $^3\Sigma$-states of O_2, so that $g_n=1$ and $\sum_{ik}|\mathbf{R}^{n_im_k}|^2=|\mathbf{R}^{nm}|^2$; using Eqs. (5), (7), and (9), one finds $|\mathbf{R}^{nm}|^2_{O_2}=9.3\times10^{-35}$ and with $\nu_{nm}=29{,}211$ cm^{-1}, A_{nm} is given by

$$A_{nm}(O_2)[PR(31,35),\ (0,14)]=7.2\times10^8\ \text{sec}^{-1}. \quad (12)$$

III. EQUILIBRIUM CONCENTRATION RATIOS

It is now necessary to calculate the equilibrium population ratio of $\text{OH}(^2\Sigma^+)$ and $O_2(^3\Sigma_u^-)$ in the rotational-vibrational levels for which the transition probabilities have been calculated above. Denoting these particular levels for brevity by the subscripts r and s for OH and O_2, respectively, one has for an equilibrium distribution,

$$\frac{N_r[\text{OH}(^2\Sigma^+)]}{N_s[O_2(^3\Sigma_u^-)]}=\frac{N_{\text{OH}}}{N_{O_2}}\frac{g_r}{g_s}\frac{\sigma_r}{\sigma_s}\frac{F_s}{F_r}\exp\left[\frac{(E_s-E_r)}{kT}\right], \quad (13)$$

where the F's are the partition functions, the σ's are the symmetry numbers ($\sigma_s=2$, $\sigma_r=1$), the g's are the appropriate statistical weights, and N_{OH}/N_{O_2} is the total equilibrium concentration ratio of OH to O_2 in the flame. This concentration ratio may be determined, for the equilibrium conditions discussed here, from a thermochemical calculation on an adiabatic hydrogen-oxygen flame. In the evaluation of g_r/g_s the rotational degeneracies must be omitted, since they are already included in the line strengths (Sec. IIc). In computing the remaining degeneracy factors one has $g_{el}\text{OH}(^2\Sigma^+)=1$, since the doublets are resolved; in the computation of the corresponding quantity for $O_2(^3\Sigma_u^-)$ one must take account of the composite nature of the $PR(31,35)$ line and the unresolved triplet structure of the components, so that $g_{el}O_2(^3\Sigma_u^-)=6$. In evaluating the electronic partition functions, f_{el}, the very small contribution of the $^1\Delta$-state of O_2 has been neglected, since it is outside the accuracy of these calculations and only introduces a complicating temperature dependence. For the same reason, no explicit account has been taken of the actual spin doublet separation and the separation of the Λ-type doublets for the $^2\Pi$-ground state of OH, so that $f_{el}(\text{OH})=4$ and $f_{el}(O_2)=3$. The $^3\Sigma_u^-$ state of O_2 and the $^2\Sigma^+$ state of OH are energetically too high to contribute to the partition functions. The evaluation of Eq. (13) then gives

$$\frac{N_r[\text{OH}(^2\Sigma^+)]}{N_s[O_2(^3\Sigma_u^-)]}=0.81\frac{N_{\text{OH}}}{N_{O_2}}\times\left[\frac{\exp(2.26\times10^4/T)-\exp(1.72\times10^4/T)}{1-\exp(-2.29\times10^3/T)}\right], \quad (14)$$

where the exponential terms arise partly from the exponential in the Boltzmann expression and partly from the vibrational partition functions.

Substitution of this population ratio [Eq. (14)] and the transition probabilities [Eqs. (11) and (12)] into Eq. (1) finally gives the calculated equilibrium intensity ratio of the $\text{OH}[R_1(10),\ (0,1)]$ and $O_2[PR(31,35),\ (0,14)]$ lines as

$$\frac{I_{\text{OH}}}{I_{O_2}}=3.2\times10^{-4}\frac{N_{\text{OH}}}{N_{O_2}}\times\left[\frac{\exp(2.26\times10^4/T)-\exp(1.72\times10^4/T)}{1-\exp(-2.29\times10^3/T)}\right]. \quad (15)$$

The adiabatic equilibrium flame temperature T and equilibrium composition ratios N_{OH}/N_{O_2} of the hydrogen-oxygen flame which are necessary for the complete evaluation of Eq. (15) were obtained from the tables of Hottel, Williams, and Satterfield;[23] they are listed in Table I.

TABLE I. Thermochemical flame temperatures and equilibrium OH/O_2 concentration ratios in the hydrogen-oxygen flame at atmospheric pressure (reference 23).

Composition	Condition	T(°K)	N_{O_2}	N_{OH}	N_{OH}/N_{O_2}
H_2+O_2	Excess O_2	2920	0.275	0.109	0.40
$H_2+\frac{1}{2}O_2$	Stoichiometric	3100	0.052	0.110	2.12
$H_2+\frac{1}{4}O_2$	Excess H_2	2825	0.00064	0.018	28.3

IV. EXPERIMENTAL

Hydrogen and oxygen were metered through calibrated flowmeters and burned off a commercial welding torch modified for use with H_2-O_2 mixtures. The

[23] Hottel, Williams, and Satterfield, *Thermodynamic Charts for Combustion Processes* (John Wiley and Sons, Inc., New York, 1949).

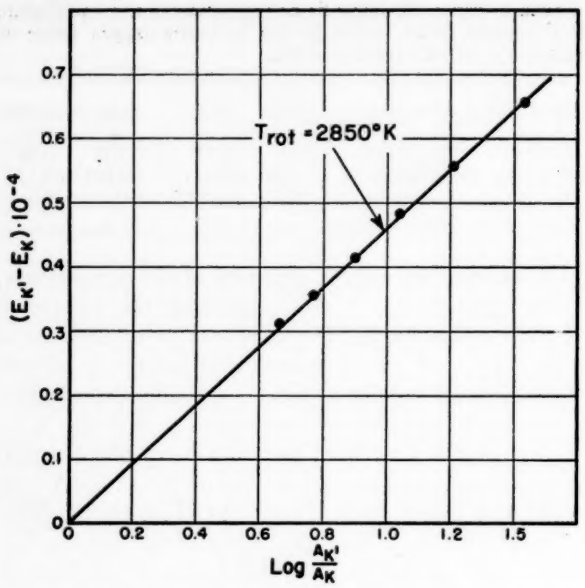

FIG. 1. A plot of $E_{k'}-E_k$ *vs* $\log(A_{k'}/A_k)$ for the R_2 branch of the (0,0) band of OH($^2\Sigma^+\rightarrow{}^2\Pi$) in the inner cone of a 1:1 hydrogen-oxygen flame.

spectra were taken in the second order of a 21-ft Jarrell-Ash grating spectrograph (Wadsworth mounting) with a dispersion of 2.4 A/mm. The exposure times using Eastman II-0 and 103-0 plates were about 10–30 minutes for the (0,0) band of OH and about 2–3 hours for the (0,14) band of O_2 and the (0,1) band of OH, the exact exposure times depending upon the particular fuel ratios. For the 4:1 hydrogen-oxygen flame a 5-hour exposure was taken on a 3-meter Jarrell-Ash grating spectrograph when it was found that no discrete Schumann-Runge bands could be detected for this mixture on the bigger and slower instrument. While the (0,1) band of OH showed up well on both spectrographs, no lines of the (0,14) band of O_2 could be found on any plate for this fuel ratio.

The spectra were all taken in the region of the inner cone of the flame about 1 cm above the nozzle opening. The geometry of the experimental set-up and the total flow rate of the gases remained the same throughout the experiments, so that the same region of the flame was being studied for all the fuel ratios. The visual appearance of the inner cone of the oxy-hydrogen flame differs from that of the oxy-acetylene flame and similar hydrocarbon flames. In place of a very bright inner cone, there is in the hydrogen-oxygen flame only a faintly luminous edge which barely delineates the inner cone. This difference is probably due to the fact that there are no strong transitions of OH or O_2 in the visible region, such as the strong Swan bands of C_2 in the hydrocarbon flames, which would give a highly luminous appearance to the inner cone. The radiation reaching a spectrograph focused on the inner cone will be due principally to the reacting gases in this luminous edge and to the hot reacted gases surrounding this combustion zone (interconal gases). The spectrum analyzed, therefore, represents some average features of the flame; and the statement that the spectrum is that of the inner cone cannot be taken to mean, for the burner used in this investigation, that the radiation is that of the reacting gases exclusively.

TABLE II. Experimental and calculated intensity ratios in the hydrogen-oxygen flame.

Composition	Condition	T_{rot}(°K)OH($^2\Sigma^+$)	I_{OH}/I_{O_2} (exp)	I_{OH}/I_{O_2} (calc)
H_2+O_2	Excess O_2	2850	1.0	0.6
$H_2+\frac{1}{2}O_2$	Stoichiometric	2950	2.5	1.6
$H_2+\frac{1}{4}O_2$	Excess H_2	2700	$>10^2$	4.1×10^1

Intensity measurements were made with a Leeds and Northrup recording photoelectric microdensitometer. The rotational distribution and temperature of OH($^2\Sigma^+$) was determined from the (0,0) band by the modified isointensity method discussed in some detail in Part II. Figure 1 shows a plot of $\log A_{k'}/A_k$ *vs* $E_{k'}-E_k$ (analogous to that of Fig. 2 in II) for a 1:1 hydrogen-oxygen fuel ratio. The good straight line which can be drawn through the experimental points indicates that the OH($^2\Sigma^+$) radicals are in a rotational equilibrium distribution and that the rotational temperature may be determined from slope. The (0,0) intercept in Fig. 1 is a further indication (see Eq. 8, Part II) of the rotational equilibrium distribution. Corresponding plots for 2:1 and 4:1 hydrogen-oxygen flames gave concordant results in indicating rotational equilibrium and thus permitted the determination of the corresponding rotational temperatures. These are listed in Table II.

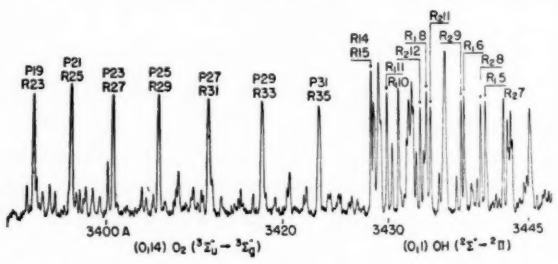

FIG. 2. Densitometer tracing of the spectrum of a 1:1 hydrogen-oxygen flame in the region between 3390A–3450A showing part of the (0,14) Schumann-Runge and (0,1) OH band.

Once the rotational temperatures had been determined, the plates were calibrated for intensity response in the overlap region of the (0,14) O_2 band and the (0,1) OH band by applying the method described in Sec. 5 of Part II to the R_1 and R_2 branches of the (0,1) band of OH. After the plates had been calibrated in the above manner, the intensity ratios of the $PR(31,35)$ "line" of O_2 and the $R_1(10)$ line of OH were determined for the various fuel ratios; since these two lines are only about 8A apart, it was not necessary to standardize the plate for wavelength response. The results of these experimental intensity ratio determinations are listed in Table II, which also gives the rotational temperatures of

$OH(^2\Sigma^+)$ and the theoretical equilibrium intensity ratios calculated from Eq. (15) using the data of Table I. The appearance of the spectrum (for a 1:1 fuel ratio) in the O_2 and OH overlap region in which the above measurements were made is shown in the densitometer tracing reproduced in Fig. 2.

V. DISCUSSION OF RESULTS

The agreement between the calculated equilibrium intensity ratios and the experimental intensity ratios (Table II) is quite good and would seem to indicate that thermal equilibrium conditions obtained in the flames. There certainly is no indication that either $OH(^2\Sigma^+)$ or $O_2(^3\Sigma_u^-)$ is in large excess of its thermal equilibrium concentration. The finding of rotational equilibrium for $OH(^2\Sigma^+)$ with a rotational temperature in good agreement with and following the trend of the calculated equilibrium flame temperature reinforces this conclusion as to the equilibrium conditions in the flame.

In a discussion of the possible thermal or chemiproduction of $O_2(^3\Sigma_u^-)$ in flames, Wolfhard and Gaydon[5] pointed out that owing to the high energy of excitation of $O_2(^3\Sigma_g^-)$ to the $^3\Sigma_u^-$ state (6.17 ev), appreciable amounts of $O_2(^3\Sigma_u^-)$ could be produced thermally only in very hot flames. However, an examination of Eqs. (11) and (12) shows that it is not at all necessary to have a high concentration of O_2 in the excited $(^3\Sigma_u^-)$ state in order to have strong Schumann-Runge bands. A rough calculation indicates that for thermal equilibrium at 3000°K the concentration ratio $OH(^2\Sigma^+)/O_2(^3\Sigma_u^-)$ is about 3.5×10^3. The ratio of transition probabilities $A_{nm}(OH)/A_{nm}(O_2)$ is, however, about 4.0×10^{-4}, so that the intensity of the Schumann-Runge bands is about equal to that of the hydroxyl bands when the concentration of $O_2(^3\Sigma^-{}_u)$ is only about 10^{-3} that of the $OH(^2\Sigma^+)$. This points up the danger of drawing conclusions as to the relative concentrations of different excited species from spectroscopic data under the tacit assumption that the total transition probabilities are of about equal magnitude.[24]

As pointed out in Sec. I, the finding of thermal equilibrium in a flame precludes the drawing of any definite conclusions as to the mode of production of the now equilibrated species. In particular, the fact that certain experimental observations indicate a state of thermal equilibrium in the flame does not necessarily point to the thermal production of the radicals. The results of this investigation do not, however, rule out this possibility; and in view of the fact that this equilibrium distribution has been found to be present in such a wide range of fuel ratios, the author is inclined to the belief that $O_2(^3\Sigma_u^-)$ is produced thermally in the hydrogen-oxygen flame.

It will be of some interest to discuss briefly some possible processes leading to electronically excited O_2 in the hydrogen-oxygen flame. In discussing the production of $O_2(^3\Sigma_u^-)$ in the CO—O_2 flame, Laidler[25] suggested, in order to account for some previous work on this flame by other investigators, the specific energy transfer process

$$CO_2^*(^3\Pi_g)+O_2(^3\Sigma_g^-)\rightarrow CO_2(^1\Sigma_g^+)+O_2^*(^3\Sigma_u^-), \quad (16)$$

which was to produce $O_2(^3\Sigma_u^-)$ in a non-equilibrium distribution. Aside from the question as to whether the chemiluminescence of the CO—O_2 flame is due to $O_2(^3\Sigma_u^-)$ or to $CO_2^*(^3\Pi_g$ or $^1\Pi_g)$, the above reaction is a plausible one on the basis that the radiative lifetime of $CO_2^*(^3\Pi_g$ or $^1\Pi_g)$ is sufficiently long for the transfer of electronic energy to $O_2(^3\Sigma_g^-)$ to be quite effective.[3] An analogous process (proceeding via a nonlinear intermediate complex)[3] in the hydrogen-oxygen flame would be

$$OH^*(^2\Sigma^+)+O_2(^3\Sigma_g^-)\rightarrow OH(^2\Pi)+O_2^*(^3\Sigma_u^-). \quad (17)$$

While some of the $O_2(^3\Sigma_u^-)$ is probably produced by this energy transfer reaction, it is very doubtful that (17) is as efficient as (16), since the radiative life time of $OH(^2\Sigma^+)$ is probably considerably shorter than that of $CO_2(^3\Pi_g, {}^1\Pi_g)$. Another reaction which may be considered to account for a possible chemi-production of $O_2(^3\Sigma_u^-)$ is

$$O(^3P)+O(^1D)+M\rightarrow O_2(^3\Sigma_u^-)+M, \quad (18)$$

which has been discussed in some detail elsewhere.[3] Reaction (18) requires a third body to produce $O_2(^3\Sigma_u^-)$ in the quantized vibrational levels which give rise to the discrete Schumann-Runge bands. There are also several bimolecular processes which may produce $O_2(^3\Sigma_u^-)$ as a stable molecule. A plausible example of this is the reaction

$$O(^3P)+OH(^2\Sigma^+)\rightarrow O_2(^3\Sigma_u^-)+H(^2S), \quad (19)$$

which is allowed by the spin correlation rules and which is endothermic by only 1.4 ev. At a temperature of about 3000°K reaction (19) might thus take place quite efficiently. Which one, if any, of these reactions plays an important role in the production of $O_2(^3\Sigma_u^-)$ in the hydrogen-oxygen flame can be decided only after further experimental and theoretical work. Such an investigation, involving the study of various flames with a number of different fuel ratios, is now being undertaken in collaboration with Dr. H. Broida of the National Bureau of Standards.

VI. ACKNOWLEDGMENTS

The author wishes to express his appreciation to the Applied Physics Laboratory of the Johns Hopkins Uni-

[24] In the case of $O_2(^3\Sigma_u^-\rightarrow{}^3\Sigma_g^-)$ and $OH(^2\Sigma^+\rightarrow{}^2\Pi)$ the difference in the values of A_{nm} is occasioned principally by the different values of the electronic matrix moments [Eqs. (4) and (5)]. This difference arises from the fact that in the O_2 transition an electron goes from a nonbonding π_g-orbital to a corresponding π_u-orbital which is a strongly allowed transition (charge transfer spectra), while in the case of OH the electron goes from a π to a noncorresponding σ-orbital, which is a much weaker transition (references 9 and 14).

[25] K. J. Laidler, J. Chem. Phys. **17**, 221 (1949).

versity for the award of a Research Fellowship during the tenure of which this investigation was conducted. He is particularly indebted to Dr. F. T. McClure of this laboratory for several helpful discussions in regard to this work. Thanks are also due Mr. George A. Hornbeck for advice and assistance in connection with some of the experimental work and to Miss M. E. Pillow of the Department of Physics, The Northern Polytechnic, London for her kind cooperation in communicating to me some of her calculations on O_2.

THE JOURNAL OF CHEMICAL PHYSICS VOLUME 19, NUMBER 7 JULY, 1951

Dissociation Energies of the Cd^{++} Vacancy Complex and of the Double Vacancy in Sodium Chloride

JOHN R. REITZ AND J. L. GAMMEL
*University of California, Los Alamos Scientific Laboratory, Los Alamos, New Mexico**

Dissociation energies for two types of lattice imperfection (namely, the impurity ion vacancy complex and the double vacancy) have been determined theoretically for NaCl, using the semiclassical model of ionic crystals developed by Born and Mayer. The procedure followed in calculating these energies was based on the method developed by Mott and Littleton for computing the formation energies of single vacancies. The numerical results which were obtained are 0.44 ev and 0.89 ev for the dissociation energies of the complex and double vacancy, respectively.

INTRODUCTION

THE theoretical work of Schottky[1] and Jost,[2] later refined by Mott and Littleton,[3] has shown that only the migration of lattice vacancies is important in explaining the ionic conductivity of alkali halide crystals. Furthermore, it is known experimentally[4,5] that below 400°C in KCl practically all of the current is transported by positive ions, and this result is believed valid also for NaCl.

Seitz[5] has suggested that because of the coulomb attraction between them, positive and negative ion vacancies will tend to combine into neutral pairs (double vacancies) or perhaps into even larger aggregates. In a similar fashion, divalent impurity atoms in an alkali halide lattice will tend to combine with positive ion vacancies to form neutral complexes. The complexes and double vacancies (shown in Fig. 1) are electrically neutral; however, the mere fact that they exist is of great importance in interpreting conductivity and diffusion data. In fact, it may be that the migration of paired vacancies is the predominant diffusion process in alkali halides at low temperatures; the low activation energy for diffusion of the pairs calculated by Dienes[6] seems to bear out this conclusion. Certainly, a determination of the dissociation energy of the pair is desirable in view of its importance in ionic conduction. Furthermore, it should be mentioned that knowledge of the dissociation energy, not only of pairs, but of larger aggregates as well, would be of interest for a quantitative treatment of the formation of dislocations by condensation of vacancies.[7]

Recently, Etzel and Maurer[8] have measured the electrical conductivity of sodium chloride in which the number of positive ion vacancies was artificially increased by the addition of cadmium impurity. From the dependence of conductivity on impurity content, they were able to determine, among other things, the equilibrium constant for the reaction between positive ion vacancies and cadmium impurity ions to form complexes. The variation of this equilibrium constant with temperature enabled them to deduce the heat of formation (dissociation energy) of the complex, which they found to be of the order of 0.3 ev.

The purpose of the present paper is to calculate theoretically the dissociation energies of both the Cd^{++} positive ion vacancy complex and the double vacancy in NaCl. The procedure followed is to calculate the work done in removing a sodium ion from the (110) lattice site to a point infinitely far from the crystal, assuming

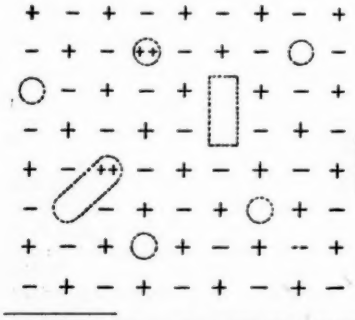

FIG. 1. Schematic representation of vacancies, divalent impurity ions, and complexes in an NaCl crystal.

* Work done under the auspices of the AEC.

[1] W. Schottky, Z. physik. Chem. **B29**, 335 (1935).

[2] W. Jost, *Diffusion and Chemische Reaktion in festen Stoffen* (Theodor Steinkopf Verlag, Dresden, 1937).

[3] N. F. Mott and M. J. Littleton, Trans. Faraday Soc. **34**, 485 (1938).

[4] C. Tubandt, *Handbuch der Experimentalphysik* Vol. XII, I. Teil (Akademische Verlagsgesellschaft M.B. H., Leipzig, 1932).

[5] F. Seitz, Revs. Modern Phys. **18**, 384 (1946).

[6] G. J. Dienes, J. Chem. Phys. **16**, 620 (1948).

[7] F. Seitz, Phys. Rev. **79**, 890 (1950).

[8] H. W. Etzel and R. J. Maurer, J. Chem. Phys. **18**, 1003 (1950).

the cadmium impurity ion at (000). This result subtracted from the work done in producing a single positive ion vacancy at some distant point in the lattice is the dissociation energy, or heat of formation, of the Cd^{++} vacancy complex. (The work to produce single vacancies in NaCl has been previously calculated by Mott and Littleton.[3]) Similarly, for the double vacancy case, the work to remove a sodium ion from the (100) position, assuming a negative ion vacancy at (000), is to be calculated. The dissociation energy may then be computed as above.

INTERACTION ENERGIES IN A SODIUM CHLORIDE LATTICE

An ion at a lattice point in an undistorted lattice experiences two types of interactions, a coulomb (the Madelung) term and a repulsive (or overlap) term. The Madelung energy, which arises from the coulomb interaction with all other ions in the lattice, can be written as $-\alpha_M(e^2/r_0)$, where α_M is the Madelung constant, and r_0 is the anion-cation distance. For the sodium chloride lattice, α_M has the value 1.7476. For small displacements of the ion from the lattice point in an otherwise undistorted lattice, the coulomb energy varies quite slowly; up to about $0.1r_0$ displacement, one can approximate the coulomb term by the Madelung energy without significant error. To obtain coulombic potentials at other points in the crystal, one must use the technique developed by Ewald.[9]

Following Born and Mayer,[10,11] the function

$$\phi(r)=c_{12}b\exp[(r_1+r_2-r)/\rho] \qquad (1)$$

has been used in the present study for the repulsive interaction between two ions. Here r_1 and r_2 are ionic radii. For sodium chloride the following constants were used:

$$\begin{aligned} c_{++}&=1.25, & r_0&=2.815\text{A},\\ c_{--}&=0.75, & r_+&=0.98\text{A},\\ c_{+-}&=1.00, & r_-&=1.81\text{A},\\ c_{Cd-}&=1.125, & r_{Cd}&=1.03\text{A},\\ \rho&=0.345\text{A}, & b&=0.229\times10^{-12}\text{ erg}. \end{aligned}$$

The + and − refer to the sodium and chloride ions, respectively. In calculating repulsive energies nearest and next-nearest neighbors were taken into account; third-nearest neighbor interactions can be shown to be negligible. For the case of a chloride ion at a lattice site, the twelve next-nearest neighbors (−−interaction) contribute almost half of the repulsive energy, almost as much as the nearest neighbors contribute. For the sodium ion, the next-nearest neighbors (++interaction) contribute only one percent of the nearest neighbor interaction.

[9] Ewald potentials needed for the present study were computed from Eq. (6) of reference 6.

[10] M. Born and J. E. Mayer, Z. Physik **75**, 1 (1932).

[11] F. Seitz, *Modern Theory of Solids* (McGraw-Hill Book Company, Inc., New York, 1940).

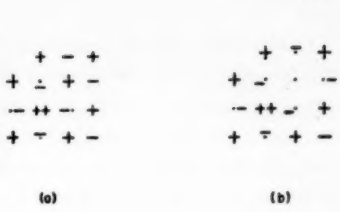

FIG. 2. Change in lattice distortion as the (110) ion is removed from the vicinity of a Cd impurity ion to form a complex. The dots represent points in the rigid lattice.

When one or more ions are missing from the lattice, not only are their coulomb and repulsive interactions with other ions lost, but there is a resultant polarization of the lattice. The ionic polarizabilities which were used are those given by Pauling,[12] and are $\alpha_-=3.66\times10^{-24}$ cm^3, $\alpha_+=0.179\times10^{-24}$ cm^3, $\alpha_{Cd}=1.05\times10^{-24}$ cm^3. The dielectric constant for NaCl for static fields[3] is $\kappa=5.62$.

CALCULATION OF THE DISSOCIATION ENERGY OF A Cd^{++}-VACANCY COMPLEX

As the sodium ion is removed from the (110) position, both the lattice distortion and polarization of neighboring ions is changed; these changes reflect a change in the potential at (110). Initially, the lattice distortion is just that due to the cadmium impurity ion; finally, it is that due to the complex (see Fig. 2).

1. Equilibrium Distortion around a Cadmium Impurity Ion

Finding the equilibrium distortion around a cadmium divalent impurity ion (Fig. 2(a)) is exactly the problem of Mott and Littleton[3] in finding the distortion around single vacancies, except that here the displacement of nearest neighbors is inward instead of outward. The problem is complicated by the long-range polarization produced in the lattice.

Mott and Littleton found for the case of an extra positive charge at (000) that the dipoles induced at distant positive and negative lattice sites are, respectively,

$$M_1'r_0^3e/r^2, \quad M_2'r_0^3e/r^2, \qquad (2)$$

where

$$M_1'=\frac{1}{4\pi}\left(1-\frac{1}{\kappa}\right)\frac{\alpha+\alpha_1}{\frac{1}{2}(\alpha_1+\alpha_2)+\alpha}, \qquad (3)$$

and a similar expression is used for M_2'. Here α_1 and α_2 stand for the α_+ and α_-, respectively, defined above, and $\alpha=e^2/p$ is a quantity which determines the displacement polarization of the medium. The p is defined as follows: $-px$ is the restoring force, due to overlap forces, on any ion in a uniformly polarized medium where each ion is displaced a distance $\pm x$.[13] For sodium chloride the quantity α has the value $4.21_5\times10^{-24}$ cm^3.

The displacement x of the ions is

$$x=M'r_0^3/r^2, \qquad (4)$$

where

$$M'=\frac{1}{4\pi}\left(1-\frac{1}{\kappa}\right)\frac{\alpha}{\frac{1}{2}(\alpha_1+\alpha_2)+\alpha}. \qquad (5)$$

[12] L. Pauling, Proc. Roy. Soc. (London) **A114**, 181 (1927).

[13] See reference 3 for further details about the quantities p and $\alpha\equiv r_0^3\beta$.

In the first-order approximation, the dipole μ and the displacement x of the nearest neighbors to the cadmium impurity ion are taken as unknowns; those of the more distant ions are computed from Eqs. (2) and (4). To simplify the algebra the displacement, which is inward, is written $x=\xi r_0$, and $\mu=mer_0$. The repulsive force on one of the (100) ions *inward* can readily be shown to be

$$\begin{aligned}F_r=&-B\exp[-(1-\xi)r_0/\rho]\\&+4Ad^{-1}(\xi+M'/2\sqrt{2})\exp[-dr_0/\rho]\\&+A\exp[-(1+\xi+M'/4)r_0/\rho]\\&-2\sqrt{2}C\exp[-\sqrt{2}(1-\xi)r_0/\rho]\\&+4C\eta^{-1}(1+\xi-2M'/5\cdot5^{\frac{1}{2}})\exp[-\eta r_0/\rho]\\&+4C\lambda^{-1}(\xi-M'/3\sqrt{3})\exp[-\lambda r_0/\rho],\end{aligned}\quad(6)$$

where

$$\begin{aligned}B&=1.125b\rho^{-1}\exp[(r_-+r_{Cd})/\rho],\\A&=b\rho^{-1}\exp[(r_++r_-)/\rho],\\C&=0.75b\rho^{-1}\exp[2r_-/\rho],\end{aligned}$$

and

$$\begin{aligned}d^2&=(1+M'/2\sqrt{2})^2+(\xi+M'/2\sqrt{2})^2,\\\eta^2&=(1+\xi-2M'/5\cdot5^{\frac{1}{2}})^2+(1-M'/55^{\frac{1}{2}})^2,\\\lambda^2&=2(1-M'/3\sqrt{3})^2+(\xi-M'/3\sqrt{3})^2.\end{aligned}$$

The electrostatic force on one of the (100) ions inward is

$$F_e=\frac{e^2}{r_0^2}\left[\frac{1-\sqrt{2}-0.25}{(1-\xi)^2}+\frac{4(1-\xi)}{(2-2\xi+\xi^2)^{\frac{1}{2}}}+\frac{1}{(2-\xi)^2}-\frac{2.3713m}{(1-\xi)^3}-1.965M_1'-0.388M_2'\right].\quad(7)$$

The equations determining m and ξ are

$$\left.\begin{aligned}F_r+F_e&=0,\\me^2r_0/\alpha_2&=F_e.\end{aligned}\right\}\quad(8)$$

This system of equations has been solved by trial and error procedure, and the results are as follows:

$$\begin{aligned}\xi&=0.068_4,\\m&=0.092_8.\end{aligned}$$

The displacement $x=\xi r_0$ is inward, and the induced dipole $\mu=mer_0$ is along the direction of the field, radially outward.

We are now in a position to compute the initial potential at the (110) lattice point, i.e., at the sodium atom which we wish to remove. The electrostatic potential can be written as follows:

$$V_1=V_1^{\text{R.L.}}+\frac{e}{r_0}\left[2\left(1-\frac{1}{(1+\xi^2)^{\frac{1}{2}}}+\frac{1}{\sqrt{3}}-\frac{1}{[2+(1-\xi)^2]^{\frac{1}{2}}}+\frac{1}{5^{\frac{1}{2}}}-\frac{1}{[1+(2-\xi)^2]^{\frac{1}{2}}}\right)-0.7428m-4.15_2M_1'-4.29_3M_2'\right]\quad(9)$$

where $V_1^{\text{R.L.}}$ is the potential which would exist in a rigid lattice without polarization effects; namely,

$$V_1^{\text{R.L.}}=-(e/r_0)[\alpha_M-1/(\sqrt{2}+M'/2)]=-1.0504(e/r_0).$$

The term in parentheses in Eq. (9) is due to the displacement of the six (100) ions from their rigid positions, and the last three terms represent the potential due to the induced polarization. Of these polarization terms, the one in m is obvious, being due to the induced dipoles on the (100) ions; the other two were computed from

$$V=-er_0^3\left[M_1'\sum_1\frac{\cos(\widehat{r_1r_2})}{r_1^2r_2^2}+M_2'\sum_2\frac{\cos(\widehat{r_1r_2})}{r_1^2r_2^2}\right].\quad(10)$$

Here r_1 denotes the distance from the lattice point in question to (000), r_2 the distance from the lattice point to (110), and the summations are over lattice points of types 1 and 2. Equation (10) is rather slowly converging; however, it was found that the individual terms approach and essentially equal the terms in the Jones and Ingham series,[14] namely,

$$M_1'\sum_1\frac{1}{r^4}+M_2'\sum_2\frac{1}{r^4},\quad(11)$$

for distances greater than $4r_0$. The value of this latter summation is known. Thus, the terms in Eq. (10) were only computed for lattice points within the sphere $r_1=4r_0$, and the remainder of the series was obtained from Eq. (11).

The repulsive energy of the (110) ion initially is

$$\Phi_1=2b\exp[(r_++r_-)/\rho]\{\exp[-(1-M'/2\sqrt{2})r_0/\rho]+\exp[-dr_0/\rho]+\exp[-r_0/\rho]\},\quad(12)$$

since the next-nearest neighbors give a negligible contribution for sodium.

Equations (9) and (12) give the initial potentials at (110). As the sodium ion is removed, the potential changes because of the changing lattice distortion and polarization. The next step, then, is to compute the (110) potential for the final configuration.

2. Equilibrium Distortion around a Cd^{++} Vacancy Complex

Finding the distortion around a complex (Fig. 2(b)) is really a difficult problem. Because of the low symmetry, there are five different displacements for the ten nearest neighbors.

In the present study a more symmetrical distortion was assumed. It was assumed that the resultant displacement of nearest neighbors was the vector sum of an inward displacement, x_1, of the six cadmium neighbors, and an outward displacement, x_2, of the six neighbors of the positive ion vacancy. As a first approximation, one could use for x_1 and x_2, the values computed in the

[14] See reference 3, p. 491.

last section and those by Mott and Littleton, respectively, for the single types of distortion. One can do better than this, however. Since for the case of the complex, the long-range polarization is essentially absent, one can again solve Eqs. (8), this time leaving out the long-range polarization terms in F_e, and obtain a value for x_1. Similarly, one can solve Mott and Littleton's equations without the terms in M_1' and M_2' and obtain an x_2. This procedure was followed here, and the displacements which were obtained are

$$x_1=0.073r_0,$$
$$x_2=0.074r_0.$$

Using these displacements, one can now compute the potential at the (110) lattice point for the final lattice configuration. Again we write the electrostatic potential as a sum

$$V_2=V_2^{\text{R.L.}}+V_2^{\text{dis}}+V_2^{\text{pol}}, \tag{13}$$

where

$$V_2^{\text{R.L.}}=-(e/r_0)[\alpha_M-1/(\sqrt{2}+M'/2)],$$

V_2^{dis} is the change in potential due to the displacement of the nearest neighbor ions, and V_2^{pol} is the potential at (110) produced by the induced polarization. Here V_2^{pol} is computed as follows: first, the polarizing field, E, can be thought of as produced by a positive charge at (000), a negative charge at (110), and displacement dipoles at each of the nearest neighbor lattice points. Then, the induced dipole at a lattice point is $\mu_i=\alpha_i E$, and V_2^{pol} can be computed from

$$V_2^{\text{pol}}=e\sum_i(\mu_i\cos\theta_i)/r_i^2, \tag{14}$$

where r_i is the distance from (110) to ion i, and θ_i is the angle between the direction of μ_i and that of r_i. In the calculation of Eq. (14), the summation was over the Cd^{++}, the ten nearest neighbors of the complex, and second- and third-nearest neighbors of (110); for ions at more distant lattice points, the contribution was negligible.

Several other effects which could influence the value of V_2 were examined. First, the second-nearest neighbors and more distant ions do not remain in their rigid lattice positions, but actually undergo slight displacements. Second, the dipole-dipole interaction of the induced dipoles and the variation of Madelung potential in the vicinity of a lattice point can affect the value of μ_i, and hence V_2^{pol}. These terms were found to be small and essentially to cancel one another out.

The repulsive energy of the (110) ion for the final lattice distortion is

$$\Phi_2=2b\exp[(r_+-r_-)/\rho]\times\{\exp[-r_0(1+\xi_2-M'/2\sqrt{2})/\rho]+\exp[-d_2r_0/\rho]+\exp[-r_0(1+\xi_2)/\rho]\}, \tag{15}$$

where

$$r_0\xi_2=x_2,\quad r_0\xi_1=x_1,$$

and

$$d_2^2=(1+\xi_2+M'/2\sqrt{2})^2+(\xi_1+M'/2\sqrt{2})^2.$$

TABLE I. Work done in removing a sodium ion from (110) position surrounding a Cd^{++} impurity to a point infinitely far from the crystal. (Result is one-half the sum of columns 1 and 2.)

	1	2
Electrostatic:		
$V^{\text{R.L.}}$	5.320 ev	5.320 ev
Displacement	0.225	−1.835
Polarization	3.16$_4$	−2.35$_4$
Repulsive:	−0.796	−0.435
	Total	4.30$_5$ ev

3. Dissociation Energy of the Complex

The work to remove a sodium ion from the (110) position surrounding the Cd^{++}, and thus the work to form a Cd^{++} ion vacancy complex, can now be computed. That part which is done against electrostatic forces is

$$-(e/2)(V_1+V_2). \tag{16}$$

Similarly, the work done against repulsive forces (a negative contribution) is

$$-(\Phi_1+\Phi_2)/2. \tag{17}$$

Substituting the values of the preceding sections into Eqs. (16) and (17), we obtain the value 4.30$_5$ ev for the total work to remove the sodium ion. A breakdown of the work is shown in Table I.

Thus far we have obtained the work needed to remove the (110) ion to a point infinitely far from the crystal. Actually, the removed sodium ion will be deposited at some distant vacant lattice site in the crystal, and a certain amount of work will be regained. If this latter work is greater than the 4.31 ev calculated above, then the complex is stable.

Mott and Littleton[3] have calculated the work needed to form a single positive ion vacancy (equivalently, the work obtained in destroying the vacancy) and have obtained the value 4.62 ev. We cannot use this value directly, however, since Mott and Littleton used a slightly different repulsive potential from the one used by us. They considered only nearest-neighbor interactions in the repulsive energy, and, consequently, had to use a somewhat larger value of b in order to insure that the crystal was in equilibrium under the combined electrostatic and repulsive forces. Using the value of b quoted in an earlier section and taking into account second-nearest neighbors, we obtain 4.75 ev for this quantity. The dissociation energy of the complex, then, is (4.75−4.31) ev equal to 0.44 ev.

This result is in fair agreement with the heat of formation of the complex which Etzel and Maurer[8] found to be of the order of 0.3 volt. It might be well to examine our theoretical calculation and see how far we can trust the 0.44 volt figure. The repulsive energies should be fairly reliable for the rather small distortions involved in the present study. The weak point in our calculation, as mentioned above, is the equilibrium

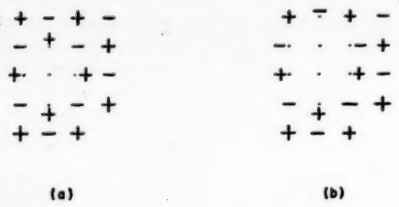

FIG. 3. Change in lattice distortion as the (100) ion is removed from the vicinity of a negative ion vacancy to form a double vacancy.

distortion around the complex. Therefore, several other displacements were chosen for x_1 and x_2 and the calculation repeated. It was found that the final result for the dissociation energy was not affected appreciably. (For example, the choice of $x_1=0.08r_0$ and $x_2=0.071r_0$ gave a final result of 0.41 ev.) Thus, we believe our calculation to be accurate to ± 0.1 ev.

DISSOCIATION ENERGY OF A DOUBLE VACANCY

In calculating the dissociation energy of a double vacancy, the procedure is essentially the same. In this case the work to remove a sodium ion from the (100) position surrounding a negative ion vacancy is computed. The initial and final distortions of the lattice are shown in Fig. 3.

The equilibrium distortion around a single negative ion vacancy has been computed by Mott and Littleton to be $\xi_i=(x_i/r_0)=0.078$. Using these distortions, we write

$$V_1=V_1^{\text{R.L.}}+V_1^{\text{dis}}+V_1^{\text{pol}}, \tag{18}$$

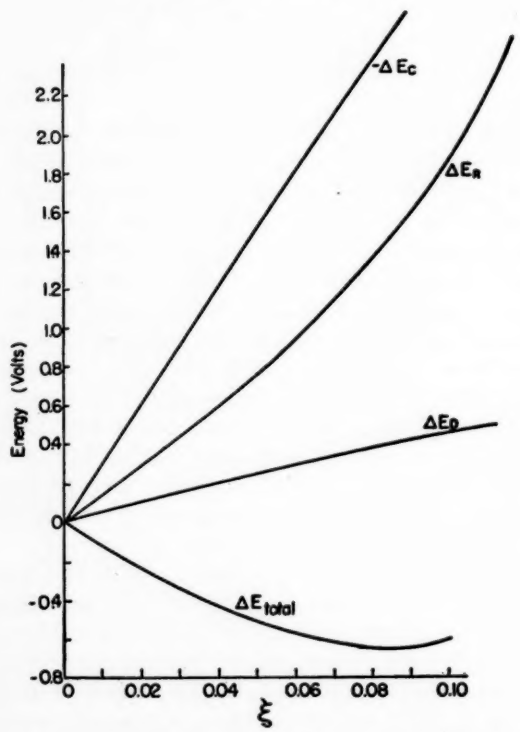

FIG. 4. Energy changes as a function of ion displacement for ions surrounding a pair of vacancies (NaCl).

where

$$V_1^{\text{R.L.}}=-(e/r_0)[1.7476-1/(1+\xi_i)],$$

V_1^{dis} is the change in potential due to the displacement of nearest neighbor ions, and

$$V_1^{\text{pol}}=-(e/r_0)[4.15_4M_1'+5.74_1M_2'+1.6642m/(1+\xi_i)^2]$$

is the potential due to the induced polarization. Here again the terms in M_1' and M_2' were obtained from a formula of type (10), in which r_1 denotes the distance from the lattice point in question to (000), and r_2 the distance from the lattice point to (100).

The repulsive energy of the sodium atom in the initial configuration is

$$\Phi_1=b\exp[(r_+-r_-)/\rho]\{4\exp[-\delta r_0/\rho]+\exp[-(1-\xi_i)r_0/\rho]\}, \tag{19}$$

where

$$\delta^2=(1-M'/2\sqrt{2})^2+(\xi_i+M'/2\sqrt{2})^2.$$

In finding the distortion around the double vacancy (Fig. 3(b)), it was assumed that each of the ten nearest neighbors was displaced outward by the same amount. Then, using the procedure followed by Dienes,[6] the change in lattice energy was plotted as a function of ion displacement (see Fig. 4). The minimum occurred at $\xi_f=(x_f/r_0)=0.083$. Using this displacement, the values, V_2 and Φ_2, for the final lattice configuration were computed. These quantities were computed in a similar fashion to that used for the "complex" case described in the preceding section.

TABLE II. Work done in removing a sodium ion from (100) position with respect to a negative ion vacancy to a point infinitely far from the crystal. (Result is one-half the sum of columns 1 and 2.)

	1	2
Electrostatic:		
$V^{\text{R.L.}}$	4.153 ev	4.153 ev
Displacement	0.574	−1.376
Polarization	3.45_7	-2.00_8
Repulsive:	−0.835	−0.392
	Total	3.86_3 ev

The work to remove the sodium ion can again be written

$$W=-(e/2)[V_1+V_2]-(\tfrac{1}{2})[\Phi_1+\Phi_2], \tag{20}$$

and was found to have the value 3.86_3 ev. (See Table II.) The work regained by destroying a positive ion vacancy somewhere in the crystal is, as before, 4.75 ev. Thus, the dissociation energy of the double vacancy is (4.75−3.86) ev, i.e., 0.89 ev.

CALCULATION OF POSSIBLE ACTIVATION ENERGY FOR THE DISSOCIATION OF THE DOUBLE VACANCY

It is also of interest to determine whether there is an activation energy for the first step in the dissociation of

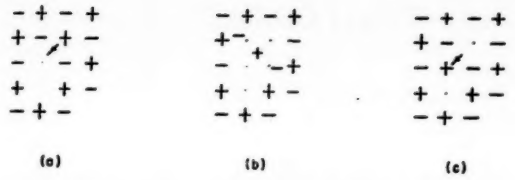

FIG. 5. The first step in dissociation of a double vacancy.

a double vacancy, namely, for the jump of a sodium ion from the (110) position to the (000) position, assuming the double vacancy at (000) and (−100). (Note the change in origin from the preceding section.) This jump is depicted in sequence in Fig. 5.

Now the saddle point, if it exists, is essentially restricted by electrostatic forces to the plane of Fig. 5. Further, the saddle point will be close to $(\frac{1}{2}\frac{1}{2}0)$, as shown in Fig. 5(b). The configuration energy was computed *in rigid lattice approximation* for the moving sodium ion at several points in the neighborhood of $(\frac{1}{2}\frac{1}{2}0)$, and the differences between these energies and that of the original configuration (Fig. 5(a)) were obtained. Indeed, the saddle point was found to be exceedingly close to $(\frac{1}{2}\frac{1}{2}0)$.

As the ion moves from state (a) to state (b) (Fig. 5), the distortion of the lattice will change. The principal change is the outward motion of the two negative ions at (100) and (010). Assuming these ions move outward by the same amount and neglecting other distortions, it is found that lattice energy is a minimum for state (b) when the two negative ions move outward a distance $x=0.1r_0$.

The difference in configuration energy of state (b), distorted, and state (a) has been calculated to be 0.22 ev. Thus it appears that there is no activation energy, but a continuous increase in energy in going from (a) to (c). It should be mentioned that activation energies cannot be calculated very accurately in terms of our simple theory, because this computation involves a knowledge of the repulsive energy at distances of the order of $0.7r_0$, where the Born-Mayer formula, Eq. (1), is not expected to be accurate.

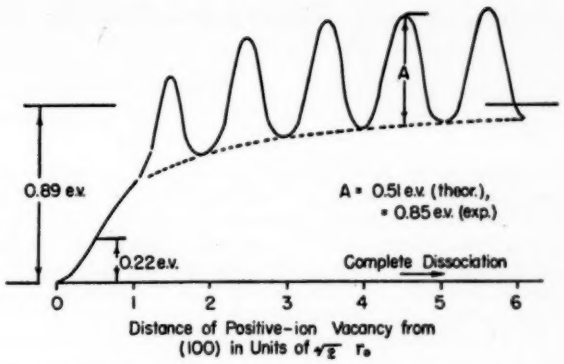

FIG. 6. Energy profile for dissociation of a double vacancy along a (110) line.

An energy profile for dissociation of the double vacancy along a (110) line is presented in Fig. 6. The dotted line, which is the approximate envelope of the energy minima, is computed from $-e^2/\kappa r$, where r is the distance between the positive and negative ion vacancies. This formula gives, of course, the energy of two "charges" (e and $-e$) in a dielectric κ. At very large separation, the two vacancies are essentially free, and the activation peaks, shown in Fig. 6, are for diffusion of the single positive ion vacancy. The theoretical value of this activation energy for diffusion is 0.51 ev (Mott and Littleton); the experimental value (see Etzel and Maurer[8]) is 0.85 ev.

ACKNOWLEDGMENT

The authors would like to express their thanks to Professor F. Seitz for many stimulating discussions and for his continued interest in the problem.

THE JOURNAL OF CHEMICAL PHYSICS VOLUME 19, NUMBER 7 JULY, 1951

Overlap and Bonding Power of 2s,2p-Hybrid Orbitals*

ROBERT S. MULLIKEN
Department of Physics, University of Chicago, Chicago, Illinois
(Received March 20, 1951)

A classification and nomenclature for $2s-2p$ hybrid *AO*'s (atomic orbitals) of any degree of hybridization is proposed, and the concepts of cohybrids, antihybrids, and orthohybrids are defined. Overlap integrals S as follows are computed and tabulated as a function of the hybridization coefficient and the interatomic-distance parameter for the case of two like first-row atoms: $S(h_\beta, h_\beta; \rho)$, $S(h_\beta, h_{o\beta}; \rho)$, and $S(1s, h_\beta; \rho)$. (See also Figs. 1 and 2.) Here h_β denotes any $2s-2p$ hybrid, and $h_{o\beta}$ the corresponding orthohybrid. Slater *AO*'s were used, and also, for selected ρ values for the case of C−C bonds, *SCF AO*'s.

In connection with this work, and extending fragmentary tables given in a previous paper, complete tables from $\rho=3$ to $\rho=14$, for the case of two like atoms, are given for the overlap integrals $S(1s, 2s)$, $S(2s, 2s)$, $S(1s, 2p\sigma)$, $S(2s, 2p\sigma)$, $S(2p\sigma, 2p\sigma)$, and $S(2p\pi, 2p\pi)$ using orthogonalized Slater $2s$ *AO*'s, and *carbon SCF* $2p\sigma$ and $2p\pi$ *AO*'s.

Tables of Slater-*AO* overlap integrals $S(1s, h_\beta)$ are given as a function of β for the radicals FH, OH, NH, and CH at their equilibrium distances, also similar tables based on *SCF AO*'s for the case of C−H bonds of lengths 1.12, 1.09, and 1.06A. (See also Fig. 3.)

The various tables and figures show that "a little hybridization goes a long way"; that is to say, a small amount of s character in a $p\sigma$ *AO*, or of $p\sigma$ character in an s *AO*, causes a large change in S. Applications of this fact to problems of chemical binding are briefly suggested. These will be developed in a following paper. (Also see *Note added in proof* at end of this paper.)

I. INTRODUCTION

WHEN a first-row atom forms one or more bonds, one usually describes these in terms of σ and π bond orbitals. Depending on the number and geometrical arrangement of the bonds, one or another set of mutually orthogonal *AO*'s is used. The most frequently used orthogonal sets are:

$$\left.\begin{array}{l}\text{For } 90° \text{ bond angles: } s,\ \sigma,\ \sigma',\ \sigma''.\\ \text{For tetrahedral bond angles: } te,\ te',\ te'',\ te'''.\\ \text{For } 120° \text{ (trigonal) bond angles: } tr,\ tr',\ tr'',\ \sigma.\\ \text{For } 180° \text{ (digonal) bond angles: } s,\ \sigma,\ \pi,\ \pi' \text{ or}\\ \qquad\qquad di,\ di',\ \pi,\ \pi'.\end{array}\right\} \quad (1)$$

The brief *AO* symbols used in (1) and elsewhere below are explained in Table I. Symbols differing by the use of one or more primes in (1) denote mutually orthogonal and geometrically equivalent but differently oriented *AO*'s.[1]

The symbols *te*, *tr*, *di*, *te'*, etc., in (1) all belong to *a class of hybrid* σ *AO*'s which may be designated by the general symbol h_β and which are defined as follows:[1]

$$h_\beta \equiv \alpha\cdot s+\beta\cdot\sigma \equiv \cos\phi\cdot s+\sin\phi\cdot\sigma. \quad (2)$$

Here ϕ may be taken as ranging from 0 to $\pm\pi$, but ordinarily we shall use only the range 0 to $\pm\frac{1}{2}\pi$. This makes $0\leq\alpha\leq 1$ but $-1\leq\beta\leq+1$. The added range from $\pm\frac{1}{2}\pi$ to $\pm\pi$ gives no new hybrids, but merely a reversal of sign of the whole *AO*. In (2), β may be called the *hybridization coefficient*. Hybrids having α and β alike in sign will be called *positive hybrids*, those with α and β different in sign, *negative hybrids*.

Except in tetravalent cases, not all the *AO*'s of any one set in (1) are used as bond orbitals. Following are some examples of molecular electron configurations (omitting $1s$ electrons) written in terms of the *AO*'s of (1) using the valence-bond method,[2] for the ground states of several molecules:

$$\left.\begin{array}{l}\mathrm{Li_2}: s\cdot s\\ \mathrm{N_2}: s)^2s)^2p\sigma\cdot p\sigma)\pi\cdot\pi)\pi'\cdot\pi') \text{ or}^3\\ \qquad di\cdot di)di')^2di')^2\pi\cdot\pi)\pi'\cdot\pi')\\ \mathrm{C_2H_2}: di\cdot h)di'\cdot h')\pi\cdot\pi)\pi'\cdot\pi')\\ F_2: s)^2s)^2\sigma\cdot\sigma)\pi)^4\pi)^4\\ \mathrm{CH_4}: te\cdot h)te'\cdot h')te''\cdot h'')te'''\cdot h''')\\ \mathrm{H_2O}: s)^2\sigma\cdot h)\sigma'\cdot h')\sigma'')^2.\end{array}\right\} \quad (3)$$

Dots connect *AO*'s for electrons forming an electron-pair bond. Lone pairs appear as $s)^2$, $di)^2$, or the like. The symbol $\pi)^4$ is equivalent to $\pi)^2\pi')^2$. The symbols h, h', etc. refer to H atom $1s$ *AO*'s (do not confuse this use of h with h_β in Eq. (2)).

As is well known, the formulations (3) are not accurate descriptions, but represent arbitrary simplifications. In some cases, for example N_2, one may question

TABLE I. Brief *AO* notation for this paper.[a]

Brief symbol	Full symbol[b]	Brief symbol	Value of β in Eq. (2)
k	$1s$	te	$(3/4)^{\frac{1}{2}}$
s	$2s$	tr	$(2/3)^{\frac{1}{2}}$
$p\sigma$	$2p\sigma$	di	$(1/2)^{\frac{1}{2}}$
π	$2p\pi$	di'	$-(1/2)^{\frac{1}{2}}$

[a] The *AO*'s k, s, $p\sigma$, te, tr, di, *relative to their respective axes of symmetry*, are all σ *AO*'s.
[b] By $2p\sigma$ is meant a $2p_z$ *AO* taken with its positive end on the positive z axis, with the latter directed toward a bond-partner.

* This work was assisted by the ONR under Task order IX of Contract N6ori-20 with the University of Chicago.

[1] The notation used here differs in one or two respects from that of a previous paper (see reference 5). The present Eq. (2) appears as Eq. (9) in reference 5; *te'* and *tr'* are there used in a different way than here. Another change is the use here of the symbol ρ to denote the parameter formerly called p.

[2] See R. S. Mulliken, J. chim. phys. 46, 497 (1949), Sec. 1, for further discussion. Reprints of this article in mimeographed form in English are available in limited numbers.

[3] As first suggested by Pauling.

which of two formulations involving different assumed degrees of hybridization is the more nearly correct. On further consideration, it is evident that the possibilities of accurate description are greatly improved by using hybrid σ *AO*'s of the general form of Eq. (2) without restricting β to the special values represented by the types $p\sigma$, *te*, *tr*, *di*, and *s*. Further, one should in general use different σ hybrids for different σ *AO*'s in one and the same molecule. The best choice of hybrid *AO*'s for a ground-state electron configuration is of course that which minimizes the total energy. Similar remarks apply to hybrid *AO*'s in general, but only hybrids of $2s$ and $2p\sigma$ *AO*'s will be considered in this paper.

In a recent paper[4] it was pointed out that the *overlap integral S* between bond orbitals of two bonded atoms

TABLE II. Hybrids related to a given hybrid h_β.[a]

Hybrid	h_β a positive hybrid α	β	h_β a negative hybrid α	β	h_β general α	β
h_β	α	$+(1-\alpha^2)^{\frac{1}{2}}$	α	$-(1-\alpha^2)^{\frac{1}{2}}$	α	β
$h_{\alpha\beta}$	α	$-(1-\alpha^2)^{\frac{1}{2}}$	α	$+(1-\alpha^2)^{\frac{1}{2}}$	α	$-\beta$
$h_{c\beta}$	$(1-\alpha^2)^{\frac{1}{2}}$	$+\alpha$	$(1-\alpha^2)^{\frac{1}{2}}$	$-\alpha$	$\lvert\beta\rvert$	$\pm\alpha$
$h_{o\beta}$	$(1-\alpha^2)^{\frac{1}{2}}$	$-\alpha$	$(1-\alpha^2)^{\frac{1}{2}}$	$+\alpha$	$\lvert\beta\rvert$	$\mp\alpha$

[a] The specifications for α and β of $h_{c\beta}$ and $h_{o\beta}$ could have been simplified in the last columns if we had not imposed the requirement that the coefficient of the *s AO* in Eq. (2) shall always be ≥ 0 (see sentences immediately following Eq. (2)). Imposition of this requirement, while not essential and sometimes awkward, appears on the whole advisable because it helps to diminish confusion in the interpretation of positive and negative values of overlap integrals.

TABLE III. Some hybrids and their orthohybrids.

AO	Hybrids α	β	*AO*	Their orthohybrids α	β
s	1	0	$p\sigma$	0	-1
cte	$(3/4)^{\frac{1}{2}}$	$(1/4)^{\frac{1}{2}}$	*ate*	$(1/4)^{\frac{1}{2}}$	$-(3/4)^{\frac{1}{2}}$
ctr	$(2/3)^{\frac{1}{2}}$	$(1/3)^{\frac{1}{2}}$	*atr*	$(1/3)^{\frac{1}{2}}$	$-(2/3)^{\frac{1}{2}}$
di	$(1/2)^{\frac{1}{2}}$	$(1/2)^{\frac{1}{2}}$	*odi*	$(1/2)^{\frac{1}{2}}$	$-(1/2)^{\frac{1}{2}}$
tr	$(1/3)^{\frac{1}{2}}$	$(2/3)^{\frac{1}{2}}$	*otr*	$(2/3)^{\frac{1}{2}}$	$-(1/3)^{\frac{1}{2}}$
te	$(1/4)^{\frac{1}{2}}$	$(3/4)^{\frac{1}{2}}$	*ote*	$(3/4)^{\frac{1}{2}}$	$-(1/4)^{\frac{1}{2}}$
$p\sigma$	0	1	*s*	1	0

should be a useful measure of the bonding powers of electrons in these orbitals. It is a simple matter using available tables[5] to compute *S* for any pair of σ hybrid orbitals.[4a] One may then use these *S* values as at least a rough guide to the choice of hybrids which minimizes the total energy.

[4] R. S. Mulliken, J. Am. Chem. Soc. **72**, 4493 (1950). See also reference 4a.

[4a] While the present paper was in preparation, a valuable article appeared by A. Maccoll (Trans. Faraday Soc. **46**, 359 (1950)) on "The principle of maximum overlapping." This is similar in part to reference 4. It also contains discussion, and a figure showing *S* values for positive hybrids for C−C and C−H, which are similar to part of the present discussion and Figs. 1 and 3. Two other important papers have also recently appeared: W. Moffitt, Proc. Roy. Soc. (London) **202A**, 534, 548 (1950). The second of these discusses among other topics the effect of a little hybridization in stabilizing CH, NH, and OH.

[5] Mulliken, Rieke, Orloff, and Orloff, J. Chem. Phys. **17**, 1248 (1949).

TABLE IV. Brief notation for overlap integrals. (See reference 1.)

Brief notation	Full notation[a]
$S_k(\rho)$	$S(1s, 1s; \rho; t=0)$
$S_s(\rho)$	$S(2s, 2s; \rho; t=0)$
$S_\sigma(\rho)$	$S(2p\sigma, 2p\sigma; \rho; t=0)$
$S_{s\sigma}(\rho)$	$S(2s, 2p\sigma; \rho; t=0)$
$S_\beta(\rho)$ or $S_\beta(\beta, \rho)$	$S(h_\beta, h_\beta; \rho; t=0)$[b]
$S_{\beta,o\beta}(\rho)$ or $S_{\beta,o\beta}(\beta, \rho)$	$S(h_\beta, h_{o\beta}; \rho; t=0)$[c]
$S_{ks}(\rho, t)$; or $S_{ks}(\omega_A\rho, t_A)$	$S(1s, 2s; \rho; t)$; $S(1s, 2s; \omega_A\rho, t_A)$[d]
$S_{k\sigma}(\rho, t)$; or $S_{k\sigma}(\omega_A\rho, t_A)$	$S(1s, 2p\sigma; \rho; t)$; $S(1s, 2p\sigma; \omega_A\rho, t_A)$[d]
$S_{k\beta}(\rho, t)$; or $S_{k\beta}(\omega_A\rho, t_A)$	$S(1s, h_\beta; \rho; t)$[e]; $S(1s, h_\beta; \omega_A\rho, t_A)$[f]

[a] In general, $S(x, y; \rho; t)$ means $\int x_a y_b d\tau$, if x and y are any two *AO*'s of overlapping atoms a and b. The case $t=0$ occurs if x and y belong to like atoms and have equal Slater μ values. In general,

$$\mu_x = Z_x/n_x,$$

Z_x and n_x being the Slater effective charge and quantum number for the x *AO of the particular atom* involved. (See reference 5.) Further (except for the special definition of ρ in Eq. (8) for use with the *second* notation above for S_{ks}, $S_{k\sigma}$, $S_{k\beta}$),

$$\rho = \tfrac{1}{2}(\mu_x+\mu_y)R/a_H;\ t = (\mu_x-\mu_y)/(\mu_x+\mu_y).$$

[b] See Eq. (2).
[c] See Table II and Eqs. (6).
[d] See first line of Eqs. (12). The second line of Eqs. (12) applies only to the special case of *AH*.
[e] See Eq. (10).
[f] See Sec. V.

As a preliminary, it is desirable to set up some further terminology for σ hybrids. (1) *The amount of* $p\sigma$ (or *s*) *character* in any *s*, $p\sigma$ hybrid may be defined as

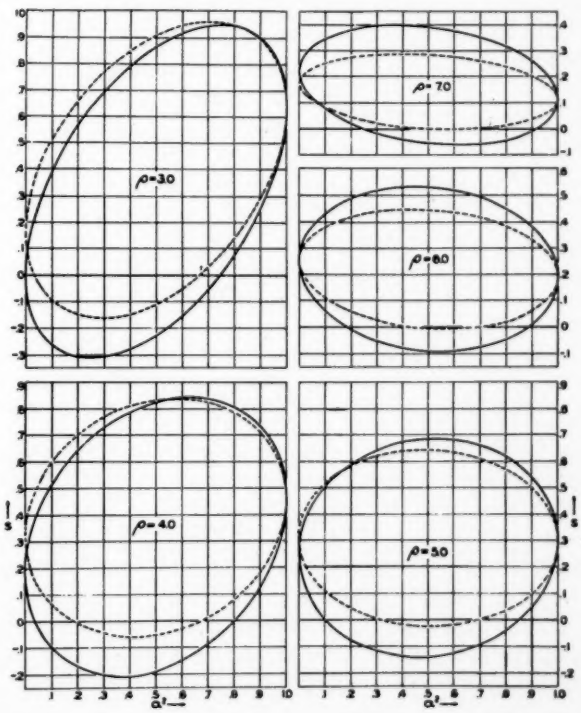

FIG. 1. Maps of overlap integrals $S_\beta(\rho)$ for $2s$, $2p$-hybrid *AO*'s in homopolar bonds, plotted against α^2. The dashed-line graphs are based on the Slater-*AO S* values of Tables VA, VB. The full-line graphs are based on *carbon SCF-AO S* values which differ only slightly from the *SCF* values of Tables VA, VB. (The slight difference is that the *S* values graphed here were computed using *SCF* $2p\sigma$ *AO*'s but *Slater* instead of orthogonalized-Slater $2s$ *AO*'s.) From the forms of Eq. (4) and the fact that $\alpha^2+\beta^2=1$, it can be shown that the curves in Fig. 1 are all ellipses.

TABLE VA. Overlap integrals $S_\beta(\beta, \rho)$ for $2s$, $2p$-hybrid AO's in homopolar bonds: negative hybrids.

ρ		$-2\alpha\beta=$ $\alpha=0$ $\beta=-1$	0.19900 $\alpha=0.1$ −0.99499	0.39192 $\alpha=0.2$ −0.97980	0.57236 $\alpha=0.3$ −0.95394	0.73322 $\alpha=0.4$ −0.91652	0.78460 0.43589 $\beta=-0.9$	0.86603 $\alpha=0.5$ −0.86603	0.96 $\alpha=0.6$ $\beta=-0.8$
		0.159	0.063	−0.021	−0.089	−0.137		−0.162	−0.157
3.0		0.159					−0.149		−0.157
	SCF	−0.001	−0.099	−0.181	−0.244	−0.284	−0.292	−0.297	−0.278
		0.208	0.112	0.027	−0.044	−0.097		−0.129	−0.133
3.2		0.208					−0.112		−0.133
		0.248	0.153	0.068	−0.005	−0.062		−0.100	−0.111
3.4		0.248					−0.078		−0.111
		0.279	0.187	0.102	0.028	−0.032		−0.074	−0.091
3.6		0.279					−0.049		−0.091
		0.303	0.212	0.129	0.055	−0.006		−0.051	−0.074
3.8		0.303					−0.025		−0.074
		0.319	0.232	0.150	0.077	0.015		−0.032	−0.058
4.0		0.319					−0.004		−0.058
	SCF	0.181	0.085	−0.002	−0.078	−0.139	−0.156	−0.180	−0.196
		0.328	0.245	0.165	0.093	0.032		−0.016	−0.046
4.2		0.328					0.013		−0.046
		0.332	0.253	0.177	0.107	0.047		−0.001	−0.033
4.4		0.332					0.028		−0.033
		0.332	0.256	0.184	0.117	0.058		0.010	−0.023
4.6		0.332					0.039		−0.023
		0.327	0.256	0.187	0.123	0.066		0.019	−0.015
4.8		0.327					0.047		−0.015
		0.319	0.252	0.187	0.126	0.071		0.026	−0.008
5.0		0.319					0.054		−0.008
	SCF	0.249	0.168	0.091	0.020	−0.042	−0.061	−0.091	−0.124
		0.289	0.233	0.178	0.125	0.077		0.036	0.005
5.5		0.289					0.062		0.005
		0.250	0.205	0.159	0.115	0.075		0.039	0.011
6.0		0.250					0.061		0.011
	SCF	0.251	0.188	0.127	0.068	0.013	−0.004	−0.033	−0.069
		0.210	0.174	0.137	0.101	0.068		0.038	0.014
6.5		0.210					0.056		0.014
		0.171	0.143	0.114	0.085	0.058		0.034	0.014
7.0		0.171					0.049		0.014
	SCF	0.222	0.177	0.130	0.085	0.041	0.026	0.002	−0.031

the value of β^2 (or α^2) in (2); for example, *te* has 75 percent $p\sigma$ (or 25 percent s) character. (2) We may conveniently distinguish between *positive hybrids* and *negative hybrids* (see text after Eq. (2)). In general, positive hybrids have strong overlap and bonding power in the direction of the positive side of $p\sigma$, while negative hybrids have weak overlap and bonding power in that direction. (3) If two hybrids have equal α and differ only in the sign of β, each may be called the *antihybrid* of the other. (4) If two hybrids which are both positive, or both negative, differ in such a way that one has the amount $\sin^2\phi$ $(=\beta^2)$ of $p\sigma$ character (and $\cos^2\phi$ of s character) and the other has an amount $\cos^2\phi$ $(=1-\beta^2)$ of $p\sigma$ character (and $\sin^2\phi$ of s character), each may be called the *cohybrid* of the other. (5) The antihybrid of a cohybrid (or what is the same, the cohybrid of an antihybrid) may be called the anti-cohybrid or *orthohybrid* of the original hybrid. (6) As is readily verified, every hybrid is orthogonal to its orthohybrid, and the antihybrid of any hybrid is orthogonal to the cohybrid.

The foregoing relations and definitions are reviewed in Table II, using the brief symbols $h_{a\beta}$, $h_{c\beta}$, and $h_{o\beta}$ for the antihybrid, the cohybrid, and the orthohybrid respectively of any *given* hybrid h_β. For maximum clarity, the case where h_β is a positive hybrid and that where it is a negative hybrid are first listed separately. In each case, the α and β of each *related* hybrid are given in terms of the α, or the α and β, of the *original* hybrid h_β.

In order to illustrate further the preceding discussion, the cohybrids, antihybrids, and orthohybrids of the familiar positive hybrid types *te*, *tr*, and *di* are listed in

TABLE VA—*Continued.*

ρ		0.99980 α=0.7 −0.71414	0.99980 0.71414 β=−0.7	0.96 α=0.8 β=−0.6	β=−0.5	α=0.9	β=−0.4	β=−0.3	β=−0.2	β=−0.1	α=1 β=0
		−0.115		−0.023		0.147					0.637
3.0			−0.106	−0.023	0.077		0.188	0.303	0.419	0.531	0.637
	SCF	−0.218	−0.205	−0.103	0.014	0.094	0.140	0.267	0.393	0.512	0.622
3.2		−0.102		−0.023		0.131					0.600
			−0.094	−0.023	0.067		0.169	0.277	0.387	0.496	0.600
3.4		−0.090		−0.023		0.117					0.563
			−0.084	−0.023	0.058		0.152	0.253	0.358	0.462	0.563
3.6		−0.078		−0.022		0.104					0.527
			−0.073	−0.022	0.050		0.136	0.230	0.329	0.429	0.527
3.8		−0.068		−0.021		0.092					0.491
			−0.064	−0.021	0.043		0.122	0.209	0.302	0.397	0.491
		−0.058		−0.020		0.082					0.456
4.0			−0.055	−0.020	0.037		0.109	0.190	0.277	0.367	0.456
	SCF	−0.180	−0.175	−0.120	−0.043	0.014	0.048	0.147	0.250	0.354	0.455
4.2		−0.051		−0.020		0.071					0.423
			−0.049	−0.020	0.031		0.096	0.171	0.252	0.337	0.423
4.4		−0.041		−0.017		0.064					0.390
			−0.040	−0.017	0.028		0.086	0.155	0.230	0.310	0.390
4.6		−0.034		−0.015		0.056					0.360
			−0.034	−0.015	0.024		0.077	0.140	0.210	0.284	0.360
4.8		−0.028		−0.014		0.049					0.330
			−0.028	−0.014	0.020		0.068	0.125	0.190	0.259	0.330
		−0.023		−0.012		0.044					0.302
5.0			−0.023	−0.012	0.017		0.060	0.113	0.172	0.236	0.302
	SCF	−0.132	−0.131	−0.108	−0.063	−0.026	−0.003	0.067	0.143	0.224	0.306
5.5		−0.013		−0.009		0.031					0.240
			−0.014	−0.009	0.012		0.044	0.086	0.133	0.185	0.240
		−0.006		−0.006		0.023					0.188
6.0			−0.007	−0.006	0.008		0.032	0.064	0.102	0.144	0.188
	SCF	−0.089	−0.090	−0.085	−0.062	−0.040	−0.026	0.020	0.073	0.131	0.193
6.5		−0.002		−0.004		0.016					0.145
			−0.003	−0.004	0.005		0.023	0.048	0.077	0.110	0.145
		0.000		−0.003		0.011					0.111
7.0			−0.001	−0.003	0.004		0.017	0.035	0.058	0.083	0.111
	SCF	−0.054	−0.061	−0.061	−0.052	−0.041	−0.032	−0.004	0.031	0.071	0.114

(1) The listed values of $S_\beta(\beta, \rho)$, at 0.1 intervals of α or of β, were computed using Eq. (4); see also Table IV and Eq. (2). (2) For convenience of reference, values of α corresponding to 0.1 intervals of β for $\beta=0$ to -0.8, and corresponding values of $|2\alpha\beta|$, are given at the top of Table VA; beyond $\beta=-0.7$, the same numbers would repeat, and so are omitted. (3) All the listed values of S_β were obtained using S_s, $S_{s\sigma}$, and S_σ values from Table VI. All except those marked "*SCF*" were based on the left-hand (Slater-*AO*) columns of Table VI. Those marked "*SCF*" are based on the right-hand columns, involving $2s^{or}$ and $2p\sigma^{SCF}$ *carbon AO*'s (see reference 7).

Table III. The table is so arranged that the *AO*'s on each line are orthohybrids of each other.

II. OVERLAP INTEGRALS FOR 2s,2p-HYBRID *AO*'S IN HOMOPOLAR BONDS

We first consider the overlap integral S_β for two like 2s,p-hybrid *AO*'s (see Eq. (2)) of two like atoms. In terms of the overlap integrals S_s and S_σ for pure 2s and pure $2p\sigma$ *AO*'s, this is:[6]

$$S_\beta(\rho)=\alpha^2S_s(\rho)+2\alpha\beta S_{s\sigma}(\rho)+\beta^2S_\sigma(\rho). \qquad (4)$$

[6] See reference 5, Eq. (78).

The value of S_β depends on β and also on a parameter ρ proportional to the internuclear distance R. The notation used here and elsewhere in this paper for overlap integrals is summarized in Table IV.

It is now necessary only to compute α^2, β^2, and $2\alpha\beta$ for each desired value of α, to look up $S_s(\rho)$, $S_{s\sigma}(\rho)$, and $S_\sigma(\rho)$ for each desired value of ρ in the tables published previously,[5] and to combine the results according to Eq. (4). This has been done for several values of ρ in the range of interest for stable homopolar bonds, and the results are presented in Table V and Fig. 1. Most of the S values in Table V are based on ordinary Slater

TABLE VB. Overlap integrals $S_\beta(\beta, \rho)$ for 2s, 2p-hybrid *AO*'s in homopolar bonds: positive hybrids.

ρ		$\alpha=1$ $\beta=0$	$\beta=0.1$	$\beta=0.2$	$\beta=0.3$	$\beta=0.4$	$\alpha=0.9$	$\beta=0.5$	$\alpha=0.8$ $\beta=0.6$	$\beta=0.7$
		0.637					0.946		0.954	
3.0		0.637	0.734	0.818	0.885	0.934		0.958	0.954	0.912
	SCF	0.622	0.720	0.802	0.865	0.906	0.914	0.919	0.899	0.839
3.2		0.600					0.920		0.942	
		0.600	0.696	0.781	0.853	0.906		0.937	0.942	0.911
3.4		0.563					0.890		0.923	
		0.563	0.658	0.744	0.817	0.874		0.911	0.923	0.901
3.6		0.527					0.856		0.898	
		0.527	0.620	0.705	0.779	0.838		0.880	0.989	0.884
3.8		0.491					0.818		0.867	
		0.491	0.581	0.665	0.739	0.800		0.845	0.867	0.861
		0.456					0.779		0.833	
4.0		0.456	0.543	0.625	0.698	0.760		0.806	0.833	0.833
	SCF	0.455	0.551	0.639	0.715	0.775	0.792	0.816	0.833	0.817
4.2		0.423					0.738		0.797	
		0.423	0.506	0.586	0.658	0.719		0.767	0.797	0.802
4.4		0.390					0.695		0.756	
		0.390	0.470	0.546	0.615	0.676		0.724	0.756	0.764
4.6		0.360					0.652		0.714	
		0.360	0.435	0.507	0.574	0.634		0.681	0.714	0.726
4.8		0.330					0.609		0.671	
		0.330	0.401	0.470	0.534	0.591		0.638	0.671	0.685
		0.302					0.568		0.629	
5.0		0.302	0.369	0.434	0.495	0.550		0.596	0.629	0.644
	SCF	0.306	0.387	0.465	0.536	0.597	0.617	0.647	0.679	0.688
5.5		0.240					0.467		0.524	
		0.240	0.296	0.351	0.403	0.452		0.493	0.524	0.542
		0.188					0.377		0.427	
6.0		0.188	0.233	0.279	0.323	0.364		0.399	0.427	0.444
	SCF	0.193	0.255	0.317	0.376	0.430	0.448	0.477	0.513	0.533
6.5		0.145					0.299		0.341	
		0.145	0.182	0.218	0.254	0.287		0.317	0.341	0.357
		0.111					0.233		0.268	
7.0		0.111	0.139	0.168	0.197	0.224		0.248	0.268	0.282
	SCF	0.114	0.159	0.206	0.251	0.295	0.310	0.334	0.367	0.390

2s and $2p\sigma$ *AO*'s, and are applicable to any first-row homopolar bond. Additional *S* values based on the use of *SCF* (self-consistent-field) *AO*'s *of the carbon atom* (see Sec. III, below) are also given in Table V. These should be roughly correct also for other second-row atoms, or at least for boron and nitrogen. Figure 1 gives a graphical comparison of the Slater and *SCF* values.[7]

The tables and figures bring out clearly an important fact which is already implicit in the form of Eq. (4): namely, a relatively small amount of *s* character in a $p\sigma$ orbital, or of $p\sigma$ character in an *s* orbital greatly increases (if $\beta>0$) or greatly decreases (if $\beta<0$) the value of the overlap integral *S*. If *S* is a measure of the bonding power of an *AO*, this means that a small amount of hybridization may be of great importance for the bond energies of chemical bonds. In other words, *a little hybridization goes a long way.*

III. SELF-CONSISTENT-FIELD OVERLAP INTEGRALS FOR CARBON ATOM 2s AND 2p *AO*'S

In the course of the computation of hybrid *SCF* overlap integrals for Table V and Fig. 1, it was found desirable to replace the brief tables[7] of 2p *SCF* and $2s^{or}$ (orthogonalized 2s) overlap integrals given in reference 5 by more complete tables, for convenience of reference in the *SCF* hybrid computations. These are given in Table VI. The $S_{s\sigma}$ *SCF* column in Table VI is entirely new.

The S_s columns in Table VI document a previous

[7] See Sec. Vb of reference 5 with regard to *SCF* 2p *AO*'s for carbon. As *SCF* 2s *AO* of carbon, an orthogonalized (see reference 5, Sec. Va) Slater 2s *AO* has been used here (see reference 11a in reference 5). It would be desirable to use *SCF S* values for all atoms, but this will require separate computations for each atom, and it will be necessary first to obtain approximate analytical expressions for the *SCF AO*'s of each atom.

TABLE VB—*Continued.*

ρ		α=0.7	α=0.6 β=0.8	α=0.5	β=0.9	α=0.4	α=0.3	α=0.2	α=0.1	α=0 β=1
		0.902	0.820	0.719		0.609	0.494	0.378	0.265	0.159
3.0			0.820		0.649					0.159
	SCF	0.827	0.725	0.607	0.527	0.482	0.354	0.229	0.109	−0.001
3.2		0.903	0.832	0.742		0.640	0.531	0.421	0.312	0.208
			0.832		0.677					0.208
3.4		0.895	0.834	0.753		0.660	0.558	0.454	0.349	0.248
			0.834		0.694					0.248
3.6		0.880	0.828	0.756		0.670	0.576	0.477	0.377	0.279
			0.828		0.702					0.279
3.8		0.858	0.815	0.750		0.672	0.584	0.492	0.397	0.303
			0.815		0.701					0.303
		0.830	0.795	0.738		0.666	0.585	0.498	0.408	0.319
4.0			0.795		0.693					0.319
	SCF	0.811	0.756	0.679	0.622	0.589	0.490	0.386	0.282	0.181
4.2		0.800	0.771	0.720		0.655	0.580	0.499	0.414	0.328
			0.771		0.680					0.328
4.4		0.763	0.739	0.695		0.637	0.568	0.492	0.413	0.332
			0.739		0.659					0.332
4.6		0.725	0.706	0.668		0.615	0.552	0.482	0.408	0.332
			0.706		0.635					0.332
4.8		0.685	0.671	0.637		0.589	0.531	0.467	0.398	0.327
			0.671		0.607					0.327
		0.645	0.634	0.604		0.561	0.509	0.449	0.385	0.319
5.0			0.634		0.578					0.319
	SCF	0.687	0.663	0.618	0.581	0.558	0.489	0.412	0.331	0.249
5.5		0.543	0.538	0.517		0.485	0.443	0.396	0.343	0.289
			0.538		0.497					0.289
		0.446	0.445	0.430		0.406	0.374	0.336	0.295	0.250
6.0			0.445		0.416					0.250
	SCF	0.534	0.529	0.506	0.484	0.470	0.424	0.371	0.312	0.251
6.5		0.358	0.359	0.350		0.332	0.307	0.278	0.245	0.210
			0.359		0.339					0.210
		0.283	0.285	0.278		0.265	0.247	0.224	0.199	0.171
7.0			0.285		0.271					0.171
	SCF	0.392	0.397	0.388	0.377	0.368	0.340	0.305	0.265	0.222

statement (see Table II of reference 5) that the use of orthogonalized 2*s* *AO*'s produces only slight changes, as compared with Slater 2*s* *AO*'s, in overlap integrals.

In a similar way, the values of $1s_H-2s_C$ and $1s_H-2p\sigma_C$ overlap integrals using $2s^{or}$ and $2p\sigma^{SCF}$ carbon atom *AO*'s are compared in Table VII with those using Slater *AO*'s, for the special case of CH. These results will be used later, in Table XI.

IV. OVERLAP INTEGRALS FOR 2s,2p HYBRID-ORTHOHYBRID OVERLAPS

According to valence-bond theory, the interaction between lone pairs on two atoms, or between a lone pair of one atom and a bonding electron on another, gives rise to an exchange repulsion of whose energy, as was pointed out in a previous paper,[4] the square of the overlap integral concerned should be a measure. For example, there should in N_2, if we accept (3), be a repulsion of this kind between a $p\sigma$ (or a *di*) bonding electron on one atom and an $s)^2$ (or a $di')^2$ (lone pair on the other. If instead of these two alternatives for N_2, one considers the more general formulation

$$k)^2k)^2h_{o\beta})^2h_{o\beta})^2h_\beta\cdot h_\beta)\pi\cdot\pi)\pi'\cdot\pi') \qquad (5)$$

and seeks the value of the hybridization coefficient β which makes the energy a minimum, one sees that the value of the overlap integral $S_{\beta,o\beta}$ (see Tables II, IV) as a function of β should be a measure of the repulsion between the h_β bonding electron on one atom and the $h_{o\beta})^2$ lone pair on the other atom.[8] Values of $S_{\beta,o\beta}(\rho,\beta)$

[8] Formulations (5) and (11), like (3), are based on the customary principle of using for each atom an orthogonal set of *AO*'s. While this is not strictly necessary, it simplifies both comprehension and computations.

TABLE VI. Comparison of Slater-*AO* with improved-*AO* overlap integrals for homopolar bonds.[a]

	S_s *AO*'s used[b]		$S_{s\sigma}$ *AO*'s used[b]			S_σ *AO*'s used[b]		S_π *AO*'s used[b]	
ρ	$2s^{Sl}$	$2s^{or}$	$2s^{Sl}$, $2p\sigma^{Sl}$	$2s^{or}$, $2p\sigma^{Sl}$	$2s^{or}$, $2p\sigma^{SCF}$	$2p\sigma^{Sl}$	$2p\sigma^{SCF}$	$2p\pi^{Sl}$	$2p\pi^{SCF}$
3.0	0.637	0.622	0.509	0.483	0.522	0.159	−0.001	0.468	0.541
3.2	0.600	0.589	0.503	0.481	0.525	0.208	0.047	0.427	0.506
3.4	0.563	0.555	0.492	0.475	0.523	0.248	0.087	0.389	0.472
3.6	0.527	0.522	0.479	0.465	0.518	0.279	0.124	0.352	0.439
3.8	0.491	0.488	0.463	0.451	0.508	0.303	0.154	0.318	0.409
4.0	0.456	0.455	0.444	0.435	0.496	0.319	0.181	0.287	0.380
4.2	0.423	0.423	0.425	0.419	0.483	0.328	0.202	0.258	0.353
4.4	0.390	0.392	0.402	0.397	0.466	0.332	0.219	0.231	0.329
4.6	0.360	0.362	0.380	0.377	0.450	0.332	0.233	0.207	0.304
4.8	0.330	0.333	0.357	0.355	0.431	0.327	0.242	0.184	0.282
5.0	0.302	0.306	0.334	0.333	0.410	0.319	0.249	0.164	0.261
5.5	0.240	0.245	0.278	0.278	0.361	0.289	0.256	0.121	0.213
6.0	0.188	0.193	0.226	0.227	0.311	0.250	0.251	0.089	0.174
6.5	0.145	0.149	0.180	0.182	0.264	0.210	0.239	0.064	0.142
7.0	0.111	0.114	0.141	0.143	0.223	0.171	0.222	0.046	0.115
8.0	0.062	0.064	0.083	0.084	0.152	0.107	0.182	0.023	0.075
9.0	0.034	0.035	0.046	0.047	0.102	0.063	0.143	0.011	0.049
10.0	0.018	0.019	0.025	0.026	0.067	0.035	0.108	0.005	0.031
11.0	0.009	0.010	0.013	0.013	0.045	0.019	0.079	0.002	0.019
12.0	0.004	0.005	0.007	0.007	0.027	0.010	0.057	0.001	0.013
13.0	0.002	0.002	0.003	0.003	0.017	0.005	0.040	0.001	0.008
14.0	0.001	0.001	0.002	0.002	0.010	0.002	0.028	0.000	0.005

[a] The left-hand (Slater) columns in Table VI are taken from the $t=0$ columns of tables in reference 5. The right-hand columns were computed in the manner indicated in Secs. Va and Vb of reference 5 (see Eq. (75) of reference 5 for S_s based on $2s^{or}$). A sampling of the results for S_σ and S_π has already been given in Table III of reference 5.

[b] The superscript "*Sl*" refers to Slater *AO*'s, "*or*" to carbon atom orthogonalized Slater $2s$ *AO*'s (see reference 2, Eq. (76)). (See reference 7.)

have therefore been computed, and are presented in Table VIII.[8a]

These are based on

$$S_{\beta,0\beta}\equiv\int(h_{\beta a})(h_{o\beta b})dv$$

$$=\int(a\cdot s_a+\beta\cdot p\sigma_a)(|\beta|\cdot s_b\mp a\cdot p\sigma_b)dv.$$

Putting $\beta=\pm(1-\alpha^2)^{\frac{1}{2}}$ or $\alpha=(1-\beta^2)^{\frac{1}{2}}$, this yields:

$$\left.\begin{aligned}S_{\beta,o\beta}&=\alpha(1-\alpha^2)^{\frac{1}{2}}(S_s-S_\sigma)\pm(1-2\alpha^2)S_{s\sigma}\quad\text{(a)}\\&=|\beta|(1-\beta^2)^{\frac{1}{2}}(S_s-S_\sigma)\mp(1-2\beta^2)S_{s\sigma},\quad\text{(b)}\end{aligned}\right\},\qquad(6)$$

where S_s, S_σ, $S_{s\sigma}$, hence $S_{\beta,o\beta}$, are functions of ρ. The upper or the lower sign in the above equations applies according as the original hybrid h_β is a positive or a negative one (See Table II).

From Eqs. (6a) and (6b), it is seen that

$$S^-(\alpha)=S^+(\beta);\quad S^+(\alpha)=-S^-(|\beta|),\qquad(7)$$

where S refers to $S_{\beta,o\beta}$ and the superscript indicates the sign of β in the original hybrid h_β. In words, the value of $S_{\beta,o\beta}$ for a negative hybrid h_β having, say, $\alpha=x$ is the same as that of $S_{\beta,o\beta}$ for the positive hybrid having $\beta=x$; and the value of $S_{\beta,o\beta}$ for a positive hybrid having $\alpha=x$ is the negative of that for the negative hybrid having $|\beta|=x$. These relations are made use of in the headings of Table VIII, and are illustrated by Fig. 2.

[8a] As a measure of the repulsion between the two $h_{0\beta})^2$ lone pairs, one may use the value of S_β^2 from Table V, taken for a value of β equal to that appropriate to $h_{o\beta}$.

V. INNER SHELL-OUTER SHELL OVERLAP INTEGRALS FOR HOMOPOLAR BONDS WITH $2s,2p$-HYBRID OUTER SHELL *AO*'S

According to valence theory, there should be exchange repulsions between inner-shell electrons (here the K shell only) and both bonding and nonbonding outer-shell electrons. Of particular interest for this paper are the k,h_β and $k,h_{o\beta}$ interactions (see e.g. (5)), of whose magnitudes the squares of the overlap integrals $S_{k\beta}$ and $S_{k,o\beta}$ (see Table IV for notation) should be a measure. These overlap integrals, although small, are nevertheless large enough to indicate that it is unwise to neglect the corresponding interactions entirely. For this reason, and also for use in a following paper, values of $S_{k\beta}$ have been computed and are given in Table X, at intervals of α and β selected to permit convenient interpolation, based on Slater *AO*'s; some *SCF* values are also included.

In connection with Table X, it is necessary to recall

TABLE VII. Comparison of Slater-*AO* with improved-*AO* overlap integrals for CH.

		S_{ks}[b,c]		$S_{k\sigma}$[b,c]	
R(A)	ρ[a]	$2s^{Sl}$	$2s^{or}$	$2p\sigma^{Sl}$	$2p\sigma^{SCF}$
1.119	2.776	0.555	0.553	0.459	0.509
1.090	2.704	0.570	0.567	0.466	0.512
1.060	2.630	0.586	0.582	0.472	0.515

[a] For CH, $\rho=1.3125\,R/a_H$; $t=-0.2381$ (see Eqs. (11)). [b] See Table VI, note b. [c] Referring to the general definitions of S_{ks} and $S_{k\sigma}$ in Table IV, the columns headed $2s^{or}$ and $2p\sigma^{SCF}$ were computed using Eq. (8) of reference 5 for $2s^{or}$ and Eq. (76) of reference 5 for $2p\sigma^{SCF}$, reducing to linear combinations of *Slater-type* integrals S_{ks} or $S_{k\sigma}$ and S_k, with various ρ and t values for the different terms, and referring to the tables of reference 5.

TABLE VIII. Overlap integrals $S_{\beta,o\beta}(\beta, \rho)$ for intratomically orthogonal 2s, 2p-hybrid *AO*'s h_β and $h_{o\beta}$ in homopolar bonds.[a, b]

	$\alpha=$ 0.8, $\beta=+0.6$ or $\alpha=$ 0.6, $\beta=-0.8$	0.7 / −0.7	0.6 / +0.8 / 0.8 / −0.6	0.5 / −0.5	0.4 / −0.4	0.3 / −0.3	0.2 / −0.2	0.1 / −0.1
ρ								
3.0 *Sl*	0.087	0.249	0.372	0.461	0.521	0.554	0.562	0.546
3.0 *SCF*	0.153	0.322	0.445	0.531	0.583	0.606	0.602	0.574
3.2	0.047	0.206	0.329	0.421	0.485	0.524	0.539	0.532
3.4	0.013	0.167	0.289	0.383	0.450	0.494	0.515	0.514
3.6	−0.015	0.133	0.253	0.347	0.417	0.464	0.489	0.494
3.8	−0.039	0.103	0.220	0.313	0.384	0.433	0.463	0.472
4.0 *Sl*	−0.058	0.078	0.190	0.282	0.352	0.404	0.436	0.449
4.0 *SCF*	−0.007	0.147	0.270	0.367	0.438	0.485	0.510	0.513
4.2	−0.074	0.056	0.164	0.253	0.324	0.376	0.410	0.426
4.4	−0.085	0.037	0.140	0.226	0.295	0.346	0.381	0.400
4.6	−0.093	0.022	0.120	0.202	0.268	0.319	0.355	0.375
4.8	−0.099	0.009	0.101	0.180	0.244	0.293	0.329	0.350
5.0 *Sl*	−0.101	−0.002	0.086	0.160	0.221	0.269	0.304	0.326
5.0 *SCF*	−0.087	0.037	0.142	0.230	0.300	0.353	0.388	0.407
5.5	−0.101	−0.019	0.054	0.118	0.171	0.214	0.246	0.267
6.0 *Sl*	−0.093	−0.027	0.033	0.086	0.131	0.167	0.196	0.215
6.0 *SCF*	−0.115	−0.023	0.059	0.130	0.190	0.238	0.275	0.299
6.5	−0.082	−0.029	0.019	0.062	0.097	0.129	0.153	0.170
7.0 *Sl*	−0.069	−0.028	0.010	0.044	0.074	0.098	0.118	0.132
7.0 *SCF*	−0.114	−0.050	0.011	0.065	0.112	0.152	0.184	0.208

	$\alpha=$ 0, $\beta=\pm1.0$ or $\alpha=$ 1.0, $\beta=$ 0.0	0.1 / +0.1	0.2 / +0.2	0.3 / +0.3	0.4 / +0.4	0.5 / +0.5	0.6 / −0.8 / 0.8 / +0.6	0.7 / +0.7	0.8 / −0.6 / 0.6 / +0.8
ρ									
3.0 *Sl*	±0.509	−0.451	−0.374	−0.280	−0.171	−0.047	0.087	0.229	0.372
3.0 *SCF*	±0.522	−0.450	−0.358	−0.250	−0.127	0.009	0.153	0.301	0.445
3.2	±0.503	−0.454	−0.386	−0.300	−0.198	−0.082	0.047	0.196	0.329
3.4	±0.492	−0.451	−0.391	−0.314	−0.219	−0.110	0.013	0.148	0.289
3.6	±0.479	−0.445	−0.392	−0.322	−0.235	−0.132	−0.015	0.114	0.253
3.8	±0.463	−0.435	−0.389	−0.326	−0.246	−0.150	−0.039	0.085	0.220
4.0 *Sl*	±0.444	−0.422	−0.382	−0.325	−0.252	−0.162	−0.058	0.060	0.190
4.0 *SCF*	±0.496	−0.459	−0.403	−0.328	−0.237	−0.129	−0.007	0.127	0.270
4.2	±0.425	−0.407	−0.373	−0.322	−0.255	−0.172	−0.074	0.039	0.164
4.4	±0.402	−0.388	−0.359	−0.313	−0.252	−0.176	−0.085	0.021	0.140
4.6	±0.380	−0.369	−0.344	−0.303	−0.248	−0.178	−0.093	0.006	0.120
4.8	±0.357	−0.349	−0.328	−0.292	−0.242	−0.177	−0.099	−0.006	0.101
5.0 *Sl*	±0.334	−0.329	−0.310	−0.279	−0.233	−0.174	−0.101	−0.015	0.086
5.0 *SCF*	±0.410	−0.396	−0.366	−0.320	−0.258	−0.180	−0.087	0.020	0.142
5.5	±0.278	−0.277	−0.265	−0.242	−0.207	−0.160	−0.101	−0.030	0.054
6.0 *Sl*	±0.226	−0.228	−0.220	−0.203	−0.177	−0.140	−0.093	−0.036	0.033
6.0 *SCF*	±0.311	−0.311	−0.297	−0.272	−0.233	−0.181	−0.115	−0.035	0.059
6.5	±0.180	−0.183	−0.178	−0.166	−0.146	−0.118	−0.082	−0.036	0.019
7.0 *Sl*	±0.141	−0.144	−0.142	−0.133	−0.118	−0.097	−0.069	−0.033	0.010
7.0 *SCF*	±0.223	−0.229	−0.226	−0.214	−0.191	−0.158	−0.114	−0.058	0.011

[a] The listed values of $S_{\beta\,o\beta}(\beta, \rho)$, at 0.1 intervals of α (upper scale) or of β (lower scale) were computed using Eqs. (6). Note that because of the relations stated in Eqs. (7), the same set of numerical values of S occurs in the α range for positive hybrids as in the $|\beta|$ range for negative hybrids, and vice versa. Note also that in the ranges α or $|\beta| = (\frac{1}{2})^{\frac{1}{2}}$ to 1, the numerical values of S repeat which occur in the ranges α or $|\beta| = 0$ to $(\frac{1}{2})^{\frac{1}{2}}$.

[b] See Notes (1) and (3) of Table VA, changing S_β to $S_{\beta,o\beta}$ and Eq. (4) to Eqs. (6).

that overlap integrals based on Slater *AO*'s *in general* depend (1) on a parameter ρ which is proportional not only to the interatomic distance R but also to the average of the Slater μ values of the particular atoms and *AO*'s involved; and (2) on a parameter t which differs from zero and depends on the particular atoms

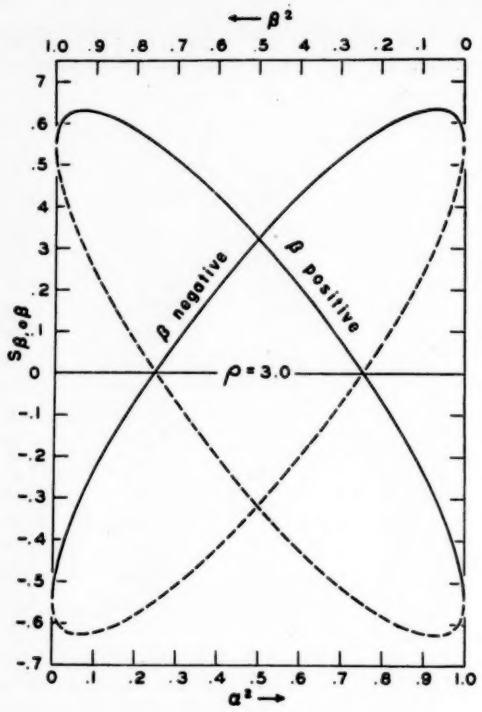

FIG. 2. $S_{\beta,o\beta}$ plotted against α^2 or β^2 for $\rho=3.0$ using numerical values from Table VIII, for the *SCF* case. Each of the two branches of the graph (β negative and β positive) forms half of an ellipse, of which the remainder is completed by the dotted lines. [If $h_{o\beta}$ were defined always as $\beta\cdot s-\alpha\cdot p\sigma$, instead of by $|\beta|\cdot s \mp\alpha\cdot p\sigma$ for positive and negative β, respectively, the sign of S in the "β negative" branch would be reversed and the two branches would combine to a single ellipse (see Table II for related comments).] Figure 2 illustrates well the relations stated in Eqs. (7).

involved, even for homopolar bonds, if *AO*'s with different μ's are involved, as is true for $S_{k\beta}$ (see Table IV). In the case of integrals such as S_β and $S_{\beta,o\beta}$ for homopolar bonds, $t=0$; here the Slater μ is the same for both of the (here two-quantum) *AO*'s involved, but depends on the particular atom A; it will here be called μ_A. For these homopolar cases, ρ is given by

$$\rho=\mu_A R/a_H, \tag{8}$$

with μ values as in Table I of reference 5. In discussing homopolar bonds between *two first-row atoms*, it will be convenient to assign this specific meaning, and the name "two-quantum ρ," to the symbol ρ.

The integrals S_{ks}, $S_{k\sigma}$, or in general $S_{k\beta}$, depend on a *different* ρ parameter, and also on a nonvanishing t parameter. These parameters will here be called $\omega_A\rho$ and t_A, where (see footnote a of Table IV)

$$\omega_A=\tfrac{1}{2}(\mu_{kA}+\mu_A)/\mu_A;\quad t_A=(\mu_{kA}-\mu_A)/(\mu_{kA}+\mu_A), \tag{9}$$

μ_A being the two-quantum A atom Slater μ mentioned above, and μ_{kA} the *one-quantum* Slater μ for atom A. Hence $S_{k\beta}$ depends not only on β and ρ, but additionally, through ω_A and t_A, somewhat on the particular atom A:

$$S_{k\beta}=S_{k\beta}(\beta,\omega_A\rho,t_A).$$

The same is of course true of S_{ks}, $S_{k\sigma}$, and $S_{k,o\beta}$.

Table IX contains values of $S_{ks}(\omega_A\rho)$ and $S_{k\sigma}(\omega_A\rho)$, *tabulated against the two-quantum* ρ, for use in computing $S_{k\beta}$. The latter is given[9] by

$$S_{k\beta}(\beta;\omega_A\rho,t_A)=\alpha S_{ks}(\omega_A\rho,t_A)+\beta S_{k\sigma}(\omega_A\rho,t_A). \tag{10}$$

Table IX also shows how S_{ks} differs for Slater and orthogonalized-Slater 2*s* *AO*'s, and how $S_{k\sigma}$ differs for Slater and *SCF* *AO*'s. Table IX shows further that, *for a given value of the two-quantum* ρ, S_{ks} and $S_{k\sigma}$ depend very appreciably on the particular atoms involved.

TABLE IX. Comparison of Slater-*AO* with improved-*AO* S_{ks} and $S_{k\sigma}$ overlap integrals as function of two-quantum ρ for homopolar bonds.

Two-qu. ρ	A	$S_{ks}(\omega_A\rho,t_A)$[a,b] 2*s* *AO*'s used: $2s^{Sl}$	$2s^{or}$	$S_{k\sigma}(\omega_A\rho,t_A)$[a,b] 2$p\sigma$ *AO*'s used: $2p\sigma^{Sl}$	$2p\sigma^{SCF}$
3.0	Li[c]	0.080	0.081	0.135	
	C	0.103	0.105	0.171	0.162
	N	0.106	0.109	0.176	
	F	0.110	0.113	0.182	
3.4	C	0.079	0.081	0.133	0.132
3.8	C	0.060	0.062	0.102	0.107
4.0	Li	0.040	0.041	0.069	
	C	0.052	0.054	0.089	0.096
	N	0.054	0.056	0.091	
	F	0.056	0.059	0.095	
4.2	C	0.046	0.047	0.077	0.087
4.6	C	0.034	0.035	0.057	0.070
5.0	Li	0.019	0.019	0.036	
	C	0.025	0.026	0.043	0.057
	N	0.026	0.026	0.044	
	F	0.027	0.027	0.046	
6.0	Li	0.008	0.009	0.015	
	C	0.010	0.011	0.019	0.033
	N	0.012	0.012	0.020	
	F	0.012	0.013	0.020	
7.0	Li	0.004	0.004	0.005	
	C	0.005	0.005	0.009	0.020
	N	0.005	0.005	0.009	
	F	0.005	0.005	0.009	
8.0	Li	0.002	0.002	0.003	
	C	0.002	0.002	0.004	0.012
	N	0.002	0.002	0.004	
	F	0.002	0.002	0.004	

[a] S_{ks} and $S_{k\sigma}$ (see Table IV) are functions of $\omega_A\rho$ and t_A (see Eq. (10)), where ρ is the "two-quantum ρ" of Eq. (8), and ω_A, t_A (see Eqs. (9)) have the values 2.577, 0.6119; 2.254, 0.5563; 2.218, 0.5491; and 2.173, 0.5398 for Li, C, N, and F, respectively.

[b] The values of S_{ks} and $S_{k\sigma}$ based on Slater 2*s* and 2$p\sigma$ *AO*'s are taken from the 1*s*, 2*s* and 1*s*, 2$p\sigma$ tables respectively (Tables V, VI) of reference 5, for p and t values in those tables equal to $\omega_A\rho$ and t_A respectively. The S_{ks} values based on $2s^{or}$ are then obtained using reference 5, Eq. (8) for $2s^{or}$, and the methods of reference 5, Sec. Va; the result is that they differ only by a factor $(1-Q_a^2)^{-\frac{1}{2}}$ from the values in the $2s^{Sl}$ column, where $Q_A=0.1663$, 0.2205, 0.2280, 0.2377 for Li, C, N, F, respectively. The $S_{k\sigma}$ values based on $2p\sigma^{SCF}$ are obtained using reference 5, Eq. (76) and the methods of reference 5, Sec. Vb.

[c] For actual application to Li–Li bonds, the Slater 2*p* *AO* of Li should be replaced by a 2*p* *AO* with a modified value of Z (reference 4, Table I, note d).

[9] See reference 5, Eq. (79), with p replaced by $\omega_A\rho$ and t put equal to t_A (see Eqs. (8)–(9)).

TABLE X. $S_{k\beta}$ overlap integrals as function of β and of two-quantum ρ for carbon-carbon bonds.

Two-qu. ρ		$\alpha=0$ $\beta=-1$	0.2	0.4	0.6 -0.8	0.8 -0.6	-0.4	-0.2
		−0.171	−0.147	−0.115	−0.074	−0.019		
3.0		−0.171			−0.074	−0.019	0.028	0.069
	SCF	−0.162	−0.138	−0.106	−0.067	−0.013	0.031	0.070
		−0.133	−0.114	−0.089	−0.058	−0.015		
3.4		−0.133			−0.058	−0.015	0.021	0.053
		−0.102	−0.088	−0.069	−0.044	−0.012		
3.8		−0.102			−0.044	−0.012	0.016	0.040
		−0.089	−0.076	−0.060	−0.039	−0.010		
4.0		−0.089			−0.039	−0.010	0.014	0.035
	SCF	−0.096	−0.083	−0.066	−0.044	−0.014	0.011	0.034
		−0.077	−0.066	−0.052	−0.033	−0.009		
4.2		−0.077			−0.033	−0.009	0.012	0.031
		−0.057	−0.049	−0.038	−0.025	−0.006		
4.6		−0.057			−0.025	−0.006	0.009	0.023
		−0.043	−0.037	−0.029	−0.019	−0.005		
5.0		−0.043			−0.019	−0.005	0.007	0.017
	SCF	−0.057	−0.051	−0.042	−0.030	−0.013	0.001	0.014
		−0.019	−0.016	−0.013	−0.009	−0.003		
6.0		−0.019			−0.009	−0.003	0.002	0.007
	SCF	−0.033	−0.030	−0.026	−0.020	−0.011	−0.003	0.004
		−0.009	−0.008	−0.006	−0.004	−0.001		
7.0		−0.009			−0.004	−0.001	0.001	0.003
	SCF	−0.020	−0.019	−0.016	−0.013	−0.008	−0.003	0.001

ρ		$\alpha=1$ $\beta=0$	0.2	0.4	0.8 0.6	0.6 0.8	0.4	0.2	0 1
		0.105			0.187	0.200	0.199	0.189	0.171
3.0		0.105	0.137	0.165	0.187	0.200			0.171
	SCF	0.105	0.135	0.161	0.181	0.193	0.190	0.180	0.162
		0.081			0.145	0.155	0.154	0.147	0.133
3.4		0.081	0.106	0.127	0.145	0.155			0.133
		0.062			0.111	0.119	0.118	0.112	0.102
3.8		0.062	0.081	0.098	0.111	0.119			0.102
		0.054			0.097	0.104	0.103	0.098	0.089
4.0		0.054	0.071	0.085	0.097	0.104			0.089
	SCF	0.054	0.072	0.088	0.101	0.109	0.110	0.105	0.096
		0.047			0.084	0.090	0.089	0.085	0.077
4.2		0.047	0.061	0.074	0.084	0.090			0.077
		0.035			0.062	0.067	0.066	0.063	0.057
4.6		0.035	0.046	0.055	0.062	0.067			0.057
		0.026			0.047	0.050	0.050	0.047	0.043
5.0		0.026	0.034	0.041	0.047	0.050			0.043
	SCF	0.026	0.037	0.047	0.055	0.061	0.063	0.061	0.057
		0.011			0.020	0.022	0.022	0.021	0.019
6.0		0.011	0.015	0.018	0.020	0.022			0.019
	SCF	0.011	0.017	0.023	0.029	0.033	0.035	0.035	0.033
		0.005			0.009	0.010	0.010	0.010	0.009
7.0		0.005	0.007	0.008	0.009	0.010			0.009
	SCF	0.005	0.009	0.013	0.016	0.019	0.020	0.021	0.020

The $S_{k\beta}$ values were computed from Eq. (10) using the S_{ks} and $S_{k\sigma}$ values *for carbon* from Table IX. For S_{ks}, *only the values based on* $2s^{or}$ in Table IX were used here; for $S_{k\sigma}$ the values based on $2p\sigma^{SI}$ were used, except in the cases marked *SCF*, where $S_{k\sigma}$'s based on $2p\sigma^{SCF}$ from Table IX were used.

TABLE XI. Overlap integrals $S_{k\beta}$ for AH molecules or bonds using 2s, 2p-hybrid *AO*'s of A atom.

Molecule	R (A)	Negative hybrids $\alpha=0$ $\beta=-1$	0.1	0.2	0.3	0.4	−0.9	0.5	0.6 −0.8	0.7
HF	0.917	−0.299	−0.250	−0.199	−0.144	−0.086		−0.023	0.043	0.116
		−0.299					−0.064		0.043	
OH	0.970	−0.345	−0.293	−0.238	−0.179	−0.116		−0.048	0.025	0.105
		−0.345					−0.092		0.025	
NH	1.038	−0.398	−0.343	−0.284	−0.221	−0.153		−0.080	−0.001	0.086
		−0.398					−0.128		−0.001	
CH	1.119	−0.459	−0.401	−0.339	−0.272	−0.199		−0.120	−0.034	0.060
		−0.459					−0.171		−0.034	
	1.119 *SCF*	−0.509	−0.451	−0.388	−0.320	−0.246		−0.164	−0.075	0.024
		−0.509					−0.217		−0.075	
	1.090 *SCF*	−0.512	−0.452	−0.389	−0.318	−0.242		−0.160	−0.070	0.031
		−0.512					−0.213		−0.070	
	1.060 *SCF*	−0.515	−0.454	−0.388	−0.316	−0.240		−0.155	−0.062	0.039
		−0.515					−0.210		−0.062	

Molecule	R (A)	Negative hybrids $\beta=-0.7$	$\alpha=0.8$ −0.6	−0.5	0.9	−0.4	−0.3	−0.2	−0.1	1 0
HF	0.917		0.198		0.294					0.471
		0.127	0.198	0.259		0.312	0.360	0.402	0.439	0.471
OH	0.970		0.194		0.301					0.501
		0.117	0.194	0.262		0.322	0.375	0.422	0.464	0.501
NH	1.038		0.184		0.302					0.529
		0.099	0.184	0.259		0.326	0.385	0.439	0.487	0.529
CH	1.119		0.168		0.299					0.555
		0.075	0.168	0.251		0.325	0.391	0.452	0.506	0.555
	1.119 *SCF*		0.137		0.276					0.553
		0.039	0.137	0.224		0.303	0.375	0.440	0.499	0.553
	1.090 *SCF*		0.147		0.288					0.567
		0.046	0.147	0.235		0.315	0.387	0.453	0.513	0.567
	1.060 *SCF*		0.157		0.299					0.582
		0.055	0.157	0.247		0.327	0.401	0.467	0.528	0.582

Table X contains values of $S_{k\beta}$, again tabulated against the two-quantum ρ, *for carbon-carbon bonds only*. The values in Table X are based on *orthogonalized* Slater 2s *AO*'s (although as already remarked, the values based on ordinary Slater 2s *AO*'s are but little different), and either Slater or *SCF* $2p\sigma$ *AO*'s. From Tables IX and X one sees that $S_{k\beta}$ (or $S_{k,o\beta}$, which is the same with different β values) may sometimes be of very appreciable magnitude.

VI. OVERLAP INTEGRALS FOR AH MOLECULES AND BONDS USING 2s,2p-HYBRID A ATOM *AO*'S

We consider now the overlap integrals for the overlap of a 1s hydrogen atom *AO* with any $2s, 2p\sigma$-hybrid *AO* of a first-row atom A. These should be valuable as guides to the determination of the true values of the hybridization coefficients in the A atom *AO*'s of hybrid molecules and bonds, for example in the OH radical with valence-bond electron configuration

$$1s_o)^2h_{o\beta})^2h_\beta\cdot 1s_H)\pi_o)^4. \qquad (11)$$

Ordinarily the configuration is taken as

$$1s_o)^2s)^2\sigma\cdot 1s_H)\pi_o)^4.$$

but it is obvious that the formulation (11) is more general.[8] A similar discussion is applicable to other molecules and bonds of the type AH.[10]

Formulation (11) indicates the desirability of a knowledge of the overlap integrals of $1s_H$ with h_β as a measure of bond strength, and (see Sec. IV) of $1s_H$ with $h_{o\beta}$ as a measure of nonbonded exchange repression. Both these integrals are of the type $S_{k\beta}$ (see Table IV for notation), and are given[11] by

$$\left.\begin{aligned} &S_{k\beta}(\beta;\rho,t)=\alpha S_{ks}(\rho,t)+\beta S_{k\sigma}(\rho,t), \\ \text{with}\quad &\rho=(\tfrac{1}{2}+\tfrac{1}{4}Z)R/a_H;\quad t=(2-Z)/(2+Z). \end{aligned}\right\} \qquad (12)$$

[10] In a more complete discussion, ionic character should of course also be considered.

[11] See reference 5, Eq. (79). In Eqs. (12), Z refers to the Slater effective nuclear charge for 2s and 2p A atom *AO*'s (see reference 5,

TABLE XI—*Continued.*

Molecule	R (A)		Positive hybrids α=1 β=0	0.1	0.2	0.3	0.4	0.9	0.5	0.8 0.6	0.7
HF	0.917		0.471					0.555		0.557	
			0.471	0.499	0.522	0.539	0.552		0.558	0.557	0.546
OH	0.970		0.501					0.602		0.608	
			0.501	0.533	0.560	0.582	0.598		0.607	0.608	0.600
NH	1.038		0.529					0.650		0.662	
			0.529	0.566	0.598	0.624	0.644		0.657	0.662	0.657
CH	1.119		0.555					0.699		0.719	
			0.555	0.598	0.635	0.667	0.692		0.710	0.719	0.718
		SCF	0.553					0.719		0.747	
			0.553	0.601	0.644	0.680	0.710		0.733	0.747	0.752
	1.090	*SCF*	0.567					0.733		0.761	
			0.567	0.615	0.658	0.694	0.724		0.747	0.761	0.763
	1.060	*SCF*	0.582					0.748		0.775	
			0.582	0.631	0.673	0.710	0.739		0.762	0.775	0.776

Molecule	R (A)		α=0.7	Positive hybrids 0.6 β=0.8	0.5	0.9	0.4	0.3	0.2	0.1	0 1
HF	0.917		0.544	0.522	0.495		0.463	0.427	0.387	0.345	0.299
				0.522		0.475					0.299
OH	0.970		0.597	0.577	0.549		0.517	0.480	0.438	0.393	0.345
				0.577		0.529					0.345
NH	1.038		0.655	0.636	0.609		0.577	0.539	0.496	0.449	0.398
				0.636		0.589					0.398
CH	1.119		0.716	0.700	0.675		0.643	0.604	0.561	0.512	0.459
				0.700		0.655					0.459
		SCF	0.751	0.739	0.717		0.688	0.651	0.610	0.562	0.509
				0.739		0.699					0.509
	1.090	*SCF*	0.763	0.750	0.726		0.696	0.658	0.615	0.566	0.512
				0.750		0.708					0.512
	1.060	*SCF*	0.775	0.762	0.737		0.704	0.666	0.621	0.571	0.515
				0.762		0.717					0.515

Explanation for Table XI. (1) The tabulated values of $S_{k\beta}$ were computed for each AH using Eq. (12), (see reference 11) with Slater S_{ks} and $S_{k\sigma}$ values taken for appropriate ρ and t values (ρ=3.120, 3.003, 2.894, 2.776, and t=−0.444, −0.389, −0.322 and −0.238 for HF, OH, NH, and CH (1.119A) respectively) from the tables of reference 5; or in the case of the CH values marked "*SCF*," from the $2s^{qr}$ S_{ks} and the *SCF* $S_{k\sigma}$ values in Table VII.

Using Eq. (12) and tabulated values[5] of S_{ks} and $S_{k\sigma}$, values of $S_{k\beta}$ are now easily obtained for any desired β value. Table XI gives values so computed for the radicals CH, NH, OH, and FH at their equilibrium R values,[10] also for C−H at approximately the R values which occur in such compounds as C_2H_6 (R=1.09A) and C_2H_2 (R=1.06A). Table XI is based on Slater $2s$ and $2p\sigma$ *AO*'s, except that in addition, values based on orthogonalized $2s$ combined with *SCF* $2p\sigma$ carbon atom *AO*'s are given for CH. The results for CH and OH are also presented graphically in Fig. 3.

Just as in the case of two first-row atom *AO*'s in Sec. II, although to a lesser extent because hybridization now affects only one of the two overlapping *AO*'s, it is seen that a small amount of s character in $p\sigma$, or of $p\sigma$ character in s, has a marked effect on the value of S. This leads to the conclusion that a little hybridization should be an important factor in stabilizing molecules of the type AH.[4a]

Eqs. (7) and Table I). In Eqs. (12), ρ and t replace $\omega_A\rho$ and t_A of Eq. (10). See Table IV, footnote a of present paper for basis of ρ and t of Eq. (12).

ACKNOWLEDGMENT

The author is very greatly indebted to Mr. Tracy J. Kinyon for his cooperation in the preparation of the tables and graphs. Mr. Kinyon carried out all the extensive numerical computations for the tables.

[*Note added in proof*. In a previous paper (See reference 4, footnote 14a) a semi-empirical "magic formula" was given for the energy of dissociation D of a molecule, containing not too strongly polar bonds, into its atoms in their ground states. This embodies in approximate quantitative form the ideas expressed above on the relations between bond energies and overlap in-

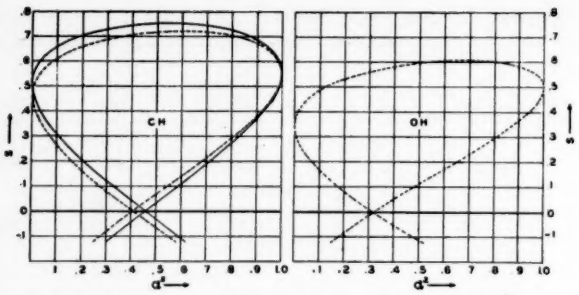

FIG. 3. Maps of overlap integrals $S_{k\beta}$ for CH and OH radicals, plotted against α^2 of the O or C atom $2s, 2p$-hybrid AO. The dashed-line graphs correspond to the Slater-AO S values in Table XI. The full-line graph for CH corresponds to the SCF-AO S values in Table XI.

[It will be noted that the graphs in Fig. 3 differ in type from those in Fig. 1. They are quartic curves instead of ellipses. For the negative hybrids, the curve of $S_{k\beta}$ plotted against α^2 goes steadily downward from $S_{k\sigma}$ at $\alpha^2=0$ to $-S_{k\beta}$ at $\alpha^2=1$, and is thus not closed. A closed curve can, however, be obtained if at the value of α^2 where S would pass through zero we begin using $-h_\beta$ instead of h_β and continue doing so for the negative hybrids until $\alpha^2=1$ is reached. Such a curve, however, reverses the sign of its slope at $S=0$.

A less arbitrary procedure would be one making use of the full range 0 to $\pm\pi$ for ϕ in Eq. (2), instead of just the range 0 to $\pm\pi/2$ which we have been using (see remarks in text immediately after Eq. (2)). This would give a closed curve of figure 8 shape, symmetrical about the line $S=0$, of which each graph in Fig. 3 shows merely the top half. The top of each graph (positive hybrids) corresponds to $\phi=0$ to $+\pi/2$; the slanting curves and their continuations for $S<0$ (negative hybrids) correspond to $\phi=0$ to $-\pi/2$ (right, $S>0$; left, $S<0$) and to $\phi=-\pi/2$ to $-\pi$ (left, $S>0$; right, $S<0$); the *bottom* of the figure 8 would be completed by a curved segment (positive hybrids) identical, except for reversal of the sign of S, with the *top* of the figure 8, and corresponding to $\phi=+\pi/2$ to $+\pi$.]

tegrals. The magic formula as now improved reads as follows:

$$D=\underset{\text{bonded electron-pairs}}{\Sigma K_i}-\underset{\text{nonbonded electron-pairs}}{\tfrac{1}{2}K_{ij}}+RE-P, \tag{13}$$

with

$$K_i=A_iS_iI_i/(1+S_i); \tag{14}$$

and with

$$K_{ij}=0.7A_{ij}S^2_{ij}I_{ij} \tag{15}$$

for nonbonded pairs i,j where both electrons are in orbitals of the same type (both σ or both π), but small and *negative* (and capable of being estimated) when i and j are of different type. The promotion energy P can often be expressed as a function of the degree of hybridization α^2 in the bonding σ orbitals, and since the S_i's and S_{ij}'s of σ type are also functions of α, one can then make a determination of the actual degree of hybridization by varying α until a minimum energy (maximum D) is obtained. Using this method, with SCF S values, it was found that on putting A (that is, A_i or A_{ij} of Eqs. (14) and (15)) equal to 1.16 for all σ–σ pairs and 1.53 for all π–π pairs, the observed D values for the molecules CH, N_2, O_2, F_2, CH_4, C_2H_6, C_2H_4, and C_2H_2 could all be fitted simultaneously with an average discrepancy of about ± 0.4 ev *per bond*. Among other results, α^2 was found to be about 0.17 for CH, 0.22 for N_2, and 0.09 for O_2, corresponding to 17 percent promotion from s^2p^2 toward sp^3 for carbon in CH, 22 percent from s^2p^3 toward sp^4 for nitrogen in N_2, and 9 percent from s^2p^4 toward sp^5 for oxygen in O_2. The magic formula also indicates that multiple bonds owe their strength to the π electrons, with the σ electrons in triple bonds making a *negative* contribution to the bond energy.]

THE JOURNAL OF CHEMICAL PHYSICS VOLUME 19, NUMBER 7 JULY, 1951

Orthonormal Sets of *LCAO* Molecular Orbitals for Second-Row Homopolar Diatomic Molecules*

ROBERT S. MULLIKEN
Department of Physics, University of Chicago, Chicago, Illinois
(Received March 22, 1951)

The forms of the *LCAO MO*'s (molecular orbitals approximated by linear combinations of atomic orbitals) of any homopolar second-row diatomic molecule are studied under the restriction that they shall form an orthogonal set. The requirement of orthogonality *per se* causes $1s-2s-2p\sigma$ hybridization (*forced hybridization*) among the *AO*'s (atomic orbitals) used in constructing the *LCAO*'s. Equations, tables, and figures are given showing how the degrees of hybridization in the members of mutually orthogonal sets of σ_g *LCAO MO*'s, likewise of σ_u *LCAO MO*'s, are related, as a function of two parameters: (a) assumed degree of hybridization in any *one* member of the set; (b) a parameter proportional to interatomic distance times effective nuclear charge. This is done using primarily Slater *AO*'s, but the effect of using *SCF* (self-consistent-field) *AO*'s is also studied.

Assuming that overlap integrals are good measures of bond strengths, it is shown that the effect of forced hybridization is to *diminish* bond strengths. It is concluded that this bond-weakening effect in *LCAO MO* valence theory is the counterpart of certain exchange repulsions which appear in the Heitler-London valence bond theory, namely those between bonding electrons on one atom and electrons in *different* (either bonding or lone-pair) *AO*'s on the other atom. The procedure used promises to give a good measure of the strengths of inner shell-outer shell interatomic repulsions; it tends to indicate that these are, in general, not large but not negligible. A paradox resulting from forced hybridization is touched on and more or less resolved; this paradox has to do with the method of counting the numbers of s and $p\sigma$ electrons per atom in a molecule described by *LCAO* methods.

I. INTRODUCTION

IN approximate molecular wave functions built from antisymmetrized products of *MSO*'s (molecular spin orbitals), it is very convenient if the *MO*'s used form an orthonormal set.[1] Ideally, the *MO*'s should be eigenfunctions of a molecular *SCF* problem ("*best MO*'s").[1,2] More practicably, they may be *MO*'s of the *LCAO* (linear combination of atomic orbitals) type, determined from solutions of an appropriate *LCAO*

* This work was assisted in part by the ONR under Task Order IX of Contract N6ori-20 with the University of Chicago.

[1] See R. S. Mulliken, J. chim. phys. **46**, 497 (1949). An *MSO* is a product of an *MO* (molecular orbital) and a one-electron spin function.

[2] C. C. J. Roothaan, to be published (see 1947–1948 and 1948–1949 ONR Reports of Spectroscopic Laboratory, Physics Department, University of Chicago).

secular equation (best, by Roothaan's *LCAO SCF* method).[2]

In symmetrical molecules, the forms of *LCAO MO*'s are partially determined by symmetry alone. The complete determination of course requires a knowledge of the matrix elements which appear in the secular equation. However, even in the absence of such knowledge, imposition of the restriction of orthonormality, alone, gives valuable information about the forms of the *LCAO MO*'s. This is particularly true in the case of homopolar-bond *LCAO MO*'s constructed from $2s,2p$-hybrid *AO*'s. A study of these will be the main subject of the present paper.

Following are the *MO* electron configurations for the ground states of several homopolar molecules:

$$\left.\begin{array}{l} H_2: 1\sigma_g)^2 \\ Li_2: 1\sigma_g)^2 1\sigma_u)^2 2\sigma_g)^2 \\ N_2: 1\sigma_g)^2 1\sigma_u)^2 2\sigma_g)^2 2\sigma_u)^2 1\pi_u)^4 3\sigma_g)^2 \\ O_2: 1\sigma_g)^2 1\sigma_u)^2 2\sigma_g)^2 2\sigma_u)^2 3\sigma_g)^2 1\pi_u)^4 1\pi_g)^2 \\ F_2: 1\sigma_g)^2 1\sigma_u)^2 2\sigma_g)^2 2\sigma_u)^2 3\sigma_g)^2 1\pi_u)^4 1\pi_g)^4. \end{array}\right\} \quad (1)$$

The *MO*'s in each configuration are given in order of increasing energy. Each *MO* symbol consists of the usual group theory species symbol, preceded by a number indicating the relative energy of the *MO* among those of its species.

The *MO*'s of (1), together with an additional excited *MO*, may be described in normalized *LCAO* approximation as follows:

$$\left.\begin{array}{l} 1\sigma_i \approx \sigma_i k = 2^{-\frac{1}{2}}(1 \pm S_k)^{-\frac{1}{2}}(k_a \pm k_b); \\ n\sigma_i \approx \sigma_i w_{ni} = 2^{-\frac{1}{2}}(1 \pm S_{wi})^{-\frac{1}{2}}(w_{nia} \pm w_{nib}); \\ 1\pi_i \approx \pi_i p = 2^{-\frac{1}{2}}(1 \mp S_\pi)^{-\frac{1}{2}}(\pi_a \mp \pi_b) \\ [n=2 \text{ or } 3;\ i=g \text{ (upper signs) or } u \text{ (lower signs).}] \end{array}\right\} \quad (2)$$

The *AO* symbols k, π, and the overlap integral symbol S_τ are explained in a preceding paper.[3,4] The *AO* symbol w denotes an *AO* hybrid consisting mainly of $2s$ and $2p\sigma$. The indices n, i on w_{ni} and $S_{wi}{}^{ni}$ (see Eqs. (5)–(7) following) are used to distinguish different hybrids w appropriate to the four different *MO*'s of type $n\sigma_i$. The main subject of the present paper will be the application of the restriction of mutual orthogonality to the determination of the forms of these four *MO*'s.

Commonly the *MO*'s $2\sigma_g$, $2\sigma_u$, and $3\sigma_g$ in N_2 are assumed to be either of the forms $\sigma_g 2s$, $\sigma_u 2s$, and $\sigma_g 2p$, respectively, or of the forms $\sigma_g 2di$, $\sigma_u 2di'$, and $\sigma_g 2di'$. These two *LCAO-MO* alternatives correspond to the two alternative valence-bond electron configurations for N_2 stated in (3) of a preceding paper.[3] But, just as was mentioned there, it is to be expected that a more accurate description of the structure of N_2 can be obtained by looking for the best hybrids of general type (here $\sigma_i w_{ni}$) instead of restricting ourselves to the two special alternatives mentioned.

II. ORTHOGONALIZATION OF $2\sigma_i$ AND $3\sigma_i$ WITH RESPECT TO $1\sigma_i$

Since any two *MO*'s of different group theory species (σ_g, σ_u, π_u, π_g, $\cdots$) are automatically orthogonal, our problem reduces to the determination of a mutually orthogonal set

$$1\sigma_g,\ 2\sigma_g,\ 3\sigma_g,$$

and of a second mutually orthogonal set

$$1\sigma_u,\ 2\sigma_u,\ 3\sigma_u.$$

To begin with, we somewhat arbitrarily take $1\sigma_g$ and $1\sigma_u$ to be of the precise forms given by the first of Eqs. (2).[4] This is justifiable on grounds of simplicity and by the fact that if the k *AO*'s used in Eq. (2) are best *SCF* $1s$ *AO*'s of the free atoms, then $1\sigma_g$ and $1\sigma_u$ are probably close to best *MO*'s.

The required orthogonality conditions may be written:

$$\int (1\sigma_i)(n\sigma_i)dv = 0; \quad (3)$$

$$\int (2\sigma_i)(3\sigma_i)dv = 0 \quad (4)$$

$$(n=2 \text{ or } 3;\quad i=g \text{ or } u).$$

Our main interest will be in the relations between the *LCAO* approximations $\sigma_i w_{ni}$ to the $n\sigma_i$'s for $n=2$ and 3; these relations can be obtained using Eqs. (3) and (4). The $\sigma_i w_{ni}$'s are linear combinations (see Eqs. (2)) of the *AO*'s w_{ni}. As already stated, the latter are essentially $2s,2p\sigma$ hybrids. However, when the condition Eq. (3) is imposed, it is found that some $1s$ must also be mixed in; not a large amount, but in general too much to be neglected in obtaining a good orthogonal set of *LCAO MO*'s. It will be convenient before using Eq. (4) to obtain a general expression for the amount of this admixture in any w_{ni} *AO*.

In terms of an (intratomically) *mutually orthogonal set of initial pure AO's* k, s, σ (i.e., $1s$, $2s$, $2p\sigma$), one can write the hybrid *AO*'s w_{ni}, *in normalized form*, as follows:

$$\left.\begin{array}{l} w_{ni} = (h_{ni} + b_{ni} \cdot k)(1 + b_{ni}{}^2)^{-\frac{1}{2}}, \\ \text{with} \\ h_{ni} = \alpha_{ni} \cdot s + \beta_{ni} \cdot \sigma. \end{array}\right\} \quad (5)$$

Here the h_{ni}'s are hybrid *AO*'s of the type h_β,[3] with $\beta = \beta_{ni}$. Since s and σ are orthogonal by symmetry, $\alpha_{ni}{}^2 = 1 - \beta_{ni}{}^2$. For the intratomically orthogonal set of *AO*'s *throughout this paper* (except as otherwise explicitly stated), Slater $1s$ *AO*'s, *orthogonalized* Slater $2s$ *AO*'s, and usually Slater, but sometimes *SCF*, $2p\sigma$ *AO*'s will be used.[5]

[3] R. S. Mulliken, J. Chem. Phys. **19**, 900 (1951). See Table I and Eq. (2) for *AO* symbols, Table IV for overlap integral notation.

[4] For $1\sigma_i$ in (2), the normalizing factor can be simplified to $2^{-\frac{1}{2}}$ for all the molecules in (1) except H_2, since S_k in the other cases is negligibly small (see R. S. Mulliken, J. Am. Chem. Soc. **72**, 4493 (1950)).

[5] See Mulliken, Rieke, Orloff, and Orloff, J. Chem. Phys. **17**, 1248 (1949). See Table I and Eqs. (7) for Slater *AO*'s. See Eqs. (8) for orthogonalized Slater $2s$ *AO*'s.

TABLE IA. Relations of hybridization coefficients for mutually orthogonal *LCAO MO*'s $2\sigma_g$ and $3\sigma_g$.[a, b] Negative hybrids.

ρ		$\alpha=0$, $\beta=-1$	0.1	0.2	0.3	0.4	0.5	0.6, −0.8	0.7
3.0	*SI*	$\alpha'=0.925$	0.963	0.991	0.999	0.969	0.880	0.724	0.518
		$\beta'=-0.381$	−0.269	−0.132	0.042	0.249	0.475	0.689	0.856
	SCF	$\alpha'=0.887$	0.939	0.980	1.000	0.967	0.848	0.645	0.406
		$\beta'=-0.461$	−0.349	−0.199	0.002	0.254	0.529	0.764	0.914
3.4	*SI*	$\alpha'=0.936$	0.968	0.992	1.000	0.979	0.913	0.785	0.593
		$\beta'=-0.353$	−0.252	−0.129	0.021	0.202	0.408	0.620	0.805
3.8	*SI*	$\alpha'=0.946$	0.973	0.993	1.000	0.983	0.929	0.820	0.647
		$\beta'=-0.326$	−0.231	−0.117	0.019	0.182	0.370	0.572	0.763
4.0	*SI*	$\alpha'=0.950$	0.976	0.994	1.000	0.984	0.934	0.832	0.667
		$\beta'=-0.312$	−0.219	−0.109	0.022	0.178	0.359	0.555	0.745
	SCF	$\alpha'=0.922$	0.956	0.984	0.999	0.989	0.931	0.802	0.595
		$\beta'=-0.386$	−0.294	−0.178	−0.033	0.148	0.365	0.597	0.804
4.2	*SI*	$\alpha'=0.954$	0.978	0.995	1.000	0.984	0.937	0.841	0.684
		$\beta'=-0.299$	−0.208	−0.101	0.027	0.177	0.351	0.541	0.730
4.6	*SI*	$\alpha'=0.963$	0.984	0.997	0.999	0.983	0.938	0.851	0.708
		$\beta'=-0.271$	−0.181	−0.077	0.044	0.185	0.347	0.525	0.706
5.0	*SI*	$\alpha'=0.970$	0.988	0.998	0.998	0.980	0.936	0.855	0.723
		$\beta'=-0.244$	−0.154	−0.052	0.065	0.199	0.351	0.518	0.691
	SCF	$\alpha'=0.950$	0.975	0.993	1.000	0.989	0.946	0.855	0.696
		$\beta'=-0.311$	−0.224	−0.121	0.002	0.150	0.324	0.519	0.718
6.0	*SI*	$\alpha'=0.984$	0.997	1.000	0.992	0.969	0.925	0.851	0.737
		$\beta'=-0.179$	−0.087	0.013	0.125	0.247	0.381	0.526	0.676
	SCF	$\alpha'=0.970$	0.988	0.998	0.998	0.983	0.943	0.867	0.740
		$\beta'=-0.241$	−0.155	−0.057	0.056	0.185	0.333	0.498	0.672
7.0	*SI*	$\alpha'=0.993$	0.999	0.997	0.984	0.955	0.909	0.838	0.736
		$\beta'=-0.121$	−0.027	0.074	0.181	0.296	0.418	0.545	0.677
	SCF	$\alpha'=0.984$	0.996	1.000	0.994	0.974	0.933	0.865	0.756
		$\beta'=-0.180$	−0.092	0.004	0.110	0.228	0.359	0.502	0.655
8.0	*SI*	$\alpha'=0.997$	1.000	0.993	0.974	0.942	0.894	0.825	0.730
		$\beta'=-0.076$	0.021	0.121	0.226	0.335	0.448	0.565	0.683
	SCF	$\alpha'=0.992$	0.999	0.998	0.987	0.963	0.921	0.855	0.757
		$\beta'=-0.128$	−0.039	0.057	0.159	0.270	0.389	0.518	0.653

The values of the coefficients b_{ni} of Eqs. (5) can be determined by substituting according to Eqs. (2) and (5) for $1\sigma_i$ and $n\sigma_i$ in Eq. (3), and evaluating; one obtains:[6]

$$\left.\begin{aligned} b_{ni} &= \mp S_{k\beta}{}^{ni} = \mp(\alpha_{ni}S_{ks} + \beta_{ni}S_{k\sigma}) \\ &\text{(upper sign for } i=g\text{, lower for } i=u\text{).}\end{aligned}\right\} \quad (6)$$

Values of $S_{k\beta}$ for any value of $\beta=\beta_{ni}$ can be obtained from Table X of reference 3; from these it is seen that b_{ni}, while never large, may be of appreciable importance.

From Eq. (6) the following useful expression for $S_w{}^{ni}$ of Eqs. (2) is obtained:[7]

$$\left.\begin{aligned} S_{wi}{}^{ni} &= [S_\beta{}^{ni} \mp 2(S_{k\beta}{}^{ni})^2][1+(S_{k\beta}{}^{ni})^2]^{-1}. \\ &\text{(The upper and lower signs apply to } S_{wg} \text{ and } S_{wu}\text{, respectively).}\end{aligned}\right\} \quad (7)$$

The definition, and tables of values, of S_β and $S_{k\beta}$ are given in a preceding paper.[3] The quantity $(S_{k\beta}{}^{ni})^2 \ll 1$ always. The notation $S_{wi}{}^{ni}$ in Eq. (7) is an abbreviation for $S_{wi}(\beta)$ with β taken as β_{ni}. Equation (7) thus describes *two functions* of β_{ni}, namely, $S_{wg}(\beta_{ni})$ and $S_{wu}(\beta_{ni})$, differing slightly because of the term $\mp 2(S_{k\beta}{}^{ni})^2$.

As discussed in Sec. V of reference 3, $S_{k\beta}$ in general depends not only on β (here β_{ni}), but also on the "two-quantum ρ," and additionally, through ω_A and t_A (see reference 3, Eq. (10)), on the particular atom A:

$$S_{k\beta}{}^{ni} = S_{k\beta}(\beta_{ni};\ \omega_A\rho,\ t_A).$$

The same is then true of b_{ni} in Eqs. (5)–(6). Hence also, w_{ni} and $S_{wi}{}^{ni}$ of Eqs. (5) and (7) depend not only on

[6] The second equality in Eq. (6) follows from $S_{k\beta}{}^{ni} \equiv \int(k_\alpha)(h_{nib})d\nu$, use of the second of Eqs. (5), and the definitions of S_{ks} and $S_{k\sigma}$ (see reference 3, Table IV).

[7] By definition, $S_w{}^{ni} \equiv \int(w_{nia})(w_{nib})d\nu$. On substituting for w_{ni} using Eqs. (5) and (6) and evaluating, dropping a negligible term in S_k,[4] Eq. (7) is readily obtained.

TABLE IA—*Continued.*

ρ		$\alpha=$ $\beta=-0.7$	0.8 −0.6	−0.5	−0.4	−0.3	−0.2	−0.1	1 0
3.0	*Sl*	$\alpha'=$ 0.486	0.290	0.138	0.020	0.075	0.153	0.219	0.277
		$\beta'=$ 0.874	0.957	0.990	1.000	−0.997	−0.988	−0.976	−0.961
	SCF	$\alpha'=$ 0.373	0.179	0.043	0.058	0.136	0.199	0.253	0.299
		$\beta'=$ 0.928	0.984	0.999	−0.998	−0.991	−0.980	−0.968	−0.954
3.4	*Sl*	$\alpha'=$ 0.562	0.357	0.189	0.054	0.055	0.145	0.221	0.287
		$\beta'=$ 0.827	0.934	0.982	0.999	−0.999	−0.989	−0.975	−0.958
3.8	*Sl*	$\alpha'=$ 0.617	0.415	0.238	0.092	0.029	0.129	0.214	0.287
		$\beta'=$ 0.787	0.910	0.971	0.996	−0.999	−0.992	−0.977	−0.958
4.0	*Sl*	$\alpha'=$ 0.638	0.440	0.262	0.111	0.014	0.119	0.207	0.284
		$\beta'=$ 0.770	0.898	0.965	0.994	−1.000	−0.993	−0.978	−0.959
	SCF	$\alpha'=$ 0.561	0.337	0.157	0.017	0.094	0.183	0.257	0.320
		$\beta'=$ 0.828	0.942	0.988	1.000	−0.996	−0.983	−0.966	−0.947
4.2	*Sl*	$\alpha'=$ 0.656	0.461	0.283	0.130	0.001	0.108	0.200	0.280
		$\beta'=$ 0.755	0.887	0.959	0.992	1.000	−0.994	−0.980	−0.960
4.6	*Sl*	$\alpha'=$ 0.682	0.499	0.324	0.169	0.035	0.080	0.179	0.265
		$\beta'=$ 0.731	0.867	0.946	0.986	0.999	−0.997	−0.984	−0.964
5.0	*Sl*	$\alpha'=$ 0.699	0.527	0.359	0.205	0.069	0.051	0.155	0.246
		$\beta'=$ 0.715	0.850	0.933	0.979	0.998	−0.999	−0.988	−0.969
	SCF	$\alpha'=$ 0.668	0.466	0.279	0.119	0.014	0.125	0.218	0.298
		$\beta'=$ 0.744	0.885	0.960	0.993	−1.000	−0.992	−0.976	−0.954
6.0	*Sl*	$\alpha'=$ 0.717	0.571	0.422	0.280	0.146	0.024	0.086	0.187
		$\beta'=$ 0.697	0.821	0.906	0.960	0.989	1.000	−0.996	−0.982
	SCF	$\alpha'=$ 0.717	0.547	0.376	0.217	0.075	0.049	0.158	0.252
		$\beta'=$ 0.697	0.837	0.927	0.976	0.997	−0.999	−0.988	−0.968
7.0	*Sl*	$\beta'=$ 0.718	0.590	0.459	0.331	0.206	0.088	0.023	0.127
		$\beta'=$ 0.696	0.807	0.888	0.944	0.978	0.996	−1.000	−0.992
	SCF	$\alpha'=$ 0.736	0.591	0.440	0.292	0.153	0.025	0.092	0.196
		$\beta'=$ 0.677	0.807	0.898	0.956	0.988	1.000	−0.996	−0.980
8.0	*Sl*	$\alpha'=$ 0.714	0.598	0.479	0.362	0.246	0.134	0.026	0.079
		$\beta'=$ 0.700	0.802	0.878	0.932	0.969	0.991	1.000	−0.997
	SCF	$\alpha'=$ 0.740	0.611	0.477	0.342	0.211	0.086	0.032	0.141
		$\beta'=$ 0.673	0.791	0.879	0.940	0.977	0.996	−1.000	−0.990

[a] The values of α' and β' were computed, at convenient intervals for interpolation, in accordance with Eqs. (16)–(19), for $i=g$. The values of S_s, $S_{s\sigma}$, and S_σ used in Eqs. (16) were taken from reference 3, Table VI, using the $2s^{or}-2s^{or}$ values of S_s in all cases, and either the $2s^{or}-2p\sigma^{Sl}$ and the $2p\sigma^{Sl}-2p\sigma^{Sl}$, *or in the cases marked SCF* the *carbon-carbon* $2s^{or}-2p\sigma^{SCF}$ and $2p\sigma^{SCF}-2p\sigma^{SCF}$, values of $S_{s\sigma}$ and S_σ. The values of S_{ks} ($2s^{or}$ values only) and of $S_{k\sigma}$ ($2p\sigma^{Sl}$, or $2p\sigma^{SCF}$ in the cases marked *SCF*) are from the values for *C–C bonds* in reference 3, Table IX.

[b] The values of α' and β' in the present table apply strictly only to C–C bonds, because S_s and S_{ks} are based on *carbon atom* $2s^{or}$ *AO's*, and also, *in the cases marked SCF*, because $S_{s\sigma}$ and S_σ are based on carbon atom $2p\sigma^{SCF}$ *AO's*. However, they should be approximately valid for other bonds, especially B–B and N–N; though less accurately so for the *SCF* than for the Slater α''s and β''s. (See Table III for further light on this.)

β_{ni} and ρ, but also (although here only to a slight extent) on the particular atom A.

Certain alternative forms of the *LCAO MO*'s $n\sigma_i$ of Eqs. (2) are of possible interest. In particular, one can write:

$$n\sigma_i \approx \sigma_i w_{ni} = l_{ni}\cdot\sigma_i h_{ni} + m_{ni}\cdot\sigma_i k, \tag{8}$$

where

$$\left.\begin{aligned}&\sigma_i h_{ni} = 2^{-\frac{1}{2}}(1\pm S_\beta{}^{ni})^{-\frac{1}{2}}(h_{nia}\pm h_{nib}).\\&\text{(Upper signs for } i=g\text{, lower for } i=u).\end{aligned}\right\} \tag{9}$$

The expressions $\sigma_i h_{ni}$, like σ_{ik} in (2), are normalized *LCAO* forms. By making use of Eqs. (2), (5), and (6), one finds:

$$\left.\begin{aligned}&l_{ni} = (1\pm S_\beta{}^{ni})^{\frac{1}{2}}[1\pm S_\beta{}^{ni} - (S_{k\beta}{}^{ni})^2]^{-\frac{1}{2}},\\&m_{ni} = \mp S_{k\beta}{}^{ni}[1\pm S_\beta{}^{ni} - (S_{k\beta}{}^{ni})^2]^{-\frac{1}{2}}.\end{aligned}\right\} \tag{10}$$

Note that $l_{ni}{}^2+m_{ni}{}^2>1$; this is because $\sigma_i h_{ni}$ is not quite orthogonal to $\sigma_i k$.

A further transformation of Eqs. (8) can be made to the form:

$$n\sigma_i \approx \sigma_i w_{ni} = q_{ni}\cdot\sigma_i s + r_{ni}\cdot\sigma_i p + m_{ni}\cdot\sigma_i k, \tag{11}$$

where

$$\left.\begin{aligned}&\sigma_i s = 2^{-\frac{1}{2}}(1\pm S_s)^{-\frac{1}{2}}(s_a\pm s_b),\\&\sigma_i p = 2^{-\frac{1}{2}}(1\pm S_\sigma)^{-\frac{1}{2}}(p\sigma_a\pm p\sigma_b).\\&\text{(Upper signs for } i=g\text{, lower for } i=u).\end{aligned}\right\} \tag{12}$$

The expressions $\sigma_i s$ and $\sigma_i p$ are normalized *LCAO* forms, frequently assumed as *LCAO MO*'s for first row diatomic molecules. Making use of the second of Eqs. (5) for h_{ni}, of Eq. (9), and of Eq. (10) for l_{ni}, one finds:

$$\left.\begin{aligned}&q_{ni} = \alpha_{ni}(1\pm S_s)^{\frac{1}{2}}[1\pm S_\beta{}^{ni} - (S_{k\beta}{}^{ni})^2]^{-\frac{1}{2}}\\&r_{ni} = \beta_{ni}(1\pm S_\sigma)^{\frac{1}{2}}[1\pm S_\beta{}^{ni} - (S_{k\beta}{}^{ni})^2]^{-\frac{1}{2}}.\\&\text{(Upper signs for } i=g\text{, lower for } i=u).\end{aligned}\right\} \tag{13}$$

Note that $q_{ni}{}^2+r_{ni}{}^2+m_{ni}{}^2>1$ (considerably), because $\sigma_i s$ and $\sigma_i p$

TABLE IB. Relations of hybridization coefficients for mutually orthogonal *LCAO MO*'s $2\sigma_g$ and $3\sigma_g$. Positive hybrids.

ρ		$\alpha=1$ $\beta=0$	0.1	0.2	0.4	0.8 0.6	0.6 0.8	0.4	0.2	0 1
3.0	*SI*	$\alpha'=$ 0.277	0.329	0.378	0.467	0.556	0.662	0.752	0.839	0.925
		$\beta'=-0.961$	−0.944	−0.926	−0.884	−0.831	−0.749	−0.659	−0.544	−0.381
	SCF	$\alpha'=$ 0.299	0.341	0.380	0.453	0.527	0.619	0.703	0.790	0.887
		$\beta'=-0.954$	−0.940	−0.925	−0.892	−0.850	−0.785	−0.712	−0.613	−0.461
3.4	*SI*	$\alpha'=$ 0.287	0.346	0.399	0.496	0.590	0.697	0.783	0.862	0.936
		$\beta'=-0.958$	−0.938	−0.917	−0.868	−0.807	−0.717	−0.623	−0.507	−0.353
3.8	*SI*	$\alpha'=$ 0.287	0.352	0.410	0.515	0.614	0.722	0.806	0.880	0.946
		$\beta'=-0.958$	−0.936	−0.912	−0.857	−0.789	−0.692	−0.592	−0.476	−0.326
4.0	*SI*	$\alpha'=$ 0.284	0.352	0.413	0.522	0.623	0.732	0.815	0.887	0.950
		$\beta'=-0.959$	−0.936	−0.911	−0.853	−0.782	−0.681	−0.579	−0.461	−0.312
	SCF	$\alpha'=$ 0.320	0.376	0.425	0.515	0.601	0.698	0.776	0.850	0.922
		$\beta'=-0.947$	−0.927	−0.905	−0.857	−0.799	−0.716	−0.630	−0.526	−0.386
4.2	*SI*	$\alpha'=$ 0.280	0.351	0.414	0.527	0.630	0.741	0.824	0.894	0.954
		$\beta'=-0.960$	−0.936	−0.910	−0.850	−0.776	−0.672	−0.567	−0.448	−0.299
4.6	*SI*	$\alpha'=$ 0.265	0.341	0.410	0.531	0.641	0.756	0.839	0.907	0.963
		$\beta'=-0.964$	−0.940	−0.912	−0.848	−0.768	−0.655	−0.545	−0.421	−0.271
5.0	*SI*	$\alpha'=$ 0.246	0.327	0.401	0.530	0.647	0.767	0.851	0.918	0.970
		$\beta'=-0.969$	−0.945	−0.916	−0.848	−0.762	−0.642	−0.525	−0.397	−0.244
	SCF	$\alpha'=$ 0.298	0.368	0.430	0.540	0.640	0.746	0.824	0.892	0.950
		$\beta'=-0.954$	−0.930	−0.903	−0.842	−0.768	−0.666	−0.566	−0.453	−0.311
6.0	*SI*	$\alpha'=$ 0.187	0.279	0.363	0.513	0.650	0.785	0.875	0.940	0.984
		$\beta'=-0.982$	−0.960	−0.932	−0.858	−0.760	−0.620	−0.485	−0.341	−0.179
	SCF	$\alpha'=$ 0.252	0.336	0.411	0.542	0.659	0.776	0.857	0.921	0.970
		$\beta'=-0.968$	−0.942	−0.912	−0.840	−0.752	−0.631	−0.515	−0.389	−0.241
7.0	*SI*	$\alpha'=$ 0.127	0.225	0.317	0.486	0.642	0.794	0.891	0.956	0.993
		$\beta'=-0.992$	−0.974	−0.948	−0.874	−0.767	−0.608	−0.454	−0.295	−0.121
	SCF	$\alpha'=$ 0.196	0.291	0.377	0.530	0.664	0.795	0.881	0.942	0.984
		$\beta'=-0.980$	−0.957	−0.926	−0.848	−0.747	−0.606	−0.474	−0.335	−0.180
8.0	*SI*	$\alpha'=$ 0.079	0.179	0.276	0.458	0.630	0.798	0.901	0.966	0.997
		$\beta'=-0.997$	−0.984	−0.961	−0.889	−0.777	−0.602	−0.433	−0.259	−0.076
	SCF	$\alpha'=$ 0.141	0.243	0.338	0.509	0.661	0.806	0.897	0.957	0.992
		$\beta'=-0.990$	−0.970	−0.941	−0.861	−0.750	−0.591	−0.443	−0.291	−0.128

are far from being orthogonal to each other, while neither is quite orthogonal to $\sigma_i k$.

The following integrals S_i are quantitative measures of the non-orthogonalities of $\sigma_i s$ and $\sigma_i p$:

$$S_i \equiv \int (\sigma_i s)(\sigma_i p)\,dv = \pm S_{s\sigma}[(1\pm S_s)(1\pm S_\sigma)]^{-\frac{1}{2}}. \quad \text{(Upper signs for } i=g\text{, lower for } i=u\text{).} \tag{14}$$

III. ORTHOGONAL *LCAO* HYBRID PAIRS $2\sigma_g$, $3\sigma_g$, AND $2\sigma_u$, $3\sigma_u$

In Sec. II the complications involved in the minor differences between the *AO* hybrid forms w_{ni} and h_{ni} of Eqs. (5) have been taken care of. We now turn to the main problem of determining relations between the coefficients β_{ni} (or α_{ni}; recall that $\alpha_{ni}^2+\beta_{ni}^2=1$ always) so that $3\sigma_g$ shall be orthogonal to $2\sigma_g$, and $3\sigma_u$ to $2\sigma_u$. Making use of Eqs. (5), (6), and (2) these four *MO*'s in *LCAO* approximation can all be reduced to the form:

$$n\sigma_i \approx 2^{-\frac{1}{2}}[1\pm S_\beta{}^{ni}-(S_{k\beta}{}^{ni})^2]^{-\frac{1}{2}}[\alpha_{ni}(s_a\pm s_b) + \beta_{ni}(p\sigma_a\pm p\sigma_b)\mp S_{k\beta}{}^{ni}(k_a\pm k_b)] \quad (n=2 \text{ or } 3;\ i=g \text{ (upper signs) or } u \text{ (lower signs)}). \tag{15}$$

On substituting by means of Eq. (15) for $2\sigma_i$ and $3\sigma_i$ in the orthogonality condition Eq. (4), and making the notation changes,[8]

$$\alpha \equiv \alpha_{2i} \text{ (or } \alpha_{3i}\text{)};\ \alpha_i' \equiv \alpha_{3i} \text{ (or } \alpha_{2i}\text{)};$$
$$\beta \equiv \beta_{2i} \text{ (or } \beta_{3i}\text{)};\ \beta_i' \equiv \beta_{3i} \text{ (or } \beta_{2i}\text{)},$$

one obtains:[9]

[8] Because of the mutuality of the orthogonality requirement, it does not matter whether we label α_{2i} as α and α_{3i} as α', or the reverse.

[9] Use is also made of the relation (see reference 6)

$$S_{k\beta}{}^{ni} = \alpha_{ni}S_{ks} + \beta_{ni}S_{k\sigma}.$$

TABLE IIA. Relations of hybridization coefficients for mutually orthogonal *LCAO MO*'s $2\sigma_u$ and $3\sigma_u$. Negative hybrids.[a]

ρ		$\alpha=0.0$ $\beta=-1.0$	0.2	0.4	0.6 -0.8	0.8 -0.6	-0.4	-0.2	-0.1	1.0 0.0
3.0	*SI*	$\alpha'=0.851$	0.846	0.842	0.837	0.831	0.825	0.818	0.813	0.807
		$\beta'=0.525$	0.533	0.540	0.547	0.556	0.565	0.575	0.582	0.590
	SCF	$\alpha'=0.875$	0.870	0.866	0.861	0.855	0.848	0.840	0.835	0.827
		$\beta'=0.484$	0.493	0.500	0.508	0.519	0.529	0.542	0.551	0.562
3.4	*SI*	$\alpha'=0.834$	0.823	0.813	0.803	0.791	0.778	0.764	0.754	0.742
		$\beta'=0.552$	0.568	0.582	0.596	0.612	0.628	0.646	0.657	0.670
3.8	*SI*	$\alpha'=0.832$	0.812	0.794	0.775	0.753	0.726	0.705	0.689	0.669
		$\beta'=0.555$	0.584	0.608	0.631	0.659	0.678	0.709	0.725	0.743
4.0	*SI*	$\alpha'=0.837$	0.811	0.788	0.764	0.735	0.707	0.675	0.655	0.631
		$\beta'=0.547$	0.585	0.616	0.645	0.678	0.707	0.738	0.756	0.776
	SCF	$\alpha'=0.850$	0.830	0.813	0.794	0.770	0.747	0.719	0.701	0.679
		$\beta'=0.526$	0.557	0.583	0.608	0.638	0.665	0.695	0.713	0.734
4.2	*SI*	$\alpha'=0.844$	0.812	0.784	0.755	0.719	0.685	0.645	0.621	0.592
		$\beta'=0.536$	0.583	0.621	0.656	0.695	0.729	0.764	0.784	0.806
4.6	*SI*	$\alpha'=0.869$	0.825	0.784	0.743	0.690	0.641	0.584	0.551	0.511
		$\beta'=0.495$	0.565	0.620	0.670	0.724	0.768	0.811	0.835	0.860
5.0	*SI*	$\alpha'=0.898$	0.844	0.792	0.737	0.666	0.601	0.527	0.484	0.434
		$\beta'=0.441$	0.537	0.611	0.676	0.746	0.799	0.850	0.875	0.901
	SCF	$\alpha'=0.876$	0.833	0.793	0.750	0.696	0.646	0.587	0.552	0.510
		$\beta'=0.482$	0.553	0.610	0.661	0.718	0.764	0.809	0.834	0.860
6.0	*SI*	$\alpha'=0.957$	0.897	0.826	0.741	0.628	0.522	0.407	0.343	0.271
		$\beta'=0.291$	0.442	0.564	0.671	0.778	0.853	0.913	0.939	0.962
	SCF	$\alpha'=0.923$	0.862	0.800	0.751	0.642	0.560	0.471	0.419	0.360
		$\beta'=0.385$	0.506	0.601	0.683	0.766	0.828	0.882	0.908	0.933
7.0	*SI*	$\alpha'=0.985$	0.936	0.860	0.757	0.610	0.470	0.323	0.244	0.159
		$\beta'=0.170$	0.353	0.511	0.653	0.793	0.883	0.947	0.970	0.987
	SCF	$\alpha'=0.961$	0.898	0.820	0.729	0.608	0.497	0.379	0.315	0.244
		$\beta'=0.276$	0.441	0.572	0.685	0.794	0.868	0.925	0.949	0.970
8.0	*SI*	$\alpha'=0.996$	0.957	0.884	0.772	0.602	0.438	0.269	0.181	0.090
		$\beta'=0.094$	0.290	0.468	0.635	0.798	0.899	0.963	0.983	0.996
	SCF	$\alpha'=0.983$	0.927	0.844	0.737	0.589	0.453	0.313	0.239	0.160
		$\beta'=0.183$	0.375	0.536	0.675	0.808	0.892	0.950	0.971	0.987

[a] Same as for Table I, except here we take the case $i=u$.

where
$$\left.\begin{aligned} A_i\alpha\alpha_i'+B_i(\alpha\beta_i'+\alpha_i'\beta)+C_i\beta\beta_i'=0,\\ A_i\equiv 1\pm S_s-S_{ks}^2;\quad B_i\equiv\pm S_{s\sigma}-S_{ks}S_{k\sigma};\\ C_i\equiv 1\pm S_\sigma-S_{k\sigma}^2.\end{aligned}\right\}\quad(16)$$

Dividing the first Eq. (16) through by $\beta\beta_i'$, letting

$$\gamma\equiv\beta/\alpha;\quad \gamma_i'\equiv\beta_i'/\alpha_i';\qquad(17)$$

and solving for γ_i', one obtains:[10]

$$\gamma_i'=-\left(\frac{A_i+B_i\gamma}{B_i+C_i\gamma}\right)=-\left(\frac{A_i\alpha+B_i\beta}{B_i\alpha+C_i\beta}\right).\qquad(18)$$

With γ_i' known, α_i' and β_i' are easily obtained[10] from

$$\alpha_i'=(1+\gamma_i'^2)^{-\frac{1}{2}};\quad \beta_i'=\gamma_i'(1+\gamma_i'^2)^{-\frac{1}{2}}.\qquad(19)$$

[10] Since the whole discussion is symmetrical (see reference 8) as regards α and α', or β and β', Eq. (18) is equally valid with γ' replaced by γ and γ, α, and β replaced by γ', α', and β'. Similarly, Eq. (19) still holds if the primes are dropped.

For any assigned values of α or β, values of α_g' and β_g', and of α_u' and β_u', can now be computed using Eqs. (16)–(19). For purposes of interpolation, it is convenient to compute and tabulate α_i' and β_i' values corresponding to 0.1 or in some cases 0.2 intervals of both α and β. This has been done, and the results are recorded in Tables I (σ_g case) and Table II (σ_u case).

The general nature of the relations between the α', β' and α, β values can best be seen from a graphical presentation. This is given, for the special ρ value 4.0 (approximately the actual value for the N_2 molecule at equilibrium), in Fig. 1 (σ_g case) and Fig. 2 (σ_u case). At the same time, Figs. 1 and 2 show how the *overlap integrals* S_{wi} (see Eqs. (2) and (7)) corresponding to mutually orthogonal *LCAO* pairs such as $2\sigma_g$, $3\sigma_g$ (β_g and β_g') or $2\sigma_u$, $3\sigma_u$ (β_u and β_u') are related. (See the caption of Fig. 1 for a more detailed explanation.)

TABLE IIB. Relations of hybridization coefficients for mutually orthogonal *LCAO MO*'s $2\sigma_u$ and $3\sigma_u$. Positive hybrids.[a, b]

ρ		$\alpha=1.0$ $\beta=0.0$	0.1	0.2	0.3	0.4	0.45	0.5	0.55	0.8 0.6
3.0	*SI*	$\alpha'=$ 0.807	0.799	0.786	0.762	0.705	0.629	0.388	0.675	0.996
		$\beta'=$ 0.590	0.602	0.619	0.648	0.709	0.778	0.922	−0.738	0.086
	SCF	$\beta'=$ 0.827	0.816	0.799	0.763	0.656	0.452	0.393	0.994	0.981
		$\beta'=$ 0.562	0.578	0.602	0.646	0.755	0.892	−0.920	−0.110	0.194
3.4	*SI*	$\alpha'=$ 0.742	0.727	0.704	0.666	0.590		0.365	0.019	0.660
		$\beta'=$ 0.670	0.687	0.710	0.746	0.807		0.931	1.000	−0.751
3.8	*SI*	$\alpha'=$ 0.669	0.644	0.608	0.553	0.456		0.243	0.026	0.329
		$\beta'=$ 0.743	0.765	0.794	0.833	0.890		0.970	1.000	−0.944
4.0	*SI*	$\alpha'=$ 0.631	0.599	0.556	0.493	0.386		0.175	0.014	0.294
		$\beta'=$ 0.776	0.801	0.831	0.870	0.923		0.985	−1.000	−0.956
	SCF	$\alpha'=$ 0.679	0.650	0.607	0.540	0.416		0.132	0.149	0.538
		$\beta'=$ 0.734	0.760	0.794	0.842	0.909		0.991	−0.989	−0.843
4.2	*SI*	$\alpha'=$ 0.592	0.555	0.506	0.434	0.320		0.114	0.054	0.286
		$\beta'=$ 0.806	0.832	0.863	0.901	0.948		0.994	−0.999	−0.958
4.6	*SI*	$\alpha'=$ 0.511	0.462	0.398	0.311	0.184		0.013		0.323
		$\beta'=$ 0.860	0.887	0.917	0.950	0.983		−1.000		−0.947
5.0	*SI*	$\alpha'=$ 0.434	0.374	0.298	0.200	0.068		0.116		0.369
		$\beta'=$ 0.901	0.928	0.955	0.980	0.998		−0.993		−0.929
	SCF	$\alpha'=$ 0.510	0.458	0.391	0.298	0.163		0.045		0.363
		$\beta'=$ 0.860	0.889	0.921	0.955	0.987		−0.999		−0.932
6.0	*SI*	$\beta'=$ 0.271	0.191	0.098	0.011	0.139		0.290		0.465
		$\beta'=$ 0.962	0.982	0.995	−1.000	−0.990		−0.957		−0.885
	SCF	$\alpha'=$ 0.360	0.292	0.209	0.107	0.022		0.188		0.399
		$\beta'=$ 0.933	0.957	0.978	0.994	−1.000		−0.982		−0.917
7.0	*SI*	$\alpha'=$ 0.159	0.068	0.031	0.139	0.257		0.385		0.523
		$\beta'=$ 0.987	0.998	−1.000	−0.990	−0.966		−0.923		−0.852
	SCF	$\alpha'=$ 0.244	0.166	0.077	0.026	0.146		0.286		0.448
		$\beta'=$ 0.970	0.986	0.997	−1.000	−0.989		−0.958		−0.894
8.0	*SI*	$\alpha'=$ 0.090	0.006	0.106	0.211	0.322		0.437		0.557
		$\beta'=$ 0.996	−1.000	−0.994	−0.977	−0.947		−0.899		−0.830
	SCF	$\alpha'=$ 0.160	0.076	0.016	0.118	0.229		0.353		0.490
		$\beta'=$ 0.987	0.997	−1.000	−0.993	−0.973		−0.936		−0.872

These relations for the S_{wi}'s have great interest in connection with bond strengths (see Sec. V).

IV. SIMPLIFIED FORMULAS FOR DETERMINING ORTHOGONAL *LCAO* HYBRID PAIRS

In view of the rather complicated forms of Eqs. (15)–(16) and of the resulting computations, a few supplementary computations have been made in which the terms in $(S_{k\beta}{}^{ni})^2$ in Eq. (15) and corresponding terms in Eqs. (16) have been neglected, and in which simple Slater $2s$ *AO*'s instead of orthogonalized Slater $2s$ *AO*'s have been used in computing S_s and $S_{s\sigma}$. For the σ_g case, the results are compared in Table III, for Slater $2p\sigma$ *AO*'s and some sample ρ values, with the more accurate results of Table I. In preparing Table III, the coefficients A_i, B_i, C_i in Eqs. (16) were replaced by

$$A_i=1\pm S_s;\quad B_i=\pm S_{s\sigma};\quad C_i=1\pm S_\sigma, \qquad (16a)$$

with Slater-*AO* values of S_s, $S_{s\sigma}$, S_σ (see left-hand columns in Table VI of reference 3). Equations (17)–(19) were then used to compute values of α' and β'.

It is seen that the results obtained for β' (hence also for α') for σ_g *LCAO MO*'s using the simplified relations (16a) do not differ appreciably, except in some cases for small ρ values, from those using the exact Eqs. (16). Thus so far as the relations of α' and β' to α and β for Slater-*AO LCAO* forms are concerned, the complications introduced in Sec. II, to make the $2s$ Slater *AO*'s orthogonal to $1s$ *AO*'s and the $2\sigma_i$ and $3\sigma_i$ *LCAO MO*'s orthogonal to $\sigma_i 1s$ *MO*'s, could just as well have been omitted at least for the σ_g case. In future work, advantage can be taken of this fact.

However, the effect of neglect of the corrections for orthogonality to $1s$ is somewhat greater for the *overlap integrals*: the $S_{wi}{}^{ni}$'s differ appreciably (although still not greatly) from the corresponding $S_\beta{}^{ni}$'s. This can be seen for example in a comparison between the $S_\beta(\beta)$ graph Fig. 1 of reference 3 for $\rho=4.0$ and the $S_{w\beta}(\beta)$

TABLE IIB—*Continued.*

ρ		$\alpha=$ $\beta=0.65$	0.7	0.7	0.6 0.8	0.5	0.4	0.3	0.2	0.1
3.0	*SI*	$\alpha'=$	0.921	0.914	0.888	0.875	0.867	0.861	0.857	0.854
		$\beta'=$	0.390	0.405	0.461	0.485	0.499	0.508	0.515	0.521
	SCF	$\alpha'=$	0.932	0.927	0.907	0.897	0.890	0.885	0.881	0.878
		$\beta'=$	0.363	0.374	0.421	0.443	0.456	0.466	0.473	0.479
3.4	*SI*	$\alpha'=$ 0.988	0.987	0.977	0.920	0.890	0.871	0.857	0.848	0.841
		$\beta'=-0.155$	0.160	0.213	0.391	0.456	0.491	0.513	0.529	0.542
3.8	*SI*	$\alpha'=$ 0.744	0.964	0.986	0.976	0.932	0.900	0.877	0.859	0.844
		$\beta'=-0.668$	−0.265	−0.167	0.218	0.363	0.436	0.481	0.512	0.536
4.0	*SI*	$\alpha'=$ 0.658	0.894	0.936	0.995	0.957	0.921	0.893	0.871	0.853
		$\beta'=-0.753$	−0.448	−0.352	0.098	0.290	0.390	0.450	0.492	0.523
	SCF	$\alpha'=$ 0.861	0.985	0.996	0.977	0.940	0.913	0.892	0.875	0.862
		$\beta'=-0.509$	−0.170	−0.093	0.214	0.340	0.409	0.452	0.483	0.507
4.2	*SI*	$\alpha'=$ 0.568	0.820	0.873	1.000	0.978	0.942	0.911	0.885	0.863
		$\beta'=-0.823$	−0.572	−0.489	−0.025	0.210	0.336	0.413	0.466	0.505
4.6	*SI*	$\alpha'=$ 0.520	0.717	0.768	0.968	0.999	0.980	0.951	0.921	0.894
		$\beta'=-0.854$	−0.697	−0.641	−0.251	0.025	0.197	0.310	0.389	0.448
5.0	*SI*	$\alpha'=$ 0.519	0.672	0.714	0.910	0.991	0.998	0.980	0.954	0.926
		$\beta'=-0.855$	−0.740	−0.700	−0.416	−0.135	0.059	0.198	0.300	0.379
	SCF	$\alpha'=$ 0.556	0.743	0.789	0.971	1.000	0.982	0.955	0.927	0.900
		$\beta'=-0.831$	−0.669	−0.614	−0.240	0.022	0.188	0.298	0.376	0.435
6.0	*SI*	$\alpha'=$	0.655	0.682	0.837	0.932	0.982	0.999	0.996	0.980
		$\beta'=$	−0.755	−0.731	−0.547	−0.360	−0.188	−0.039	0.089	0.198
	SCF	$\alpha'=$	0.643	0.678	0.868	0.965	0.998	0.996	0.978	0.952
		$\beta'=$	−0.766	−0.735	−0.496	−0.262	−0.066	0.089	0.210	0.306
7.0	*SI*	$\alpha'=$	0.668	0.688	0.810	0.896	0.953	0.985	0.999	0.998
		$\beta'=$	−0.744	−0.725	−0.586	−0.443	−0.303	−0.171	−0.048	0.066
	SCF	$\alpha'=$	0.628	0.654	0.810	0.914	0.972	0.997	0.998	0.985
		$\beta'=$	−0.778	−0.751	−0.586	−0.406	−0.234	−0.078	0.058	0.175
8.0	*SI*	$\alpha'=$	0.680	0.697	0.802	0.880	0.925	0.972	0.993	0.999[9]
		$\beta'=$	−0.733	−0.717	−0.597	−0.475	−0.354	−0.235	−0.121	−0.011
	SCF	$\alpha'=$	0.637	0.658	0.788	0.883	0.947	0.983	0.999	0.997
		$\beta'=$	−0.771	−0.753	−0.615	−0.469	−0.323	−0.181	−0.049	0.072

[a] Note that in each row, as β increases, β' first increases to $+1$ (which means the same hybrid as -1), then rises from -1 through 0 to positive values. For small ρ values, the passage to ± 1 and from there back through zero to positive values occurs very rapidly in a narrow range of β values.

[b] The column $\alpha=0$, $\beta=1$ at the extreme right of Table IIB has been omitted; it would be identical with the column $\alpha=0$, $\beta=-1$ of Table IIA.

and $S_{wu}(\beta)$ graphs Figs. 1 and 2 of the present paper. (See also Eq. (7) of the present paper, for the algebraic relations involved.)

If *SCF AO*'s are used instead of Slater *AO*'s, the relations of α' and β' to α and β, and the overlap integrals, are considerably altered (see Tables I and II).

V. FORCED HYBRIDIZATION AND ITS SIGNIFICANCE FOR BOND STRENGTHS

We may conveniently refer to *AO* hybrid pairs β_i, β_i' which correspond to mutually orthogonal σ_i *LCAO MO*'s as σ_i-*LCAO*-orthogonal hybrids ($i=g$ or u). A striking relation appearing for the σ_g hybrids in Fig. 1 is that the *totality* of positive hybrids ($\beta \geqslant 0$) is σ_g-*LCAO*-orthogonal to *only a portion* of the negative hybrids, leaving two ranges of the negative hybrids (one adjacent to $p\sigma$, the other to s) to be σ_g-*LCAO*-orthogonal *to each other*. For the σ_u hybrids (see Fig. 2), the roles of positive and negative hybrids are reversed.

The foregoing results appear in an interesting light when applied to a question raised earlier, as to the actual forms of the *MO*'s $2\sigma_g$ and $3\sigma_g$ for the N_2 molecule in (1). Suppose we knew $2\sigma_g$ to have $\beta=0$. In terms of $2s-2p\sigma$ hybridization (neglecting $1s$ admixture) $2\sigma_g$ would then be built from pure $2s$ *AO*'s, that is, it would be $\sigma_g s$ in the notation of Eqs. (2). Figure 1 would then show that $3\sigma_g$ (again neglecting $1s$ admixture) would by no means be built from pure $2p\sigma$ *AO*'s, that is, it would not be $\sigma_g p$, but would be built from negative hybrid *AO*'s with a considerable amount of $2s$ character. In a similar way, if we knew $3\sigma_g$ (neglecting $1s$) to be pure $\sigma_g p$, that is, $\beta'=1$, then, according to Fig. 1,

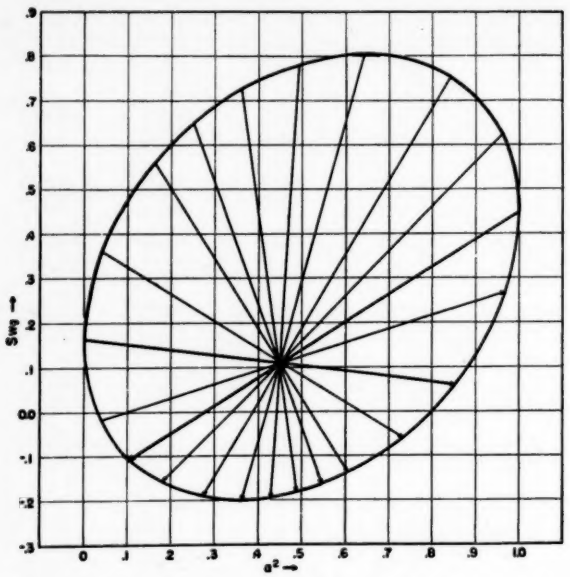

FIG. 1. $S_{wg}(\beta)$ plotted against $\alpha^2(\alpha^2=1-\beta^2)$, for $\rho=4.0$, with cross lines connecting sample pairs of hybrid $2s-2p\sigma$ *AO*'s which correspond to mutually orthogonal σ_g *LCAO MO*'s. The values of $S_{wg}(\beta)$ were computed using Eq. (7), referring to Table V of reference 3 for the S_β values and to Table X of reference 3 for the $S_{k\beta}$ values. For the graph, *carbon-carbon SCF* values of S_β and $S_{k\beta}$ from the tables mentioned were used. The upper segment of the graph, involving positive hybrids ($\beta \geqslant 0$), is drawn with an extra heavy line; the lower segment (negative hybrids, $\beta \leqslant 0$), with a lighter line. It should be noted that the $S_{wg}(\alpha^2)$ graph shown here differs only slightly—due only to the $S_{k\beta}$ terms in Eq. (7)—from an $S_\beta(\alpha^2)$ graph drawn for $\rho=4.0$ (see Fig. 1 of reference 3 for S_β graphs for several ρ-values).

The present Fig. 1 serves to illustrate certain relations which follow from the imposition of the condition of orthogonality (Eq. (4)) between the *LCAO MO*'s $2\sigma_g$ and $3\sigma_g$ of Eqs. (2): namely, (1), the relation between the hybridization coefficients of the two $2s-2p\sigma$ hybrid *AO*'s involved in Eq. (5); (2), the relation between the corresponding overlap integrals S_{wg} (see Eqs. (2) and (7)). The general character of these relations is displayed by the slanting arrows drawn in Fig. 1. Each of these goes from a selected sample point α, β (the points used were $\alpha=-0.2$, 0, $+0.2$, $+0.4$, $+0.5$, $+0.6$, $+0.7$, $+0.8$, and $\beta=+0.4$, $+0.2$, 0) to the corresponding *LCAO*-orthogonal point α', β' taken from Table I ($\beta=\pm(1-\alpha^2)^{\frac{1}{2}}$, $\beta'=\pm(1-\alpha'^2)^{\frac{1}{2}}$).

$2\sigma_g$ would of necessity be built from negative hybrid *AO*'s containing a rather large amount of $2p\sigma$ character. In an actual molecule, presumably $2\sigma_g$ will not have $\beta=0$ nor $3\sigma_g\,\beta'=1$, but σ_g-*LCAO*-orthogonality will still in general require relations similar to those just discussed.

This *forced hybridization*, as it may be called (see abstract for a summary), is a necessary corollary of the orthogonality requirement, and occurs without regard to and entirely aside from the usual expectation in valence-bond theory that hybridization occurs when thereby a bond can be strengthened. Indeed, the forced hybridization noted above to occur in $3\sigma_g$ if $2\sigma_g$ is assumed to be pure $\sigma_g 2s$ (or in $2\sigma_g$ if $3\sigma_g$ is assumed to be pure $\sigma_g 2p$) here causes very marked bond *weakening* rather than strengthening, since the overlap integral S_{wg} involved in $3\sigma_g$ (or in $2\sigma_g$ in the second assumed case) is much smaller than if $3\sigma_g$ had been pure $\sigma_g 2p$ (or pure $\sigma_g 2s$, in the second case). In general, the effect

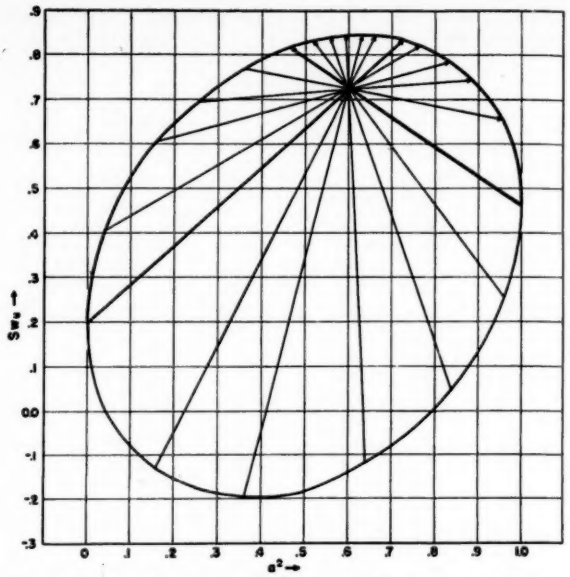

FIG. 2. $S_{wu}(\beta)$ plotted against α^2 for $\rho=4.0$, with cross lines connecting sample pairs of hybrid $2s-2p\sigma$ *AO*'s which correspond to mutually orthogonal σ_u *LCAO MO*'s. For further details, see caption of Fig. 1, changing g to u everywhere.

of forced hybridization, as judged by S_{wi} values, is to *weaken* very considerably the bonding power of bonding *MO*'s (σ_g here) but to *strengthen* markedly the antibonding power of *antibonding MO*'s (σ_u here—see Fig. 2).

An interpretation of the phenomenon of forced hybridization caused by the *LCAO* orthogonality requirement can be sketched along the following lines. In *AO electron-pair bond* theory, the total energy of interaction of two neutral atoms a and b is given approximately by a sum of terms of two kinds. These are: (1) bonding terms corresponding to pairwise exchange between a and b electrons; (2) nonbonded exchange terms between *all other* pairs of electrons one of which is on a and one on b; these correspond to repulsions, some of them strong, if both electrons are in *AO*'s of the same species (both σ, or both π), but to attractions (not very strong) for pairs one of which is σ, the other π. The net effect of the numerous terms in (2) is to diminish considerably the bond strength given by the term or terms in (1). The magnitudes of the repulsive nonbonded exchange terms in (2) may be estimated for molecules involving first and second row atoms by using the overlap integrals of the preceding paper[3] in connection with a semi-empirical procedure outlined earlier (proportionality of exchange repulsions to squares of corresponding overlap integrals: see reference 4 and Secs. IV and V of reference 3). Further details and applications will be given in another paper.

In *LCAO MO* theory, on the other hand, the bonding terms analogous to (1) of the *AO* theory are essentially resonance terms (simplest example,[1] the bonding electon in H_2^+); numerous exchange terms are also present but these very likely have no great effect on the bonding. In addition, there may be antibonding resonance terms which after subtracting related bonding terms

TABLE III. Relations of hybridization coefficients for mutually orthogonal *LCAO MO*'s $2\sigma_g$ and $3\sigma_g$ using simplified formulas.[a, b]

ρ			$\alpha=0$ $\beta=-1$	0.2	0.4	0.6 -0.8	0.8 -0.6	-0.4	-0.2	1 0
3.0	*Si*	β'	−0.402	−0.163	0.214	0.679	0.961	−1.000	−0.985	−0.955
	Sl	β'	−0.381	−0.132	0.249	0.689	0.957	1.000	−0.988	−0.961
4.0	*Si*	β'	−0.319	−0.119	0.168	0.549	0.900	0.995	−0.992	−0.956
	Sl	β'	−0.312	−0.109	0.178	0.555	0.898	0.994	−0.993	−0.959
5.0	*Si*	β'	−0.245	−0.054	0.196	0.516	0.849	0.979	−0.999	−0.969
	Sl	β'	−0.244	−0.052	0.199	0.518	0.850	0.979	−0.999	−0.969
6.0	*Si*	β'	−0.178	0.014	0.246	0.524	0.820	0.960	1.000	−0.982
	Sl	β'	−0.179	0.013	0.247	0.526	0.821	0.960	1.000	−0.982
7.0	*Si*	β'	−0.120	0.075	0.296	0.545	0.806	0.943	0.996	−0.992
	Sl	β'	−0.121	0.074	0.296	0.545	0.807	0.944	0.996	−0.992
8.0	*Si*	β'	−0.075	0.122	0.335	0.564	0.801	0.932	0.991	−0.997
	Sl	β'	−0.076	0.121	0.335	0.565	0.802	0.932	0.991	−0.997
ρ			$\alpha=1$ $\beta=0$	0.2	0.4	0.8 0.6	0.6 0.8	0.4	0.2	0 1
3.0	*Si*	β'	−0.955	−0.919	−0.878	−0.826	−0.748	−0.663	−0.555	−0.402
	Sl	β'	−0.961	−0.926	−0.884	−0.831	−0.749	−0.659	−0.544	−0.381
4.0	*Si*	β'	−0.956	−0.908	−0.851	−0.781	−0.681	−0.581	−0.466	−0.319
	Sl	β'	−0.959	−0.911	−0.853	−0.782	−0.681	−0.579	−0.461	−0.312
5.0	*Si*	β'	−0.969	−0.915	−0.847	−0.761	−0.641	−0.525	−0.397	−0.245
	Sl	β'	−0.969	−0.916	−0.848	−0.762	−0.642	−0.525	−0.397	−0.244
6.0	*Si*	β'	−0.982	−0.932	−0.858	−0.759	−0.618	−0.483	−0.340	−0.178
	Sl	β'	−0.982	−0.932	−0.858	−0.760	−0.620	−0.485	−0.341	−0.179
7.0	*Si*	β'	−0.992	−0.949	−0.874	−0.766	−0.606	−0.453	−0.293	−9.120
	Sl	β'	−0.992	−0.948	−0.874	−0.767	−0.608	−0.454	−0.295	−0.121
8.0	*Si*	β'	−0.997	−0.961	−0.889	−0.776	−0.601	−0.431	−0.258	−0.075
	Sl	β'	−0.997	−0.961	−0.889	−0.777	−0.602	−0.433	−0.259	−0.076

[a] See notes to Table I, except that here Eqs. (16a) are used instead of the second line of Eqs. (16), and the values of S_s, $S_{s\sigma}$, and S_σ are taken from the left-hand columns of Table VI of reference 3, corresponding to Slater *AO*'s only, with the Slater $2s$ *AO*'s *not* made orthogonal to $1s$. Unlike the Slater-*AO* results in Table I, the slightly less exact results here are valid equally for *all* homopolar 2-quantum bonds.

[b] For given values of α and β listed at the top of the table, computed values of β' are given in the table. For each ρ-value, *Si*β' denotes values computed using the *simplified* Slater-*AO* formula (16a), while *Sl*β' denotes *accurate Slater-AO* values (taken from Table I) computed using Eqs. (16). Corresponding α' values can be obtained if desired by using the relation $\alpha'=(1-\beta'^2)^{\frac{1}{2}}$.

give a net repulsion effect corresponding to the nonbonded repulsions between closed shells ("lone pairs") in the *AO* theory. It now seems fairly clear that in the *LCAO* theory the effects of forced hybridization are the counterpart of those nonbonded exchange repulsions in the *AO* theory which involve unlike *AO*'s in the two atoms. If in the given bonding (or antibonding) *LCAO MO* constructed from hybrid *AO*'s, the overlap integral S_{wi} between the latter is an approximate measure of bonding (or antibonding) power of the *MO*, then as we have seen above, the effect of forced hybridization is precisely to diminish (considerably) the total bond strength.

For example, in the ground state of an hypothetical molecule formed from two like atoms each with one $2s$ and one $2p\sigma$ electron, there would be two σ bonds in *AO* theory, or two doubly-occupied bonding orbitals ($2\sigma_g$ and $3\sigma_g$) in *LCAO MO* theory. In *AO* theory, there would be two strong bonding terms ($2s_a-2s_b$ and $2p\sigma_a-2p\sigma_b$), and two fairly strong exchange repulsion terms ($2s_a-2p\sigma_b$ and $2s_b-2p\sigma_a$). In *LCAO MO* theory, if one disregarded forced hybridization, there would be two resonance attractions corresponding to the bonding effect of two electrons in a $\sigma_g 2s$ and two in a $\sigma_g 2p$ *MO*. But forced hybridization in either or both[11] of $2\sigma_g$ and $3\sigma_g$ *prevents* them from being the one pure $\sigma_g 2s$ and the other pure $\sigma_g 2p$, and (as judged by the corresponding overlap integrals) diminishes their total bonding effect.

A further example of forced hybridization is the occurrence of some $1s$ in both $2\sigma_g$ and $3\sigma_g$ (see Eqs. (2), (5)); this has been neglected in the discussion just given. It will be seen from Eqs. (5) that its effect is to decrease S_{wg} still further, and so presumably to weaken bonding. For σ_u *MO*'s, Eq. (5) indicates an analogous effect in strengthening antibonding. This forced $1s$ hybridization can now be interpreted as the counterpart of the exchange repulsions which the *AO* theory predicts between the $1s$ shell of each atom and the $2s$ and $2p\sigma$ electrons of the other atom, in molecules such as for

[11] It can be shown that in this particular case (both $2\sigma_g$ and $3\sigma_g$ *MO*'s filled with two electrons) the complete antisymmetrized wave function is not changed except in superficial appearance, and its energy is not changed at all, by a change in the degrees of hybridization assumed, so long as $2\sigma_g$ and $3\sigma_g$ are orthogonal.

example N_2. The magnitude of this inner-shell effect on the bond energy, as judged by the S_{wi} values,[12] is perhaps not large, but far from negligible.[13]

The phenomenon of forced hybridization leads to a curious paradox. In a molecule such as N_2, to which Fig. 1 is approximately applicable, the $2\sigma_g$, $2\sigma_u$, and $3\sigma_g$ MO's (see Eqs. (1)) are each filled with two electrons. If these MO's are approximated by *LCAO* forms, and we then ask how much $2s$ and how much $2p\sigma$ population the above distribution corresponds to *for the two separate atoms*, we may obtain what at first seem like strange results. If we should assume no hybridization and then ignore the requirements of orthogonality, there would be two electrons each in $\sigma_g 2s$, $\sigma_u 2s$, and $\sigma_g 2p$; and, since each *LCAO MO* belongs equally to both atoms, we would say that this corresponds to two $2s$ and one $2p\sigma$ electron on each atom. On requiring *LCAO* orthogonality, it would still be allowable to assume that $2\sigma_g$ is pure $\sigma_g 2s$ and $2\sigma_u$ is pure $\sigma_u 2s$, but $3\sigma_g$ would then have to be a hybrid containing a considerable amount of $\sigma_g 2s$ mixed into $\sigma_g 2p$. If now we count each *LCAO MO* as divided equally between the two atoms, we obtain *more than two* $2s$ electrons on each atom. Why does this not violate the Pauli principle? It might be argued that there *is* a violation, resulting from unjustified initial assumptions. But this can be disproved, since, (1), with both the shells $2\sigma_g$ and $3\sigma_g$ filled, as here, the total wave function when antisymmetrized can be shown to be independent of how $2\sigma_g$ is chosen with respect to degree of hybridization,[11] and, (2), the form of $2\sigma_u$ is not subject to any direct restrictions depending on the numbers of electrons in $2\sigma_g$ and $3\sigma_g$.

The answer to the paradox undoubtedly lies in the implications of the fact that the pure forms $\sigma_g 2s$ and $\sigma_g 2p$ are *not orthogonal* (see Eq. (14)), or of the related fact that $2s$ of one atom is not orthogonal to $2p\sigma$ of the other. The importance of the paradox is as a warning that caution is needed in any attempt to conduct a census of $2s$ and $2p\sigma$ electrons in the separate atoms of a stable molecule on the basis of the *LCAO MO* method.

With regard to the specific question raised above for the configuration $2\sigma_g^2 2\sigma_u^2 3\sigma_g^2$ of N_2, it is to be noted that if $2\sigma_u$ were pure $\sigma_u 2s$, then, regardless[11] of what forms are used for $2\sigma_g$ and $3\sigma_g$, the best answer would appear to be that there are precisely two $2s$ and one $2p\sigma$ electrons on each atom. However, if (as is in principle possible, and in fact to be expected, for the best —energy-minimizing—wave function of N_2) the $2\sigma_u$ corresponds to some degree of $2s-2p\sigma$ hybridization, then the number of $2s$ electrons per atom is *less* than two and the number of $2p\sigma$ electrons correspondingly greater than one.

A more thorough analysis of the matters touched on in this Section will be postponed to a later paper.[14]

ACKNOWLEDGMENT

The author is very greatly indebted to Mr. Tracy J. Kinyon for his cooperation in the preparation of the tables and graphs. Mr. Kinyon carried out all the extensive numerical computations for the tables.

[12] Compare Figs. 1 and 2 with the $\rho=4.0$ figure in Fig. 1 of reference 3.

[13] This discussion is relevant to the question of Van Vleck's "nightmare of inner shells" (J. H. Van Vleck and A. Sherman, Revs. Modern Phys. **7**, 185 (1935)), and to the discussion of inner-shell-outer-shell repulsions in reference 4 and by Pitzer in an earlier paper.

[14] Reference should be made to P. O. Löwdin, J. Chem. Phys. **18**, 365 (1950) for a discussion of certain closely related problems and methods.

THE JOURNAL OF CHEMICAL PHYSICS VOLUME 19, NUMBER 7 JULY, 1951

The Properties of the Interstitial Compounds of Graphite. I. The Electronic Structure of Graphite Bisulfate

GERHART HENNIG
Argonne National Laboratory, Chicago, Illinois

(Received April 4, 1951)

1. The electrical resistance, its temperature dependence, and the Hall coefficients of graphite bisulfate compounds have been determined at various oxidation stages. The measurements have indicated that the oxidation removes electrons from a nearly full conduction band.

2. Reduction of the lamellar bisulfate compounds produces residue compounds which retain about a third of the bisulfate ions and half the sulfuric acid originally present in the lamellar compounds. The formula of the residue compounds is approximated by $C_n \cdot HSO_4 \cdot 4H_2SO_4$.

3. The model of a hypothetical graphite which has lost electrons from its conduction band, is approximated closely by these residue compounds, since the impurities are distributed in a state of high disorder. The lamellar compounds, on the other hand, may distort the band structure of graphite because they form a superlattice.

INTRODUCTION

GRAPHITE is a semiconductor in which the empty and full conduction bands are separated by either a small[1] or vanishing[2] energy gap. Those properties of graphite which depend on the conduction electrons should therefore be very sensitive to small amounts of impurities which change the number of electrons in the conduction bands. A strong dependence of properties on the purity of graphite has, in fact, been known for a long time. It was therefore decided to investigate the

[1] S. Mrozowski, Phys. Rev. **78**, 644 (1950).
[2] P. R. Wallace, Phys. Rev. **71**, 622 (1947).

relations between the electrical properties and the band structure experimentally by adding known amounts of electron donors or acceptors to graphite.

Nearly all chemical reactions of graphite produce either lamellar compounds or residue compounds.

Lamellar Compounds

In these substances, planes of carbon atoms alternate in a definite periodic sequence with single planes of the reactant. The period of alternation becomes smaller as the activity of the reactant is increased, but, with the exception of the ferric chloride compound, the concentration of the reactant remains constant in those planes which it has already invaded. A review of these substances has been published by Riley.[3] Numerous additional lamellar compounds, some of which will be described in subsequent papers, have been observed in this laboratory. It has always been assumed that all the lamellar compounds except the graphite salts were unionized. This will be shown in subsequent papers to be incorrect. The graphite salts, however, are known to be ionized,[4] i.e., the reactants are intercalated as negative ions, and the graphite planes share the positive charge.

Residue Compounds

Most of the reactant in the lamellar compounds can be removed by essentially reversing the procedure by which the lamellar compounds were formed. In all cases examined, however, a small amount of reactant remains which cannot be removed without resorting to fairly drastic procedures. The amount of reactant remaining is dependent upon the amount of reactant present in the original lamellar compound. Compounds of this type, in which the reactant is held very strongly in the graphite and cannot be removed by cathodic reduction or chemical washing, have been termed "residue" compounds. These substances have not been described previously. In residue compounds, the reactant is distributed more irregularly through the graphite than in lamellar compounds. It is likely that the reactant in the residue compounds becomes trapped at imperfections and twinning planes of the lattice. This irregular structure of the residue compounds has been established by x-ray diffraction measurements which will, however, be reported in a subsequent paper.

In both lamellar graphite salts and in the corresponding residue compounds, the reactant is present as negative ions, and the graphite planes share the positive charges. Such a charge distribution is typical of electron acceptor impurities. However, in a study of graphite, the residue compounds are more important than the lamellar compounds, since they do not distort the band structure of graphite as much as do the lamellar compounds. The electrical properties of both

[3] H. L. Riley, Fuel **24**, 1, 43 (1945).
[4] W. Rüdorff and U. Hofman, Z. Anorg. Allgem. Chem. **238**, 1 (1938).

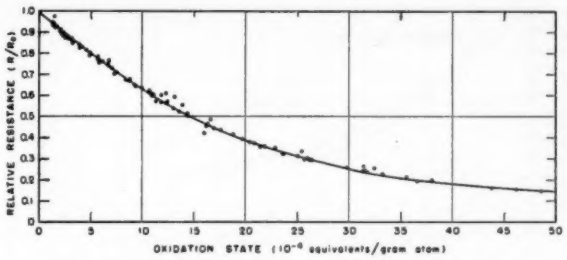

FIG. 1. Effect of oxidation in sulfuric acid on the electrical resistance of graphite.

lamellar and residue graphite salts have been investigated. The results of the investigation on the graphite bisulfates are reported in this paper.

Graphite bisulfates are prepared by the oxidation of graphite in concentrated sulfuric acid. Numerous oxidizing agents, as well as an electric current, will cause this oxidation. The fully oxidized compound has the composition[4] $C_{24}^{+}\cdot HSO_4^{-}\cdot 2H_2SO_4$. In the present investigations, various lamellar and residue graphite bisulfates were prepared by electrolytic oxidation and reduction in concentrated sulfuric acid.

The electrical resistance, its temperature dependence, and the Hall coefficient were measured for various graphite bisulfates. The resistance and its temperature dependence are obviously important properties of the conduction electrons. The Hall coefficient is a measure of the number of conduction electrons. A negative coefficient is obtained if the conduction electrons move near the bottom of an empty band; a positive coefficient is obtained if the electrons move near the top of an almost full band.

EXPERIMENTAL

Materials

The graphite used was Acheson graphite similar in properties to the National Carbon Company's Spectroscopic Electrodes except that it showed a high anisotropy. All except specially designated samples were cut so that the current direction and the Hall direction were perpendicular to the axis of extrusion, i.e., the direction of lowest resistivity.

A few samples of natural graphite from Ticonderoga were obtained from Ward's Natural Science Establishment, Rochester, New York. The samples were thin plates about 1 cm long. They were purified by alternate washing with hydrochloric and hydrofluoric acids. The platelets cleaved very easily, but showed many striations on the basal planes.

The sulfuric and nitric acids used were Baker Analyzed Chemicals.

Electrical Resistance and Oxidation State

Samples of graphite were mounted in such a way that their resistance could be determined during oxidation in sulfuric acid. The samples weighed about 0.4 g and

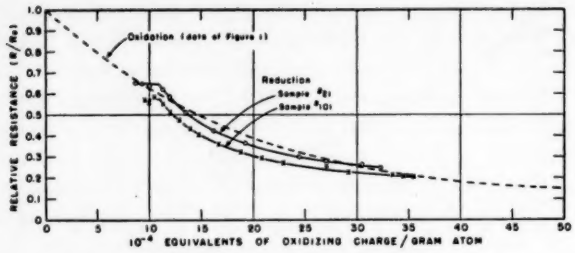

FIG. 2. The electrical resistance of graphite during oxidation and reduction in sulfuric acid.

their dimensions were 2 mm×2 mm×40 mm. Several millimeters from each end, a very small hole was drilled through the sample to accommodate platinum potential leads. The current leads were sturdy platinum wires, which fitted into recesses at the ends of the sample. Resistance measurements were reproducible to 0.5 percent. The whole assembly was lowered into a tube containing concentrated sulfuric acid. The tube communicated through a sintered glass disk with a cathode compartment which contained concentrated sulfuric acid and a platinum electrode. The graphite was oxidized by a current which varied for different experiments from 2 to 10 milliamperes. The oxidation state in equivalents of electrons per gram atom of carbon was calculated from the formula:

$$tI(60)(12)/96500w,$$

where t is the time in minutes, I is the current in amperes, and w is the weight of the sample in grams.

The resistance decreased as the graphite became oxidized. In a few cases this decrease was delayed, presumably because of traces of oxidizable impurities present in the acid or in the sample. In such cases the zero time was chosen to coincide with the first decrease in the resistance. The choice also eliminated the small error in the measurements of the resistance which was caused by that fraction of the oxidizing current which flowed through the graphite. Each resistance measurement was corrected for a relatively small potential recorded by the potentiometer immediately after the resistance measuring current had been discontinued. This potential, which is probably caused by temperature fluctuations and strains in the graphite, was usually quite small, but occasionally rose to several hundred microvolts.

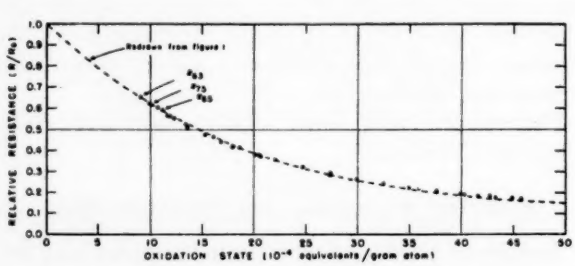

FIG. 3. Effect of reoxidation on the electrical resistance of graphite bisulfate "residue" compounds.

The resistance data obtained for twelve separate runs on twelve different samples are plotted in Fig. 1. All resistances are reported relative to the resistance of the unoxidized sample in sulfuric acid.

One parallel cut and six perpendicular cut samples were run at five milliamperes in concentrated sulfuric acid, and one parallel cut sample was run at 10 milliamperes in concentrated acid. The other samples were all perpendicular cut samples and differed from each other by the fact that two were run at two milliamperes and ten milliamperes, respectively, one was oxidized in 13 molar sulfuric acid, one was oxidized while a stream of helium was passed through the acid, and one was oxidized while a stream of sulfur dioxide was passed through the acid. The agreement, seen in Fig. 1, between such a number of runs under different conditions demonstrates that the current efficiency of the oxidation is very probably close to unity. If it were not unity it would have changed with the current density. Furthermore if it were less than unity due to a concurrent oxidation of sulfur dioxide, for example, the presence of excess sulfur dioxide should have decreased the current efficiency considerably.

TABLE I. Properties of the graphite bisulfate residue compounds.

Sample no.	Oxidation state of lamellar compound (10^{-4} equivalent/g atom)	Oxidation state of corresponding residue compound (10^{-4} equivalent/g atom)	$10^2\times$ fractional weight gain in residue compound	H_2SO_4/HSO_4^- ratio in residue compound
17	17.8	5.3	2.15	4.0
19	10.55	3.55	1.79	5.2
21	29.6	9.35	3.40	3.5
27	43.5	9.75	4.29	4.4
29	19.75	6.5	2.94	4.6
35	11.2	4.0	1.96	5.1
53	25.4	7.5	3.19	4.3
57	31.5	9.1	3.71	4.1
63*a*	31.1	9.2		
63*b*	40.6	11.15		
63*c*	42.7	11.70	4.88	4.2
69	20.85	6.65	2.66	4.0
71	32.5	9.85	3.46	3.4
73*a*	33.7	9.95		
97	37.75	11.15	4.37	3.8
101	35.6	12.00	4.59	3.7
105*a*	36.65	10.2		

At any oxidation level, the lamellar graphite bisulfate compound could be decomposed by a current which made graphite the cathode. The progress of this reduction was followed again by resistance measurements. Fig. 2 represents two typical runs. At the beginning of the reduction, the rate at which the resistance increased was less than the rate at which it had decreased during oxidation, but later the rate was higher than the corresponding rate during oxidation. After approximately two-thirds of the missing electrons had been restored, the resistance quite suddenly reached a constant value unaffected by further passage of current. At this point the material had the characteristics of a residue compound. The constant resistance ultimately reached in the reduction is dependent only on the degree of oxida-

tion of the original lamellar compound. Thus, for every lamellar compound there is a corresponding residue compound.

The current efficiency during the reduction of the lamellar compound was not always unity as evidenced by a lack of reproducibility. Therefore a reliable determination of the number of electrons trapped in the residue compound was not possible from measurements made during the reduction. Fortunately the reoxidation of the residue compound proceeded at unit current efficiency. In fact, the rate of the resistance change during reoxidation was identical with the rate during the original oxidation when compared at equal resistances. This indicates that the resistance of a lamellar compound and a residue compound are identical if they are oxidized to the same oxidation state, and that the number of electrons missing from the graphite in the residue compound is the same as the number of electrons lost in the formation of a lamellar compound having the same resistance. This fact was used in drawing Fig. 3. The dashed line in Fig. 3, which is the resistance *vs* oxidation state curve for lamellar compounds, also applies to residue compounds, as was just shown. In this way the oxidation states for residue compounds were determined, for which only the resistance was known. The experimental points represent the resistances of residue compounds as they were gradually oxidized.

The chemical composition of residue compounds was determined in the following manner: The material was washed in running water for 24 hours, dried and weighed. Rewashing for several days in running water, or in boiling sodium hydroxide, affected the weight only slightly. It was assumed that the excess weight above the original weight of graphite was due to trapped bisulfate ions and sulfuric acid only. Since the number of bisulfate ions should be equal to the number of electrons lost during oxidation, the weight of these ions could be calculated from the oxidation state. The rest of the weight gain was assumed due to sulfuric acid. The number of molecules of sulfuric acid associated with each bisulfate ion is listed in Table I, column 5, and is roughly four molecules per ion. The second column of Table I lists the number of equivalents of electrons missing from the corresponding lamellar compound from which the residue compound was produced by reduction. The entries in the third column were determined from the measured resistance of the residue compound, by referring to Fig. 1.

It was found that the resistance of artificial graphite which had been oxidized more than 0.005 equivalent per gram atom began to increase gradually. At the same time the samples became bent and distorted. A few samples were sealed into glass tubes to provide a rigid support. The tubes were perforated in six places to admit platinum leads and acid. The resistance ratio of one of these samples passed through a minimum of

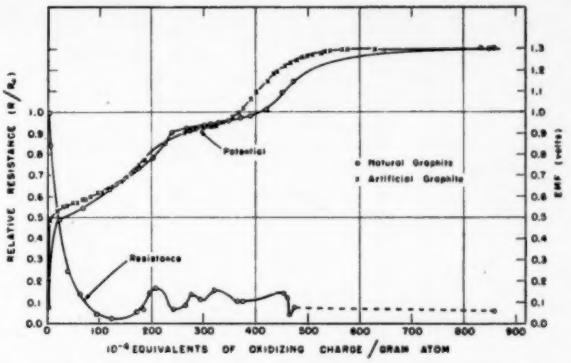

FIG. 4. The electrical resistance of graphite during oxidation in concentrated sulfuric acid, and the corresponding electromotive force of the cell $Hg|Hg_2SO_4|H_2SO_4|C_nHSO_4 \cdot 2H_2SO_4$.

0.106, corresponding roughly to 0.007 equivalents of oxidation, but increased again beyond this value.

It was anticipated that natural graphite of large crystal size would not distort as badly as fine-grained artificial graphite. Accordingly, a plate of natural graphite (#37) was set in plaster of Paris so that it was supported on three sides for reinforcement. The plate was about 3 mm wide, 10 mm long, and 0.2 mm thick. Platinum wires bent into clamps provided current leads. Fine platinum wires were threaded through holes in the plate for potential leads. The resistance of this plate is shown in Fig. 4. The resistance decreased 50-fold before it began to fluctuate. It is reasonable to conclude that the resistance would continue to decrease even further if more rigid and more perfect samples were available.

A plate of natural graphite (#119) mounted without the plaster of Paris backing was oxidized 0.00286 equivalents/g atom. Its resistance ratio dropped to 0.262. On reduction, a residue compound was formed, but its exact resistance was uncertain. The resistance

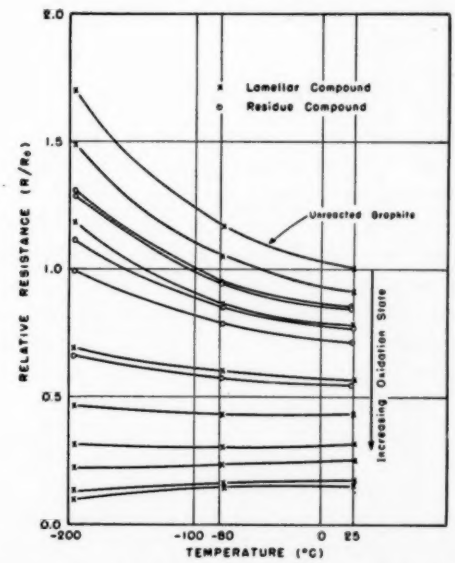

FIG. 5. The electrical resistance of graphite bisulfates as a function of temperature.

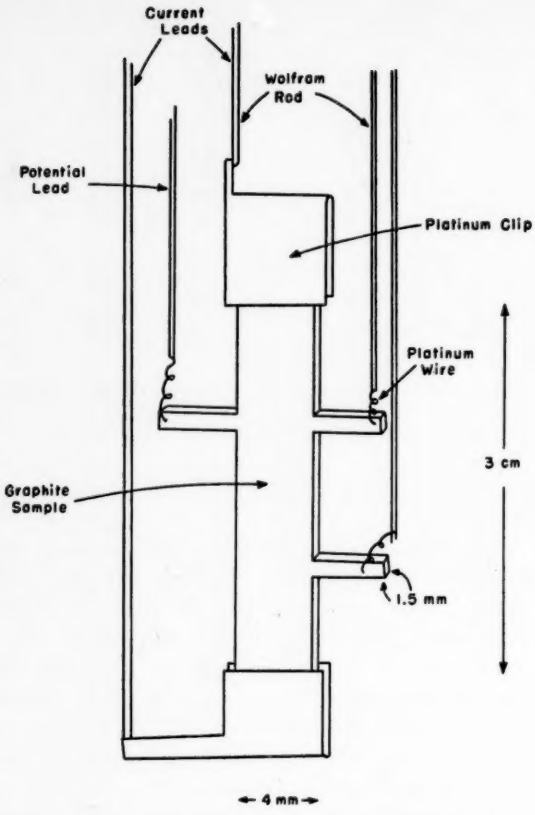

FIG. 6. Graphite sample used for Hall coefficient and resistance measurements in sulfuric acid.

kept increasing very slightly, as long as a reducing current was passed. The sample was therefore washed in running water, and its resistance ratio rose from 0.656 to 0.762 after three days of washing. Obviously, then, the residue compounds of natural graphite are not as stable as those formed from artificial graphite, probably because the imperfections in natural graphite are not very efficient traps.

The Electrode Potential

The electrode potentials of artificial and natural graphite against a standard mercurous sulfate electrode were measured at various oxidation states. Graphite itself was sometimes slightly positive and sometimes slightly negative but became consistently negative after a very small reducing current had passed. The lamellar compounds were always strong oxidizing agents and produced large potentials against the standard electrode. During the reduction of lamellar compounds, the potential decreased, passed through zero close to the end of the reduction and became negative. The residue compound itself was always a weaker oxidizing agent than the mercurous sulfate electrode. The potentials for a sample of artificial and a sample of natural graphite have been plotted in the upper part of Fig. 4. The current efficiency of this oxidation was incidentally not always unity because of the gradual disintegration of the material. Detailed measurements of the electrode potentials and their temperature coefficients will be published later.

The Temperature Dependence of the Resistance

A resistance sample was placed in sulfuric acid containing a few drops of nitric acid as an oxidizing agent and the resistance was measured as the sample oxidized. The sample was withdrawn periodically, washed with sulfuric acid, and, still wet with acid, dipped into liquid nitrogen. The resistance was redetermined. The sample was next transferred to a dry ice-petroleum ether mixture and the resistance remeasured. Finally the petroleum ether was washed off with sulfuric acid, the sample was reoxidized further, and the above measurements repeated. The resistances have been plotted in Fig. 5 as a function of temperature. The resistance of various residue compounds was also determined at these temperatures on samples prepared by electrolytic oxidation followed by reduction. These samples were washed and dried before measurement. The results of these measurements are also plotted in Fig. 5.

TABLE II. The effect of temperature on the electrical resistance of a natural graphite bisulfate compound.

Sample	Relative resistance at 25°C	−75°C	−195°C	Average temperature coefficient between −195 and 25°C $\left(\frac{\Delta R \times 10^3}{(\Delta T)(R_{25})}\right)$
Unreacted	1	0.896	0.602	+1.8
Bisulfate residue compound	0.756	0.620	0.388	+2.2

The temperature coefficient of the natural graphite sample described previously (#119) was also determined, both on the unreacted sample and on its washed and dried residue compound. The resultant data are shown in Table II.

The Hall Coefficient

The resistance and Hall coefficient were measured on a sample which was cut and mounted as shown in Fig. 6. The current leads were rigid platinum clips, while all potential leads consisted of platinum wire. Stray potentials, and particularly the Ettingshausen potential, were reduced considerably by leaving stubs of graphite attached to the sample at the desired points and making contact to these stubs. All platinum leads were gold soldered to wolfram rods which were sealed through a ground glass cap. The whole assembly fitted into a flattened glass tube of 1 cm o.d. which was mounted between the round pole pieces, 5 cm in diameter, of an electromagnet.

The magnet was calibrated between 4 and 15 kilogauss with a search coil and ballistic galvanometer. The Hall measurements were always made at 14 kilogauss and a current of two amperes. The field was reversed at

least seven times and the average value of the differences in the induced potentials was determined. The Hall coefficient (A_H) was calculated from the following formula:

$$A_H = \frac{(\Delta E)d(10^9)}{2IH},$$

where ΔE is the average potential difference (volts); d is the thickness of sample (cm); I is the current (amp); H is the magnetic field (gauss); and 10^9 is the conversion factor from practical units to emu. To insure that the Hall coefficient referred to the same number of carbon atoms even after a chemical reaction, any changes in the dimensions of the sample during the reaction were ignored, and the coefficient was calculated from the thickness of the sample before reaction. The precision of the measurements was *ca* ± 0.005 emu.

The following experimental procedure was used. A sample was immersed completely in concentrated sulfuric acid and its properties were measured. It was oxidized briefly by a current to a platinum electrode. Its properties were then remeasured. Subsequent reduction converted it to a residue compound. This cycle of oxidation and reduction was repeated so that the sample was alternately measured as a lamellar and as a residue compound. A separate set of experiments was performed in which the sample was oxidized in dilute sulfuric acid by a few drops of nitric acid added to the sulfuric acid. It was found that little oxidation occurred in 12 molar or more dilute acid, but a very small increase in the acid concentration near 12 molar changed the final oxidation state of graphite considerably.

The Hall coefficients obtained after chemical or electrical oxidation have been plotted in Fig. 7 against the corresponding resistance. Two quite distinct curves were obtained for the lamellar and the residue compounds.

DISCUSSION

Reaction Mechanisms

It is probable that the cause for the formation of lamellar graphite bisulfates with the bisulfate planes occurring with a definite periodicity[5] is an electrostatic phenomenon. A layer plane filled with bisulfate ions constitutes such a concentration of charge that, in spite of the dielectric action of sulfuric acid, the concentration of bisulfate ions at the graphite surface will be low near this plane. Therefore, the next layer of bisulfate ions enters as far away as possible, namely, exactly midway between planes already filled, thus giving rise to the stepwise or periodic reaction. Such a mechanism would not apply to those lamellar compounds which are not ionic. Most lamellar compounds are formed in this stepwise fashion, and it seeems reasonable that such lamellar compounds should also be ionic in character. That this was found to be true will be shown in subsequent papers.

The conversion of lamellar to the corresponding residual graphite bisulfate compounds may involve a transitory reduction of the bisulfate ions. When Fig. 2 was discussed earlier, the peculiar delay in the resistance increase was mentioned. The lamellar compounds act on reduction as if the electrons were at first "stored away" without entering the graphite conduction band, but electrons can only be "stored away" by reducing the bisulfate or sulfuric acid. Later during the reduction when the ions and molecules are ejected from the graphite they release these electrons to the graphite. This mechanism would also explain why the current efficiency during reduction is often not unity. If the reduced ions escape too rapidly they may fail to return some of the "borrowed" electrons to the graphite and may, in the presence of even a weak oxidizing agent, release the electrons to this agent. It must be emphasized that this mechanism is highly tentative and has been postulated only to explain the behavior of the resistance during the reduction of lamellar compounds.

Two alternate explanations are possible to explain why a residue compound is formed at all in preference to complete expulsion of interstitials. Isolated ions may simply be trapped with the graphite planes collapse. Once trapped, the isolated ions and molecules are certainly unable to move because the energy required to separate two carbon planes is enormously large, due to the number of carbon atoms involved per ion. As an alternate explanation of residue compounds, it may be postulated that the bisulfate ions and acid molecules in

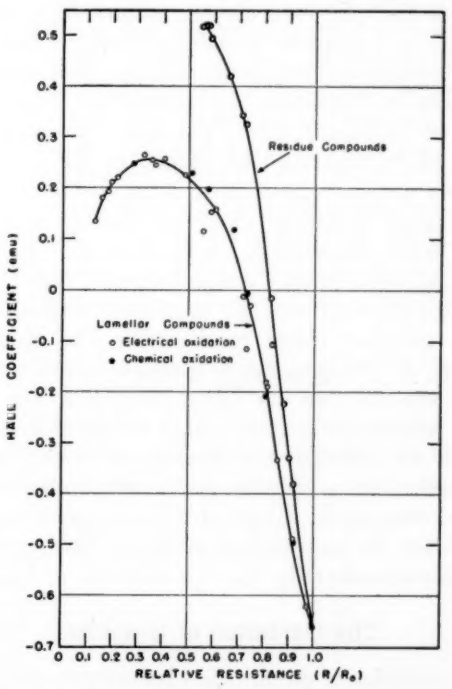

FIG. 7. Hall coefficient of graphite bisulfates as a function of oxidation state.

[5] W. Rüdorff, Z. physik. Chem. **B45**, 42 (1940).

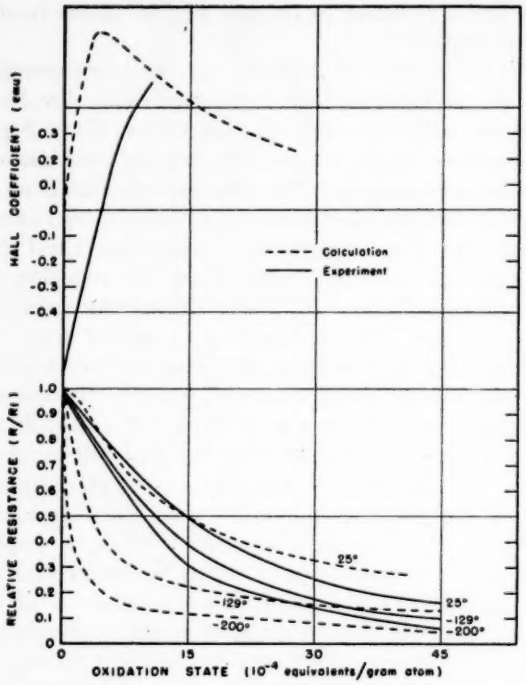

FIG. 8. Calculated and experimental resistances and Hall coefficients of oxidized graphite.

a layer plane have also invaded adjacent cracks and imperfections. On reduction they are trapped in these positions. Evidence in favor of this second view will be advanced in subsequent papers.

Comparison of Compounds

One of the purposes of this investigation was the preparation of graphite containing acceptor impurities. Their distribution should be uniform, but statistical, to prevent the formation of a superlattice, which would change the band structure of the parent compound.

It is likely that lamellar bisulfates are not ideally suited as acceptor impurities. The bisulfate ions are concentrated in widely separated layers, where they are probably arranged in planar lattices. The residue compounds are certainly more dilute and very probably more disordered than the lamellar compounds and should, therefore, have more nearly the same band structure as graphite itself, perhaps differing from it only in the effective number of electrons. The experimental results confirm that either the band structure is different for lamellar and residue compounds or that the lamellar compounds are not as homogeneous as the residue compounds. Either of these explanations could account for the large difference in the Hall coefficients of the compounds (Fig. 7).

The Oxidation of Graphite

The oxidation of graphite has been shown to diminish its resistance and change the sign of the Hall coefficient. These changes are in agreement with the commonly accepted theory that the electrons in graphite fill one conduction band completely except for a small number of electrons which are excited into a nearly empty band. The excited electrons and the "missing electrons" in the lower band constitute the current carriers. Removal of electrons by oxidation increases the number of unpaired electrons in the lower band but decreases the number of excited electrons in the upper band by a smaller amount. Therefore, the net number of current carriers increases, and the resistance decreases. Since the carriers are predominantly in the lower band, the Hall coefficient is positive. The number of positive carriers depends only slightly on temperature and therefore the temperature coefficient of resistivity becomes small and even changes sign, because eventually the temperature fluctuations of the lattice increase the resistances more than the temperature excitation of electrons into the empty band can compensate for. The temperature coefficient of natural graphite is already positive,[6] because of the smaller number of permanent scattering centers,[2] and increases further on oxidation.

A quantitative comparison of the experimental results with Wallace's[2] band theory of graphite was attempted. For the purpose of this comparison it was assumed that the intercalation of ions and molecules into graphite reduces the number of electrons in the graphite lattice without distorting the electron bands and without increasing the effective number of scattering centers appreciably. Furthermore, it was assumed that the distribution of electrons in the graphite lattice is uniform on a microscopic scale and does not change in the vicinity of an intercalated negative ion layer.

With these restricting assumptions the resistance and Hall coefficient of oxidized graphite were calculated. Wallace has derived equations for the energy and conductivity of electrons both in a two-dimensional and a three-dimensional model of graphite. The calculations have been extended to a two-dimensional model of oxidized graphite only.

The following symbols have been used by Wallace: E_c is the energy at the corners of the Brillouin zone, E E is the energy of an electron, γ_0 is an exchange energy of magnitude 0.9 ev, f_0 is the Fermi distribution, $N(E)dE/N_a$ is the density per atom of electronic energy states between E and $E+dE$, $d\sigma$ is a surface element in the surface of constant energy, ρ is the resistivity, $1/\tau$ is the probability per unit time of scattering an electron wave, a and c are fundamental lattice displacements in graphite. We define the additional terms: m is the number of electrons per atom removed from the graphite lattice by oxidation, Δ is the difference between Fermi energy and E_c, and A_H is the Hall coefficient.

The Fermi energy of electrons coincides in graphite with the energy at the corners of the Brillouin zone.

[6] D. E. Roberts, Phil. Mag. **26**, 159 (1913).

Oxidation, i.e., removal of m electrons, lowers the Fermi energy by an amount Δ, which is a function of the number of electrons removed and of the temperature. This relation between Δ and m can be calculated by equating the number of empty states created ($m/2$) to the total number of states available before oxidation minus the available electrons after oxidation:

$$m/2=\int_{-\infty}^{E_c}\frac{N(E)}{N_a}dE-\int_{-\infty}^{\infty}\frac{N(E)}{N_a}f(E)dE$$

$$\frac{\pi\sqrt{3}\gamma_0^2}{2}m=\int_{-\infty}^{E_c}(E_c-E)dE$$

$$-\int_{-\infty}^{E_c}\frac{E_c-E}{1+e^{(E-E_c+\Delta)/kT}}dE-\int_{E_c}^{\infty}\frac{E-E_c}{1+e^{(E-E_c+\Delta)/kT}}dE$$

$$2.2m=\tfrac{1}{2}\Delta^2+\frac{k^2T^2\pi^2}{6}$$

$$-2k^2T^2(e^{-\Delta/kT}-\tfrac{1}{4}e^{-2\Delta/kT}+\tfrac{1}{9}e^{-3\Delta/kT}-\cdots).$$

From this equation, Δ in units of ev can be computed at a given temperature for various values of m.

For a given value of Δ, the resistivity can be calculated from Wallace's equation (3.12):

$$\frac{8\pi e^2\tau}{h^2c}\int_{-\infty}^{\infty}|E-E_c|\frac{df_0}{dE}dE$$

$$=-\frac{8\pi e^2\tau}{h^2c}(\Delta-2kT\ln[1+e^{\Delta/kT}]).$$

The resistance relative to unoxidized graphite at a given temperature is then

$$R/R_t=-2kT\ln 2/(\Delta-2kT\ln[1+e^{\Delta/kT}]).$$

The Hall coefficient was calculated from the equations:[7]

$$A_H=\frac{-1}{2eN_xN_y}\int\frac{df_0}{dE}\int\left(\left(\frac{\partial E}{\partial k_y}\right)^2\frac{\partial^2E}{\partial k_x^2}-\frac{\partial E}{\partial k_x}\frac{\partial E}{\partial k_y}\frac{\partial^2E}{\partial k_x\partial k_y}\right)\frac{d\sigma}{|\mathrm{grad}E|}dE$$

$$N_x=\int\int\frac{df_0}{dE}\left(\frac{\partial E}{\partial k_x}\right)^2\frac{d\sigma}{|\mathrm{grad}E|}dE$$

$$N_y=\int\int\frac{df_0}{dE}\left(\frac{\partial E}{\partial k_y}\right)^2\frac{d\sigma}{|\mathrm{grad}E|}dE.$$

Substitution of Wallace's relations

$$E_c-E=+\sqrt{3}\pi\gamma_0a|(k_c-k)| \quad \text{for } E<E_c$$
$$E-E_c=\sqrt{3}\pi\gamma_0a|(k-k_c)| \quad \text{for } E>E_c$$

results in

$$A_H=-\frac{1}{2ec}(\sqrt{3}\pi\gamma_0a)^2\frac{(1-2f_0)_{E_c}(c/2)^2}{\pi(\Delta+2kT\ln[1+e^{-\Delta/kT}])^2}.$$

This must be multiplied by (3×10^{10}) to convert to emu.

Calculated and experimental values of the Hall coefficient at room temperature and of the resistance at three temperatures have been plotted in Fig. 8 against the oxidation level m. The resistances have been plotted as R/R_t, where R_t is the resistance of unoxidized graphite at the temperature stated. The experimental values were obtained from Figs. 1 and 5.

Comparison of the calculated and the measured resistances shows fairly good agreement at room temperature, but progressively larger deviations at lower temperatures. The calculated Hall coefficient differs considerably from the experimental one obtained for the residue compounds. They differ, however, by a nearly constant value of m, as if a certain fraction of the positive carriers behaved in reality as negative carriers.

Qualitatively, the calculated values agree with the general trend of the electrical properties of graphite observed during oxidation, but quantitatively, the measured and calculated properties differ considerably. The difference may be due in part to the choice of the two-dimensional model of graphite for these calculations. However, the assumptions which were made earlier about the nature of oxidized graphite may also be inadequate. These assumptions will be tested in subsequent papers which deal with the effects of other acceptor impurities, and of donor impurities, on graphite.

ACKNOWLEDGMENT

It is a pleasure to thank O. C. Simpson and J. R. Gilbreath for numerous discussions and for their invaluable help in editing this paper.

[7] H. Jones and C. Zener, Proc. Roy. Soc. (London) **A145**, 269 (1934).

Discrete Energy Levels Associated with the Lennard-Jones Potential

JOHN E. KILPATRICK AND MYRA F. KILPATRICK
Department of Chemistry, The Rice Institute, Houston, Texas
(Received March 29, 1951)

The radial wave equation for two particles with a Lennard-Jones relative potential energy, in the reduced form, $-(R\psi)''+25b^2(R^{-12}-R^{-6})R\psi=-\lambda^2R\psi$, has been examined for discrete eigenvalues by both variation and perturbation theory. The largest eigenvalue, λ_0 (corresponding to the lowest energy level), has been followed, as a function of b, until it disappears into the positive energy continuum. A short table of λ_0 and λ_1 has been computed.

INTRODUCTION

THE Lennard-Jones potential has frequently been used to represent the intermolecular potential energy of two atoms of helium or of some other inert gas. From the solutions of the resulting wave equation various interesting quantities such as the collision cross section and the second virial coefficient of the gas may be calculated. In such calculations the presence or absence of discrete energy levels, in addition to the usual positive continuum of energy, can be of considerable importance. As a consequence of the rapid approach to zero of the Lennard-Jones potential with increase of the intermolecular distance, there can be only a finite number of discrete energy levels. For a sufficiently shallow potential or a sufficiently small reduced mass, discrete levels may be absent entirely.

There seems to be general agreement that a pair of normal He^4 atoms possess at most one discrete energy level. Opinion is divided, however, as to whether there is a single level very close to zero or no discrete level at all. Beth and Uhlenbeck[1] feel that the behavior of the second virial coefficient of He^4 at about 3°K indicates the presence of a discrete energy level near zero. De-Boer and Michels[2] think it is probable that no discrete level exists. Kahn[3] agrees with Beth and Uhlenbeck. Such a low-lying level would imply a very weakly bonded He_2 molecule. This hypothetical molecule is not to be confused with the moderately stable He_2 molecule formed from one excited and one normal helium atom.

This uncertainty led us to study the general problem of the location of the discrete energy levels associated with the Lennard-Jones potential. Unfortunately, we have found that the question of the presence or absence of a discrete level in He_2 cannot be answered on the basis of the available experimental data. The two Lennard-Jones parameters for He are not known with sufficient accuracy to distinguish between the two choices. Indeed, He is so close to the dividing line, according to the Lennard-Jones potential, that the actual potential of interaction of the two real atoms would have to be determined to a very high accuracy in order that a choice could be made with certainty.

[1] E. Beth and G. E. Uhlenbeck, Physica 4, 915 (1937).
[2] J. de Boer and A. Michels, Physica, 6, 409 (1939).
[3] B. Kahn, thesis, Utrecht (1938).

SOLUTION OF WAVE EQUATION

The radial wave equation for the system consisting of two point mass atoms with relative potential energy $V(r)=4\epsilon[(r/\sigma)^{-12}-(r/\sigma)^{-6}]$ is

$$-\frac{\hbar^2}{2m}\frac{d^2r\psi}{dr^2}+\left\{\frac{l(l+1)\hbar^2}{2mr^2}+V(r)\right\}r\psi=Er\psi, \quad (1)$$

where ψ is the radial factor of the complete wave function and m is the reduced mass of the system. By means of the substitutions

$$r=\sigma R \quad (2)$$

$$\lambda^2=-2m\sigma^2E/\hbar^2 \quad (3)$$

$$25b^2=8\epsilon\sigma^2m/\hbar^2 \quad (4)$$

one obtains the reduced equation

$$-(R\psi)''+[l(l+1)R^{-2}+25b^2(R^{-12}-R^{-6})]R\psi=-\lambda^2R\psi. \quad (5)$$

We have considered only the case $l=0$ since, except for large values of b, there are no discrete levels if $l>0$. Our problem then is to examine the equation

$$-(R\psi)''+25b^2(R^{-12}-R^{-6})R\psi=-\lambda^2R\psi \quad (6)$$

for discrete eigenvalues, i.e., discrete positive values of λ^2. We are particularly interested in determining how λ_0 varies with b in the region where λ_0 is very small. Since the terms in R^{-6} and R^{-12} make the equation quite intractable to an analytic solution, we have employed variation in the region of small b, perturbation in the region of large b, and both techniques in the intermediate range.

Variation

The expression $\Sigma C_nR^n\exp(-aR-b'R^{-1})$ is a reasonable form for a trial variation function. This function satisfies the boundary conditions for $R\psi$ but does not become small fast enough as R approaches zero. The elements of the resulting secular equation can readily be evaluated in terms of certain bessel functions (K_n). A few trial calculations indicated that this form would not give good results without the use of a secular equation of high degree.

The limiting behavior of $R\psi$, both for very large and very small values of R led us to adopt the varia-

tion function $\varphi=\Sigma C_n\varphi_n$, where

$$\varphi_n=R^n\exp(-aR-bR^{-5}), \tag{7}$$

and a is an estimated value for λ. This form, with only two or three terms, results in good values for λ_0, even with a rather poor choice for a.

The elements of the secular equation, $|H_{mn}+\lambda^2\Delta_{mn}|=0$, are given by the expressions

$$\begin{aligned}H_{mn}=&\beta^{1/5(m+n+1)}(a^2-5/2a\beta)U_{m+n}(x)\\&+\beta^{1/5(m+n)}[5/4(m+n)\beta\\&-a(m+n)+6a]U_{m+n-1}(x)\\&+\beta^{1/5(m+n-1)}[(m-3)(n-3)-6]U_{m+n-2}(x),\end{aligned} \tag{8}$$

$$\Delta_{mn}=\beta^{1/5(m+n+1)}U_{m+n}(x), \tag{9}$$

where

$$\beta=2b,\quad x=2a\beta^{1/5},$$

and

$$U_n(x)=\int_0^\infty R^n\exp(-xR-R^{-5})dR. \tag{10}$$

Neither $U_n(x)$ nor any other function from which $U_n(x)$ can be derived has been tabulated. $U_n(x)$ is a particular case of the more general function

$$W_n{}^q(x)=\int_0^\infty t^n\exp(-xt-t^{-q})dt. \tag{11}$$

$W_n{}^q$ is a sort of generalized bessel function. It satisfies the differential equation

$$x\frac{d^{q+1}W_n{}^q}{dx^{q+1}}+(n+q+1)\frac{d^qW_n{}^q}{dx^q}+(-1)^qqW_n{}^q=0 \tag{12}$$

and the recursion relation

$$xW_{n+1}{}^q=(n+1)W_n{}^q+qW_{n-q}{}^q. \tag{13}$$

Faxén[4] has discussed in considerable detail the properties of a function closely related to $W_n{}^q$. His equations reduce to the expression

$$W_n{}^q(x)=\frac{1}{q}-(P_1+P_1')+P_2+P_2', \tag{14}$$

where

$$P_1=\sum_{s=0}^{\infty}\left[\frac{s+n+1}{q}+1\neq\text{positive integer}\right]\frac{(-1)^s}{s!}x^s\Gamma\left(-\frac{s+n+1}{q}\right), \tag{15}$$

$$P_1'=\sum_{s=0}^{\infty}\left[\frac{s+n+1}{q}+1=r+1=\text{pos. int.}\right]\frac{(-1)^{r+s}}{r!s!}x^s[\psi(r+1)-\ln x], \tag{16}$$

$$P_2=\sum_{s=0}^{\infty}[sq-n\neq\text{pos. int.}]\frac{(-1)^s}{s!}x^{sq-n-1}\Gamma(-sq+n+1), \tag{17}$$

$$P_2'=\sum_{s=0}^{\infty}[sq-n=r+1=\text{pos. int.}]\frac{(-1)^{r+s}}{r!s!}x^{sq-n-1}[\psi(r+1)-\ln x], \tag{18}$$

and $\psi(r)=\Gamma'(r)/\Gamma(r)$, the usual psi function. This series is absolutely convergent for all values of n, q, and x. However, for $U_n(x)\equiv W_n{}^5(x)$, the labor of summation becomes prohibitive for $x>2$.

The series of Eq. (14), together with the recursion relation of Eq. (13), was used to tabulate $U_n(x)$ to seven significant figures, at numerous selected values of x between zero and 1.88 and for each order (n) between -15 and 4, inclusive.

In order to calculate $U_n(x)$ for large values of x, we derived an asymptotic series by the method of steepest descent:

$$U_n(x)\sim\pi^{\frac{1}{2}}(5/y)^{(2n+7)/12}\exp(-6/5(5)^{1/6}y)\times\{\sum_{i=0}^{3}Q_iy^{-i}+O(y^{-4})\}, \tag{19}$$

where

$$y=x^{5/6}$$

$$Q_0=1$$

$$Q_1=\frac{5^{5/6}}{720}(12n^2+72n+77)$$

$$Q_2=-\frac{5^{10/6}}{1{,}036{,}800}(144n^4+2496n^3+12{,}504n^2+16{,}272n-3311)$$

$$Q_3=\frac{5^{15/6}}{11{,}197{,}440{,}000}(8640n^6+293{,}760n^5+3{,}380{,}400n^4+14{,}525{,}920n^3+9{,}784{,}980n^2-43{,}985{,}160n-25{,}592{,}567).$$

This expression was used for $x>32$.

In the early stages of this investigation a considerable amount of exploratory work was necessary in order to determine first, an approximate value of λ_0 for a given value of b, and second, the best values of n to use in the variation function.

Since preliminary calculations showed that $\lambda_0{}^2$ is small but definitely positive for $b=1$, we decided to explore this case thoroughly.

Table I shows how a and $\lambda_0{}^*$ (the *largest* root of the secular equation and a *lower* limit for λ_0) vary with x when the simple one-term variation function φ_0 is used. For computational simplicity, x rather than a was selected as the independent variable. The maximum

[4] Hilding Faxén, Arkiv for Math., Astr., och Fysik **15**, 1 (1920).

TABLE I. Values of λ_0^* resulting from the use of a one-term variation function $\varphi_0=\exp(-aR-bR^{-5})$ with $b=1$.

x	a	λ_0^*
0.10	0.0435	0.0739
0.12	0.0522	0.0759
0.13	0.0566	0.0761
0.15	0.0653	0.0754
0.16	0.0696	0.0744
0.17	0.0740	0.0729
0.18	0.0784	0.0709
0.20	0.0871	0.0653
0.22	0.0958	0.0569
0.26	0.1132	0.0206
0.50	0.2176	imag.

value of λ_0^* is well below our best value for λ_0 (0.114) and the agreement between a and λ_0^* at this maximum is not good. However, φ_0 is the best one-term variation function of the form φ_n, since any value of n other than zero gives an imaginary λ_0^*. Table II shows how λ_0^* varies with the number of terms in the variation function

$$\varphi=\sum_n C_n R^n \exp(-aR-bR^{-5}), \qquad (20)$$

and with the values of a and n that are used, again for the case $b=1$. In the left half of Table II, $a=0.07835$ and in the right half, $a=0.11317$. Since $\lambda_0=0.114$ at $b=1$, the former choice is a poor approximation for λ_0 and the latter choice a very good approximation. However, even in the case of the poor choice of a, the best λ_0^* obtained differs from λ_0 by only a few percent.

Very poor results are obtained with a variation function that does not contain φ_0. Addition of terms with n positive does not improve λ_0^* very much. Small negative values of n are quite useful. The best two term function is $C_0\varphi_0+C_{-2}\varphi_{-2}$. The addition of more terms, with n positive or negative, effects little improvement in λ_0^*.

With the value of λ_0 at $b=1$ as a starting point, b was slowly decreased until at $b=0.9460$, λ_0 is just equal to zero. This critical value of b was determined in two ways, (1) by extrapolation of the values of λ_0 at $b=1.0$, 0.98, 0.97, 0.96, and 0.95, (2) by solving a third degree secular equation whose terms were evaluated from the limiting form of the $U_n(x)$ function as λ_0 (and therefore x) approaches zero.

TABLE II. Values of λ_0^* resulting from the use of various one-, two-, three-, and four-term linear variation functions of the form $\Sigma_n C_n\varphi_n$ where $\varphi_n=R^n\exp(-aR-bR^{-5})$, with $b=1$.

$x=0.18$,	$a=0.07835$	$x=0.26$,	$a=0.11317$
n	λ_0^*	n	λ_0^*
0	0.0709	0	0.0206
0, +1	0.0773	0, −1	0.1098
0, +2	0.0716	0, −2	0.1131
		0, −3	0.1114
0, −1	0.1018	0, −4	0.1066
0, −2	0.1070		
0, −3	0.1081	0, +1, −3	0.1116
0, −4	0.1064	0, −1, −2	0.1132
		0, −1, −3	0.1127
−1, −2	imag.		
		0, −2, −3	0.1131
0, −1, −2	0.1099	0, −2, −4	0.1131
		0, −1, −2, −3	0.1134
		0, −2, −3, −4	0.1135

It is interesting to compare this critical value of b with the value of b for two normal He^4 atoms. De Boer and Michels[2] give $h^2/m\epsilon\sigma^2=7.05$. This factor corresponds to $b=0.9466$, with an uncertainty of at least 0.001. The question of the presence of a discrete energy level for He^4 is therefore unresolved. Our value of b at the vanishing point of λ_0, 0.9460, is certainly an upper limit for this quantity and is probably correct to within 0.0002. A generous estimate, then, is that $\lambda_0<0.002$ for two ground-state He^4 atoms, assuming a Lennard-Jones potential of interaction and de Boer's values for ϵ and σ. This limit corresponds to a binding energy of less than 1.4×10^{-5} cal/mole, which is striking in comparison to the depth of the potential minimum, 20 cal/mole. It is a very curious coincidence that the discrete energy level of this system, if it exists at all, is so close to vanishing into the positive continuum of energy.

TABLE III. λ_0 and λ_1, from variation and from perturbation, as a function of b.

b	λ_0(var.)	λ_0(pert.)	λ_1(var.)	λ_1(pert.)
0.9460	0.0000			
0.95	0.0086			
0.96	0.0294			
0.97	0.0504			
0.98	0.0716			
1.0	0.114	0.316		
1.1	0.331	0.422		
1.2	0.555	0.603		
1.3	0.785	0.814		
2.5		3.680		
5	9.87	9.876	4.03	5.30
6		12.368		7.62
7	14.84	14.862	10.09	10.013
8		17.358		12.436
9		19.854		14.879
10	22.353	22.351		17.335
15	34.843	34.843	29.77	29.710
20		47.339		42.151
25		59.837		54.616
30		72.335		67.093

The independent variable x of the function $U_n(x)$ increases rapidly with b. At $b=1.3$, x is about 1.88, and it was not practicable to use the convergent series for $U_n(x)$ beyond this point. On the other hand, the asymptotic series for $U_n(x)$ is not sufficiently accurate for x less than about 32, corresponding to $b=5$. There is a gap, therefore, in our values for λ_0 in this intermediate region. However this omission is not serious, since λ_0 turns out to be very nearly linear in b.

The second column of Table III gives a summary of our best values for λ_0 as determined by variation. In the region of small b, four-term variation functions were necessary to assure constancy in the last figure of λ_0 quoted. For b in the neighborhood of 7 or greater, φ_0

alone as a variation function gives very nearly as good results as a multi-term expression.

The fourth column of Table III gives three values for λ_1, the last two of which were determined with a variation function of the form $\varphi=C_1\varphi_0(b, a_0)+C_2\varphi_{-2}(b, a_0)+C_3\varphi_0(b, a_1)+C_4\varphi_1(b, a_1)$, where a_0 and a_1 are estimates for λ_0 and λ_1. A secular equation of prohibitively high degree would be necessary in order to attain the same accuracy for λ_1 as we were able to achieve for λ_0. We were not able to determine the value of b for which λ_1 vanishes.

Perturbation

The energy levels of the anharmonic oscillator with the wave equation

$$-\frac{\hbar^2}{2m}\frac{d^2\psi}{dx^2}+(A_0+2\pi^2 m\nu_0^2x^2+\sum_{i=3}^{\infty}A_ix^i)\psi=E\psi \quad (21)$$

are given by perturbation theory in the form

$$E_n=A_0+(n+\tfrac{1}{2})h\nu_0+\sum A_i\beta^{i/2}P^i$$
$$-\sum\sum\frac{A_iA_j\beta^{(i+j)/2}}{h\nu_0}P^{ij}$$
$$+\sum\sum\sum\frac{A_iA_jA_k\beta^{(i+j+k)/2}}{(h\nu_0)^2}P^{ijk}$$
$$-\sum\sum\sum\sum\frac{A_iA_jA_kA_l\beta^{(i+j+k+l)/2}}{(h\nu_0)^3}P^{ijkl}+\cdots, \quad (22)$$

where $\beta=\hbar/4\pi m\nu_0$ and the P's are certain polynomials in n. On substituting $x=(2\beta\gamma)^{\frac{1}{2}}z$, one obtains the reduced equation

$$-\psi''+\gamma^2(C_0+z^2+C_3z^3+C_4z^4+\cdots)=\Lambda\psi. \quad (23)$$

If the C_i's are pure numbers, as they are for the reduced Lennard-Jones potential (Eq. (6)), the terms of Λ_n should be arranged as a descending power series in γ:

$$\Lambda_n=C_0\gamma^2+(2n+1)\gamma+\left(\frac{C_4}{4}P^4-\frac{C_3^2}{16}P^{33}\right)$$
$$+\left[\frac{C_6}{8}P^6-\frac{C_4^2}{32}P^{44}-\frac{C_3C_5}{32}(P^{35}+P^{53})\right.$$
$$\left.+\frac{C_3^2C_4}{128}(P^{334}+P^{343}+P^{433})-\frac{C_3^4}{512}P^{3333}\right]\gamma^{-1}+0(\gamma^{-2}), \quad (24)$$

where

$$P^4=6n^2+6n+3$$
$$P^{33}=30n^2+30n+11$$
$$P^6=20n^3+30n^2+40n+15$$
$$P^{44}=68n^3+102n^2+118n+42$$
$$P^{35}+P^{53}=280n^3+420n^2+400n+130$$
$$P^{334}+P^{343}+P^{433}=1800n^3+2700n^2+2268n+684$$
$$P^{3333}=2820n^3+4230n^2+3270n+930.$$

When the reduced Lennard-Jones potential is expanded about its minimum in the form

$$V=25b^2[R^{-12}-R^{-6}]=\sum_{i=0}^{\infty}\gamma^2C_i(\Delta R)^i, \quad (25)$$

the coefficient of $(\Delta R)^i$ in the ascending power series is

$$\gamma^2C_i=\frac{25b^2(-1)^i}{2\cdot 2^{i/6}}\left[\frac{1}{2}\binom{i+11}{i}-\binom{i+5}{i}\right]. \quad (26)$$

The coefficient C_2 is unity in accordance with the convention of Eq. (23).

We can now employ Eqs. (24) and (26) to obtain the eigenvalues of Eq. (6):

$$-\lambda_n^2=-6.25\,b^2+13.363\,481\,(2n+1)\,b$$
$$+(6.134\,643\,P^4-2.430\,708\,P^{33})$$
$$+[1.874\,488\,P^6-1.408\,086\,P^{44}$$
$$-1.106\,819\,(P^{35}+P^{53})$$
$$+0.557\,921\,(P^{334}+P^{343}+P^{433})$$
$$-0.221\,063\,P^{3333}]\,b^{-1}+0\,(b^{-2}). \quad (27)$$

For the two most interesting cases $n=0$ and $n=1$, we have

$$\lambda_0^2=6.25\,b^2-13.363\,481\,b$$
$$+8.333\,859-1.120\,612\,b^{-1} \quad (28)$$

$$\lambda_1^2=6.25\,b^2-40.090\,433\,b$$
$$+80.560\,623-41.434\,03\,b^{-1}. \quad (29)$$

A few values of λ_0 and λ_1 obtained from Eqs. (28) and (29) are given in Table III. The accuracy of these two equations is shown by the agreement with the variation results at $b=7$, 10, and 15. The agreement for λ_0 persists at least as low as $b=5$. The value of λ_1 by variation at $b=5$ is probably quite low, since the root $\lambda_1=4.03$ was determined as a by-product of a variational equation designed to give λ_0 accurately.

ACKNOWLEDGMENT

The numerical calculations and a considerable portion of the algebra of this work were performed on a calculating machine that was very kindly loaned to us by the Los Alamos Scientific Laboratory, Los Alamos, New Mexico.

The Overlap Average and Central Field Approximations

CHARLES R. MUELLER AND HENRY EYRING
Chemistry Department, University of Utah, Salt Lake City, Utah
(Received November 16, 1950)

A series of approximations, which achieve a considerable simplification in molecular orbital calculations, is discussed. The method is to replace some of the more complex integrals in some cases by an "overlap average" of simpler integrals; in other cases to use a "central field" approximation. The effective charge of the central field point source is calculated by application of Gauss' theorem. These approximations are applied to diatomic lithium hydride.

ONE of the chief difficulties in the application of quantum mechanics to chemical problems is in the evaluation of the integrals representing the energy arising from the interelectronic repulsions.

The purpose of this paper is to discuss, extend, and estimate the accuracy of a series of approximations applied here to the *LCAO* molecular orbital method which achieve a considerable simplification in the calculation of numerical values for these "repulsive integrals." In connection with this purpose, we have found it necessary to discuss the theory of the "central field" approximation, replacement of an electric field of several sources by a field from a single source.

The more difficult of these "repulsive integrals" have the form

$$\int\int \frac{\varphi_a(1)\varphi_b(1)\varphi_a(2)\varphi_b(2)}{R_{12}} d\tau_1 d\tau_2 = \int ab/ab, \quad (1)$$

$$\int\int \frac{\varphi_a^2(1)\varphi_a(2)\varphi_b(2)}{R_{12}} d\tau_1 d\tau_2 = \int aa/ab, \quad (2)$$

where φ_a and φ_b are hydrogenic[1] or Slater-like[2] atomic orbitals. R_{12} is the distance between electrons 1 and 2 and $d\tau_1$ and $d\tau_2$ are the volume elements over which the integration is performed.

The integrals of these types which are discussed in this paper arise from two sources; the interaction of K shell electrons with bonding electrons; and the interaction of the bonding electrons with one another.

Since the eigenfunctions of the K shell electrons are spherically symmetric with respect to the nucleus, the potential arising from the system of a nucleus and its K shell electrons should, to a high degree of accuracy, be represented as originating from a single point source coincident with the nucleus. In the first section, the determination of the charge of this point source and the accuracy of this "central field" approximation is discussed, with emphasis on diatomic lithium hydride.

The two nonbonding electrons in this molecule are assigned to lithium 1s orbitals. If we use the customary linear combination of atomic orbitals for the bond eigenfunction:

$$\psi = a\varphi_a + b\varphi_b \quad (3)$$

where:

$$a^2 + 2abs + b^2 = 1 \quad (4)$$

$$s = \int \varphi_a \varphi_b d\tau.$$

The interaction of bonding electrons, having eigenfunctions like those of Eq. (3), has been discussed by Mulliken,[3] and for the heteropolar diatomic case, the interaction energy, the energy arising from interelectronic repulsion, is:

$$E_i = a^2 \int u_s aa + 2ab \int u_s ab + b^2 \int u_s bb, \quad (5)$$

where

$$\int u_s aa \cong \tfrac{1}{2}(1-Q)J_{aa} + \tfrac{1}{2}(1+Q)J_{ab} \quad (6)$$

$$\int u_s ab \cong \tfrac{1}{2}(1-Q)\int aa/ab + \tfrac{1}{2}(1+Q)\int bb/ab \quad (7)$$

$$\int u_s bb \simeq \tfrac{1}{2}(1+Q)J_{bb} + \tfrac{1}{2}(1-Q)J_{ab}, \quad (8)$$

φ_a and φ_b being atomic orbitals.

$$Q = b^2 - a^2 \quad (9)$$

$$J_{aa} = \int\int \frac{\varphi_a^2(1)\varphi_a^2(2)}{R_{12}} d\tau_1 d\tau_2 \quad (10)$$

$$J_{bb} = \int\int \frac{\varphi_b^2(1)\varphi_b^2(2)}{R_{12}} d\tau_1 d\tau_2 \quad (11)$$

$$J_{ab} = \int\int \frac{\varphi_a^2(1)\varphi_b^2(2)}{R_{12}} d\tau_1 d\tau_2. \quad (12)$$

Because J_{aa}, J_{bb}, and J_{ab} are much more easily evaluated than the other integrals, and can be reduced to algebraic functions, it is advantageous to introduce the

[1] L. Pauling and E. Wilson, *Introduction to Quantum Mechanics* (McGraw-Hill Book Company, Inc., New York, 1935), p. 132.
[2] J. C. Slater, Phys. Rev. **36**, 57 (1930).
[3] R. S. Mulliken, J. Chim. Phys. **46**, 497 (1949), Eqs. (104)-(106).

approximations*

$$\int aa/ab \cong s/2\{J_{aa}+J_{ab}\} \tag{13}$$

$$\int bb/ab \cong s/2\{J_{ab}+J_{bb}\}. \tag{14}$$

The accuracy of these "overlap average" approximations for the energy arising from the interaction of bonding electrons is considered in detail in Sec. II.

Finally in Sec. III the bond energy and charge distribution of diatomic lithium hydride are calculated, using the previously considered approximations.

The atomic orbitals in formula (3) are, for the lithium $2s$ electron

$$\varphi_a=\left(\frac{Z_2^5}{96\pi}\right)^{\frac{1}{2}}\exp-(Z_2r_a/2)r_a, \tag{15}$$

for the hydrogen $1s$ electron

$$\varphi_b=\frac{1}{\pi^{\frac{1}{2}}}e^{-r_b}, \tag{16}$$

for the lithium $1s$ electron

$$\varphi_1=\frac{Z_1^{\frac{3}{2}}}{\pi^{\frac{1}{2}}}\exp-(Z_1r_a), \tag{17}$$

all expressed in atomic units.

I. CENTRAL FIELD AND THE *K*-SHELL ELECTRONS

To the extent that the K-shell electrons are not polarized by the adjacent atom, the charge distribution of the innermost shell is spherically symmetric. Since Coulomb's law is valid for atomic and molecular dimensions, it seems safe to assume the validity of Gauss's theorem,

$$\int_S \mathbf{E}\cdot\mathbf{dS}=4\pi q, \tag{18}$$

where $\mathbf{E}$ is the electric field intensity, $\mathbf{dS}$, the surface element of integration and q, the net charge within the surface $\mathbf{S}$.

For a spherical charge distribution, integrating over a sphere of radius r

$$4\pi r^2\mathbf{E}=4\pi q, \tag{19}$$

$$V=q/r. \tag{20}$$

Now, the average net charge, q, within a sphere of radius r centered on the nucleus is the difference between the nuclear charge, Z_n, and the average number of electrons enclosed by the sphere. Our effective nuclear charge, Z_e, for the system of a nucleus and its K-shell electrons is, at r units from the nucleus,

$$Z_e=Z_n-2\int_0^r \varphi_K^2 d\tau, \tag{21}$$

where φ_k is the eigenfunction of the K-shell electrons.

For the diatomic lithium hydride molecule,

$$Z_e=3-2\int_0^r \varphi_1^2 d\tau$$

$$=3-8Z_1^3\left[\frac{2}{(2Z_1)^3}-\frac{r^2e^{-2Z_1r}}{2Z_1}-\frac{2re^{-2Z_1r}}{(2Z_1)^2}-\frac{2e^{-Z_1r}}{(2Z_1)^3}\right]. \tag{22}$$

The average distance of the lithium $2s$ electron from the nucleus is

$$\bar{r}=\int \varphi_a^2 r_a d\tau=5/Z_2 \text{ a.u.} \tag{23}$$

The effective charge, Z_1, of the lithium $1s$ electrons can be assigned as 2.688 by a variational treatment of the lithium atom.[4]

If (23) is substituted into (22), it is seen that Z_e is very close to one atomic unit of charge.

This charge for the single point source, replacing the nucleus and K-shell electrons, can be verified in a more complicated but direct way.

The average value of Z_e for the lithium $2s$ electron is

$$\bar{Z}_e=\int \varphi_a Z_e \varphi_a d\tau \tag{24}$$

where Z_e is given by Eq. (22).

Integrating, we have

$$\bar{Z}_e=1+\frac{4!}{6}\left(\frac{30Z_2^5Z_1^2}{(Z_2+2Z_1)^7}+\frac{5(Z_2^5Z_1)}{(Z_2+2Z_1)^6}+\frac{Z_2^5}{2(Z_2+Z_1)^5}\right)=1.0076. \tag{25}$$

Since, as a result of the calculations in Sec. IV, it is found that 66 percent of the charge of the bonding electrons is on the hydrogen atom (b^2 in Eq. (3) is 0.66) it is important that the effect of using a Z_e of 1.00 on these electrons be discussed. It is more convenient in this case to make a comparison of energies.

Let $H^{(1)}$ be the complete and exact hamiltonian for the two bonding electrons.

$$H^{(1)}=-\tfrac{1}{2}(\nabla_1^2+\nabla_2^2)-\frac{3}{R_{a1}}-\frac{3}{R_{a2}}-\frac{1}{R_{b1}}-\frac{1}{R_{b2}}+\frac{1}{R_{12}}+\frac{3}{R_{ab}}+\frac{2}{R_{k1}}+\frac{2}{R_{k2}} \tag{26}$$

* These approximations are suggested by Eq. (63) of Mulliken, reference 3.

[4] V. Guillemin and C. Zener, Z. Physik **61**, 199 (1930).

TABLE I. Validity of the approximations for $\int aa/ab$ and $\int bb/ab$.

Z_2	$\int aa/ab$ Approx.	$\int aa/ab$ Integration	$\int bb/ab$ Approx.	$\int bb/ab$ Integration
1.00	0.0899	0.0799	0.1806	0.1882
1.25	0.1171	0.1136	0.2051	0.2161
1.50	0.1414	0.1357	0.2203	0.2277
1.75	0.1547	0.1493	0.2210	0.2291
2.00	0.1647	0.1572	0.2171	0.2225
2.30	0.1688	0.1584	0.2046	0.2057

where the subscripts 1 and 2 refer to the electrons, subscript a to the lithium nucleus; b to the hydrogen nucleus; k to the lithium 1s electrons and R_{ab} is the distance between nuclei.

Similarly, for our central field approximation, the hamiltonian is

$$H^{(2)}=-\tfrac{1}{2}(\nabla_1^2+\nabla_2^2)-\frac{1}{R_{a1}}-\frac{1}{R_{a2}}-\frac{1}{R_{b1}}-\frac{1}{R_{b2}}+\frac{1}{R_{12}}+\frac{1}{R_{ab}}. \quad (27)$$

The total energy for the systems described by these hamiltonians are

$$E^{(1)}=\int \psi H^{(1)}\psi d\tau \quad (28)$$

$$E^{(2)}=\int \psi H^{(2)}\psi d\tau. \quad (29)$$

On integration it is found that

$$\int \psi_b H^{(1)}\varphi_b d\tau = 0.9910 \int \varphi_b H^{(2)}\varphi_b d\tau. \quad (30)$$

It is estimated that, because of this discrepancy, the approximation which we have introduced will cause a 3 percent increase in bond energy over that obtained by direct integration.

Several comments can be made on the equations of this section.

We can use the preceding equations to find the accuracy of assigning an effective nuclear charge of Z_n-2 to the point source representing the K-shell electrons and the nucleus to which they belong. This is, of course, equivalent to a field in which the two electrons and nucleus are confident.

For example, to digress for a moment the average effective nuclear charge for the carbon 2s electrons in the free atom is, by a method exactly analogous to that previously used,

$$\bar{Z}_e=4+\frac{4!}{6}\left(\frac{30Z_2^5Z_1^2}{(Z_2+2Z_1)^7}+\frac{5Z_2^5Z_1}{(Z_2+2Z_1)^6}+\frac{Z_2^5}{2(Z_2+Z_1)^5}\right). \quad (31)$$

The eigenfunctions for carbon 1s and 2s electrons have the same functional form as given in Eqs. (15) and (17) except that Z_1 and Z_2 are considerably higher.

A variational treatment of the C^{4+} ion gives a Z_1 of 5.688 and it is found that a simultaneous variation of Z_1 and Z_2 changes the value but slightly. The independence of Z_1 from the presence of surrounding electrons is, in fact, the basis of Slater's rule[2] that "the shielding constant, s, is formed, for any group of electrons, from the following contributions:

(a) Nothing from any shell outside the one considered. . . ."

As a first approximation, let Z_2 be 4.00. The value of the average effective nuclear charge is, from Eq. (31), 4.053. This provides some justification of the use of 4.00 by Goeppert-Mayer and Sklar.[5]

For atoms possessing a greater number of outer shell electrons, it is probably better to calculate an explicit value.

II. THE REPULISVE FIELD OF THE BONDING ELECTRONS

The approximations which Mulliken[3] has suggested for the interaction energy of the two bonding electrons in heteropolar diatomic molecules have already been given in Eqs. (5) to (8). Additional approximations are introduced in Eqs. (13) and (14) for $\int aa/ab$ and $\int bb/ab$ (compare Eq. (2)).

These approximations are applied in this section to diatomic lithium hydride, and tabular comparisons are made of the values of the integrals obtained by the various approximations and by direct integration. The values of the integrals are obtained from the tables of Kotani, Amemiya, and Simose,[6] Kotani and Amemiya,[7] or were evaluated by the authors.

This is the first application of the approximations suggested by Mulliken to a molecular orbital which is a linear combination of 1s and 2s atomic orbitals.

Table I gives the values for $\int aa/ab$ and $\int bb/ab$ obtained by the approximations,

$$\int aa/ab \cong s/2(J_{aa}+J_{ab})$$

and

$$\int bb/ab \cong s/2(J_{bb}+J_{ab}).$$

The errors which result are, in some cases, of appreciable magnitude. In Table II, where the validity of the approximations for $\int u_s aa$, $\int u_s ab$, and $\int u_s bb$ are considered, it appears that there is, to some extent, a cancellation of errors. In the calculations of Table II,

[5] M. Goeppert-Mayer and A. L. Sklar, J. Chem. Phys. 14, 259 (1942).

[6] Kotani, Amemiya, and Simose, Proc. Phys.-Math. Soc. Japan 22, 20, Extra Number (1938).

[7] M. Kotani and A. Amemiya, Proc. Phys.-Math. Soc. Japan 22, Extra Number (1940).

the coefficients of the atomic orbitals, in the molecular orbital given by Eq. (7), are taken equal; a is equal to b. In this way, a more typical comparison is made than those which follow for the specific case of lithium hydride.

In Table III, Z_2 is assigned a value of 1.00 and the quantity R is a^2/b^2, the ratio of the squares of the coefficients of the atomic orbitals. The worst error is about 5 percent of the bond energy, and this occurs for a highly ionic bond. The cause is not difficult to ascertain. Any process which depends on some sort of average of two quantities to obtain the value of a third, as this method repeatedly does, is more and more susceptible to error, the more different in magnitude the first two quantities are.

An enormous advantage of the preceding approximations is that it reduces the calculation of the energy arising from the repulsion of the two bonding electrons to a function of J_{aa}, J_{bb}, and J_{ab}. J_{aa} and J_{bb} can be evaluated by direct integration in spherical coordinates, and this integration, while sometimes tedious, is quite straightforward. J_{ab} is evaluated by a method described in the article by Kotani, Amemiya, and Simose,[6] and reduces to a function of $A_n(\alpha)$'s and $B_m(\beta)$'s where

$$A_n(\alpha)=\int_1^\infty e^{-\alpha\lambda}\lambda^n d\lambda, \tag{32}$$

$$B_m(\beta)=\int_{-1}^{+1} e^{-\beta\mu}\mu^m d\mu, \tag{33}$$

λ and μ being the elliptic coordinates. $A_n(\alpha)$ and $B_m(\beta)$ are in turn easily calculated by the recursion formulas,

$$A_n(\alpha)=1/\alpha\{e^{-\alpha}+nA_{n-1}(\alpha)\} \tag{34}$$

$$B_m(\beta)=1/\beta\{(-1)^m e^{\beta}-e^{-\beta}+mB_{m-1}(\beta)\}. \tag{35}$$

For example, J_{ab} for diatomic lithium hydride is[6]

$$J_{ab}=\frac{1}{24}\delta^5R^4\Big\{(A_3'B_0'+3A_1'B_2'+3A_2'B_1'+A_0'B_3') -(A_3B_0+3A_1B_2+3A_2B_1+A_0B_3) -\frac{R}{2}(A_4B_0-2A_1B_3+2A_3B_1-A_0B_4)\Big\} \tag{36}$$

R is the internuclear distance.

$$\delta=Z_2/2,$$
$$A_m'=A_m(\delta R),\quad A_m=A_m((\delta+1)R),$$
$$B_m'=B_m(\delta R),\quad B_m=B_m((\delta-1)R).$$

While the integration of J_{ab} is quite tedious, it is not nearly as difficult as the remaining integrals, and the application of the approximations previously considered effect a tremendous reduction in labor.

TABLE II. Validity of the approximations for $\int u_s aa$, $\int u_s ab$, and $\int u_s bb$ with equal atomic orbital coefficients.

	Z_2	1.50	1.75	2.00
$\int u_s aa$	Approx.	0.2896	0.3184	0.3493
	Integration	0.2856	0.3147	0.3438
$\int u_s ab$	Approx.	0.1808	0.1879	0.1910
	Integration	0.1887	0.1933	0.1932
$\int u_s bb$	Approx.	0.4512	0.4549	0.4607
	Integration	0.4563	0.4602	0.4636

III. THE DIATOMIC LITHIUM HYDRIDE MOLECULE

Using the approximations previously considered, a calculation of the binding energy and charge distribution of diatomic lithium hydride was made, using the hamiltonian of Eq. (27).

The effective charges, Z_2 of the lithium atomic orbital and Z_h of the hydrogen atomic orbital, were taken as 1.00. The coefficients, a and b, of the atomic orbitals in the molecular orbital were obtained by graphical variation. The internuclear distance observed by Nakamura[8] (1.6A) was used.

The calculated binding energy was 1.855 electron-volts in comparison with the experimental value of 2.56 ev.[8] The calculated value is 72.5 percent of the experimental binding energy and 82.3 percent of that obtained by Knipp,[9] using a very complicated eigenfunction, in the best quantum-mechanical calculation.

Binding energy, in the sense that we have used the term, is the difference between the total energy of the two bonding electrons, including the energy of repulsion of the lithium and hydrogen cores, and the total energy of a lithium $2s$ and a hydrogen $1s$ electron. The energy of the lithium $2s$ electron and the hydrogen $1s$ electron are assigned values corresponding to the first

TABLE III. The repulsive energy from approximation and integration.

	R	1	4	8
$a^2\int u_s aa$	Approx.	0.0740	0.0319	0.0189
	Integration	0.0709	0.0310	0.0184
$2ab\int u_s ab$	Approx.	0.0948	0.0927	0.0808
	Integration	0.0961	0.0905	0.0840
$b^2\int u_s bb$	Approx.	0.1485	0.3056	0.3829
	Integration	0.1497	0.3084	0.3855
Total	Approx.	0.3173	0.4303	0.4826
	Integration	0.3167	0.4298	0.4879

[8] G. Nakamura, Z. Physik 59, 218 (1930).
[9] J. Knipp, J. Chem. Phys. 4, 300 (1936).

ionization potentials of the lithium and hydrogen atoms respectively.

In the case of the lithium 2*s* electron, this is probably a quite accurate estimate of total energy, since the energy of the *K* shell is almost unaffected by the presence or absence of *L* shell electrons. For the hydrogen 1*s* electron, the ionization potential is, of course, equal to the electronic energy.

The value of *a*, the coefficient of the lithium 2*s* atomic orbital was found to be 0.332 and *b*, the coefficient of the hydrogen 1*s* atomic orbital was 0.812.

About 11 percent of the electronic charge cloud of the bonding electrons is on the lithium atom, 23 percent in the overlap, and 66 percent on the hydrogen atom. This is about what one would expect from the saline character of the compound.

THE JOURNAL OF CHEMICAL PHYSICS VOLUME 19, NUMBER 7 JULY, 1951

The Microwave Spectrum of Sulfur Dioxide*

M. H. SIRVETZ†‡
Mallinckrodt Chemical Laboratory, Harvard University, Cambridge, Massachusetts
(Received March 14, 1951)

The *K*-band microwave spectrum of sulfur dioxide has been reinvestigated with results which are in agreement with the main points of the previously reported analysis by Dailey, Golden, and Wilson. Some additional lines have been assigned, and new rotational constants have been derived which permit considerably closer agreement between observed and computed frequencies. From two of these the structural parameters $r(S-O)=1.432$A and $\measuredangle(O-S-O)=119.53°$ can be obtained. The remaining discrepancy (of the order of 15 mc for ten lines involving J values up to $J=35$) has been attributed to inaccuracies in the centrifugal distortion computation.

INTRODUCTION

THE *K*-band microwave spectrum of sulfur dioxide has been observed and partially analyzed by Dailey, Golden, and Wilson.[1] Using the Stark effect pattern[2] for the lines at 29321.46 and 23414.24 mc, they were able to assign six of the eleven strongest lines. From these assigned frequencies, they found the structure of the molecule to be very close to that previously obtained by other methods.[3,4] In making this structure determination, they used the rigid rotor formula corrected roughly for centrifugal stretching effects.

Although the structural result was satisfactory, the agreement between observed frequencies and those computed according to the quantum-mechanical formulas was disappointingly poor, i.e., of the order of 60 mc. At that time no other asymmetric top molecule had been subjected to extensive analysis, so that the question was open as to whether additional effects needed to be taken into account which might make the agreement better. Because of this discrepancy, the molecule has been reinvestigated with more accurate frequency measuring equipment and with a further extension of the calculations in an effort to see whether a better fit with the theory could be obtained. As a result, it has been found that the frequency measurements made earlier with a cavity wave meter were not as accurate as had been believed and that there was an error in sign in the centrifugal distortion formula used.[5] Furthermore, it now appears that the correction for centrifugal distortion cannot be made with an accuracy comparable to the accuracy of measurement on the basis of existing information regarding the force constants. The final result of the present study has been to confirm the quantum number assignments previously made and to reduce the discrepancy between theory and experiment to about 15 mc, a value which is compatible with the uncertainty in the centrifugal distortion correction. The structure resulting from this improved analysis differs very little from that previously reported.

EXPERIMENTAL DETAILS

Most of the experimental work was performed on a Stark effect microwave spectroscope, of the type described by McAfee, Hughes, and Wilson,[6] which covered the frequency range 20,000 to 30,000 mc. The frequencies, given in Table I, were measured by the usual technique of beating the microwave radiation against harmonics of an accurately known fundamental fre-

* The research reported in this paper was made possible by support extended to Harvard University by the ONR under Contract N5ori-76, Task Order V.
† Present address: Brookhaven National Laboratory, Upton, Long Island, New York.
‡ AEC Predoctoral Fellow.
[1] Dailey, Golden, and Wilson, Phys. Rev. **72**, 871 (1947); for more detail see also S. Golden, thesis, Harvard University, Cambridge, Massachusetts, 1948.
[2] S. Golden and E. B. Wilson, Jr., J. Chem. Phys. **16**, 669 (1948).
[3] W. G. Penney and G. B. B. M. Sutherland, Proc. Roy. Soc. (London) **156**, 654 (1936).
[4] V. Schomaker and D. P. Stevenson, J. Am. Chem. Soc. **62**, 1267 (1940).
[5] S. Golden, J. Chem. Phys. **16**, 250 (1948); and erratum, *ibid.* **17**, 586 (1949).
[6] McAfee, Hughes, and Wilson, Rev. Sci. Instr. **20**, 821 (1949).

quency. The new measurements have a precision of about 0.1 mc (estimated standard deviation).

Relative intensities were measured by a technique developed by Dr. D. H. Baird[7] consisting essentially of comparing the alternating current component of the signal from the detecting crystal at the peak of the absorption line with a standard signal of the same frequency and of variable magnitude. Comparison of intensity of absorptions at widely separated frequencies is not at present possible by this method, so that in Table I the notation S, M, W for strong, medium, and weak is used to give a rough indication of relative intensities. For the intensity of a single line at different temperatures, or for two nearby lines ($\delta\nu\sim$a few 100 mc), however, it is believed that the accuracy of comparisons is of the order of 10 percent.

The ratio of relative intensities of a line at two different temperatures (room temperature and dry ice temperature, usually) gives the energy of the initial level involved, according to the relation

$$E_i=[kT_1T_2/(T_2-T_1)][\ln I(T_2)/I(T_1) +3\ln(T_2/T_1)], \quad (1)$$

where the factor 3 depends upon the assumptions made concerning the effect of temperature on line breadth and may be somewhat in error. Because of a certain cancellation of errors, the difference in initial energies of two different nearby lines is determined with somewhat greater accuracy by this type of measurement than are the E_i's themselves. We have

$$\Delta E_i=E_i-E_i'=[T_1T_2/(T_1-T_2)] \times k\ln[I(T_1)I'(T_2)/I(T_2)I'(T_1)]. \quad (2)$$

Equations (1) and (2) proved useful in two specific cases in the course of the analysis.

It will be observed that there are two strong lines (at 24039.50 and 24083.38 mc) very close to one another. The analysis up to this point called for the appearance of the $9_{1,9}\rightarrow 8_{2,6}$ transition in this frequency region, but making a definite assignment on the basis of frequency considerations alone seemed impossible. For example, a change in θ of only 0.02° would shift the predicted frequency from one position to the other. Using Eq. (2), it was found experimentally that the line at 24083.38 was the one for which E_i was lower, and that $\Delta E_i\cong 4.97\times 10^6$ mc. The conclusion is that the line at 24083.38 mc is to be assigned to $9_{1,9}\rightarrow 8_{2,6}$, and that the other corresponds to a transition with J of the order of 22. Detailed computation then showed that the transition $22_{4,18}\rightarrow 21_{5,17}$ should, indeed, appear at approximately the observed frequency (24039.50 mc), and that the ΔE_i is then 4.81×10^6 mc, in good agreement with the experimental value.

Intensity measurements were used again near the end of the analysis. A systematic program of computation of all transitions ($J\leq 25$) for which a symmetric-rotor energy equation had indicated a possibility of a transition in the K-band led to assignments for nine of the eleven strong lines observed. The lines at 25049.13 and 23034.83 mc remained unassigned, and we wanted to confirm the conjecture that they were of higher J than the highest J for which computations had been made. Using Eq. (1), it was found that E_i for the first was $\sim 1.1\times 10^7$ mc; for the second, $\sim 2.4\times 10^7$ mc. The latter has, accordingly, been dismissed as being of "high" J ($J=50$ or so), while the former appeared to be of J not much higher than 30. On extending the range of calculation beyond $J=25$, it was found that the transition $34_{7,27}\rightarrow 35_{6,30}$ should appear near the observed frequency (25049.13 mc). Its E_i is 1.4×10^7 mc, the agreement with the experimental value being about as good as can be expected, especially in view of the uncertainty regarding the variation of line breadth with temperature.

TABLE I. Observed frequencies in the spectrum of sulfur dioxide.

Frequency (mc)	Intensity
20335.40	S
20460.05	W
22220.32	W
22482.51	S
22733.83	M
22904.95	M
22928.45	W
23034.83	S
23414.24	S
23733.03	W
24039.50	S
24083.38	S
24319.67	M
25049.13	S
25170.97	W
25392.81	S
26777.20	S
28858.11	S
29321.46	S

ANALYSIS OF THE SPECTRUM

It is well known that because of the interaction of rotation and vibration the effective principal moments of inertia of a planar molecule do not obey the sum rule, $I_c=I_a+I_b$. In particular, the rotational spectrum of sulfur dioxide is determined by three independent parameters which must be determined empirically and which bear no simple exact relationship to the equilibrium structural parameters of the molecule. To a certain approximation, however, the effective aplanarity may be neglected, in which case the frequency of any transition considered is given as a function of the two structural parameters, r and θ. Such an ideally rigid model was adopted as a basis for computation in the early stages of the analysis. The two lines whose Stark effects had been resolved were assigned in turn to each of those pairs of transitions which might provide Stark effect patterns similar to those observed. Each such assignment provided values of r and θ which were used in turn to predict other transitions in the K-band. The con-

[7] D. H. Baird, Ph.D. thesis, Harvard University, Cambridge, Massachusetts, 1950.

TABLE II. The centrifugal distortion coefficients, $\tau_{\alpha\beta\gamma\delta}$ (erg^{-3} sec^{-4}).

$\alpha\beta\gamma\delta$	$\tau_{\alpha\beta\gamma\delta}\times10^{-86}$
aaaa	−470.5
bbbb	−2.288
cccc	−0.7645
aabb	+21.52
aacc	+5.728
bbcc	−1.195
abab	−2.954

clusion was that only a single, uniquely determined structure could explain the K-band spectrum as a whole.

Sulfur dioxide may be shown to be a nearly prolate symmetrical top with its unique axis lying in the plane and perpendicular to the (principal) axis along which the dipole moment lies. Because of the zero spin of the O^{16} nucleus, only the levels $J_{e,e}$ and $J_{o,o}$ are permitted.[8] The selection rules, $\Delta J=0$, ±1, and $\Delta K=\pm1$, ±3, $\cdots$, apply.

The symmetric-top energy equation is, in this case,

$$E^{J}{}_{-K_1,\,K_{+1}}\,(\mathrm{mc})=9500J(J+1)+51000K_{-1}^{2}. \quad (3)$$

It is clear that the Q-branch transitions of lowest frequency (i.e., $\Delta J=0$, $K_{-1}=0$ to $K_{-1}=1$) occur well above the maximum frequency observed. Even if the numerical factor 51000 were in such error as to cause these transitions to fall in the K-band, all of them (only $J=$even occur) would appear at the same frequency except for a shift, increasing monotonically with J, due to the asymmetry. Such a series would be easily recognizable and has not been observed. The important transitions are of the form $\Delta J=+1$; $\Delta K=-1$; and $\Delta J=-1$, $\Delta K=+1$. (Transitions with $|\Delta K|>1$ are of much lower intensity.) The approximate frequency of such a transition is given by

$$\nu=|19000J-51000(1+2K_{-1})|, \quad (4)$$

where both quantum numbers refer to the state of higher J. From the condition $0\leqq K_{-1}\leqq J$, it may be inferred that for any value of J, no matter how high, there will be a value of K_{-1} giving rise to a transition of frequency lying in, or not far removed from, the K-band. Because of the degeneracy factor $(2J+1)$ occurring in the expression for the level population, the intensity is expected to be high even for quite large values of J. Actually, only at roughly $J>50$ does an appreciable decrease in intensity occur because of the Boltzmann factor.

Equation (4) cannot be used in the detailed analysis. It was used, however, to pick out those transitions for each value of J which might conceivably fall in the observable region. Further selection from among these still very numerous possibilities may be made by a perturbation calculation (expansion of the energy levels in a power series in the asymmetry parameter) or, for high J, by using Golden's[9] convenient method of employing the tabulated characteristic values of Mathieu's differential equation as approximations to the roots of the energy matrix. The exact frequencies were computed by expansion of the secular equations in the form of continued fractions[8] and solution by successive approximations. A systematic investigation in this way of all levels through $J=35$ led to assignments for ten of the eleven strong lines observed. As mentioned previously, there is experimental evidence that the remaining line should be of J higher than $J=35$. It should also be mentioned that the extensive computations predict the appearance of no lines other than those observed, for this range of J.

The effect of centrifugal distortion was taken into account, according to the method developed by Wilson.[10] The energy matrices were modified by small terms, quartic in the angular momentum components and depending on the force constants and the assumed structure of the molecule; and the resulting matrices were diagonalized. Carrying out this computation exactly, however, is made very difficult by the fact that centrifugal distortion not only modifies the (K, K) and $(K, K\pm2)$ matrix elements, which alone are different from zero in the case of a rigid molecule, but also introduces non-zero $(K, K\pm4)$ elements; and the latter make the usual method of continued fractions inapplicable. The method adopted was suggested by the fact that the $(K, K\pm4)$ elements produce only a small contribution to the total correction. This can be verified in any particular case by comparing this contribution, as evaluated by Golden's approximate method,[5] with the value of the diagonal perturbing element. It then seemed a reasonable procedure to set the troublesome $(K, K\pm4)$ elements equal to zero in performing the diagonalization (in which case the continued fraction method of computation is similar to that for a rigid molecule), and to take them into account finally in a pure correction term evaluated by Golden's Mathieu function method. This was done in every case except for the $34_{7,27}\rightarrow35_{6,30}$ transition where the required fourier transformation coefficients were not available.

The centrifugal distortion coefficients are defined by the equation

$$\tau_{\alpha\beta\gamma\delta}=-\tfrac{1}{2}\sum_k(\partial\mu_{\alpha\beta}/\partial Q_k)_0(\partial\mu_{\gamma\delta}/\partial Q_k)_0/\lambda_k, \quad (5)$$

where $\lambda_k=4\pi^2\nu_k^2$, the $\mu_{\alpha\beta}$ are the elements of the matrix inverse to the inertial matrix, and the summation is over the normal coordinates, Q_k. In the case of sulfur dioxide, symmetry considerations show that seven independent τ's are different from zero. Since this is more than the number of lines of moderately high J, it seemed impractical to obtain these coefficients empirically. Instead, they were computed once and for all from the approximate structural and vibrational data available. The fundamental frequencies adopted were 1150.5,

[8] King, Hainer, and Cross, J. Chem. Phys. **11**, 27 (1943).

[9] S. Golden, J. Chem. Phys. **16**, 78 (1948).

[10] E. B. Wilson, Jr., J. Chem. Phys. **5**, 617 (1937).

524.5, and 1336.0 cm^{-1}. Assuming a pure valence force field, the coefficients given in Table II were computed. Considering the errors in the data used as well as the many approximations involved in the computation, it is doubtful whether these quantities are to be trusted to more than a few percent.

RESULTS AND COMPARISON WITH THEORY

If we assume that the centrifugal distortion coefficients, $\tau_{\alpha\beta\gamma\delta}$, are correct, the problem of fitting the observed spectrum reduces to finding the three rotational parameters by a least-squares computation. This has been done, using nine of the assigned lines; the results are presented in Table III. Along with the assignments and the observed frequencies, we give in column I the frequencies computed from the "best" set of moments obtained by a calculation that weights the low J levels heavily. We see that for the six lines of lowest J (those which had previously been assigned) the mean discrepancy has been reduced from over 50 mc to about 3.4 mc. The transitions of high J, however, fit quite badly because of their greater sensitivity to small errors in the moments. (Frequencies, of the order of 25,000 mc, are computed as the difference of two terms each of the order of 500,000 mc.) It seemed worth while to compute another "best" set of moments weighting the high J levels heavily, and the computed frequencies so obtained are given in column II. In this way the best over-all fit is obtained, the mean deviation being of the order of 15 mc.

Actually, the two sets of moments differ by no more than 0.01 percent. The mean values of the effective moments of inertia (in units of 10^{-40} g cm^2) are

$$I_a=13.8046,$$
$$I_b=81.3067,$$
$$I_c=95.3376.$$

Evidence for the correctness of the analysis is obtained by considering the value of $I_c-I_b-I_a=0.226$. The value computed from vibrational data, using an equation given by Darling and Dennison,[11] is 0.23. It is believed that the chief source of the remaining discrepancy lies in errors in the coefficients, $\tau_{\alpha\beta\gamma\delta}$, which depend on force constant information. For $J\sim20$, the contribution to the energy levels by centrifugal distortion is of the order of 3000 mc. Thus errors in the τ's of only a percent or so could cause the observed discrepancy.

It is not possible to obtain structural parameters from effective moments of inertia with the same accuracy with which the moments themselves are known. If, however, a pair of moments is used, the aplanarity thus being neglected, approximate values may be calculated. From I_a and I_b are thus derived the values

$$r=1.432\text{A},$$
$$\theta=119.53°.$$

[11] B. T. Darling and D. M. Dennison, Phys. Rev. **57**, 128 (1940).

TABLE III. Comparison of observed and predicted frequencies (mc).

Transition	ν (observed)	ν (computed) I	II
$3_{1,3}\rightarrow 4_{0,4}$	29321.46	29320.9	29336.9
$6_{1,5}\rightarrow 5_{2,4}$	23414.26	23411.6	23379.2
$7_{2,6}\rightarrow 8_{1,7}$	25392.81	25391.1	25439.1
$9_{1,9}\rightarrow 8_{2,6}$	24083.39	24080.9	24090.9
$13_{2,12}\rightarrow 12_{3,9}$	20335.47	20339.2	20313.0
$16_{3,13}\rightarrow 17_{2,16}$	28858.11	28867.1	28858.5
$22_{4,18}\rightarrow 21_{5,17}$	24039.50	24153.3	24039.5
$23_{5,19}\rightarrow 24_{4,20}$	22482.51	22352.8	22490.1
$24_{5,19}\rightarrow 25_{4,22}$	26777.20	26674.9	26768.3
$34_{7,27}\rightarrow 35_{6,30}$	25049.13		

The extent to which these may be considered meaningful is indicated by the values of these quantities computed from I_b and I_c:

$$r=1.435\text{A},$$
$$\theta=119.13°.$$

THE UNASSIGNED LINES

The analysis has been concerned only with the eleven strong lines. There remain several considerably weaker lines, the frequencies of some of which are given in Table I. They are believed to arise in rotational transitions of several different types: (1) transitions involving isotopic variants of sulfur dioxide, especially $S^{34}O_2$; (2) transitions of molecules in excited vibrational states (the first bending mode is appreciably populated); (3) transitions of the type already used in the analysis but of higher J; (4) transitions with $|\Delta K|>1$. The last two classes are intrinsically of rather slight interest, since they give information only of the sort already obtained. An attempt was made to assign lines in the first two classes, but no definite conclusions were reached. This was essentially because of the characteristic property of this type of asymmetric rotor molecule that rather slight changes in structural parameters produce, through changes in the asymmetry of the molecule, quite unexpectedly large frequency shifts. Thus, calculation indicates that none of the assigned strong lines of moderately low J should have an isotopic "satellite" in the K-band. On the other hand, measurements of the effect of change of temperature on intensity of some of the observed weak lines indicate that they are "satellites" of unknown main lines presumably falling outside the observable region.

ACKNOWLEDGMENTS

The author would like to express his gratitude to Professor E. Bright Wilson, Jr., who suggested this problem, and to Drs. D. H. Baird and R. M. Fristrom for much helpful advice during the course of this research.

Intensities of Some Characteristic Infrared Bands of Ketones and Esters*

S. A. FRANCIS
Beacon Laboratories of The Texas Company, Beacon, New York
(Received March 21, 1951)

Integrated intensities of the 2900, 1720, 1460, 1370, and 1200 cm^{-1} bands are reported for four ketones and five esters, and grating spectra are shown for the 2780–3060 and 1300–1500 cm^{-1} spectral regions. CH_3 and CH_2 structural group integrated intensities are derived from the data which are adequate for predicting the integrated molecular intensities of the bands in the 2900, 1460, and 1370 cm^{-1} spectral regions. The data show that the carbonyl and ester structural groups reduce the intensities of the stretching modes and increase the intensities of the deformation modes of adjacent CH_3 and CH_2 groups. A number of empirical correlations are pointed out between positions of absorption maxima in the 2900, 1460, and 1370 cm^{-1} regions and the internal molecular environment of CH_3 and CH_2 groups.

INTRODUCTION

IN a previous paper[1] unit structural group integrated intensities were obtained for $-CH_3$, $\diagdown CH_2 \diagup$ and $-\diagdown\!\diagup CH$ structural groups of paraffin hydrocarbons in the 2900, 1460, and 1370 cm^{-1} spectral regions. The internal molecular environment of a structural group was found to have very little effect upon the structural group integrated intensities for the hydrocarbons studied. In the present work the effects of the carbonyl ($\diagdown C{=}O \diagup$) group of ketones and of the ester ($O{=}C{-}O$) group upon the CH_3 and CH_2 structural group intensities are investigated.

The infrared absorption spectra of a large number of ketones and esters, including those studied here, have been reported previously by Thompson and Torkington[2] and by Titeica.[3] Relatively strong bands are found in the spectra of all the ketones and esters in the 2800–3000 and the 1330–1500 cm^{-1} regions which are very probably associated with the stretching and deformational modes of CH_3 and CH_2 groups, respectively. A strong band is observed in the spectra of ketones near 1720 cm^{-1} and of esters near 1740 cm^{-1} which is almost surely associated with the stretching vibration of the carbonyl bond. Thompson and Torkington reported a strong band in the spectra of esters in the vicinity of 1200 cm^{-1} which they associated with the C–O bond between the carbonyl group and the part of the ester derived from an alcohol. A relatively strong band is also found in the ketone spectra near this position.

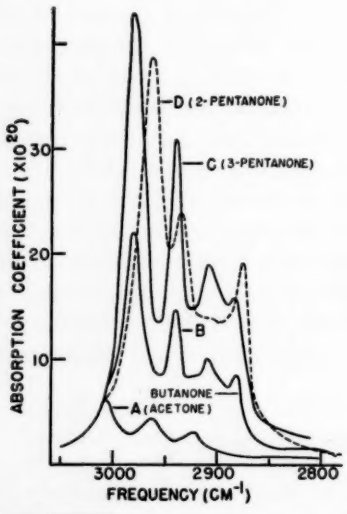

FIG. 1. Grating spectra for ketones in 2900 cm^{-1} region. A. Acetone. B. Butanone. C. 3-pentanone. D. 2-pentanone.

Integrated intensity data have been reported previously for three bands in the spectrum of acetone vapor by Price.[4]

In the present work the integrated intensities of the 2900, 1720, 1460, 1370, and 1200 cm^{-1} bands were measured for four ketones and five esters. The results indicate that the carbonyl and the ester groups strongly affect the absorption intensities of the stretching and deformation bands of adjacent CH_3 and CH_2 groups. Some correlations are pointed out also between the positions of absorption maxima in the 2900, 1460, and 1370 cm^{-1} regions and the structural groups present in the molecules.

EXPERIMENTAL

The spectral data were obtained with the evacuated spectrometer described previously.[1,5] A 4×6 inch echelette replica grating ruled with 3610 lines per inch was used in the 2900, 1720, 1460, and 1370 cm^{-1} regions, and a sodium chloride prism was used in the 1200 cm^{-1} region. The spectral slit widths were 1.4 cm^{-1} in the 2900 cm^{-1} region, 1.1 cm^{-1} in the 1720, 1460, and 1370 cm^{-1} regions, and 2.6 cm^{-1} in the 1200 cm^{-1} region. The cells consisted of two NaCl plates separated by either a platinum or a lead spacer. Cell thicknesses

* Presented in part at the 1951 Pittsburgh Conference on Analytical Chemistry and Applied Spectroscopy, March, 1951.

[1] S. A. Francis, J. Chem. Phys. **18**, 861 (1950).

[2] H. W. Thompson and P. Torkington, J. Chem. Soc. **1945**, 640 (1945).

[3] Radu Titeica, Ann. phys. (11) **1**, 533 (1934).

[4] Donna Price, J. Chem. Phys. **9**, 725 (1941). Since Price's results are about twenty times as large as those reported later in this paper, it seems likely that an error was made by Price in stating the intensity units employed.

[5] R. A. Oetjen, J. Opt. Soc. Am. **35**, 743 (1945).

were determined by an interference method,[6] and the variation in cell thickness over the area used was not more than about one percent. The spectral data were recorded on a Brown strip-chart recorder and the integrated intensities were calculated directly from the spectral records with the logarithmic integrator referred to previously.[1] Data obtained with the grating were corrected for stray radiation. No correction was required for the prism data, since the instrument was operated as a double monochromator.

The ketones were prepared by The Pennsylvania State College Standards Project on Oxygenated Compounds under the direction of Dr. Newell C. Cook, and their purities exceed 99 percent. The methyl acetate, ethyl acetate, and methyl propionate were

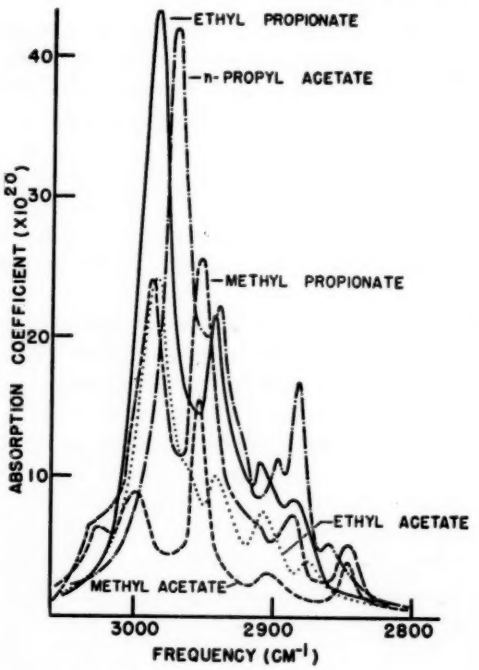

FIG. 2 Grating spectra for esters in 2900 cm^{-1} region – – – – – – Methyl acetate. ····· Ethyl acetate. –·–·– n-propyl acetate. – – – – Methyl propionate. ——— Ethyl propionate.

Eastman Kodak samples which were freshly distilled prior to use, a middle fraction being used. The n-propyl acetate and ethyl propionate were kindly supplied by Professor E. J. Serfass of Lehigh University, and their physical properties indicate they are of high purity.

Carbon tetrachloride solutions of the compounds were examined in either a 0.1- or 0.5-mm cell. Solution concentrations varied in the range 0.05–1.0 molar depending upon the strength of the absorption band being studied. Data were obtained at a series of solution concentrations in a number of cases to determine if there was any effect of dilution upon the integrated intensity. Within the limits of reproducibility of the results, which was about ±5 percent, no such effects

[6] D. C. Smith and E. C. Miller, J. Opt. Soc. Am. **34**, 130 (1944).

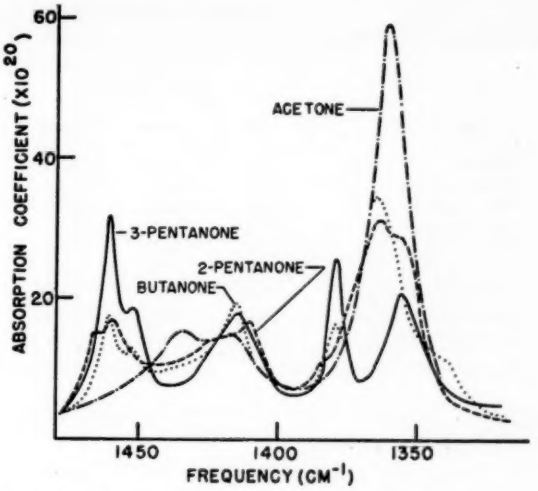

FIG. 3. Grating spectra for ketones in 1400 cm^{-1} region. ·—·— Acetone. ····· Butanone. – – – – – – 2-plantanone. ——— 3-pentanone.

were observed. The transmission of the cell filled with sample was compared in each case with the transmission of the same cell filled with pure solvent.

CH_3 AND CH_2 GROUP INTENSITIES

Since only prism spectra for most of the compounds studied have been published, the grating spectra in the 2780–3060 and the 1300–1500 cm^{-1} spectral regions are shown in Figs. 1 to 4 for the nine compounds. The ordinates are the absorption coefficients calculated from the Lambert-Beer absorption equation,

$$\alpha(\nu) = (1/NL)\ln(I_0/I), \qquad (1)$$

where $\alpha(\nu)$ = absorption coefficient in cm^2/molecule, N = number of molecules per cm^3, L = cell thickness in cm, I_0 = transmission through cell filled with CCl_4, and I = transmission through cell filled with sample. Correlations between the heights and spectral positions of a number of the absorption maxima shown in these figures will be discussed later after the data on the

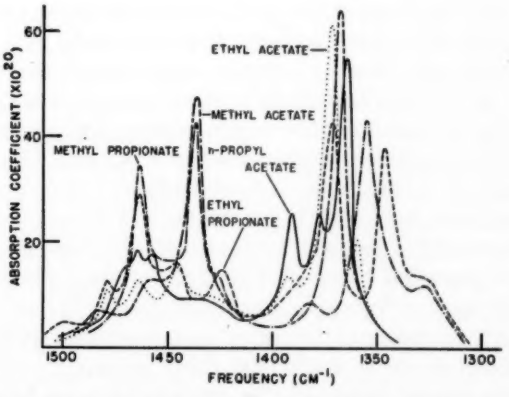

FIG. 4. Grating spectra for esters in 1400 cm^{-1} region. – – – – Methyl acetate. ····· Ethyl acetate. ——— n-propyl acetate. –·–·– Methyl propionate. – – – – – – Ethyl propionate.

TABLE I. Integrated intensities of 2900, 1460, and 1370 cm^{-1} bands.

	Integrated intensity (cm^2/molecule sec)($\times 10^7$)								
	Experimental			Calculated					
Compound	2900	1460	1370	2900	Percent Δ	1460	Percent Δ	1370	Percent Δ
Acetone	1.76	2.64	3.82	1.48	−15.9	2.62	−0.8	3.88	1.6
Butanone	5.39	2.92	3.10	5.63	4.5	3.02	3.4	3.16	1.9
3-pentanone	9.70	3.45	2.37	9.78	0.8	3.42	−0.9	2.44	3.0
2-pentanone	9.15	3.28	3.34	9.44	3.2	3.25	−0.9	3.16	−5.4
Methyl acetate	3.24	3.32	2.52	3.28	1.2	3.31	−0.3	2.55	+1.2
Ethyl acetate	4.94	2.51	3.56	4.79	−3.0	2.50	−0.4	3.49	−1.7
n-propyl acetate	8.37	2.63	3.65	8.60	2.7	2.73	3.8	3.49	−4.4
Methyl propionate	6.49	3.86	3.19	6.45	−0.6	3.90	1.0	3.14	−1.6
Ethyl propionate	8.04	3.15	3.93	7.96	−1.0	3.09	−1.9	4.08	+3.8

integrated intensities of these bands have been presented and discussed.

The integrated absorption intensity, A, over a spectral region is defined as

$$A = \int_{\nu_1}^{\nu_2} \alpha(\nu) d\nu, \tag{2}$$

where ν_1 and ν_2 are the spectral frequencies between which the integration is performed. The need for such a practical definition of the integrated intensity arises from the fact that some choice is usually involved in the determination of integration limits. The integrated intensity data for the 2900, 1460, and 1370 cm^{-1} spectral regions are summarized in Table I. Integrations were carried out over the spectral intervals 2800–3060, 1395–1500, and 1330–1395 for the ketones and 2800–3060, 1410–1500, and 1334–1410 for the esters.

It is readily demonstrated that the unit structural group intensities obtained for paraffin hydrocarbons[1] are not satisfactory for calculating the integrated intensities for the compounds studied in the present work. For example, for acetone, which contains two CH_3 groups, one calculates 8.82×10^{-7}, 1.08×10^{-7}, and 0.78×10^{-7} cm^2/molecule sec for the integrated intensities in the 2900, 1460, and 1370 cm^{-1} regions, respectively, from the CH_3 structural group intensities for paraffins. One sees from Table I that the calculated value for the 2900 cm^{-1} region is much too large and for the 1460 and 1370 cm^{-1} regions much too small. This indicates that the effect of the carbonyl group upon the structural group intensities must be considered.

It is possible to calculate the integrated intensities for the ketone molecules with reasonable accuracy if the assumption is made that the CH_3 and CH_2 unit structural group intensities are affected only by adjacent structural groups. On the basis of this picture the CH_3 and CH_2 groups in ketones can be divided into two kinds according to whether they are or are not adjacent to the carbonyl group. The nonadjacent CH_3 and CH_2 groups are assigned the same unit structural group intensities as were found for these groups in paraffin hydrocarbons,[1] since all the structural groups adjacent to them in the molecule are hydrocarbon groups. Best values for the unit structural group intensities for CH_3 and CH_2 groups adjacent to the carbonyl group are then calculated from the experimental integrated intensity data.

These two sets of structural group intensities for CH_3 and CH_2 groups are given in the top two rows of Table II, and the integrated intensities for the ketone molecules, calculated by summing the group intensities over the groups in the molecule, are given in Table I in the columns headed "Calculated intensities." The agreement between calculated and experimental intensities, expressed as the percentage differences in Table I, is within the accuracy of the experimental results.

There are three different environmental situations for CH_3 and CH_2 groups in an ester molecule, and the experimental data indicate that different unit structural group intensities must be associated with the CH_3 and CH_2 groups for each of the three situations. For CH_3 and CH_2 groups bonded only to other CH_3 and CH_2 groups the structural group intensities obtained for paraffin hydrocarbons are assumed to hold. CH_3 and CH_2 structural group intensities can then be calculated from the experimental data for groups bonded to the carbon atom and for groups bonded to the oxygen atom of the $-COO-$ structural group. There is no unique set of CH_3 and CH_2 structural group intensities, however. This results from the fact that only three independent relations can be obtained between the measured molecular intensities and the four types of structural groups (CH_3 and CH_2 each bonded to either carbon or oxygen).[7] Consequently, the intensity for one of the structural groups can be chosen arbitrarily for each spectral region. All the possible sets of CH_3 and CH_2 structural group intensities which are consistent with the data were obtained graphically. A consideration of these solutions showed that at least one of the CH_2 structural group intensities was always negative for the 2900 cm^{-1} region. The values obtained for the CH_3 groups adjacent to the carbonyl in ketones were chosen

[7] If a and b are the CH_3 and CH_2 intensities for groups bonded to the carbon of the ester group and c and d the similar intensities for groups bonded to the oxygen atom, only the combinations $a+c$, $a+d$, $b+c$, and $b+d$ can be measured experimentally. Since the determinant of these four equations is zero, the four relations are not independent.

TABLE II. CH_3 and CH_2 structural group intensities (cm^2/molecule sec).

Structural group environment	Unit structural group intensity ($\times 10^7$) 2900 cm^{-1} region CH_3	2900 cm^{-1} region CH_2	1460 cm^{-1} region CH_3	1460 cm^{-1} region CH_2	1370 cm^{-1} region CH_3	1370 cm^{-1} region CH_2
Paraffin hydrocarbon	4.41	3.81	0.54	0.23	0.39	0
Adjacent carbonyl, ketone	0.74	0.48	1.31	1.17	1.94	0.83
Adjacent carbonyl, ester	0.74	−0.50	1.31	1.36	2.55	2.75
Adjacent oxygen, ester	2.54	−0.36	2.00	0.65	0	0.55

for the similar group in esters for the 2900 and 1460 cm^{-1} regions. This choice was based upon the apparent similarity of the structural group environments in the two cases and the fact that this choice results in negative values for the CH_2 intensities for the 2900 cm^{-1} region which are small. For the 1370 cm^{-1} region a value of zero was chosen for the $-OCH_3$ group, since, as discussed later, the absorption curves suggest that this group does not absorb in this region. The set of structural group intensities for esters are given in Table II. The molecular intensities calculated from these structural group intensities are compared in Table I with the experimental intensities, and good agreement is observed. However, this comparison between experimental and calculated intensities is not a very severe test, since there are for each spectral region four arbitrary parameters which can be adjusted to fit five pieces of data. Measurements on additional compounds would be desirable to test further the agreement between experimental and calculated intensities for esters.

DISCUSSION OF INTENSITY DATA

It is not possible at this time to assess with any certainty the physical significance of the unit structural group intensities given in Table II. The assignment of structural group intensities represents an empirical approach to the problem of interpreting the integrated intensity data for the relatively complex molecules studied. This approach is supported by the observation that integrated intensities can be calculated for the molecules which agree well with the measured integrated intensities. Some further support is indicated by the correlations between the positions and intensities of absorption maxima and the structural groups present in the molecules, which are discussed in the following section.

It seems fairly certain that the carbonyl and ester groups decrease the absorption intensity of the stretching vibrations and increase the intensity of the deformation vibrations of the nearby CH_3 and CH_2 structural groups. However, it is entirely possible that this effect is not confined to the CH_3 and CH_2 groups adjacent to the carbonyl and ester groups, but may extend with decreasing magnitude to the CH_3 and CH_2 groups two or more carbon atoms removed. The negative structural group intensities obtained for CH_2 groups adjacent to the ester group suggests very strongly that this hypothesis is true. It appears, therefore, that the effects of the carbonyl and ester groups on the absorption intensities of nearby CH_3 and CH_2 groups are established qualitatively but not quantitatively by this work. Accordingly, only a qualitative discussion of the interpretation of these effects is given.

One possible explanation for the effects of ketone and ester groups on the absorption intensities of nearby CH_3 and CH_2 groups is that there is considerable interaction between the motions of the ketone or ester groups and the adjacent CH_3 and CH_2 groups. The highly polar nature of the former groups then might affect appreciably the intensities of the bands associated with the CH_3 and CH_2 groups. This explanation seems much less likely than an explanation based upon the polarization of the bonds in nearby groups by the highly polar ketone and ester groups. The reduction in intensity of CH stretching vibrations indicates a decrease in the derivative of the CH bond dipole moment with respect to CH bond length; the increase in intensity of the deformation vibrations indicates an increase in bond dipole moment. This result does not follow from the simple picture of the oscillation of point charges, for which one expects an increase in bond dipole moment to be associated with an increase in the derivative of the bond dipole moment with respect to internuclear distance.

It might be expected that the electrons in the CH bonds near a carbonyl group would, on the average, be nearer the carbon atom than the electrons in CH bonds in a hydrocarbon molecule as a result of the considerable electronegative character of the nearby oxygen atom. The structural group intensities indicate a larger CH bond dipole moment for groups near a carbonyl group. There are then two possibilities. Either the CH bond dipole moment is directed toward the hydrogen atom in hydrocarbons and merely has an increased magnitude in the groups adjacent to a ketone or ester group, or it is directed toward the carbon atom in hydrocarbons and its direction is reversed as well as its magnitude increased by the proximity of a ketone or ester group. The former possibility seems more reasonable, since it requires a smaller alteration of the CH moment and since, to date, no cases have been found where the CH moment appears to be smaller than in paraffin hydrocarbons. Such a conclusion is in agreement with electronegativity considerations[8] and with

[8] Linus Pauling, *Nature of the Chemical Bond* (Cornell University Press, Ithaca, New York, 1939), p. 64.

TABLE III. Correlation of absorption maxima in 1370 cm^{-1} region with structural groups of ketones and esters.

CH_3COCH_3	CH_3COOCH_3
1361 1361	1370 1438
$CH_3CH_2COCH_3$	$CH_3COOCH_2CH_3$
1379 1360* 1365	1373 1360 1393
$CH_3CH_2CH_2COCH_3$	$CH_3COOCH_2CH_2CH_3$
1383* 1357 1364	1378 1365 1391
$CH_3CH_2COCH_2CH_3$	$CH_3CH_2COOCH_3$
1379 1356 1356 1379	1383 1356 1438
$CH_3CH_2COOCH_2CH_3$	
1385* 1347 1372 1385*	

Cole and Thompson's results for aromatic CH bonds,[9] but is in disagreement with the theoretical predictions of Coulson.[10]

DISCUSSION OF ABSORPTION CURVES

A study of the absorption curves shown in Figs. 1–4 suggests that a number of absorption maxima can be correlated with particular structural groups in the molecules. A complete set of such correlations are shown below in Table III for the 1300–1400 cm^{-1} region. The position of the absorption maximum is written underneath the structural group with which it is believed to be associated. Absorption maxima which are not resolved but whose existence is indicated by the presence of a shoulder or a widening of the adjacent band (see Figs. 3 and 4) are indicated by an asterisk.

No serious ambiguities occur in the above correlations for the ketones. The band near 1363 cm^{-1} is present in the spectra of the three methyl ketones and its maximum absorption coefficient is approximately 30×10^{-20} cm^2/CH_3 group. The band associated with a CH_3 group nonadjacent to the carbonyl group occurs at about the same position as it is observed in *n*-paraffin hydrocarbons. The appearance of a band which can be correlated with the presence of a CH_2 group adjacent to a carbonyl group confirms the conclusion arrived at from a consideration of the integrated intensity data that a CH_2 group so situated in a molecule absorbs in the 1370 cm^{-1} spectral region.

The correlations are somewhat less satisfactory for the ester molecules. Methyl acetate (see Fig. 4) shows a single band in this region at 1370 cm^{-1}. The fact that ethyl acetate also has a band of comparable intensity with a maximum at 1373 cm^{-1} indicates that this band is associated with the CH_3 group adjacent to the carbonyl group. It appears that the CH_3 group bonded to the oxygen atom does not absorb in this region. Both methyl acetate and methyl propionate have a strong sharp band near 1438 cm^{-1}, and it seems likely that this is the CH_3 symmetrical deformation mode of the $O-CH_3$ group. The similar vibrational mode for the CH_3 group in *n*-paraffins absorbs near 1379 cm^{-1}. The other correlations proposed above for ethyl acetate and for methyl propionate appear reasonable from an inspection of the spectral curves in Fig. 4. However, the correlations proposed for *n*-propyl acetate and ethyl propionate are less satisfactory in that the maximum absorption coefficients of the bands correlated with the same structural group show considerable variation. Thus the 1360 cm^{-1} band correlated with the $O-CH_2$- group in ethyl acetate is quite weak, while the bands correlated with this group in *n*-propyl acetate and ethyl propionate are quite strong. Similarly, the 1378 cm^{-1} band of *n*-propyl acetate is much weaker than the bands correlated with the similarly placed group in methyl acetate and ethyl acetate.

A study of the 1460 cm^{-1} region of Figs. 3 and 4 suggests a number of correlations, although they are by no means so complete as for the 1370 cm^{-1} region. The CH_2 deformation vibration is expected in this region as well as the doubly degenerate deformation vibration of the CH_3 group. However, since the molecules do not contain a threefold axis of symmetry, this degenerate vibration will be split and may appear as a doublet.

The absorption maximum at 1415 cm^{-1} in the spectra of butanone and 3-pentanone and at 1410 cm^{-1} in the spectrum of 2-pentanone in Fig. 3 is probably characteristic of the CH_2 group adjacent to the carbonyl group in ketones. The similar group in esters can probably be associated with the 1425 cm^{-1} maximum of ethyl propionate and the 1427 cm^{-1} shoulder in the methyl propionate spectrum. The only other maxima observed in this region in the 3-pentanone spectrum are at 1452 and 1461 cm^{-1} so these maxima are probably associated with the terminal methyl groups of this molecule. They are also observed with about one-half the intensity in the butanone spectrum which contains only one methyl group nonadjacent to the carbonyl group. It is therefore inferred that the maxima near 1452 and 1461 cm^{-1} result from the splitting of the doubly degenerate deformation mode of the isolated CH_3 group. A number of other maxima are observed in this region but they are probably masked by other stronger bands in a number of cases, so that any generalizations made about them could not be strongly supported.

TABLE IV. Absorption data for molecules containing $-CH_2CH_3$ structural group.

Molecule	No. of groups	2980 cm^{-1} band ν_{max}	2980 cm^{-1} band α_{max} ($\times10^{20}$)	2940 cm^{-1} band ν_{max}	2940 cm^{-1} band α_{max} ($\times10^{20}$)
Butanone	1	2981	22	2941	15
3-pentanone	2	2982	43	2940	31
Ethyl acetate	1	2984	24	2942	10
Methyl propionate	1	2988	24	2952	26
Ethyl propionate	2	2985	44	2943	21

[9] A. R. H. Cole and H. W. Thompson, Trans. Faraday Soc. **46**, 103 (1950).
[10] C. A. Coulson, Trans. Faraday Soc. **38**, 433 (1942).

A few correlations can be indicated for the 2900 cm^{-1} spectral region, although the interpretation for this region is by no means complete. The three maxima near 3008, 2963, and 2922 cm^{-1} in the acetone spectrum in Fig. 1 may be identified with the three CH stretching modes of the CH_3 structural group. If this assignment is correct, it can be inferred that the degenerate vibration of free CH_3 is split in the molecule, and that the interaction between the two CH_3 groups is not sufficient to produce a further noticeable splitting of the energy levels. The spectra of butanone and 3-pentanone (see Fig. 1) are quite similar in this region, but the peak heights are roughly twice as great for 3-pentanone. Since the structural group intensities indicate that the structural groups adjacent to the carbonyl groups are relatively weak absorbers, the four maxima might be associated with the methyl group nonadjacent to the carbonyl. It seems best at this time, however, merely to indicate some generalizations for this region and not to attempt to correlate the observed maxima with particular structural groups. Maxima are observed near 2980 and 2940 cm^{-1} for every compound containing a CH_3CH_2-group adjacent to either a carbonyl group or an oxygen atom (see Figs. 1 and 2). The positions and maximum absorption coefficients of these bands are summarized in Table IV. The relatively strong maximum at 2954 cm^{-1} in the methyl acetate spectrum in Fig. 2 is probably associated with the $O-CH_3$ group and the 2952 cm^{-1} band of methyl propionate may be due to the combination of CH_3CH_2- and $O-CH_3$ groups.

1720 AND 1200 CM^{-1} BAND INTENSITIES

The frequencies of maximum absorption and the integrated intensities are given in Table V for the bands in the 1720 and 1200 cm^{-1} regions for the nine molecules studied. The integrated intensities of the 1720 cm^{-1} bands are relatively constant for all the compounds of the same type, but the ester intensities average approximately seventy percent higher than the ketone intensities. A normal coordinate treatment of the skeletal modes of the acetone molecule indicates this band is associated with a vibrational mode which is mainly a stretching of the C=O bond but which includes about twenty percent C—C stretching. The nature of the normal vibration is illustrated schematically in Fig. 5A. The increased intensity of the band for the esters may be due to the substitution of the polar C—O bond for one of the C—C bonds in the ketones as illustrated in Fig. 5B.

TABLE V. Frequencies and integrated intensities of bands in 1720 and 1200 cm^{-1} regions.

Compound	1720 cm^{-1} band $\nu(cm^{-1})$	1720 cm^{-1} band $A^a(\times 10^7)$	1200 cm^{-1} band $\nu(cm^{-1})$	1200 cm^{-1} band $A^a(\times 10^7)$
Acetone	1717	8.3	1218	3.84
Butanone	1718	8.4	1172	2.37
3-pentanone	1720	8.0	1122	1.67
2-pentanone	1717	7.8	1170	2.27
Methyl acetate	1749	12.8	1245	13.9
Ethyl acetate	1742	14.9	1240	17.6
n-propyl acetate	1744	14.0	1234	17.7
Methyl propionate	1746	13.2	1178 1202	12.9
Ethyl propionate	1740	13.3	1190	15.0

[a] Units of A —cm^2/molecule sec.

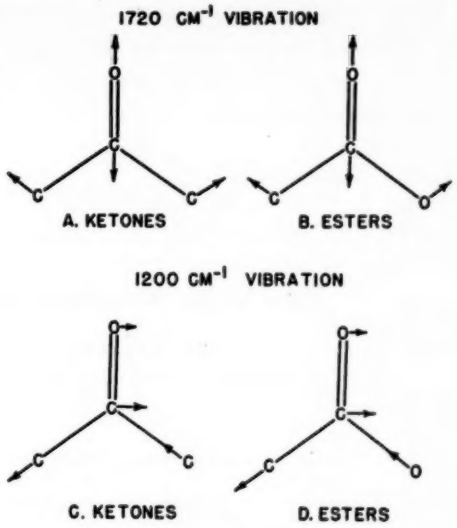

FIG. 5. Illustration of probable vibrational motions associated with 1720 and 1200 cm^{-1} bands of ketones and esters.

The intensity of the 1200 cm^{-1} band for the ketones decreases from acetone to 3-pentanone. The intensity appears to decrease with increasing size of the alkyl groups attached to the carbonyl group. This band in acetone was assigned by Kohlrausch[11] to the nonsymmetric C—C stretching vibration; the vibrational motion is illustrated in Fig. 5C. The decrease in intensity with increase in size of the alkyl groups suggests that either other C—C bonds in the molecule contribute to the normal mode in the more complex molecules or that the electron distribution around the carbonyl group is altered by an increase in the size of the alkyl groups.

The 1200 cm^{-1} bands of both the ketones and the esters are appreciably broadened on the high frequency side by the addition of a small amount of methyl alcohol to the CCl_4 solutions. This indicates that an appreciable amount of deformation of the carbonyl bond is involved in the vibrational motion for both types of molecules. This suggests that the 1200 cm^{-1} ester band is associated with a vibrational mode analogous to that shown in Fig. 5C for the ketones. The motion is illustrated in Fig. 5D. The greatly increased intensity of the ester band compared to the ketone band may be due to the replacement of one of the C—C bonds of ketones by the more polar C—O bond of esters.

Substitution of an ethyl group for a methyl group bonded to the oxygen atom of the ester group results in an appreciable increase in intensity of the 1200 cm^{-1} band, while a similar substitution of the alkyl group

[11] K. W. F. Kohlrausch, *Ramanspektren* (Akademische Verlagsgesellschaft Becker and Erler, Leipzig, 1943), p. 103.

bonded to the carbonyl group results in a decrease in intensity. This may be a consequence of changes in the nature of the vibrational motion associated with this band in the various molecules.

ACKNOWLEDGMENT

I wish to thank Dr. L. C. Roess for many helpful discussions and Mr. J. E. Scardefield for making many of the measurements and preparing the figures.

THE JOURNAL OF CHEMICAL PHYSICS VOLUME 19, NUMBER 7 JULY, 1951

The Vapor Pressure and Critical Constants of Neopentane

JAMES A. BEATTIE, DONALD R. DOUSLIN, AND SAMUEL W. LEVINE
Department of Chemistry, Massachusetts Institute of Technology, Cambridge, Massachusetts
(Received April 16, 1951)

The vapor pressure of neopentane has been measured from 50° to the critical point. The equation,

$$\log_{10}p(\text{atmos}) = 3.901633 - \frac{1136.462}{T} + 4.99118\times10^{-4}T \quad (T = t°\text{C} + 273.16),$$

gives a fair representation of the observations.

A study of the compressibility of neopentane in the critical region gives for the critical temperature, pressure, volume, and density the values: $t_c = 160.60° \pm 0.05°$C (Int.), $p_c = 31.57 \pm 0.03$ normal atmospheres, $V_c = 0.303$ liter per mole (4.20 ml per g), $d_c = 3.30$ mole/liter (0.238 g per ml). The uncertainty in the critical volume and density is 1 percent.

WE have measured the vapor pressure of neopentane, $C(CH_3)_4$, from 50° to the critical temperature, 160.60°; and have studied the compressibility in the critical region at a sufficient number of isotherms to locate the critical point. The apparatus and experimental procedure[1] for determining pressure, volume, mass, and temperature has been described earlier. The bomb with a glass linear was used for the study of neopentane. The properties of a number of other hydrocarbons have been measured in the same apparatus.[2]

The vapor pressure of neopentane has been measured from −42.0° to 9.4° by Whitmore and Fleming,[3] and from −15° to 10° by Aston and Messerly.[4]

The neopentane used was a sample of API–NBS hydrocarbon which was made available to us by the American Petroleum Institute and the National Bureau of Standards through the API Research Project 44 on the "Collection, analysis, and calculation of data on the properties of hydrocarbons." These samples were purified at the National Bureau of Standards by the API Research Project 6, under the supervision of Frederick D. Rossini, from materials supplied by the California Research Corporation, Richmond, California. We are greatly indebted to Dr. Rossini for supplying us with the neopentane and for stating the purity: 99.982±0.012 mole percent neopentane.

No further purification of the sample was attempted except for the removal of permanent gases. The liquid was frozen with liquid nitrogen and the head space evacuated, then allowed to melt with continued evacuation. Six alternate freezings and meltings were made. The substance was then transferred by distillation into the weighing bomb and finally to the compressibility bomb.

TABLE I. Variation of the measured vapor pressure with vapor volume for the sample of neopentane at 50°C.

Vapor volume ml	Observed vapor pressure normal atmos
94	3.512
78	3.507
64	3.509
50	3.510
20.5	3.507
6.1	3.509
0.9	3.509
0.2	3.508
0.11	3.509

TABLE II. Vapor pressure of neopentane.

Temp., °C (Int.)	Vapor pressure, normal atmos Obs.	Obs–Calc from Eq. 1 atmos.	percent
50	3.509	+0.008	+0.23
57	4.214	−0.004	−0.09
75	6.494	−0.019	−0.29
100	11.033	−0.008	−0.07
125	17.565	+0.058	+0.33
150	26.673	+0.068	+0.25
158	30.294	−0.024	−0.08
158[a]	30.292	−0.022	−0.07
160.60	31.572	−0.087	−0.28

[a] Made after completion of a study of the compressibility of neopentane to 275°.

[1] J. A. Beattie, Proc. Am. Acad. Arts Sci. **69**, 389 (1934).
[2] J. A. Beattie and S. Marple, Jr., J. Am. Chem. Soc. **72**, 1449 (1950).
[3] F. C. Whitmore and G. H. Fleming, J. Am. Chem. Soc. **55**, 3803 (1933).
[4] J. G. Aston and G. H. Messerly, J. Am. Chem. Soc. **58**, 2355 (1936).

TABLE III. Isotherms of neopentane (C_5H_{12}) in the critical region. Molecular weight = 72.0924.

Temp., °C (Int.)		160.00	160.40	160.50	160.58	160.60	160.62	160.70
Volume liter/mole	Density mole/liter	Pressure, normal atmospheres						
0.4000	2.500	31.232						
0.3846	2.600	31.251						
0.3774	2.650		31.444	31.483	31.522	31.534	31.544	31.580
0.3704	2.700	31.260		31.498	31.532	31.543	31.554	31.595
0.3636	2.750		31.455	31.507	31.538	31.550	31.560	31.605
0.3571	2.800	31.267	31.453	31.512	31.545	31.557	31.568	31.608
0.3509	2.850			31.513			31.571	31.610
0.3472	2.880		31.459		31.549	31.564		
0.3401	2.940		31.459	31.517	31.551	31.566	31.574	31.616
0.3333	3.000	31.264	31.462	31.522	31.552	31.564	31.574	31.617
0.3288	3.042		31.464	31.519	31.554	31.567	31.575	31.619
0.3226	3.100			31.521				
0.3195	3.130		31.465	31.521	31.556	31.569	31.578	31.621
0.3125	3.200		31.465	31.526	31.558	31.568	31.580	31.622
0.3049	3.280		31.467	31.524	31.557	31.570	31.581	31.627
0.2985	3.350		31.469	31.523	31.559	31.572	31.581	31.630
0.2924	3.420			31.522	31.558	31.574	31.584	31.630
0.2857	3.500	31.268	31.470	31.525	31.563	31.576	31.588	31.634
0.2817	3.550			31.523				
0.2778	3.600		31.468	31.526	31.570	31.583	31.592	31.640
0.2740	3.650		31.470	31.528				
0.2703	3.700	31.272	31.476	31.540	31.577	31.591	31.606	31.657
0.2667	3.750		31.480	31.546	31.593	31.604	31.618	31.669
0.2597	3.850	31.275	31.513	31.583	31.625	31.641	31.658	31.708
0.2532	3.950	31.311						
0.2500	4.000	31.358						
0.2439	4.100	31.450						

Critical constants from Fig. 1: $t_c = 160.60 \pm 0.05$°C (Int.); $p_c = 31.57 \pm 0.03$ normal atmos.; $V_c = 0.303$ liter/mole (4.20 ml/g); $d_c = 3.30$ mole/liter (0.238 g/ml). The uncertainty in the critical volume and density is 1 percent.

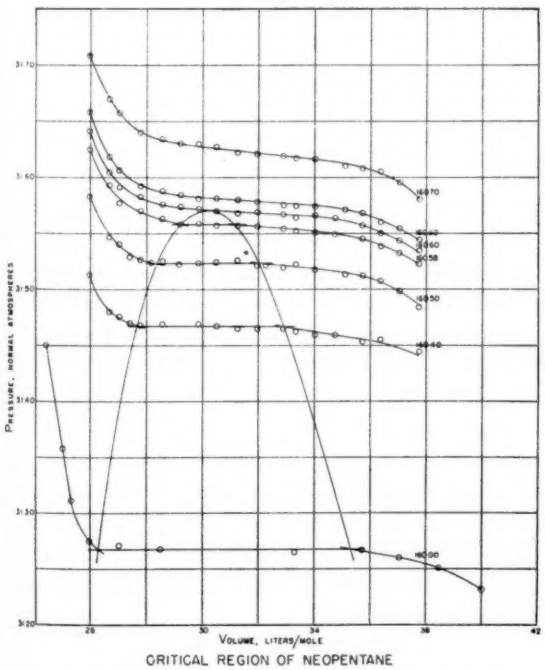

FIG. 1. Isotherms of neopentane in the critical region. The radius of each circle is 0.002 atmos.

An indication of the purity of the sample is given by the variation of the vapor pressure with vapor volume shown in Table I. The variation is within the error of determination of pressure.

The vapor pressure of neopentane is given in Table II. Since the temperature range is not great the results were expressed in terms of the equation:

$$\log_{10} p(\text{atmos}) = 3.901633 - (1136.462/T) + 4.99118 \times 10^{-4} T \quad (T = t°\text{C} + 273.16). \quad (1)$$

The second vapor pressure at 158° was determined after a study of the critical region and of the compressibility of the sample to 275° had been completed. It indicates that any decomposition of the neopentane was negligibly small.

The results of our measurements on the compressibility of neopentane in the critical region are listed in Table III, and these values are plotted in Fig. 1. The critical constants determined by inspection of the plot are: $t_c = 160.60° \pm 0.05$°C (Int.), $p_c = 31.57 \pm 0.03$ normal atmospheres, $V_c = 0.303$ liter per mole (4.20 ml/g), $d_c = 3.30$ mole/liter (0.238 g/ml). The uncertainty in the critical volume and density is 1 percent.

The Magnetic Susceptibility of Uranium Tetrachloride*

R. STOENNER AND N. ELLIOTT
Chemistry Department, Brookhaven National Laboratory, Upton, Long Island, New York
(Received April 23, 1951)

The magnetic susceptibility of UCl_4 has been measured in the temperature range 76°–354°K. The molar susceptibility is given by the equation,

$$\chi_{mole}=1.22/(T+39°).$$

THE magnetic susceptibility of anhydrous uranium tetrachloride, UCl_4, as a function of temperature has been measured by Bommer.[1] A Weiss-Curie law was reported for temperatures above 300°K with

$$\chi_{mole}=0.92/(T-55°).$$

The magnetic moment calculated for the U^{4+} ion from Bommer's data is 2.73 Bohr magnetons, in fair agreement with the value calculated for two spinning electrons, which is 2.83 Bohr magnetons. However, if the U^{4+} ion is a member of a $5f$ transition group, analogous to the rare earth series, its spectroscopic ground state is $^3H_4$, and one would expect a moment closer to 3.62 Bohr magnetons.[2]

Examination of Bommer's data indicated the possibility of a structural transformation in the neighborhood of room temperature with one value of the magnetic moment above room temperature and another value below. This is shown in Fig. 1. Therefore we prepared some UCl_4 and repeated the magnetic measurements.

Anhydrous uranium tetrachloride was prepared by a method reported by Mezey.[3] It was stored in a vacuum desiccator and all transfer operations were performed in a dry box.

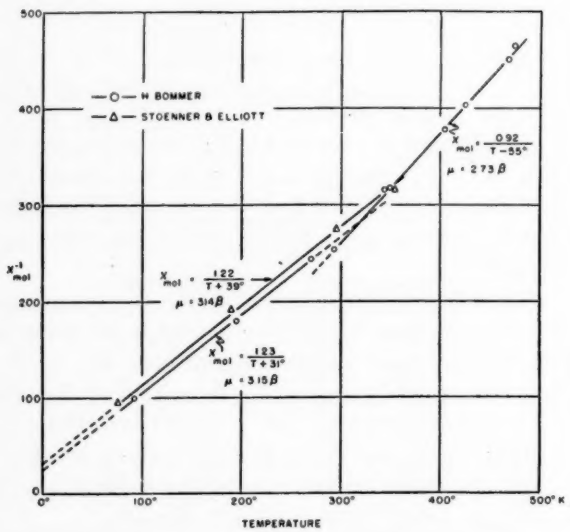

FIG. 1. The magnetic susceptibility of UCl_4 as a function of temperature. (In the figure all x's should be χ.)

Uranium analyses were done by dissolution of the samples in dilute H_2SO_4, addition of an appropriate quantity of ferric sulfate solution, and titration of the resulting ferrous iron with standard ceric sulfate. This method gave low and somewhat variable results unless precautions were taken to exclude air and keep the solutions cold while the samples were being dissolved. Good results were obtained if the dilute H_2SO_4 was cooled with an ice bath prior to the solution of the UCl_4, and if the sample bottles were opened beneath the surface of the solution. Two analyses gave 62.12 percent and 62.16 percent U^{4+}. The theoretical value is 62.63 percent.

Magnetic susceptibility measurements were made on a Gouy balance over a considerable temperature range.

TABLE I.

Temp. °K	76°	191°	295°	354°
$\chi_{mole}\cdot 10^6$	10536	5223	3636	317

No dependence of susceptibility on field strength was observed. The data are given in Table I and in Fig. 1 for comparison with Bommer's results. Corrections have been made for the diamagnetism of the ions, using the values -29×10^{-6} and -24×10^{-6}, respectively, for the gram ionic susceptibilities of the U^{4+} and Cl^- ions.

As shown in Fig. 1, the present data and those of Bommer are in fairly good agreement in the temperature range 76°–270°K. We find the Weiss-Curie law to be followed from 76°K to 354°K, the highest temperature used in this experiment. The molar susceptibility is given by the equation,

$$\chi_{mole}=1.22/(T+39°).$$

This leads to a magnetic moment of 3.14 Bohr magnetons. UCl_4 therefore behaves magnetically like other tetravalent uranium salts which have been recently measured.[2,4]

* Work carried out under the auspices of the AEC.
[1] H. Bommer, Z. anorg. u. allgem. chem. **247–249**, 249 (1941).
[2] C. A. Hutchison and N. Elliott, J. Chem. Phys. **16**, 920 (1948).
[3] R. Mezey, Manhattan Project Report C-1139.
[4] N. Elliott, Phys. Rev. **76**, 431 (1949).

The magnetic moments of all U^{4+} salts which have been examined are found to lie in the range 2.73–3.75 Bohr magnetons. This is approximately the range of values to be expected if the U^{4+} ion is in a $^3H_4$ state with more or less quenching of the orbital moment by the crystalline fields, the predicted range being 2.83–3.62 Bohr magnetons. The situation is very different if one supposes tetravalent uranium to have two 6 *d* electrons unpaired and the ground state $^3F_2$. By analogy with the corresponding ions of the first row transition elements, the magnetic moment of U^{4+} should then be found in the range 1.63–2.83 Bohr magnetons.[5]†

[5] E. C. Stoner, *Magnetism and Matter* (Methuen & Company, Ltd., London, 1934), p. 312.

† *Added Footnote:*—Some magnetic measurements of uranium halides by J. K. Dawson in the *Journal of the Chemical Society*, pp. 429–431 (1951) have just come to our attention. The difference in Dawson's results and ours for UCl_4 is somewhat larger than can be accounted for by experimental error, but not much. The magnetic moment and Curie temperature calculated for UCl_4 from our data are in close agreement with Dawson's values for UBr_4. Such agreement is fairly general for the chlorides and bromides of the first row transition elements.

THE JOURNAL OF CHEMICAL PHYSICS VOLUME 19, NUMBER 7 JULY, 1951

The Dipole Moments and Structures of a Series of Alkyl Polysulfides*

CARROLL C. WOODROW,† MARVIN CARMACK, AND JOHN G. MILLER
Department of Chemistry and Chemical Engineering, University of Pennsylvania, Philadelphia, Pennsylvania

The dipole moments of *n*-hexadecyl mono-, di-, tri-, and tetrasulfides at 30°C are 1.47, 2.00, 1.63, and 2.16*D*, respectively. These values provide evidence in favor of non-branched sulfur chains in the polysulfides and are also in accord with fixed non-planar configurations for these chains. It is possible that the disulfide exists as mixture of two non-superimposable mirror-image forms, the trisulfide as a mixture of one highly polar form together with a pair of nearly non-polar enantiomorphs, and the tetrasulfide as a mixture of three different pairs of enantiomorphs, all three pairs being polar.

INTRODUCTION

THE arrangement of the sulfur atoms in the higher polysulfides has long been debated. Most of the physical evidence has favored a non-branched chain arrangement of the sulfur atoms. From the characteristic Raman frequencies of trisulfides, Pai[1] concluded that these have the $R-S-S-S-R$ structure. Donohue and Schomaker[2] reached the same conclusion from an electron-diffraction study of dimethyl trisulfide as did also Dawson and Robertson[3] as a result of an x-ray investigation of the structure of 2,2′-diiododiethyl trisulfide. By measurements of their ultraviolet absorption spectra, Koch[4] found strong evidence that diphenyl tetrasulfide and dicyclohexyl hexasulfide likewise contain non-branched chains of sulfur atoms.

A survey of the literature revealed that no attempt had been made to investigate the structures of higher polysulfides by means of dipole moment measurements. Accordingly, a systematic study of the moments of the mono-, di-, tri-, and tetrasulfides of the *n*-hexadecyl series was undertaken. This choice of sulfides appeared advantageous because, as contrasted with the lower alkyl sulfides, they are crystalline compounds which can be obtained in a high state of purity.

Shortly after the start of our preparation of this paper, Westlake, Laquer, and Smyth[5] and Kushner, Gorin, and Smyth[6] published studies of the dipole moments of methyl, ethyl, and *n*-propyl disulfides and methyl and ethyl trisulfides. Their values are consistent with a non-branched chain structure for the trisulfides. Our results are in agreement with theirs and extend the studies to the structure of the tetrasulfide. The values are also considered from the standpoint of fixed nonplanar configurations caused by the directional properties of the sulfur bonds.

EXPERIMENTAL

The *n*-hexadecyl sulfides were prepared and purified by methods described previously.[7] The dipole moments in benzene solution were measured at 30±0.01°C using an apparatus and method of measurement reported earlier.[8] The refractive indices of the benzene solutions were measured at the same temperature with a Pulfrich refractometer, using the Na_D line.

RESULTS

Table I shows the mole fractions of the solute, N_2, the dielectric constant, ϵ_{12}, density, d_{12}, and the square of

* This paper is based on a portion of a dissertation submitted in December, 1949 by C. C. Woodrow in partial fulfillment of the requirements for the degree of Doctor of Philosophy at the University of Pennsylvania.

† Harrison Fellow and Rohm and Haas Research Assistant, 1948–1949; Present address: Viscose Rayon Research Section, E. I. duPont de Nemours Company, Inc., Richmond, Virginia.

[1] G. N. Pai, Indian J. Phys. **9**, 231 (1935).
[2] J. Donohue and V. Schomaker, J. Chem. Phys. **16**, 92 (1948).
[3] I. M. Dawson and J. M. Robertson, J. Chem. Soc. 1256 (1948).
[4] H. P. Koch, J. Chem. Soc. 394 (1949).
[5] Westlake, Jr., Laquer, and Smyth, J. Am. Chem. Soc. **72**, 436 (1950).
[6] Kushner, Gorin, and Smyth, J. Am. Chem. Soc. **72**, 477 (1950).
[7] J. E. Baer and M. Carmack, J. Am. Chem. Soc. **71**, 1215 (1949).
[8] J. G. Miller, J. Am. Chem. Soc. **64**, 117 (1942); J. G. Miller and H. S. Angel **68**, 2358 (1946).

TABLE I. The dielectric constant, density, and refractive index of benzene solutions of *n*-hexadecyl sulfides at 30°C.

N_2	ϵ_{12}	d_{12}	$n^2_{12}D$
Monosulfide			
0.001342	2.2683	0.86716	2.22851
0.002243	2.2707	0.86689	2.22821
0.003745	2.2739	0.86650	2.22708
0.006275	2.2788	0.86570	2.22520
0.010509	2.2867	0.86462	2.22216
$\epsilon_{12}=2.26613(\pm0.00022)+1.980(\pm0.035)N_2$, $d_{12}=0.86752(\pm0.00025)-0.2788(\pm0.0043)N_2$, $n^2_{12}D=2.22965-0.7099N_2$.			
Disulfide			
0.001362	2.2738	0.86731	2.23105
0.002272	2.2748	0.86725	2.23048
0.003800	2.2836	0.86707	2.22965
0.006346	2.2972	0.86703	2.22821
0.010588	2.3180	0.86680	2.22729
$\epsilon_{12}=2.26524(\pm0.00080)+4.974(\pm0.137)N_2$, $d_{12}=0.86735(\pm0.00003)-0.0508(\pm0.0049)N_2$, $n^2_{12}D=2.23134-0.4118N_2$.			
Trisulfide			
0.001364	2.2699	0.86759	2.23048
0.002275	2.2725	...	2.23021
0.003794	2.2759	0.86797	2.22992
0.006326	2.2867	0.86829	2.22935
0.010636	2.2980	0.86894	2.22821
$\epsilon_{12}=2.26542(\pm0.00066)+3.110(\pm0.112)N_2$, $d_{12}=0.86740(\pm0.00002)+0.1443(\pm0.0024)N_2$, $n^2_{12}D=2.23081-0.2411N_2$.			
Tetrasulfide			
0.001371	2.2728	0.86789	2.23219
0.002282	2.2755	0.86825	2.23219
0.006379	2.3013	0.86955	2.23248
0.010634	2.3286	0.87089	2.23284
$\epsilon_{12}=2.26285(\pm0.00085)+6.135(\pm0.133)N_2$, $d_{12}=0.86748(\pm0.00002)+0.3212(\pm0.0034)N_2$, $n^2_{12}D=2.23205+0.0722N_2$.			

the refractive index, $n^2_{12}D$, at 30°C for the solutions of the sulfides in benzene.

The values in Table II have been computed from the data in Table I. The Hedestrand[8,9] formulation was used to obtain the infinite dilution values of the molar refractivity, MR_D, and of the total polarization, P_{20}. The dipole moments, μ, were calculated by the equation,

$$\mu=0.01281[(P_{20}-MR_D)T]^{\frac{1}{2}},$$

and are estimated to be in error by no more than ±0.02 unit in any case. All moment values stated in this paper are given in Debye units. Rough measurements of the dielectric constant and density of the solid sulfides showed that there is little difference between the solution values of MR_D and the total polarizations in the solid state at the same temperature.

TABLE II. The refractivities, polarizations and dipole moments of *n*-hexadecyl sulfides in benzene solution at 30°C.

	MR_D	P_{20}	μ
Monosulfide	158.41	202.02	1.47
Disulfide	167.90	248.65	2.00
Trisulfide	176.05	299.43	1.63
Tetrasulfide	187.01	280.39	2.16

[9] G. Hedestrand, Z. physik. Chem. **2B**, 428 (1929).

Working with benzene solutions at 25°C, Westlake, Laquer, and Smyth[5] obtained the value 1.99 for the dipole moment of ethyl disulfide and 1.64 for ethyl trisulfide. Kushner, Gorin, and Smyth[6] found the values 1.95, 1.96, and 1.96 for the moments of methyl, ethyl, and *n*-propyl disulfides, respectively, and the value 1.66 for methyl trisulfide. Their values were also obtained from measurements in benzene at 30°C.

DISCUSSION

In addition to their stability and purity, the sulfides studied here provide a series in which the alkyl groups are the same throughout, so that the only change in composition in passing through the series is the increase in the number of sulfur atoms.

The effect of concentration on the polarization of the ethyl and *n*-amyl sulfides in benzene reported by Walls and Smyth[10] was ascribed by them to the large size of the sulfur atom which prevented screening by the alkyl groups and permitted greater interaction of the solute molecules than is shown by ethers. In the case of the hexadecyl sulfides such interaction is apparently negligible in the concentration range of our measurements. This was revealed by plots of P_2N_2 against N_2 in accordance with the suggestion of Hoecker,[11] P_2 being the molar polarization of the solute at the concentration N_2. For each compound a good straight line was obtained which passed through the origin, as typified by the behavior of the monosulfide shown in Fig. 1. The large alkyl groups apparently provide adequate screening in these solutions.

The dipole moment values obtained here are additional evidence that disulfides do not have a *Y* structure and that in tri- and tetrasulfides the sulfur atoms are combined in a non-branched chain. This conclusion, in accord with that reached by Kushner, Gorin, and Smyth[6] for the sulfides they studied, is based on the small changes in dipole moment that result with increase in the number of sulfur atoms as one passes through the series from mono- to tetrasulfide. Large changes would be expected if the added sulfur atoms were held by coordinate linkages.

Additional interpretations of the moment values may be made with reference to the structures of the individual members of the series, especially in view of recent discoveries concerning sulfur chains.[6,12,13]

As pointed out by Kushner, Gorin, and Smyth, there is steric hindrance to intramolecular rotation in methyl trisulfide and those authors concluded that it is possible that the trisulfide exists in two more or less fixed nonplanar configurations. The small effect of the bulk of the

[10] W. S. Walls and C. P. Smyth, J. Chem. Phys. **1**, 337 (1933).
[11] F. E. Hoecker, J. Chem. Phys. **4**, 431 (1936).
[12] L. Pauling, Proc. Nat. Acad. Sci. **35**, 495 (1949).
[13] J. Donohue, J. Am. Chem. Soc. **72**, 2701 (1950).

alkyl groups as shown by the close agreement of our moment values with their values for both the di- and trisulfides indicates even more strongly the existence of fixed nonplanar structures. Rotation of the two alkyl-sulfur linkages with respect to one another would be affected by the bulk of the alkyl groups, and the alkyl-sulfur linkages are the only apparent source of moment for these molecules.

Pauling[12] has recently reviewed a large amount of evidence supporting non-planar configurations for polysulfides. He has shown that nonplanarity is clearly the rule, being due principally to the strong repulsion between the $p\pi$ electrons of the linked sulfur atoms and has concluded that the normal value of the dihedral angle for the sulfur-sulfur bonds is in the neighborhood of 100°. The approach of the dihedral angles to this normal value is apparently one of the strongest factors in deciding the stability of different configurations of compounds containing sulfur-sulfur linkages. In view of this, Donohue[13] re-examined the data of Dawson and Robertson[3] on the crystal structure of 2,2′-diiododiethyl trisulfide and showed that the $S-S-S-C$ grouping is not co-planar in that molecule as originally proposed, but forms a dihedral angle close to 90°.

The dipole moment of *n*-hexadecyl disulfide is consistent with a skew structure for the $C-S-S-C$ section of the molecule. The minimum moment of the alkyl disulfides would be zero, corresponding to a *trans* co-planar configuration where the dihedral angle is 180°, and the maximum moment would be $2m\sin\theta$, corresponding to a *cis* co-planar configuration with a dihedral angle of 0°, where m is the moment of the alkyl-sulfur link and θ is the $C-S-S$ bond angle. For a dihedral angle of 90° the calculated moment is the same as the free-rotation value, $1.414m\sin\theta$. Taking the bond angle as 105° in the monosulfide, a value of m equal to 1.21 is found from the observed moment of the monosulfide, 1.47. If the same reasonable value for the bond angle is chosen for the disulfide, the moments corresponding to 0°, 90°, and 180° for the dihedral angle are 2.34, 1.65, and 0 for this value of m. While these calculations definitely exclude the *trans* co-planar configuration, they support the *cis* coplanar, the right-angle skew, and the freely-rotating structures equally well.

Fortunately, a decision can be made in this situation by reconsideration of the alkyl-sulfur linkage moment, m. While at first glance the monosulfide moment appears well suited for the estimation of m because the monosulfide structure is not complicated by rotation, nevertheless the close proximity of the dipoles and the resultant mutual induction will render this estimate too low. In contrast to this, the effective m value for the disulfide should be little affected by mutual induction because of the greater separation of the dipoles and it should be considerably greater than 1.21. If m is calculated from the observed moment of the disulfide, the value 1.04 is obtained for a *cis* co-planar structure, and 1.47 for the skew or free-rotation structure. This clearly

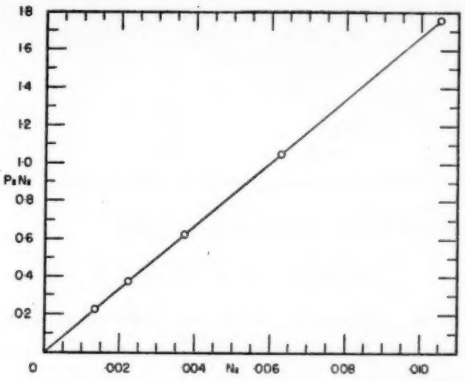

FIG. 1. The Hoecker plot for *n*-hexadecyl monosulfide.

excludes the co-planar structure and we may next call on the earlier discussion in favor of a fixed skew configuration to establish that form in preference to the structure in which the internal rotation is free. It should be noted that two non-superimposable mirror-image forms of the same moment can be formed with the same dihedral angle and that the disulfide should therefore be resolvable into two optically active forms.

We are now in a position to discuss the higher polysulfides by use of m obtained from the disulfide. In view of the values reported for the dihedral angles in other compounds containing sulfur-sulfur bonds, we have a preference for a value of 105°, rather than 90°, for this angle. This leads to a value of 1.70 for m, and this value will be used for the alkyl-sulfur linkage moment throughout the remainder of the discussion. This arbitrary choice of the dihedral angle when followed consistently has no important effect on the results of these discussions, which is fortunate in view of the uncertainty expressed by other workers in their estimates of the dihedral angles.

A model of the trisulfide molecule is shown in Fig. 2. We have developed the following formula for the moment, μ, of any instantaneous configuration in terms of the dihedral angles φ_1 and φ_2, and the bond angle θ, assuming the three bond angles equal.

$$\mu^2 = m^2\{\sin^2(180-\theta)(\sin\varphi_1+\sin\varphi_2)^2+\sin^2(180-\theta)\times\cos^2(\theta/2)(\cos\varphi_1-\cos\varphi_2)^2+[2\cos(180-\theta)\times\cos(\theta/2)+\sin(180-\theta)\sin(\theta/2)\times(\cos\varphi_1+\cos\varphi_2)]^2\}\cdots. \quad (1)$$

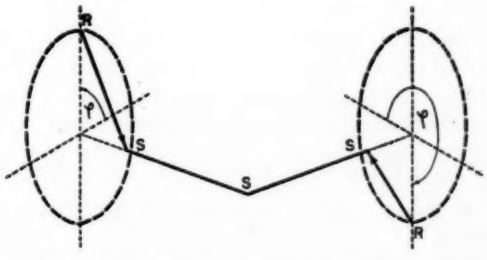

FIG. 2. The trisulfide, showing rotation of the $R-S$ linkages.

TABLE III. Three fixed configurations for *n*-hexadecyl trisulfide.

	φ_1	φ_2	μ
A	105	255	0.14
B	255	105	0.14
C	105	105	3.17

This leads to the free-rotation value

$$\mu = m[2 - 2\cos^3(180 - \theta)]^{\frac{1}{2}}$$

which is in agreement with the free-rotation formulas given by Smyth and Walls[14] and Kumler and Halverstadt.[15]

Taking each bond angle equal to 105°, we find that free-rotation would produce a moment of 2.38, compared to the observed value 1.63. For the several co-planar structures possible, the lowest moment calculated by Eq. (1) would be 2.07, for a *trans-trans* ($\varphi_1 = \varphi_2 = 180°$) or a *cis-trans* ($\varphi_1 = 180°$, $\varphi_2 = 0°$) arrangement, which is too high, in agreement with the other evidence ruling against coplanarity.

Taking the preferred dihedral angle (corresponding to $\varphi = 105°$ or 255°), three fixed non-planar configurations are obtained as shown in Table III. If these structures possess sufficient rigidity, it is possible that the substance may be considered a mixture of all three. Equal amounts of each would produce a moment of 1.83, and a mixture composed of 37 percent each of *A* and *B* and 26 percent of *C* would give the observed moment, 1.63. Such mixtures may be expected to yield to separation by chromatographic adsorption first into a polar fraction composed largely of the *C* form and a non-polar fraction made up largely of the other two forms. These two forms, *A* and *B*, are mirror images and this fraction could then be resolved into the separate, optically active molecules. An effort to carry out such separations is being undertaken. It is interesting to note that zero moment for the trisulfide should result if one dihedral angle is 102° and the other 258°.

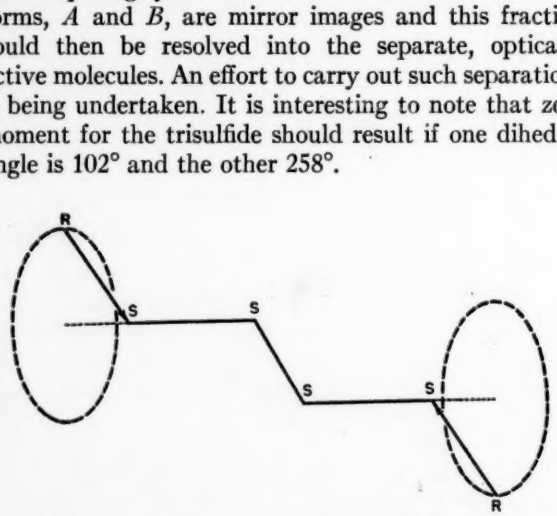

FIG. 3. The tetrasulfide showing rotation of the *R*—*S* linkages about a fixed co-planar chain of sulfur atoms.

The tetrasulfide has a moment which is only slightly greater than that of the disulfide. A moment equal to that of the disulfide might be expected if the four sulfur atoms were in a fixed *trans*-co-planar arrangement with the two *S*—*S*—*S* bond angles the same, no matter what value is chosen for these angles. In this case the axes of rotation for the two *R*—*S* moment vectors would be parallel as shown in Fig. 3 and the moment would have the same dependence on the rotation of these linkages as for the disulfide. Thus, the observed value of the moment, 2.16, is the same as would be calculated for a fixed structure in which the sulfurs are *trans* co-planar and the *R*—*S* linkages describe an azimuthal angle of approximately 96° with respect to each other. This is nearly the same as if the rotation of these links were completely free.

In view of the evidence against co-planar arrangements for the sulfur atoms, all of the fixed configurations

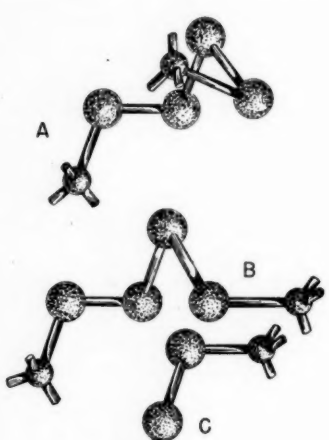

FIG. 4. Members of the three different pairs of enantiomorphs for *n*-hexadecyl tetrasulfide.

of the tetrasulfide molecule that would be obtained by application of a constant bond angle of 105° and dihedral angles of 105° to the *C*—*S*—*S*—*S*—*S*—*C* chain have been considered. Six non-superimposable forms are obtained in this way and these comprise three pairs of mirror images. Figure 4 shows one member of each of these pairs of enantiomorphs. The most tightly-coiled structure, *A*, would have a moment of 2.93. The others, such as *B* and *C*, would have equal moments, 2.01, although they differ in extent of coiling.

Similar to the result obtained for the trisulfide, equal amounts of each of these six forms would nearly account for the observed moment, the root-mean-square value for such a mixture being 2.36. A mixture composed of 86 percent of the lower moment forms and 14 percent of the higher would give exactly the observed value, 2.16.

[14] C. P. Smyth and W. S. Walls, J. Am. Chem. Soc. **54**, 2261 (1932).
[15] W. D. Kumler and I. F. Halverstadt, J. Am. Chem. Soc. **63**, 2182 (1941).

The Quantum Mechanics of Assemblies of Interacting Particles

H. S. GREEN
Dublin Institute for Advanced Studies, Dublin, Ireland
(Received January 22, 1951)

The quantum mechanics of fluids at moderately high and very low temperatures is investigated by the extension of a method due to Wigner. The fundamental equation satisfied by the phase space distribution function is solved, on the basis of classical statistics, by two different methods, and quantum corrections for thermodynamical equilibrium are obtained. It is shown that the effective molecular interaction becomes very weak near absolute zero. An estimate is made of the zero-point energy. Corrections due to quantum statistics are obtained.

I. INTRODUCTION

A GOOD deal of work has been done on the evaluation of quantum corrections to thermodynamical quantities, mostly based on a method of Kirkwood[1] of developing the Slater sum. Assuming the validity of classical statistics, quantum corrections to the virial coefficients of gases have been computed by Uhlenbeck and Beth,[2] and de Boer[3] subsequently extended these calculations to a number of thermodynamical quantities. This work is, however, based on an expansion in powers of Planck's constant, which fails at low temperatures. A method of potentially wider application was initiated by Wigner,[4] who derived the fundamental equation for the phase-space distribution function, which is essentially a fourier transform of the density matrix of von Neumann, and, as pointed out by Moyal,[5] replaces the velocity distribution function of the classical theory. Mayer and Band[6] have since put Wigner's work on a more rigorous footing.

In this paper an attempt has been made to obtain direct solutions of the fundamental integral equation. One solution is a power series in $\hbar^2$, and leads to thermodynamical expressions identical with those obtained by other methods, though rather more general than those resulting from Kirkwood's expansion, since they are applicable to condensed systems as well as gases. Another solution, in powers of the force constant, is better applicable to the region at very low temperatures. To obtain explicit results without undue labor, an approximation has been made, on the basis of which it would appear that effective molecular interaction becomes very small at very low temperatures. This is in agreement with some previous work by the author,[7] in which it was shown that the radial distribution function does not possess the usual high coordination peaks near absolute zero. It also helps to account for several puzzling properties of liquid helium.

Little has yet been done to examine the effect of quantum statistics on the statistical mechanics of assemblies of interacting particles. In the last section of this paper, an approach has been made to this problem. It is shown that, near absolute zero, the corrections for quantum statistics are approximately additive to the corrections already obtained.

II. PHASE SPACE DISTRIBUTIONS

In the classical theory of fluids, the value of any physically observable quantity is conveniently determined by means of the velocity distribution function f_q, defined in such a way that

$$f_q(\xi, \mathbf{x}, t)d^q\xi d^q\mathbf{x}$$

is the probability, at time t, of finding q molecules, with velocities in the ranges $\xi^{(i)}, d\xi^{(i)}$ $(i=1\cdots q)$, respectively, with their mass centers in the volume elements $\mathbf{x}^{(i)}$, $d\mathbf{x}^{(i)}$ $(i=1\cdots q)$. The mean value $\bar{\theta}_q$ at time t of any function θ_q of the velocities (and positions) of the q molecules is then given by

$$n_q(\mathbf{x}, t)\bar{\theta}_q(\mathbf{x}, t)=\int^q f_q(\xi, \mathbf{x}, t)\theta_q(\xi, \mathbf{x})d^q\xi, \qquad (1)$$

where

$$n_q(\mathbf{x}, t)=\int^q f_q(\xi, \mathbf{x}, t)d^q\xi \qquad (2)$$

is the density distribution function for q molecules with assigned positions $\mathbf{x}^{(i)}$ $(i=1\cdots q)$.

In the quantum theory, the statistical concept defining f_q is illegitimate, since the position and velocity of a molecule cannot, even in principle, be measured simultaneously. It has, however, been pointed out by Moyal[5] that a *phase space* distribution function f_q can be defined which allows mean values to be calculated from the classical formulas 1 and 2. In fact, the only property of the classical velocity distribution function which is not also possessed by the quantum-mechanical phase space distribution function is the essentially positive character of a probability.

The phase space distribution function is defined in terms of the density matrix $\rho_q(\mathbf{x}', \mathbf{x}'', t)$ by means of

[1] J. G. Kirkwood, Phys. Rev. **44**, 31 (1931).
[2] G. E. Uhlenbeck and E. Beth, Physica **3**, 729 (1936); **4**, 915 (1937).
[3] J. de Boer, Amsterdam Dissertations (1940).
[4] E. Wigner, Phys. Rev. **40**, 749 (1932).
[5] J. E. Moyal, Proc. Cambridge Phil. Soc. **45**, 99 (1949).
[6] J. E. Mayer and W. Band, J. Chem. Phys. **15**, 141 (1947).
[7] H. S. Green, Proc. Roy. Soc. (London) **A194**, 244 (1948).

the equations,

$$f_q(\xi, \mathbf{x}, t)=\left(\frac{m}{h}\right)^{3q}\int^q g_q(\mathbf{x}, \mathbf{y}, t) \times\exp(im\sum\xi^{(i)}\cdot y^{(i)}/\hbar)d^q\mathbf{y} \quad (3)$$

and

$$g_q(\mathbf{x}, \mathbf{y}, t)=\rho_q(\mathbf{x}-\tfrac{1}{2}\mathbf{y}, x+\tfrac{1}{2}\mathbf{y}, t), \quad (4)$$

in which m is the molecular mass and $h=2\pi\hbar$ is Planck's constant. The density matrix ρ_q was introduced into quantum mechanics by von Neumann.[8] For a system *in a pure state*, it can be represented as a product of Schrödinger wave functions,

$$\psi_q(\mathbf{x}', t)\psi_q^*(\mathbf{x}'', t).$$

This circumstance has been exploited by Price.[9] However, a cluster of molecules in a fluid, or even the entire fluid if it is in statistical interaction with its environment, cannot be in a pure state, and the use of the density matrix is then compulsory. It is necessary further to pay close attention to the boundary conditions.

Unless one supposes that the fluid occupies the whole of space, the wall must be represented by a potential barrier, and the molecules are then under the influence of an external field of force as well as their mutual interactions. The potential energy $\chi(\mathbf{x})$ of a molecule in this external field rises from the value zero inside the volume V occupied by the fluid to some very large or infinite value outside. The precise form of the function $\chi(\mathbf{x})$ is unimportant, except that it must permit the existence of a complete set of normal solutions of the Schrödinger equation. If $\chi(\mathbf{x})$ has any discontinuity, the second space derivative of the Schrödinger wave function and therefore of the density matrix will also be discontinuous at the wall. As a matter of convenience, $\chi(\mathbf{x})$ will here be assumed symmetrical about the origin of coordinates:

$$\chi(-\mathbf{x})=\chi(\mathbf{x}). \quad (5)$$

If $\phi(\mathbf{x}^{(j)}-\mathbf{x}^{(i)})$ is the mutual potential energy of a pair of molecules at the positions $\mathbf{x}^{(i)}$ and $\mathbf{x}^{(j)}$, the total potential energy of the molecules of the fluid will be

$$\Phi(\mathbf{x})=\tfrac{1}{2}\sum\sum\phi^{(ij)}+\sum\chi^{(i)}, \quad \phi^{(ij)}=\phi(\mathbf{x}^{(j)}-\mathbf{x}^{(i)}), \quad \chi^{(i)}=\chi(\mathbf{x}^{(i)}). \quad (6)$$

Assuming that the fluid consists of N identical molecules, the density matrix ρ_N satisfies

$$i\hbar\frac{\partial\rho_N}{\partial t}+\frac{\hbar^2}{2m}\sum\left\{\left(\frac{\partial}{\partial\mathbf{x}^{(i)'}}\right)^2-\left(\frac{\partial}{\partial\mathbf{x}^{(i)''}}\right)^2\right\}\rho_N =\{\Phi(\mathbf{x}')-\Phi(\mathbf{x}'')\}\rho_N \quad (7)$$

and the function g_N defined by (4) therefore satisfies

$$i\hbar\frac{\partial g_N}{\partial t}-\frac{\hbar^2}{2n}\sum\frac{\partial^2 g_N}{\partial\mathbf{x}^{(i)}\cdot\partial\mathbf{y}^{(i)}}=\{\Phi(\mathbf{x}-\tfrac{1}{2}\mathbf{y})-\Phi(\mathbf{x}+\tfrac{1}{2}\mathbf{y})\}g_N. \quad (8)$$

By fourier transformation, the equation satisfied by the phase space distribution function is obtained in the form,

$$\frac{\partial f_N(\xi)}{\partial t}+\sum\xi^{(i)}\cdot\frac{\partial f_N(\xi)}{\partial\mathbf{x}^{(i)}} =\frac{2}{\hbar}\int X(\mathbf{n})\sin(m\sum\mathbf{n}^{(i)}\cdot\mathbf{x}^{(i)}/\hbar)f_N(\xi-\tfrac{1}{2}\mathbf{n})d^N\mathbf{n}, \quad (9)$$

where

$$X(\mathbf{n})=\left(\frac{m}{h}\right)^{3N}\int^N\Phi(\mathbf{y})\cos(m\sum\mathbf{n}^{(i)}\cdot y^{(i)}/\hbar)d^N\mathbf{y}. \quad (10)$$

From (10) it follows that

$$\Phi(\mathbf{x})=\int^N X(\xi)\cos(m\sum\xi^{(i)}\cdot\mathbf{x}^{(i)}/\hbar)d^N\xi; \quad (11)$$

hence, if $f_N(\xi-\frac{1}{2}\mathbf{n})$ is expressed as a Taylor's series in powers of $\mathbf{n}$, thus:

$$f_N(\xi-\tfrac{1}{2}\mathbf{n})=f_N-\tfrac{1}{2}\sum\mathbf{n}^{(i)}\cdot\frac{\partial f_N}{\partial\xi^{(i)}} +\tfrac{1}{8}\sum\sum\mathbf{n}^{(i)}\cdot\frac{\partial^2 f_N}{\partial\xi^{(i)}\partial\xi^{(j)}}\cdot\mathbf{n}^{(j)}-\cdots, \quad (12)$$

Eq. (9) reduces to

$$\frac{\partial f_N}{\partial t}+\sum\xi^{(i)}\cdot\frac{\partial f_N}{\partial\mathbf{x}^{(i)}}=\frac{1}{m}\left\{\sum\frac{\partial\Phi}{\partial\mathbf{x}^{(i)}}\cdot\frac{\partial f^N}{\partial\xi^{(i)}} -\frac{\hbar^2}{24m^2}\sum\sum\sum\frac{\partial^3\Phi}{\partial\mathbf{x}^{(i)}\partial\mathbf{x}^{(j)}\partial\mathbf{x}^{(k)}} \cdot\frac{\partial^3 f_N}{\partial\xi^{(i)}\partial\xi^{(j)}\partial\xi^{(k)}}+\cdots\right\}. \quad (13)$$

In the classical limit, as $\hbar\to 0$, it is clear that one obtains the classical equation,

$$\frac{\partial f_N{}^c}{\partial t}+\sum\xi^{(i)}\cdot\frac{\partial f_N{}^c}{\partial\mathbf{x}^{(i)}}=\frac{1}{m}\sum\frac{\partial\Phi}{\partial\mathbf{x}^{(i)}}\cdot\frac{\partial f_N{}^c}{\partial\xi^{(i)}}, \quad (14)$$

which determines the velocity distribution function. The additional terms in (13) determine quantum corrections to the formulas of the classical theory of fluids.

III. MODERATELY HIGH TEMPERATURES

At sufficiently high temperatures, the phase space distribution function f_N can be expanded in powers of

[8] J. v. Neumann, *Grundlagen der Quantenmechanik* (Verlag. Julius Springer, Berlin, 1932).
[9] P. J. Price, Phil. Mag. **61**, 448 (1950).

$\hbar^2$. The expansion is most conveniently obtained by substituting

$$f_N = f_N{}^c(1+\hbar^2 A_1+\hbar^4 A_2+\cdots) \tag{15}$$

into (13). Then $f_N{}^c$ is the classical velocity distribution function, which satisfies (14); by separating powers of $\hbar^2$ from (13), one obtains for A_1

$$\frac{\partial A_1}{\partial t}+\sum\left(\boldsymbol{\xi}^{(i)}\cdot\frac{\partial A_1}{\partial \mathbf{x}^{(i)}}-\frac{1}{m}\frac{\partial\Phi}{\partial \mathbf{x}^{(i)}}\cdot\frac{\partial A_1}{\partial \boldsymbol{\xi}^{(i)}}\right)$$

$$=-\frac{1}{24m^3 f_N{}^c}\sum\sum\sum\frac{\partial^3\Phi}{\partial \mathbf{x}^{(i)}\partial \mathbf{x}^{(j)}\partial \mathbf{x}^{(k)}}\cdot\frac{\partial^3 f_N{}^c}{\partial \boldsymbol{\xi}^{(i)}\partial \boldsymbol{\xi}^{(j)}\partial \boldsymbol{\xi}^{(k)}}. \tag{16}$$

In the present paper, attention will be limited to fluids in thermal and mechanical equilibrium, for which it is known that

$$\partial A_1/\partial t=0, \quad f_N{}^c=\exp\beta(F-\Phi-\textstyle\sum\frac{1}{2}m\boldsymbol{\xi}^{(i)2}) \tag{17}$$

where F is the free energy. Then the right-hand side of (16) reduces to

$$\frac{\beta^3}{24}\left(\sum\boldsymbol{\xi}^{(i)}\cdot\frac{\partial}{\partial \mathbf{x}^{(i)}}\right)^3\Phi-\frac{\beta^2}{8m}\left(\sum\boldsymbol{\xi}^{(i)}\cdot\frac{\partial}{\partial \mathbf{x}^{(i)}}\right)\left(\sum\frac{\partial^2\Phi}{\partial \mathbf{x}^{(j)}\partial \mathbf{x}^{(j)}}\right),$$

and the solution of (16) is

$$\frac{\beta^3}{24}\left(\sum\boldsymbol{\xi}^{(i)}\cdot\frac{\partial}{\partial \mathbf{x}^{(i)}}\right)^2\Phi$$

$$-\frac{\beta^2}{8m}\sum\left(\frac{\partial^2\Phi}{\partial \mathbf{x}^{(i)}\partial \mathbf{x}^{(i)}}-\frac{\beta}{3}\frac{\partial\Phi}{\partial \mathbf{x}^{(i)}}\cdot\frac{\partial\Phi}{\partial \mathbf{x}^{(i)}}\right). \tag{18}$$

The coefficients A_2, A_3, etc., in (15) can be determined in a similar way, but naturally their complexity increases greatly with the power of $\hbar^2$ which they multiply.

The density distribution function n_N, derived from (15) in accordance with (2), is

$$n_N=n_N{}^c(1+\hbar^2 B_1+\hbar^4 B_2+\cdots), \tag{19}$$

where $n_N{}^c$ is the classical function

$$n_N{}^c=\lambda^N\exp\beta(F-\Phi), \qquad \lambda=(2\pi/\beta m)^{\frac{1}{2}}, \tag{20}$$

and

$$B_n=\lambda^{-N}\int^N\exp(-\beta\textstyle\sum\frac{1}{2}m\boldsymbol{\xi}^{(i)2})A_n d^N\boldsymbol{\xi}. \tag{21}$$

Using (18), one has

$$B_1=\frac{\beta^2}{24m}\sum\left(\beta\frac{\partial\Phi}{\partial \mathbf{x}^{(i)}}\cdot\frac{\partial\Phi}{\partial \mathbf{x}^{(i)}}-2\frac{\partial^2\Phi}{\partial \mathbf{x}^{(i)}\partial \mathbf{x}^{(i)}}\right). \tag{22}$$

This is the result obtained by Wigner.[4] It has been pointed out by Mayer and Band[6] that the analysis is not perfectly rigorous, since the initial terms of the series (19) increase rapidly in magnitude. Assuming, however, that the free energy can be expanded in powers of $\hbar^2$, this defect is corrected in (26) below.

Now, it will be supposed that the n_q are normalized in such a way that

$$\int n_{q+1}d\mathbf{x}^{(q+1)}=(N-q)n_q, \tag{23}$$

with $n_0=1$. Then it follows from (19) and (20) that

$$\exp(-\beta F)=\frac{\lambda^N}{N!}\int^N\exp(-\beta\Phi)$$

$$\cdot(1+\hbar^2 B_1+\cdots)d^N\mathbf{x}=\frac{\lambda^N}{N!}\int^N\exp(-\beta\Phi)$$

$$\cdot\left(1-\frac{i\hbar^2\beta^2}{24m}\sum\frac{\partial^2\Phi}{\partial \mathbf{x}^{(i)}\partial \mathbf{x}^{(i)}}+\cdots\right)d^N\mathbf{x} \tag{24}$$

after an integration by parts.

In this section the terms arising from the existence of the external potential function $\chi(\mathbf{x})$ will be neglected, except in so far as it limits the spatial integration to a region of volume V. Then, substituting from (6) into (24), the latter reduces to

$$\exp(-\beta F)=\exp(-\beta F^c)\left\{1-\frac{\hbar^2\beta^2}{24m}\right.$$

$$\left.\times\int\int n_2{}^c\frac{\partial^2\phi(\mathbf{r})}{\partial\mathbf{r}\cdot\partial\mathbf{r}}d\mathbf{x}^{(1)}d\mathbf{x}^{(2)}+\cdots\right\}, \tag{25}$$

where F^c and

$$n_2{}^c=\frac{\lambda^N}{(N-2)!}\int^{N-2}\exp\beta(F^c-\Phi)\prod_{i=2}^{N}d\mathbf{x}^{(i)}$$

are the classical values of F and the number distribution function n_2, and $\mathbf{r}=\mathbf{x}^{(2)}-\mathbf{x}^{(1)}$. Hence

$$F=F^c+\frac{\hbar^2\beta V}{24m}\int n_2{}^c\frac{\partial^2\phi}{\partial\mathbf{r}\cdot\partial\mathbf{r}}d\mathbf{r}+\cdots. \tag{26}$$

The thermodynamic pressure and internal energy may be derived in the usual way by differentiating with respect to $V=N/n_1$ and β, respectively, thus:

$$p=p^c+\frac{\hbar^2\beta}{24m}\int\left(n_1\frac{\partial n_2{}^c}{\partial n_1}-n_2{}^c\right)\frac{\partial^2\phi}{\partial\mathbf{r}\cdot\partial\mathbf{r}}d\mathbf{r}+\cdots, \tag{27}$$

and

$$U=U^c+\frac{\hbar^2\beta V}{24m}\int\left(\beta\frac{\partial n_2{}^c}{\partial\beta}+2n_2{}^c\right)\frac{\partial^2\phi}{\partial\mathbf{r}\cdot\partial\mathbf{r}}d\mathbf{r}+\cdots. \tag{28}$$

These formulas are correct for both liquids and gases. The classical radial distribution function $n_2{}^c$ may to a

first approximation be replaced by the actual radial distribution function n_2 obtained, for example, by the analysis of the x-ray scattering experiments. In *rare gases*,

$$\beta p^c = n_1 - \tfrac{1}{2}n_1^2 \int \{\exp(-\beta\phi)-1\} d\mathbf{r} + 0(n_1^3),$$
$$n_2^c = n_1^2 \exp(-\beta\phi) + 0(n_1^3); \tag{29}$$

so

$$p = p^c + \frac{\hbar^2\beta^2 n_1^2}{24m} \int \exp -\beta\phi \left(\frac{\partial\phi}{\partial \mathbf{r}}\right)^2 d\mathbf{r} + 0(n_1^3). \tag{30}$$

This expression, which gives the quantum correction to the second virial coefficient, was obtained by Uhlenbeck and Beth[2] by another method, and has been evaluated by de Boer[3] for a general potential function of the Leonard-Jones type.

The phase space distribution function of f_1 appropriate to a single molecule in the fluid can be obtained from (15) by integrating over all positions and velocities except $\mathbf{x}^{(1)}$ and $\boldsymbol{\xi}^{(1)}$:

$$f_1 = \frac{1}{(N-1)!} \int^{2(N-1)} \{f^{Nc}(1+\hbar^2 B_1 + \cdots)$$
$$+ h^2 f_N{}^c (A_1 - B_1) + \cdots\} \prod_{i=2}^{N} d\boldsymbol{\xi}^{(i)} d\mathbf{x}^{(i)}$$
$$= \lambda^{-1} \exp(-\tfrac{1}{2}\beta m \xi^{(1)2}) \left\{ n_1 + \frac{\hbar^2\beta^2}{24m} (\tfrac{1}{3}\beta m \xi^{(1)2} - 1) \right.$$
$$\left. \times \int n_2{}^c \frac{\partial^2\phi}{\partial \mathbf{r}\cdot\partial\mathbf{r}} d\mathbf{r} + \cdots \right\}. \tag{31}$$

Since

$$\int^{N-1} \exp(-\beta\Phi)\cdot(A_1 - B_1) d^{N-1}\mathbf{x}$$
$$= \sum \frac{\beta^2}{24m} (\tfrac{1}{3}\beta m \xi^{(i)2} - 1)$$
$$\times \int^{N-1} \exp(-\beta\Phi) \cdot \frac{\partial^2\Phi}{\partial \mathbf{x}^{(i)} \partial \mathbf{x}^{(i)}} d^{N-1}\mathbf{x}.$$

The mean kinetic energy of a molecule, obtained from (1) with the help of this formula, is

$$\tfrac{3}{2}kT_1 = \frac{3}{2\beta} \left\{ 1 + \frac{\hbar^2\beta^2}{36m} \int n_2{}^c \frac{\partial^2\phi}{\partial \mathbf{r}\cdot\partial\mathbf{r}} d\mathbf{r} + \cdots \right\}, \tag{32}$$

showing that the "kinetic" temperature T_1 differs in the quantum theory from the "thermodynamic" temperature $1/(k\beta)$.

Owing to the factor β which they contain, the quantum corrections proportional to $\hbar^2$ in the formulas (26)–(28) and (32) become very large at very low temperatures. It is not hard to verify that this feature is reproduced to an even greater degree in the corrections proportional to higher powers of $\hbar^2$. The procedure of expansion in powers of $\hbar^2$ will therefore fail near absolute zero, and another method of approximation has to be devised.

IV. VERY LOW TEMPERATURES

At very low temperatures, the differential equation (13) is no longer useful, and it is necessary to return to the integral equation (9) in order to determine the phase space distribution function. A solution exists of the following form:

$$f^N = \exp(\beta F)(C_0 + C_1 + C_2 + \cdots),$$
$$C_k = \int^{kN} E_k(\boldsymbol{\xi}, \mathbf{H}_k) \cos(m \sum \mathbf{H}_k{}^{(i)} \cdot \mathbf{x}^{(i)}/\hbar)$$
$$\times \prod_{l=1}^{k} \{X(\mathbf{n}_l) d^N \mathbf{n}_l\}, \tag{33}$$

where E_k is a function, to be determined, of $\boldsymbol{\xi}$,

$$\mathbf{H}_k = \sum_{l=1}^{k} \mathbf{n}_l,$$

and in general the relative velocities $\mathbf{n}_l - \mathbf{n}_m$ as well. Since one must obtain the classical solution in the limit $X(\mathbf{n}) \to 0$,

$$C_0 = E_0 = \exp(-\tfrac{1}{2}\beta m \sum \xi^{(i)2}). \tag{34}$$

Substituting (33) in the integral equation (9), one finds that the latter is in fact satisfied, provided

$$(m \sum \boldsymbol{\xi}^{(i)} \cdot \mathbf{H}_{k+1}{}^{(i)} E_{k+1}(\boldsymbol{\xi}, \mathbf{H}_{k+1})$$
$$= E_k(\boldsymbol{\xi} - \tfrac{1}{2}\mathbf{n}_{k+1}, \mathbf{H}_k) - E_k(\boldsymbol{\xi} + \tfrac{1}{2}\mathbf{H}_k, -\mathbf{n}_{k+1}). \tag{35}$$

With the help of (34),

$$(\tfrac{1}{2}m \sum \boldsymbol{\xi}^{(i)} \cdot \mathbf{n}^{(i)}) E_1(\boldsymbol{\xi}, \mathbf{n}) = -\exp\{-\tfrac{1}{2}\beta m \sum (\xi^{(i)2}$$
$$+ \tfrac{1}{4}\mathbf{n}^{(i)2})\} \sinh(\tfrac{1}{2}\beta m \sum \boldsymbol{\xi}^{(i)} \cdot \mathbf{n}^{(i)}). \tag{36}$$

In this formula it is convenient to write

$$\sinh(\tfrac{1}{2}\beta m \sum \boldsymbol{\xi}^{(i)} \cdot \mathbf{n}^{(i)}) = (\tfrac{1}{2}\beta m \sum \boldsymbol{\xi}^{(i)} \cdot \mathbf{n}^{(i)})$$
$$\times \int_0^1 \cosh(\tfrac{1}{2} z \beta m \sum \boldsymbol{\xi}^{(i)} \cdot \mathbf{n}^{(i)}) dz.$$

Then (33) gives, on substitution from (10),

$$C_1 = -\beta \int_0^1 \int^N \left(\frac{2\pi m}{\beta h^2}\right)^{3N/2}$$
$$\times \exp[-\tfrac{1}{2}\beta m \sum \{(1-z^2)\xi^{(i)2} + \mathbf{y}^{(i)2}/(\beta\hbar)^2\}]$$
$$\times \cos(mz \sum \boldsymbol{\xi}^{(i)} \cdot \mathbf{y}^{(i)}/\hbar) \Phi(\mathbf{x} + \tfrac{1}{2}\mathbf{y}) d^N\mathbf{y} dz. \tag{37}$$

By integrating Eq. (33) over all velocities, one obtains

$$n_N = \lambda^N \exp(\beta F) \cdot (1 - \beta\Phi_1 + \tfrac{1}{2}\beta^2\Phi_2 - \tfrac{1}{6}\beta^3\Phi_3 + \cdots), \tag{38}$$

where

$$\lambda^N(-\beta)^k\Phi_k=k!\int^N C_k d^N\xi. \tag{39}$$

The convergence of the series in (38) is satisfactory because, although β is very large at very low temperatures, it will appear in the following calculation that the coefficients Φ_k in this temperature range are of order β^{-k}. The value of Φ_1 can be determined immediately from (39) and (37); it is*

$$\Phi_1=\int_0^1\int^N\left(\frac{2\pi m}{\beta\hbar^2}\right)^{3N/2}\times\exp\left(-\frac{\beta\sum\mathbf{y}^{(i)2}}{2\beta\hbar^2}\right)\Phi\{\mathbf{x}+(1-z^2)^{\frac{1}{2}}\mathbf{y}\}d^N\mathbf{y}dz. \tag{40}$$

Equations (37) and (40) can be reduced with the help of (6); one obtains

$$C_1=-\beta(\tfrac{1}{2}\sum\sum c_1^{(ij)}+\sum d^{(i)})C_0$$

$$c_1^{(ij)}=\int_0^1\int\left(\frac{\pi m}{\beta\hbar^2}\right)^{\frac{3}{2}}\exp-\tfrac{1}{4}\beta m\{-z^2\rho^2+\mathbf{s}^2/(\beta\hbar)^2\}\times\cos(\tfrac{1}{2}mz\boldsymbol{\varrho}\cdot s/\hbar)\phi(\mathbf{r}+\tfrac{1}{2}\mathbf{s})d\mathbf{s}dz,$$

$$\mathbf{r}=\mathbf{x}^{(j)}-\mathbf{x}^{(i)},\quad \boldsymbol{\varrho}=\boldsymbol{\xi}^{(j)}-\boldsymbol{\xi}^{(i)},$$

$$d^{(i)}=\int_0^1\int\left(\frac{2\pi m}{\beta\hbar^2}\right)^{\frac{3}{2}}\times\exp-\tfrac{1}{2}\beta m\{-z^2\xi^{(i)2}+\mathbf{y}^{(i)2}/(\beta\hbar)^2\}\times\cos(mz\boldsymbol{\xi}^{(i)}\cdot\mathbf{y}^{(i)}/\hbar)\chi(\mathbf{x}^{(i)}+\tfrac{1}{2}\mathbf{y}^{(i)})d\mathbf{y}^{(i)}dz, \tag{41}$$

and

$$\Phi_1=\tfrac{1}{2}\sum\sum\phi_1^{(ij)}+\sum\chi_1^{(i)},$$

$$\phi_1^{(ij)}=\int_0^1\int\left(\frac{\pi m}{\beta\hbar^2}\right)^{\frac{3}{2}}\times\exp\left(-\frac{ms^2}{4\beta\hbar^2}\right)\phi\{\mathbf{r}+(1-z^2)^{\frac{1}{2}}\mathbf{s}\}d\mathbf{s}dz,$$

$$\chi_1^{(i)}=\int_0^1\int\left(\frac{2\pi m}{\beta\hbar^2}\right)^{\frac{3}{2}}\exp\left(-\frac{m\mathbf{y}^{(i)2}}{\beta\hbar^2}\right)\times\chi\{\mathbf{x}^{(i)}+(1-z^2)^{\frac{1}{2}}\mathbf{y}^{(i)}\}d\mathbf{y}^{(i)}dz. \tag{42}$$

The values of Φ_2, Φ_3, etc., remain to be determined. This will not at present be attempted in detail; but it can be seen from (41) that, since each term of C_1 differs from C_0 only by a factor involving the coordinates and velocities of at most two molecules, Φ_2 will differ from Φ_1^2 only in the value of terms, such as $(\phi_1^{(ij)})^2$ and $2\phi_1^{(ij)}\phi_1^{(jk)}$, whose factors refer repeatedly to a single molecule. Similarly Φ_3 differs from Φ_1^3 only in the value of terms such as $6\phi_1^{(ij)}\phi_1^{(jk)}\phi_1^{(kl)}$. As such terms are statistically much less numerous than the others, and in any case involve increasing powers of β^{-1}, it seems reasonable to suppose that

$$n_N=\lambda^N\exp\beta(F-\Phi_1) \tag{43}$$

is a good approximation to (38). This is especially so near absolute zero, where Φ_1 is of order β^{-1}. A probable exception to the validity of the approximation will occur when two molecules are so close that they are in the very strongly repulsive region of the field of their mutual interaction.

A few consequences of (43) will be immediately obvious. The free energy and all the density distribution functions will be the same as one would expect on the basis of the classical theory, if the potential energy were Φ_1 instead of Φ. The actual form of the effective interaction $\phi_1(\mathbf{r})$ is evidently of interest. From (42) it follows that

$$\phi_1(r)=\frac{m}{\hbar^2\beta r}\int_0^\infty\int_{|r-a|}^{|r+a|}\phi(s)sds\exp\left(-\frac{ma^2}{\beta\hbar^2}\right)da, \tag{44}$$

and at very low temperatures the exponential factor is practically unity over most of the range of integration. Assuming†

$$\begin{aligned}\phi(r)&=-\mu r^{-6}+A\exp(-r/r_0), && r>b,\\ &=-\mu b^{-6}+A\exp(-r/r_0), && r<b,\end{aligned} \tag{45}$$

so that b is the molecular diameter, one obtains

$$\begin{aligned}\phi_1(r)&=\frac{m}{6\hbar^2\beta}[-\mu r^{-1}(8b^{-3}-r^{-3})\\ &\quad+12A\{2r_0-(r+2r_0)\exp(-r/r_0)\}], && r>b,\\ &=\frac{m}{6\hbar^2\beta}[-\mu(9b^{-4}-2r^2b^{-6})\\ &\quad+12A\{2r_0-(r+2r_0)\exp(-r/r_0)\}], && r<b.\end{aligned} \tag{46}$$

The terms neglected are proportional to β^{-2}, and the approximation is valid only up to moderately large distances, and for $\beta\hbar^2>mb^2$, i.e., at temperatures less than 2°K in helium.

The fact that $\phi_1(r)$ is proportional to β^{-1}, with its corollary that Φ_k is proportional to β^{-k}, justifies the expansion represented by (38), and shows that the method of approximation is particularly well adapted to the temperature range near absolute zero. What is

* The formula,

$$\int\exp(-\tfrac{1}{2}\xi^2/\sigma)\cos(\tau\boldsymbol{\xi}\cdot\mathbf{y})d\boldsymbol{\xi}=(2\pi\sigma)^{\frac{1}{2}}\exp(-\tfrac{1}{2}\sigma\tau^2y^2),$$

is used here, and on several subsequent occasions.

† The use of a potential with a strong singularity at the origin would lead to difficulties, associated with the lack of definition of the hamiltonian operator—see K. M. Case, Phys. Rev. **79**, 220 (1950).

chiefly required in this range is to expand the free energy in powers of the absolute temperature.

The effect of the approximation (43) is to exclude the contribution to the free energy of quantum jumps involving more than two molecules at a time. As the amount of energy available for such transitions is small near absolute zero, it may be expected that the error involved is not large in this region, and there would in any event be no difficulty in developing the first- and second-order corrections.

On account of the factor β^{-1} which it contains, the effective interaction is very weak at low temperatures. Only the fact the long-range attractive term $4\mu m/(3h^2\beta b^3 r)$ is effective to moderately large distances (it will be remembered that (46) is not a good approximation to (44) at *very* large distances) will indeed explain the cohesion of the liquid. Since the minimum of the effective potential energy between two molecules is at a consideraly greater distance than in the classical theory, so one would expect the density of the liquid to be abnormally low. The viscosity of the liquid, which depends almost entirely on the effective action of the intermolecular forces, will also be abnormally low. The effective interaction of a molecule with any wall bounding the fluid may be represented by the last equation of (42), and is also proportional to β^{-1} near absolute zero.

An estimate of the zero-point energy of the fluid can be obtained by computing the mean kinetic energy of a molecule directly with the help of (41). Neglecting the term containing $d^{(i)}$, which becomes important only near the boundary of the fluid, one has

$$\int^N f_N\cdot\tfrac{1}{2}m\xi^{(i)2}d^N\xi$$

$$=n_N\int\lambda^{-1}\exp(-\tfrac{1}{2}\beta m\xi^{(i)2})\cdot\Big\{1+\sum_j\int\lambda^{-1}$$

$$\times\exp(-\tfrac{1}{2}\beta m\xi^{(j)2})\cdot(c^{(ij)}+\beta\phi_1{}^{(ij)})d\xi^{(j)}$$

$$\cdot\tfrac{1}{2}m\xi^{(i)2}d\xi^{(i)}\Big\}. \quad (47)$$

After some elementary integrations, the right-hand side of this equation reduces to

$$n_N\Big\{\frac{3}{2\beta}+\tfrac{1}{4}\sum_j(\phi_1{}^{(ij)}-\phi^{(ij)})\Big\}.$$

The mean kinetic energy of a molecules is therefore

$$\tfrac{3}{2}kT_1=\tfrac{3}{2}\beta^{-1}+\tfrac{1}{4}\int\frac{n_2}{n_1}\{\phi_1(r)-\phi(r)\}d\mathbf{r}. \quad (48)$$

At absolute zero, this tends to the limit

$$-\tfrac{1}{4}\int n_1{}^{-1}n_2\phi(r)d\mathbf{r}$$

equal to one-half of the negative potential energy of a molecule in the fluid. In passing from the liquid to the gas a molecule must lose kinetic energy equal to one-half of the potential energy which it gains. The heat of vaporization is therefore only one-half of the classical value.

To obtain an exact theory, it will be necessary to determine the coefficients Φ_2, Φ_3, etc., of the series (38) more exactly. Another limitation to the validity of the results obtained in this section is that classical statistics have been employed. The influence of quantum statistics on the behavior of systems of interacting particles is probably less than one would suppose from the theory of non-interacting systems; this is indicated, for example, by the work of de Boer,[10] who has successfully predicted the values of molar quantities in a way which is independent of the statistics. On the other hand, there is a significant difference in the superfluid behavior of liquefied He^4 and He^3 which cannot be accounted for solely by the difference in mass. It is very desirable, therefore, to examine the effect of quantum statistics on the theory developed in the last two sections.

V. QUANTUM STATISTICS

The quantitative effect of quantum statistics on the theory of assemblies of identicle particles is most readily exhibited in the form of the density matrix. For non-interacting particles this has been shown by Husimi.[11] In what follows, $\rho_N(\mathbf{x}', \mathbf{x}'')$ continues to represent the density matrix determined on the basis of classical statistics, and the corresponding density matrices for particles satisfying Bose and Fermi statistics respectively are denoted by $\rho_N{}^+(\mathbf{x}', \mathbf{x}'')$ and $\rho_N{}^-(\mathbf{x}', \mathbf{x}'')$.

If I_{rs} is the "space exchange" operator which interchanges the coordintes $\mathbf{x}^{(r)'}$ and $\mathbf{x}^{(s)'}$, the relation of $\rho_N{}^+$ and $\rho_N{}^-$ to ρ_N may be specified with the help of the symmetrization operators

$$S^+=(1+I_{NN-1})\cdots(1+I_{32}+\cdots+I_{N2})$$
$$\times(1+I_{21}+I_{31}+\cdots+I_{N1})$$
$$S^-=(1-I_{NN-1})\cdots(1-I_{32}-\cdots-I_{N2})$$
$$\times(1-I_{21}-I_{31}-\cdots-I_{N1}). \quad (49)$$

One has, in fact,

$$\rho_N{}^+(\mathbf{x}', \mathbf{x}'')=c^+S^+\rho_N(\mathbf{x}', \mathbf{x}''),$$
$$\rho_N{}^-(\mathbf{x}', \mathbf{x}'')=c^-S^-\rho_N(\mathbf{x}', \mathbf{x}''), \quad (50)$$

where c^+ and c^- are constants determined by the normalizing conditions.

$$\int^N\rho_N{}^+(\mathbf{x}, \mathbf{x})d^N\mathbf{x}=\int^N\rho_N{}^-(\mathbf{x}, \mathbf{x})d^N\mathbf{x}=N!. \quad (51)$$

[10] J. de Boer, Proc. of the International Conference on the Physics of Very Low Temperatures (Cambridge, Massachusetts, 1949).

[11] K. Husimi, Proc. Phys.-Math. Soc. Japan **22**, 264 (1940).

The free energies F^+ and F^- for Bose and Fermi statistics are related to the free energy F determined on the basis of classical statistics by means of

$$c^+=\exp\beta(F^+-F),\quad c^-=\exp\beta(F^--F). \tag{52}$$

As formulas for Fermi particles are obtainable by a trivial modification of those for Bose particles, attention will henceforth be restricted to the latter. Some investigations concerning the radial distribution function n_2 have been made in this connection by F. London.[12] Combining Eqs. (50)–(52), we have

$$N!\exp\beta(F-F^+)=\int^N (S^+\rho_N)(\mathbf{x},\mathbf{x})d^N\mathbf{x}$$
$$=\int^N (S^+g_N)(\mathbf{x},0)d^N\mathbf{x}, \tag{53}$$

where g_N is defined by (4).

Any term of the symmetrization operator S^+ can be expressed as the product of a number of cyclic permutation operators of the type

$$C_{rstu\ldots z}=I_{rs}I_{st}I_{tu}\cdots I_{yz}. \tag{54}$$

There are, in fact,

$$\frac{N!}{k_1!\cdots k_q!}\cdot\frac{1}{2^{k_2}\cdots q^{k_q}}$$

terms of S^+ which factorize into k_2 cyclic permutations of 2 coordinates, k_3 cyclic permutations of 3 coordinates, etc., and leave k_1 of the coordinates $\mathbf{x}^{(i)'}$ unchanged. Hence

$$\int^N (S^+g_N)(\mathbf{x},0)d^N\mathbf{x}=N!\sum{}'\left(\frac{Q_{k_1k_2\cdots k_q}}{k_1!k_2!\cdots k_q!}\right), \tag{55}$$

where the summation is over those values of the k's for which

$$\sum qk_q=N \tag{56}$$

and

$$(2^{k_2}\cdots q^{k_q})Q_{k_1k_2\cdots k_q}$$
$$=\int^N (P_{k_1k_2k_3\cdots k_q}g_N)(\mathbf{x},0)d^N\mathbf{x}, \tag{57}$$

where $P_{k_1k_2\cdots k_q}$ is a typical product of cyclic permutations.

The effect of a cyclic permutation $C_{12\ldots q}$ on a function $g_q(\mathbf{x}^{(1)},\cdots\mathbf{x}^{(q)};\ \mathbf{y}^{(1)},\cdots\mathbf{y}^{(q)})$ of the $\mathbf{x}^{(i)}=\frac{1}{2}(\mathbf{x}^{(i)'}+\mathbf{x}^{(i)''})$ and $\mathbf{y}^{(i)}=\mathbf{x}^{(i)''}-\mathbf{x}^{(i)'}$ is easily determined; one has, in fact,

$$(C_{12\ldots q}g_q)(\mathbf{x}^{(1)},\cdots\mathbf{x}^{(q)};0,\cdots 0)$$
$$=g_q(\mathbf{x}^{(12)},\cdots\mathbf{x}^{(q1)};\mathbf{r}^{(12)},\cdots\mathbf{r}^{(q1)}), \tag{58}$$

where

$$\mathbf{x}^{(ij)}=\tfrac{1}{2}(\mathbf{x}^{(i)}+\mathbf{x}^{(j)})\quad\text{and}\quad\mathbf{r}^{(ij)}=\mathbf{x}^{(j)}-\mathbf{x}^{(i)}.$$

The functions g_q to which (58) will be applied are defined by (4); with the normalization indicated by (23), one has

$$(N-q)!g_q(\mathbf{x},\mathbf{y})$$
$$=\int^{2(N-q)} g_N(\mathbf{x},\mathbf{y})\prod_{i=q+1}^{N}\{\delta(\mathbf{y}^{(i)})d\mathbf{y}^{(i)}d\mathbf{x}^{(i)}\}. \tag{59}$$

At moderately high temperatures, the value of g_N as a power series in $\hbar^2$ can be inferred from (15) with the help of the formula,

$$g_N(\mathbf{x},\mathbf{y})=\int^N f_N(\mathbf{x},\boldsymbol{\xi})\exp(-im\textstyle\sum\boldsymbol{\xi}^{(i)}\cdot\mathbf{y}^{(i)}/\hbar)d^N\boldsymbol{\xi}, \tag{60}$$

which follows from (3). One obtains

$$g_N(\mathbf{x},\mathbf{y})=\lambda^N\exp\beta\{F-\Phi-\tfrac{1}{2}m\textstyle\sum(y^{(i)}/\beta\hbar)^2\}$$
$$\times(1+\hbar^2D_1+\hbar^4D_2+\cdots), \tag{61}$$

where

$$D_1=-\frac{\beta}{24}\left(\sum\frac{\mathbf{y}^{(i)}}{\hbar}\cdot\frac{\partial}{\partial\mathbf{x}^{(i)}}\right)^2\Phi$$
$$-\frac{\beta^2}{24m}\sum\left(2\frac{\partial^2\Phi}{\partial\mathbf{x}^{(i)}\cdot\partial\mathbf{x}^{(i)}}-\beta\frac{\partial\Phi}{\partial\mathbf{x}^{(i)}}\frac{\partial\Phi}{\partial\mathbf{x}^{(i)}}\right). \tag{62}$$

On account of the factor

$$\exp\{-\tfrac{1}{2}\beta m\textstyle\sum(\mathbf{r}^{(ii+1)}/\beta\hbar^2)\}$$

which it contains, $(C_{12\ldots q}g_q)(\mathbf{x},0)$ will be negligible if any of the positions $\mathbf{x}^{(i)},\cdots\mathbf{x}^{(q)}$ are far apart. The fluid is therefore divided by the product $P_{k_1}\cdots_{k_q}$ of cyclic permutations into clusters of molecules, and (57) reduces to

$$Q_{k_1\cdots k_q}=(VJ_1)^{k_1}\cdots(VJ_q)^{k_q},$$
$$qVJ_q=\int^q (C_{12\ldots q}g_q)(\mathbf{x},0)d^q\mathbf{x} \tag{63}$$

if one neglects the small interference between different clusters.

From (53), (55), (56), and (63) it follows that

$$\exp\beta(F-F^+)=\text{coefficient of }\zeta^N\text{ in }\exp(V\textstyle\sum J_q\zeta^q)$$
$$=\frac{1}{2\pi i}\oint\zeta^{-(N+1)}\exp(V\textstyle\sum J_q\zeta^q)d\zeta, \tag{64}$$

where the contour is one surrounding only the singularity at the origin. By the method of steepest descents[13]

[12] F. London, J. Chem. Phys. **11**, 203 (1943).

[13] See Born and Fuchs, Proc. Roy. Soc. (London) **A166**, 391 (1938).

this reduces to

$$z^{-N}\exp\{V\sum J_q z^q+0(\ln V)\},$$

where z is the real root of the transcendental equation,

$$\sum qJ_q z^q=n_1=N/V. \tag{65}$$

Hence

$$\beta(F-F^+)=-N\ln z+V\sum J_q z^q. \tag{66}$$

It remains to evaluate the J_q. From (59), (61), and (62) it follows that, at moderately high temperatures,

$$g_q(\mathbf{x},\mathbf{y})=n_q\left\{1-\frac{\hbar^2\beta}{24}\left(\sum_q \frac{\mathbf{y}^{(i)}}{\hbar}\cdot\frac{\partial}{\partial\mathbf{x}^{(i)}}\right)^2\Phi_q+\cdots\right\}$$
$$\times\exp\{-\tfrac{1}{2}\beta m\textstyle\sum_q(\mathbf{y}^{(i)}/\beta\hbar)^2\}, \tag{67}$$

where

$$\Phi_q=\tfrac{1}{2}\textstyle\sum_q\sum_q\phi^{(ij)}$$
$$+n_q^{-1}\int n_{q+1}(\phi^{(iq+1)}+\phi^{(jq+1)})d\mathbf{x}^{(q+1)} \tag{68}$$

is the mean potential energy of the cluster of q molecules, and the suffix q to $\sum_q$ indicates that the summation is limited to the cluster. Now, n_q is practically zero if any two molecules of the cluster are closer together than a molecular diameter. But the factor

$$\exp\{-\tfrac{1}{2}\beta m(\mathbf{r}^{(ii+1)}/\beta\hbar)^2\}$$

of $(C_{12}\ldots_q g_q)(\mathbf{x},0)$, as determined from (58) and (67) will also be very small if the distance between the molecules of the clusters is much greater than $(2\beta/m)^{\frac{1}{2}}\hbar$. Hence the corrections due to quantum statistics are completely negligible, except in the very low temperature range where the series (61) is divergent.

At very low temperatures, g_N must be determined by substituting (33) in (60). One thus obtains

$$g_N=\exp\beta F\cdot(G_0+G_1+G_2+\cdots), \tag{69}$$

where, with the help of (34) and (41),

$$G_0=\lambda^N\exp\{-\tfrac{1}{2}\beta m\textstyle\sum(\mathbf{y}^{(i)}/\beta\hbar)^2\} \tag{70}$$

and

$$G_1=-\beta(\tfrac{1}{2}\textstyle\sum\sum g^{(ij)}+\sum h^{(i)})G_0,$$

$$g^{(ij)}=\int_0^1\int\left(\frac{\pi m}{\beta\hbar^2}\right)^{\frac{3}{2}}\exp\left\{-\frac{1}{4}\frac{\beta m}{(1-z^2)}\left(\frac{z\mathbf{s}-\mathbf{s}'}{\beta\hbar}\right)^2\right\}$$
$$\times\phi(\mathbf{r}+\tfrac{1}{2}\mathbf{s}')d\mathbf{s}'dz,$$

$$\mathbf{s}=\mathbf{y}^{(j)}-\mathbf{y}^{(i)},$$

$$h^{(i)}=\int_0^1\int\left(\frac{2\pi m}{\beta\hbar^2}\right)^{\frac{3}{2}}\exp\left\{-\frac{1}{2}\frac{\beta m}{(1-z^2)}\left(\frac{z\mathbf{s}-\mathbf{s}'}{\beta\hbar}\right)^2\right\}$$
$$\times\psi(\mathbf{r}+\tfrac{1}{2}\mathbf{s}')d\mathbf{s}'dz. \tag{71}$$

From this it follows that

$$g_q(\mathbf{x},\mathbf{y})=n_q\{1-\beta(\tfrac{1}{2}\textstyle\sum_q\sum_q g^{(ij)}+\sum_q h^{(i)})+\cdots\}$$
$$\times\exp\{-\tfrac{1}{2}\beta m\textstyle\sum_q(\mathbf{y}^{(i)}/\beta\hbar)^2\}. \tag{72}$$

The series may be approximated by

$$\exp-\beta(\tfrac{1}{2}\textstyle\sum_q\sum_q g^{(ij)}+\sum_q h^{(i)}),$$

but it can be seen from (71) that the exponent is numerically small at very low temperatures, so this factor may probably be neglected. Then

$$qVJ_q=\int^q n_q\exp\left\{-\frac{1}{2}\frac{m}{\beta\hbar^2}(\mathbf{r}^{(12)2}\right.$$
$$\left.+\mathbf{r}^{(23)2}+\cdots+\mathbf{r}^{(q1)2})\right\}d^q\mathbf{x}. \tag{73}$$

At sufficiently low temperatures, the factor n_q is equal to n^q in most numerically significant configurations, and the J_q will have the same values as for a system of non-interacting particles:

$$qJ_q=(2\pi\beta\hbar^2/qm)^{\frac{3}{2}}+0(1/V). \tag{74}$$

Thus, the effects of quantum-mechanical interaction and quantum statistics on the classical theory may, to a fair degree of approximation, be superposed. To obtain a more exact theory, it will be necessary to proceed to a higher degree of approximation in the calculation of §4, and also to improve the approximation represented by (63). The methods developed by Mayer and his collaborators[14] probably will be very useful in this task.

[14] J. E. Mayer, J. Chem. Phys. **5**, 67, 74; **6**, 87, 101 (1937).

A Seemingly Forbidden Octacovalent Structure

GEORGE H. DUFFEY
Department of Chemistry, South Dakota State College, Brookings, South Dakota
(Received April 4, 1951)

About a metal atom in the $Ta_6Cl_{12}^{+a}$-like structure, one cannot set up *spd* hybrid orbitals directed toward all eight neighboring atoms. One can set up *spd* hybrid orbitals with four orbitals directed toward neighboring halogen atoms and with four orbitals directed towards the middles of neighboring faces of the octahedron. Using such bond orbitals in the over-all structure and assigning two electrons to each set of overlapping bond orbitals, one gets the value two for a. The degree of overlapping seems favorable.

THE x-ray diffraction data of Vaughan, Sturdivant, and Pauling[1] uphold an octahedral structure for the ions $Ta_6Cl_{12}^{+a}$, $Ta_6Br_{12}^{+a}$, and $Nb_6Cl_{12}^{+a}$. In this structure a metal atom is put at each corner of the octahedron and a halogen atom is put symmetrically over the middle of each edge. Let us call this structure the $Ta_6Cl_{12}^{+a}$ structure.

About a given metal atom in this structure the symmetry is C_{4v}. If the bonds lie along the lines joining the atom to its nearest neighbors, then the angular coordinates of the maxima in its bond orbitals are apparently the angular coordinates in Table I. The bond orbitals yield a reducible representation[2,3] which may be broken down as follows:

$$\sigma=2A_1+2B_1+2E. \tag{1}$$

In *spdf* hybridization all these irreducible representations are available. However in *spd* hybridization, only one B_1 is available[3] and the arrangement is forbidden. Inasmuch as the available f orbitals in tantalum and niobium (columbium) are relatively unstable, the arrangement should be forbidden in complexes of these metals. Let us work out a possible solution to this problem.

In a constrained system the maxima in the bond orbitals need not lie along the lines joining nearest neighbors.[4] An arrangement consistent with the symmetry and constraints of the structure is described in Table II. This arrangement might be called a distorted tetragonal antiprism arrangement. The corresponding bond vectors are defined in Table III. For the eight bond orbitals

$$\sigma=2A_1+B_1+B_2+2E, \tag{2}$$

and all irreducible representations needed are available[3] in *spd* hybridization.

A ninth valence orbital may be directed along bond vector nine. This ninth orbital may very likely be empty (free of unshared electrons) since the ninth valence orbital may be considered empty in[5] TaF_8^{-3} and in OsF_8. However, the ninth valence orbital is not empty in[5] $W(CN)_8^{-4}$ and in $W(CN)_8^{-3}$.

In the over-all structure we now have three equivalent bond orbitals overlapping above the middle of each face of the octahedron. For an electron on a given face the eigenfunction may be written as a linear combination of the three overlapping atomic orbitals. This approximation gives the secular equation,[6]

$$\begin{vmatrix} q-E & \beta & \beta \\ \beta & q-E & \beta \\ \beta & \beta & q-E \end{vmatrix}=0, \tag{3}$$

where q is the coulombic integral, β the exchange integral, and E the energy of the electron. The lack of orthogonality between the three atomic orbitals is neglected. We get the three roots

$$E=q-\beta, \tag{4}$$

$$E=q-\beta, \tag{5}$$

TABLE I. Angular coordinates of the atoms bound to a given metal atom in the $Ta_6Cl_{12}^{+a}$ structure.

Atom number[a]	θ	φ
1	θ_1'	0°
2	θ_1'	90°
3	θ_1'	180°
4	θ_1'	270°
5	θ_5''	0°
6	θ_5''	90°
7	θ_5''	180°
8	θ_5''	270°

[a] Atoms 1–4 are halogen atoms; atoms 5–8 are metal atoms.

TABLE II. Possible angular coordinates of the maxima in the bond orbitals belonging to a given metal atom in the $Ta_6Cl_{12}^{+a}$ structure.

Bond orbital number	θ	φ
1	θ_1	0°
2	θ_1	90°
3	θ_1	180°
4	θ_1	270°
5	θ_5	45°
6	θ_5	135°
7	θ_5	225°
8	θ_5	315°

[1] Vaughan, Sturdivant, and Pauling, J. Am. Chem. Soc. **72**, 5477 (1950).
[2] J. H. Van Vleck, J. Chem. Phys. **3**, 803 (1935).
[3] G. E. Kimball, J. Chem. Phys. **8**, 188 (1940).
[4] J. E. Kilpatrick and R. Spitzer, J. Chem. Phys. **14**, 463 (1946).
[5] More examples are to be found in the list of Marchi, Fernelius, and McReynolds, J. Am. Chem. Soc. **65**, 329 (1943). By the way, the trigonal prism arrangement suggested by Marchi, Fernelius, and McReynolds is forbidden in *spd* hybridization.
[6] S. Glasstone, *Theoretical Chemistry* (D. Van Nostrand Company, Inc., New York, 1944).

TABLE III. Possible angular coordinates of the bond vectors about a given metal atom in the $Ta_6Cl_2^{+a}$ structure.

Bond vector number[a]	θ	φ
1	θ_1'	0°
2	θ_1'	90°
3	θ_1'	180°
4	θ_1'	270°
5	θ_5'	45°
6	θ_5'	135°
7	θ_5'	225°
8	θ_5'	315°
9	0°	...

[a] Bonds 1–4 are directed to halogen atoms; bonds 5–8 are directed to the middles of adjacent faces of the octahedron. If there is a ninth bond, it is directed away from the center of the octahedron on a line joining the center with the metal atom.

TABLE IV. Colatitudes[a] calculated from the data of Pauling and co-workers. (See reference 1.)

Ion	θ_1'	θ_5''	θ_5'
$Ta_6Cl_{12}^{+a}$	81°10′	135°0′	144°44′
$Ta_6Br_{12}^{+a}$	78°50′	135°0′	144°44′
$Nb_6Cl_{12}^{+a}$	81°15′	135°0′	144°44′

[a] See Tables I and III for the definitions of θ_1', θ_5'', and θ_5'.

$$E=q+2\beta. \tag{6}$$

Since β is negative, only one of the face orbitals is stabilized by exchange. This orbital can hold only two electrons. Hence, let us put only two electrons into each set of three overlapping atomic orbitals.*

When we leave the ninth valence orbitals of the metal atoms empty and put two electrons into each set of overlapping orbitals, we find that a in the formula $Ta_6Cl_{12}^{+a}$ is two. The result should be considered tentative.

Each ninth valence orbital may be used for binding an additional atom. To the over-all structure as many as six atoms might be added. If a is two, the ion need pick up only two halide ions to give the neutral molecule.

We may wonder whether the proposed arrangement about a metal atom is distorted too much from the tetragonal antiprism arrangement.[7] See Table IV for the observed angles. Define the s, p, and d functions as before[7] and set up the following functions:

$$\psi_1=[1/(8)^{\frac{1}{2}}]s+\{[1/(8)^{\frac{1}{2}}]\cos\beta\}p_z +[(1/\sqrt{2})\cos\alpha]p_x-\{[1/(8)^{\frac{1}{2}}]\sin\beta\}d_z +(1/2)d_{xy}+[(1/\sqrt{2})\sin\alpha]d_{x+z}, \tag{7}$$

$$\psi_2=[1/(8)^{\frac{1}{2}}]s+\{[1/(8)^{\frac{1}{2}}]\cos\beta\}p_z +[(1/\sqrt{2})\cos\alpha]p_y-\{[1/(8)^{\frac{1}{2}}]\sin\beta\}d_z -(1/2)d_{xy}+[(1/\sqrt{2})\sin\alpha]d_{y+z}, \tag{8}$$

$$\psi_3=[1/(8)^{\frac{1}{2}}]s+\{[1/(8)^{\frac{1}{2}}]\cos\beta\}p_z -[(1/\sqrt{2})\cos\alpha]p_x-\{[1/(8)^{\frac{1}{2}}]\sin\beta\}d_z +(1/2)d_{xy}-[(1/\sqrt{2})\sin\alpha]d_{x+z}, \tag{9}$$

* In some molecules three atomic orbitals not all equivalent may overlap. Thus, in the bridge model for diborane the 1s orbital of a bridge hydrogen may overlap a hybrid orbital from each boron. Only two electrons are put into this set of three overlapping orbitals.

[7] G. H. Duffey, J. Chem. Phys. **18**, 746 (1950).

TABLE V. Properties[a] of some bond orbitals fitting[b] a metal atom in $Ta_6Cl_{12}^{+a}$ and $Ta_6Br_{12}^{+a}$.

Function maximized	$\cos\alpha$	$\cos\beta$	S_1'	S_5'	S_9
S_1'	0.9322	0.2836	2.961	2.656	2.295
$S_1'+S_5'$	0.9048	0.6262	2.930	2.767	2.751
S_5'	0.8771	0.7845	2.877	2.786	2.828

[a] Here S_i' is the value of ψ_i in the direction of the i-th bond vector; $S_9=S_9'$. The composition of each orbital could readily be calculated from $\cos\alpha$ and $\cos\beta$.
[b] In the calculations $\theta_1'=80°0'$ and $\theta_5'=144°44'$.

$$\psi_4=[1/(8)^{\frac{1}{2}}]s+\{[1/(8)^{\frac{1}{2}}]\cos\beta\}p_z -[(1/\sqrt{2})\cos\alpha]p_y-\{[1/(8)^{\frac{1}{2}}]\sin\beta\}d_z -(1/2)d_{xy}-[(1/\sqrt{2})\sin\alpha]d_{y+z}, \tag{10}$$

$$\psi_5=[1/(8)^{\frac{1}{2}}]s-\{[1/(8)^{\frac{1}{2}}]\cos\beta\}p_z +[(1/2)\sin\alpha]p_x+[(1/2)\sin\alpha]p_y +\{[1/(8)^{\frac{1}{2}}]\sin\beta\}d_z+(1/2)d_{x+y} -[(1/2)\cos\alpha]d_{x+z}-[(1/2)\cos\alpha]d_{y+z}, \tag{11}$$

$$\psi_6=[1/(8)^{\frac{1}{2}}]s-\{[1/(8)^{\frac{1}{2}}]\cos\beta\}p_z -[(1/2)\sin\alpha]p_x+[(1/2)\sin\alpha]p_y +\{[1/(8)^{\frac{1}{2}}]\sin\beta\}d_z-(1/2)d_{x+y} +[(1/2)\cos\alpha]d_{x+z}-[(1/2)\cos\alpha]d_{y+z}, \tag{12}$$

$$\psi_7=[1/(8)^{\frac{1}{2}}]s-\{[1/(8)^{\frac{1}{2}}]\cos\beta\}p_z -[(1/2)\sin\alpha]p_x-[(1/2)\sin\alpha]p_y +\{[1/(8)^{\frac{1}{2}}]\sin\beta\}d_z+(1/2)d_{x+y} +[(1/2)\cos\alpha]d_{x+z}+[(1/2)\cos\alpha]d_{y+z}, \tag{13}$$

$$\psi_8=[1/(8)^{\frac{1}{2}}]s-\{[1/(8)^{\frac{1}{2}}]\cos\beta\}p_z +[(1/2)\sin\alpha]p_x-[(1/2)\sin\alpha]p_y +\{[1/(8)^{\frac{1}{2}}]\sin\beta\}d_z-(1/2)d_{x+y} -[(1/2)\cos\alpha]d_{x+z}+[(1/2)\cos\alpha]d_{y+z}, \tag{14}$$

$$\psi_9=(\sin\beta)p_z+(\cos\beta)d_z. \tag{15}$$

In these angular wave functions the coefficients of s, p_z, and d_z are not so general as they could be.[8] The orbitals are general enough, however, for our purpose. They fall into three groups of equivalent orbitals: $\psi_1, \cdots \psi_4$; $\psi_5, \cdots \psi_8$; ψ_9.

Some properties of three sets of these bond orbitals are given in Table V. Here S_1' is the value of ψ_1 in the direction of bond vector one, S_5' is the value of ψ_5 in the direction of bond vector five, and S_9 is the maximum value of ψ_9, the value in the direction of bond vector nine. For θ_1' and θ_5', 80°0′ and 144°44′, respectively, were used.

Following Kilpatrick and Spitzer[4] in part,[9] we may consider S_1' as the effective strength of orbital one. Also, S_5' might be considered a rough measure of the overlapping in bond five. Although these are moot generalizations of Pauling's index, the largeness of S_1' and S_5' when $S_1'+S_5'$ is maximized gives some support to the proposed arrangement of orbitals.

[8] The general coefficients are like those derived in G. H. Duffey, J. Chem. Phys. **19**, 92 (1951).

[9] The author has used Pauling's index of bond-forming power in the form of Eq. (13) of G. H. Duffey, J. Chem. Phys. **18**, 510 (1950). When the bonds to an atom are not all alike, some difficulties arise. Thus, one can only make plausible assumptions in dividing among the differing bonds the energy needed to form the molecular valence state of the atom (to get W for each bond).

The Microwave Spectra and Molecular Structures of Trifluorosilane Derivatives*

JOHN SHERIDAN† AND WALTER GORDY
Department of Physics, Duke University, Durham, North Carolina

(Received March 27, 1951)

Pure rotational spectra have been measured for the molecules $Si^{28}F_3H$, $Si^{29}F_3H$, $Si^{30}F_3H$, $Si^{28}F_3Cl^{35}$, $Si^{28}F_3Cl^{37}$, $Si^{28}F_3Br^{79}$, $Si^{28}F_3Br^{81}$, and $Si^{28}F_3CH_3$. Values of B_0 and moments of inertia, I_B, are tabulated. The nuclear quadrupole couplings of Cl^{35}, Br^{79}, and Br^{81} in these molecules have been determined from their hyperfine structures as -43, 440, and 370 Mc/sec, respectively. Molecular dimensions, calculated by assuming the first parameter mentioned to be within the stated limits, are, for SiF_3H, $d_{SiH}=1.55\pm0.05$A, $d_{SiF}=1.561\mp0.005$A, $\angle FSiF=108°6'\mp30'$; for SiF_3Cl, $\angle FSiF=108°30'\pm1°$, $d_{SiF}=1.560\mp0.005$A, $d_{SiCl}=1.989\pm0.018$A; for SiF_3Br, $\angle FSiF=108°30'\pm1°$, $d_{SiF}=1.560\mp0.005$A, $d_{SiBr}=2.153\pm0.018$A. The special shortness of silicon-halogen bonds is discussed and shown to be related to the electronic structure of silicon. The spectrum of SiF_3CH_3 shows lines caused by molecules in excited torsional vibrational states, which show additional splitting caused by the doubling of the torsional vibrational levels. From relative intensities the height of the barrier opposing free rotation about the SiC bond is estimated as 1200 cal/mole. From the variations of B_0 with torsional vibration, the separations of the doublets in the ground, first, and second torsional vibration levels are estimated as 0.1 cm^{-1}, 1.4 cm^{-1}, and 12 cm^{-1}, respectively.

INTRODUCTION

THE molecular structures of few fluorinated silanes have been studied. Silicon tetrafluoride and trifluorochlorosilane have been measured by electron diffraction,[1] and recently the microwave spectrum of fluorosilane has been reported.[2] In a preliminary communication[3] we have outlined results for the microwave spectra of the symmetric top molecules SiF_3H, SiF_3Cl, SiF_3Br, and SiF_3CH_3. The present paper gives a fuller account of the results for these molecules.

EXPERIMENTAL

Trifluorosilane, SiF_3H, was prepared by the method of Emeleus and Maddock.[4] Methyl trifluorosilane, SiF_3CH_3, was prepared in essentially the same way, by passing methyl trichlorosilane vapor over antimony trifluoride and antimony pentachloride.[5] Trifluorochlorosilane, SiF_3Cl, was made as described by Booth and Swinehart[6] and trifluorobromosilane, SiF_3Br, by the method of Schumb and Anderson.[7] All samples were purified by vacuum fractionation in conjunction with gas density measurements.

The microwave spectra were measured using a video sweep spectroscope described in earlier communications from this laboratory.[8] All measurements were made at -70°C and at gas pressures of about 10^{-3} mm. Frequencies were measured with a frequency standard monitored by comparison with station WWV.

RESULTS

Table I lists the unperturbed frequencies of the indicated transitions, the values of B_0, the moments of inertia I_B, the distortion coefficients D_{JK}, and the nuclear quadrupole coupling factors eqQ for the chlorine and bromine nuclei.

The values of D_{JK} and eqQ are those used to calculate the hyperfine structures which are compared with those measured for SiF_3Cl and SiF_3Br in Tables II, III, and IV. Though the crowding of the lines is too marked for a precise evaluation of D_{JK} and eqQ, the values chosen give the best agreement with observation. The absorption caused by SiF_3Cl is quite weak, and insufficient hyperfine structure caused by SiF_3Cl^{37} in natural concentration was observed to obtain the nuclear coupling of Cl^{37} in this molecule.

The transitions of $Si^{28}F_3H$, $Si^{29}F_3H$, and $Si^{30}F_3H$ were observed in their natural concentrations, and showed no resolvable hyperfine structure, in agreement with the accepted nuclear spins of 0, $\frac{1}{2}$, and 0 for Si^{28}, Si^{29}, and Si^{30}, respectively.[3]

TABLE I. Molecular constants.

Molecule	Transition	Unperturbed frequency Mc/sec ±0.1	B_0 Mc/sec	I_B[a] $\times10^{-40}$ g cm²	D_{JK} kc/sec	eqQ for halogen Mc/sec
$Si^{28}F_3H$	1→2	28,831.90	7207.98	116.386		
$Si^{29}F_3H$	1→2	28,782.65	7195.66	116.585		
$Si^{30}F_3H$	1→2	28,734.80	7183.70	116.779		
$Si^{28}F_3Cl^{35}$	9→10	49,555.75	2477.7_9	338.57_0	1.8	-43
$Si^{28}F_3Cl^{37}$	7→8	38,608.9$_6$	2413.0_6	347.65_2		-34[b]
$Si^{28}F_3Br^{79}$	15→16	49,599.5$_1$	1549.9_8	541.23_6	0.8	+440
$Si^{28}F_3Br^{81}$	15→16	49,092.6$_0$	1534.1_4	546.82_4	0.8	+370
$Si^{28}F_3CH_3$	3→4	29,725.04	3715.63	136.033		

[a] Calculated using Planck's constant $=6.62373\times10^{-27}$ erg/sec and 1 amu $=1.65972\times10^{-40}$ g, from J. W. M. Dumond and E. R. Cohen, Revs. Modern Phys. 21, 651 (1949). In view of possible error in Planck's constant, the last two figures quoted for I_B have relative significance only.
[b] Calculated from the value for Cl^{35}.

* The research reported in this document has been made possible through support and sponsorship extended by the Geophysical Research Directorate of the Air Force Cambridge Research Laboratories under Contract No. W19-122-ac-35. It is published for technical information only and does not represent recommendations or conclusions of the sponsoring agency.

† Present address: Department of Chemistry, University of Birmingham, Birmingham, England.

[1] P. W. Allen and L. E. Sutton, Acta Cryst. **3**, 46 (1950).
[2] Sharbaugh, Thomas, and Pritchard, Phys. Rev. **78**, 64 (1950).
[3] J. Sheridan and W. Gordy, Phys. Rev. **77**, 719 (1950).
[4] H. J. Emeleus and A. G. Maddock, J. Chem. Soc. **1944**, 293 (1944).
[5] See also H. S. Booth and W. F. Martin, J. Am. Chem. Soc. **68**, 2655 (1946).
[6] H. S. Booth and C. F. Swinehart, J. Am. Chem. Soc. **57**, 1333 (1935).
[7] W. C. Schumb and H. H. Anderson, J. Am. Chem. Soc. **58**, 994 (1936).
[8] E.g., W. Gordy and M. Kessler, Phys. Rev. **72**, 644 (1947).

TABLE II. Observed and calculated hyperfine structure of the $J=9\rightarrow10$ transition of $Si^{28}F_3Cl^{35}$. Lines are calculated for $D_{JK}=1.8$ kc/sec and $eqQ=-43$ Mc/sec.

Observed frequency Mc/sec	Calculated frequency Mc/sec	Transition $F\rightarrow F'$	K
49,555.72	The principal theoretical components of this broad line include all K components for $F=15/2\rightarrow17/2$, K=0 to 6 for $21/2\rightarrow23/2$, $K=0$, 1, and 2 for $F=17/2\rightarrow19/2$, $19/2\rightarrow21/2$. These range in frequency from 49,555.41 mc to 49,556.06		
49,555.20	49,555.33	21/2→23/2	7
	49,555.19	21/2→23/2	8
	49,555.15	19/2→21/2	3
	49,555.11	17/2→19/2	3
49,554.70	49,554.69	17/2→19/2	4
	49,554.61	19/2→17/2	4
49,554.10	49,554.15	17/2→19/2	5
	49,553.94	19/2→21/2	5
49,553.54	49,553.49	17/2→19/2	6
49,553.12	49,553.12	19/2→17/2	6
49,552.70	49,558.71	17/2→19/2	7
49,552.10	49,552.14	19/2→21/2	7

TABLE III. Observed and calculated hyperfine structure of the $J=15\rightarrow16$ transition of $Si^{28}F_3Br^{79}$. Lines are calculated for $D_{JK}=0.8$ kc/sec and $eqQ=+440$ Mc/sec.

Observed frequency Mc/sec	Calculated frequency Mc/sec	Transition $F\rightarrow F'$	K
49,603.30	49,603.43	31/2→33/2	8
	49,603.20	29/2→31/2	9
49,601.56	49,601.59	31/2→33/2	6
	49,601.41	29/2→31/2	6
49,600.90	49,601.04	29/2→31/2	4
	49,600.95	29/2→31/2	5
	49,600.86	31/2→33/2	5
49,599.86	49,600.27	31/2→33/2	4
	49,600.26	29/2→31/2	3
	49,600.05	29/2→31/2	2
	49,599.91	29/2→31/2	1
	49,599.88	29/2→31/2	0
	49,599.88	27/2→29/2	0
	49,599.82	31/2→33/2	3
	49,599.75	27/2→29/2	1
49,599.22	49,599.49	31/2→29/2	2
	49,599.47	27/2→29/2	2
	49,599.28	31/2→33/2	1
	49,599.21	33/2→35/2	0
	49,599.21	31/2→31/2	0
	49,599.12	33/2→35/2	1
	49,598.84	33/2→35/2	2
	49,598.80	27/2→29/2	3
49,598.42	49,598.36	33/2→35/2	3
49,597.80	49,597.97	27/2→29/2	0
	49,597.69	33/2→35/2	4
49,596.60	49,596.90	27/2→29/2	5
	49,596.83	33/2→35/2	5
49,595.72	49,595.77	33/2→35/2	6
	49,595.59	27/2→29/2	6
49,594.38	49,594.52	33/2→35/2	7
	49,594.06	27/2→29/2	7
49,593.00	49,593.09	33/2→35/2	8
49,592.25	49,592.27	27/2→29/2	8
49,591.66	49,591.44	33/2→35/2	9

As at present isotopic substitutions have been made at only one nuclear position in all these molecules, it is necessary to assume one parameter in each case. Table V shows sets of combinations of parameters which are in accord with the moments of inertia. Table VI shows the most probable values of the molecular structure parameters calculated from the I_B values for SiF_3H, SiF_3Cl, and SiF_3Br.

In SiF_3H the structure is not very sensitive to the value of d_{SiH}; and if this is given the wide range 1.550 $\pm$0.05A (which includes the values found in other silane derivatives), we obtain, neglecting zero-point vibration effects, $d_{SiF}=1.561\mp0.002$A and $\angle FSiF=108°6'\mp4'$. The structure of the SiF_3 group can thus be rather closely determined. The value of $\angle FSiF$ agrees well with that found by electron diffraction in SiF_3Cl, 108.5°$\pm$1°.[9]

Accepting $\angle FSiF=108.5\pm1°$ in SiF_3Cl from electron diffraction, we obtain $d_{SiF}=1.560\mp0.005$A and $d_{SiCl}=1.989\pm0.018$A. Therefore, d_{SiF} is again rather closely determined and very close to that in SiF_3H, but there is more uncertainty in d_{SiCl}. This length, however, must be less than that in SiH_3Cl, 2.048A,[10,11] for if $d_{SiCl}=2.048$A, then it follows that $d_{SiF}=1.550$A and $\angle FSiF=111°37'$. This angle is outside the range consistent with the electron diffraction data. Perhaps the best set of parameters for SiF_3Cl is obtained by assuming $\angle FSiF=108°6'$ as in SiF_3H, when we obtain $d_{SiF}=1.561$A and $d_{SiCl}=1.983$A.

In SiF_3Br, the assumption of the same value for $\angle FSiF$ as given for SiF_3Cl, namely, 108.5°$\pm$1°, gives $d_{SiF}=1.560\mp0.005$A and $d_{SiBr}=2.153\pm0.018$A. Again, d_{SiF} is rather closely determined and very close to that in SiF_3H and SiF_3Cl, but a greater variation in d_{SiBr} is permitted. This length, however, is almost certainly shorter than d_{SiBr} in SiH_3Br, 2.209A,[12] for if this value is assumed, we find $d_{SiF}=1.550$ and $\angle FSiF=111°32'$. Such a greater value of $\angle FSiF$ as compared with that in SiF_3H and SiF_3Cl is very unlikely, since the replacement of H or Cl by the larger Br should not increase $\angle FSiF$. If we make $\angle FSiF$ in SiF_3Br the same as in SiF_3H, 108°6', we obtain $d_{SiF}=1.560$A and $d_{SiBr}=2.147$A as the other probable best parameters.

The value of I_B for SiF_3CH_3 has been shown[3] to be consistent with $d_{SiC}=1.88$A if the SiF_3 and CH_3 configurations are assumed to be as found in other mole-

[9] R. L. Livingston and L. O. Brockway, J. Am. Chem. Soc. 66, 94 (1944).
[10] A. Harry Sharbaugh, Phys. Rev. 74, 1870 (1948).
[11] Dailey, Mays, and Townes, Phys. Rev. 76, 136 (1949).
[12] Sharbaugh, Bragg, Madison, and Thomas, Phys. Rev. 76, 1419 (1949).

TABLE IV. Observed and calculated hyperfine structure of the $J=15\rightarrow16$ transition of $Si^{28}F_3Br^{81}$. Lines are calculated for $D_{JK}=0.8$ kc/sec and $eqQ=+370$ Mc/sec.

Observed frequency Mc/sec	Calculated frequency Mc/sec	Transition $F\rightarrow F'$	K
49,094.20	49,094.20	31/2→33/2	6
	49,094.06	29/2→31/2	6
49,093.60	49,093.70	29/2→31/2	5
	49,093.64	31/2→33/2	5
	49,093.42	29/2→31/2	4
49,092.88	49,093.19	29/2→31/2	3
	49,093.18	31/2→33/2	4
	49,093.04	29/2→31/2	2
	49,092.93	29/2→31/2	1
	49,092.91	29/2→31/2	0
	49,092.91	27/2→29/2	0
	49,092.82	31/2→33/2	3
	49,092.80	27/2→29/2	1
49,092.38	49,092.57	31/2→33/2	2
	49,092.50	27/2→29/2	2
	49,092.40	31/2→33/2	1
	49,092.36	31/2→33/2	0
	49,092.36	33/2→35/2	0
	49,092.27	33/2→35/2	1
49,091.70	49,091.60	33/2→35/2	3
49,091.00	49,091.24	27/2→29/2	4
	49,091.00	33/2→35/2	4
49,090.22	49,090.30	27/2→29/2	5
	49,090.24	33/2→35/2	5
49,089.18	49,089.31	33/2→35/2	6
	49,089.16	27/2→29/2	6
49,088.01	49,088.21	33/2→35/2	7
	49,087.81	27/2→29/2	7

cules. This is an acceptable value for a C—Si bond, but we defer discussion of the dimensions of this molecule until I_B values are measured for farther isotopic combinations.

The spectrum of SiF_3CH_3 shows an interesting structure which has been concurrently reported by Minden, Mays, and Dailey.[13] For the $J=3\rightarrow4$ transition we have measured the lines shown in Table VII, which also gives their relative intensities at 200°K. The spectrum differs from that described by Minden, Mays, and Dailey in that certain lines show a doublet structure; this fact, and the spectrum generally, can be accounted for by the theory of torsional vibrations, as discussed below.

DISCUSSION

I. Molecular Structures

The distance d_{SiF}, which can hardly be longer than 1.563A in SiF_3H, SiF_3Cl, or SiF_3Br, is distinctly shorter in these molecules than in fluorosilane, SiH_3F,[2] where $d_{SiF}=1.593$A. This is similar to the case of CF bonds, d_{CF} in methyl fluoride being 1.385A[14] as compared with about 1.33A in trifluoromethyl derivatives. The contraction in the bond Si—F, however, caused by substitution of two further fluorine atoms, is smaller than the contraction similarly induced in the C—F bond. While in methyl fluoride d_{CF} is that predicted by the Schomaker-Stevenson rule,[15] d_{SiF} in SiH_3F is already 0.1A shorter than the 1.69A predicted by this rule; the statement by Sharbaugh, Thomas, and Pritchard[2] that the rule is obeyed in SiH_3F arises from their use of Pauling's single-bond radius for fluorine (0.64A) instead of the value 0.72A, which should be used with this rule. It seems, therefore, that an additional bond-shortening factor is already operative in SiH_3F which is not present in methyl fluoride; and this is explained by contributions from state (I) in SiH_3F, the analog of which cannot occur in methyl fluoride, since the valency shell of the carbon cannot expand. We expect state (I) to be significant in view of the stability of double bonds

(I) (II)

to first-row elements such as fluorine. The further con-

TABLE V. Parameters consistent with I_B values.

Molecule	$d_{SiX}(A)$ (x=H, Cl, Br)		$d_{SiF}(A)$	∠FSiX	∠FSiF
SiF_3H	1.500		1.563	110°45′	108°10′
	1.550	SiH	1.561	110°49′	108°6′
	1.600		1.559	110°52′	108°2′
SiF_3Cl	2.007		1.557	109°30′	109°27′
	1.989		1.560	110°30′	108°26′
	1.983	SiCl	1.561	110°49′	108°6′
	1.971		1.563	111°30′	107°22′
	(2.048		1.550	107°14′	111°37′)
SiF_3Br	2.171		1.557	109°30′	109°27′
	2.153		1.560	110°30′	108°26′
	2.147	SiBr	1.560	110°49′	108°6′
	2.135		1.563	111°30′	107°22′
	(2.209		1.550	107°20′	111°32′)

Atomic masses assumed were
Silicon: 27.99581, 28.98567, and 29.98290 [H. E. Duckworth and R. S. Preston, Phys. Rev. **79**, 402 (1950); Duckworth, Preston, and Woodcock, *ibid.*, **79**, 188 (1950)].
Fluorine: 19.00452 [M. S. Livingston and H. A. Bethe, Revs. Modern Phys. **9**, 373 (1937)].
Hydrogen: 1.00813.
Chlorine: 34.98107 and 36.97829 [E. Pollard, Phys. Rev. **57**, 1186 (1940)].
Bromine: 78.9417 and 80.9400 [F. W. Aston, Nature **141**, 1096 (1938)].

TABLE VI. Dimensions of SiF_3X molecules.

	d_{SiX}	d_{SiF}	∠FSiF
SiF_3H	1.55 ±0.05A (assumed)	1.561 ±0.005A	108°6′ ±30′
SiF_3Cl	1.989 ±0.018	1.560 ±0.005	108°30′ ±1° (assumed)*
SiF_3Br	2.153 ±0.018	1.560 ±0.005	108°30′ ±1° (assumed)

* This value for the angle is indicated by electron diffraction, reference 9. The limits of error are estimated from the effects of zero-point vibration in other molecules and from the limits given for the assumed parameter. Actually, a much larger variation in d_{SiH} than ±0.05 would be required to shift the other two parameters of SiF_3H outside the limits indicated.

[13] Minden, Mays, and Dailey, Phys. Rev. **78**, 347 (1950).
[14] Gilliam, Edwards, and Gordy, Phys. Rev. **75**, 1014 (1949).
[15] V. Schomaker and D. P. Stevenson, J. Am. Chem. Soc. **63**, 37 (1941).

TABLE VII. Lines measured in the $J=3\rightarrow4$ transition of $Si^{28}F_3CH_3$.

Frequency Mc/sec ±0.1		Relative intensities at 200°K
29,729.14		10
29,725.04	A	70
29,724.87		30
29,704.70		3
29,704.12		10
29,690.07	B	15
29,689.70		20
29,659.05	C	8
29,656.06		8

traction in d_{SiF} which occurs as two more fluorine atoms are attached to the silicon atom is presumably to be explained in the same way as the analogous contraction in CF bonds, for example, by the advent of contributions from structures of type (II); since, however, SiF in SiH_3F has already considerable double-bond character, the further contraction is less marked in SiF than in CF.

The angle FSiF in SiF_3H is slightly less than the tetrahedral angle, as is found also in SiF_3Cl[9] and for $\angle$FGeF in GeF_3Cl.[16]

The distance d_{SiCl} in SiF_3Cl is unlikely to exceed the lower limit of 2.00A proposed from the electron diffraction data,[9] and this bond and the Si—Br bond in SiF_3Br both appear at least 0.04A shorter than the same bonds in SiH_3Cl and SiH_3Br. The contraction caused by substitution of three fluorine atoms for hydrogen atoms is presumably due to causes such as increased contributions from forms of type (III) or to a shrinkage of the silicon bond-radius on account of the formal charge in forms of type (IV). The contraction is greater than that found when a

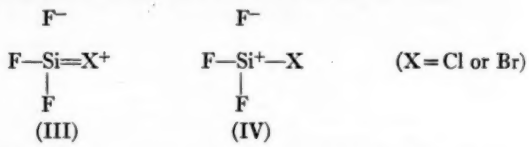

(III) (IV)

similar fluorine substitution is made in methyl chloride[17] or bromide,[18,19] which is presumably due to the greater ionic character in Si—F bonds as compared with C—F bonds.

The nuclear quadrupole coupling factors of chlorine and bromine in SiF_3Cl and SiF_3Br are somewhat greater numerically than in SiH_3Cl and SiH_3Br.[11,12] While increased contributions of type (III) would be expected to reduce the coupling, it is possible that this is balanced by the encouragement of states such as (V) or (VI), in which the coupling would be increased, and the discouragement of (VII), by the extreme electronegativity of the fluorine atoms. It is notable that the Cl and Br couplings are also slightly greater in CF_3Cl and CF_3Br than in CH_3Cl and CH_3Br.[17,19]

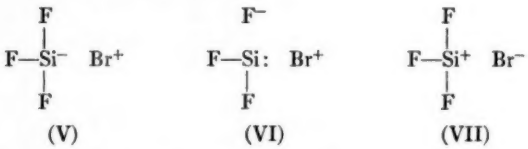

(V) (VI) (VII)

A profitable comparison can be made between the available data on bonds from halogens to carbon, silicon, and germanium. The lengths of such bonds are summarized in Table VIII, which also includes for comparison purposes the lengths predicted by the Schomaker-Stevenson rule.[15] The quantity $d_{obs}-d_{calc}$, i.e., the deviation from the rule, is plotted for the three elements in Fig. 1. While the rule is not usually obeyed exactly in these compounds, this figure shows clearly the special tendency of bonds to silicon to be shorter than might be expected from the position of silicon between carbon and germanium. In each series of compounds there is an increase in the negative deviation from the rule with the descent from carbon to silicon; and, in all cases where data are available, this is followed by a decrease in the negative deviation from the rule from silicon to germanium.

The extra shortening in the case of silicon is accounted for by silicon's position in the second row of the periodic table. For, in such an atom, the ability to expand the valency shell beyond eight (absent in carbon) is combined with a greater ability to form multiple bonds than is found in subsequent rows of the table, for example in germanium. States of type (VIII) are therefore permitted easily with silicon, but not at all with carbon, and only to a minor degree with ger-

TABLE VIII. Observed bond lengths (d_{obs}) compared with those calculated by the Schomaker-Stevenson rule (reference 15).

Molecule	$d_{MF}(A)$ obs	calc	$d_{MCl}(A)$ obs	calc	$d_{MBr}(A)$ obs	calc
CF_3Cl (CF_3H)	1.323[a,b]	1.38	1.765[a]	1.74		
SiF_3Cl (SiF_3H)	1.561	1.69	1.983	2.05		
GeF_3Cl	1.68[a,c]	1.73	2.067[c]	2.09		
CF_3Br	1.32[d,e]	1.38			1.93[d,e]	1.90
SiF_3Br	1.560	1.69			2.147	2.22
CH_3X	1.384[b]	1.38	1.779[g]	1.74	1.936[g]	1.90
SiH_3X	1.593[f]	1.69	2.048[h,i]	2.05	2.209[j]	2.22
GeH_3X (X=F, Cl, Br)	...	...	2.147[i]	2.09	2.297[k]	2.26

[a] Reference 17.
[b] Reference 14.
[c] Reference 16.
[d] Reference 18.
[e] Reference 19.
[f] Reference 2.
[g] Gordy, Simmons, and Smith, Phys. Rev. 74, 243 (1948).
[h] Reference 10.
[i] Reference 11.
[j] Reference 12.
[k] Reference 20.

[16] Anderson, Sheridan, and Gordy, Phys. Rev. 81, 819 (1951).

[17] D. K. Coles and R. H. Hughes, Phys. Rev. 76, 858 (1949).
[18] J. Sheridan and W. Gordy, Phys. Rev. 77, 292 (1950).
[19] Sharbaugh, Pritchard, and Madison, Phys. Rev. 77, 302 (1950).

manium. The greater double-bond character present in

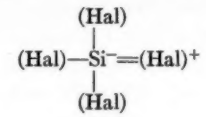

(VIII)

silicon-halogen bonds is indicated by their extra shortening.

The same peculiarity of silicon is implied in the contributions of various states which can account[11,12,20] for the lower nuclear quadrupole couplings of the halogens in SiH_3Cl and SiH_3Br as compared with the analogous carbon and germanium compounds. The decrease in electronegativity of the central atom as we pass from carbon through silicon to germanium would lead us to expect a steady fall in the halogen coupling in that sequence, caused by a steady increase in ionic character of the bond to the halogen. The extra tendency for double bonded states to occur in the silicon compounds, however, leads to an extra lowering of the coupling in their case.

II. Hindered Internal Rotation in Methyl Trifluorosilane

The spectrum of the $J=3\rightarrow4$ transition of SiF_3CH_3 (Table VI) can be accounted for in terms of the expected torsional vibration of the molecule about the C–Si bond. From their relative intensities and their roughly equal frequency separations, the pairs of lines marked A, B, and C can be assigned to molecules in the ground state and in the first and second torsional vibration states, respectively. The other lines are ascribed to molecules in other vibrational states. As the torsional vibration level rises, B_0 falls and the moment of inertia I_B increases, presumably on account of an increased repulsion between the CH and SiF bonds as torsion brings them closer to the "eclipse" position. This interpretation is essentially that described by Minden, Mays, and Dailey.[13]

An additional observation, however, which is not mentioned by these authors, is that pairs of lines, and therefore two B_0 and I_B values, are found for each torsional level. These show wider separations as the torsional quantum number is increased. This is expected if the doublets are due to the anticipated splitting of the torsional vibration levels caused by the finite height of the barrier opposing free rotation.[21] In this case we have molecules with $K=0$, 1, 2, and 3; and it has been shown[22] that the torsional levels will be doubled for $K=0$, but in general tripled for other K-values.[23] The fact that only pairs of lines are observed, however, can be understood, since the SiF_3 group contributes 96 percent of the moment of inertia of the molecule about the symmetry axis; and when a light group (CH_3) undergoes torsional oscillations against a heavy one (SiF_3), it is predicted[22] that the splitting of a given torsional level will change only slowly as K is varied. Accordingly, the pair of sublevels which are degenerate when $K=0$ remain very close when $K=1$, 2, or 3; and we observe only two different B_0 values for each torsional state.

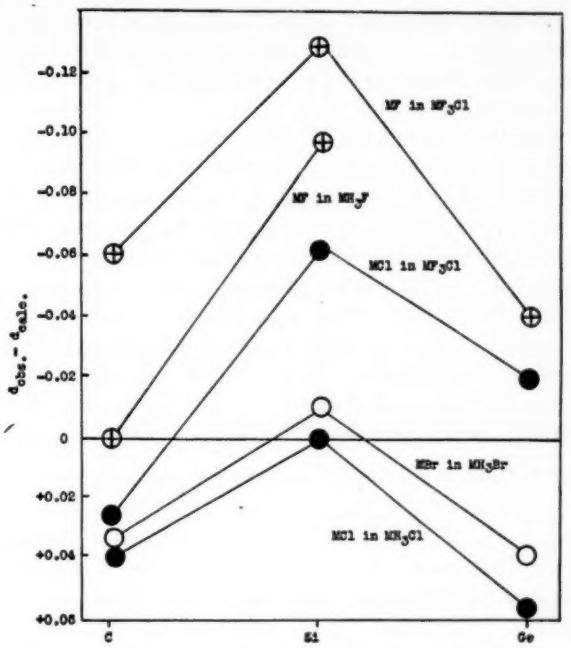

FIG. 1. Deviations from Schomaker-Stevenson rule for halogen bonds to carbon, silicon, and germanium.

The height of the barrier opposing free formation can be estimated from the relative intensities of the lines at 200°K given in Table VI. From the fact that lines caused by the third excited torsional state were not observable at this temperature, we can estimate their intensity at less than 5 percent of that of the strongest pair. The splitting within the levels is neglected here, the intensities being summed for each pair of lines. If the torsional vibration frequency is ω_t, application of the Boltzmann relationship to the ground and first three excited states gives $\omega_t=145$ cm^{-1}, $2\omega_t=255$ cm^{-1}, and $3\omega_t\gtrsim416$ cm^{-1}, which yield a mean value of ω_t of 140 cm^{-1}. If we assume a cosine form for the barrier, its height, V_0, will be given by[24]

$$V_0=(\omega_t^2/9)A/A_1A_2,$$

where A, A_1, and A_2 are the rotational constants respectively associated with the total moment of inertia of the molecule about the symmetry axis, and the separate moments of the SiF_3 and SiH_3 groups (I_1 and I_2) about that axis. Taking $A=0.133$ cm^{-1}, we have $A_1=0.136$ cm^{-1}, and $A_2=5.21$ cm^{-1} in accordance with

[20] Sharbaugh, Pritchard, Thomas, Mays, and Dailey, Phys. Rev. **79**, 189 (1950).

[21] G. Herzberg, *Infrared and Raman Spectra of Polyatomic Molecules* (D. Van Nostrand Company, Inc., New York, 1945), p. 225.

[22] J. S. Koehler and D. M. Dennison, Phys. Rev. **57**, 1006 (1940).

[23] See also D. R. Lide and D. K. Coles, Phys. Rev. **80**, 911 (1950).

[24] Reference 21, p. 226.

a probable molecular model; and substituting for ω_t, we obtain $V_0=410$ cm^{-1} or 1200 cal/mole. This agrees with the barrier weight very recently reported by Minden and Dailey.[25]

From the separation of the doublets the extent of the splitting of the torsional levels can be estimated. The lowering of frequency (and B_0) is approximately proportional to the energy present in the torsional vibration; each torsional quantum (ignoring splitting), represented by ω_t (140 cm^{-1}) causes a fall in frequency of some 35 Mc/sec. This approximate relationship is expected over a limited range of vibrational energy because the potential energy curve for the torsional oscillation is a cosine curve.[21,22] The separation of the doublet for the second excited state is 3 Mc/sec, which corresponds to a separation of 12 cm^{-1} in the energy levels into which this state is split. The frequency separation in the first excited state is much smaller, in agreement with theory,[22] being about 370 kc/sec, which corresponds to a splitting into components about 1.4 cm^{-1} apart. The splitting in the ground level will be much smaller than this, and we may estimate it as 0.14 cm^{-1} on the assumption that a further reduction by a factor of 10 occurs as compared with the splitting in the level above. This would correspond to a doublet frequency separation of only 37 kc/sec, which is hardly resolvable, whereas the separation observed in the main doublet, 170 kc/sec, is much larger. The latter splitting may therefore by the normal K-splitting, which would also be present but unresolved for the weaker lines of the other molecular states.

[25] H. T. Minden and B. P. Dailey, Phys. Rev. **82**, 338A (1951).

THE JOURNAL OF CHEMICAL PHYSICS VOLUME 19, NUMBER 7 JULY, 1951

The Limiting Negative Pressure of Acetic Acid, Benzene, Aniline, Carbon Tetrachloride, and Chloroform

LYMAN J. BRIGGS
National Bureau of Standards, Washington, D. C.
(Received May 21, 1951)

The limiting negative pressure of acetic acid, benzene, aniline, carbon tetrachloride, and chloroform has been measured in relation to temperature. A centrifugal method was employed, the liquid being contained in a capillary tube, the ends or legs of which were bent sharply back parallel to the straight central part. The tube was cemented to a horizontal spinner, with its midpoint intersecting the spin axis. Both ends of the tube were open, which facilitated filling and cleaning. The volume of liquid was so chosen that the menisci were located in the legs of the tube near the bends.

The maximum values observed were: CH_3COOH, −288 bars; C_6H_6, −150 bars; $C_6H_5NH_2$, −300 bars; CCl_4, −276 bars; $CHCl_3$, −317 bars. Excepting benzene, the limiting negative pressure of these liquids has not heretofore been measured. All except benzene equal or exceed that of water (−275 bars). Acetic acid, benzene, and aniline show a decrease in the limiting negative pressure as the freezing point is approached, like water, but the effect is much less marked.

The higher values observed for the polar liquids in comparison with their nonpolar relatives suggests that the dipoles are contributing markedly to the cohesion of the liquid. An investigation of the *cis*- and *trans*-forms of the *same* liquid is now under way.

IN a recent paper[1] I gave the results of direct measurements, by a centrifugal method, of the limiting negative pressure of water at various temperatures. The maximum observed was −275 bars at 8°C (1 bar $=10^6$ dynes/cm^2=0.987 atmosphere). Below 5°C, the negative pressure decreased rapidly, and near the freezing point was less than 10 percent of the maximum value.

The present paper presents the results of measurements of the limiting negative pressure of five organic liquids. Inasmuch as their behavior near the freezing point was of special interest, the following liquids with melting points near that of water were selected: acetic acid, CH_3COOH, (mp, 16.7°C); benzene, C_6H_6, (mp, 5.5°C); and aniline, $C_6H_5NH_2$, (mp, −6.4°C). This also afforded an opportunity to compare the limiting negative pressure of nonpolar benzene with its strongly polarized derivative, aniline. When it was found that the maximum value of aniline was twice that of benzene, a second pair of nonpolar and polar liquids was examined, namely, carbon tetrachloride, CCl_4, and chloroform, $CHCl_3$.

The experimental apparatus was similar to that used for water, but the capillary tube, open at both ends, which contains the liquid, was modified. The legs of the Z-shaped tube beyond the bends were greatly lengthened, and bent sharply back parallel to the straight central part. At the hub of the spinner these legs were bent horizontally outward at right angles, and after clearing the hub, bent downward 1 cm parallel to the spin axis. The Pyrex glass capillary was cemented

[1] L. J. Briggs, J. Appl. Phys. **21**, 721 (1950).

to the web of the invar spinner (of channel cross section) by flooding the channel with thinned Duco, and was so located that *its midpoint intersected the spin axis.* Narrow notches milled in the side walls of the channel at the hub provided exits for the legs of the tube.

The volume of liquid in the tube was so chosen that the menisci were located in the legs, about 5 mm from the bend. In the centrifugal field, one-half of the liquid column pulls against the other. The maximum stress is at the center. Here a minute section is visible, even at the highest speeds, because the spin axis intersects the tube. The rupture of the column is signalized by a marked change in the refraction of the tube at its center, when viewed by a side light.

The negative pressure at the spin axis in dynes/cm^2 at T°C is $\frac{1}{2}\rho\omega^2 r^2$, where ρ is the density at T°, ω is the spin velocity in radians per sec, and r is one-half the distance in cm between the two menisci (measured at room temperature, but corrected to T°). It is believed that the observation error does not exceed 3 percent (0.5 percent for r, 1 percent for ω).

The capillary tubes used in the course of the work had bore diameters ranging from 0.6 to 0.8 mm at the midpoint, and external diameters of from 1.5 to 1.8 mm. The mortality of the tubes is rather high. At the highest speeds, the centrifugal load on the empty capillary is approaching the values commonly given for the tensile strength of glass. As long as the liquid column is intact, it does not contribute to this load, save for a small amount of liquid in the bends. But when the column finally breaks, the tube receives a severe shock.

Before filling the capillary tube, the liquid under investigation was boiled vigorously (reducing the volume about one-fourth) to remove as much air as possible. The liquid was then delivered directly from the boiling flask to the capillary through a siphon with the lower end of its outside leg bent upward, into which one leg of the capillary was inserted. The liquid was permitted to *flow through* the capillary for some minutes, flushing it thoroughly.

It is known that the solubility of air in a liquid decreases with increase in temperature. Since the liquid was boiled vigorously, it is assumed that at *lower* temperatures the residual air content is *below* the saturation level and that the remaining air is in true solution. Boiling does not remove all the air. After the column breaks, the two halves are usually found separated by a small bubble. This is often quickly reabsorbed when the column is tilted or it may be shaken out.

The open-ended capillary has the great advantage of being easy to clean. Concentrated sulfuric acid freshly saturated with Cr_2O_3 has been used for this purpose, first flushing the tube and then letting it stand filled over night. The importance of cleanliness cannot be over-emphasized. Fouling is indicated by a progressive decrease in the readings. If this persists, a new capillary should be used. All of which raises the question as to whether we are measuring the cohesion of the molecules in the free liquid or their adhesion to the glass wall of the tube.

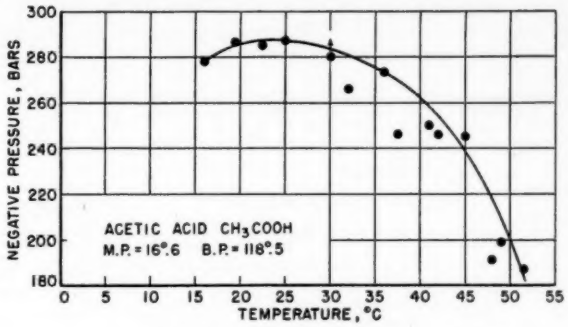

FIG. 1. Limiting negative pressure of acetic acid.

The spinner was enclosed in a glass-topped container, in which the pressure was reduced approximately to the vapor pressure of the liquid under investigation. The work done by the spinner on the surrounding air gradually raises its temperature. Consequently, there is some uncertainty, particularly for volatile liquids, regarding the temperature of the liquid column at its center at the instant of rupture.

ACETIC ACID

Glacial acetic acid meeting A.C.S. reagent specifications was used. After boiling at atmospheric pressure, it was cooled until 85–90 percent was crystallized. The liquid portion was discarded, the remaining crystals melted, boiled vigorously and introduced promptly into the experimental capillary. Observed melting point, 16.58°–16.60°.

The results are given in Fig. 1. Each point represents an individual measurement. A point with an arrow attached means either that the column did not break at the indicated stress or that the tube broke. The graph represents the locus of the *highest* values observed, i.e., the limiting negative pressure at various

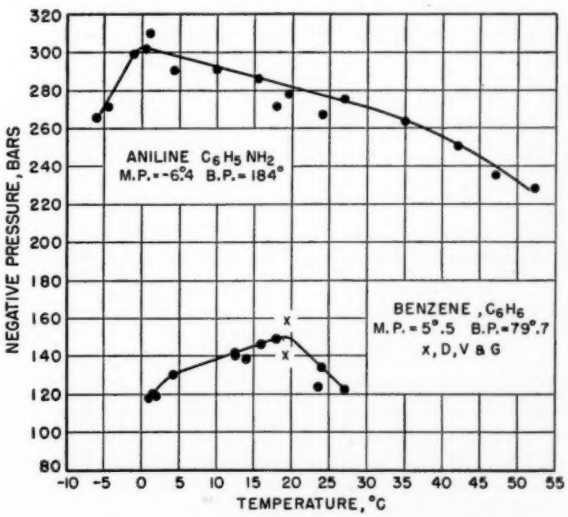

FIG. 2. Limiting negative pressure of benzene and aniline.

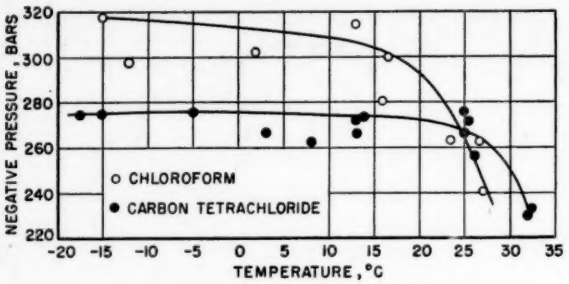

FIG. 3. Limiting negative pressure of carbon tetrachloride and chloroform.

temperatures. Observations lower than those shown have been omitted.

Acetic acid, like water, exhibits a maximum (−287 bars) a few degrees above its melting point, but the effect is not marked. At higher temperatures, the limiting negative pressure falls off rapidly. This is to be expected, because at the critical temperature (or below) the negative pressure must be zero.

BENZENE AND ANILINE

Benzene is a nonpolar liquid with a flat symmetrical molecule. Aniline differs structurally from benzene by the substitution of an NH_2 group for a hydrogen atom. It has a dipole moment of $\mu=1.48\times10^{-18}$ in the gas phase.

The aniline and benzene used were water free, prepared[2] by vacuum distillation, discarding the first and last quarters. The results are given in Fig. 2.

Like water and acetic acid, the limiting negative pressure of benzene and aniline decreases as the freezing point is approached. The maximum for aniline is 300 bars or 25 bars greater than that observed for water. This is in great contrast with the maximum observed for benzene, namely 150 bars. It suggests that the dipoles in aniline may be contributing markedly to the cohesion of the liquid.

Donaghue, Vollrath, and Gerjuoy[3] have also measured the limiting negative pressure of benzene. These authors used sealed tubes and went to great pains to reduce the partial pressure of the air in equilibrium with benzene to as little as 7×10^{-5} cm Hg. Their two highest values are shown by crosses in Fig. 2 and bracket my observations. This agreement lends support to my assumption that the gas remaining in the liquid after vigorous boiling is in true solution.

CARBON TETRACHLORIDE AND CHLOROFORM

The great difference in the limiting negative pressure of aniline and benzene suggests that the dipoles in aniline may be contributing markedly to the cohesive forces. Accordingly, nonpolar CCl_4 and polar $CHCl_3$ were selected for further measurement and comparison. Both liquids were of reagent quality, meeting A.C.S. specifications. The results are given in Fig. 3.

Again, the polar liquid $CHCl_3$ sustains the greater negative pressure, 318 bars as compared with 277 bars for CCl_4, with a tetrahedral structure. The difference in this case is not so marked, but $CHCl_3$ is not strongly polarized ($\mu=1.02\times10^{-18}$). However, these two pairs of liquids are of different (though related) chemical composition. A more satisfying approach would be the comparison of the *cis-* and *trans-*forms of the same liquid. This is under investigation.

The freezing points of CCl_4 and $CHCl_3$ are below the limit of the present apparatus (−18°C), and their behavior as the freezing point is approached could not be studied.

[2] Through the courtesy of C. A. Hewitt and T. J. Murphy of the Chemistry Division, NBS.

[3] Donaghue, Vollrath, and Gerjuoy, J. Chem. Phys. **19**, 55 (1951).

Letters to the Editor

THIS section will accept reports of new work, provided these are terse and contain few figures, and especially few half-tone cuts. The Editorial Board will not hold itself responsible for opinions expressed by the correspondents. Contributions to this section should not exceed 600 words in length and must reach the office of the Managing Editor not later than the 15th of the month preceding that of the issue in which the letter is to appear. No proof will be sent to the authors. The usual publication charge ($8.00 per page) will not be made and no reprints will be furnished free.

Calculation of Degree of Crystallinity in Polymers from Density Measurements

FRASER P. PRICE
Research Laboratory, General Electric Company, Schenectady, New York
(Received April 30, 1951)

LINEAR polymers which crystallize show a variation of thermodynamic properties such as heat content and specific volume of the general type illustrated in Fig. 1.

T_m is the melting temperature, T_g the glass transformation temperature, and T_x is determined by the intersection of the extrapolated liquid curve with the extrapolated liquid+crystal curve. T_x is the temperature where the specific volume of the crystals is equal to that of the liquid, and hence equal to the specific volume of a mixture of the two. It is, in general, an experimentally unattainable point but if the extrapolations are not too long it can be determined. The equality of liquid and specific volumes at T_x is independent of the extent of crystallinity in the sample. If it were completely crystallized the volume *versus* temperature curve would lie below the crystal+liquid and crystal+glass curves, but would meet the extrapolated liquid curve at T_x.

At the glass transformation temperature there is a discontinuity in the slopes of both the liquid and the liquid+crystal curves. This discontinuity will be greater the smaller the fraction of crystals present. Since the thermal expansion coefficients of the glass and the crystals are substantially identical below T_g, the glass, glass+crystal, and crystal curves very nearly parallel each other.[1]

Now let X=volume fraction of crystals in mixture with liquid or glass, V=specific volume of mixture, Vlg=specific volume of liquid or glass, whichever is appropriate to the given temperature, Vs=specific volume of crystals.

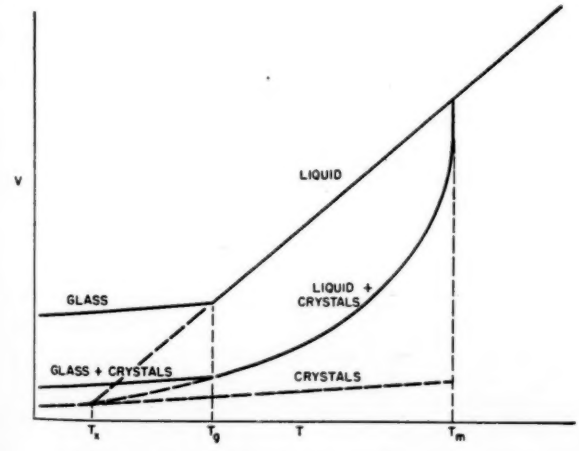

FIG. 1. Variation of specific volume with temperature.

TABLE I. Degree of crystallinity in polyethylene.

	Temp. (°C)	0	40	60	80	90	100	105	110	115
X	This method	0.85	0.77	0.72	0.63	0.57	0.48	0.42	0.33	0.14
	H+O[2]	0.55	0.55	0.55	0.50	0.45	0.40	0.35	0.25	0.10
	R, $R+R^3$	...	...	0.70	0.60	0.55	0.45	0.40	0.30	0.15

Then at any given temperature

$$X=(Vlg-V)/(Vlg-Vs). \quad (1)$$

If measurements have been made below T_g, all the terms in the right-hand member of the above equation are determinable. If measurements have not been made below T_g, a maximum X is obtained by assuming the crystal curve tangent to the liquid+crystal one at T_x, and a minimum X obtained by assuming zero coefficient of expansion of the crystals. It should be noted that below T_g, X is constant because in the glassy state the polymer cannot crystallize in the time of the experiment.

Using this method the density data on polyethylene[2] have been recalculated and compared in Table I with those from calorimetric data[3] and with the calculations of Hunter and Oakes.

The method of this note checks the calorimetric method very well, but gives higher values of X than those of Hunter and Oakes who assumed too low a value of Vs.

A study of the specific volume of polychlorotrifluoroethylene, the details of which will be published later, showed T_g to be very near T_x. Here measurements were not made below T_g and the limiting degrees of crystallinity shown in Fig. 2 were calculated.

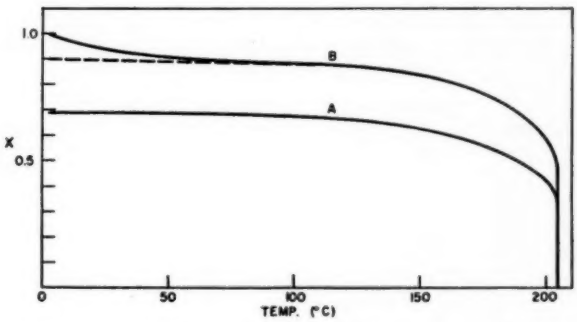

FIG. 2. Degree of crystallinity in polychlorotrifluoroethylene as a function of temperature.

These curves indicate that a maximum degree of crystallinity of between 70 and 90 percent were attained and that approximately $\frac{2}{3}$ of the crystals melt over a 5°C range just below T_m. These observations are in accord with Flory's predictions on melting of crystalline polymers.[4]

[1] W. Kauzmann, Chem. Revs. **43**, 219 (1948). G. Borelius, Arkiv. Mat. Astron. Fys. **33**, 1 (1946).
[2] E. Hunter and W. G. Oakes, Trans. Faraday Soc. **41**, 49 (1945).
[3] Raines, Richards, and Ryder, Trans. Faraday Soc. **41**, 56 (1945).
[4] P. J. Flory, J. Chem. Phys. **17**, 223 (1949).

Ultraviolet Absorption Spectrum of Fluoranthene

WILLIAM FRANCIS MADDAMS AND ROBERT SCHNURMANN
Physics Department, Manchester Oil Refinery, Limited, Manchester, England
(Received May 8, 1951)

THE ultraviolet absorption spectrum of fluoranthene has received some attention in recent years in connection with work on "aromatic cyclo-dehydrogenation"[1] and in conjunction with the cracking of petroleum. In an attempt to ascertain the quantitative aspects of the spectrum of fluoranthene a number of measurements were made on solutions of a synthesized specimen[2] in three solvents (isooctane, ethylalcohol, and chloroform). These

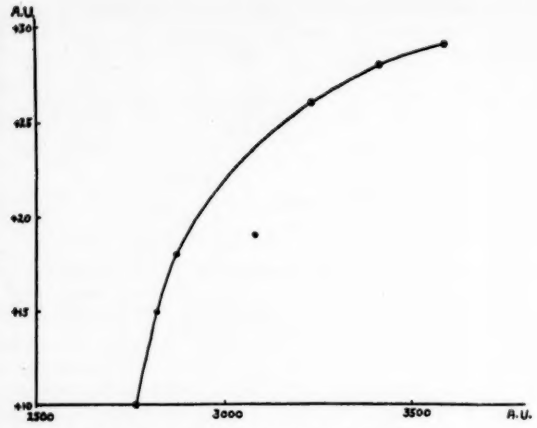

FIG. 1. Red shift of the absorption bands of a solution of synthesized fluoranthene in chloroform B.P. at the wavelengths indicated by the abscissas for the absorption bands of the same specimen of fluoranthene dissolved in iso-octane.

show an interesting red shift of increasing magnitude toward longer wavelengths of the bands (Fig. 1) with chloroform as the solvent and with iso-octane as the reference solvent. There is no

TABLE I. Absorption characteristics of fluoranthene.

Synthesized fluoranthene (reference 2) in						Fluoranthene (reference 1) in	
Iso-octane		Ethylalcohol		Chloroform		ethylalcohol	
A.U.	ϵ	A.U.	ϵ	A.U.	ϵ	A.U.	ϵ
—	—	—	—	—	—	2170	23550
2293	43400	—	—	—	—	—	—
2357	59500	2358	55800	—	—	2345	37070
2614	17500	2613	17800	—	—	2619	12680
2765	29100	2769	27400	2775	32700	2759	22810
2820	24100	2823	21900	2835	24700	2808	17420
2872	57100	2871	49400	2890	47500	2862	35080
3084	4050	3099	3750	3103	4380	3078	3451
3234	6150	3238	5800	3260	7630	3217	6266
3415	8060	3425	8090	3443	9590	3414	8531
3590	9230	3592	8900	3619	9730	3586	8337

appreciable wavelength shift on passing from the iso-octane solution to the ethylalcohol solution (see Table I) whereas there is a similar parallelism in the changes of absorption intensity of the

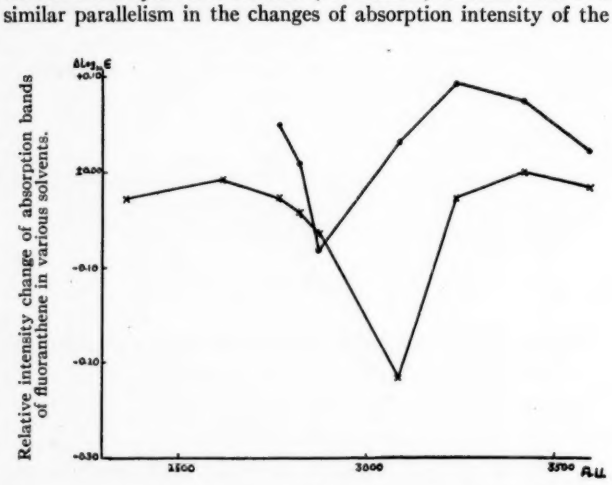

FIG. 2. Position of absorption bands of fluoranthene in iso-octane. X—in ethylalcohol. ●—in chloroform.

various bands (Fig. 2) as had been previously described with phenanthrene in various solvents.[3]

The spectrum of fluoranthene in iso-octane is illustrated by

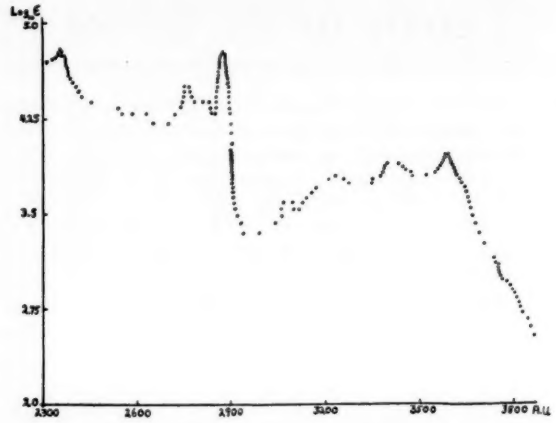

FIG. 3. Ultraviolet absorption spectrum of fluoranthene (G.L. 49) in iso-octane.

Fig. 3 since it shows some appreciable quantitative deviations from the spectrum published earlier by Orchin and Reggel.

[1] M. Orchin and L. Reggel, J. Am. Chem. Soc. **69**, 505 (1947).
[2] The authors express their thanks to Dr. M. Sulzbacher of the Grosvenor Laboratory, London, for the preparation of fluoranthene by the diene reaction between acenaphthylene and butadiene with subsequent dehydrogenation of tetrahydrofluoranthene. The fluoranthene was obtained as light yellow needles of melting point 110°C.
[3] W. F. Maddams and R. Schnurmann, J. Chem. Phys. **17**, 108 (1949).

Integrated Absorption of the Fundamental of CO from Measurements Using Self-Broadening of Rotational Lines*

D. WEBER AND S. S. PENNER
Jet Propulsion Laboratory, California Institute of Technology, Pasadena, California
(Received April 26, 1951)

THE results of quantitative infrared-intensity and line-width measurements on CO have been described in recently published articles.[1]

Quantitative intensity measurements were carried out for the first overtone of CO by two independent series of investigations. In one group of tests an infrared-inactive gas was used to produce adequate pressure-broadening of the rotational lines in order to facilitate quantitative intensity measurements. In another series of investigations, it was shown that self-broadening can be used

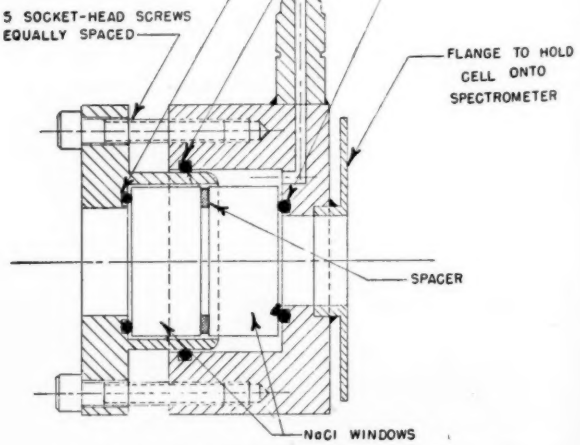

FIG. 1. Assembly drawing of variable space, high pressure gas absorption cell.

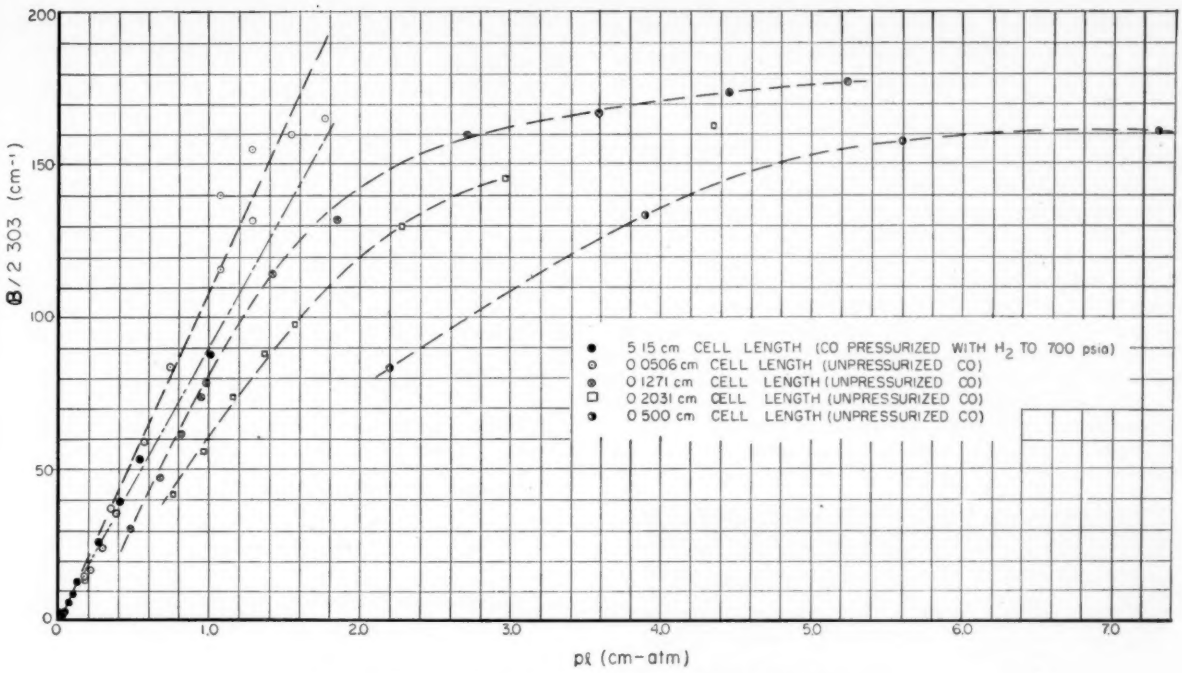
B/2 303 (cm⁻¹)
pℓ (cm-atm)
5 15 cm CELL LENGTH (CO PRESSURIZED WITH H2 TO 700 psia)
0 0506 cm CELL LENGTH (UNPRESSURIZED CO)
0 1271 cm CELL LENGTH (UNPRESSURIZED CO)
0 2031 cm CELL LENGTH (UNPRESSURIZED CO)
0 500 cm CELL LENGTH (UNPRESSURIZED CO)

FIG. 2. The quantity $B/2.303$ as a function of optical density pl.

to achieve the conditions necessary for quantitative measurements. The agreement between integrated absorption measurements obtained by the two independent methods was within the limits of experimental error.[1]

The results of quantitative infrared intensity studies on the fundamental of CO have been described only for measurements using infrared inert gases to achieve pressure broadening. Absorption cells suitable for quantitative studies on intense vibration-rotation bands must be exceedingly short. However, in view of the large discrepancies between values for the integrated absorption on the fundamental of CO reported by different investigators, it is evidently desirable to obtain an independent check of the mixed gas studies reported previously. Accordingly, a small infrared absorption cell, with variable path length, has been constructed for use at elevated pressures.

A sketch of the small infrared absorption cell used for the present studies is shown in Fig. 1. Accurately machined stainless steel gaskets served as spacers. Experimental results obtained for the fundamental of CO using self-broadening are shown in Fig. 2 together with the mixed gas data used to obtain the value 237 cm^{-2} $atmos^{-1}$ for the integrated absorption[1] of the fundamental. The abscissa in Fig. 2 represents the optical density pl, whereas the ordinate is

$$B/2.303=\int \log(T_{0\nu}/T_\nu)d\nu,$$

where $T_{0\nu}$ and T_ν denote, respectively, the apparent incident and transmitted intensities in the wave number interval between ν and $\nu+d\nu$. In accordance with the analysis presented previously,[1] the integrated absorption α_{01} is given by the relation

$$\alpha_{01}=2.303\frac{d(B/2.303)}{d(pl)}$$

as pl goes to zero or as the total pressure is increased without limit.

Reference to Fig. 2 shows that as the cell length is reduced, the data utilizing self-broadening approach the mixed gas data obtained previously. For the smallest absorption cell (cell length =0.0506 cm) $B/2.303$ appears to exceed the mixed gas data for a given value of pl by perhaps 15 percent. Since special precautions were not taken to assure the absence of small surface cracks for the sodium chloride windows under pressure, the agreement between experimental results must be considered to be satisfactory. Our estimate for the integrated absorption of the fundamental of CO remains unchanged at 237 ± 12 cm^{-2} $atmos^{-1}$.

* This paper presents the results of one phase of research carried out at the Jet Propulsion Laboratory, California Institute of Technology, under U. S. Army Ordnance Department Contract No. W-04-200-ORD-455.

[1] S. S. Penner and D. Weber, J. Chem. Phys. 19, 807, 817 (1951).

Erratum: Structure and Dipole Moment of Isothiocyanic Acid

[J. Chem. Phys. 18, 1437 (1950)]

C. I. BEARD*
Research Laboratory of Electronics, Massachusetts Institute of Technology, Cambridge, Massachusetts
AND
B. P. DAILEY†
Department of Chemistry, Harvard University Cambridge, Massachusetts

THE identifications of the first two lines in Table I are interchanged and should read:

$1_{1,0;+1}\rightarrow 2_{1,1;0}$	HNCS	23,499.5
$1_{1,1;0}\rightarrow 2_{1,2;-1}$	HNCS	23,424.5

Likewise, in Fig. 4 the frequencies of the lines labeled B and C should be interchanged.

Because of an arithmetical error, the values of the rotational constants B and C given just above Table I are in error. With $\frac{1}{2}(B+C)=5865.5$ mc/sec and $(B-C)=37.5$ mc/sec, as given in the article, the correct constants are:

$$B=5884.3 \text{ mc/sec}$$
$$C=5846.8 \text{ mc/sec}$$
$$I_B=142.58\times10^{-40} \text{ g cm}^2$$
$$I_C=143.49\times10^{-40} \text{ g cm}^2.$$

The value of I_A obtained from the relation $I_A=I_C-I_B$ (*if applicable*, as mentioned in the article) is $I_A=0.9\times10^{-40}$ g cm², and $A=900{,}000$ mc/sec.

* Now with Applied Physics Laboratory, The Johns Hopkins University, Silver Spring, Maryland.
† Now with Department of Chemistry, Columbia University, New York, New York.

Evidence for the Noncubic High Temperature Phase of $BaTiO_3$

ELIZABETH A. WOOD
Bell Telephone Laboratories, Murray Hill, New Jersey
(Received May 8, 1951)

BARIUM titanate crystals grown by B. T. Matthias at 1200°C from melts of barium chloride, barium carbonate, and titanium dioxide, with small amounts of boron trioxide[1] are of two types: (a) Cubic-habit, multiply-twinned crystals a few hundredths of a millimeter on an edge and (b) irregularly shaped thin plates, relatively untwinned, which may be several millimeters in diameter. Their major faces are normal to the optic axis (c) of the tetragonal crystal. Many of the plates show etch pits, like those shown in Fig. 1, the arrangement of whose facets is found to have only a twofold axis of symmetry, which is normal to the plate. Most of these platey crystals are pitted and embayed as though by solution; whereas the very small cubic-habit crystals have crystallographically perfect shapes—that is, they are euhedral.

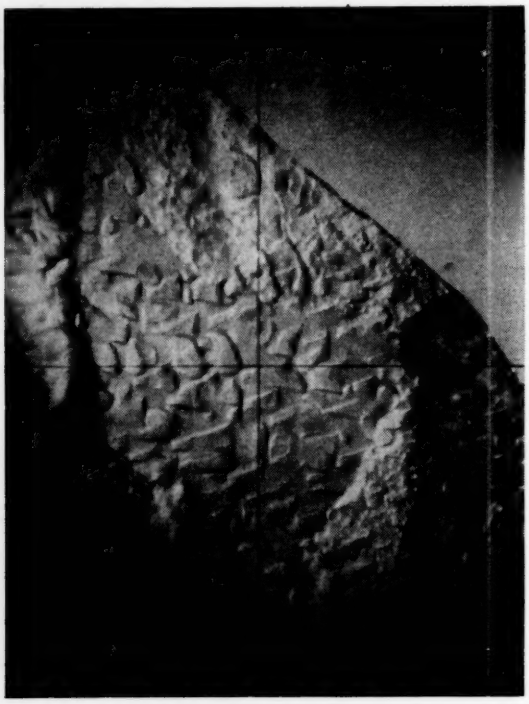

FIG. 1. Low symmetry etch pits on (001) face of tetragonal barium titanate.

This evidence indicates that the symmetry of the platey crystals at the time of their crystallization was not that of the cubic system since the symmetry of the etch pits is at least as low as orthorhombic; that the platey crystals were subsequently subjected to conditions unfavorable for their existence and began to disintegrate; and that, at some time, probably during the rapid cooling of the melt at the end of the experiment, there was a "shower" of truly cubic crystals, a great many nuclei forming at once. What is suggested is a noncubic form of barium titanate, stable at a higher temperature than the cubic form, with a sluggish transition to the cubic form.

This suggestion was made by the writer at a meeting of the American Society for X-ray and Electron Diffraction at Cornell University in June, 1949, and the above evidence was presented there at that time. Others at the meeting considered the existence of a high temperature noncubic phase very unlikely on theoretical grounds and since efforts to obtain crystals of it by quenching were unsuccessful the writer did not publish the observations described above. However, W. O. Statton[2] now concludes that such a phase exists and this letter is offered as supporting evidence for his conclusions.

The lower limit of the stability range of this phase in a pure $BaTiO_3$ melt, according to Statton, is about 1450°C. In the presence of fluxes, however, that limit might be much lower. Matthias found that the addition of small amounts of B_2O_3 resulted in the production of the large, relatively untwinned plates. The fact that the tetragonal axis is oriented normal to the plate throughout suggests that the crystal "remembers" a noncubic symmetry which it had during growth. Apparently imperfections or impurities included in the platey crystals during their growth in the lower symmetry form gave them a preference for a single *c*-axis direction when they underwent the cubic-tetragonal inversion at about 120°C.

The very small, cubic-habit crystals, however, growing with cubic symmetry, were free to choose any of their three cubic axes for the *c* tetragonal axis at 120° and were therefore multiply twinned.

[1] For example: 59 g $BaCl_2$; 26 g $BaCO_3$; 5.6 g TiO_2; 2 g B_2O_3.
[2] W. O. Statton, J. Chem. Phys. **19**, 33 (1951).

Rotational Isomerism in 2-Methyl Butane and 2:3-Dimethyl Butane

J. K. BROWN AND N. SHEPPARD
Department of Colloid Science, Free School Lane, Cambridge, England
(Received May 2, 1951)

THE crystallization of liquid straight chain hydrocarbons produce a very marked simplification of their infrared and Raman spectra.[1–4] These molecules exist in a number of rotational isomeric configurations in the liquid state, each configuration having its own set of infrared and Raman frequencies. In the crystalline state only one form exists, and consequently the frequencies of the other forms disappear from the spectrum on crystallization of the liquid. However, previous spectroscopic investigations of the simple branched chain hydrocarbons 2-methyl butane and 2:3-dimethyl butane[3, 5] have shown that all the infrared and Raman frequencies remain on passing from the liquid to the solid state. This observation has been interpreted in two different ways,[5] either (a) there is a large energy difference between the configurations in the liquid state, i.e., virtually only one form exists in the liquid and solid states or, (b) there is a small energy difference leading to the presence of two forms in the liquid state which persist on solidification.

The alternative (b) might give rise to either an ordered or to a disordered solid solution,[5] and this has important thermodynamic consequences.[6, 7]

During an infrared investigation of other molecules existing in isomeric configurations we have found that rapid freezing of the liquid sometimes leads to a glassy solid,[8] both liquid and glass having virtually identical spectra. On controlled warming of this glass to near the melting point a slow transition to the crystalline state takes place which is easily observable. It seemed possible that glasses had also been produced in the previous studies of the spectra of the two branched paraffins in the solid state. We have therefore applied this method in the re-investigation of the infrared spectra of these substances, and have been able to crystallize both of them. The infrared spectrum of liquid 2:3-dimethyl butane was greatly simplified on crystallization, a number of strong absorptions disappearing, and the spectrum of the crystalline state indicated that the configuration stable in the lattice has a center of symmetry. There is thus little doubt that, for this molecule, the interpretation of a small, approximately zero, energy difference between the two isomers in the liquid state is the correct one.

The evidence for 2-methyl butane is less clear cut. On crystallization the infrared spectrum showed a change in the relative intensity of a few absorption bands when compared with the spec-

trum of the cold liquid, and one well-marked band at 912 cm^{-1} disappeared. Although the simplification is not as extensive as that for 2:3-dimethyl butane, this might arise from overlapping of absorptions due to different configurations in the liquid state, particularly as both possible forms have low symmetry in this case. It is not thought that the changes observed are extensive enough to justify unequivocally the assumption of a small energy difference. On the other hand, the observation of some simplification does not allow us to rule out this possibility on the spectroscopic evidence alone, particularly as the existence of two strong, polarized Raman lines between 700 and 800 cm^{-1} in liquid 2-methyl butane is very readily explained in terms of two isomers present in comparable concentration.[5] A re-investigation of the Raman spectrum in the solid state under conditions of complete crystallization may settle this problem. A marked weakening or complete disappearance of one of the aforementioned lines would certainly be in favor of a small energy difference in the liquid state, but if both of these persisted a single form would be indicated, and then the two strong Raman lines would probably be attributable to Fermi resonance.[6] A more detailed account of the work on these and other branched paraffins will be published shortly.

[1] Rank, Sheppard, and Szasz, J. Chem. Phys. **17**, 83 (1949).
[2] S. Mizushima and T. Simanouti, J. Am. Chem. Soc. **71**, 1320, (1949).
[3] D. W. E. Axford and D. H. Rank, J. Chem. Phys. **18**, 51, (1950).
[4] Brown, Simpson, and Sheppard, Disc. Faraday Soc., September, 1950 (to be published).
[5] G. J. Szasz and N. Sheppard, J. Chem. Phys. **17**, 93 (1949).
[6] Scott, McCullough, Williamson, and Waddington, J. Am. Chem. Soc. **73**, 1707 (1951).
[7] J. G. Aston, Disc. Faraday Soc. April, 1951 (to be published).
[8] J. K. Brown and N. Sheppard, Disc. Faraday Soc. September, 1950 (to be published).

The Pyrolysis of *iso*-Propyl Bromide

ALLAN MACCOLL AND P. T. THOMAS
University College, London, England
(Received April 30, 1951)

IN continuation of the work in this Laboratory on the pyrolysis of organic bromides,[1,2] the kinetics of the decomposition of *iso*-propyl bromide have now been investigated. Previous work on this substance by Lessig[3] showed that the reaction may be represented by

$$C_3H_7Br \rightarrow C_3H_6+HBr, \qquad (1)$$

although the ratio of the final to initial pressure was found to be less than the two, as demanded by Eq. (1). Lessig used clean vessels and found that the rate constants were not particularly reproducible. The reaction was concluded to be of the first order, and the rate constants would appear to depend upon the initial pressure of the *iso*-propyl bromide.

In the present work, in which the reaction was followed both by the measurement of the rate of pressure increase and analytically by the estimation of the HBr produced, the first-order character of the decomposition has been confirmed. Reproducibility was only obtained when aged vessels were used and all traces of oxygen completely excluded. In particular, care was taken not to allow oxygen into the reaction vessel between runs. The reaction is uncomplicated in that no products uncondensable in liquid air were obtained. However, considerable evidence was found for the existence of the equilibrium

$$C_3H_7Br \rightleftharpoons C_3H_6+HBr.$$

In the first place, the first-order constants began to fall off after about 50 percent of the reaction had taken place. For this reason only the first 30 percent of the reaction was used for the calculation of the rate constant. Secondly, the falling off was more marked at high initial pressures, and also in those runs carried out in the presence of added propylene.

In the initial pressure range 30 to 450 mm, there was no variation of the first-order constants. Similarly the addition of propylene did not affect the initial rate. The addition of either allyl bromide or bromine had no marked effect upon the rate. For these reasons, it is concluded that *iso*-propyl bromide decomposes by a unimolecular splitting off of molecular HBr. The rate constants were well represented by the expression,

$$k=4.07\times10^{13}e^{-47,800/RT}.$$

This raises the question as to why a chain mechanism is preferred in the case of *n*-propyl bromide, whereas a direct unimolecular split is of prime importance in the case of *iso*-propyl bromide. A relevant factor may lie in the chain propagating step

$$Br+C_3H_7Br \rightarrow C_3H_6Br+HBr.$$

For in the case of *n*-propyl bromide the principal attack of the bromine atom is upon a secondary hydrogen atom, whereas in the case of *iso*-propyl bromide it would be upon a primary hydrogen atom, and there is a certain amount of evidence for the secondary C—H bond strength being less than the primary. This point will be taken up again elsewhere in a subsequent publication.

The mechanism of the oxygen-catalyzed reaction is by no means clear. It seems probable that chains are started on the walls and ended in the gas phase, since partial inhibition of the catalyzed reaction may be brought about by the addition of propylene.

The behavior of the butyl bromides is of interest. Kistiakowsky and Stauffer[4] have shown that *t*-butyl bromide decomposes by a unimolecular splitting out of HBr. Here again, attack of a bromine atom can only be upon a primary C—H bond, and so that chain mechanism would be rendered energetically unfavorable. The pyrolysis of the butyl bromides is at present under investigation.

[1] A. Maccoll, J. Chem. Phys. **17**, 1350 (1949).
[2] P. Agius and A. Maccoll, J. Chem. Phys. **18**, 158 (1950).
[3] Lessig, J. Phys. Chem. **36**, 225 (1932).
[4] Kistiakowsky and Stauffer, J. Am. Chem. Soc. **59**, 165 (1937).

Studies of Zeeman Effects from Solutions of Europium and Neodymium Salts

GEORGE J. ROTARIU*
University of Illinois, Urbana, Illinois
(Received May 15, 1951)

THE effect of a high magnetic field on solutions of salts of trivalent europium and neodymium was investigated spectrographically in the hope of checking the J-values of the energy levels between which the absorptions occur, and arriving at an understanding of the symmetry of arrangement of ions in solutions.

Gobrecht[1] has interpreted the spectra of the trivalent europium ion in crystals at 4650A as due to a $J=0$ to a $J=3$ transition. A partial check on this assignment has been made by Schmillan[2] who obtained five lines in this region from an inverse Zeeman effect on europic sulfate crystals using a magnetic field of 40,000 gauss. An earlier work by Freed and co-workers[3] on aqueous solutions of europic nitrate showed that a Zeeman effect can be obtained from these solutions with a field of 33,000 gauss; four lines were obtained which checked in position four of the five lines Schmillan obtained.

An attempt was first made to check this latter result for solutions. A transverse inverse Zeeman effect was sought at room temperature (23.0°C) using a 1.21M aqueous solution of europic nitrate in a 23.52-mm-long Pyrex cell. A Littrow-type, Hilger quartz prism spectrograph was used which had a dispersion of 2.22A per mm at 4650A; the electromagnet used[4] gave a field of 31,000±1200 gauss with two-inch-diameter polefaces separated at a distance of 4.7 mm. This solution did not appear to exhibit a Zeeman splitting under these conditions.

Lower temperatures were resorted to in the hope of sharpening up the lines. Absorption Zeeman spectra were then taken of a 0.233M solution of europic nitrate in absolute ethyl alcohol at room temperature, at −22°C and at −80°C in a paraffined, silver-plated, copper cell built within a copper bar. This solution did reveal such an effect in the 4658A component. A lowering of the temperature to −80°C in the no-field cases caused the original doublet to change into a triplet; this indicated a change in the structure of the alcohol about the europic ion from the alcohol-

type at room temperature to a "water-type"[5] which possesses less symmetry than the former. This can possibly be explained in the increased stability of the hydrogen bonding in the alcohol as the temperature was lowered. At −22°C and at −80°C, the spectra of this solution, both with and without the field of 31,000 gauss, seemed to reveal a fine structure in each of the three components (4648A, 4652A, 4658A). This would indicate a still lower symmetry in the alcohol at these temperatures than suspected.

Recent work by Moeller and Brantley[6] and Moss[7] has revealed that formation of the ethylenediamine tetraacetate (Sequestrene, *S*) complexes of neodymium chloride, erbium chloride, and gadolinium chloride splits the original bands into more components. However the bands of praeseodymium chloride were not split by such complexing. This complexing agent was used in the hope of obtaining further splitting of the europic ion lines at 4650A similar to the results obtained by Freed and Weissman with europic acetylacetonate.[8] A 1:1 aqueous mixture of 0.466M europic nitrate and 0.466M ethylenediamine tetraacetate was photographed in the 4500–5300A region. Only *one* line (1.6A wide) was obtained at 4652A and no lines in the 5250A region. No definite statement concerning the symmetry of this europic complex can be made, although if the same selection rules for the transitions hold, the symmetry indicated is very high. The magnetic field of 31,000 gauss did not alter this spectrum.

X-ray photos also indicate the existence of a 1:1 Eu^{+++}−*S* crystalline compound (*insoluble* in water), and spectral evidence points to the existence of a probable 4/3 Eu^{+++}−*S* complex (*soluble* in water), both of which are supposedly analogous to the neodymium complexes. This latter solution exhibited essentially the same spectra as that for the 1:1 compound mentioned above. No effect of the field of 31,000 gauss was observed in the room temperature spectra of any of the Eu^{+++}−*S* mixtures.

The spectra of a 0.466M aqueous solution of neodymium nitrate, investigated in the region of 5300–6300A, revealed two sharp lines at 6256A and 6222A, in addition to the main band at 5770A (200–300A wide). A solution of 4/3 mole ratio of Nd^{+++}−*S* in water exhibited a spectrum with lines at 6270A, 6252A (?), 6235A, and at 6222A. These lines appear as sharp as the europic ion triplet at 4650A; furthermore, the middle component (6235A) seems to be made up of 3 or 4 very sharp lines itself. A 1:1 aqueous mixture of 0.466M neodymium nitrate and 0.466M *S* revealed a spectrum which resembled that of the 4/3 complex in intensity, but with lines at 6274A and at 6230A (?). No effect of the field of 31,000 gauss was noted in the spectra of these neodymium solutions. The main band at 5770A for the neodymium ion seemed unaffected by the complexing and by the influence of the high magnetic field at the exposure times used.

The author wishes to acknowledge the guidance and aid of Professor W. H. Rodebush, under whom this work was conducted, and the generosity and assistance of Professor G. W. Almy (Physics).

* Submitted as partial fulfillment for the degree of Doctor of Philosophy, University of Illinois, Urbana, Illinois, October, 1950. Present address: Department of Chemistry, University of California, Berkeley, California.

[1] H. Gobrecht, Ann. Physik **28**, 673 (1937).
[2] A. Schmillan, Ann. Physik **39**, 502 (1941).
[3] Freed, Weissman, and Rotariu, J. Chem. Phys. **8**, 291 (1940).
[4] E. J. Shaw, Rev. Sci. Instr. **2**, 611 (1931).
[5] Freed, Weissman, Fortess, and Jacobson, J. Chem. Phys. **7**, 824 (1939).
[6] T. Moeller, and J. C. Brantley, J. Am. Chem. Soc. **72**, 5447 (1950).
[7] F. Moss, private communication (Professor Moeller's group).
[8] Freed, Weissman, and Fortess, J. Am. Chem. Soc. **63**, 1079 (1941).

Errata: Contributions to the Theoretical Treatment of Ammonium. II

[J. Chem. Phys. **16**, 857–864 (1948)]

J. I. HORVÁTH
Department of Theoretical Physics, University of Debrecen, Debrecen, Hungary

IN Part I, I have discussed the problem of the stability of the neutral ammonium molecule, which is experimentally unknown. Equation (23) gives the binding energy of the valence electron, which is by definition negative. Unfortunately I have not noticed this trivial fact and so the first term of this equation has a negative sign, which causes a mistake in Table I.

Paragraph C of this Part, where the energy of the binding of the valence electron is calculated numerically, contains a further error of calculation, which is important in point of view of the discussed energy. The effective charge Z^* with increased r tends to +1 and the function, by which Z^* is approximated, decreases exponentially. The analytical approximation of the effective charge is correctly

$$Z^*=1+B\cdot r^b\cdot e^{-\beta r},$$

where

$$B=540.38087,\quad b=1.80142,\quad \beta=4.09740.$$

The calculations show in this case that we have a nonbinding state, consequently the neutral ammonium molecule is unstable, which is in excellent agreement with the experimental facts.

Finally we have to remark that the mentioned errors and corrections do not influence the principal part of our investigation, which deals with the theoretical treatment of the ammonium molecule-ion.

I am very indebted to Professor A. Kónya and Dr. T. A. Hoffmann who kindly called my attention to this fact.

Dielectric Constant and Loss Factor of Ethyl Alcohol and Water at λ=3.24 cm Obtained by Free Wave Method

MASASI YASUMI, HIDEO OKABAYASHI, MICHIO SHIRAI, AND SAN-ICHIRO MIZUSHIMA
Institute of Science and Technology and Faculty of Science of Tokyo University, Tokyo, Japan

(Received May 7, 1951)

WE have measured the dielectric constant (ϵ') and loss factor (ϵ'') of ethyl alcohol and water at several temperatures by improved free wave method, which removes the difficulties in the earlier measurements and yields reliable values of ϵ' and ϵ''.

If the linearly polarized plane wave of the wave length λ is emitted to free space and is reflected by the liquid dielectric layer of the thickness d placed on mercury, the reflection coefficient will be expressed as

$$R^2=\frac{\sinh\left(\frac{2\pi kd}{\lambda}+\frac{1}{2}\ln R_{12}\right)-\cos^2\left(\frac{2\pi nd}{\lambda}-\frac{\gamma}{2}\right)}{\sinh\left(\frac{2\pi kd}{\lambda}-\frac{1}{2}\ln R_{12}\right)+\cos^2\left(\frac{2\pi nd}{\lambda}+\frac{\gamma}{2}\right)},$$

where n is the refractive index, k the absorption coefficient, and

$$R_{12}^2=\frac{(n-1)^2+k^2}{(n+1)^2+k^2}$$

$$\tan\gamma=\frac{2k}{(n^2-1)+k^2}.$$

At each of the three temperatures shown in Table I, about forty measurements have been made to determine the values of R^2 for ethyl alcohol in the range of d/λ from 0 to 0.523 and about thirty measurements for water in the range of d/λ from 0 to 0.15.

In Table I are shown the values of n and k which explain most satisfactorily the experimental relation of R^2 *vs* d/λ. The probable error of n is 0.3 percent for ethyl alcohol and 0.4 percent for water. The error of k is estimated as 1 percent for ethyl alcohol and 2 percent for water.

TABLE I.

	Ethyl alcohol (λ=3.24 cm)			Water (λ=3.24 cm)		
t(°C)	10	18	24	6	11	19
n	2.00	2.05	2.11	7.50	7.51	7.60
k	0.48	0.54	0.61	2.22	2.11	1.96
ϵ'	3.77	3.91	4.08	51.3	51.9	53.9
ϵ''	1.92	2.22	2.58	33.3	31.7	29.8

From these values of n and k the dielectric constant ϵ' and loss factor ϵ'' are calculated according to the following formula,

$$\epsilon'-i\epsilon''=(n-ik)^2,$$

and tabulated also in Table I.

Discussions of these experimental data on the basis of molecular theory will be given elsewhere, with detailed description of experiment and method of calculation.

New Absorption Bands of the NO Molecule in the Extreme Ultraviolet Region

Y. TANAKA,* M. SEYA, AND K. MORI
Optical Institute, Tokyo University of Education, Tokyo, Japan
(Received April 30, 1951)

THE 6000A bands of the NO molecule which appear strongly in a Geissler discharge of NO_2 or NO gases have the appearance of a triplet structure. At first Grillet[1] and his co-workers attributed these bands to the NO^+ molecule. Very recently, however, Feast[2] studied the same bands with large dispersion equipment and after making a rotational analysis of them he came to the conclusion that these bands are due to the transition between a new electronic level ($E^2\Sigma^+$) and the upper state of the γ-bands of NO. According to him, the apparent triplet structure is due to the closeness of the bands in the sequence (0, 0), (1, 1), and (2, 2), each of which consists of a P and a R branch.

Recently, in a series of studies[3] on the absorption of NO in the extreme ultraviolet region, we observed a band progression which corresponds to the $v'-0$ progression in the electronic transition between the ground state $X^2\pi_{\frac{1}{2}, \frac{3}{2}}$ and the upper state of the 6000A band ($E^2\Sigma^+$). These bands are very similar to the γ-bands in their appearance, each one being composed of 4-heads shaded toward the violet. $\Delta\nu$ between the shortest wavelength head (Q_1) and the third head (Q_2) is about 120 cm^{-1} which is nearly equal to the doublet separation of the ground state $^2\pi$.

In Table I, the observed wavelengths and wave numbers are shown in the second and third columns respectively. In the last column, the expected locations of the band origins are shown which were calculated using the general formula and the molecular constants obtained by Feast. As shown in Table I, there is good agreement between observed and calculated values for the lower members of the progression, but the discrepancy becomes great for the higher vibrational bands. The measurements were done on the head of the bands so that such a discrepancy is to be expected. The first two bands appear free from obstruction by other bands but the following four are obscured, so that the accuracy of the measurement of the latter is not good compared with the other two.

TABLE I.

v'	λ(A) head	$\nu(cm^{-1})$ head	I	Calculated band origin $\nu(cm^{-1})$
	1646.92	60719.4		
0	46.30	742.3	2	
	43.62	841.3		
	42.97	865.4		60862.8
	1585.86	63057.3		
1	85.15	085.5	3	
	82.71	182.8		
	82.15	205.1		63204.8
	1529.98	65360.3		
2	29.29	389.8	2	
	27.40	470.7		
	26.69	501.2		65514.9
	1478.41	67640.2		
3	77.55	679.6	1	
	75.35	780.5		
	74.83	804.4		67793.4
	1431.83	69840.7		
4	31.40	861.7	1	
	29.42	958.4		
	29.07	975.6		70040.1
	1386.52	72123.0		
5	85.82	159.4	1	
	84.01	253.8		
	83.45	283.1		72255.0

* Present address: Physics Department, University of Chicago, Chicago, Illinois.

[1] M. Duffieux and L. Grillet, Compt. rend. **201**, 1338 (1935); **202**, 938 (1936); **205**, 39 (1937).
[2] M. W. Feast, Can. J. Research **A28**, 488 (1950).
[3] Y. Tanaka, Sc. Pap. I. P.C.R. **39**, 456 (1942); **43**, 160 (1949).

The Nature of the Scale Factor Occurring in the Quantum-Mechanical Treatment of Systems by the Variational Method*

P. TORKINGTON
British Rayon Research Association, Urmston, Lancashire, England
(Received April 16, 1951)

A SOMEWHAT unsatisfactory feature in the quantum-mechanical treatment of all systems governed by central force fields, other than the hydrogen atom or hydrogenlike ions, is the arbitrary scale factor found necessary in the wave functions. The accepted interpretation of this factor is that it is an effective nuclear charge. Thus, in the helium atom,[1] to approach the true binding energy the real nuclear charge $Z=2$ must be replaced by $Z'=1.6875$ and in the hydrogen molecule[2] $Z=1$ must be replaced by $Z'=1.17$, in the first improvements on the simplest functions. In the first case, the usual explanation is that each electron partially screens the nucleus from the other, and in the second that the mutual repulsion of the two electrons effectively increases the repulsion of the nuclei. It is suggested here that if there is not a correspondence between parameters in the wave function and those occurring in the hamiltonian of the system, then the electron distribution given by the function is actually for a "ghost" having the same energy as the real system, the deviation of Z/Z' from unity being a measure of the difference between the ghost and the real system; if the scale factor were really an effective nuclear charge, then one would expect that a better approximation would be attained by using a common Z' in the function and the hamiltonian. The fact that this is not so† is surely an indication that functions in which scale factors occur should not be interpreted as due to there being an "effective" nuclear charge. In the treatments of the hydrogen molecule-ion and helium atom outlined below, the scale factors arise from very simple considerations in a quite straightforward manner.

In the ion H_2^+ it is significant that in two of the functions found satisfactory, two scale factors (Z' and Z''), occur.[3] The best of these, due to Guillemin and Zener, gives the binding energy correct to within 0.01 ev; it has the form,

$$\psi=\exp(-Z'r_A)\cdot\exp(-Z''r_B)+\exp(-Z''r_A)\cdot\exp(-Z'r_B), \quad (1)$$

where r_A, r_B are the two electron-nucleus distances. The best values of the parameters are 1.13, 0.23. It will be noted that $|Z'-Z''|$ is approximately unity. Now if we assume that for each value of the internuclear distance R there is a critical ellipsoid $\mu=1+2a^0/R$ (where μ is the elliptical coordinate $(r_A+r_B)/R$ and $R+2a^0$ is the major axis of the ellipsoid) within which the electron-density is higher than that given by the simple function $\psi=\exp(-r_A)+\exp(-r_B)$, and outside which it is lower, and further that the deviation from the simple function is governed by an exponential law, the function obtained is

$$\psi=\exp[c(R+2a^0-\mu R)][\exp(-r_A)+\exp(-r_B)], \quad (2)$$

where c is a positive constant. The expression a^0 is presumably a function of R; it is related to the eccentricity e of the critical ellipsoid by

$$2ea^0=R(1-e). \quad (3)$$

Equation (2) reduces to

$$\psi=N(\phi_A\phi_B)^c(\phi_A+\phi_B), \quad (4)$$

where ϕ_A and ϕ_B are the two 1s hydrogen orbitals and N is a

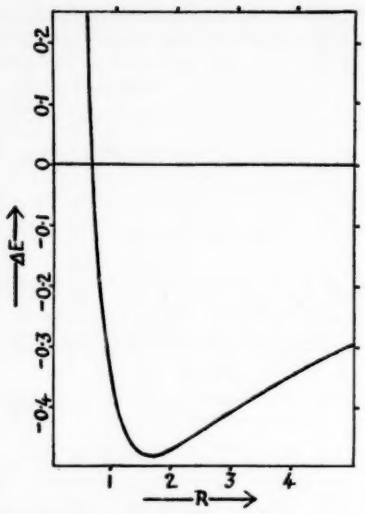

FIG. 1. The hydrogen molecule-ion; plot of binding energy against internuclear distance R for the hypothetical system with $\psi=\exp[-(r_A+r_B)]$. (R in units of a_0, ΔE in units of (e^2/a_0).) $\Delta E_{\min}=-0.477$, $R_{\min}=1.65$. Values in real system: $\Delta E_{\min}=-0.102_5$, $R_{\min}=2.00$. Values with $1s$ hydrogen functions: $\Delta E_{\min}=-0.065$, $R_{\min}=2.49$. Values with effective atomic number 1.23: $\Delta E_{\min}=-0.083$, $R_{\min}=2.00$. The binding energy (total energy minus energy of $1s$ hydrogen atom) is given here by the formula:

$$\Delta E=R^{-1}-6(2R+1)(4R^2+6R+3)^{-1}.$$

normalizing factor, including the term in a^0. Equation (4) reduces to Guillemin and Zener's function (1) to a very good approximation if c has a value of the order 0.18 ± 0.05; presumably $|Z'-Z''|$ is not quite unity because the critical surface is not an exact ellipsoid. The single scale factor in the Wang-type treatment would on the above view arise from a critical spherical surface around each nucleus, within which the electron-density was higher and outside which it was lower than that given by the hydrogen functions, the two nuclei being treated independently. Clearly, this approximation can only be expected to hold for intermediate-to-large nuclear separations. The analog of Eq. (2) is

$$\psi=\phi_A\cdot\exp[c(r^0-r_A)]+\phi_B\cdot\exp[c(r^0-r_B)], \qquad (5)$$

where r^0, the critical radius, is again presumably a function of R, but is absorbed in the normalizing factor. The relation to the scale factor is $Z'=1+c$; variation of c with R is to be expected here, as it is, of course, not justifiable to treat the two nuclei independently.

Finally, it may be observed that the polarization, producing a charge-density characteristic of the bond, should give rise to functions in which the density is in inverse ratio to both elliptical coordinates μ and ν. The form of James' function[4] and the present considerations suggest that in this function the μ-component exaggerates the contraction normally reached by using a scale factor (which is used as well, however), and that this effect is then corrected by balancing against the term in ν^2, which effectively sends charge towards the nuclei. (Compare the hydrogen molecule,[5] in which a scale factor *less* than unity is used in addition to a term in ν.) This suspicion is at least not removed by calculations with the simple elliptical function $\psi=\exp[-(r_A+r_B)]$. The curve obtained is shown in Fig. 1; it is effectively that of a highly unstable system with a strong contraction. The presence of this elliptical component in the molecular orbital (presumably for H_2 as well as for H_2^+), will thus easily give the energy; and it flattens the minimum. In H_2, the simple combination of hydrogen functions gives too sharp a minimum, and this defect is increased when a scale factor is used.[6]

The helium atom is complicated by electron-repulsion, which at first sight is not allowed for in the simple scale-factor function. If we take the ratio ρ of the electron-densities given by the functions with and without scale factor, we obtain the result

$$\rho=(Z'/Z)^6\exp[2(Z-Z')(r_1+r_2)], \qquad (6)$$

where r_1 and r_2 are the two electron-nucleus distances. It is found that $\rho=1$ at $r_1+r_2=-3[Z(1-\alpha)]^{-1}\ln\alpha$, where $\alpha=Z'/Z$. Substituting $Z'=27/16$, given by the simplest variational treatment, we obtain $\rho=1$ at $r_1+r_2=1.63a_0$ (a_0 is the Bohr radius). Thus, there is a critical spherical surface of radius $0.815a_0$ within which the electron-density is always lower than in the system with hydrogen functions ($Z=2$) and another with radius $1.63a_0$ outside which it is always higher, and the scale factor is seen to be a first approximation for electron-repulsion, not a screening factor. It might be observed that in any case the screening here would be more likely to be that of one electron with respect to the other, by the interposing nucleus.

* This letter arises from part of the program of fundamental research undertaken by the British Rayon Research Association.

† Unpublished calculations of the author.

[1] L. C. Pauling and E. B. Wilson, Jr., *Introduction to Quantum Mechanics* (McGraw-Hill Book Company, Inc., New York, 1935), pp. 184ff., or any other standard text on quantum mechanics.

[2] Reference 1, p. 345.

[3] Reference 1, pp. 331ff.

[4] Reference 1, p. 333.

[5] Reference 1, p. 350.

[6] Reference 1, p. 349.

Solvent Induced Frequency Shifts for Cata-Condensed Aromatics

NORMAN D. COGGESHALL AND ABBOTT POZEFSKY
Gulf Research and Development Company, Pittsburgh, Pennsylvania

(Received May 23, 1951)

BAYLISS[1] has discussed the interaction between solute and solvent whereby electronic transition frequencies are reduced by electrostatic interaction effects. The purpose of the present note is to present certain data on this effect observed for cata-condensed aromatics. These data were obtained with a Beckman DU spectrophotometer.

In the first phase of this work the low frequency band of naphthacene (*circa* 22,000 cm^{-1}) was correlated with the index of refraction of the solvent. For this the solvent was varied to have values of n_D between 1.3915 and 1.6219 by using 2,2,4-trimethylpentane, benzene, styrene, naphthalene, α-methylnaphthalene, anthracene, and phenanthrene in various combinations and concentrations. The results may be seen in Fig. 1. Here are plotted the observed frequency *versus* $(1/2)(1-1/n_D^2)$, which corresponds to Bayliss' Eq. (2), and *versus* $(n_D^2-1)/(2n_D^2+1)$, which corresponds to his Eq. (3). Here K, the dielectric constant, has been replaced by n_D^2. It is seen that there is a definite relation between the frequency and the n_D of the solvent. Throughout the central

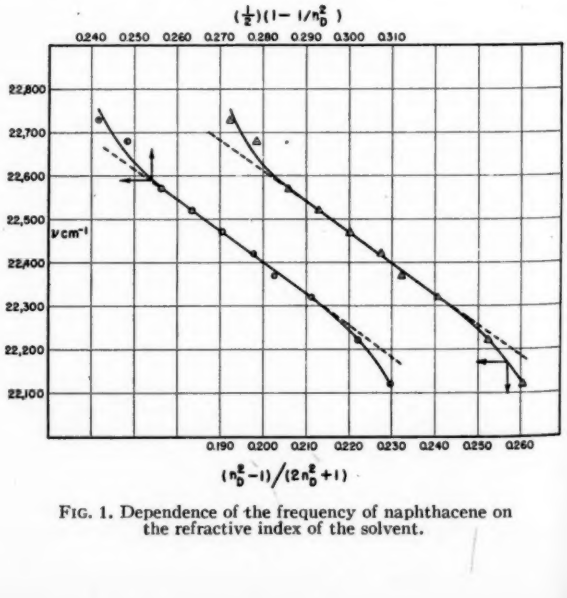

FIG. 1. Dependence of the frequency of naphthacene on the refractive index of the solvent.

TABLE I. Assignment of frequencies in cm^{-1} observed in 2,2,4-trimethylpentane solution.

Compound	$'L_a$	$'L_b$	$'B_b$
Phenanthrene	26670 28090	28900 29540 30300 30960 31700	34130 35590
Anthracene	26670 28090 29500 30960	...	...
1,2 benzanthracene	27970 29330 30670 31950	26010 26700	34780 36180
9,10-dimethyl-1,2-benzanthracene	26280 27590 28940	...	33730 35030
1,2,5,6-dibenzanthracene	28740 29990 31250	25410 26080 26810 27510	33610 34970
Methylcolanthrene	27820 29240 30630	25450 26390 26880	33730 35090
Naphthacene	21320 22780 24180	25310	...

portion of the data the curves are linear in accordance with Bayliss' equations, and the representations are essentially equivalent for the data at hand. It would be necessary to have the vapor phase frequency to obtain a more complete check of the theory. There is a question regarding the appropriateness of the n_D values used rather than index of refraction values for frequencies in the range of the absorption band. This introduces doubt as to the absolute value of the slopes of the curves. However, the dependence of frequency upon index of refraction is definitely displayed, and the concept of the effect as originating in the polarization of the solvent is thereby confirmed.

The second phase of this investigation was concerned with the correlation of magnitude of frequency shift with type of transition being observed. The terminology used in identifying the transitions is that described by Platt[2] in his classification of the spectra of cata-condensed hydrocarbons. In this work a series of aromatics was examined in 2,2,4-tri-methylpentane solution and in benzene solution. The shifts toward lower frequencies induced by the change of solvent were then correlated with type of transition.

In Table I are given the observed frequencies in the paraffin solution and the tentative assignments using Platt's classification. The transitions are from the ground level to the state indicated. As these data were obtained at wavelength points separated by at least 0.5 $m\mu$ on the instrument named above, they do not possess the precision obtainable with more refined equipment. However, they are adequate for the purposes of this note, which is to point out the order-of-magnitude variations in the shifts observed for the different transitions.

In Table II are given the average values of $\Delta\nu$ for each transition induced by the change in solvent. These are averaged in each case over the individual values obtained for the separate

TABLE II. Average frequency shifts between paraffin and benzene solution for the assigned transitions.

Compound	$\Delta\nu('L_a)$	$\Delta\nu('L_b)$	$\Delta\nu('B_b)$
Phenanthrene	295	118	310
Anthracene	275	...	...
1,2 benzanthracene	312	155	570
9,10-dimethyl-1,2-benzanthracene	313	...	470
1,2,5,6-dibenzanthracene	297	150	440
Methylcolanthrene	340	210	470
Naphthacene	323	120	...

TABLE III. $\langle\Delta\nu\rangle_{Av}$ values observed for paraffin solutions.

Compound	$\langle\Delta\nu\rangle_{Av}('L_a)$	$\langle\Delta\nu\rangle_{Av}('L_b)$	$\langle\Delta\nu\rangle_{Av}('B_b)$
Phenanthrene	1320	705	1460
Anthracene	1430	...	...
1,2-benzanthracene	1350	690	1400
9,10-dimethyl-1,2-benzanthracene	1325	...	1300
1,2,5,6-dibenzanthracene	1250	697	1360
Methylcolanthrene	1410	725	1380
Naphthacene	1430	...	...

bands as listed in Table I. It is clear from the table that the $\Delta\nu$ for any transition remains of the same order of magnitude throughout the series of materials. Note also that $\Delta\nu('L_a)$ is generally of the order of twice the $\Delta\nu('L_b)$ and that $\Delta\nu('B_b)$ is of the order of three times $\Delta\nu('L_b)$. The approximate constancy of $\Delta\nu$ for a given transition thus provides a basis for the assignment of the bands to the various transitions for molecules not yet investigated.

Another correlation which may also serve in the assignments for further molecules resides in the separations between individual bands for any particular transition. In Table III are given the values of $\langle\Delta\nu\rangle_{Av}$ for the various transitions for each material. Here $\langle\Delta\nu\rangle_{Av}$ is the average frequency separation between the individual bands for any transition, as examined in the paraffin solution. Here it is evident that $\langle\Delta\nu\rangle_{Av}$ is always of the order of 1300 cm^{-1} for either $'L_a$ or $'B_b$ transitions whereas $\Delta\tilde{\nu}$ is always of the order of 700 cm^{-1} for the $'L_b$ transitions.

Following the reasoning of Jones,[3] the $\langle\Delta\nu\rangle_{Av}$ values as observed for the $'L_a$ and the $'B_b$ may tentatively be assigned to in-plane C—H bending vibrations. The $\langle\Delta\nu\rangle_{Av}$ values as observed for the $'L_b$ transitions are then tentatively assigned to out-of-plane C—H bending vibrations.

Acknowledgment is made to Mr. A. S. Glessner, who aided in obtaining some of the data.

[1] N. S. Bayliss, J. Chem. Phys. **18**, 292 (1950).
[2] J. R. Platt, J. Chem. Phys. **17**, 484 (1949).
[3] R. N. Jones, Chem. Revs. **41**, 353 (1947).

Concerning Cyclic Polyenes

JOHN F. TINKER
Converse Laboratory, Harvard University, Cambridge, Massachusetts
(Received May 10, 1951)

HÜCKEL has suggested that,[1] for optimum stabilization of a resonating system, $4n-2$ electrons (n is an integer) be involved. Applied to neutral compounds, this "rule" requires the presence of an odd number of conjugated double bonds, as in benzene. It is interesting to note that recent values[2] for resonance energy (in excess of benzene resonance) in styrene, a system of four double bonds, is about zero; that of stilbene, a system of seven, is about 6 kcal. This criterion augurs that heptalene and pentalene be less stable than azulene, contrary to some other calculations.[3] One attempt to prepare a heptalene[4] yielded instead an azulene, although the conditions were not mild. The criterion, applied to the proposed cyclic polyenes of Sworski[5] suggests that I would be more stable than II (Fig. 1).

Besides the consideration of resonance stabilization, steric effects must be taken into account. Figure 2 illustrates qualitatively the importance of resonance energy (ΔE_R in the figure) and destabilization due to unfavorable steric requirements (ΔE_s). The

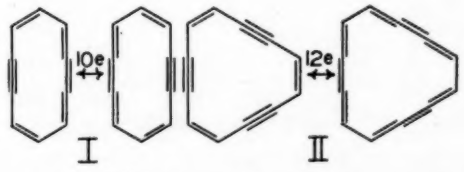

FIG. 1. Proposed polyenes of Sworski (see reference 5).

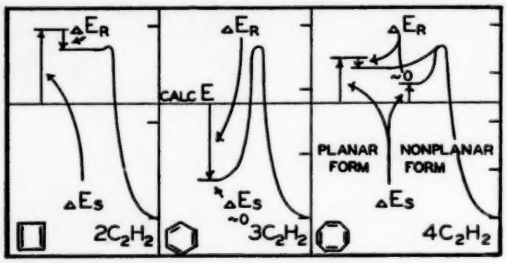

FIG. 2. Energy diagrams for the formation of three cyclic polyenes from acetylene.

three sections of Fig. 2, referring to cyclobutadiene, benzene, and cyclooctatetraene are on different scales, so as to be more readily comparable. The energy level near the center of the figure is the calculated energy content of the nonresonating system. The resonance energy is drawn small for the first (2 double bonds), large for the second (3 double bonds), and small for the third (4 double bonds); in the last case, the nonplanar form, with less strain and no resonance stabilization, is more stable than the planar, resonating form.

These considerations might be applied to various other cyclic polyenes. For instance, 1,3,5,7,9,11,13-tricyclo [9.3.0.0^{2,8}] tetradecaheptaene (III, Fig. 3) might be a stable compound, since

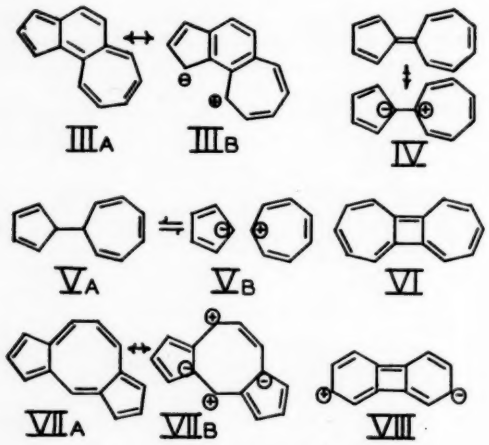

FIG. 3. Proposed cyclic polyenes.

(a) its steric requirements are the same as those of azulene, and (b) it has a system of *seven* conjugated double bonds. The resonance contributor IIIb has a sextet of electrons in each ring, and is analogous to phenanthrene.

Cycloheptatrienylidine cyclopentadiene[6] (IV) might similarly be considered the azulene analog of biphenyl.

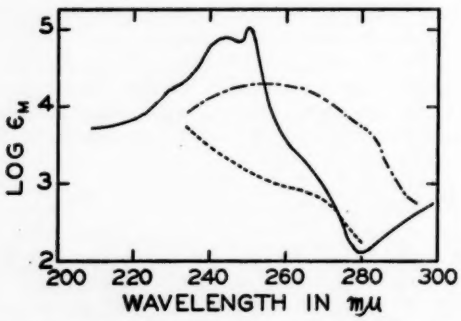

FIG. 4. Ultraviolet absorption spectra of ——— biphenylene (reference 7); — · — · — 4,4′-dimethylbiphenyl (reference 8); and - - - - - - - - 2,2′-dimethylbiphenyl (reference 8).

Cycloheptatrienyl cyclopentadiene (Va) would itself afford little resonance stabilization; but it might be in equilibrium with the fragments formed by breaking one bond, cycloheptatrienylinium cyclopentadienate (Vb); both fragments have a sextet of π-electrons.

None of the proposed compounds III, IV, V, have steric requirements different from those of azulene. The steric destabilization resulting from ring-size smaller than five or larger than seven might be assessed by studying compounds embodying an odd number of conjugated double bonds. Such a compound, containing a four-membered ring, is 1,3,5,7,9,11-tricyclo [7.5.0.0^{2,8}] tetradecaheptaene (VI). That the fused four-membered ring of VI might not entirely inhibit resonance is indicated by the ultraviolet absorption spectrum of biphenylene,[7] which shows absorption due to the increased contribution of the form VIII (Fig. 4).

A similar compound containing an eight-membered ring is 1,3,5,7,9,11-tricyclo [9.3.0.0^{8,7}] tetradecaheptaene (VII). The resonance contributors with separated charges (VIIb) have two sextets and one pair of π-electrons, although they bear two like charges.

Syntheses of several of these new compounds are under way.

[1] E. Hückel, Z. Physik **70**, 204 (1931); Chem. Abstracts **26**, 25 (1932).
[2] J. L. Franklin, J. Am. Chem. Soc. **72**, 4278 (1950).
[3] D. P. Craig and A. Maccoll, Nature **161**, 481 (1950).
[4] Horn, Nunn, and Rapson, Nature **160**, 829 (1947); D. H. S. Horn and W. S. Rapson, J. Chem. Soc. **1949**, 2421.
[5] T. J. Sworski, J. Chem. Phys. **16**, 550 (1948).
[6] First suggested by James H. Gardner III.
[7] Carr, Pickett, and Voris, J. Am. Chem. Soc. **63**, 3231 (1941).
[8] M. T. O'Shaughnessy and W. H. Rodebush, J. Am. Chem. Soc. **62**, 2906 (1940).

Kinetic Energy Matrix Elements for Linear Molecules

SALVADOR M. FERIGLE AND ARNOLD G. MEISTER
Spectroscopy Laboratory, Department of Physics, Illinois Institute of Technology, Chicago, Illinois
(Received May 24, 1951)

THE elements of the g matrix, as given by Wilson,[1] are

$$g_{mn}=\sum_{i=1}^{N}\mu_i\mathbf{s}_{mi}\cdot\mathbf{s}_{ni}, \tag{1}$$

where the sum is extended over the N atoms of the molecule, μ_i is the reciprocal of the mass of the ith atom, and $\mathbf{s}_{mi}$ is defined by

$$R_m=\sum_{i=1}^{N}\mathbf{s}_{mi}\cdot\mathbf{r}_i, \tag{2}$$

where R_m is the mth internal coordinate and $\mathbf{r}_i$ is the displacement vector of the ith nucleus from its equilibrium position. Wilson,[1] Decius,[2] and Lohman[3] have given expressions for the $\mathbf{s}$ vectors; and g matrix elements have been tabulated for the most common type of coordinates used in vibrational frequency calculations.[2,3]

As pointed out by Decius,[2] a deficiency occurs in the tables when a molecule contains a chain of three or more collinear nuclei. The expressions for the $\mathbf{s}$ vectors given by Wilson[1] cannot be used, since for the bending coordinates the denominator becomes zero. However, it is possible to obtain expressions for the $\mathbf{s}$ vectors for linear molecules in a very simple manner.

The following nomenclature will be used:

Q_{ij} = reciprocal of the equilibrium distance between the ith and the jth nuclei;

q_{ij} = change in the bond distance between the ith and jth nuclei from the equilibrium value;

γ_{jk}^{i} = equilibrium value of the angle having the ith nucleus as its apex and the jth and kth nuclei at the ends;

α_{jk}^{i} = change in the $j-i-k$ interbond angle from its equilibrium value;

$\mathbf{e}_{ij}$ = unit vector directed along the $i-j$ bond from the ith nucleus to the jth;

$\mathbf{f}_{jk}{}^{i}$ = unit vector in the plane $i-j-k$ perpendicular to the bond $i-j$ and directed towards the kth nucleus.

For small displacements of the nuclei from the equilibrium configuration the following approximate relations given by Eliashevich[4] follow from geometrical considerations:

$$\left.\begin{aligned} q_{ij} &= \mathbf{e}_{ij}\cdot(\mathbf{r}_j-\mathbf{r}_i), \\ \text{and} \quad \alpha_{jk}{}^{i} &= Q_{ij}(\mathbf{r}_i-\mathbf{r}_j)\cdot\mathbf{f}_{jk}{}^{i}+Q_{ik}(\mathbf{r}_i-\mathbf{r}_k)\cdot\mathbf{f}_{kj}{}^{i}. \end{aligned}\right\} \tag{3}$$

From Eqs. (2) and (3) one obtains

$$\left.\begin{aligned} &\mathbf{s}q_{ij},\, i = -\mathbf{e}_{ij} = \mathbf{e}_{ji}, \\ &\mathbf{s}q_{ij},\, j = \mathbf{e}_{ij}, \\ &\mathbf{s}\alpha_{jk}{}^{i},\, j = -Q_{ij}\mathbf{f}_{jk}{}^{i}, \\ &\mathbf{s}\alpha_{jk}{}^{i},\, k = -Q_{ik}\mathbf{f}_{kj}{}^{i}, \\ &\mathbf{s}\alpha_{jk}{}^{i},\, i = Q_{ij}\mathbf{f}_{jk}{}^{i}+Q_{ik}\mathbf{f}_{kj}{}^{i}. \end{aligned}\right\} \tag{4}$$

When the nuclei i, j, and k are not collinear, one obtains

$$\left.\begin{aligned} \mathbf{f}_{jk}{}^{i} &= (1/\sin\gamma_{jk}{}^{i})(\mathbf{e}_{ik}-\mathbf{e}_{ij}\cos\gamma_{jk}{}^{i}), \\ \mathbf{f}_{kj}{}^{i} &= (1/\sin\gamma_{jk}{}^{i})(\mathbf{e}_{ij}-\mathbf{e}_{ik}\cos\gamma_{jk}{}^{i}). \end{aligned}\right\} \tag{5}$$

Substitution of Eq. (5) into Eq. (4) leads to the **s** vectors given by Wilson:[1]

$$\left.\begin{aligned} &\mathbf{s}\alpha_{jk}{}^{i},\, j = (Q_{ij}/\sin\gamma_{jk}{}^{i})(\mathbf{e}_{ij}\cos\gamma_{jk}{}^{i}-\mathbf{e}_{ik}), \\ &\mathbf{s}\alpha_{jk}{}^{i},\, k = (Q_{ik}/\sin\gamma_{jk}{}^{i})(\mathbf{e}_{ik}\cos\gamma_{jk}{}^{i}-\mathbf{e}_{ij}), \\ &\mathbf{s}\alpha_{jk}{}^{i},\, i = (1/\sin\gamma_{jk}{}^{i})[Q_{ij}(\mathbf{e}_{ik}-\mathbf{e}_{ij}\cos\gamma_{jk}{}^{i}) \\ &\qquad\qquad +Q_{ik}(\mathbf{e}_{ij}-\mathbf{e}_{ik}\cos\gamma_{jk}{}^{i})]. \end{aligned}\right\} \tag{6}$$

For linear molecules the expressions given in Eq. (6) no longer hold, because the equations (5) for the **f** vectors are not valid. For this case it is difficult to define the **f** vectors, because an infinite number of planes can be passed through the nuclei i, j, and k. However, for linear molecules, normal coordinates corresponding to bending vibrations are formed by combination of displacements of the nuclei in a plane. Hence, one may define the **f** vectors in this plane, the **f** vectors of all the bonds being in the same direction. Equations (3) and (4) then hold for linear molecules, and one also has $\mathbf{f}_{jk}{}^{i}=\mathbf{f}_{kj}{}^{i}=\mathbf{f}$, where **f** is a unit vector, perpendicular to the axis of the molecule and in the plane in which the nuclei move for a particular normal vibration. From Eq. (1) one obtains the following expressions for the g matrix elements for the bending coordinates:

$$g_{\phi\phi}{}^{3} = \mu_2(Q_{12}+Q_{13})^2+\mu_3Q_{23}{}^2+\mu_1Q_{12}{}^2; \tag{7}$$

$$g_{\phi\phi}{}^{2}(^{1}_{0}) = -\mu_1(Q_{12}+Q_{14})Q_{12}-\mu_2(Q_{12}+Q_{23})Q_{12}; \tag{8}$$

$$g_{\phi\phi}{}^{1}(^{2}_{2}) = \mu_1Q_{12}Q_{14}. \tag{9}$$

The numbering of the nuclei and the angles involved follows that of Decius and is shown in Fig. 1.

One notices that Eqs. (7)–(9) agree with the corresponding relations given in the Decius tables, providing one lets $\gamma_{jk}{}^{i}=180°$ and $\tau=0°$. However, this substitution is not permissible in the tables, since the Decius relations were obtained from Eqs. (6), which are not valid for $\gamma_{jk}{}^{i}=180°$. The reason for the agreement is that the Decius relations can be obtained directly by use of Eqs. (4), which are valid for linear molecules and also are easier to work with than the more complicated Eqs. (6). Then, and that has been done in this communication, the difficulty in treating linear molecules disappears. However, the present justification seems necessary.

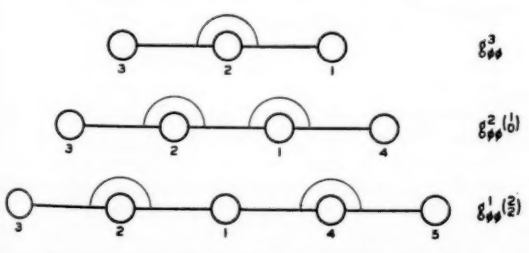

FIG. 1. The numbering of the atoms and bond angles involved for Eqs. (7)–(9).

[1] E. B. Wilson, Jr., J. Chem. Phys. **7**, 1047 (1939); **9**, 76 (1941).
[2] J. C. Decius, J. Chem. Phys. **16**, 1025 (1948).
[3] J. B. Lohman, Technical Report No. 17 ONR (1951).
[4] M. Eliashevich, Compt. rend. acad. sci. U.R.S.S. **28**, 604 (1940).

Effect of a Gaussian Distribution on Flow Birefringence

HAROLD A. SCHERAGA
Department of Chemistry, Cornell University, Ithaca, New York
(Received May 24, 1951)

THE use of Sadron's equations[1] for the extinction angle, χ, and the magnitude of the birefringence, Δn, in double refraction of flow measurements in polydispersed systems is relatively simple for a small, discrete number of particle sizes[2] (e.g., a binary system of monomers and dimers). For systems having a wide distribution of sizes as in the case of gelatin[3] or soap micelles[4] the calculations become quite extensive; besides, it is conceivable that a unique solution for the distribution may not always be possible in some cases. To obtain some idea of the behavior to be expected from varying degrees of polydispersity some calculations involving a gaussian distribution of elongated ellipsoidal particles are presented.

Since measurements over a wide range of velocity gradients are required to characterize a polydispersed system, the discussion is restricted to the case of rigid ellipsoidal particles for which a theory for both small and large gradients exists, *viz.*, the orientation theory of Peterlin and Stuart[5] with the numerical solutions of Scheraga, Edsall, and Gadd.[6] Also, since many polydispersed systems are polymers of some single fundamental unit, it seems reasonable to assume that all particles in such systems possess the same optical factor,[5] thereby enabling the birefringence for any single species of particles to be characterized by its volume fraction and the orientation factor it would have if present alone in the system.

The distribution function for the volume fraction may be written as

$$(h/\pi^{\frac{1}{2}})\exp[-h^2(\Delta L/L_0)^2], \tag{1}$$

where L is the length of the particle, L_0 the mean length, $\Delta L = L-L_0$, and h is a constant characterizing the spread of the distribution. For a monodispersed system $h=\infty$; as the system becomes more polydispersed, h approaches zero.

For such a distribution Sadron's equations require the evaluation of

$$A = (h/\pi^{\frac{1}{2}})\int f\sin 2\varphi\cdot\exp[-h^2(\Delta L/L_0)^2]dL \tag{2}$$

and

$$B = (h/\pi^{\frac{1}{2}})\int f\cos 2\varphi\cdot\exp[-h^2(\Delta L/L_0)^2]dL, \tag{3}$$

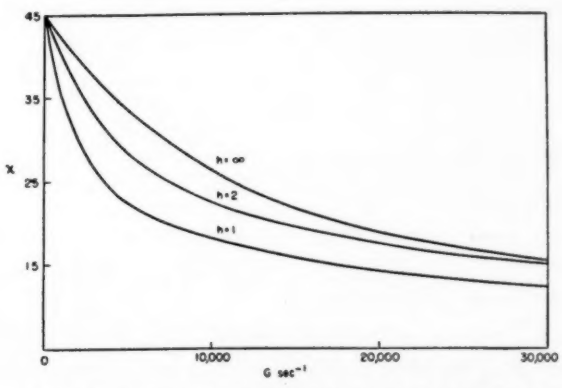

FIG. 1. Dependence of extinction angle on velocity gradient for several values of the parameter h.

where f and φ are the orientation factor and extinction angle, respectively, for each particle length if present alone in the solution. The resultant extinction angle is given by

$$\tan 2\chi = A/B \tag{4}$$

with a similar expression for the orientation factor. For low gradients the limiting laws of Peterlin and Stuart may be used to obtain f and φ as functions of L. For a wide range of gradients the data of Scheraga, Edsall, and Gadd may be used, performing the integration graphically. This latter procedure is illustrated for a particle distribution where $L_0 = 2000$A, minor axis $= 50$A, and $h = 1$, 2, and ∞. Figure 1 shows the calculated dependence of χ on velocity gradient, thereby illustrating the effects to be expected in polydispersed systems having the assumed distribution of particle sizes. The behavior of the birefringence shows the orientation character of a monodispersed system of rigid particles with similar deviations due to polydispersity.

The available data[6] are not sufficiently extensive for calculations for values of h close to zero. However, it may be inferred that as h approaches zero, the relative concentration of extremely long particles (for which $L \to \infty$, or rotary diffusion constant, $\theta \to 0$) becomes large, so that the observed birefringence is due essentially to the long particles. Thus, the value of θ at $G = 0$ and $h = 0$ is probably zero, so that the χ *vs* G curve for $h = 0$ has a vertical tangent at $G = 0$.

For small h the χ *vs* G curve becomes relatively horizontal as G increases. For a gaussian distribution, all experimental curves would lie lower than the curve for a monodispersed system of particles of length L_0 showing the effect of the longer particles. Thus, in a polydispersed system the experimental data give a rotary diffusion constant smaller than that corresponding to L_0; therefore, one knows at least the maximum value of L_0. As G approaches infinity, all the curves approach the one for $h = \infty$ and the mean rotary diffusion constant results.

In treating experimental data such calculations can give some idea of the distribution in polydispersed systems, the existence of the polydispersity in a system of rigid particles being suggested by the variation of θ with G. It should be kept in mind that the precision of the experimental data may not always permit the choice of a unique pair of parameters h and L_0 to characterize the distribution.

[1] C. Sadron, J. Phys. Radium (7) **9**, 381 (1938).
[2] C. Sadron and H. Mosimann, J. Phys. Radium (7) **9**, 384 (1938).
[3] J. T. Edsall and J. F. Foster (unpublished results). These results were referred to in Scatchard, Oncley, Williams, and Brown, J. Am. Chem. Soc. **66**, 1980 (1944), and reported at the Fourth Conference on Gelatin, Subcommittee on Blood Substitutes, National Research Council, March 3, 1944.
[4] H. A. Scheraga and J. K. Backus, J. Am. Chem. Soc., to be published.
[5] A. Peterlin and H. A. Stuart, Hand. u. Jahrb. chem. Physik (1943), Vol. 8, Part 1B.
[6] Scheraga, Edsall, and Gadd, submitted to J. Chem. Phys.

The Dependence of the Diffusion Coefficient on Concentration in Dilute Polymer Solutions*

LEO MANDELKERN AND P. J. FLORY
Department of Chemistry, Cornell University, Ithaca, New York
(Received May 22, 1951)

ONSAGER and Fuoss[1] have shown that the diffusion coefficient, D, is related to the frictional coefficient f, and the activity coefficient γ_2 by

$$D = (RT/f)(1 + d\ln\gamma_2/d\ln c_2), \tag{1}$$

where c_2 is the concentration in moles per unit volume. For a binary system it follows that

$$D = (M/f)\partial\pi/\partial c, \tag{2}$$

where M is the solute molecular weight, c the concentration in grams per cc, and π the osmotic pressure.

A recent statistical treatment of dilute polymer solutions[2] has led to the following relation:

$$(\pi/c) = (\pi/c)_0[1 + \Gamma_2 c + \tfrac{5}{8}\Gamma_2^2 c^2 + \cdots] \tag{3}$$

for $(\pi/c)/(\pi/c)_0 < 3$, where Γ_2 depends explicitly on the molecular weight and thermodynamics of polymer-solvent interaction. The application of this equation to the interpretation of osmotic pressure, and of the related equation to light scattering data, has been discussed recently.[3] Equation (3) can be combined with Eq. (2) to give

$$Df/RT \cong [1 + 2\Gamma_2 c + (15/8)\Gamma_2^2 c^2 + \cdots]. \tag{4}$$

The right-hand side of Eq. (4) is equal to $(c/\tau)/(c/\tau)_0$, where τ is the excess turbidity of the solution over that of the solvent.

If Γ_2 for the given polymer and solvent is established from osmotic or from light scattering measurements, the diffusion constant at a given (low) concentration may be computed according to Eq. (4) from the frictional coefficient determined at the same concentration. The latter ordinarily is determined from sedimentation velocity measurements, and may be expressed satisfactorily at low concentrations by

$$f = f_0(1 + k_1 c). \tag{5}$$

It follows that

$$D/D_0 = [1 + 2\Gamma_2 c + (15/8)\Gamma_2^2 c^2]/(1 + k_1 c) \tag{6}$$

providing the solution is sufficiently dilute to justify use of Eqs. (3) and (5). Although diffusion coefficients generally have been assumed to vary linearly with concentration, Eq. (6) indicates that this assumption may introduce a serious error in the extrapolated D_0.

Values of D/D_0 have been computed as a function of concentration from this equation for fractions of polystyrene in toluene and in methyl ethyl ketone. The values of the parameters used are listed in Table I. The Γ_2's, in units of 100 cc per gram, were

TABLE I. Values of Γ_2 and k_1 used to calculate the diffusion coefficient of polystyrene in solution.

Molecular weight	Solvent	Γ_2 in 100 cc/g	k_1 in 100 cc/g
1,240,000	Toluene	2.45	4.0
254,000	Toluene	0.84	1.5
1,240,000	Methyl ethyl ketone	0.78	2.3

obtained from the osmotic pressure data of Mark and Frank,[4] and of Bawn, Freeman, and Kamaliddin,[5,6] while the values of k_1, in the same units, were taken from the sedimentation studies of Newman and Eirich.[7] Plotted in Fig. 1 are the results of this calculation; D/D_0 is decidedly nonlinear with c at very low concentrations, although it is approximately linear over a limited

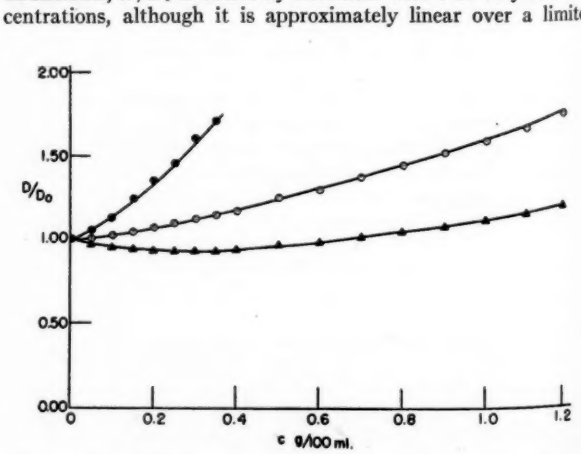

FIG. 1. D/D_0 as a function of concentration for polystyrene solutions. $M = 1{,}240{,}000$ in toluene (●); $M = 254{,}000$ in toluene (⊙); $M = 1{,}240{,}000$ in MEK (▲).

portion of the curve at higher concentrations. The value of D_0 obtained by linear extrapolation through this portion would be appreciably in error. In fact, for polystyrene in methyl ethyl ketone, the initial slope $(2\Gamma_2-k_1)$ is negative, as has been noted previously;[7,8] a minimum is reached at a rather low concentration, beyond which the curve rises with concentration.

The above analyses cast serious doubt on the reliability of D_0 values reported in the literature for randomly coiled polymers, since these invariably have been obtained by *linear* extrapolation. Equation (6) can be rewritten as

$$[1+2\Gamma_2 c+(15/8)\Gamma_2^2 c^2]/D=(1+k_1 c)/D_0. \quad (7)$$

If Γ_2 is known and diffusion measurements are made in the concentration range for which Eq. (7) is valid, a plot of the left side of (7) against c should be linear and the intercept should equal $1/D_0$. In this manner reliable values of D_0 can be obtained. Having established Γ_2 from thermodynamic measurements, values of f and of s, the sedimentation velocity constant, can be obtained from D; experimental determination of both D and s is unnecessary.

* This work was carried out at Cornell University as part of a research program supported by the Allegany Ballistics Laboratory, Cumberland, Maryland, an establishment owned by the United States Navy and operated by the Hercules Powder Company under Contract NOrd 10431.

[1] L. Onsager and R. M. Fuoss, J. Phys. Chem. **36**, 2689 (1932).
[2] P. J. Flory and W. R. Krigbaum, J. Chem. Phys. **18**, 1086 (1950).
[3] Fox, Flory, and Bueche, J. Am. Chem. Soc. **73**, 285 (1951).
[4] H. P. Frank and H. Mark, J. Polymer Sci. **6**, 243 (1950).
[5] Bawn, Freeman, and Kamaliddin, Trans. Faraday Soc. **46**, 862 (1950).
[6] We are indebted to Dr. W. R. Krigbaum for the calculation of the values of Γ_2.
[7] S. Newman and F. Eirich, J. Colloid Sci. **5**, 541 (1950).
[8] A. F. Schick and S. J. Singer, J. Phys. and Colloid Chem. **54**, 1028 (1950).

The Role of Chlorine in the Luminescence of ZnS:Cu Phosphors

RICHARD H. BUBE
Radio Corporation of America, RCA Laboratories Division, Princeton, New Jersey
(Received May 21, 1951)

A CORRELATION between the proportion of copper and the proportion of chlorine incorporated in ZnS:Cu phosphors, prepared in an atmosphere of H_2S and HCl, has been reported by Kroeger, Hellingman, and Smit.[1] This letter presents the result of analyses for incorporated chlorine made on a series of cubic and hexagonal ZnS:Cu phosphors prepared with 2 percent NaCl by weight. The present study was undertaken (1) to determine if the incorporation of chlorine is independent of whether NaCl or HCl is used as a source of chlorine, and (2) to obtain values for the proportion of chlorine incorporated over a wider range of copper proportions than that previously reported. The luminescence characteristics of the phosphors used in this study have been previously published.[2]

Approximately 2 grams of the sample to be tested was placed in a Soxhlet extractor in which it was washed about once every two minutes with hot water which was originally triple-distilled. The sample was washed in this way for six hours and was then dried at 150°C. The dried sample was treated with dilute HNO_3 until about 10 percent of the sample by weight had been dissolved. This treatment with HNO_3 was suggested by H. W. Leverenz to remove any chlorine bound too tightly to the surfaces of phosphor particles to be removed by water washing. The sample was then washed three times by decantation with triple-distilled water, dried, and returned to the extractor for four more hours of hot water washing. Finally, the sample was dried, and a portion was completely dissolved with HNO_3. One drop of 1 N $AgNO_3$ was added to a 3-ml solution of the sample. The turbidity of the resulting solution was compared with standard 3-ml solutions containing known amounts of NaCl and one drop of 1 N $AgNO_3$.

The variation of the proportion of chlorine incorporated with the proportion of copper is given in Table I for both the cubic and the hexagonal phosphors. The values of chlorine concentration have a possible error of about ±20 percent. The blank spaces in the table occur for samples which had been used up in previous measurements.

TABLE I. Determination of chlorine concentration.

	Cubic		Hexagonal	
Cu conc. mol ppm*	Cl conc. mol ppm	Cl conc. / Cu conc.	Cl conc. mol ppm	Cl conc. / Cu conc.
1.5	130	87	125	83
15	250	17	190	13
45	150	3.3	185	4.1
155	...	...	375	2.4
460	360	0.78	590	1.3
1530	445	0.29	...	...
4590	2070	0.45	1630	0.36

* 1 mole part per million (mol ppm) = 1 microgram atom per mole of phosphor.

These results are a confirmation of the major thesis of Kroeger, Hellingman, and Smit, that chlorine is actually incorporated in ZnS:Cu phosphors, and that the proportion of chlorine incorporated is a function of the copper proportion. Approximately the same results are found regardless of whether NaCl or HCl is used as a source of chlorine. The analytical procedure used to obtain the values given in Table I insures that the chlorine detected is incorporated as a part of the phosphor crystal, and is not simply adsorbed on surface layers.

These results also support a previously reported hypothesis[2] correlating the luminescence emission of ZnS:Cu phosphors with the location of the Cu ions in the crystal structure. It was proposed that, at low copper proportions, interstitially located copper ions are responsible for a green luminescence emission and for the formation of deep electron traps. The location of copper ions (possibly Cu^+) in interstitial positions is expedited by the incorporation of at least an equal number of chloride ions. If the copper proportion exceeded a certain limit, however, a blue luminescence emission was found together with the green emission, and the deeper traps were destroyed. This blue emission is associated with the substitutional location of copper ions (possibly Cu^{++}) for which corresponding chloride ions are not available in the crystal.

If this hypothesis is correct, the blue band should appear when the ratio of chlorine to copper concentration becomes less than unity. For very low copper proportions, for which the ratio of chlorine to copper concentration is much greater than unity, the major portion of the incorporated chloride ions are involved in the formation of host crystal emission centers.

The blue luminescence emission appears for a copper concentration between 155 and 460 mol ppm for cubic phosphors, but between 460 and 1530 mol ppm for hexagonal phosphors. It may be noted from Table I that the ratio of chlorine to copper concentration has fallen below unity for a Cu concentration of 460 mol ppm for the cubic phosphors, but does not fall below unity for the hexagonal phosphors until Cu concentrations of greater than 460 mol ppm have been obtained.

Kroeger, Hellingman, and Smit report approximately one chlorine for each two copper atoms in the range of copper proportions for which a blue emission is found. The data of Table I indicate that a ratio of approximately this value is found for the phosphors analyzed in the present study. Inasmuch as only a green emission is found for the phosphors with 4590 mole ppm of copper, however, it does not seem that a definite association between the blue-emitting centers and the ratio of one chlorine to two coppers can be claimed.

The author wishes to thank Dr. S. M. Thomsen for assistance in organizing the analytical procedure.

[1] Kroeger, Hellingman, and Smit, Physica **15**, 990 (1949).
[2] R. H. Bube, Phys. Rev. **80**, 655, 764 (1950); **81**, 633 (1951).

Energy Transfer between Complex Molecules

MARGARET M. MOODIE AND C. REID
Department of Chemistry, University of British Columbia, Vancouver, Canada
(Received May 21, 1951)

RECENTLY, observations have been made[1-3] of the transfer of energy absorbed by one kind of molecule to a different molecular species from which it is subsequently emitted as light. Experiments hitherto reported, whether made on absorbing crystals containing impurities or on substances dissolved in absorbing solvents, have one feature in common. The process can always be visualized as a succession of transfer steps between adjacent molecules; and it is impossible unambiguously to decide whether the mechanism is one of "resonance fluorescence" or involves an electron transfer step.

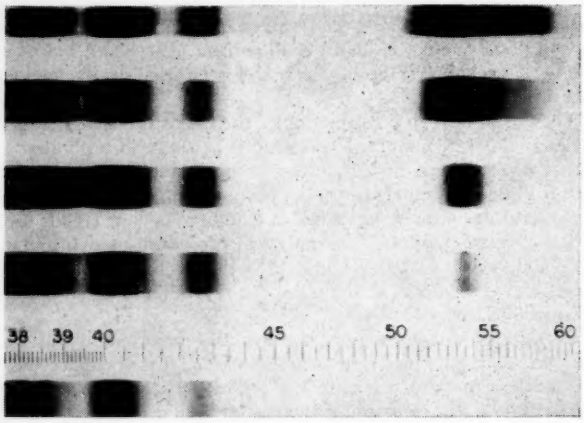

FIG. 1. Emission of suspended naphthacene crystals in the presence of varying amounts of dissolved anthracene. The anthracene emission (on left in picture) shows little variation as its concentration increases from 10^{-4} mole/liter in the bottom picture to 7.5×10^{-4} in the top one. The naphthacene emission (on right in picture) shows a very large increase in intensity as the anthracene concentration increases, although the amount of naphthacene is the same in all cases. Hilger E_2 spectrograph. Exposure time—5 minutes. Source—General Electric A.H. 6 mercury arc. Slit 0.2 mm. Scale in hundreds of A.

In order to study possible energy transfer processes over greater distances the authors have examined the low temperature emission spectra of systems containing two different substances dissolved in a rigid glassy medium, irradiated with light of a wavelength absorbed by one of the substances, but not by the other, or by the solvent. It has been found that when the emission region of the primary absorber overlaps the absorption region of the second substance, a transfer of energy may occur.

Lack of reproducibility in our earlier experiments has been traced to a surprising phenomenon. When the second substance is present in microcrystalline form rather than in true solution, the efficiency of the transfer process is enormously increased. Figure 1 shows the effect of increasing amounts of dissolved anthracene on the emission of an ether-isopentane-alcohol glass containing suspended microcrystals of naphthacene. Although the emission observed lies in the same region as that of crystalline naphthacene alone, it is not identical with that of the crystals, showing that the process is not the trivial one of absorption followed by re-emission. In fact, the band occurs exactly where the 0—0 transition of the crystal band is predicted by comparison of the absorption and emission spectra. This transfer process appears to be more efficient by a factor of at least 1000 than that occurring when both substances are dissolved.

Examination of several other pairs of substances shows that the phenomenon is quite a general one. Energy transfer has been shown to occur to such molecules as dibenzanthracene, rhodamine G, and pinacyanol. In a few cases—e.g., that of *p* amino-azobenzene—no emission is observed in the spectral region examined (up to 7500A) although the emission of the primary absorber is quenched. Whether this is because the emission lies in the infrared or because of some kind of quenching process has not been determined.

The explanation of the highly efficient transfer to microcrystals must be either that the dissolved absorber molecules become oriented in the field of the crystal before the glass has become rigid, or that the effect is actually due to adsorption on the microcrystal surface. We have as yet found no evidence for the latter process. If the former one is correct—i.e., there is orientation but no local concentration of absorber molecules around the microcrystals—transfer of energy must be occurring over distances greater than 100A and is therefore probably taking place by the mechanism suggested by Forster.[4]

It is felt, in view of the above result, that the importance of the state of aggregation of the components of the biologically important systems concerned with energy transfer (e.g., in photosynthesis or the respiration process) has not in the past been sufficiently well appreciated. Conflicting results (such as those concerning the possible long-lived phosphorescent state of chlorophyll)[5] may be attributable to the neglect of this fact. We propose to reinvestigate such processes using the technique described above. Details of the above work including lifetimes and (it is hoped) absolute quantum yields will be given in a forthcoming paper.

[1] Bowen, Mikiewiez, and Smith, Proc. Phys. Soc. (London) **A62**, 26 (1949).
[2] H. Kallman and M. Furst, Phys. Rev. **79**, 857 (1950); **81**, 853 (1951).
[3] A. J. Dekker and F. Lipsett, private communication.
[4] C. Forster, Ann. Physik **2**, 55 (1948).
[5] J. Frank and W. E. Loomis, *Photosynthesis in Plants*, p. 182.